THE JOURNAL OF

PHYSICAL CHEMISTRY

Volume 74, Number 3 February 5, 1970

Lattice Contributions to Electric Field Gradient Calculations in Heavy Metal Chlorides . . . **Thomas B. Brill, Z Z. Hugus, Jr., and A. F. Schreiner** 469

On the Calculation of Intramolecular Radiationless Relaxation Rates . . . **S. E. Webber** 475

A Statistical Treatment of Micellar Solutions . . . **H. S. Chung and I. J. Heilweil** 488

Adsorption from Solution. III. A New Model for the Kinetics of Adsorption–Desorption Processes . . . **F. T. Lindstrom, R. Haque, and W. R. Coshow** 495

Diffusion and Solubility of Hydrogen in Palladium and Palladium–Silver Alloys . . . **Gerhard L. Holleck** 503

The Crystal Structure of the *cis*-1,2-Cyclohexanedicarboxylic Acid . . . **Ettore Benedetti, Carlo Pedone, and Giuseppe Allegra** 512

Antagonistic Interactions between Copper Sulfate and Tetra-*n*-butylammonium Salts in Water at 25° . . . **Joseph Steigman and Mario Della Monica** 516

Study of Ionic Surfactants by Membrane Osmometry . . . **H. Coll** 520

The Time Dependence of Effusion Cell Steady-State Pressures of Carbon Monoxide and Calcium Vapors Generated by the Interaction of Calcium Oxide and Graphite . . . **Juey Hong Rai and N. W. Gregory** 529

Spectroscopic Studies of Ionic Solvation in Pyridine Solutions . . . **William J. McKinney and Alexander I. Popov** 535

Infrared Matrix Isolation Spectrum of the Methyl Radical Produced by Pyrolysis of Methyl Iodide and Dimethyl Mercury . . . **Alan Snelson** 537

Structure and Conformations of Free Radicals. II. Radical Ions from Nitrophenyl Aromatic Hydrocarbons . . . **Graham R. Underwood, Don Jurkowitz, and S. Carlton Dickerman** 544

Reactions of Electrons Photoejected from Aromatic Amino Acids in Frozen Aqueous Solutions of Divalent Metal Salts . . . **René Santus, Annie Hélène, Claude Hélène, and Marius Ptak** 550

The Single Crystal Spectra of Dichlorotetrapyrazolenickel(II), Dibromotetrapyrazolenickel(II), and Hexapyrazolenickel(II) Nitrate . . . **Curt W. Reimann** 561

The Photochemistry of N_3^- in Aqueous Solution at 2288 and 2139 Å . . . **I. Burak, D. Shapira, and A. Treinin** 568

Photochemistry of Methylfurans. Selectivities of Ring Contraction Reactions . . . **H. Hiraoka** 574

Radiolysis of Water Vapor in a Wide Range Radiolysis Source of a Mass Spectrometer. I. Individual and Total Cross Sections for the Production of Positive Ions, Negative Ions, and Free Radicals by Electrons . . . **Charles E. Melton** 582

Ionic Reactions in Gaseous Methylsilane . . . **P. Potzinger and F. W. Lampe** 587

Effect of Association with Phenol on Rotation around the (Thio) Carbonyl-to-Nitrogen Bond in an Amide and a Thionamide . . . **T. H. Siddall, III, E. L. Pye, and W. E. Stewart** 594

The Use of Differential Reaction Kinetics in Determining Rate Constants of Hydroxyl–Isocyanate Reactions . . . **Friso Willeboordse** 601

Ionic Polymerization under an Electric Field. XIII. Living Anionic Polymerization of Styrene in the Binary Mixtures of Benzene and Dimethoxyethane by the Three-State Mechanism . . . **Norio Ise, Hideo Hirohara, Tetsuo Makino, Katsuhiko Takaya, and Masatoshi Nakayama** 606

Addition of Oxygen Atoms to Olefins at Low Temperature. IV. Rearrangements . . . **Ralph Klein and Milton D. Scheer** 613

A Concentration-Jump Relaxation Method Study on the Kinetics of the Dimerization of the Tetrasodium Salt of Aqueous Cobalt(II)–4,4′,4″,4‴-Tetrasulfophthalocyanine . . . **Z. A. Schelly, R. D. Farina, and E. M. Eyring** 617

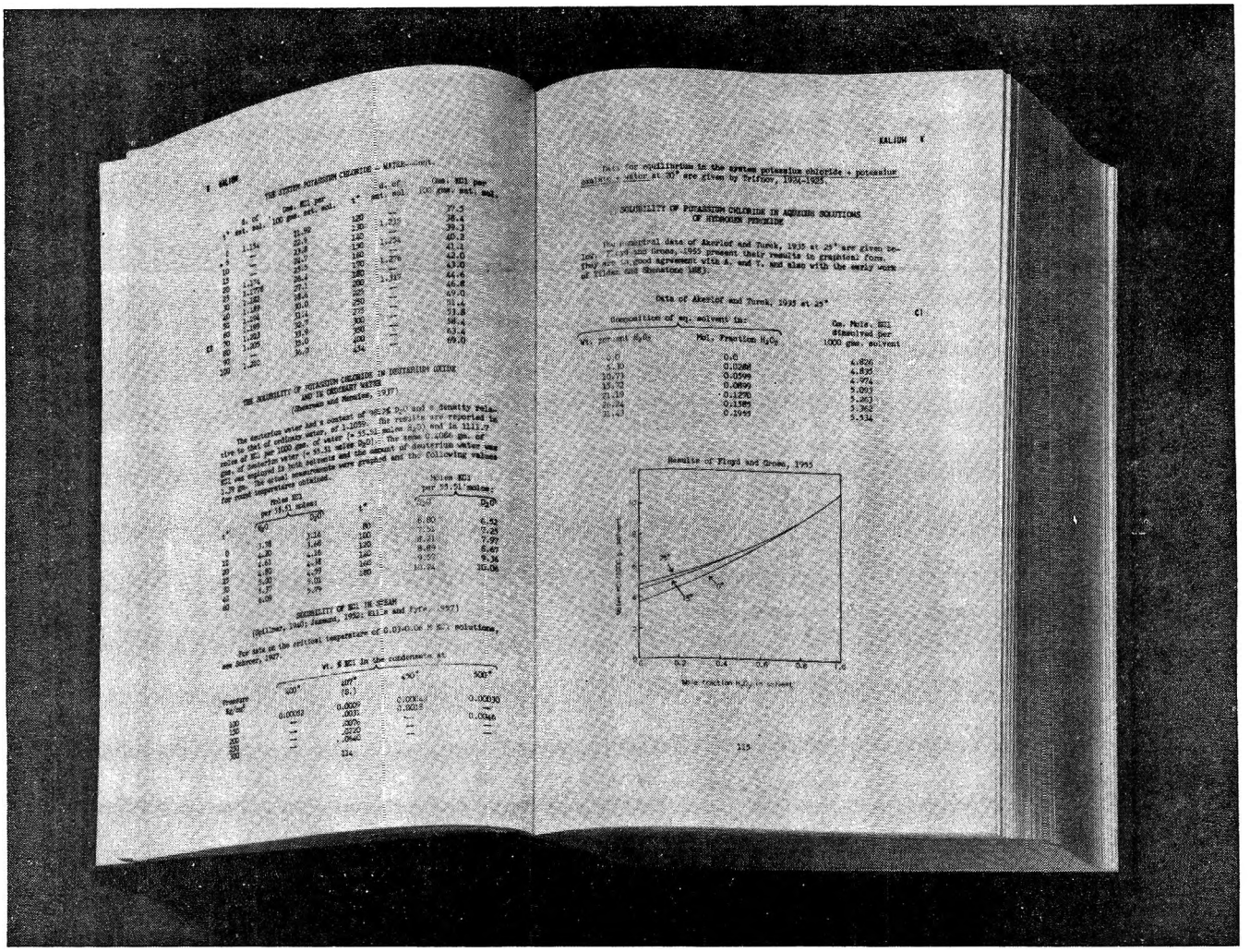

NOW AVAILABLE ..... FROM THE AMERICAN CHEMICAL SOCIETY

A valuable, new edition of an essential chemical reference—

Volume II of the Fourth Edition of Seidell's SOLUBILITIES OF INORGANIC AND METAL ORGANIC COMPOUNDS

Illustrated above are two of the 57 pages of data on solubilities of only *one* inorganic compound, potassium chloride, in various solvents and with various compounds. Volume II has a total of 1,914 pages of critically evaluated data, with tables, values at various temperatures, and melting point references . . . all systematically arranged for quick reference. And data are given for 1,281 other compounds besides potassium chloride and for 26 elements as well, covering the elements with symbols from K through Z.

Volume I appeared in 1959. With the appearance of Volume II in 1966 the data for inorganic and metal organic compounds in the Fourth Edition is now complete . . . a painstaking revision by Dr. William F. Linke, American Cyanamid Company, continuing the compendium started by the late Dr. Atherton Seidell.

The book is a time-saving work aid, clearly indexed, and carefully cross-referenced with Volume I in terms of subject matter and literature cited in both volumes.

Seidell-Linke, "Solubilities of Inorganic and Metal Organic Compounds," Fourth Edition, Vol. II. iii 1,941 pages. Cloth bound. (1966) . . . **$32.50**

Order from:
Special Issues Sales Dept. J
AMERICAN CHEMICAL SOCIETY
1155 Sixteenth Street, N.W.
Washington, D. C. 20036

Angular Dependence of Long-Range Proton Hyperfine Coupling Constants in Aliphatic Radicals . . . **Michael Barfield** 621

The Relative Stabilities of Perchlorate, Perbromate, and Periodate Ions . . . **Margaret M. Cox and John W. Moore** 627

Surface and Interfacial Tensions of Polymer Melts. II. Poly(methyl methacrylate), Poly(*n*-butyl methacrylate), and Polystyrene . . . . . **Souheng Wu** 632

Electron Acceptor–Electron Donor Interactions. XV. Examination of Some Weak Charge-Transfer Interactions and the Phenomenon of Thermochromism in These Systems . . . . . **P. R. Hammond and L. A. Burkardt** 639

Electron Acceptor–Electron Donor Interactions. XVI. Charge-Transfer Spectra for Solutions of Tungsten and Molybdenum Hexafluorides and Iodine Heptafluoride in *n*-Hexane and Cyclohexane. Donor Properties of the Aliphatic Hydrocarbons . . . . . **P. R. Hammond** 647

Acid–Base Catalysis of Dielectric Relaxation of Zwitterions . . . . . **Gerhard Schwarz** 654

Volume–Temperature Relationships of Hydrophobic and Hydrophilic Nonelectrolytes in Water . . . **J. L. Neal and D. A. I. Goring** 658

NOTES

Secondary Valence Force Catalysis. X. Fluorine-19 Chemical Shifts as a Probe for Localization of Organic Substrates in Micellar Systems . . . **Paul A. Arrington, A. Clouse, David Doddrell, R. B. Dunlap, and E. H. Cordes** 665

On the Interaction of Solute Molecules with Porous Networks . . . . . **A. G. Ogston** 668

An Electron Spin Resonance Study of Acetate Dianion and Acetamide Anion . . . . . **Michael D. Sevilla** 669

Ultrasonic Attenuation in Aqueous Triethylamine . . . . . **Robert Scott Brundage and Kenneth Kustin** 672

Retention of Configuration during Recoil Tritium Reactions at Asymmetric Carbon Positions in 2,3-Dichlorobutane . . . **Yi-Noo Tang, C. T. Ting, and F. S. Rowland** 675

A Multilayer Isotherm with Sensible Spreading Pressure Limits . . . . . **C. M. Greenlief and G. D. Halsey** 677

Radiation-Induced Chain Decomposition of Hexachloroethane in Cyclohexane Solutions. Reactions of the Pentachloroethyl Radical . . . . . **A. Horowitz and L. A. Rajbenbach** 678

The Wavelength Dependence of the Primary Processes in the Photolysis of Sulfur Dioxide . . . **T. Navaneeth Rao and Jack G. Calvert** 681

COMMUNICATIONS TO THE EDITOR

Entropies of Sodium and Hydroxide Ions and the Thermodynamics of Ionization of Water . . . **John W. Larson** 685

AUTHOR INDEX

Allegra, G., 512
Arrington, P. A., 665

Barfield, M., 621
Benedetti, E., 512
Brill, T. B., 469
Brundage, R. S., 672
Burak, I., 568
Burkardt, L. A., 639

Calvert, J. G., 681
Chung, H. S., 488
Clouse, A., 665
Coll, H., 520
Cordes, E. H., 665
Coshow, W. R., 495
Cox, M. M., 627

Della Monica, M., 516
Dickerman, S. C., 544
Doddrell, D., 665
Dunlap, R. B., 665

Eyring, E. M., 617

Farina, R. D., 617

Goring, D. A. I., 658
Greenlief, C. M., 677
Gregory, N. W., 529

Halsey, G. D., 677
Hammond, P. R., 639, 647
Haque, R., 495
Heilweil, I. J., 488
Hélène, A., 550
Hélène, C., 550
Hiraoka, H., 574
Hirohara, H., 606
Holleck, G. L., 503
Horowitz, A., 678
Hugus, Z Z., Jr., 469

Ise, N., 606

Jurkowitz, D., 544

Klein, R., 613
Kustin, K., 672

Lampe, F. W., 587
Larson, J. W., 685
Lindstrom, F. T., 495

Makino, T., 606
McKinney, W. J., 535
Melton, C. E., 582
Moore, J. W., 627

Nakayama, M., 606
Neal, J. L., 658

Ogston, A. G., 668

Pedone, C., 512
Popov, A. I., 535
Potzinger, P., 587
Ptak, M., 550
Pye, E. L., 594

Rai, J. H., 529
Rajbenbach, L. A., 678
Rao, T. N., 681
Reimann, C. W., 561
Rowland, F. S., 675

Santus, R., 550
Scheer, M. D., 613
Schelly, Z. A., 617
Schreiner, A. F., 469
Schwarz, G., 654
Sevilla, M. D., 669
Shapira, D., 568
Siddall, T. H., III, 594
Snelson, A., 537
Steigman, J., 516
Stewart, W. E., 594

Takaya, K., 606
Tang, Y.-N., 675
Ting, C. T., 675
Treinin, A., 568

Underwood, G. R., 544

Webber, S. E., 475
Willeboordse, F., 601
Wu, S., 632

THE JOURNAL OF
PHYSICAL CHEMISTRY

Registered in U. S. Patent Office © Copyright, 1970, by the American Chemical Society

VOLUME 74, NUMBER 3 FEBRUARY 5, 1970

Lattice Contributions to Electric Field Gradient Calculations in Heavy Metal Chlorides[1a]

by Thomas B. Brill,[1b] Z Z. Hugus, Jr., and A. F. Schreiner

North Carolina State University, School of Physical Sciences and Applied Mathematics, Department of Chemistry, Raleigh, North Carolina 27607 *(Received July 25, 1969)*

Electric field gradients at ^{35}Cl nuclei were interpreted for K_2PtCl_4, K_2PtCl_6, K_2ReCl_6, and $HgCl_2$ by taking into account extramolecular fields (lattice contributions), intramolecular fields, and the Sternheimer effect. Lattice field gradients were determined, using a point charge model, for all extramolecular charges within a chosen sphere whose origin was at the chlorine nucleus in question. Intramolecular field gradients were computed from atomic orbital occupations and the Townes and Dailey relationship. It was found that the lattice makes small but variable contributions to the experimentally observed nuclear quadrupole coupling constants. In K_2PtCl_4 the lattice was found to have a pronounced effect on the asymmetry parameter of the field gradient. For $HgCl_2$ the results of our calculations are consistent with the asymmetry parameters measured by Negita, *et al.*, for the chlorine atoms in $HgCl_2$ and do not concur with those of Dinesh, *et al.*, and Ramakrishna.

Introduction

The electric field gradient (EFG) is defined by a symmetric second rank tensor, **q**, with components

$$q_{ij} = \frac{\partial^2 V}{\partial x_i \partial x_j}$$

where V is the electrostatic potential at the nucleus due to surrounding charges, and in cartesian coordinates, x_i, x_j correspond to x, y, and z. If **q** is expressed in the principal axis coordinate system, only diagonal elements remain, and Laplace's equation requires that

$$q_{xx} + q_{yy} + q_{zz} = 0 \quad (1)$$

As is usually done,[2] we have chosen the axes, x, y, and z, so that

$$|q_{zz}| \geq |q_{yy}| \geq |q_{xx}| \quad (2)$$

The asymmetry parameter associated with **q** is defined as

$$\eta = \frac{q_{xx} - q_{yy}}{q_{zz}} \quad (3)$$

In the solid state, contributions to **q** at the site of the nucleus of an atom A in a molecule arise from (a) valence electrons of A, (b) other intramolecular charge distributions, (c) distortions of the core electron distribution of A by its valence electrons, (d) charges in the crystal lattice wholly external to the molecule, and (e) polarization of valence and core electron distributions of A by the charges in the lattice. Hereinafter, (a), (b), and (c) will be termed the "molecular contribution," and (d) and (e) the "lattice contribution."

For a nucleus in a solid the explicit calculation of **q** requires an accurate evaluation of (a), (b), (c), (d), and (e). Unfortunately, there are considerable difficulties in computing each of these terms, and an explicit calculation which includes (a)–(e) has not yet been carried out. For example, the lack of highly accurate wave functions[3] affects the values of terms (a)

(1) (a) This work will be submitted by T. B. B. to the Graduate School of the University of Minnesota as part of a thesis in partial fulfillment of a Doctor of Philosophy degree; (b) NDEA Predoctoral Fellow at the University of Minnesota, 1966–1969.

(2) C. Dean, *Phys. Rev.*, **96**, 1053 (1954).

and (b). The accuracy of computing (d) is surely limited by assuming a nonoverlapping charge model for the lattice.[4] The terms (c) and (e), frequently referred to as the internal and external Sternheimer effects,[5] are extremely difficult to calculate. For these reasons, several approximate methods have been developed to interpret nuclear quadrupole coupling constants in terms of intramolecular bonding parameters.[6,7] We have calculated intramolecular EFG's by the direct substitution of hole populations, determined by evaluating orbital occupations,[8] into the Townes and Dailey relationship.[6]

Although lattice EFG calculations have been carried out with varying degrees of success in highly ionic crystals,[9] none have been attempted as corrections to intramolecular EFG's calculated from a molecular orbital model. Thus, it was our objective to interpret EFG's and asymmetry parameters by not only using results of intramolecular LCAO–MO computations, but by also including the lattice contribution. We have evaluated the effect of the lattice on both the EFG and the asymmetry parameter in several representative compounds. Since the models described below are approximate ones, the absolute numbers obtained from them cannot be considered to be of prime importance. They are, however, an indication of the potential importance of the lattice in interpreting NQR coupling constants and asymmetry parameters using these models.

The Lattice Contribution

The calculation of the lattice EFG was carried out using a general lattice summation program. Charges at distance r from the quadrupole nucleus contribute q_{ij} to the EFG tensor, $\mathbf{q}$

$$(q_{ij})_{r=0} = \sum_k e_k \sum_{i,j} \frac{(3x_i x_j - \delta_{ij} r^2)}{r^5}$$

$\delta_{ij} = 1$ if $i = j$ and 0 otherwise. e_k is the charge on the kth ion. The lattice tensor was generated by computing six of the nine q_{ij}'s for each charge in a spherical volume of a chosen radius. Depending on the crystallographic point group, the summation might have been performed in a nonorthogonal axis system. When necessary, therefore, after summation, the axis system was transformed into a cartesian one. One obtains the eigenvalues and eigenvectors of the lattice EFG principal axes by diagonalizing the resulting tensorial matrix.

To be certain that the program was functioning correctly, calculations, which could be carried through by hand, were performed on a distorted NaCl lattice. Precise agreement was obtained. In addition, Madelung's constant for NaCl was calculated by the same scanning procedure. The convergence is slow by this method,[10] but a value of 1.74 in agreement with the accepted value[11] of 1.75 was obtained in a sphere with scanning radius 60 Å.

To properly calculate the principal axes orientation and the asymmetry parameter of the EFG, it is necessary to know the eigenvectors of $\mathbf{q}$ both with and without the intramolecular contribution present. We have found the point charge model can be useful for making a reliable estimate of the orientation of the principal axes. The program was written to exclude contributions to the lattice EFG from atoms in the molecule containing the nucleus at $r = 0$. The resulting tensor was labeled $\mathbf{q}'_{\text{lat}}$. The excluded contributions were stored in a separate tensor called $\mathbf{q}_{\text{bound}}$. A variable parameter, ϵ, was used to weight $\mathbf{q}_{\text{bound}}$

$$\mathbf{q}_{\text{sum}} = \mathbf{q}'_{\text{lat}} + \epsilon\,\mathbf{q}_{\text{bound}}$$

For values of ϵ from 0 to 10, the two tensors were added, and the resulting matrix of $\mathbf{q}_{\text{sum}}$ was diagonalized. ϵ has no theoretical significance and was used only to provide an understanding of how the molecular principal axes relate to those of the lattice. When $\epsilon = 0$, $\mathbf{q}_{\text{sum}}$ represents the lattice contribution only. When $\epsilon > 0$, the eigenvalues and eigenvectors of $\mathbf{q}_{\text{sum}}$ represent a mixture of the lattice and molecular systems. Figures 1, 2, 3, and 4 are intended to show how the eigenvalues of the lattice principal axes relate to those of the intramolecular system in the compounds studied. It is not necessary to continue the plots past the value of ϵ at which the lines no longer cross one another even though in reality $\epsilon \gg 1$. Using these graphs one knows how the eigenvalues of the lattice EFG should be added to the eigenvalues of the intramolecular EFG (*vide infra*).

For simplicity, we will adopt the convention that q_{xx}, q_{yy}, and q_{zz} refer to the eigenvalues of $\mathbf{q}'_{\text{lat}}$ whose eigenvectors correspond, respectively, to the eigenvectors of q_{xx}, q_{yy}, and q_{zz} from the intramolecular system. q_{xx}, q_{yy}, and q_{zz} of $\mathbf{q}'_{\text{lat}}$, therefore, do not necessarily conform to eq 2. Care was taken to use the proper sign of $(q_{ij})_{\text{lat}}$ since the lattice principal axes in the compounds studied may either be aligned with or exactly opposite in direction to those of the intramolecular system.

(3) W. H. Flygare, J. M. Pochan, G. I. Kerley, T. Caves, M. Karplus, S. Aung, R. M. Pitzer, and S. I. Chan, *J. Chem. Phys.*, **45**, 2793 (1966).

(4) R. Bersohn and R. G. Shulman, *ibid.*, **45**, 2298 (1966).

(5) R. M. Sternheimer and H. M. Foley, *Phys. Rev.*, **102**, 731 (1956), and references therein.

(6) C. H. Townes and B. P. Dailey, *J. Chem. Phys.*, **17**, 782 (1949).

(7) F. A. Cotton and C. B. Harris, *Proc. Nat. Acad. Sci. U. S.*, **56**, 12 (1966).

(8) R. S. Mulliken, *J. Chem. Phys.*, **23**, 1841 (1955).

(9) G. G. Belford, R. A. Bernheim, and H. S. Gutowsky, *ibid.*, **35**, 1032 (1961), and references therein.

(10) H. M. Evjen, *Phys. Rev.*, **39**, 675 (1932).

(11) L. Pauling, "The Nature of the Chemical Bond," Cornell University Press, Ithaca, N. Y., 1960, p 508.

As pointed out before, lattice charges can polarize electron shells of the atom containing the quadrupole nucleus and produce an additional EFG (the external Sternheimer effect). Burns and Wikner[12] suggest that multiplying the calculated EFG by an empirical value of 10 best explains experimental results. This value is consistent with very recent experimental work on lattice effects.[13] When the EFG is converted into a coupling constant, the components of $\mathbf{q}_{lat}$ are

$$(e^2Qq_{ij}/h)_{lat} = 10(e^2Qq'_{ij}/h)_{lat}, \text{ MHz}$$

where Q is the quadrupole moment of the nucleus.

The Molecular Contribution

The basic assumption of all approximate models is that the EFG at the nucleus of an atom chemically bonded in a molecule is related to the EFG in the atom in its purely atomic state by a variable parameter, ρ

$$\mathbf{q}_{mol} = \rho\mathbf{q}_{at} \tag{4}$$

The quantity ρ has been assumed to be related to the occupations of the atomic orbitals comprising the valence shell of the atom being studied.[6,7] If p orbitals are used, and the p_z orbital is oriented so that it is σ-bonding, the EFG from p_x and p_y orbitals is related to that of the p_z by[14]

$$q_{zz} = -2q_{xx} = -2q_{yy}$$

ρ may then be replaced in eq 4 by the quantity,[15] $N_z - \frac{N_x + N_y}{2}$, where N_x, N_y, and N_z are the "number" of holes in the p_x, p_y, and p_z atomic orbitals, respectively.[7,16] $\mathbf{q}_{mol}$ will now simplify to the molecular EFG along the Z principal axis and can be expressed as a coupling constant

$$(e^2Qq_{zz}/h)_{mol} = \left(N_z - \frac{N_x + N_y}{2}\right)(e^2Qq_{zz}/h)_{at}, \text{ MHz} \tag{5}$$

For chlorine, $(e^2Qq_{zz})_{at}$ may be replaced by -109.7 MHz,[17] and after adding in the lattice contribution, one obtains

$$(e^2Qq_{zz}/h)_{tot} = -109.7\left(N_z - \frac{N_x + N_y}{2}\right) + (e^2Qq_{zz}/h)_{lat}, \text{ MHz} \tag{6a}$$

The internal Sternheimer effect is approximately eliminated by using -109.7 MHz for the ^{35}Cl coupling constant.[7] Although $(e^2Qq_{zz}/h)_{tot}$ and $(e^2Qq_{yy}/h)_{tot}$ are not observables, they may be derived in the same way as eq 5 was;[15] they are needed in order to compute η and must satisfy eq 1

$$(e^2Qq_{xx}/h)_{tot} = -109.7\left(N_x - \frac{N_y + N_z}{2}\right) + (e^2Qq_{xx}/h)_{lat}, \text{ MHz} \tag{6b}$$

$$(e^2Qq_{yy}/h)_{tot} = -109.7\left(N_y - \frac{N_x + N_z}{2}\right) + (e^2Qq_{yy}/h)_{lat}, \text{ MHz} \tag{6c}$$

Substitution of eq 6a, b, and c into eq 3 gives the total asymmetry parameter

$$\eta_{tot} = \frac{(e^2Qq_{xx}/h)_{tot} - (e^2Qq_{yy}/h)_{tot}}{(e^2Qq_{zz}/h)_{tot}}$$

Computations

Lattice Calculation. K_2PtCl_4 is known to crystallize in a tetragonal lattice[18] with one formula unit per cell, with space group P4/mmm, and with cell dimensions $a = 6.93$ Å and $c = 4.13$ Å. The $PtCl_4^{2-}$ ion is planar and has four equivalent Pt–Cl bonds of length 2.33 Å. The lattice EFG was calculated using the self-consistent charges of Pt = 0.45 and Cl = −0.61 from the molecular calculation. Several maximum scanning radii were chosen to check the convergence of the sum. In going from a radius of 50 to 60 Å, the diagonal elements of $\mathbf{q}'_{lat}$ changed by no more than 0.03%. A radius of 50 Å was chosen. Figure 1 shows how the lattice and intramolecular principal axes relate to one another. $(q_{zz})_{lat}$ is essentially constant since it is ⊥ to the $PtCl_4^{2-}$ plane. The eigenvector of $(q_{yy})_{lat}$ is exactly opposite those of $(q_{yy})_{bound}$. Therefore, $(q_{yy})_{lat}$ should be taken with the opposite sign when it is combined with $(q_{yy})_{mol}$.

K_2PtCl_6 crystallizes in an antifluorite lattice of space group Fm3m, with cell dimensions of 9.725 Å and with four formula units per unit cell.[19] All six Pt–Cl bonds are crystallographically equivalent. K_2ReCl_6 is isomorphous with K_2PtCl_6[20] and has cell dimensions of 9.861 Å. The lattice EFG was calculated with a scanning radius of 50 Å using the self-consistent charges from the molecular calculation of Pt = 0.69, Cl = −0.45 and Re = 1.30, Cl = −0.55. For these compounds simple addition of the eigenvalues of the lattice and intramolecular principal axes, X, Y, and Z suffices (see Figure 2).

$HgCl_2$ has been the subject of two X-ray studies.[21,22]

(12) G. Burns and E. G. Wikner, *Phys. Rev.*, **121**, 155 (1961).

(13) T. B. Brill, Z Z. Hugus, Jr., and A. F. Schreiner, to be published.

(14) C. H. Townes and A. L. Schawlow, "Microwave Spectroscopy," McGraw-Hill Book Co., Inc., New York, N. Y., 1955, p 233.

(15) T. P. Das and E. L. Hahn, "Nuclear Quadrupole Resonance Spectroscopy, Solid State Physics, Supplement 1," Academic Press, Inc., New York, N. Y., 1958.

(16) A similar expression may be derived for d orbitals

$$(q_{zz})_{mol} = \left(N_{z^2} + \frac{N_{xz} + N_{yz}}{2} - N_{x^2-y^2} - N_{xy}\right)(q_{zz})_{at}$$

(17) V. Jaccarino and J. G. King, *Phys. Rev.*, **83**, 471 (1951).

(18) R. G. Dickenson, *J. Amer. Chem. Soc.*, **44**, 2404 (1922).

(19) F. J. Ewing and L. Pauling, *Z. Krist.*, **68**, 223 (1928).

(20) B. Aminoff, *ibid.*, **94**, 246 (1936).

(21) H. Braekken and W. Scholten, *ibid.*, **89**, 448 (1934).

(22) D. Grdenić, *Ark. Kemi*, **22**, 14 (1950).

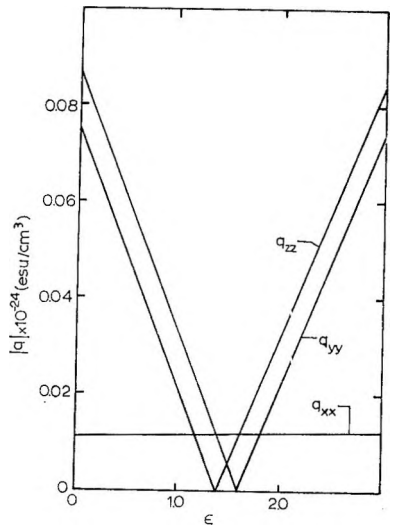

Figure 1. The eigenvalues of the principal axes in K_2PtCl_4 as a function of the importance of the intramolecular contribution.

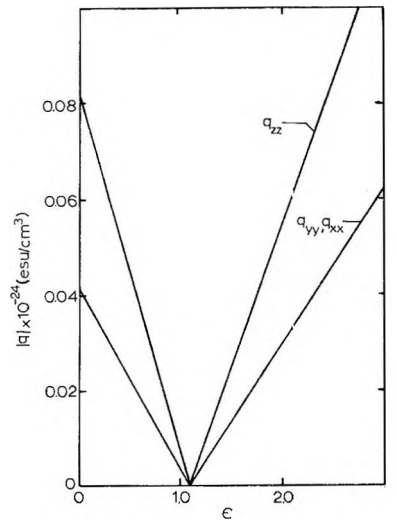

Figure 2. The eigenvalues of the principal axes in K_2PtCl_6 and K_2ReCl_6 as a function of the importance of the intramolecular contribution.

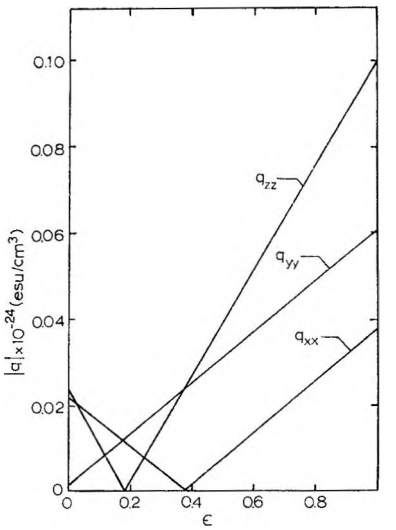

Figure 3. The eigenvalues of the principal axes of the chlorine at 2.27 Å from the mercury in $HgCl_2$ as a function of the importance of the intramolecular contribution.

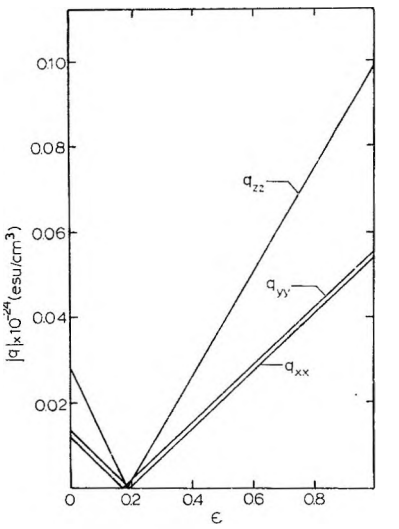

Figure 4. The eigenvalues of the principal axes of the chlorine at 2.23 Å from the mercury in $HgCl_2$ as a function of the importance of the intramolecular contribution.

The lattice unit cell was found to be orthorhombic containing four approximately linear molecules. The cell has a space group of symmetry Pmnb, and its dimensions are a = 5.963 Å, b = 12.735 Å, and c = 4.325 Å. Packing forces cause a difference in the Hg–Cl bond lengths; Hg–Cl_a = 2.27 Å, Hg–Cl_b = 2.23 Å. The two X-ray studies differ slightly in their positioning of the chlorine atoms. The lattice EFG was calculated at both chlorine atoms using self-consistent charges of Hg = 0.77, Cl_a = −0.40, and Cl_b = −0.37 in a sphere of radius 50 Å. Figures 3 and 4 show how the lattice and intramolecular principal axes of Cl_a and Cl_b relate to one another. The atomic coordinates of Braekken, *et al.*, were used for these plots, but Grdenić's data give the same general pattern.

Molecular Calculation. Orthogonal molecular orbitals were generated as linear combinations of oblique atomic orbital basis sets. Right-hand coordinate systems were employed for both local atomic and molecular coordinates. All valence electrons were included. The single-term analytical basis functions for 5d and 6s orbitals of platinum and rhenium had been obtained previously[23,24] by comparing overlap integrals with those obtained using the numerical functions of Herman and Skillman.[25] The orbital exponent of the 6p

(23) F. A. Cotton and C. B. Harris, *Inorg. Chem.*, 6, 369 (1967).

(24) F. A. Cotton and C. B. Harris, *ibid.*, 6, 376 (1967).

(25) F. Herman and S. Skillman, "Atomic Structure Calculations," Prentice-Hall, Inc., Englewood Cliffs, N. J., 1963.

orbital was chosen to be slightly smaller than the 6s orbital.

We have obtained the single-term mercury radical wave functions, $\psi(r)$, for 5d, 6s, and 6p orbitals in the following manner

$$\psi(r) = \frac{(2\alpha)^n}{\sqrt{2(n-1)!}} r^n \exp(-\alpha r/n)$$

n is the principal quantum number. The α's (5d, 6s, 6p) were first evaluated for Pt^{2+} using Burns' rules,[26] but the resulting radial functions were too diffuse. These α's (5d, 6s, 6p) were, however, found to differ from α_0's, as derived in ref 23 and 24, by a multiplicative factor, γ, *i.e.*

$$\alpha_0(i) = \alpha(i)\gamma(i) \quad (i = 5d,6s)$$

The assumption was made that the mercury functions can be fitted in a similar manner. On this basis, values of $\alpha(i)$ were first obtained for mercury functions using Burns' rules. These orbitals were then contracted by $\gamma(i)$ as determined by the platinum fitting procedure. We also compared graphs of $\psi(r)$ *vs.* r up to 3 Å. The single-term mercury functions differed from their numerical Herman–Skillman counterparts in a manner very similar to the analogous deviations of the platinum functions. Therefore, these mercury functions (α/n (5d) = 2.93, α/n (6s) = 2.65, α/n (6p) = 2.30) are considered as good as the platinum and rhenium functions. The chlorine orbitals, if used as they were for $PtCl_6^{2-}$ and $ReCl_6^{2-}$, were too diffuse. Therefore, Clementi–Raimondi functions were employed.[27]

Diagonal and off-diagonal Hamiltonian matrix elements between the oblique basis functions for platinum and rhenium were used as previously described.[23,24] Diagonal elements, H_{ii}, for mercury were chosen 1.4 eV lower than those of platinum in keeping with mercury's higher ionization potential. Values of H_{ii} for Hg and Cl in $HgCl_2$ were charge-adjusted by −3 eV per unit positive charge.

Population analyses were carried out with the oblique basis sets in the usual manner.[8] Calculations proceeded iteratively as described elsewhere[28] until self-consistent charges and orbital occupations resulted.

Orbital occupations of p_π orbitals in the bent $HgCl_2$ were obtained by perturbation of the degenerate π-molecular orbitals in the linear molecule. This was effected by inducing a two-degree bend of one of the Hg–Cl bonds, and obtaining occupations from

$$\rho(p_k\pi) = \sum_i^{\pi\text{-MO}} N_i C_{ki}^2 + \sum_{m\neq k}^{\text{AO}} \sum_i^{\pi\text{-MO}} N_i C_{ki} C_{mi} S_{km}$$

where, for example, C_{ki}, is the Kth component of the ith π-MO and S_{km} is the overlap integral between the Kth and mth AO. N_i is the population of the ith MO.

Results and Discussion

Calculated and experimental coupling constants and calculated asymmetry parameters for K_2PtCl_4, K_2PtCl_6, and K_2ReCl_6 are summarized in Table I. Calculated and experimental data for $HgCl_2$ are tabulated in Table II.

The lattice EFG for K_2PtCl_4 is seen to be about 6% of the total calculated EFG and has the effect of decreasing the asymmetry parameter to about one-sixth of that which would be expected if the isolated $PtCl_4^{2-}$ were considered. The agreement between the calculated and experimental EFG's is fortuitous in view of the approximations in both the lattice and molecular models. The contribution of the lattice to the asymmetry parameter is, however, significant. This contribution is probably greater than the error in the asymmetry parameter calculated from the molecular orbital model.

The lattice contribution in K_2PtCl_6 and K_2ReCl_6 is about the same order of magnitude as that in K_2PtCl_4. This correlates well with the fact that the unit cell volume in the hexachloro compounds is about four times greater than that in K_2PtCl_4. The hexachloro compounds have, however, four times as many formula units per cell than does K_2PtCl_4. Adding the lattice contribution to the molecular contribution in K_2PtCl_4 and K_2PtCl_6 is seen to improve the agreement between the calculated and experimental coupling constants. For K_2ReCl_6 the discrepancy between the calculated and experimental coupling constants cannot be accounted for by the lattice and appears to arise from the molecular calculation. The lattice does not destroy the axial symmetry of the metal–chlorine bond in the hexachloro compounds and therefore gives rise to no asymmetry parameter. Our calculated values are in agreement with the experimental asymmetry parameter of 0.000 ± 0.008 measured for iodine in Rb_2PtI_6 which has the same structure.[29]

As a result of differing Hg–Cl bond lengths in $HgCl_2$, there are two ^{35}Cl NQR signals.[30] These resonances have been the subject of several studies to determine the chlorine EFG asymmetry parameters.[31–33] Dinesh, *et al.*, used a powder method and determined approximate η values for the two chlorine atoms of 0.30 and

(26) G. Burns, *J. Chem. Phys.*, **39**, 1521 (1964).

(27) E. Clementi and D. L. Raimondi, *ibid.*, **38**, 2686 (1963).

(28) A. F. Schreiner and T. L. Brown, *J. Amer. Chem. Soc.*, **90**, 3366 (1968).

(29) D. Nakamura and M. Kubo, *J. Phys. Chem.*, **68**, 2986 (1964).

(30) It is interesting to note that, although the molecular calculation said that the 2.27-Å chlorine was more ionic than the 2.23-Å chlorine, slight variations in the populations caused the higher frequency resonance to be due to the 2.27-Å chlorine. This is probably an artifact of the approximations in the LCAO–MO method or the assumption in eq 6a that the atomic coupling constant is −109.7 MHz regardless of the orbital type.

(31) J. Ramakrishna, *Phil. Mag.*, **14**, 589 (1966).

(32) H. Negita, T. Tanaka, T. Okuda, and H. Shimada, *Inorg. Chem.*, **5**, 2196 (1966).

(33) Dinesh and P. T. Narasimkan, *J. Chem. Phys.*, **45**, 2170 (1966).

Table I: A Summary of Calculated and Experimental Coupling Constants (MHz) and Their Asymmetry Parameters for K_2PtCl_4, K_2PtCl_6, and K_2ReCl_6

Compound	Principal axes	$(e^2Qq/h)_{mol}$	$(e^2Qq/h)_{mol}$	$(e^2Qq/h)_{lat}$	$(e^2Qq/h)_{tot}$	$(e^2Qq/h)_{exp}$	η_{mol}	η_{tot}
	X	15.5		0.33	15.8			
K_2PtCl_4	Y	18.0		−2.35	15.4			
	Z	−33.4	34.0[a]	−2.02	35.4	35.8[c]	0.075[d]	0.013
	X	24.5		1.12	25.6			
K_2PtCl_6	Y	24.5		1.12	25.6			
	Z	−49.0	51.0[b]	−2.24	51.2	51.6[e]	0.0	0.0
	X	16.7		1.10	17.8			
K_2ReCl_6	Y	16.7		1.10	17.8			
	Z	−33.5	32.0[b]	−2.20	35.7	27.8[f]	0.0	0.0

[a] Reference 23. [b] Reference 24. [c] E. P. Marram, E. J. McNiff, and J. L. Ragle, *J. Phys. Chem.*, **67**, 1719 (1963). [d] Reference 23, calcd $\eta_{mol} = 0.072$; reference 7, calcd $\eta_{mol} = 0.025$. [e] D. Nakamura, Y. Kurita, K. Ito, and M. Kubo, *J. Amer. Chem. Soc.*, **82**, 5783 (1960). [f] R. Ikeda, D. Nakamura and M. Kubo, *J. Phys. Chem.*, **69**, 2101 (1965).

Table II: A Summary of Calculated and Experimental Coupling Constants (MHz) and Asymmetry Parameters for $HgCl_2$

Atom	Principal axes	$(e^2Qq/h)_{mol}$	$(e^2Qq/h)_{lat}$	$(e^2Qq/h)_{tot}$	$(e^2Qq/h)_{exptl}$	η_{tot}	η_{exptl}[a]
		Coupling constants using atomic coordinates of Grdenić (Cl–Hg–Cl angle = 180°)					
Cl_a,	X	20.85	0.61	21.46			
2.27 Å	Y	20.85	0.34	21.19			
	Z	−41.75	−0.95	42.70	44.45	0.006	0.087
Cl_b,	X	20.63	0.87	21.50			
2.23 Å	Y	20.63	0.14	20.77			
	Z	−41.25	−1.01	42.26	44.07	0.017	0.085
		Coupling constants using atomic coordinates of Braekken, *et al.* (Cl–Hg–Cl angle = 178°)					
Cl_a,	X	21.12	0.92	22.04			
2.27 Å	Y	20.32	0.01	20.33			
	Z	−41.45	−0.93	42.38	44.45	0.041	0.087
Cl_b,	X	20.87	0.38	21.25			
2.23 Å	Y	20.07	0.37	20.44			
	Z	−40.95	−0.75	41.70	44.07	0.018	0.085
		Coupling constants using Cl–Hg–Cl angle = 176°					
Cl_a,	X	22.23	0.92	23.15			
2.27 Å	Y	18.09	0.01	18.01			
	Z	−40.31	−0.93	41.24	44.45	0.125	0.087
Cl_b,	X	21.98	0.38	22.36			
2.23 Å	Y	17.84	0.37	18.21			
	Z	−39.81	−0.75	40.56	44.07	0.102	0.085

[a] Reference 32.

0.28. Ramakrishna, using the Zeeman method, obtained η values of 0.70 and 0.40 for the two chlorine atoms. Negita, *et al.*, reported values of $\eta = 0.087$ and 0.085 for the two chlorine atoms using the Zeeman method. Obviously, there is a wide variation in the experimentally determined η's. Negita, *et al.*, pointed out that the crystal structure determination of Braekken, *et al.*, generally agreed better with their Zeeman study than did that of Grdenić. However, they considered that the Z principal axis of the EFG lay along the Hg–Cl bond and therefore obtained a Cl–Hg–Cl bond angle of 180° in agreement with Grdenić's crystal structure value. The lattice may cause the Z principal axis to be slightly off the bond and give rise to the possibility that the $HgCl_2$ molecule is not exactly linear in the solid state. In fact, Braekken, *et al.*, found that the Cl–Hg–Cl angle was 178°. If the molecule were linear, any asymmetry of the chlorine EFG would have to be due entirely to the lattice. We found that the lattice contributes too little to the total EFG to cause asymmetry parameters for the chlorine atoms which are comparable to any experimental ones. Table II shows that the calculated chlorine coupling constant is not particularly sensitive to the Cl–Hg–Cl angle

providing the angle is small. On the other hand, the asymmetry parameter, which arises due to variations in the population of atomic orbitals with π-bonding symmetry, is extremely sensitive to the angle. Bending the molecule two degrees in accordance with Braekken, *et al.*, produces calculated asymmetry parameters which are 25 to 50% of the values measured by Negita, *et al.* Bending the molecule two degrees more increases the asymmetry parameters to values larger than those of Negita, *et al.* It seems reasonable that the packing forces in the $HgCl_2$ lattice could cause the Cl–Hg–Cl angle to be a few degrees less than 180° particularly since the packing forces cause the Hg–Cl bond lengths to differ.

Our calculations appear to concur best with the data of Negita, *et al.* Chlorine EFG asymmetry parameters as large as those reported by Ramakrishna and Dinesh, *et al.*, can be rationalized only be resorting to enormous bending of the molecule and reshaping of the lattice. This would be in sharp disagreement with the available crystal structure data.

In summary, the contribution of the lattice to the observed coupling constant in these covalently bonded compounds using the point charge model is 5 or 6% of the total field gradient. The lattice contribution to the asymmetry parameter can be considerably more however.

Acknowledgment. The use of the computer facilities at North Carolina State University and the Triangle Universities Computation Center, and the financial support of the North Carolina Board of Science and Technology for the purchase of a Wilks NQR-1A spectrometer are gratefully acknowledged.

On the Calculation of Intramolecular Radiationless Relaxation Rates

by S. E. Webber

Department of Chemistry, The University of Texas at Austin, Austin, Texas 78712 *(Received August 12, 1969)*

The time evolution of systems with a discrete energy level spectrum is discussed by means of a density matrix formalism and some perturbative operator techniques. In particular the case of a "two-level system" interacting *via* a discrete field is analyzed, and it is shown that the relaxation rates depend on a correlation function which in turn depends on the distribution of matrix elements that couple the two "coarse" levels of the system. It is argued that it is the properties of the intramolecular correlation function that determine if an irreversible intramolecular relaxation process can occur. Also some exact results are derived for the time evolution of a discrete, finite system, and it is shown that (a) for short times the relaxation processes will not be exponential and (b) to the lowest order in t the perturbation and exact results agree. In Appendix II the exact time evolution of some finite model systems is compared to the perturbation calculation for the same system.

I. Introduction

During the past few years a number of authors have discussed the problem of radiationless transitions between molecular excited states from various points of view.[1] The basic problem to be understood is the fate of that portion of electronic energy of an excited molecule that does not reappear as an emitted photon. Previous studies have tended to emphasize (1) the magnitude of the rate of the radiationless processes[2-5] and (2) the nature of the interaction that leads to irreversible processes.[6-12] The first aspect of this problem has been treated by evoking the Golden Rule[13] for the transition rate between two states

$$P_{i\to j} = \frac{2\pi}{\hbar^2} |\langle \psi_i | V | \psi_f \rangle|^2 \rho(E_j)\delta(E_j - E_i)$$

and then estimating the matrix element and density of states that appear in this equation. An exact

(1) See the review by S. K. Lower and M. A. El-Sayed, *Chem. Rev.*, **66**, 199 (1966), especially section II where references to earlier work are given.

(2) G. W. Robinson and R. P. Frosch, *J. Chem. Phys.*, **37**, 1962 (1962); *ibid.*, **38**, 1187 (1963).

(3) W. Siebrand and D. F. Williams, *ibid.*, **49**, 1860 (1968), and other references to earlier work by these authors therein.

(4) S. H. Lin, *ibid.*, **44**, 3759 (1966).

(5) G. R. Hunt, E. F. McCoy, and I. G. Ross, *Aust. J. Chem.*, **15**, 591 (1962).

(6) M. Bixon and J. Jortner, *J. Chem. Phys.*, **48**, 715 (1968).

(7) J. Jortner and R. S. Berry, *ibid.*, **48**, 2757 (1968).

(8) D. P. Chock, J. Jortner, and S. A. Rice, *ibid.*, **49**, 610 (1968).

(9) K. F. Freed and J. Jortner, to be published in *J. Chem. Phys.*

(10) K. F. Freed, "Resonance Fluorescence in Polyatomic Molecules," preprint.

(11) M. Gouterman, *J. Chem. Phys.*, **36**, 2846 (1962).

evaluation of these quantities is very difficult, but some very useful qualitative discussions have accounted for systematic differences in rates for related classes of molecules (especially for planar aromatics).

The second aspect involves a study of the time evolution of a system with discrete energy levels. Previous work[6-10] has clearly shown that under certain circumstances a molecule may contain a sufficiently high density of states such that it may act as its own "heat bath" with respect to dissipation of excess electronic energy. It has also been shown in the case of a sparse intramolecular density of states "quantum beat" or other complex (*i.e.*, nonexponential) decay phenomena may occur, and further information about spectroscopically inaccessible molecular states may be obtained.[14]

It is the purpose of the present article to study the validity of the Golden Rule result for a system with discrete levels and to present a method for calculating the transition rate. The usual derivation of the Golden Rule assumes the existence of a continuum of final states, $\{\psi_f\}$, with a smooth variation of matrix elements $\langle\psi_i|V|\psi_f\rangle$ *vs.* E_f.[15] In isolated molecules such a situation does not generally exist, yet it is known that some molecules undergo radiationless processes even at very low pressures,[16-18] which implies that the molecule provides its own "continuum." It has also been observed that larger molecules tend to have the same fluorescence rates and quantum yields regardless of phase, indicating that the intramolecular continuum is the dominant "heat bath" for electronic relaxation in all states of matter. Thus studying the application of the Golden Rule for discrete systems will be of equal importance for understanding radiationless rates in condensed phases, where strictly speaking we recover a continuum of final states.

In section II a brief discussion of the nature of the coupling between zeroth-order molecular states is presented, primarily to clarify the nature of the coupling that leads to an intramolecular heat bath. Section III presents some formal aspects of the time evolution of a discrete system which emphasizes the nonexponential behavior generally expected. In section IV a density matrix formalism is presented which displays the usual exponential decay of an excited state under certain well-defined conditions. It is these conditions (discussed in section V) that determine when the intramolecular states have the correct properties to provide a "dissipative field" or "heat bath." The present formalism provides a straightforward method for the calculation of a rate (which may generally be time dependent) for any arbitrarily discontinuous variation of the elements $\langle\psi_i|V|\psi_f\rangle$.

II. The Intramolecular Coupling of Zeroth-Order Molecular Stages

In general the calculation of intramolecular coupling between the members of any zeroth-order basis set is expected to be very difficult and inexact. It is most likely that simple models for the coupling will have to be employed, and a general intuition developed before intramolecular relaxation processes can be successfully interpreted. In what follows we will consider a particular choice for a zeroth-order basis set and discuss the coupling of the members of this set for the purpose of illustrating the nature of the interactions that lead to the phenomenon of intramolecular relaxation processes. It should be noted that the equations to be derived later are independent of the present considerations, but application of these equations to calculate relaxation rates *will* be sensitive to the choice of zeroth-order states. This will be true of any theory that involves the projection of some zeroth-order state onto the (in principle) complete set of molecular eigenstates.

The choice of zeroth-order states will be the same as that employed in the Herzberg–Teller theory[19,20] of vibronic transitions, in which the electronic and vibrational wave function is written as

$$\Phi_{kj} = \Theta^0{}_k(X,Q)\phi_j{}^k(Q) \tag{1}$$

where $\phi_j{}^k(Q)$ is a product of harmonic oscillator functions that belong to the electronic potential of the kth electronic state. The index j refers to a particular set of quantum numbers of the independent oscillator functions. It is implied that the normal coordinates, Q, are derived from the potential surface of the kth electronic state. The function $\Theta_k{}^0(X,Q)$ may be expanded as a linear combination of electronic wave functions suitable for any arbitrary nuclear configuration Q^0 (for absorption strength calculations this choice is the equilibrium configuration of the kth electronic state). The dependence on Q comes from the coefficients of mixing, so we may write

$$\Theta_k{}^0(X,Q) = \sum_s \lambda_{ks}(Q - Q^0)\Theta_s{}^0(X,Q^0) \tag{2}$$

In general each $\lambda_{ks}(Q - Q_0)$ could be expanded as a power

(12) C. Coulson and K. Zalewski, *Proc. Roy. Soc.*, **A268**, 437 (1962).

(13) See, for example, E. Merzbacher, "Quantum Mechanics," John Wiley & Sons, Inc., New York, N. Y., 1961, Chapter 20, eq (20.10).

(14) Reference 7 stresses this point in particular.

(15) See ref 13 for example.

(16) P. Pringsheim, "Fluorescence and Phosphorescence," Interscience Publishers, Inc., New York, N. Y., 1949, p 271 (anthracene).

(17) R. J. Watts and S. J. Strickler, *J. Chem. Phys.*, **44**, 2423 (1966) (naphthalene).

(18) R. Williams and G. J. Goldsmith, *ibid.*, **39**, 2008 (1963) (tetracene).

(19) See A. C. Albrecht, *ibid.*, **33**, 156 (1960), and references therein.

(20) A. D. Liehr, "Advances in Chemical Physics," Vol. 5, Interscience Publishers, Inc., New York, N. Y., 1963, p 241, and references to earlier work therein.

series in the normal coordinates. We also assume that all $\lambda_{ks}(Q - Q_0)$ vanish as $Q \rightarrow Q^0$, except for $\lambda_{kk}(Q - Q^0)$. The Herzberg–Teller theory of vibronically allowed electronic transitions uses perturbation theory to calculate $\lambda_{ks}(Q - Q^0)$, but an explicit expression for $\lambda_{ks} \cdot (Q - Q^0)$ is not required for this discussion. Except in the limit that the set $\{\Theta_s^0(X,Q^0)\}$ becomes very large (*i.e.*, approximately complete), eq 2 is not expected to be very accurate for quantitative calculations. Note that the functions $\{\Theta_s^0(X,Q^0)\}$ do not follow the nuclei but remain fixed in space as the nuclei vibrate. In principle the function $\Theta_k^0(X,Q^0)$ can be of mixed multiplicity, but it is expected that one would usually prefer to treat both the spin–orbit (SO) and Born–Oppenheimer (BO) coupling simultaneously. The perturbation operator may be written

$$V(Q) = V_{SO}(Q) + V_{BO}(Q) \tag{3}$$

where

$$V_{SO}(Q) = V_{SO}(O) + V'_{SO}(O)Q + \ldots \tag{4}$$

and

$$V_{BO}(Q) = \frac{-\hbar^2}{2M}\left\{\frac{\partial^2}{\partial Q^2}\right\}_{el} - \frac{\hbar^2}{M}\left\{\frac{\partial}{\partial Q}\right\}_{el}\frac{\partial}{\partial Q} \tag{5}$$

Some comparisons of the first and second term of eq 4 made by Albrecht[21] for benzene indicate that the second term (the so-called "spin–vibronic" term) is 1/3 of the first. In some cases this term might be important, if for example the spin–orbit coupling of two states were "symmetry-forbidden." Equation 5 is the BO coupling term (all these equations are written symbolically for one normal coordinate), where $\{\}_{el}$ implies that the electronic matrix element is computed for the quantity inside the brackets before the integration over the vibrational wave function is carried out.

In general we will have to couple an initial state, $\Theta_i^0(X,Q)$, with some particular final state, $\Theta_f^0(X,Q)$, using the operator $V(Q)$. Note that in this static atomic orbital approximation $\Theta_f^0(X,Q)$ will be obtained for the equilibrium configuration of the ith electronic state. The function $\Theta_f^0(X,Q)$ represents a Taylor expansion of the true BO electronic function, $\Theta_f(X,Q)$, around the most important point of its full space for calculating matrix elements with respect to the true BO function $\Theta_i(X,Q)$. The function $\Theta_i(X,Q)$ is in turn expanded around $Q = Q^0 = 0$. This is the usual approximation of the Herzberg–Teller theory. We might comment that this formulation would be unsatisfactory if the initial state Φ_{ij} is highly excited vibrationally, such that large Q values were important in $\Theta_i^0(X,Q)$.

We assume that the $\lambda_{ks}(Q - Q^0)$ in eq 2 are expanded as a power series in Q, and that the series may be differentiated with respect to Q (eq 5) or multiplied by any power of Q (eq 4). The integration over the electronic coordinates is carried out, leaving a polynomial in Q. One then carries out the integration over Q, using the harmonic oscillator functions $\phi_j^t(Q)$ and $\phi_j^f(Q)$. These integrals are equivalent to Franck–Condon overlaps modified by certain constants characteristic of the $V_{SO}(Q)$ or $V_{BO}(Q)$ operator. It is not surprising, therefore, that semiquantitative discussions of these processes based on the magnitude of the Franck–Condon factors have been very successful in accounting for relative radiationless rates in related classes of molecules.[2,3]

The above discussion serves to illustrate the nature of the coupling of zeroth-order molecular states. In what follows we need to assume only that such coupling exists and will discuss the time-dependent behavior induced by these interactions. We will use the notation that

$$\Theta_i^0(X,Q)\phi_\omega^t(Q) \equiv |i,\omega\rangle \tag{6}$$

where ω represents a particular set of harmonic oscillator quantum numbers such that

$$\omega = \sum_k \omega_k^{(t)} v_k \tag{7}$$

where the sum goes over all the normal modes of the ith electronic state. The state $\omega = 0$ represents the zero point energy of the oscillators. In this discussion we have ignored the coupling with the radiation field states, as this is not an intramolecular coupling. Formally the kets corresponding to states with photons present are identical with 6, where ω has the meaning of a single-photon energy.

III. The Time Evolution of a Matrix Representation of a Discrete System

A. General Properties. We may define a set of zeroth-order kets

$$\mathbf{H}_0|i,\omega\rangle = (\epsilon_i + \omega)|i,\omega\rangle \tag{8}$$

The full Hamiltonian may be written as

$$\mathbf{H} = \hbar(\mathbf{H}_0 + \mathbf{V}) \tag{9}$$

where $\mathbf{V}$ connects zeroth-order kets and is responsible for the apparent relaxation of a system prepared in a pure zeroth order ket.

The time-dependent ket that describes a system may be written as

$$|t\rangle = e^{-i\mathbf{H}t}|0\rangle \tag{10}$$

where $|0\rangle$ is the ket at $t = 0$. The operator $e^{-i\mathbf{H}t}$ is defined by the expansion

$$e^{-i\mathbf{H}t} = \sum_{n=0}^{\infty} \frac{(-it)^n}{n!}\mathbf{H}^n \tag{11}$$

We will require the projection of $|0\rangle$ on $|t\rangle$ and the magnitude of this projection squared. This latter

(21) A. C. Albrecht, *J. Chem. Phys.*, **38**, 354 (1963).

quantity is the probability of observing the zeroth-order ket $|0\rangle$. We may assume that there exists a set of eigenkets of **H** which we define by the equation

$$\mathbf{H}|\lambda\rangle = \lambda|\lambda\rangle \tag{12}$$

Expanding the kets in eq 10 in terms of this set we obtain the result that

$$\begin{aligned}\langle 0|t\rangle &= \sum_{\lambda}|\langle 0|\lambda\rangle|^2 e^{-i\lambda t} \\ &= \sum_{\lambda} \mathcal{G}(\lambda)e^{-i\lambda t}\end{aligned} \tag{13}$$

where we have defined a quantity

$$\mathcal{G}(\lambda) = |\langle 0|\lambda\rangle|^2 \tag{14}$$

This quantity may be regarded as a normalized distribution function, and $\langle 0|t\rangle$ represents the characteristic function of this distribution function. The property of normalization follows from

$$\langle 0|0\rangle = \sum_{\lambda} \mathcal{G}(\lambda) = 1 \tag{15}$$

This distribution function can be used to calculate moments of energy eigenvalue spectrum as follows

$$\langle \lambda^n \rangle = \sum_{\lambda} \mathcal{G}(\lambda)\lambda^n \tag{16}$$

All these moments exist so long as the number of eigenvalues is finite and the eigenvalues themselves are all finite. Those moments may also exist even if these conditions are not met, depending on the characteristics of $\mathcal{G}(\lambda)$.

In general we need to diagonalize explicitly a matrix representation of a system, obtain $\mathcal{G}(\lambda)$, and study its characteristic function in order to analyze the time evolution of a discrete system. For problems of real physical interest, this would not be a practical means for solving time-dependent problems, as the dimensionality would be enormous.[22] However, this method is suitable for testing the general validity of a weak coupling time-dependent theory for short times.

B. Behavior of $\langle 0|t\rangle$ for Short Times. One is able to compute the value of $\langle 0|t\rangle$ to any arbitrary order in t by application of the cumulant theorem.[23] We observe that the exponential function on the right-hand side of eq 13 may be expanded so that

$$\begin{aligned}\langle 0|t\rangle &= \sum_{n=0}^{\infty} \frac{(-it)^n}{n!} \sum_{\lambda} \mathcal{G}(\lambda)\lambda^n \\ &= \sum_{n=0}^{\infty} \frac{(-it)^n}{n!} \langle \lambda^n \rangle\end{aligned} \tag{17}$$

If we take the natural logarithm of both sides of this equation and rearrange the series, we obtain

$$\ln\{\langle 0|t\rangle\} = \sum_{n=1}^{\infty} \frac{(-it)^n}{n!} \langle \lambda^n \rangle_c \tag{18}$$

where $\langle \lambda^n \rangle_c$ is the nth cumulant. If we choose our energy levels so that $\langle \lambda \rangle = 0$, then

$$\begin{aligned}\langle \lambda^2 \rangle_c &= \langle \lambda^2 \rangle \\ \langle \lambda^3 \rangle_c &= \langle \lambda^3 \rangle \\ \langle \lambda^4 \rangle_c &= \langle \lambda^4 \rangle - 3\langle \lambda^2 \rangle^2\end{aligned} \tag{19}$$

and so on. The quantity of physical interest is $|\langle 0|t\rangle|^2$. From eq 18 we see that

$$|\langle 0|t\rangle|^2 = \exp\left\{2 \sum_{n=1}^{\infty} \frac{(it)^{2n}}{(2n)!} \langle \lambda^{2n} \rangle_c\right\} \tag{20}$$

This means that for short times the relaxation of a finite discrete system will be of the form

$$|\langle 0|t\rangle|^2 \simeq e^{-t^2\langle \lambda^2 \rangle_c} \tag{21}$$

This is not the usual form of exponential decay. It will be seen that essentially exponential decay of the form

$$|\langle 0|t\rangle|^2 \simeq e^{-kt} \tag{22}$$

occurs on a longer time scale than the result (eq 21).

Equation 20 has a practical advantage however. All the moments may be directly obtained from $\mathbf{H}_0$ and **V** without explicitly diagonalizing **H**. We may see this by using the invariance of the trace of a matrix to the choice of representation. We may write

$$\begin{aligned}\langle \lambda^n \rangle &= \sum_{\lambda} |\langle 0|\lambda\rangle|^2 \lambda^n \\ &= tr\{|0\rangle\langle 0|\mathbf{H}^n\} \\ &= \langle 0|(\mathbf{H}_0 + \mathbf{V})^n|0\rangle\end{aligned} \tag{23}$$

The latter equality was obtained by evaluating the trace in the original zeroth-order representation. The explicit value of each moment is easy to obtain. For simplicity we will assume a prediagonalization of the $|i,\omega'\rangle$ states, so

$$\begin{aligned}\langle 2,0|\mathbf{V}|2,0\rangle = \langle 1,\omega|\mathbf{V}|1,\omega'\rangle = 0 \\ \langle 2,0|\mathbf{V}|1,\omega\rangle \neq 0\end{aligned} \tag{24}$$

We also define our energy levels relative to ϵ_2, so

$$\langle 2,0|\mathbf{H}_0|2,0\rangle \equiv 0 \tag{25}$$

Using the notation

$$\begin{aligned}|0\rangle &= |2,0\rangle \\ |\tilde{\omega}\rangle &= |1,\omega\rangle \\ \tilde{\omega} &= \epsilon_1 + \omega - \epsilon_2 \\ \langle 1,\omega|\mathbf{V}|2,0\rangle &= V(\tilde{\omega})\end{aligned} \tag{26}$$

we obtain the following results

(22) References 6–10 have treated radiationless transitions in essentially this way, using a scattering theory formalism and suitable models to make the resulting equations tractable.

(23) See, for example, H. Cramer, "Mathematical Methods of Statistics," Princeton University Press, Princeton, N. J., 1946, Chapter 15.

$$\langle\lambda\rangle = 0$$
$$\langle\lambda^2\rangle = \sum_{\tilde{\omega}} V(\tilde{\omega})^2$$
$$\langle\lambda^3\rangle = \sum_{\tilde{\omega}} V(\tilde{\omega})^2\tilde{\omega}$$
$$\langle\lambda^4\rangle = \sum_{\tilde{\omega}} V(\tilde{\omega})^2\tilde{\omega}^2 + \langle\lambda^2\rangle^2 \qquad (27)$$

and so on. Thus for smaller values of t where eq 20 is of practical interest one may obtain the value of $|\langle 0|t\rangle|^2$ directly from the presumably known values of the zeroth-order energies and coupling matrix elements.

IV. The Weak-Coupling Relaxation Equation

A. Derivation of the First-Order Equation. We now turn to the problem of an approximate equation of motion for a system with a well-defined boundary condition at $t = 0$ in terms of some zeroth-order set of states. The derivation of this weak-coupling equation will differ in detail, but not in physical content, from previous work or relaxation processes (especially in spin systems).[24-28] We present this derivation in order to clearly show the origin of certain of the quantities whose properties essentially determine the relaxation rate of the system. In a sense the present treatment is in the same spirit as Gouterman's[11] in which the analogy between a photon field and a phonon field was exploited to obtain spontaneous and stimulated radiationless relaxation. It is our aim to isolate the essential property of a physical system that determines the validity of a kinetic equation with time-independent transition probabilities between zeroth-order states. It will be seen that such an equation is possible even if the "field" that induces transitions between states has discontinuities or is made up of discrete states. It follows that the discrete set of molecular states may itself act as a dissipative field and in fact would be expected to provide the dominant nonradiative relaxation channel for many systems of interest.

The present analysis will enable a general discrete field to be classified as dissipative or nondissipative, and in the former case, a rate can be calculated. In the latter case the present theory is thought to be inadequate, as will be discussed.

We assume that the zeroth-order kets of a system can be written as $|i,\omega\rangle = |i\rangle|\omega\rangle$. The indices $i,j,k,l,\ldots$ refer to the "coarse-grained" states of the system and ω refers to the zeroth-order energy of the "fine-grained" states. These latter states may be considered to constitute a "heat bath" or a dissipative medium and will include photon states, phonon states, and intramolecular states. We may write our Hamiltonian as

$$\mathbf{H} = \hbar(\mathbf{H}_0 + \mathbf{V}) \qquad (28)$$

where $\mathbf{V}$ represents a perturbation that mixes the kets $|i,\omega\rangle$. The energy levels of $\mathbf{H}_0$ are given by

$$\mathbf{H}_0|i,\omega\rangle = (\epsilon_i + \omega)|i,\omega\rangle \qquad (29)$$

We may assume some operator exists that is diagonal in ω. The expectation value of such an operator is obtained by taking the trace

$$\begin{aligned}\langle\mathcal{P}(t)\rangle &= tr\{\varrho(t)\mathcal{P}\} \\ &= \sum_{i,\omega}\sum_{j,\omega'}\langle i,\omega|\varrho(t)|j,\omega'\rangle\langle j,\omega'|\mathcal{P}|i,\omega\rangle \\ &= \sum_{i,j}\mathcal{P}_{ji}\sum_{\omega}\langle i,\omega|\varrho(t)|j,\omega\rangle \\ &= \sum_{i,j}\sigma(t)_{ij}\mathcal{P}_{ji} \qquad (30)\end{aligned}$$

It was assumed in eq 30 that

$$\begin{aligned}\langle j,\omega|\mathcal{P}|i,\omega\rangle &= \delta_{\omega,\omega'}\langle j|\mathcal{P}|i\rangle \qquad (31)\\ &\equiv \delta_{\omega,\omega'}\mathcal{P}_{ji}\end{aligned}$$

The symbol $\sigma(t)_{ij}$ in eq 30 is an element of a "reduced" or "condensed" density matrix. It is useful, therefore, to obtain an equation of motion for this density matrix.

We may derive the time-dependent equation for $\sigma(t)$ by use of some operator techniques first introduced by Fano[24,25] and later elaborated by Kubo.[26,29] The results of this derivation are the same as obtained by other workers by a variety of techniques. The results will be cast in a form which is most easily compared to Kubo's work.

The time-dependent density matrix may be written in the following equivalent forms

$$\begin{aligned}\varrho(t) &= e^{-i\mathbf{H}t/\hbar}\varrho(0)e^{i\mathbf{H}t/\hbar} \\ &= e^{-i\mathbf{H}^x t/\hbar}\varrho(0) \\ &= e^{-i\mathbf{H}_0{}^x t}\exp_0\{-i\int_0^t dt'\mathbf{V}(t')^x\}\varrho(0) \qquad (32)\end{aligned}$$

where we have used the notation of Kubo[26] for Heisenberg operators, which is

$$e^{-i\mathbf{A}^x}\mathbf{B} = e^{-i\mathbf{A}}\mathbf{B}e^{i\mathbf{A}} \qquad (33)$$

The last equality in eq 32 uses the ordered exponent and the "disentangled" form of $e^{-i\mathbf{H}^x t/\hbar}$. We presume that the effect of $e^{i\mathbf{H}_0 t}$ on $\varrho(0)$ is already known. We may transform $\varrho(t)$ to a form that eliminates this time dependence, by multiplying through by $e^{i\mathbf{H}_0{}^x t}$. We thereby obtain the desired form of the density matrix

(24) U. Fano, *Phys. Rev.*, **96**, 869 (1954).
(25) U. Fano, *Rev. Mod. Phys.*, **29**, 74 (1957).
(26) R. Kubo, *J. Phys. Soc. Jap.*, **17**, 1100 (1962).
(27) P. Hubbard, *Rev. Mod. Phys.*, **33**, 249 (1961).
(28) A. Abragam, "Principles of Nuclear Magnetism," Oxford University Press, New York, N. Y., 1961, see Chapter 8 especially.
(29) R. Kubo, *J. Phys. Soc. Jap.*, **17**, 1100 (1962).

$$\varrho'(t) \equiv e^{iH_0 t}\varrho(t) = \exp_0\{-i\int_0^t dt' \mathbf{V}(t')^x\}\varrho(0) \quad (34)$$

We wish to reduce $\varrho'(t)$ to $\sigma'(t)$ by combining together all elements of $\varrho'(t)$ with the same indices ω but different indices i,j. We may represent this operation by an operator A. The dimensionality of $\varrho(t)$ is $D_c \times D_f$, where D_c is the dimensionality of the coarse-grained states and D_f is the dimensionality of the fine-grained states. The dimensionality of $A\varrho(t) = \sigma(t)$ is D_c. Thus we may write that

$$\langle i|\sigma(t)|j\rangle = A\sum_{\omega,\omega'}\langle i,\omega|\varrho(t)|j,\omega'\rangle = \sum_{\omega}\langle i,\omega|\varrho(t)|j,\omega\rangle \quad (35)$$

where A selects out only those elements such that $\omega = \omega'$. If $\mathbf{1} = \mathbf{1}_c \times \mathbf{1}_f$ represents the identity operator in the full $D_c \times D_f$ representation, then

$$A\mathbf{1} = \mathbf{1}_c \quad (36)$$

Thus the operator $\mathbf{A}$ satisfies the requirements for application of the "generalized cumulant theorem" of Kubo.[29] We assume the general boundary condition

$$\varrho(0) = \sigma(0) \times \varrho^T \quad (37)$$

where in particular ϱ^T will often be taken to be a thermal equilibrium density matrix (of dimensionality D_f). No specification of ϱ^T is required at this point. We may define an operator $\bar{A}$, where

$$\bar{A}\mathbf{B} = A\mathbf{B}(\varrho^T \times \mathbf{1}_c) \quad (38)$$

So long as

$$tr\{\varrho^T\} = 1 \quad (39)$$

$\bar{A}$ will also satisfy the requirements for the application of the "generalized cumulant theorem." If we apply A to $\varrho'(t)$ in eq 37, we obtain

$$A\varrho'(t) \equiv \sigma'(t) = \bar{A}\exp_0\left\{-i\int_0^t \mathbf{V}(t')^x dt'\right\}\sigma(0) = \exp\left\{-\frac{\vartheta}{2}\int_0^t dt_1\int_0^t dt_2 \bar{A}(\mathbf{V}(t_1)^x \cdot \mathbf{V}(t_2)^x)\right\}\sigma(0) \quad (40)$$

In applying the cumulant theorem, we have assumed that $\bar{A}V(t) = 0$, which ignores an energy shift term. We have also truncated the cumulant moment series in eq 40. While not proved, it is probable that this truncation limits the validity of the following results to essentially dissipative cases.

Equation 40 assumes a more tractable form if we take the time derivative of both sides. The result is

$$\frac{\partial}{\partial t}\sigma'(t) = -\frac{\partial}{\partial t}\frac{\vartheta}{2}\int_0^t dt_1\int_0^t dt_2 A[\mathbf{V}(t_1) - [\mathbf{V}(t_2), \sigma'(t) \times \varrho^T]] \quad (41)$$

where ϑ is the time-ordering operator. We may use the following transformation of the time integral to replace the more formal expression above

$$\frac{\vartheta}{2}\int_0^t dt_1\int_0^t dt_2 = \int_0^t dt_1\int_0^{t_1} dt_2 = \int_0^t d\tau\int_\tau^t dt_1 \quad (42)$$

where $\tau = t_1 - t_2$.

To proceed further, one must evaluate matrix elements of the above equation. The algebra is tedious but straightforward, and the results have appeared other places.[27,28] We will write down the results for the i,jth element, primarily to introduce notation. The results are

$$\frac{\partial}{\partial t}\langle i|\sigma'(t)|j\rangle \equiv \frac{\partial}{\partial t}\sigma'(t)_{ij} = -\sum_k\{k^{(1)}{}_{ij;ik}(t)\sigma'(t)_{ik} + k^{(2)}{}_{ij;kj}(t)\sigma'(t)_{kj}\} + \sum_{k,l} k_{ij;kl}(t)\sigma'(t)_{kl} \quad (43)$$

where

$$k^{(1)}{}_{ij;ik}(t) = e^{i(\epsilon_k-\epsilon_j)t}\int_0^t \psi^{(1)}{}_{ij;ik}(\tau)d\tau$$

$$k^{(2)}{}_{ij;kj}(t) = e^{i(\epsilon_i-\epsilon_k)t}\int_0^t \psi^{(2)}{}_{ij;kj}(\tau)d\tau$$

$$k_{ij;kl}(t) = e^{i(\epsilon_i-\epsilon_j+\epsilon_k-\epsilon_l)t}\int_0^t \psi_{ij;kl}(\tau)d\tau \quad (44)$$

The quantities $\psi_{ij;mn}(\tau)$ are *correlation functions* for a particular transition. Explicit evaluation of these quantities yields

$$\psi^{(1)}{}_{ij;ik}(\tau) = \sum_\omega\sum_{l,\omega'} e^{i(\epsilon_l-\epsilon_k+\omega'-\omega)\tau}\langle k,\omega|\mathbf{V}|l,\omega'\rangle \times \langle l,\omega'|\mathbf{V}|j,\omega\rangle\rho^T(\omega)$$

$$\psi^{(2)}{}_{ij;kj}(\tau) = \sum_\omega\sum_{l,\omega} e^{i(\epsilon_k-\epsilon_l+\omega-\omega')\tau}\langle i,\omega|\mathbf{V}|l,\omega'\rangle \times \langle l,\omega'|\mathbf{V}|k,\omega\rangle\rho^T(\omega)$$

$$\psi_{ij;kl}(\tau) = \sum_{\omega,\omega'}\{e^{i(\epsilon_j-\epsilon_l+\omega-\omega')\tau} + e^{i(\epsilon_k-\epsilon_i+\omega'-\omega)\tau} \times \langle i,\omega|\mathbf{V}|k,\omega'\rangle\langle l,\omega'|\mathbf{V}|j,\omega\rangle\rho^T(\omega') \quad (45)$$

In evaluating terms of eq 41, the following types of equalities were used

$$e^{iat_1}e^{ibt_2} = e^{i(a+b)t_1}e^{-ib\tau}$$

$$\frac{\partial}{\partial t}\int_0^t d\tau f(\tau)\int_\tau^t e^{iat_1}dt_1 = e^{iat}\int_0^t f(\tau)d\tau \quad (46)$$

The replacement of $\langle\omega|\varrho^T|\omega'\rangle$ by $\delta_{\omega,\omega'}\varrho^T(\omega)$ has been used throughout. This affects only the explicit form of the $\psi_{ij;mn}(\tau)$ and can be generalized.

Equation 43 represents a form of the quantum mechanical equation of motion. If the "rate constants" $k_{ij;mn}(t)$ are assumed to be constant in time, and one

assumes all off-diagonal elements of $\dot{\sigma}(t)$ are zero, then eq 43 is known as a master or *kinetic equation*[30] and represents a set of states which are relaxing into one another due to well-defined transition rates. In the next section we will examine eq 43 for the special case $\rho^T(\omega) = \delta_{\omega,0}$ and only two coarse-grained states.

B. The Two-Level System. For many cases of physical interest one may consider an initial excited electronic state to undergo a transition into one other electronic state. The vibrational modes of the final electronic state act as the heat sink for the excess electronic energy. We may designate the electronic states as our coarse-grained states and consider all the vibrational quantum states of the final electronic state to form the set of states $\{|\omega\rangle\}$. For this model the boundary condition would be $\rho^T(\omega) = \delta_{\omega,0}$ as no vibrational quanta of the lower state were excited at $t = 0$ (assuming low kT). We may take our initial state of the system to be $|2,0\rangle$ ($\equiv|0\rangle$ of section III) and consider transitions into states $|1,\omega\rangle$. This model is denoted as the two-level system (TLS). Moreover we will assume that $\mathbf{V}$ in eq 41 is nondiagonal in the coarse-grained indices. That is

$$\langle 1,\omega|\mathbf{V}|1,\omega'\rangle = \langle 2,\omega|\mathbf{V}|2,\omega'\rangle = 0 \tag{47}$$

These assumptions greatly simplify the form of eq 43. Due to eq 47 we see that terms such as $\langle 2,\omega|\mathbf{V}|l,\omega'\rangle \cdot \langle l,\omega'|\mathbf{V}|1,\omega\rangle$ will vanish identically. This will result in a decoupling of the equations for diagonal and off-diagonal elements of $\dot{\sigma}$. It should be noted that this decoupling is not required to obtain solutions to eq 43, but does simplify the form of the solution. If we form a matrix from the elements of (43) by considering the elements $\sigma'(t)_{ij}$ to be elements of a vector, then for this model TLS we will obtain

$$\frac{\partial}{\partial t}|\sigma'(t)\rangle = \mathbf{K}(t)|\sigma'(t)\rangle \tag{48}$$

where

$$\mathbf{K}(t) = \begin{pmatrix} -k_{11}(t) & k_{22;11}(t) & 0 & \\ k_{11;22}(t) & -k_{22}(t) & & \\ & & -k_{12}(t) & k_{21;12}(t) \\ 0 & & k_{12;21}(t) & -k_{21}(t) \end{pmatrix}$$

$$|\sigma'(t)\rangle = \begin{pmatrix} \sigma'(t)_{11} \\ \sigma'(t)_{22} \\ \sigma'(t)_{12} \\ \sigma'(t)_{21} \end{pmatrix}$$

$$k_{ij}(t) = k^{(1)}{}_{ij;ij}(t) + k^{(2)}{}_{ij;ij}(t) \tag{49}$$

In more general cases there will not be a factorization of the relaxation equation for diagonal and nondiagonal elements of $\dot{\sigma}'(t)$. This factorization will not occur with a system with more than two levels even if an assumption like (47) is made, so the TLS has an inherent mathematical advantage. The present TLS is analogous to an isolated resonance state interacting with a single continuum, $\{|l,\omega\rangle\}$. In general, a multilevel problem would be represented by multiple resonances interacting with one or more continua. As Mies[31] has pointed out, complex effects occur when resonances are separated by less than their line width. In the present formulation this added complexity would result in the additional importance of the off-diagonal terms of $\dot{\sigma}(t)$ in determining the evolution of the diagonal terms, and in the need to retain higher cumulant terms in (40). The theoretical approach discussed herein is most appropriate for isolated resonances.

Solution of an equation like (48) is of itself a difficult mathematical problem. For any finite system, the time-dependent matrix $\mathbf{K}(t)$ will be expected to have a recursion time such that

$$\mathbf{K}(t + T) = \mathbf{K}(t) \tag{50}$$

Unfortunately this property does not simplify the solution of eq 48. One may use a numerical method as follows. If $\mathbf{K}(t)$ can be considered constant over a time interval Δt, the solution to eq 22 over such an interval is

$$|\sigma'(t)\rangle = \sum_{\lambda} c_\lambda(t)|\lambda(t)\rangle e^{\lambda(t)\tau} \tag{51}$$

where

$$\mathbf{K}(t)|\lambda(t)\rangle = \lambda(t)|\lambda(t)\rangle \tag{52}$$

The coefficients $c_\lambda(t)$ are obtained from the boundary value of $|\sigma'(t)\rangle$. The symbol τ is time elapsed since $t(\tau \leq \Delta t)$. If the explicit form of $\mathbf{K}(t)$ is known at all values of t, then a series of solutions of the form of (51) can be joined and the vector $|\sigma'(t)\rangle$ can be obtained for the range of time of interest.

Certain other simplifications of (49) are possible. If one inspects the various correlation functions defined by eq 45, one finds that terms of the form $e^{i(\epsilon_1-\epsilon_2-\omega)\tau}V(\omega)^2$ or $e^{i(\epsilon_2-\epsilon_1-\omega)\tau}V(\omega)^2$ appear, where $V(\omega)^2$ is some matrix element squared. If $\epsilon_2 > \epsilon_1$, then only the second term will have a "resonance," *i.e.*, a value of ω such that $\epsilon_2 - \epsilon_1 - \omega = 0$. If we denote the resonance case correlation function by

$$\psi(\tau) = \sum_{\omega} e^{i(\epsilon_2-\epsilon_1-\omega)\tau}V(\omega)^2 \tag{53}$$

then in the nonresonance case the correlation function would be $e^{-i2\omega_0\tau}\psi(\tau)$, where $\omega_0 = \epsilon_2 - \epsilon_1$. If $\psi(\tau)$ decays slowly compared to the oscillations of $e^{-i2\omega_0\tau}$, then the integral of $e^{-i2\omega_0\tau}\psi(\tau)$ may safely be neglected (see eq 44). This condition must be met in cases appropriate for the present treatment. Stated most simply,

(30) See, for example, E. Montroll and K. Shuler, *Advan. Chem. Phys.*, 1, 361 (1958).

(31) F. H. Mies, *Phys. Rev.*, 175, 164 (1968).

neglect of the nonresonance terms is equivalent to neglect of transitions that do not conserve energy.

If we neglect the nonresonance terms, we will find the following equalities for a TLS

$$k_{11}(t) = k_{11;22}(t) = 0 \tag{54}$$

If we use the $\rho^T(\omega) = \delta_{\omega,0}$ boundary condition, we may define

$$\begin{aligned}\psi(\tau) &= \sum_{\omega} e^{i(\epsilon_1+\omega-\epsilon_2)\tau}|\langle 2,0|\,\mathbf{V}\,|1,\omega\rangle|^2 \\ &= \sum_{\tilde{\omega}} e^{i\tilde{\omega}\tau}V(\tilde{\omega})^2\end{aligned} \tag{55}$$

where the notation of eq 26 has been used in the second equality. In terms of the correlation function $\psi(\tau)$ we may write

$$\begin{aligned}k_{22}(t) = k_{22;11}(t) &= 2\int_0^t Re\{\psi(\tau)\}\,d\tau \\ k_{12;21}(t) = k_{12}(t) &= \int_0^t \psi(\tau)d\tau \\ k_{21;12}(t) = k_{21}(t) &= \int_0^t \psi(\tau)^*d\tau\end{aligned} \tag{56}$$

We may study the solution for the $\sigma(t)_{22}$ element, as it is this element that describes the decay of the initial state. Since $k_{11;22}(t)$ is zero, the matrix equation for $\sigma(t)_{22}$ (eq 48) becomes

$$\frac{\partial}{\partial t}\sigma(t)_{22} = -k_{22}(t)\sigma(t)_{22} \tag{57}$$

with the solution

$$\begin{aligned}\sigma(t)_{22} &= \exp\left\{-\int_0^t k_{22}(t')dt'\right\}\sigma(0)_{22} \\ &= \exp\left\{-2\int_0^t dt'\int_0^{t'} Re\{\psi(t'')\}dt''\right\}\end{aligned} \tag{58}$$

where $\sigma(0)_{22}$ was assumed equal to unity for the second equality. From eq 58 we see that the normal exponential decay is obtained if $k_{22}(t)$ becomes constant for larger t values. In general such a decay law for $\sigma(t)_{22}$ will not be obtained.

We may verify that eq 58 agrees with eq 20 for very short lines. From eq 55 we see that

$$\psi(\tau) \approx \sum_{\tilde{\omega}} V(\tilde{\omega})^2 + \mathcal{O}(\tau) \tag{59}$$

so

$$\int_0^{\tau'} \psi(\tau)d\tau \approx \sum_{\tilde{\omega}} V(\tilde{\omega})^2\tau' \tag{60}$$

and

$$\begin{aligned}\int_0^t k_{22}(\tau')d\tau' &= \sum_{\tilde{\omega}} V(\tilde{\omega})^2t^2 \\ &= \langle\lambda^2\rangle t^2\end{aligned} \tag{61}$$

in agreement with eq 21 for $|\langle 0|t\rangle|^2$ (note that $|\langle 0|t\rangle|^2$ and $\sigma(t)_{22}$ have the same meaning, in different notations). We may also observe that $\sigma(t)_{22}$ cannot be shown to be equal to $|\langle 0|t\rangle|^2$ to higher order (*i.e.*, see eq 27). The reason for this disagreement is the truncation of the cumulant expansion in eq 40. It would appear from these results that the present results embodied in eq 58 would be correct only in the very short time range, and then be identical with the previously derived exact results in section III. Yet eq 58 does yield the normal exponential decay commonly encountered experimentally and expected to result from a weak-coupling theory. As we will see in Appendix II calculations of $|\langle 0|t\rangle|^2$ for some finite matrices yields essentially exponential decay for "intermediate" time scales. Thus for this time scale the result of combining all the terms in eq 20 is essentially the appearance of a simple linear dependence on t in the argument of the exponential. This is certainly not obvious from the form of the expression and would suggest that the results of section III are of practical interest for very short t only. The fact that eq 58 agrees with the normal exponential decay law, if $k_{22}(t)$ approaches a constant for intermediate times, suggests that the truncation of the cumulant expansion in deriving eq 43 will be a valid approximation for systems that show dissipative behavior. We may now investigate in more detail the requirements for validity of an exponential decay law.

V. The Relation of the Spectral Distribution Function, the Correlation Function, and the Exponential Decay Law

The conditions for the validity of an exponential decay law are obvious from eq 58. There must exist a correlation time, τ_c, such that

$$\lim_{\tau\to\tau_c} \psi(\tau) \longrightarrow \epsilon \tag{62}$$

where ϵ is a small constant, and it follows that

$$\lim_{\tau\to\tau_c} k_{22}(\tau) = 2\int_0^{\tau} Re\{\psi(\tau')\}d\tau' = k \tag{63}$$

where k is a constant. For all $t > \tau_c$, the normal exponential decay law holds. From eq 55 we see that the behavior of the correlation function as a function of time depends on the properties of the matrix elements, $V(\tilde{\omega})$. We may denote the function $V(\tilde{\omega})^2$ as the spectral distribution function, or SDF. If the SDF is a smooth function of the relative energy $\tilde{\omega}$, then $\psi(\tau)$ will have a short τ_c and the conditions for exponential decay will be met. On the other hand, if some particular matrix element, $V(\tilde{\omega}')$, has a very large magnitude, oscillations will appear in $\psi(\tau)$, and highly nonexponential decay may result. If $\psi(\tau)$ is found to oscillate strongly for a model SDF, one may be certain that nonexponential decay will result, but the truncation of the cumulant series in eq 40 is apparently not justified (see Appendix

II). If the higher terms in the cumulant expansion are retained, the resulting equations become very unwieldy and the present approach is difficult to apply. While the range of validity of eq 40 for finite systems deserves further study, it is thought that eq 58 will be an adequate approximation for testing a model SDF for its dissipative properties. In the case that eq 62 and 63 obtain, then eq 58 will allow the rate of relaxation to be calculated. It is important to realize that it is the property 62 that determines if a set of states, $|\omega\rangle$, may serve as a dissipative "field." All fine-grained states appear in the sum 55, including purely molecular vibrations, lattice phonons and photons. If the intramolecular SDF is sufficiently smooth, then there will be a significant intramolecular contribution to the observed rate. For this case, the rate of relaxation and quantum yield of all processes of the excited electronic state of the molecule should be essentially independent of the state of matter (in the absence of external heavy atom effects or other interactions that change the electronic wave function in an important way).

The practical advantage of the present formulation is that the evaluation of $\psi(\tau)$ (eq 55) is a straightforward project and may be undertaken for any assumed SDF. Thus, the calculation of a relaxation rate is not limited to a particular model for the function $V(\tilde{\omega})^2$, and one may take account of structure in the SDF in a simple way.

It is interesting to investigate the time evolution of $\sigma(t)_{22}$ for two simple model SDF's. The first is the same as discussed by Bixon and Jortner[6] and later by Chock, *et. al.*[8] In this model, the states $|\tilde{\omega}\rangle$ are each separated by energy $\hbar x$, and the matrix elements are all equal. If these are $N/2$ states above and below the $\tilde{\omega} = 0$ level, the eq 55 becomes

$$\psi(\tau) = v^2 \sum_{n=-N/2}^{N/2} (e^{ix\tau})^n = v^2 \frac{\sin\{(N+1)x\tau/2\}}{\sin\{x\tau/2\}} \tag{64}$$

Defining the variable

$$y = x\tau/2 \tag{65}$$

the integral of $\psi(\tau)$ becomes

$$\frac{1}{2}k(\tau) = \frac{2v^2}{x}\int_0^{\tau x/2} \frac{\sin\{(N+1)y\}}{\sin\{y\}}dy \approx \frac{2v^2}{x}\int_0^{\infty} \frac{\sin(N+1)y}{y}dy = \frac{\pi v^2}{x} \tag{66}$$

In order to obtain this result, $\sin(y)$ was expanded, and only the first term was retained. Since the most important contribution to the integral is for small y, we may safely extend the upper boundary to infinity. Substituting eq 66 into eq 58 we obtain the expected result

$$\sigma(t)_{22} = \exp\left\{-\frac{2\pi v^2 t}{x}\right\} \tag{67}$$

Note that x^{-1} is the density of states for this model. Equation 67 is the same result obtained by Bixon and Jortner by another method.[6]

The second model that we discuss is rather artificial but has the advantage that $\psi(\tau)$ may be obtained explicitly. As before we assume that all the states $|\tilde{\omega}\rangle$ are equally spaced in energy, with separation $\hbar x$. The matrix elements are taken to have the form

$$V(\tilde{\omega})^2 = v^2 y^{|n|} \tag{68}$$

where

$$\tilde{\omega} = nx \tag{69}$$

The integer n may take all values between $\pm\infty$ and y is a constant ($y \leq 1$). Since $\tilde{\omega}$ is the energy relative to the energy of the $|2,0\rangle$ state, this model has the maximum matrix element between the isoenergetic kets $|2,0\rangle$ and $|1,\epsilon_2 - \epsilon_1\rangle$. We may evaluate eq 55 by use of the geometric series as follows

$$\psi(\tau) = v^2\left[\sum_{n=1}^{\infty}(e^{-ix\tau}y)^n + \sum_{n=1}^{\infty}(e^{ix\tau}y)^n + 1\right] = v^2\frac{1-y^2}{1+y^2-2y\cos(x\tau)} \tag{70}$$

We may use the standard integral

$$\int \frac{dz}{a+c\cos z} = \frac{2}{(a^2-c^2)^{1/2}}\tan^{-1}\left\{\frac{(a-c)\tan(z/2)}{(a^2-c^2)^{1/2}}\right\} \tag{71}$$

for $x\tau$ in the range $[0,\pi]$. We will assume that we may write

$$y = e^{-\Delta} \approx 1 - \Delta \tag{72}$$

where the latter equality holds for small Δ. We obtain the result that

$$k(\tau)_{22} = \frac{4v^2}{x}\tan^{-1}\left\{\frac{2}{\Delta}\tan\left(\frac{x\tau}{2}\right)\right\} \tag{73}$$

We see that at $\tau = 0$, $k(0)_{22} = 0$ and

$$\lim_{x\tau\to\tau} k(\tau)_{22} = \frac{2\pi v^2}{x} \tag{74}$$

which is the Golden Rule result. We could obtain (74) by using the identity

$$\lim_{\tau\to\infty}\int_0^{\tau} e^{i\omega\tau'}d\tau' = \pi\delta(\omega) + i\mathcal{P}/\omega \tag{75}$$

in eq 44 and 45. We now see that the validity of (75) for this model will depend not only on the time, τ, but the parameters Δ and x, which are characteristic of the model SDF. We expect that in general the *smoothness* of the SDF (characterized by Δ for this model) will play the dominant role in determining the nonexponen-

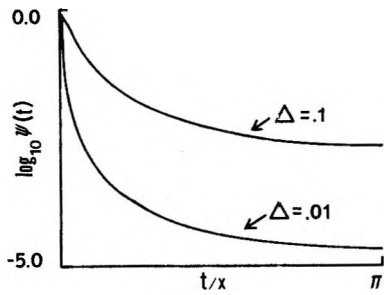

Figure 1. $\psi(\tau)$ *vs.* the "reduced time" t/x for the model discussed in section V.

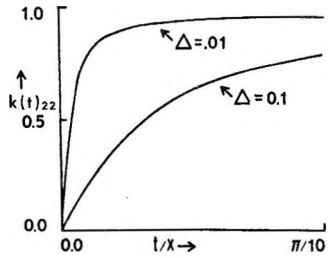

Figure 2. $k(t)_{22}$ *vs.* the "reduced time" t/x for the model discussed in section V, where constants have been chosen so $k(\infty)_{22} = 1.0$.

tial range of decay. For short times the decay rate of the system will be less than the asymptotic rate. The properties of $\psi(\tau)$ and $k(\tau)_{22}$ for this model are displayed in Figures 1 and 2. We may also note that this model has a recursion time, $\tau_r = 2\pi/x$, as would be expected for any finite system. From (70) we see that

$$\psi(0) = \psi(2\pi/x) \tag{76}$$

We would expect that a recursion would occur for $\sigma(t)_{22}$ at longer times, that is for some time T

$$\sigma(0)_{22} = \sigma(T)_{22} \tag{77}$$

We see that in general our first-order theory will not yield a result like (77), unless $\psi(\tau)$ changes sign for longer τ, resulting in a cancellation of terms in (56). This is not true for the two models discussed above and is not expected to be true for most SDF's. We conclude that a relation like (77) can only come from higher terms in the cumulant expansion. Thus the present formulation is unable to account for possible long t quantum beats or recursion signals.

There is one practical point that should be made about the *width* (*i.e.*, the range of energies $\tilde{\omega}$) that needs to be considered. As can be seen from (55), evaluating $\psi(\tau)$ requires a sum that includes all states $|\omega\rangle$. For real systems this would be an impossible task. It is expected that the "wings" of the SDF will only contribute to the very short time behavior of $\psi(\tau)$, which may be neglected in the time integral to obtain $k(\tau)_{22}$. For practical calculations, one would start with the narrowest reasonable SDF and would calculate $k(\tau)_{22}$. One would then expand the range of energies, $\tilde{\omega}$, considered and recalculate $k(\tau)_{22}$ until this function has converged. Of most interest is the long τ asymptotic behavior of $k(\tau)_{22}$ which will tend to require only a narrow segment of the SDF. In a sense the present work shows how to calculate the correct "average value" of an arbitrary SDF for application of the Golden Rule. As should be clear from the previous comments, the exponential decay law will only hold in the region $\tau_c < t < \tau_r$, but this is the time scale of normal experimental interest.

The present results have been obtained for a TLS which obeys eq 47. If one makes a random phase approximation in eq 43 by ignoring the off-diagonal elements of $\mathfrak{d}(t)$, then eq 58 will hold for a many-level system. The rate $k(t)_{22}$ will be a sum of terms, each due to a transition $|2,0\rangle \rightarrow |i,\omega\rangle$. Each coarse-grained state generates an independent dissipative field due to the fine-grained states, $|\omega\rangle$, that may accompany it. The correlation function for each coarse-grained state SDF may be examined separately, and its contribution to the overall rate computed. It may be that certain coarse-grained states contribute an SDF that leads to an oscillating correlation function. This circumstance may be denoted as a nondissipative interaction. By studying the correlation functions for each transition, one may treat both the nondissipative and dissipative interactions within the molecular set of states consistently. In the former case a new basis set must be found such that the SDF for transitions between these states will be sufficiently smooth for exponential decay to obtain and for there to exist a kinetic equation for transitions between these states. This would be analogous to "intensity stealing" in the case of radiative transitions. In the dissipative case, the results of the weak-coupling, time-dependent theory may be used, and the kinetic equation considered to be a valid description of the relaxation of the system.

VI. Conclusions

The present formulation of intramolecular relaxation processes employs rather different mathematical procedures than recent work by other authors.[6-10] It is felt that the present formalism is simpler to apply to realistic models of intramolecular coupling of electronic and vibrational degrees of freedom, but its validity is limited to the so-called statistical[7,32] and intermediate cases.[7,9,10,32] As is especially demonstrated in Appendix II, the present "weak-coupling" approach will fail to predict the correct magnitude for quantum beats, but can categorize a model SDF as "dissipative" (≡ statistical) or "nondissipative" (≡ resonant). In recent work by Freed and Jortner,[9] more emphasis has been placed on the "smoothness" of functions describing

(32) Robinson has denoted the various cases for intramolecular dissipation as the "small molecule" or "α" limit and "large molecule" or "ω" limit (*J. Chem. Phys.*, **47**, 1967 (1967)). Reference 7 uses the terms "resonance" and "statistical" limit, while we prefer the terms "nondissipative" and "dissipative" limit.

the intramolecular interactions. While these authors use a completely different formalism, it is similarly concluded that the presence of reasonably strong, sparsely spaced interactions can lead to important interference effects in the intramolecular relaxation process. It is not clear to the present author if these workers could apply their results to an arbitrarily discontinuous SDF. We have not explicitly discussed absorption or emission lines shapes or emission quantum yields in this article. While the former quantities are related to the time evolution of the system (see section IIIA, for example), it is not generally possible to work backwards from the time evolution to obtain a unique absorption line shape. From the point of view of the present theory, absorption line widths (described by $\mathcal{G}(\lambda)$ if only the state $|0\rangle$ carries oscillator strength) are taken to be Lorentzian with the half-height width given by the relaxation rate (see Bixon and Jortner[6] for example). Likewise the emission quantum yield would be calculated in the usual way, with the overall relaxation rate separated into rates for independent channels.[33] Thus if k_r is the radiative rate, and k_q is the sum of all radiationless (*i.e.*, quenching) processes, then the quantum yield would be taken to be

$$Q = \frac{k_r}{k_r + k_q} \tag{78}$$

Again we emphasize that the present treatment is designed to test the validity of a relation like (78) and to calculate k_q from realistic molecular models. In nondissipative cases, neither Lorentzian line-shapes nor quantum yield expressions like (78) are expected to hold.

How might the present formalism be applied to experimental data? Admittedly the construction of a molecular SDF appears quite formidable. However, it is quite clear that molecular vibrations will differ in their efficiency in coupling electronic states due to symmetry requirements and "local" amplitudes, (*i.e.*, specific bond stretches). Consequently partial isotopic substitution may affect the radiationless processes differently, depending on the position of the isotopes.[34,35] The same comment holds for other chemical substitutions on the basic chromophores. The most consistent way to study these effects would be to analyze the resultant perturbation on the molecular SDF in the energy range around the $|0\rangle$ state. It would seem unreasonable to consider only the changes in the strictly isoenergetic portion of this function, as is implied by the Golden Rule, unless one is willing to replace the real SDF by a suitably smoothed representation.

One might well enquire if experimental intramolecular relaxation rates are in fact known for any molecule. As is pointed out by Bixon and Jortner,[6] a number of large molecules evidently undergo electronic relaxation even at very low gas pressures, where collisions are thought to play a very small role.[16-18] Strictly speaking, the statistical limit implies that the emission quantum yield and lifetime for a given electronic state would be invariant to state of matter, in the absence of energy transfer, and external heavy atom effects (or other specific perturbations on the electronic state). A great many molecules show some dependence of emission on solvent, but it does not follow that the intramolecular contribution to the relaxation rate is negligible. On the contrary, the main effect of the solvent is to broaden the zeroth-order molecular states and consequently change the SDF (see Appendix I). If the isolated molecule SDF were known, then the solvent dependence of the SDF could be estimated by the solvent dependence of the vibrational relaxation times. Quantitative studies of the solvent dependence of fluorescence lifetime and quantum yields and comparison to gas phase studies would clarify the experimental situation considerably.

Acknowledgments. The author would like to acknowledge a helpful conversation with Dr. D. Chock and Dr. S. A. Rice and to thank Dr. K. Freed for providing a preprint of his work in this area.

Appendix I. A Simple Model for a Pressure Broadened Intramolecular Field

We assume that the SDF for a transition may be written as a sum

$$\mathcal{g}(\tilde{\omega}) = \sum_\alpha v_\alpha{}^2 \frac{\gamma_\alpha}{\pi} [(\tilde{\omega} - \omega_\alpha)^2 + \gamma_\alpha{}^2]^{-1} \tag{I-1}$$

where γ_α represents the broadening of the αth molecular state due to gas phase collisions or interactions with phonon states, etc. These molecular states α would generally be taken to be vibrational levels belonging to a different electronic state. The function $\mathcal{g}(\tilde{\omega})$ is a continuous function of $\tilde{\omega}$, which is the energy parameter relative to ϵ_2. By use of standard integrals we obtain the result

$$\begin{aligned} \psi(\tau) &= \int d\tilde{\omega} e^{i\tilde{\omega}\tau} \mathcal{g}(\tilde{\omega}) \\ &= \sum_\alpha v_\alpha{}^2 e^{i\omega_\alpha \tau} e^{-|\gamma_\alpha|\tau} \end{aligned} \tag{I-2}$$

We see that $\psi(\tau)$ is a sum of damped oscillating functions. The effect of increased broadening is to increase the damping rate. This illustrates how an intramolecular field may become dissipative at higher pressures or in a condensed phase. The integral of the real part of (I-2) is

(33) In the present formalism, the perturbation operator V may be expressed as a sum of commuting operators for the independent channels. In this case $\kappa(t)_{22}$ is a sum of functions, each with its own correlation time.

(34) S. H. Lin and R. Bersohn, *J. Chem. Phys.*, 48, 2732 (1968).

(35) T. E. Martin and A. H. Kalantar, "Molecular Luminescence," W. A. Benjamin, Inc., New York, N. Y., 1969, p 437.

$$k(t) = 2\int_0^t Re\{\psi(\tau)\}d\tau$$

$$= \sum_\alpha 2v_\alpha^2 \frac{\gamma_\alpha}{\gamma_\alpha^2 + \omega_\alpha^2} \times \{1 - e^{-\gamma_\alpha t}[\cos\omega_\alpha t - (\omega_\alpha/\gamma_\alpha)\sin\omega_\alpha t]\} \quad \text{(I-3)}$$

$$= \sum_\alpha 2v_\alpha^2\gamma_\alpha(\gamma_\alpha^2 + \omega_\alpha^2)^{-1}$$

where the second equality occurs for $t\gamma_\alpha \gg 1$ for all γ_α. From (I-3) we see that if $\gamma_\alpha \ll \omega_\alpha$ we will have a nondissipative case, such that $k(t)$ will be an oscillating function of time, unless the set of frequencies, ω_α is sufficiently closely spaced such that the oscillating terms effectively cancel out. We also note that the second equality in (I-3) is exactly what would obtain if eq 75 had been used. As usual, the use of an integral operator relation like (75) is valid on a time scale such that the correlation function has converged. In order to recover the Golden Rule in its usual form from (I-3) we may assume that the set of states lie very close together and replace the sum by an integral. If we use the identity

$$\lim_{\epsilon\to 0+} \frac{\epsilon}{x^2 + \epsilon^2} = \pi\delta(x) \quad \text{(I-4)}$$

then making some obvious assumptions we obtain

$$\lim_{\substack{t\gg\tau_c \\ \gamma\alpha(\tilde{\omega})\to 0+}} k(t) = \lim_{\gamma(\tilde{\omega})\to 0+} \int 2v(\tilde{\omega})^2 \left(\frac{\gamma(\tilde{\omega})}{\gamma(\tilde{\omega})^2 + \tilde{\omega}^2}\right)\rho(\tilde{\omega})d\tilde{\omega}$$

$$= 2\pi v(0)^2\rho(0) \quad \text{(I-5)}$$

This limit corresponds to a molecule which is statistical in the unperturbed state (*i.e.*, no broadening). The more interesting case would be (I-3), where the rate would be a function of both intramolecular interactions (v_α^2) and interaction with a true heat bath (γ_α).

Appendix II. Comparison of the Exact and "Weak-Coupling" Time Evolution for Some Finite Matrices

As was discussed in section III, one may obtain the exact time evolution of a quantum mechanical system if one has obtained all the eigenvectors and eigenvalues of **H**. For real physical systems this procedure is not generally practical, but for smaller matrices (50 × 50) one may use standard mathematical methods to obtain these quantities. In particular some results of calculations of this type for the TLS will be presented in this section. For our assumed prediagonalized set of states (see eq 47) with the boundary conditions $|0\rangle = |2,0\rangle$ the matrix **H** will have diagonal elements $\tilde{\omega}$ ($\tilde{\omega} = 0$ corresponds to the energy of the $|2,0\rangle$ ket) and only one column and one row of off-diagonal elements between $|0\rangle$ and $|\tilde{\omega}\rangle$. After this matrix is diagonalized the projection of all the eigenvectors, $|\lambda\rangle$, on $|0\rangle$ may be obtained and $|\langle 0|t\rangle|^2$ obtained directly.

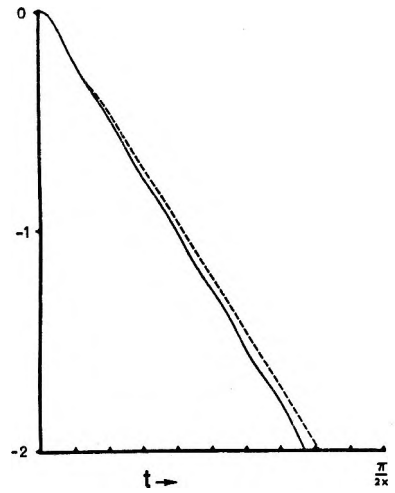

Figure 3. Semilog plot of $\sigma(t)_{22}$ (– – –) and $\nu\langle 0\nu t\rangle^2$ (——) *vs.* time for "square wave" model. The maximum value of t in all the plots that follow is $\pi/2x$. The recursion time would be $\tau_t = 2\pi/x$ for a constant energy separation of $\hbar x$.

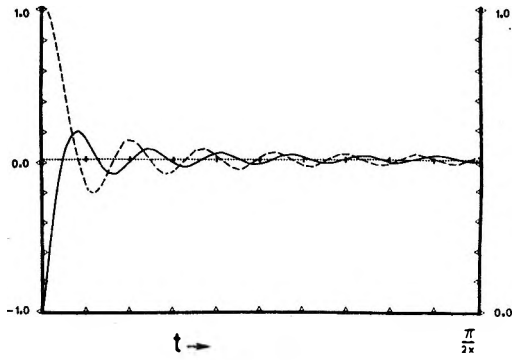

Figure 4. $\psi(t)$ (– – –) and $k(t)_{22}$ (——) (in arbitrary units) *vs.* t for the "square wave" model. The left-hand ordinant refers to $\psi(\tau)$ and the right-hand ordinant refers to $k(t)_{22}$.

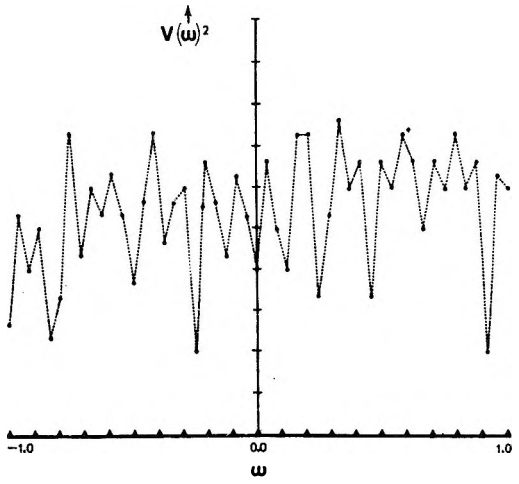

Figure 5. The discontinuous SDF assumed for the calculations presented in Figures 6 and 7 (in arbitrary units). The SDF was normalized such that $\langle\lambda^2\rangle = 0.05$, which is the same normalization as the "square wave" model. The values of the matrix elements $(V(\omega)^2)$ are essentially a random number set.

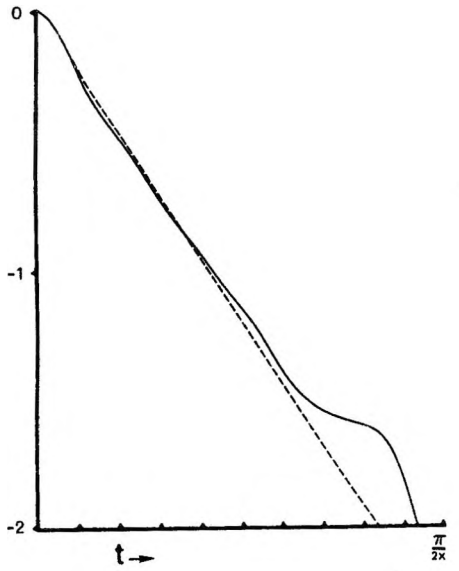

Figure 6. Semilog plot of $\sigma(t)_{22}$ (- - -) and $|\langle 0|t\rangle|^2$ *vs.* time for discontinuous model (compare to Figure 3).

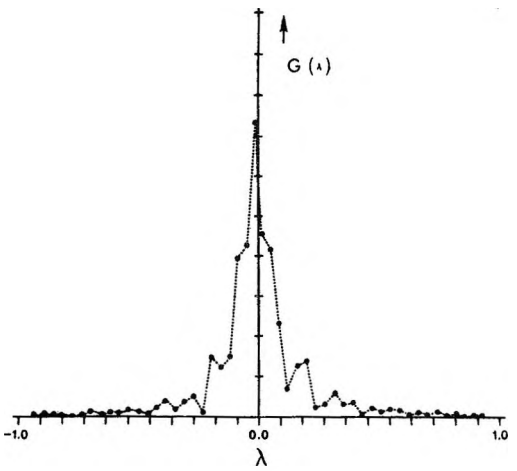

Figure 7. Plot of $\mathcal{G}(\lambda)$ (arbitrary units) *vs.* λ (exact energy eignevalues) for discontinuous model.

This is the exact result for the particular model of the SDF.

The "weak-coupling" results follow from eq 55. The real part of $\psi(\tau)$ can be evaluated for any SDF, and $k_{22}(t)$ can be obtained by a numerical integration. The perturbation solution, $\sigma(t)_{22}$, follows from eq 58 and a second numerical integration. These operations are easily programmed and quite easy to extend to a large number of states $|\tilde{\omega}\rangle$. In what follows we will compare $|\langle 0|t\rangle|^2$ (the exact solution) and $\sigma(t)_{22}$ (the weak-coupling result) for three different SDF's.

The first SDF will be the constant value model discussed in section V. The SDF is a "square wave" function, symmetric about $\tilde{\omega} = 0$. The upper and lower $\tilde{\omega}$'s were taken arbitrarily to be ± 1.0 and 49 states $|\tilde{\omega}\rangle$ were assumed (which with the addition of $|0\rangle$ leads to a 50×50 matrix). All time-dependent

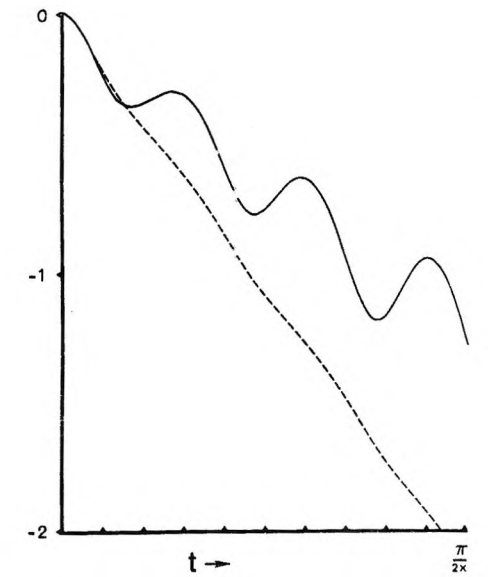

Figure 8. Semilog plot of $\sigma(t)_{22}$ (- - -) and $|\langle 0|t\rangle|^2$ (——) *vs.* t for the "square wave plus two strong discontinuities" model.

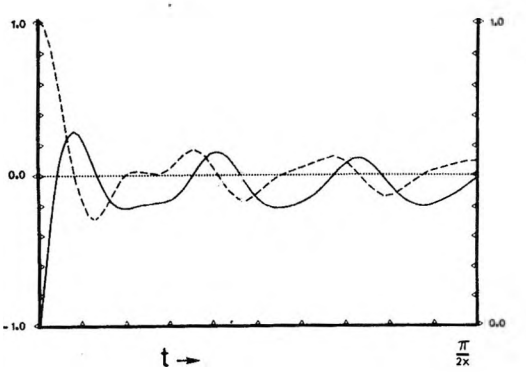

Figure 9. $\psi(t)$ (- - -) and $k(t)$ (——) (in arbitrary units) *vs.* t for "square wave plus two strong discontinuities" model.

results depend on the parameter τx, so the time scale was such that $\tau_{max}\, x = \pi/2$ for all models discussed. For this model $\mathcal{G}(\lambda)$ is a Lorentzian function, peaked at $\lambda = 0$, as expected In Figure 3 $|\langle 0|t\rangle|^2$ and $\sigma(t)_{22}$ are plotted on a semilog scale. As can be seen the agreement is quite good, with $\sigma(t)_{22}$ tending to underestimate the oscillations in the exact solution. In Figure 4 $\psi(\tau)$ and $k(\tau)$ are presented for this model. Despite the slight oscillations in $k(t)$, the rate of relaxation of $\sigma(t)_{22}$ very quickly becomes constant on the scale of Figure 3. Note the perfect agreement of these curves for short t, as discussed in section IVB.

A second SDF was considered which was rough and discontinuous, much as a molecular SDF would be. This SDF is displayed in Figure 5. Again the SDF extended only to ± 1.0 on the energy scale. The matrix elements were scaled such that $\langle \lambda^2 \rangle$ was equal to that of the previous model (see eq 27). The "weak-coupling" result for $\sigma(t)_{22}$ was virtually the same as the "square wave" model. Likewise $\psi(\tau)$ and $k(\tau)$ were very similar to those functions presented in Figure 4.

The comparison to the exact result is not so good for this model, especially at longer t (see Figure 6). The weak-coupling result does reproduce the general rate of decay, but does not reproduce the full set of oscillations present in the exact solution. In Figure 7 the function $\mathcal{G}(\lambda)$ for this model is presented. Note that $\mathcal{G}(\lambda)$ would correspond to the absorption line shape for a transition to the $|0\rangle$ state, assuming that the states $|\tilde{\omega}\rangle$ carry no oscillator strength.

The third model considered was a "square wave" SDF with two matrix elements with magnitude five times the rest, symmetrically disposed around $\tilde{\omega} = 0$. In this case the "weak-coupling" result fails to duplicate the strong oscillations found in the exact solution (see Figure 8). As shown in Figure 9, strong oscillations show up in both $\psi(\tau)$ and $k(\tau)$. This model represents a case of a nondissipative interaction between a set of states. As discussed in the main body of this paper, one way to proceed is to obtain new zeroth-order states which are mixtures of $|0\rangle$ and the two nondissipative states, and use a weak-coupling formulation in terms of these new zeroth-order states. This is essentially the same procedure as discussed by Douglas[36] with regard to "anomalously long lifetimes" of small molecules. Note that in Figure 8 this effect is operative, as the rate of decay of $|\langle 0|t\rangle|^2$ is less than $\sigma(t)_{22}$.

In all these calculations the exact solution will show a recursion (*i.e.*, $|\langle 0|t\rangle|^2$ will increase) at $\tau_r \approx 2\pi/x$. This behavior is not reproduced by $\sigma(t)_{22}$, although $\psi(\tau)$ will show a similar recursion. In general $\sigma(t)_{22}$ will tend to underestimate all oscillations in the exact time-dependent solution. It is probable that any model SDF that results in even slight oscillations in $\sigma(t)_{22}$ may not be properly treated in the weak-coupling limit.

(36) A. E. Douglas, *J. Chem. Phys.*, **45**, 1007 (1966).

A Statistical Treatment of Micellar Solutions

by H. S. Chung and I. J. Heilweil

Central Research Division Laboratory, Mobil Research and Development Corporation, Princeton, New Jersey 08540
(Received June 16, 1969)

A statistical treatment of micellar solutions is given. It is based upon a Flory analysis of the ideal associated solution model of Prigogine and coworkers. In part A, which is mostly applicable to aggregating nonaqueous solutions, a new definition of the critical micelle concentration (cmc) is proposed; it is defined as the inflection point of the osmotic coefficient *vs.* concentration curve. The dependence of the average degree of aggregation on the solute concentration is derived from the minimization of the Helmholtz free energy of the solution. The results indicate that the theory can account for all the essential features (including the so-called "anomalies") of micellar solutions. A comparison between theory and experiment shows the agreement is satisfactory. In part B, solvation phenomena are considered. It is found that empirical formulas previously employed for the correlation of the properties of solvating systems may be obtained by a straightforward application of the Flory formalism.

I. Introduction

In binary liquid mixtures, one often encounters situations in which molecules of one component may associate with themselves or with those of the other component. The resulting molecular aggregates, especially those made up of amphipathic molecules, are sometimes referred to as micelles. The practical importance of these associating systems has long been fully recognized. The characterization of their behavior, for example, is central to the understanding of such diverse phenomena and technological processes as solubilization, detergency, biological actions, and some phases of secondary oil recovery and of catalysis.

Although many attempts have been made to construct theoretical frameworks for the description of micellar systems, the present state of affairs cannot be regarded as satisfactory. As a case in point, we may mention the fact that the currently available theories cannot even account for some of the most basic, distinguishing, qualitative features of micellar solutions such as the relative sharpness of the critical micelle concentration (cmc), the polydispersity and the average size of the micelles and their variations with temperature, and the so-called "second anomaly,"[1] that is, the

(1) See, for example, C. W. Davis, "Ion Association," Butterworth and Co., Washington, D. C., 1962, p 120.

apparently abnormal rise of some properties of the system (*e.g.*, the osmotic coefficient) at higher solute concentrations.

Both phenomenological and molecular approaches have been employed in portraying micellar systems. Among the former, we may cite the mass action schemes of Jones and Bury,[2] Murray and Hartley,[3] Phillips,[4] and Vold[5] and the phase separation models of Stainsby and Alexander,[6] Shinoda and Hutchinson,[7] and Matijevic and Pethica.[8] Since these works have only peripheral relevance to our discussion and since their difficulties have been thoroughly recounted in a recent, excellent review article by Hall and Pethica,[9] we shall not refer to them any further here. Among the latter, the statistical mechanical theories of Aranow,[10] Hoeve and Benson,[11] and Poland and Scheraga[12] come immediately to mind. Aranow's formulation, which is based upon the grafting of the exact physical cluster theory of Hill unto the constant pressure ensemble, suffers from the fact that, in spite of its formal elegance, relatively little information may be derived from it. The Mayer–McMillan-like treatment of Hoeve and Benson, on the other hand, makes use of, among other approximations, the macroscopic liquid-drop model inherent in the nucleation theory of Becker, Döring, and Zeldovich.[13] Therefore, the justifications for assigning a macroscopic surface tension to aggregates of molecular dimensions and for regarding even aggregates composed of a few molecules as having a well-defined spherical shape are once again called into question. Finally, the method of Poland and Scheraga has, in addition to the drawbacks just listed, the disadvantages of having (a) considered, instead of a size distribution of micelles, only micelles of one size, (b) used the gas phase partition functions for molecules in the liquid solution, and (c) introduced the concept of "hydrophobic bonding" which some investigators[14] felt to be unnecessary in the study of associated systems. Although perhaps it can be argued that the idea of hydrophobic bonding has been found on some occasions to be useful in dealing with aqueous solutions, its extension to aggregating nonaqueous systems is by no means obvious.

It is the main purpose of this work to examine the behavior of micellar solutions through a Flory analysis of the ideal associated solution model of Prigogine and coworkers.[15] The dependence of the aggregation number on solute concentration is derived from the minimization of the Helmholtz free energy of the solution. A new definition of the cmc is proposed which, unlike that of Phillips, does not include any reference to ideal colligative properties. On the basis of this model, it is found that the essential features of micellar systems are reproduced. The "anomaly" mentioned previously is seen to be, in reality, one of the fundamental characteristics of associating systems. Limited comparison of the theory with experimental data indicates that the agreement is adequate. Lastly, solvation phenomena in multicomponent solutions are examined by a direct application of the Flory formalism.

II. Theory

A. Nonsolvating System. Consider a binary system composed of N_A molecules of A (solute) and N_B molecules of B (solvent). In the particular case in which only the molecules of A can associate with one another to form complexes ("micelles"), A_2, A_3, $\cdots$ and other oligomers (which we shall simply denote by the set $\{A_k\}$), then

$$M = N_A + N_B = \sum_{i=1} iN_{Ai} + N_B \qquad (1)$$

where M is the total number of molecules. We shall suppose that only interactions that lead to the formation of the existing set of complexes need to be considered; all the dispersion forces between the complexes and between the complexes and the solvent are assumed to be negligible. The model described is the ideal associated solution of Prigogine, *et al.* If we view our problem from the standpoint of a lattice model and let the molecular partition function of species k be f_k, the partition function of the solution may be expressed as

$$Q = g(N_B; \{N_{Ai}\})\, f_B{}^{N_B} \prod_{i=1} f_{Ai}{}^{N_{Ai}} \qquad (2)$$

where g is the combinatorial factor for placing N_B monomeric solvent molecules and the set $\{A_k\}$ (where A_k occupies k lattice sites) on a quasi-lattice of M sites. There are several ways in which one can estimate this function g. One may, if the differences in the size of the complexes can be ignored, use the random mixing approximation, or he may employ the more accurate quasi-chemical method[16] which does take into account

(2) E. R. Jones and C. R. Bury, *Phil. Mag.*, **4**, 841 (1927).

(3) G. S. Hartley, "Aqueous Solutions of Paraffin Chain Salts," Hermann and Cie, Paris, 1936.

(4) J. N. Phillips, *Trans. Faraday Soc.*, **51**, 561 (1955).

(5) M. J. Vold, *J. Colloid Sci.*, **5**, 506 (1950).

(6) G. Stainsby and A. E. Alexander, *Trans. Faraday Soc.*, **46**, 587 (1950).

(7) K. Shinoda and E. Hutchinson, *J. Phys. Chem.*, **66**, 577 (1962).

(8) E. Matijevic and B. A. Pethica, *Trans. Faraday Soc.*, **54**, 587 (1958).

(9) D. G. Hall and B. A. Pethica, "Nonionic Surfactants," M. J. Schick, Ed., Marcel Dekker, New York, N. Y., 1967.

(10) R. H. Aranow, *J. Phys. Chem.*, **67**, 556 (1963).

(11) C. A. T. Hoeve and G. C. Benson, *ibid.*, **61**, 1149 (1957).

(12) D. C. Poland and H. A. Scheraga, *ibid.*, **69**, 2431 (1965); D. C. Poland and H. A. Scheraga, *J. Colloid Interfac. Sci.*, **21**, 273 (1966).

(13) R. Becker and W. Döring, *Ann. Phys.*, **24**, 719 (1935); Ya. B. Zeldovich, *J. Exp. Theor. Phys.*, **12**, 525 (1942).

(14) J. H. Hildebrand, *J. Phys. Chem.*, **72**, 1841 (1968); G. Nemethy, H. A. Scheraga, and W. Kauzmann, *ibid.*, **72**, 1842 (1968).

(15) I. Prigogine, V. Mathot, and A. Desmyter, *Bull. Soc. Chim. Belg.*, **58**, 547 (1949); I. Prigogine and A. Desmyter, *Trans. Faraday Soc.*, **47**, 1137 (1951); L. Sarolea-Mathot, *ibid.*, **49**, 8 (1953); I. Prigogine and R. Defay, "Chemical Thermodynamics," John Wiley & Sons, New York, N. Y., 1954, Chapter 26.

(16) E. A. Guggenheim, "Mixtures," Oxford University Press, New York, N. Y., 1952, p 196.

size variations. Alternatively, if the aggregates are presumed to be chainlike, the factor g derived by Flory in his treatment of polydisperse polymer solutions is much more tractable.[17] In the present study, we shall adopt the Flory approximation. Thus

$$\ln g = -N \ln \sigma + N_B \ln (M/N_B) - \sum_{i=1} N_{A_i} \ln (N_{A_i}/M) + \sum_{i=1} (i-1) N_{A_i} [\ln (z-1) - 1]; N = \sum_{i=1} N_{A_i} \quad (3)$$

Here, z is the coordination number of the lattice, N the total number of complexes, and σ the symmetry number which will be set equal to unity (there is no reason to believe that the complexes have any symmetry). From the thermodynamic relations for the Helmholtz free energy, A, the chemical potential of B, μ_B, and the definition of the activity of the solvent, a_B

$$A = -kT \ln Q \quad (4)$$

$$\mu_B = [\partial A/\partial N_B]_{T, \{N_{A_i}\}} \quad (5)$$

$$\ln a_B = [\mu_B - \mathring{\mu}_B]/kT \quad (6)$$

one finds that

$$\ln a_B = \ln \varphi_B + \sum_{i=1} (1 - i^{-1}) \varphi_{A_i} \quad (7)$$

The quantities φ_B and φ_{A_i} are the volume fractions of B and of A_i defined, respectively, by $\varphi_B = N_B/M$ and $\varphi_{A_i} = iN_{A_i}/M$. Equation 7 is precisely what Flory obtained for a solution of polydisperse polymers in a monomeric solvent. This is also what one anticipates on physical grounds for our system because whether one calls the aggregate a micelle or a polymer molecule (both occupying the same number of sites) is immaterial so far as the combinatorial analysis is concerned. [In addition to the well-known derivations of Hildebrand and of Longuet-Higgins, it is interesting to find that eq 7 may be obtained by *still* another method. Thus, Prigogine and Defay[15] have shown that, by purely thermodynamic arguments (*i.e.*, without any recourse to statistical models), the activity coefficient of the solvent φ_B of an ideal associated solution can be expressed in the form (see eq 26.20 and 26.21 of ref 15)

$$\gamma_B = [x_B + x_A \langle i \rangle_N^{-1}]^{-1}$$

where $\langle i \rangle_N$ is given by eq 9. Using the definition $a_B = x_B \gamma_B$ and upon taking the logarithm of both sides of the above equation, we have

$$\ln a_B = \ln x_B - \ln [1 - (1 - x_B)(1 - \langle i \rangle_N^{-1})]$$

For dilute solutions, we may expand the second term on the right hand side in a series and retain only the leading member. The final result is

$$\ln a_B = \ln x_B + (1 - x_B)[1 - \langle i \rangle_N^{-1}]$$

which is just an alternate form of eq 7.] This adaptation of the Flory technique to associating systems has been suggested and utilized in the recent works of Scott[18] and of Lacmann.[19] However, these authors chose to formulate their problems in terms of a set of equilibrium constants and then proceeded to examine such aspects and properties of the solution as the heat and energies of mixing, entropy effects, phase separation, conditions for the occurrence of azeotropes, etc. In many systems, particularly solutions of surfactants, these may not be the primary concerns. Instead, one is generally more interested in such quantities as the osmotic coefficient ϕ, the values of the cmc and of the average degree of association, their temperature and concentration dependence, ... and so on. We wish to investigate these questions and would therefore want to recast eq 7 in terms of parameters more germane to the discussion of micellar solutions. The result is

$$\phi \equiv -[\ln a_B/(x_A/x_B)] = -x_B[1 - \langle i \rangle_N^{-1} + (\ln x_B)/x_A] \quad (8)$$

where x_k is the mole fraction of the kth species and $\langle i \rangle_N$ is the number average degree of aggregation of A defined as

$$\langle i \rangle_N = \sum_{i=1} iN_{A_i} / \sum_{i=1} N_{A_i} \quad (9)$$

From eq 8, it is evident that in order to consider the dependence of ϕ on the solute concentration, and consequently to locate the cmc, one needs to know the detailed behavior of the function $\langle i \rangle_N$. To construct $\langle i \rangle_N$ according to eq 9, one must have the equilibrium size distribution of the micelles. We propose to specify this distribution $\{N_{A_i}\}$ uniquely by a variational principle: the most probable distribution of the micelles is one which corresponds to the lowest Helmholtz free energy of the solution. Formally, this means the minimization of A with respect to N_{A_i} subject to the "normalization" constraint $N_A = \sum_{i=1} iN_{A_i}$. We may also summarize this by the statement

$$\partial/\partial N_{A_i} [-A/kT - \alpha \sum_{i=1} iN_{A_i}]|_{T, N_B} = 0 \quad (10)$$

where k is the Boltzmann constant, T the absolute temperature, and α the Lagrange multiplier which is to be determined by the normalization. Before proceeding further, we find it convenient to write f_{A_i} in the form (see section III)

$$f_{A_i} = f_{A_1}{}^i \exp[-(i-1)\Delta E/kT] \quad (11)$$

which merely asserts that the free energy of A_i is the

(17) P. J. Flory, *J. Chem. Phys.*, **12**, 425 (1944); combinatorial factors for self-winding and branched chains, which approximate quite well the conventional conception of roughly spherical micelles, have been derived by Huggins and by Guggenheim (M. L. Huggins, *J. Phys. Chem.*, **46**, 151 (1942); E. A. Guggenheim, *Proc. Roy. Soc.*, **A133**, 213 (1944)).

(18) R. L. Scott, *J. Phys. Chem.*, **69**, 261 (1965).

(19) R. Lacmann, *Z. Phys. Chem.* (Frankfurt am Main), **23**, 313 (1960); R. Lacmann, *ibid.*, **23**, 324 (1960).

sum of the free energies of all the individual components and of their interactions. The function ΔE is the energy change accompanying the aggregation process, *i.e.*, the energy of micellization (or of association); it is assumed to be independent of i. The extremalization of A can now be performed with the result that

$$N_{A_i} = K_1 y^i \tag{12}$$

where

$$K_1 = [M/(z - 1)] \exp[\Delta E/kT] \tag{13}$$

and

$$K_2 = x_B + (N/M) + \ln (z - 1) - 1 - \alpha - \Delta E/kT + \ln f_{A_1} \tag{14}$$

where $y = \exp[K_2]$. With the aid of these equations, one may readily show that

$$N_A = K_1 \sum_{i=1} i y^i = K_1 y/(1 - y)^2 \tag{15}$$

$$N = K_1 \sum_{i=1} y^i = K_1 y/(1 - y) \tag{16}$$

so that

$$\langle i \rangle_N = [1 \pm (1 + 4x_A M/K_1)^{1/2}]/2 \tag{17}$$

From the physical requirement that $\langle i \rangle_N$ should approach the asymptotic value of unity as the solute concentration becomes vanishingly small, the sign of the square root must always be chosen to be positive. Similarly, the weight average degree of aggregation of A, $\langle i \rangle_W$, assumes the form

$$\langle i \rangle_W = \sum_{i=1} i W_{A_i} / \sum_{i=1} W_{A_i} = \sum_{i=1} i^2 N_{A_i} / \sum_{i=1} i N_{A_i} = 2\langle i \rangle_N - 1 \tag{18}$$

where W_{A_i} is the weight of species A_i. The foregoing analysis then permits us to study the concentration dependence of both the degree of aggregation and the osmotic coefficient. In addition, the osmotic pressure, which often is of interest, may be obtained from the well known thermodynamic formula relating it to the chemical potential of the solvent.

Next, we consider the cmc. Perhaps it should first be noted that there is no universally accepted definition. Operationally, it has usually been associated with the concentration at which some property of the system undergoes a drastic change. Mathematically, it has been defined by Phillips[20] as the concentration at which the *third* derivative of an *ideal* colligative property, say P°, equals zero

$$\partial^3 P^\circ/\partial C^3 \,|_{C = \text{cmc}} = 0$$

where C is the concentration. It is difficult to interpret this in an unambiguous fashion in terms of the experiments one conducts with micellar solutions. Aside from the question of expressing the property of the solution in an idealized form, the reasons for the vanishing of the third derivative are not entirely clear. It appears to mean the inflection point in the $(\partial P^\circ/\partial C) - C$ plane; yet $(\partial P^\circ/\partial C)$ is not one of the experimentally observed quantities.[21] In view of the formulation we have just outlined, it seems natural, both experimentally and theoretically, to define the cmc as the inflection point in the property *vs.* the concentration curve; this would be appropriate regardless of the sharpness of the cmc. Thus, if we take the solution property of interest to be ϕ, then we may have either

$$\partial^2\phi/\partial x_A^2|_{x_A = \text{cmc}} = 0 \tag{19a}$$

or

$$\partial^2\phi/\partial(\ln x_A)^2|_{x_A = \text{cmc}} = 0 \tag{19b}$$

For the reason that the cmc normally occurs at exceedingly low concentrations, it is more convenient to adopt the latter definition. Thus, the combination of eq 8, 17, and 19b yields

$$\partial^2\phi/\partial(\ln x_A)^2\,|_{x_A = \text{cmc}} = -[(1 - \phi^\circ)/(1 - x_A)] - x_A[\langle i \rangle_N^{-1} - 1 + (1 - 3x_A)\langle i \rangle_N^{-2}(\partial\langle i \rangle_N/\partial x_A) + x_A(1 - x_A)\langle i \rangle_N^{-2}\{(\partial^2\langle i \rangle_N/\partial x_A^2) - 2\langle i \rangle_N^{-1}(\partial\langle i \rangle_N/\partial x_A)^2\}]\,|_{x_A = \text{cmc}} = 0 \tag{20}$$

$$\phi^\circ = \lim_{\langle i \rangle_N \to 1} \phi; \quad \lim_{x_A \to 0} [\partial\phi/\partial x_A] = 0 \tag{21}$$

$$\partial\langle i \rangle_N/\partial x_A = [K_1(2\langle i \rangle_N - 1)/M]^{-1} \tag{22}$$

$$\partial^2\langle i \rangle_N/\partial x_A^2 = -2(K_1/M)^{-2}(2\langle i \rangle_N - 1)^{-3} \tag{23}$$

B. Solvating System. Within the context of the preceding section, we shall discuss next a binary solution in which the interactions are such that the solute (A) and the solvent (B) molecules may associate to form solvates. From the outset, we wish to state that the purpose here is merely one of demonstrating how solvation can be taken into consideration from the present standpoint. Solvation phenomena, of course, have been the subject of study of many physical chemists for a long time. Our own interest in them was stimulated by the experimental work of Robinson and Stokes (RS)[22] and by the recent theoretical studies of Kozak, Knight, and Kauzmann.[23] In their derivation of the RS equation, which has been employed to account for the properties of aqueous solutions, Kauzmann, *et al.*, enumerated the total number of configurations accessible to the solution in a manner completely analogous to

(20) A definition of the cmc along lines similar to Phillips has been discussed also by Hall and Pethica (see ref 9).

(21) It has been stated that Phillips' definition corresponds to the point of maximum curvature. For a function $f(x)$, the curvature is given by $[f''(x)/(1 + f'(x)^2)^{3/2}]$. Thus, this interpretation appears to be incorrect since $f'(x)$ is not negligibly small.

(22) R. A. Robinson and R. H. Stokes, *J. Phys. Chem.*, **65**, 1954 (1961).

(23) J. J. Kozak, W. S. Knight, and W. Kauzmann, *J. Chem. Phys.*, **48**, 675 (1968).

that of Flory. Thus, for the system in which both A and B molecules are monomeric, and in which each A molecule can solvate or "tie down" H of the B molecules, their combinatorial analysis leads to the following expression for the activity of B

$$a_B = [1 - (1 + H)x_A] \exp(Hx_A) \quad (24)$$

which in the limit of small x_A reduces to the RS equation

$$a_B = [1 - (1 + H)x_A]/(1 - Hx_A) \quad (25)$$

From the physical picture of the complexes we have advanced, it is evident that the solution just described can be viewed also as an "effective" binary system composed of monomeric B and a solute whose molecules are made up of $(1 + H)$ segments—one A and H solvated B molecules. Thus, the Flory formalism for the r-mer–monomer system can be adopted in its totality and a_{B_1} then becomes (see eq 7)

$$\ln a_{B_1} = \ln \varphi_{B_1} + [1 - (1 + H)^{-1}]\varphi_{A_1B_H} \quad (26)$$

where φ_k is the volume fraction of species k, *i.e.*

$$\varphi_{B_1} = N_{B_1}/M; \quad \varphi_{A_1B_H} = (1 + H)N_{A_1B_H}/M \quad (27)$$

In contrast to the model used in section IIA, we should note that here we have only complexes of one size, namely, those consisted of $(1 + H)$ segments. Consequently, in this simpler system, the problem of obtaining the distribution through the variational principle does not arise. From the "conservation" of the number of molecules of each species in the solution, we have

$$M = N_A + N_B; \quad N_A = N_{A_1B_H}; \quad N_B = N_{B_1} + HN_{A_1B_H} \quad (28)$$

By combining eq 26–28 *and* noting the relations for associated equilibrium, one obtains the Kauzmann equation (24) immediately.

The advantages of the above interpretation becomes more evident when one considers the case in which each solute molecule may associate with a variable number of solvent molecules. If the solution is composed of B_1 and the solvate "subspecies" A_1B_1, A_1B_2, $\cdots$, A_1B_n, we find, after considerable manipulations, that a_B has exactly the same form as eq 24 except that H is now replaced by

$$\langle H \rangle = \sum_{H=1}^{n} HN_{A_1B_H} / \sum_{H=1}^{n} N_{A_1B_H} \quad (29)$$

where $\langle H \rangle$ is the average number of solvent molecules per complex. This result, which is analogous to that for a polydisperse polymer solution, is clearly more realistic and encompassing than the previous one, for here we are concerned with a distribution rather than a single type of solvates.

To conclude this section, we mention briefly the extension of the present method to multicomponent monomeric solute–monomeric solvent systems. If we have a solution composed of solute species 1, 2, 3, $\cdots$, n, each of whose molecules can associate with H_1, H_2, H_3, $\cdots$, H_n solvent molecules, respectively, the equation describing the solvent activity is found to be

$$a_B = [1 - \sum_{i=1}^{n} (1 + H_i)x_i] \exp[\sum_{i=1}^{n} H_i x_i] \quad (30)$$

which at low concentrations and for ternary systems reduces to the empirical formula used by Robinson and Stokes for representing the behavior of sucrose–mannitol–water solutions (see eq 19 of ref 22).

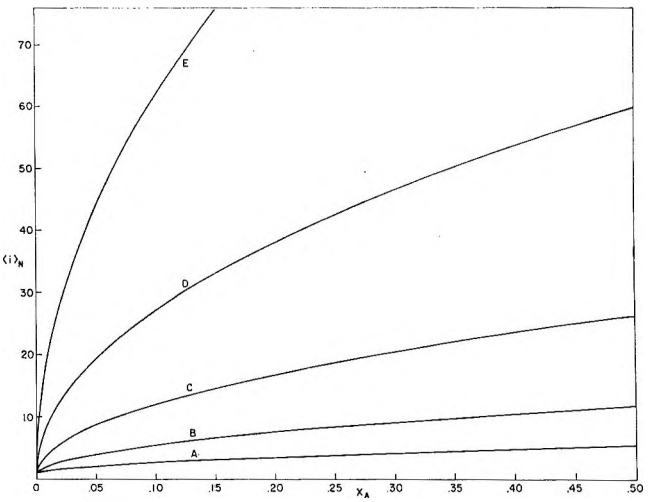

Figure 1. The dependence of the number average degree of aggregation on the mole fraction of the solute. The letters A, B, C, D, and E denote, respectively, the results for $\Delta E = -1$, -2, -3, -4, and -5 kcal/mol at 300°K (or for $\Delta E/T = -1.67$, -3.33, -5.00, -6.67, and -8.33 at temperature T). $z = 10$; the value of z has little effect upon the calculated properties. For example, if z is increased from 10 to 14, the resulting change in the cmc is such that it corresponds to an increase of only about 150 cal/mol in ΔE (see Figure 3), *i.e.*, cmc ($z = 10$, ΔE) $\cong$ cmc ($z = 14$, $\Delta E = \Delta E + 150$ cal/mol).

III. Discussion and Conclusions

All the calculations were performed on an IBM 7040 digital computer using "double precision" arithmetic. In Figure 1, the dependence of $\langle i \rangle_N$ upon x_A at various association energies is presented. As expected, at a fixed concentration, systems with higher ΔE's contain correspondingly larger aggregates. From our computations, we see the model predicts the existence of a wide range of micelles the distribution of which depends on the energy, concentration, and temperature. This is at variance with the prevailing notion that the solution is composed of monomers and micelles of one type only (*i.e.*, without any intermediates). The basis of this belief seems to have rested heavily on the interpretations for the comparative sharpness of the cmc. Thus, in analogy to the theories of irreversible condensation, the cmc is construed as the concentration at which large micelles ("embryos") are beginning to form,

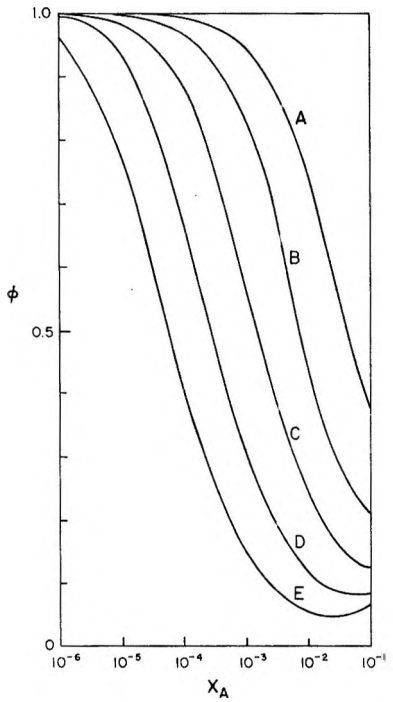

Figure 2. The variation of the osmotic coefficient at low solute concentrations. The letters A, B, C, $\cdots$ and so on have the same meaning as in Figure 1.

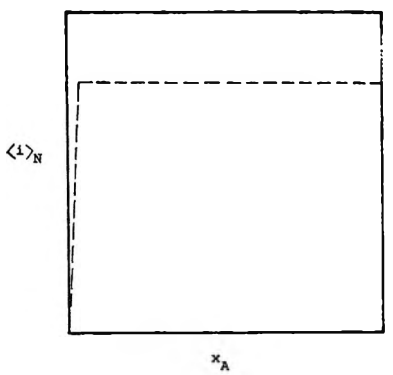

Figure 3. Concentration dependence of the average aggregation number.

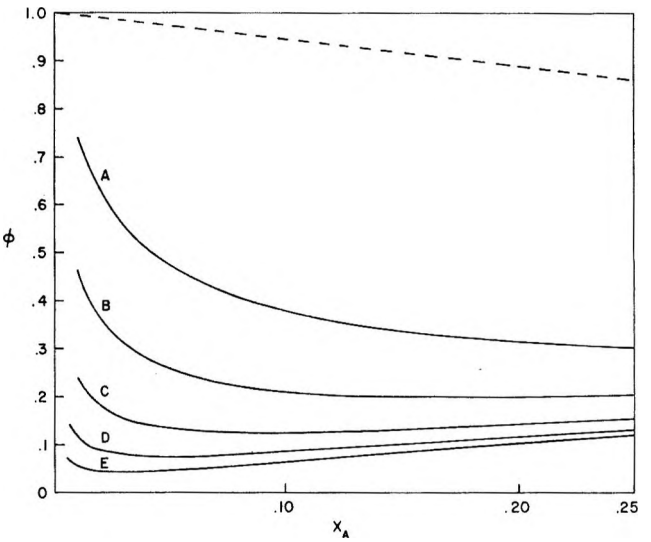

Figure 4. The variation of the osmotic coefficient at the higher solute concentrations. All symbols are identical in meaning with those of Figure 2. The dotted curve describes ϕ for non-associating systems (note the absence of the "second anomaly").

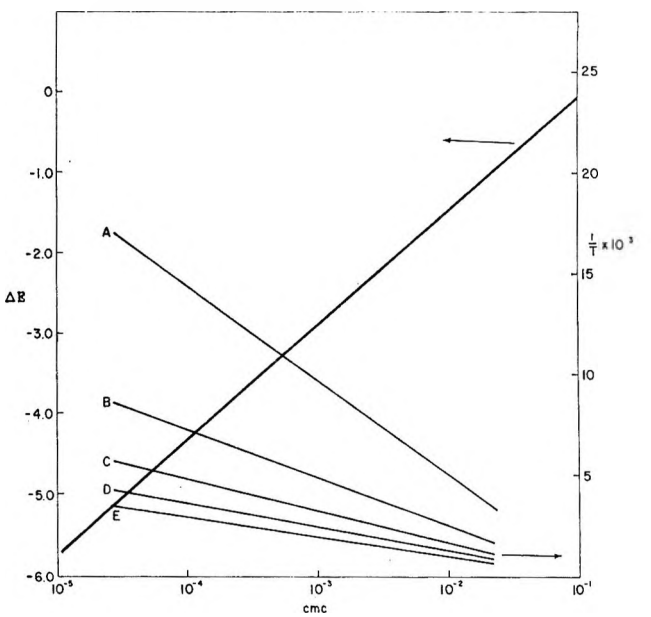

Figure 5. The dependence of the cmc on ΔE at 300°K (heavy line) and on $(1/T)$; $z = 10$.

but somehow with the restriction that they ultimately grow to one particular size only. From Figure 2, where we have plotted the decrease of the osmotic coefficient at the lower concentrations, we find the above interpretation may be misleading in that quite sharp cmc's (note that we have used an expanded abscissa—log x_A rather than the usual x_A or $x_A^{1/2}$ (or C and $C^{1/2}$)—to show the details of this region) are obtained without implying any parallel drastic changes in $\langle i \rangle_N$. Furthermore, it should be recognized that the cmc's are not invariably clear-cut and that many systems do exhibit a spectrum of micelles; this is especially true of nonionics in nonaqueous solvents. Although, strictly speaking, our conclusions are valid only for the present noninteracting model, we believe its basic tenor would not be materially affected by the inclusion of intermicellar interactions. For solutions which display the kind of distribution in Figure 3, that is, for systems in which the concentrations of all micelles of intermediate size are small, we suspect that the solvent must have played a role more prominent than that implicit in the model.

The distribution may also be somewhat influenced by what may be referred to as "orientational degeneracies" of the monomer segments. If a monomer can be in any one of the Ω conformations of the same energy (*e.g.*, Ω may be taken as the z rotational states of the monomer), then instead of eq 11, the partition function is now

Table I: Comparison of Theory and Experiment

	Dodecylammonium benzoate in cyclohexane at 30°					Zn O,O-di-*n*-octylphosphorodithioate in benzene at 38°					Ba O,O-di-*n*-dodecylphosphorodithioate in benzene at 38°				
x_A[a]	2.38–3	2.92–3	3.90–3	4.65–3	5.85–3	1.15–3	2.30–3	3.45–3	4.60–3	5.75–3	2.0–4	4.0–4	8.3–4	1.7–3	2.5–3
$\langle i\rangle_N^{obsd}$	2.9	3.8	4.2	4.4	5.3	1.07	1.15	1.23	1.26	1.29	1.56	2.75	4.45	6.67	7.80
$\langle i\rangle_N^{calcd}$	3.3	3.8	4.2	4.4	5.1	1.08	1.14	1.20	1.25	1.31	2.5	3.2	4.4	6.0	7.1
ΔE_{obsd}, kcal/mol		−1.9 to −5.9						...					...		
ΔE_{calcd}, kcal/mol		−3.55						−1.18					−4.5		
$c_{mc_{obsd}}$		5.50 to 15.0 mmol/l.						11 g/dl					~1 g/l.		
$c_{mc_{calcd}}$		3.3 mmol/l.						14.8 g/dl					0.97 g/l.		

[a] The last digit in x_A denotes the powers of ten; thus, 2.38–3 means 2.38×10^{-3}.

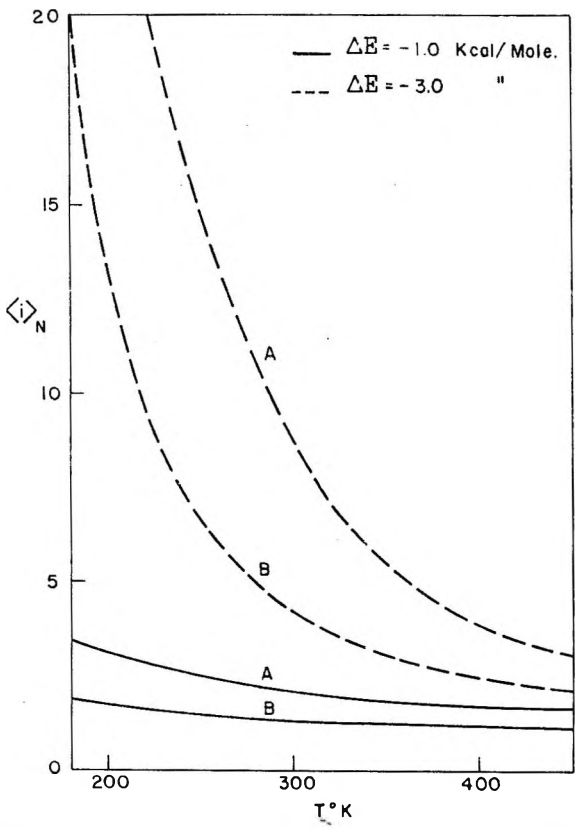

Figure 6. The dependence of $\langle i\rangle_N$ on the temperature at two energies. The curves A and B denote, respectively, the concentrations $x_A = 0.05$ and $x_A = 0.01$; $z = 10$.

expressed by $f_{A_i} = \Omega_i q_{A_1}{}^i \exp[-(i-1)\Delta E/kT]$ where $\Omega_i = \Omega$ if $i = 1$ and $= 1$ otherwise. Subsequent numerical analysis indicated that this leads to results not significantly different from those presented. Thus, the curve for $\langle i\rangle_N$ *vs.* x_A for a solution with energy ΔE now corresponds closely to that of an earlier solution with ΔE equal to $(0.85\text{–}0.95)\Delta E$.

Figure 4 illustrates the variation of ϕ at the higher solute concentrations. Of special interest are the differences in the behavior of ϕ between the associating and nonassociating systems and the appearance of the "second anomaly" for the micellar solutions. We have established mathematically that the nonassociating solutions do not possess a cmc as we have defined it. From this graph, it should be clear that the "second anomaly" is in actuality one of the intrinsic features of aggregating systems.

In Figure 5, the curves for the cmc *vs.* ΔE and cmc *vs.* $(1/T)$ are provided. The concentration at which rapid changes in ϕ are observed (cmc) varies directly with temperature and inversely with the energy of micellization. This is indeed in accord with experimental results on many surfactant solutions.

Figure 6 describes the temperature dependence of the aggregation number at different concentrations and energies. The size of the micelles decreases with increasing temperature, a fact which is again observed.

Next, we compare our calculations with experiment. The utility of the formulas derived in section IIB has already been amply demonstrated[22] so we shall be focusing our attention exclusively on the results of section IIA. Since the theory is based on the assumption that the solvent molecules remain monomeric, aqueous solutions are not suitable for our purpose. This is unfortunate because the amount of data on nonaqueous micellar systems is limited. In order to test the model, we have chosen the data of Kitahara on dodecylammonium benzoate in cyclohexane[24] and our more recent work on Zn and Ba dialky phosphorodithioates in benzene.[25] We found that by properly selecting the energies of micellization, we were able to reproduce faithfully the experimental aggregation numbers. From these energies and from Figure 5, the values of the cmc's were obtained. The results are summarized in Table I. We see that our calculated ΔE is in accord with Kitahara's value obtained from the temperature dependence of the cmc. In view of the approximate nature of the model, the manner of defining the cmc, and the differences in the size of the solute and solvent molecules in these solutions, the agreement between the calculated and observed properties can be considered to be reasonably good. For the theory to be more generally applicable, intermicellar interactions, solvation, and other effects must be simultaneously incorporated. The study of these extensions is now in progress.

(24) A. Kitahara, *Bull. Chem. Soc. Jap.*, 31, 288 (1958).

(25) I. J. Heilweil, 150th National Meeting of the American Chemical Society, Division of Petroleum Chemistry, Preprint, No. 10, Atlantic City, N. J., 1965, p D19. The cmc's were obtained by ir, solubilization, and interfacial tension measurements.

Adsorption from Solution. III. A New Model for the Kinetics of Adsorption–Desorption Processes[1]

by F. T. Lindstrom, R. Haque, and W. R. Coshow

Department of Agricultural Chemistry, Oregon State University, Corvallis, Oregon 97331
(Received October 7, 1969)

A detailed study of the kinetics of adsorption from solution has been made. A rate expression for the adsorption process which takes into account both the forward and backward reaction and the sticking probability of the adsorbate on the surface has been derived. The theory has been tested for the adsorption of three biologically active organic compounds, 2,4-D, isocil, and bromacil, from aqueous solution onto illite clay and silica gel surfaces. The rate constants and other kinetic parameters for the adsorption and desorption process have been calculated. One of the main advantages of the approach used in the paper is that it enables the simultaneous determination of the rate constants for adsorption and desorption from the adsorption data. The theory has been extended to predict the desorption of adsorbates as well. The theory can be applied to many other adsorption processes.

Introduction

The kinetics of adsorption is one of the fundamental studies necessary for better understanding of the mechanism of adsorption. This is especially true for the adsorption of chemicals from solution. Various workers have used different approaches to elucidate the rate mechanism involved in the adsorption from solution. Swearingen and Dickinson[2] introduced the term "distance from equilibrium" for the adsorption of acids from aqueous solution on silica gel and charcoal. They found that the rate constant is proportional to this term. The equation developed by Roginsky and Zeldovich,[3] commonly known as the Elovich equation,[4,5] has been used widely to study the chemisorption rates. However, unrealistic boundary conditions were observed and the equation was modified by Micale and Zettlemoyer[6] and McLintock.[7] Other rate equations for the chemisorption process have been developed by Kingman[8] and Barrer.[9] The Langmuir model is often used to explain the adsorption of polymers from solution,[10] while the idea of free energy change with the surface coverage was incorporated by Eley.[11]

However, most of the above approaches are not applicable to adsorption from solution. They do not take into account the backward reaction, *i.e.*, the desorption rate. Fava and Eyring[12] have derived an equation which takes into account the backward reaction as well, for the adsorption of dodecyl benzenesulfonate on cotton. Their equation can be represented as

$$\frac{d\phi}{dt} = 2k_1(1 - \phi) \sinh b(1 - \phi) \qquad (1)$$

where ϕ is the fraction sorbed (amount sorbed at time t divided by the total amount sorbed), k_1 is the rate constant for adsorption, and b is a constant which yields a measure of the surface stressing energy due to loading with molecules. This equation fits many adsorption data satisfactorily. However, there are two drawbacks to this equation. First, while deriving this equation it was assumed that the product of the free concentration of the adsorbate and the forward rate constant is equal to the product of the sorbed concentration with the backward rate constant. Although this is true for equilibrium, it may not be true at any other time of the reaction. Secondly, in deriving this equation it has been assumed that the sticking probability[13] for the adsorbate on the surface is unity for all values of ϕ, $0 \leq \phi \leq 1$, which may not be true. In the present study we have tried to derive an equation which takes into account both the sticking probability factor as a function of coverage ϕ and the simultaneous backward reaction rate. The derivation is based on a general

(1) (a) Research Supported by U. S. Public Health Service Grant No. ES00040-04. (b) Issued as Technical Paper No. 2557 from Oregon Agricultural Experiment Station. (c) Presented in part at 23rd American Chemical Society Northwest Regional Meeting held at Portland, Ore. June 1968. (d) For Part II see R. Haque and R. Sexton, *J. Colloid Interfac. Sci.*, **25**, 818 (1968).

(2) L. E. Swearingen and B. N. Dickinson, *J. Phys. Chem.*, **36**, 534 (1932).

(3) S. Z. Roginsky and J. Zeldovich, *Acta Physiochem. (USSR)*, **1**, 554 (1934).

(4) M. J. D. Low, *Chem. Rev.*, **60**, 267 (1960).

(5) G. A. Taylor and N. Thon, *J. Amer. Chem. Soc.*, **74**, 4169 (1952).

(6) F. J. Micale and A. C. Zettlemoyer, *J. Colloid Interfac. Sci.*, **24**, 464 (1967).

(7) I. S. McLintock, *Nature*, **216**, 1204 (1967).

(8) F. E. T. Kingman, *Trans. Faraday Soc.*, **28**, 269 (1932).

(9) R. M. T. Barrer, *J. Chem. Soc.*, 1261 (1936).

(10) C. Peterson and T. K. Kwei, *J. Phys. Chem.*, **65**, 1330 (1961).

(11) D. D. Eley, *Trans. Faraday Soc.*, **49**, 643 (1953).

(12) A. Fava and H. Eyring, *J. Phys. Chem.*, **60**, 890 (1956).

(13) (a) I. Langmuir, *J. Amer. Chem. Soc.*, **40**, 1361 (1918). (b) D. O. Hayward and B. M. W. Trapnell, "Chemisorption," Butterworth and Co., Ltd., London, 1964, p 91.

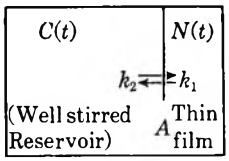

Figure 1. Schematic diagram of the adsorption microenvironment.

Langmuir approach. It has been applied to the adsorption of some sparingly soluble, biologically active organic compounds on illite clay and silica gel. One of the main advantages of the present approach is that it gives kinetic parameters for both adsorption and desorption simultaneously by using the data obtained from the adsorption experiment. It could be applied to many other adsorption–desorption processes occurring in solution.

Theory

Let the surface and the adsorbate be represented by S and A, respectively. The equilibrium in such a system could be written as

$$A(H_2O)_x + S(H_2O)_y \underset{k_2'}{\overset{k_1'}{\rightleftharpoons}} A(H_2O)_z{}^s \qquad (2)$$

where x, y, and z are the hydration numbers. In the adsorbed state, the adsorbate could come either into direct contact with the surface ($a = 0$), or it is separated by a thin layer of water between the adsorbate and the surface ($z > 0$). The quantities k_1' and k_2' are the rate constants for the forward and the backward adsorption process.

Consider the physical system sketched above in Figure 1. It is assumed that at time $t = 0$ we have an adsorbate concentration C_0 existing in the bulk of the solution and no adsorbate in the thin film, *i.e.*, no chemical sorbed. It is also assumed that for the complete reaction or mass transfer process from the free phase $C(t)$, to the sorbed phase $N(t)$, no mass is lost. Hence, we have a mass conserving system. This leads to the mass balance equation

$$M_0 = C(t)V + \chi AN(t) \qquad (3)$$

where M_0 = initial mass in system (in g), C = free adsorbate concentration (g/cm³), V = volume of adsorbate (cm³), χ = ratio of active sorbing surface area to total surface area of sorber (dimensionless). A = total surface area of sorber (cm²), $N(t)$ = surface concentration (g/cm²), and $C(t)$ = free adsorbate concentration (g/cm³). If we use the Langmuir approach,[13] the velocities of the adsorption μ and desorption μ' can be written, respectively, as

$$\mu = \frac{\phi C}{\sqrt{2\,mRT}} f(\phi) e^{\frac{-\Delta G^{\pm}}{RT}} \qquad (4)$$

and

$$\mu = Kf'(\phi) e^{\frac{-\Delta G^{\pm\prime}}{RT}} \qquad (5)$$

where σ = condensation coefficient, m = molecular mass, $f'(\phi)$ = sticking probability, C = concentration of adsorbate, $f'(\phi)$ = desorption probability, K = proportionality coefficient, $\Delta G^{\pm}$ = free energy of activation for adsorption, $\Delta G^{\pm}$ = free energy of activation for desorption, and R = gas constant.

Let

$$f(\phi) = (1 - \phi/2) \qquad (6)$$

$$f'(\phi) = \phi/2 \qquad (7)$$

represent the adsorption and desorption sticking probabilities, respectively. We choose f and f' this way because we feel these to be the easiest and simplest probability functions to begin with. Also, at $\phi = 0$ we want $f = 1$ and $f' = 0$, and at $\phi = 1$ we want both the adsorption and desorption sticking probabilities to be equal. The forward rate coefficient, k_1, and the backward coefficient, k_2, can be written as

$$k_1 = \frac{\sigma}{\sqrt{2\,mRT}} \qquad (8)$$

and

$$k_2 = \frac{k_0}{\sqrt{T}} \qquad (9)$$

where k_0 is a constant. The net gain of the sorbed concentration can be written as

$$\frac{dN(t)}{dt} = \frac{Vk_1}{\chi A} C(t)\left(1 - \frac{\phi}{2}\right) e^{-\Delta G^{\pm}/RT} - k_2 N(t) \frac{\phi}{2} e^{-\Delta G^{\pm\prime}/RT} \qquad (10)$$

Let the free energies $\Delta G^{\pm}$ and $\Delta G^{\pm\prime}$ for adsorption and desorption, respectively, vary[11] with increasing surface coverage ϕ according to the expressions

$$\Delta G^{\pm} = \Delta G_0{}^{\pm} + \alpha\phi \qquad (11)$$

$$\Delta G^{\pm\prime} = \Delta G_0{}^{\pm\prime} + (1 - \phi)\alpha \qquad (12)$$

where α is an energy stress constant for the sorbing surface. $\Delta G_0{}^{\pm}$ and $\Delta G_0{}^{\pm\prime}$ are some initial free energies of activation required for adsorption and desorption. Define them in such a way that $\Delta G_0{}^{\pm\prime} > \Delta G_0{}^{\pm}$. According to eq 11 and 12 at three limiting conditions of ϕ, the values of $\Delta G^{\pm}$ and $\Delta G^{\pm\prime}$ are

$$\phi = 0; \quad \Delta G^{\pm} = \Delta G_0{}^{\pm}; \; \Delta G^{\pm} = \Delta G_0{}^{\pm\prime} + \alpha$$

$$\phi = 0.5; \quad \Delta G^{\pm} = \Delta G_0{}^{\pm} + \frac{\alpha}{2}; \; \Delta G^{\pm\prime} = \Delta G_0{}^{\pm\prime} + \frac{\alpha}{2}$$

$$\phi = 1; \quad \Delta G^{\pm} = \Delta G_0{}^{\pm} + \alpha; \; \Delta G^{\pm\prime} = \Delta G_0{}^{\pm}$$

Under these conditions, $\Delta G^{\pm\prime}$ is always greater than $\Delta G^{\pm}$ at $\phi = 0$ and $\phi = 0.5$. At the extreme case when

$\phi = 1$, $\Delta G^{\ddagger\prime}$ is greater than or at least equal to $\Delta G^{\ddagger}$ if $\Delta G_0^{\ddagger\prime} \geq \Delta G_0^{\ddagger} + 2\alpha$. Substituting (11) and (12) into (10) we obtain

$$\frac{dN}{dt} = \frac{V}{\chi A} k_1'C(t)\left(1 - \frac{\phi}{2}\right)e^{-\alpha\phi/RT} - k_2'N(t)\frac{\phi}{2}e^{\alpha\phi/RT} \tag{13}$$

where

$$k_1' = k_1 e^{-\Delta G_0^{\ddagger}/RT}$$

and (14)

$$k_2' = k_2 e^{-\Delta G_0^{\ddagger}/RT}$$

Upon multiplying through both sides of (13) by $1/N(\infty)$, by solving for $C(t)$ in (3), and with subsequent substitution of this result into (13) we find

$$\frac{d\phi}{dt} = k_1'(\beta - \phi)\left(1 - \frac{\phi}{2}\right)e^{-b\phi} - k_2'\frac{\phi^2}{2}e^{b\phi} \tag{15}$$

where

$$\beta = \frac{VC_0}{XAN(\infty)}; \quad b = \frac{\alpha}{RT} \tag{16}$$

Require that $d\phi/dt \to 0$ as $t \to \infty$, *i.e.*, equilibrium is attained and that $\phi \to 1$ as $t \to \infty$. Thus, we have

$$\beta = 1 + \frac{k_2'}{k_1'}e^{2b} \tag{17}$$

Substituting (17) into (16) gives

$$\frac{d\phi}{dt} = k_1'\left(1 + \frac{k_2'}{k_1'}e^{2b} - \phi\right) \times \left(1 - \frac{\phi}{2}\right)e^{-b\phi} - k_2'\frac{\phi^2}{2}e^{b\phi} \tag{18}$$

or

$$\frac{d\phi}{dt} = k_1'\left\{(1 - \phi)\left(1 - \frac{\phi}{2}\right)e^{-b\phi}\right\} + k_2'\left\{\left(1 - \frac{\phi}{2}\right)e^{b(2-\phi)} - \frac{\phi^2}{2}e^{b\phi}\right\} \tag{19}$$

Equation 19 is the final expression for the rate of adsorption process. Once good estimates of the values of k_1', k_2', and b at constant temperature are determined using the experimental ϕ's and a curve-fitting technique described in the Appendix, $\phi(t)$ can be obtained from (19) by using a numerical integration scheme such as the Runge–Kutta technique.

Experimental Section

Material. The adsorbates used were 2,4-dichlorophenoxy acetic acid (2,4-D), 3-*sec*-butyl-5-bromo-6-methyl uracil (bromacil), and 3-isopropyl-5-bromo-6-methyl uracil (isocil). The chemical formulas of these compounds are

2,4-D

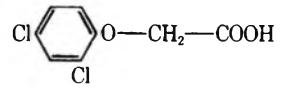

Isocil

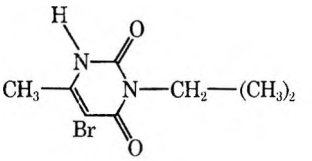

Bromocil

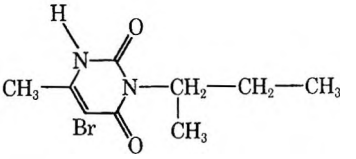

The samples of isocil and bromocil used were of analytical grade, while the 2,4-D used was ^{14}C radioactive and purchased from Aluphram Chemicals, New Orleans, La. Solutions of these three chemicals were prepared by dissolving a known quantity in a pH 6 buffer (phosphate) solution. The adsorbents used were silica gel and illite; their properties are given in Table I.

Table I: Characteristic Properties of the Surface under Consideration

Surface	Source	Particle size, mm	Amount of buffer solution required for saturation of 1 g of surface, ml
Illite	No. 35 Fithian, Illinois	0.83	0.5
Silica gel	Grace Division Chemical, Baltimore, Maryland	0.59–0.07	1.0

Procedure. Before starting the kinetics experiments, the surfaces were saturated with phosphate buffer solutions of pH 7 as indicated in Table I. This saturation was necessary in order to take into account the change in concentration of the adsorbate due to the sorption of solvent. After this saturation process, the sorbing material was put into an erlenmeyer flask and a known volume of adsorbate solution of certain concentration was added. The mixture was stirred vigorously throughout the experiment so as to minimize any diffusion gradients which for this experiment would be undesirable in the free solution. Any error which may arise due to intraparticle diffusional effects will be very small (see Appendix B). An aliquot of the mixture was taken out at different time intervals and analyzed for the concentration of adsorbate. The total volume of the aliquot taken at different time intervals was negligible when compared to the entire volume of the adsorbate solution. Preliminary adsorption studies

at different time intervals indicated that 24 hr was sufficient to attain equilibrium. Hence, the equilibrium value for the adsorption was taken after 24 hr of continuous stirring. The sorbed concentration $N(t)$ was calculated according to the equation

$$N(t) = (C_0 - C(t))\frac{V}{\chi A} - \frac{V_b}{\chi A} C(t) \qquad (20)$$

where V_b is the volume of the buffer solution required for the saturation of surface material, C_0 is the initial free chemical concentration, and the other terms have been previously defined. Define the fraction of the adsorbate sorbed ϕ as

$$\phi = \frac{N(t)}{N(\infty)} = \frac{(C_0 - C(t))\frac{V}{\chi A} - \frac{V_b}{\chi A}C(t)}{(C_0 - C(\infty))\frac{V}{\chi A} - \frac{V_b}{\chi A}C(\infty)} \qquad (21)$$

where $N(\infty)$ is the equilibrium concentration on the surface. Defining $C_0' = C_0(V/V^b + V)$ and substitution of this expression into the above equation obtains

$$\phi(t) = \frac{C_0' - C(t)}{C_0' - C(\infty)} \qquad (22)$$

The experiments were carried out at 0 and 25°.

The analysis of isocil and bromacil was carried out using a uv spectrophotometric method, while the 2,4-D concentration was estimated by a ^{14}C radioactive counting technique. The optical density measurements were performed at 296-mμ wavelengths. Before analyzing the samples it was determined that these compounds do obey the Beer–Lambert law. The measurements were made on a Cary Model 11 adsorption spectrophotometer, and they were accurate up to ±5%. For estimation of 2,4-D, 0.1 ml of solution was put into a scintillation vial and 10 ml of scintillation media (consisting of 2:1 toluene and methyl cellulose mixture) was added. The radioactivity was measured on a Packard TRICARB liquid scintillation spectrophotometer. By comparing the counts per minute with that for the solution of a known concentration, the concentration of the unknown was determined. The accuracy of the measurements was ±10%. In view of the difficulties involved in the adsorption experiments, an error of ±5–10% is acceptable.

Results and Discussion

In most of the adsorbent–adsorbate systems considered, the time required for greater than 50% completion of the adsorption was less than 1 hr. A typical experimental result is shown in Figure 2, where ϕ has been plotted as a function of time t and the 10% estimated uncertainty in each point has been included.

We now show the results of the modified[2] technique (Appendix) in the case of bromacil–illite adsorption–desorption at 26°. The results can be seen in Table II.

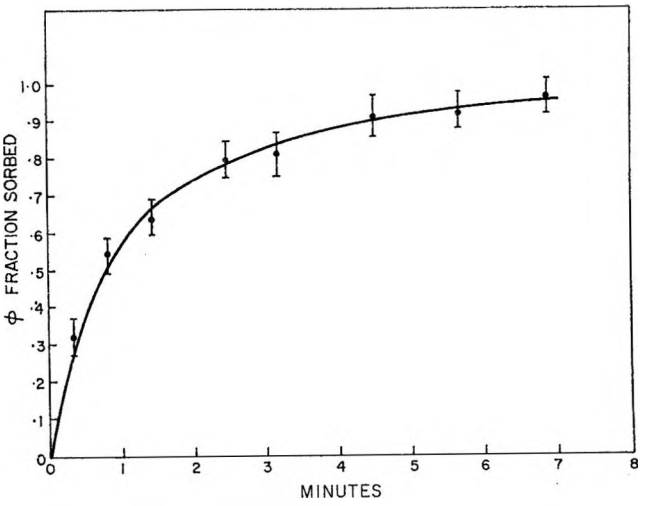

Figure 2. Graph showing the change in ϕ as a function of time for the adsorption of Bromacil (300 ppm) on illite surface at 25° ("eye ball curve")[a]

Table II: Comparison of Observed and Calculated ϕ Values for the Absorption of Bromacil on Illite at 25°[a]

Time, min	ϕ obtained from smooth curve through exptl points	ϕ calcd, Runge–Kutta method	$\phi_{obsd} - \phi_{calcd}$
0	0	0	0
0.25	0.215	0.214	0.001
0.50	0.375	0.379	−0.004
0.75	0.490	0.484	0.006
1.00	0.573	0.560	0.013
1.25	0.630	0.618	0.012
1.50	0.673	0.664	0.009
1.75	0.707	0.703	0.004
2.00	0.738	0.734	0.004
2.25	0.762	0.762	0
2.50	0.788	0.785	0.003
2.75	0.805	0.806	−0.001
3.00	0.825	0.824	0.001

[a] $b = 1.4$; $k_1' = 2.5 \times 10^{-2}\,sec^{-1}$; $k_2' = 2.0 \times 10^{-4}\,sec^{-1}$.

For this particular experiment, the choice of b at $b = 1.4$ arises from the criterion the $E_c = \min_{b>0} E$ was obtained at this particular b value. The numerical integration scheme has an inherent truncation error in it, but this error is $\sim 10^{-4}$ for this particular choice at Δt. All the computations were carried out on the CDC 3300 computer at the Oregon State University Computer Center. Thus, it is seen that the fit is quite good for more than 80% of the maximum sorbed concentration $N(\infty)$. While we recognize that other schemes for obtaining k_1', k_2', and b may exist, it can be shown (see ref 17 and 18 in Appendix) that the so obtained values of k_1', k_2', and b do yield a minimum in the sum of the squares of the deviations of the observed and calculated ϕ values.[14] Consequently, the three values obtained

Table III

A. Kinetic Parameters for the Adsorption Processes

System	T, °K	Rate constant k_1', sec^{-1}	Activation energy, ΔE kcal/mol	Enthalpy of activation, $\Delta H^{\pm}$, kcal/mol	Entropy of activation, $\Delta S^{\pm}$, eu	Free energy of activation, $\Delta G^{\pm}$, kcal/mol	b
Silica gel	273	5.9×10^{-2}		5.5	−43.8	17.4	4.2
			6.0				
2,4-D (10 ppm)	298	1.5×10^{-1}		5.4	−43.5	18.4	2.2
Silica gel	273	2.7×10^{-4}		5.5	−54.5	20.4	1.9
Isocil			6.0				
(100 ppm)	298	7.0×10^{-4}		5.4	−54.0	21.5	1.2
Silica gel	273	2.0×10^{-5}		7.4	−54.0	22.0	4.0
Bromacil			7.9				
(300 ppm)	298	6.8×10^{-5}		7.3	−52.0	22.7	3.8
Illite	273	1.5×10^{-2}		2.8	−56.5	18.2	4.4
			3.3				
2,4-D (10 ppm)	298	2.5×10^{-2}		2.7	−56.5	19.5	3.5
Illite	273	1.1×10^{-2}		−0.54	−69.0	18.3	0.4
Isocil			0				
(100 ppm)	298	1.1×10^{-2}		−0.55	−70.0	20.3	0.4
Illite	273	2.0×10^{-2}		0.95	−62.5	18.0	1.7
Bromacil			1.5				
(300 ppm)	298	2.5×10^{-2}		0.94	−63.0	19.7	1.4

B. Kinetic Parameters for the Desorption Processes

Silica gel	273	4.0×10^{-6}		6.5	−61	23.1	4.2
			7.0				
2,4-D (10 ppm)	298	1.2×10^{-5}		6.4	−62	24.9	2.2
Silica gel	273	2.2×10^{-7}		8.0	−59.4	24.2	1.9
Isocil			8.5				
(100 ppm)	298	8.2×10^{-7}		7.9	−58.5	25.3	1.2
Silica gel	273	8.6×10^{-8}		14.8	−36.4	24.7	4.0
Bromacil			15.3				
(300 ppm)	298	9.2×10^{-7}		14.7	−38.4	26.3	3.8
Illite	273	4.5×10^{-7}		5.1	−68.7	23.9	4.4
			5.6				
2,4-D (10 ppm)	298	1.1×10^{-6}		5.0	−68.2	25.3	3.5
Illite	273	1.0×10^{-3}		−0.54	−74.6	19.8	0.4
Isocil			0				
(100 ppm)	298	1.0×10^{-3}		−0.55	−74.8	21.8	0.4
Illite	273	1.0×10^{-4}		4.0	−32.2	21.0	1.7
Bromacil			4.5				
(300 ppm)	298	2.0×10^{-4}		3.9	−62.0	23.4	1.4

are quite reasonable. Furthermore, as we have discussed in the latter part of the paper, these values do explain the kinetics of adsorption from solution satisfactorily.

The values of the rate constants k_1' and k_2' calculated in such a manner are given in Tables IIIA and IIIB. The values of k_1' and k_2' at 0 and 25° give us an opportunity to calculate the Arrhenius activation energy ΔE for the adsorption and desorption processes. These values are also included in Tables IIIA and IIIB. It is interesting to note that the rate constant for the adsorption process is always greater than the desorption value. Similarly, the activation energy for the desorption process is always greater than the value for adsorption. This we should expect because the desorption process always requires more energy. The rate constants k_1' and k_2' could be represented in terms of transition state theory by

$$k_1' = \left(\frac{kT}{h}\right)\exp\left(\frac{-\Delta G_a^{\pm}}{RT}\right) = \left(\frac{kT}{h}\right)\exp\left(\frac{-\Delta H_a^{\pm}}{RT}\right)\exp\left(\frac{\Delta S_a^{\pm}}{R}\right) \quad (23)$$

$$k_2' = \left(\frac{kT}{h}\right)\exp\left(\frac{-\Delta G_d^{\pm}}{RT}\right) = \left(\frac{kT}{h}\right)\exp\left(\frac{-\Delta H_d^{\pm}}{RT}\right)\exp\left(\frac{\Delta S_d^{\pm}}{R}\right)$$

(14) Also, we have available copies of the FORTRAN program used in obtaining k_1', k_2', and b.

where k and h are the Boltzmann and Plank constants, respectively, and $\Delta G^{\ddagger}$, $\Delta H^{\ddagger}$, and $\Delta S^{\ddagger}$ are the corresponding values of free energy of activation, enthalpy of activation, and entropy of activation for the adsorption and desorption processes. The enthalpy of activation, $\Delta H^{\ddagger}$, is related to activation energy as follows.

$$\Delta E = \Delta H^{\ddagger} + RT \tag{24}$$

Hence, a knowledge of k_1' and k_2' and ΔE could be used to calculate $\Delta S^{\ddagger}$, $\Delta H^{\ddagger}$, and $\Delta G^{\ddagger}$. These values calculated from the above expressions are given in Tables IIIA and IIIB. An examination of the above tables indicates that $\Delta G^{\ddagger}$ for the desorption process is always greater than the corresponding value for adsorption.

Some interesting conclusions can be drawn regarding the mechanism of the adsorption. The adsorbate 2,4-D is a weak acid and has 600 ppm solubility in water at 20° with a heat of solution of about 6 kcal/mol. The other adsorbates isocil and bromacil, however, are of a different nature. They are neutral molecules of slightly higher solubility (500–1000 ppm) and a lower value of the heat of solution (2 kcal/mol).

Earlier isotherm studies of 2,4-D,[15] isocil, and bromacil[16] on these surfaces indicated that the isosteric heat of adsorption $\Delta H^{\ddagger}$, as a function of the amount of chemical sorbed x, calculated by the following expression[16]

$$\Delta H = R\left(\frac{\partial \ln c}{\partial\left(\frac{1}{T}\right)}\right)_x \tag{25}$$

where c is the equilibrium concentration), was higher for silica gel than illite (Table IV). The low magnitude

Table IV: Changes in the Isoteric Heat of Adsorption for Various Systems at High and Low Surface Coverage, ϕ

Surface	Adsorbate	ΔH, kcal/mol
Silica gel	2,4-D	0 to −8.0
	Isocil	0 to −13.0
	Bromacil	0 to −7.0
Illite	2,4-D	−1 to 0
	Isocil	0 to −10
	Bromacil	−1 to 0

of $\Delta H^{\ddagger}$ ruled out the possibility of a chemisorption. The most probable nature of the adsorption was of the physical type. A hydrogen bond formation between the silica gel surface and the chemical was suggested to explain the higher value of $\Delta H^{\ddagger}$ for the surface.

Extension of the Theory to the Desorption Process. The theory could be easily extended to study the kinetics of desorption process. For the desorption experiment at time $t = 0$, $N(0) = N_{max}$, $\phi = 1$, $C(0) = 0$, and $M_0 = \chi A N_{max}$. Assuming the mass balance equation

$$\chi A N_{max} = C(t)V + \chi A N(t) \tag{26}$$

the rate equation for the desorption process is the same as (13), *i.e.*

$$\frac{dN}{dt} = \frac{V}{\chi A} C(t) k_1'(1 - \phi/2) e^{\frac{-\alpha\phi}{RT}} - k_2' \frac{N(t)}{\chi A} \frac{\phi}{2} e^{\frac{\alpha\phi}{RT}} \tag{27}$$

where all the terms are as previously defined.

Substituting for $C(t)V$ the so obtained value from the mass balance equation, use of the initial condition $M_0 = \chi A N_{max}$, and the multiplication through this rate equation (13) by $1/N_{max}$ we obtain

$$\frac{d\phi}{dt} = k_1'(1 - \phi)\left(1 - \frac{\phi}{2}\right) e^{-b\phi} - k_2' \frac{\phi^2}{2} e^{b\phi} \tag{28}$$

as the equation for the rate of desorption from a previously equilibrated surface, *i.e.*, desorption from a surface which initially has $\phi = 1$ at $t = 0$.

As before, beginning with $\phi(0) = 1$, $t \to \infty$ implies that $d\phi/dt \to 0$ and $\phi \to \phi_{min}$. Mathematically, this is

$$k_1'(1 - \phi_{min})\left(1 - \frac{\phi_{min}}{2}\right) e^{-b\phi_{min}} = k_2' \frac{\phi_{min}^2}{2} e^{b\phi_{min}} \tag{29}$$

or

$$\frac{2(1 - \phi_{min})\left(1 - \frac{\phi_{min}}{2}\right)}{\phi_{min}^2} \frac{k_1'}{k_2'} = e^{2b\phi_{min}} \tag{30}$$

Equation 30 is an interesting transcendental equation in ϕ_{min}. For particular realistic values of k_1', k_2', and b we show later in the discussion of the results of (30) the graphical solution to find ϕ_{min} for those particular values of k_1', k_2', and b.

By solving for k_1' in (30), and with subsequent substitution of this value into (28), we obtain

$$\frac{d\phi}{dt} = -k_2' \frac{\phi^2}{2} e^{b\phi}\left\{1 - e^{2b(\phi_{min} - \phi)} \times \left(\frac{\phi_{min}}{\phi}\right)^2\left(\frac{1 - \phi}{1 - \phi_{min}}\right)\left(\frac{2 + \phi}{2 - \phi_{min}}\right)\right\} \tag{31}$$

as the alternate rate equation for the desorption experiment. Again, for the previously obtained k_1', k_2', b and subsequently ϕ_{min}, we exhibit the numerical solution to (31) graphically in the discussion of the results.

In Figure 3 we show the graphical solution to the transcendental equation (30). Hypothetical, yet realistic, values of k_1', k_2', and b are assumed and the solution, ϕ_{min}, for each combination, is seen as the intersection point of the two curves.

Figure 4 shows the numerical solution of (31) for the

(15) R. Haque and R. Sexton, *J. Colloid Interfac Sci.*, **25**, 818 (1968).
(16) W. R. Coshow and R. Haque, unpublished work.

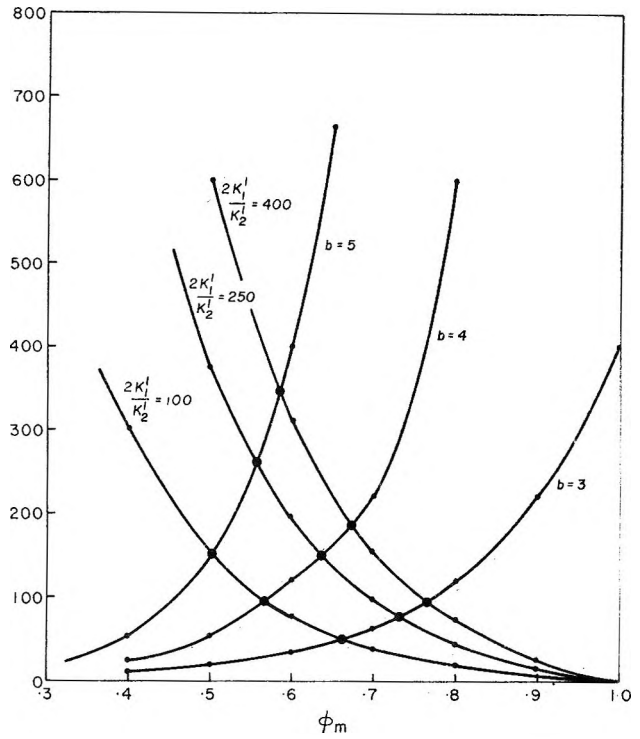

Figure 3. Graph of each side component in eq 22 for various realistic values of b and ratios of k_1'/k_2'. The intersection points yield ϕ_m.

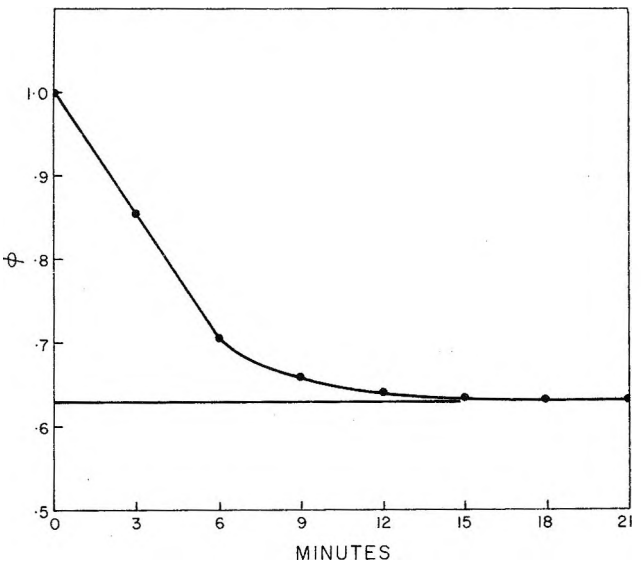

Figure 4. Graph of hypothetical desorption experiment for $b = 2$, $k_1'/k_2' = 150$, and $\phi_m = 0.63$.

particular choice of k_1', k_2', and b stated in the caption of the figure. It is interesting to note that this curve asymptotically approaches ϕ_{min} from above: $0 < \phi_{min} \leq \phi(t) \leq 1, t \geq 0$ for desorption. That $\phi_{min} > 0$ brings out the interesting feature that after performing an adsorption experiment, a desorption experiment is then carried out with the reservoir volumes remaining unchanged. The chemical desorbs down to some ϕ_{min} which is greater than $\phi = 0$. This indicates some residual chemical remaining sorbed. This residual chemical is in good agreement with many data reported elsewhere in the literature.

Summary

1. A rate expression for the kinetics of adsorption based on: (i) the adsorption process as a net result of two opposing reactions, adsorption and desorption; (ii) the change of free energy of activation with surface coverage; and (iii) the inclusion of the sticking probability of the adsorption on the surface has been derived.

2. The equation has been tested for the adsorption from solution of three organic compounds on surfaces.

3. The rate expression enables us to determine simultaneously the rate constants of adsorption and desorption from only the adsorption data.

4. From the temperature dependence of the rate constants, various thermodynamic parameters have been calculated.

5. The theory has been extended to predict the desorption of adsorption from the surface.

Acknowledgment. We thank Mr. R. J. Murray, O. S. U. Computer Center, for his most able assistance in writing the computer programs for this work.

Appendix A

We are given a nonlinear differential equation of the form

$$\frac{d\phi}{dt} = k_1'f(\phi,b) + k_2'g(\phi,b) \qquad \text{(i)}$$

where $0 \leq \phi \leq 1, 0 \leq t < \infty, \phi(0) = 0$, and k_1, k_2', and b are real nonnegative constants to be determined. Let

$$f(b,\phi) = (1 - \phi)\left(1 - \frac{\phi}{2}\right)e^{-b\phi}$$
$$g(b,\phi) = \left(1 - \frac{\phi}{2}\right)e^{b(2-\phi)} - \frac{\phi^2}{2}e^{b\phi} \qquad \text{(ii)}$$

Clearly, both f and g are bounded measurable functions of ϕ, for fixed b, defined on the strip

$$\{0 \leq \phi \leq 1\} \times \{0 \leq t \leq T\}, T \text{ finite}$$

Thus, f and g are integrable Lebesgue; consequently, at least one solution to D.E. (i) exists. Define

$$\phi(t) - \phi(t_0) = k_1' \int_{t_0}^{t} (1 - \phi)\left(1 - \frac{\phi}{2}\right)e^{-b\phi}d\tau + k_2' \int_{t_0}^{t} \left(1 - \frac{\phi}{2}\right)e^{b(2-\phi)} - \frac{\phi^2}{2}e^{b}d\tau \qquad \text{(iii)}$$

for $\{t \mid 0 \leq t_0 < t \leq T \infty\}$. Since we do not know k_1', k_2', and b at this time, a Piccard type of solution approach yields nothing useful. Therefore, we propose to l^2 (least squares) fit k_1', k_2' for each given b value using the experimental data. Note! This process is also known as least-square imbedding in a direct search op-

eration. In this way an acceptable region of b values is thus generated. Since for every b value chosen, k_1' and k_2' are obtained in l^2, we then use Runge–Kutta numerical integration to generate a curve which is pointwise checked against the experimental curve. This check will be explained in greater detail later on.

Partition up the interval (t_0, t) into N equally spaced intervals.

Define

$$\text{(a) } Y_i = \phi(t_0 + i\Delta t) - \phi(t_0)$$

$$\text{(b) } X_i^{(1)} = \int_{t_0}^{t_0+i\Delta t} (1 - \phi)\left(1 - \frac{\phi}{2}\right) e^{-b\phi} d\tau \qquad \text{(iv)}$$

$$\text{(c) } X_i^{(2)} = \int_{t_0}^{t_0+1\Delta t} \left(\left(1 - \frac{\phi}{2}\right) e^{b(2-\phi)} - \frac{\phi}{2} e^{b\phi}\right) d\tau$$

where Δt is the length of each sub interval, *i.e.*

$$\Delta t = \frac{t - t_0}{N}$$

and i is the running index, $i = 1, 2 \ldots, N$.

Define for every b

$$E = \sum_{i=1}^{N} (Y_i - k_1' X_i^{(1)} - k_2' X_i^{(2)})^2 \qquad \text{(v)}$$

Observe that E is really a convex function of k_1', k_2', and b[17] (quadratic hypersurface). It therefore possesses a unique set of values $(\bar{k}_1', \bar{k}_2', \bar{b})$ which do indeed cause E to assume its minimum value on the positive quadrant of the three-dimensional vector space (k_1', k_2', b).[18]

Minimizing E with respect to k_1' and k_2' gives the system of equations

$$k_1' \sum_1^N (X_i^{(1)})^2 + k_2' \sum_1^N X_i^{(1)} X_i^{(2)} = \sum_1^N X_i^{(1)} Y_i$$

$$k_1' \sum_1^N X_i^{(1)} X_i^{(2)} + k_2' \sum_1^N (X_i^{(2)2}) = \sum_1^N X_i^{(2)} Y_i$$

Solutions to this system k_1', k_2' always exist and are unique, for the determinant of the coefficients of k_1' and k_2' in (vi) never vanishes. However, we require the constraint k_1' and k_2' must be real nonnegative numbers for the system to be physically reasonable. Therefore, though any real nonnegative b value will give a k_1' and k_2', only a certain range of b values will satisfy this real nonnegativity constraint. Furthermore, of all the physically acceptable b, k_1', and k_2' values obtained, we are restricted again in the choice of the best b value in l^2 (and hence k_1' and k_2' value) when the numerical integrated values are compared with the experimental values. This check can be stated as follows. From among the class of physically acceptable b values we select that value which gives the least value of E, *i.e.*

$$E_0 = \min_{\substack{b \geq 0 \\ k_1', k_2' \geq 0}} E$$

For purposes of ease in programming for the computer, we chose to begin b at $b = 0$ say, compute k_1' and k_2' for $b = 0$, and check the algebraic sign on both k_1' and k_2'. If the signs are both positive then the R–K integration is applied. The computed curve of ϕ (t) *vs.* t is then checked against the experimental curve and E is calculated. b is increased by Δb and the procedure is repeated.

If previously upon checking the signs of k_1' and k_2' it is found that one or both signs are negative, then immediately we increment b by Δb, *i.e.*, $b = b + \Delta b$ and compute a new set k_1' and k_2'. Again, signs are checked and the whole process repeats itself, thus generating an interval of b values which are physically acceptable. We, in the course of our experimental testing, found every interval of acceptable b values to lie in the interval $0 \leq b \leq 10$.

It should be noted here that the accuracy of the method depends heavily upon the accuracy of the quadrature formula used in $X_i^{(1)}$ and $X_i^{(2)}$. We used a third-order polynomial formula and a small Δt so that accuracy would be high. Note also that the whole process could be systematized to obtain a very good value of b by using nonlinear least squares and a Newton type convergence sequence; however, no guarantee is given that for this particular b value, k_1' and k_2' will both be positive.

Appendix B

From diffusion in solids we have the following equation[19]

$$X_{16\%} \cong 2\sqrt{Dt} \qquad \text{(vi)}$$

where $X_{16\%}$ is the concentration of the chemical expected at the center of the solid, t the time, and D the diffusion coefficient. The value[19] of D varies generally from 10^{-8} to 10^{-10} cm^2/sec^{-1}. Using a value of 10^{-8} for the diffusion coefficient of the adsorbate and 0.5 mm as an average particle size of the adsorbent under investigation, the time required for the chemical concentration to reach 16% of the surface concentration will be about 20 hr. For the adsorption experiments under investigation 90% of the adsorption is complete within 15 min. Hence the error due to neglect of intraparticle diffusion in this time range is very small.

(17) W. Firey, "Some Means of Convex Bodies," Tech. Rept. 17, Sept 1963, Department of Mathematics, Oregon State University, Corvallis, Ore.

(18) P. M. Anselone and R. H. Moore, An Extension of the Newton–Kautorovic Method for Solving Nonlinear Equations, MRC Tech. Report No. 510, Jan 1965. University of Wisconsin, Madison, Wis.

(19) J. Crank and G. S. Parks, "Diffusion in Polymers," Academic Press, New York, N. Y., 1968.

Diffusion and Solubility of Hydrogen in Palladium and Palladium–Silver Alloys

by Gerhard L. Holleck

Tyco Laboratories, Inc., Waltham, Massachusetts *(Received June 6, 1969)*

Diffusion coefficients and heats of solution for hydrogen in Pd and Pd–Ag alloys at low hydrogen concentration were determined from 260 to 640°. The change in activation energy for hydrogen diffusion with increasing mole fraction of silver (X_{Ag}) from Pd to $Pd_{0.5}Ag_{0.5}$ can be represented empirically by $E = 3800X_{Ag}^4 + 1500X_{Ag}^2 + 5260$ cal. The preexponential factor, D_0 showed only a slight linear decrease $D_0 = -2.65 \times 10^{-3}X_{Ag} + 2.9 \times 10^{-3}$. The molar heat of desorption, ΔH_{H_2}, increased with rising Ag concentration from 4000 cal (Pd) to a maximum between 8020 ($Pd_{0.6}Ag_{0.4}$) and 7090 cal ($Pd_{0.5}Ag_{0.5}$). The entropy of desorption, ΔS_{H_2}, remained quite constant at values between 23.3 and 24.4 cal/deg mol.

Introduction

The diffusion of hydrogen in Pd and Pd alloys is of great interest because of its fundamental importance as one of the best defined examples of interstitial diffusion in transition metals. It also has considerable technological importance. Membranes, especially of Pd alloys, are widely used for separation and purification of hydrogen gas. Despite this, there has been no systematic investigation of the hydrogen diffusion behavior in Pd–Ag alloys at elevated temperatures. The diffusion of hydrogen in Pd between 200 and 700° has, however, been studied by several authors.[1–5] Most measurements were based on results of hydrogen permeation and solubility data from Sieverts, *et al.*,[3,7] or Gillespie and Galstaun (210–313°).[8]

There are only a few limited measurements[5,9] on hydrogen diffusion and solubility in Pd–Ag alloys above 250°. Investigations of hydrogen diffusion in Pd at approximately room temperature were reported recently by many authors.[10–16] Electrochemical methods were primarily employed,[10–14] but more recently gas volumetric methods were used successfully as well.[15,16] In this temperature range, several investigators reported also on hydrogen diffusion in Pd–Ag membranes.[14,15,17–20]

Two more recent publications[14,15] discuss the electrochemical and gas volumetric hydrogen diffusion measurements in Pd and Pd–Ag alloys between 0 and 100°, with special reference to the hydrogen concentration in the metal lattice. However, some uncertainty remained about the effect on hydrogen diffusion of increasing Ag content in Pd–Ag alloys at low hydrogen concentrations.

The aim of this investigation was to clarify this point and to examine changes in hydrogen diffusion and solubility parameters with Ag content over a larger temperature range. Special care was taken to avoid inhibition at the interface which often led to erroneous results in the past.

Principle of Measurement and Diffusion Theory

Consider one-dimensional diffusion in a membrane of thickness, s, bounded by two parallel planes (this means in practice that effectively all the diffusing substance enters and leaves through the plane faces, and a negligible amount through the edges).

The initial and boundary conditions for the diffusion equation $\partial c/\partial t = D\,\partial^2 c/\partial^2 x$ are

$$c = c_0 \text{ for } 0 < x < s \text{ and } t = 0$$

$$c = 0 \text{ for } x = 0 \text{ and } c = c_1 \text{ for } x = s \text{ and } t > 0$$

(1) W. Jost and A. Widmann, *Z. Phys. Chem.*, **B29**, 247 (1935); **B45**, 285 (1940).

(2) W. P. Davis, USAEC Report KAPL-1227, U. S. Atomic Energy Commission, Washington, D. C., 1954.

(3) G. I. Toda, *Res. Inst. Catalysis, Hokkaido Univ.*, **6**, 13 (1958).

(4) O. M. Katz and E. A. Gulbransen, *Rev. Sci. Instrum.*, **31**, 615 (1960).

(5) L. R. Rubin, *Engelhard Ind., Tech. Bull.*, **8**, 18 (1967).

(6) A. Sieverts, *Z. Metallk.*, **21**, 44 (1929).

(7) A. Sieverts and G. Zapf, *Z. Phys. Chem.*, **A174**, 359 (1935).

(8) L. J. Gillespie and L. S. Galstaun, *J. Amer. Chem. Soc.*, **58**, 2565 (1936).

(9) A. Sieverts, E. Jurisch, and A. Metz, *Z. Anorg. Chem.*, **92**, 328 (1915).

(10) M. A. V. Devanathan and Z. Stachurski, *Proc. Roy. Soc.*, **A270**, 90 (1962).

(11) M. von Stackelberg and P. Ludwig, *Z. Naturforsch.*, **19a**, 93 (1964).

(12) J. W. Simons and T. B. Flanagan, *J. Phys. Chem.*, **69**, 3581 (1965).

(13) E. Kahrig, D. Kirstein, and Fr. Lange, *Ber. Bunsenges. Phys. Chem.*, **70**, 592 (1966).

(14) G. Holleck and E. Wicke, *Z. Phys. Chem.*, (Frankfurt am Main), **56**, 155 (1967).

(15) G. Bohmholdt and E. Wicke, *ibid.*, **56**, 133 (1967) (G. Bohmholdt, Dissertation, Münster, 1966); *Z. Physik. Chem.*, (Frankfurt am Main), **42** 115 (1964).

(16) D. N. Jewett and A. C. Makrides, *Trans. Faraday Soc.*, **61**, 932 (1965); *Engelhard Ind. Tech. Bull.*, **7**, 51 (1966).

(17) A. Küssner, *Z. Phys. Chem.*, (Frankfurt am Main), **36**, 383 (1963).

(18) F. von Sturm and H. Kohlmüller, *Naturwissenschaften*, **52**, 31 (1965).

(19) E. Wicke and G. Holleck, *Z. Physik. Chem.*, (Frankfurt am Main), **46**, 123 (1965).

(20) A. Küssner, *Z. Naturforsch.*, **21a**, 515 (1966).

where c is the H concentration in the metal.

The more general case ($c = c_{00} \neq 0$ at $x = 0$ for $t > 0$) is reduced to the above by substituting $c' = c - c_{00}$. The resulting boundary conditions are

$$c' = c_0 - c_{00} \text{ for } 0 < x < s \text{ and } t = 0$$

$$c' = 0 \text{ for } x = 0 \text{ and } c' = c_1 - c_{00} \text{ for } x = s \text{ and } t > 0$$

This diffusion problem was dealt with by Daynes[21] and Barrer.[22]

If we solve the diffusion equation with the stated boundary conditions for the total amount of gas, Q, which emerges from the face ($x = 0$), we obtain for the time lag, L (which is represented by the intercept on the t axis of a plot Q *vs.* t[23])

$$L = \frac{s^2}{6D} - \frac{c_0 s^2}{2Dc_1} \tag{1}$$

and, for the more general case

$$L = \frac{s^2}{D(c_1 - c_{00})}\left(\frac{c_1}{6} + \frac{c_{00}}{3} - \frac{c_0}{2}\right) \tag{2}$$

In the measurements reported here, the initial membrane concentration was always 0. Thus, the diffusion coefficient is defined by

$$D = \frac{s^2}{6L} \tag{3}$$

if we can neglect the concentration c_{00} at the low pressure side of our membrane. If we take c_{00} into consideration, we obtain

$$D = \frac{s^2}{6L}\frac{c_1 + 2c_{00}}{c_1 - c_{00}} \tag{4}$$

When measuring the rate of permeation, J, *vs.* time, the quantity of hydrogen which has permeated the membrane at various times is obtained by integrating the rising curve.

Devanathan[24] showed that the time lag can also be obtained by determining the time at which the rate of permeation is 0.6299 times the steady-state value. He also defined the equation for the rising transient by

$$\ln\left(\frac{J_t - J_\infty}{J_\infty}\right)_{x=0} = \ln\left(1 - e^{-3t/t_0} + e^{-8t/t_0} \ldots\right) + \ln 2 - \frac{t}{t_0} \tag{5}$$

where the rise-time constant, t_0, is given by

$$t_0 = \frac{s^2}{\pi^2 D}$$

Thus, for times greater than 0, a plot of $\ln [(J_t - J_\infty)/J_\infty]_{x=0}$ against t should have a gradient of $1/t_0$. Since the time lag, L, is equal to the sum of the rise-time constant and the breakthrough time, t_b, we obtain for the latter

$$t_b = \frac{s^2}{D}\left(\frac{1}{6} - \frac{1}{\pi^2}\right) = \frac{s^2}{15.3D} \tag{6}$$

Thus, the diffusion coefficient D can be determined by evaluating the transient behavior.

Solubility data can be obtained from the steady-state flux, J_∞, by

$$J_\infty = -D\frac{\partial c}{\partial x} = -D\frac{c_{00} - c_1}{s} \tag{7}$$

If the reaction ($H_{2gas} \rightleftarrows 2\ H_{ads} \rightleftarrows 2\ H_{Me}$) at the interface is fast compared with the diffusion rate, the hydrogen concentration in the metal lattice at the surface is in equilibrium with the gas phase and can be expressed by the hydrogen pressure. For low hydrogen concentrations in the metal, we obtain as a good approximation Sieverts' equation

$$(P/P_0)^{1/2} = K(T)n \tag{8}$$

The atomic ratio, n, and the concentration, c, are related by

$$c = n\frac{m_{Me}}{qs}\left(\frac{\text{g-atom}}{\text{cm}^3}\right)$$

where P_0 = 1 Torr, $K(T)$ = Sieverts' constant, n = mole ratio of H in the metal, m_{Me} = g-atom of metal in the membrane, and q = membrane area.

From eq 7 and 8, Sieverts' constant is

$$K = \frac{D\left[\left(\frac{P_1}{P_0}\right)^{1/2} - \left(\frac{P_2}{P_0}\right)^{1/2}\right]}{2J_\infty V_{Me} s} \tag{9}$$

where P_1, P_2 = high and low hydrogen pressure in Torr, V_{Me} = volume of 1 g-atom of metal, and J_∞ = steady-state flux in g-atoms of H_2/cm^2.

The system described in the following paragraphs was designed to approach the initial and boundary conditions of the time lag method as closely as possible. The measurement of the hydrogen flow emerging from the low-pressure side of the membrane is based on monitoring the pressure difference across a calibrated capillary. Generally, these pressures were between 0 and 100 μ. The extent and effect of deviations from the boundary conditions stated above will be discussed later.

Experimental Section

Apparatus. The apparatus is shown schematically in Figure 1. The vacuum side consists of a thermistor, two capillaries, and the pumping system with an oil diffusion pump (Speedivac Model 403A from Edwards High Vacuum Ltd.) and a high flow rate liquid nitrogen cold

(21) H. A. Daynes, *Proc. Roy. Soc.*, A97, 286 (1920).

(22) R. M. Barrer, *Trans. Faraday Soc.*, 35, 628 (1939).

(23) W. Jost, "Diffusion," Academic Press, New York, N. Y., 1960.

(24) M. A. V. Devanathan, O.N.R. Technical Report No. ONR/551/22-NR026-028, Feb 28, 1961.

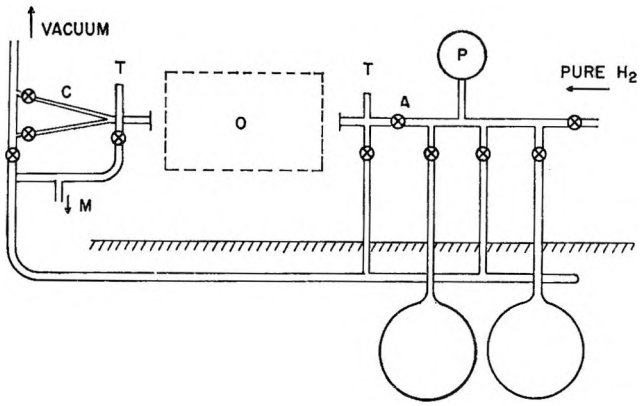

Figure 1. Hydrogen diffusion apparatus: T, thermistor; O, furnace and sample holder; P, absolute pressure gauge; M, McLeod gauge; A, wide-bore glass stopcocks, and C, capillaries.

trap. The high-vacuum part also contained an NRC ion gauge and a McLeod gauge for continuous pressure monitoring and thermistor calibration. The high-pressure side of the apparatus consisted of two 5-l. flasks and a precision absolute pressure gauge (Wallace and Tiernan, Model No. FA129).

Short, wide glass tubing and large-bore stopcocks were used throughout the system to avoid any undesired pressure gradients. The total volume of the high-pressure part of the apparatus was 14150 cm^3; the volume between the sample and the capillaries was $\sim$20 cm^3.

The sample holder (Figure 2) was machined out of stainless steel and was connected to the vacuum apparatus by two O-ring joints. A stainless steel bellows provided the necessary flexibility. The sample, a disk of 2.5 cm ϕ, was clamped between the two parts of the sample holder which were pressed together by four stainless steel bolts, leaving a well defined area of 3.14 cm^2. An aluminum ring and thick walled copper tubing provided uniform temperature distribution all around the sample. The sample holder was inserted into a 25-cm long tube furnace controlled by a Wheelco furnace control unit.

A chromel–alumel thermocouple for measuring the sample temperature was positioned to touch the side of the sample, as indicated in Figure 2. The sample temperature was measured to $\pm 0.2°$. There was no temperature drift during short runs. During runs extending over a longer time, the temperature variation stayed within $\pm 0.2°$ of the preset value. At the furnace exits, the sample holder was cooled by water flowing through two windings of copper pipe.

Pressure Measurement. The measuring principle is based on the high-temperature coefficient of the thermistor resistance. A glass bead thermistor (G108, 40 kilohms at 25°, 1–2 sec time constant from Fenwal Electronics) was mounted in a glass tube with a water jacket thermostated to 25 $\pm$ 0.1° by a Haake thermostat. The thermistor was part of a Wheatstone bridge arrangement connected to a stabilized dc power supply. The bridge was balanced at high vacuum, and under our conditions the thermistor resistance was 815 kilohms. During measurements, the imbalance was followed by a variable speed compensation strip recorder (Sargent). A variable resistor was used for the fine adjustment of the zero point at high vacuum, and a similar thermistor arrangement in a very insensitive setting was used at the high-pressure side to indicate the start of the run. The thermistor bridge output was calibrated with hydrogen against a McLeod gauge. It showed an almost completely linear relationship between resistance and pressure in the range from 0 to 200 μ with a slope of 375 mV/100 μ.

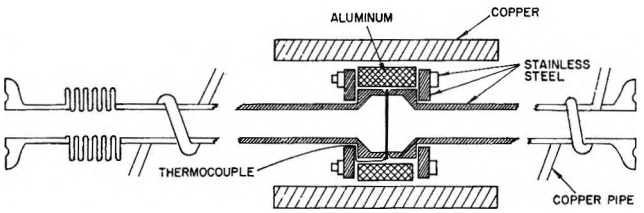

Figure 2. Sample holder.

Flux Measurement. For the calibration of flux through the capillaries, a flask of known volume was connected to the low-pressure part of the system. Since the pressure change with time was recorded during evacuation through a capillary, a calibration curve for each capillary was thus determined. The flow rate at low pressures was 4×10^{-3} and 6×10^{-3} cm^2 of H_2 (STP)/min μ. For the actual determination of H_2 flow, the calibration curve was used because of deviations from linearity at higher pressures.

Materials. Tank hydrogen was purified by passing it through an Engelhard hydrogen purifier (this apparatus is based on the principle of hydrogen diffusion through a Pd–Ag alloy at elevated temperatures). The Pd samples (99.9+) were obtained from Engelhard Industries. The Pd–Ag alloys were prepared at Tyco Laboratories from a Pd sponge (99.95%+, Engelhard Ind.) and silver (99.999%) under a positive argon pressure and then rolled into sheets. Four different membranes of Pd and two to four different membranes of each Pd–Ag alloy were employed. The thickness ranged from 0.0800 to 0.2025 cm.

Preparation of the Samples and Experimental Procedure. A disk 2.5 cm in diameter was punched out, washed with acetone, mechanically cleaned with fine emery paper, etched for a short time in concentrated nitric acid, and electrolytically palladized in an acidic palladium nitrate solution. After careful washing with triply distilled water, the sample was mounted in the sample holder, connected to the vacuum system, and evacuated. Before starting the furnace, the arrangement was checked for leaks. After the sample reached a constant temperature, it was treated with hydrogen

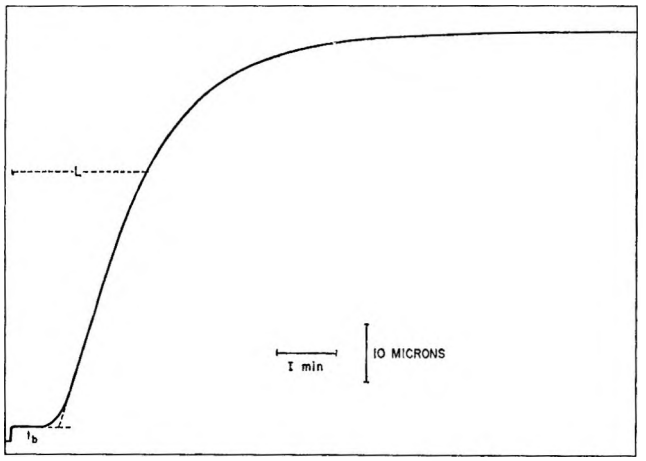

Figure 3. Typical recording of pressure rise with time. The first step marks the start of the run; hydrogen permeation through 0.11-cm $Pd_{0.9}Ag_{0.1}$ at 263°.

and evacuated. The stopcocks to the vacuum line were then closed, the capillaries opened, and the recorder started. By opening stopcock A (Figure 1), a constant H_2 pressure was applied to the high-pressure side of the sample. This starting point was indicated by a small thermistor signal on the recorder. After an induction time, the pressure on the opposite side of the membrane started to rise and finally reached a constant value, indicating a steady-state flux. A typical recording is shown in Figure 3. Before the next run at different pressure, the sample was again completely evacuated.

Results

The results reported here are based on permeation measurements in the temperature range of 250 to 640° and hydrogen pressures between 30 and 500 Torr. A typical recording of hydrogen flux against time is shown in Figure 3.

Values for the time lag, L, were evaluated from plots of Q *vs.* t and from the time elapsed until the flux was equal to 0.63 of the steady-state value (Q was obtained by graphical integration of the flux *vs.* time curve). Both methods led to the same result for L. Diffusion coefficients calculated from L, t_b, and t_0, according to eq 4, 5, and 6, agree within experimental error. However, values for D obtained from t_b were generally slightly higher (~5%) than those from L and t_0, and showed a larger scatter. The breakthrough time, t_b, reflects the time elapsed until the first hydrogen appears at the low-pressure side of the foil. Since $t_b \sim s^2$, it is very sensitive to differences in sample thickness and will have a value corresponding to the thinnest parts of the membrane. If the membrane thickness is not completely uniform, values of t_b will tend to be too short compared with the average sample thickness, thus leading to values of D which are too large. Due to the rolling of relatively small sheets, some samples are indeed not completely uniform in thickness over the whole 3.14 cm^2. The fact that a commercially obtained Pd sheet with more uniform thickness yielded the same values for D from L and t_b seems to confirm this explanation. The results are therefore generally based on the evaluation of L. Values obtained for L were between 10 and 2000 sec, depending on sample composition, thickness, and temperature.

The response time of the thermistor arrangement was determined to establish its influence on small values of L. When measuring the steady-state reflux through a membrane, a pressure change follows the opening or closing of the second capillary. From this transient, one obtains a value for the time constant of the measuring system. It can be shown that the evaluated time constants of 1.4 to 1.8 sec change the smallest values of L less than 1%. Table I shows an example of measured values for the 0.110-cm $Pd_{0.9}Ag_{0.1}$ membrane. Diffusion coefficients, D', are calculated from eq 3. Values for D are obtained from eq 4 by substituting the ratio of the hydrogen concentrations in the metal by the ratio of the square roots of the hydrogen pressures.

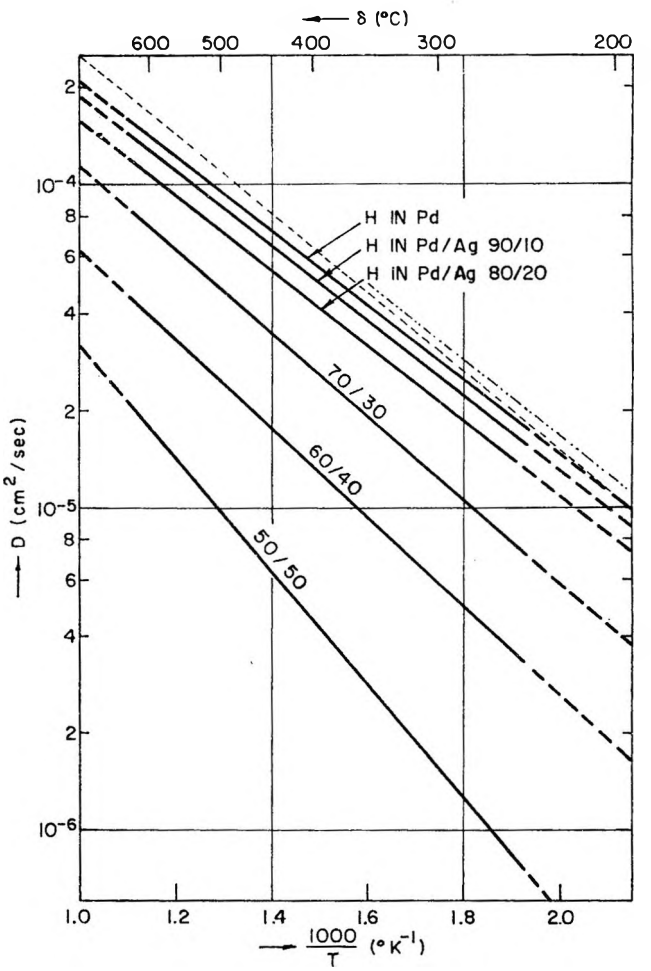

Figure 4. Diffusion coefficients of hydrogen in Pd and Pd–Ag alloys at low hydrogen concentrations. Arrhenius diagram: —, this investigation, – – –, H in Pd ref 2, –·–·– H in Pd ref 4.

Table I: Evaluation Example, Hydrogen Diffusion through 0.11-cm $Pd_{0.9}Ag_{0.1}$

δ[a]	P_1, Torr	P_2, Torr × 10^{-8}	J, cm³/cm² sec × 10^{-3}	L, sec	D', cm²/sec × 10^{-5}	D, cm²/sec × 10^{-5}
245.0	45.0	45.3	1.4278	163.0	1.24	1.36
263.0	85.5	68.0	2.1762	135.0	1.49	1.62
265.0	202.0	68.3	3.4607	124.0	1.63	1.72
265.0	399.0	149.2	5.0849	119.0	1.69	1.79
416.0	42.6	95.2	3.1263	44.3	4.55	5.23
416.0	201.0	131.3	7.1125	41.9	4.81	5.19
416.0	400.0	178.5	10.0159	40.4	4.99	5.31
416.0	112.5	97.2	5.0425	43.4	4.65	5.07
416.0	33.5	82.5	2.6805	45.6	4.42	5.12
614.0	36.0	84.5	4.3418	17.5	11.52	13.28
614.0	52.5	101.2	5.2601	16.5	12.22	13.91
614.0	91.0	132.6	7.1921	16.5	12.22	13.68
614.0	150.0	167.0	9.3047	15.4	13.10	14.45
614.0	200.0	182.3	10.5679	15.1	13.36	14.60

[a] δ = temperature in °C.

Table II: Diffusion and Solubility Parameters of Hydrogen in Pd and Pd–Ag Alloys between 260 and 640° at Low Hydrogen Content in the Metal

	No. of measurements	D_0, cm²/sec × 10^{-3}	E, cal/g-atom	ΔH_{H_2}, cal/g-atom	ΔS_{H_2}, cal/deg g-atom
Pd	57	2.94 ± 0.2	5260 ± 50	4000	23.3
$Pd_{0.9}Ag_{0.1}$	43	2.69 ± 0.2	5300 ± 60	5535	23.6
$Pd_{0.8}Ag_{0.2}$	30	2.33 ± 0.2	5335 ± 100	6740	24.0
$Pd_{0.7}Ag_{0.3}$	31	2.21 ± 0.2	5900 ± 100	7330	23.5
$Pd_{0.6}Ag_{0.4}$	19	1.50 ± 0.2	6300 ± 150	8020	24.4
$Pd_{0.5}Ag_{0.5}$	19	1.82 ± 0.2	8000 ± 150	7090	24.1

The example clearly illustrates the difference in the calculated diffusion coefficients. Values of D' are somewhat smaller than values of D and show a noticeable pressure dependence leading to increasing values of D' with rising hydrogen pressure. Since D' approaches D at higher pressures, and the latter shows no systematic pressure dependence, this indicates that the pressure dependence of the diffusion coefficient is a reflection of the deviations from the boundary condition $c = 0$ at $x = 0$ for $t > 0$ and does not represent a true concentration dependence of the hydrogen diffusion coefficient in the membrane. The latter would also be unlikely in view of the low hydrogen concentration in the metal lattice during all measurements.[14,15] The average concentration extremes were $n \approx 5 \times 10^{-5}$ for Pd at 640° and $n \approx 4 \times 10^{-2}$ for $Pd_{0.6}Ag_{0.4}$ at 250°.

All diffusion coefficients reported here were obtained by eq 4, and are independent of membrane thickness. The temperature dependence of the diffusion coefficients can be expressed by

$$D = D_0 \exp(-E/RT) \qquad (10)$$

where D_0 = frequency factor and E = activation energy.

An Arrhenius plot of log D against $1/T$ is shown in Figure 4. It can be seen that there is little change in the absolute values and in the activation energy of the hydrogen diffusion coefficients from pure Pd up to $Pd_{0.8}Ag_{0.2}$. With an increase of Ag content, the hydrogen diffusion coefficients decrease progressively and the activation energy increases. Values of D_0 and E for Pd and the Pd–Ag alloys were obtained by a least-squares fit of log D against $1/T$, and are given in Table II with the number of measurements upon which they are based. Figure 5 shows a typical example of the statistical distribution of experimental values for D around the calculated least-squares line. The change in activation energy with the mole fraction of Ag (X_{Ag}) up to $Pd_{0.5}Ag_{0.5}$ can be approximately described by

$$E = 3800X_{Ag}^4 + 1500X_{Ag}^2 + 5260 \text{ (cal)} \qquad (11)$$

The frequency factor, D_0, decreases slightly with increasing Ag content. Its change between Pd and $Pd_{0.5}Ag_{0.5}$ can be described by a linear relationship between D_0 and X_{Ag}

$$D_0 = -2.65 \times 10^{-3}X_{Ag} + 2.9 \times 10^{-3} \qquad (12)$$

Figure 6 shows a typical plot of the steady-state hydrogen flux at constant temperature *vs.* the difference of the square roots of the hydrogen pressures. The

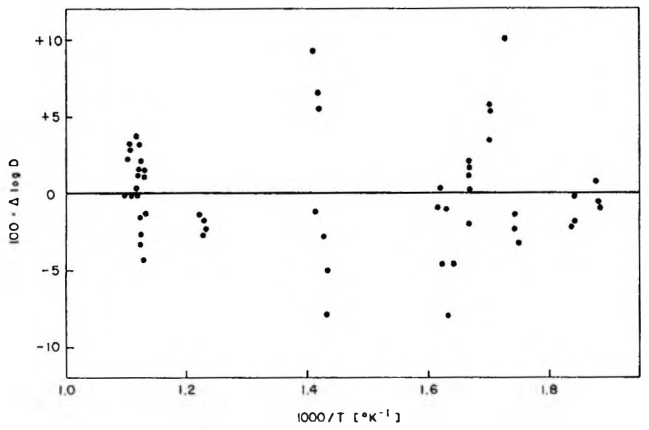

Figure 5. Typical distribution of experimental values of the hydrogen diffusion coefficient around the straight line calculated by a least-squares fit. Values obtained at four Pd membranes of different thickness.

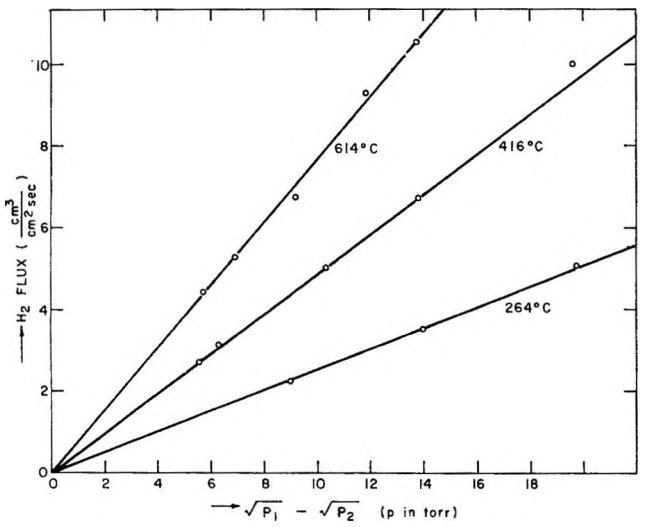

Figure 6. Hydrogen flux at different temperatures against the square root of the pressure; $Pd_{0.9}Ag_{0.1}$ membrane of 0.11 cm thickness.

measured points fall on straight lines which intersect the origin. There were no systematic deviations. The slopes, which depend on the membrane and the temperature, were used to calculate values of Sieverts' constant K (eq 9). The diffusion flux was found to be directly proportional to $1/s$ in accordance with eq 7.

This has two important implications; (1) it suggests that there is no significant inhibition at the interface, and (2) that the whole sample area is active for diffusion. The lack of dependence of D and $J_\infty s$ on membrane thickness and the reproducibility indicates that the diffusion equations (with the stated boundary conditions) can be applied to the experiments reported here.

Figure 7 shows the temperature dependence of Sieverts' constant K in an Arrhenius plot. The hydrogen solubility at very low hydrogen content in the lattice increases considerably from Pd to $Pd_{0.8}Ag_{0.2}$; this is

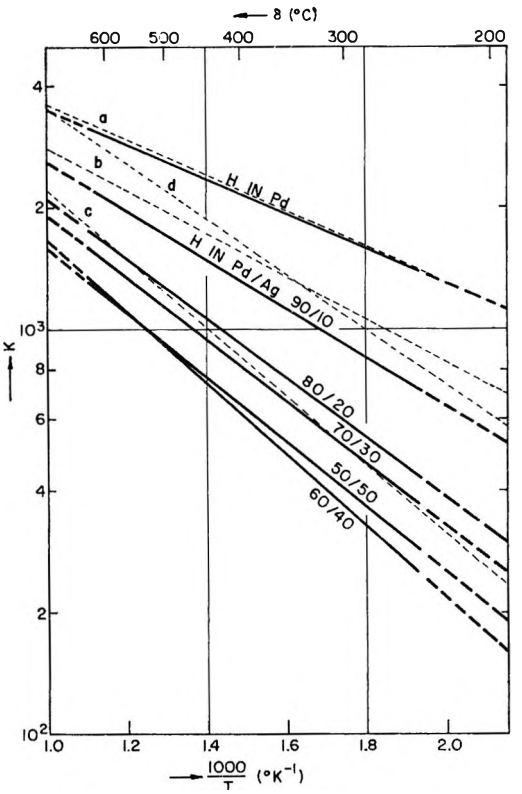

Figure 7. Temperature dependence of Sieverts' constant K for Pd and Pd–Ag alloys: —, this investigation; ----, Sieverts, *et al.*; a, Pd; b, $Pd_{0.9}Ag_{0.1}$; c, $Pd_{0.6}Ag_{0.4}$; d, $Pd_{0.5}Ag_{0.5}$.

followed by a slower increase with a maximum between $Pd_{0.6}Ag_{0.4}$ and $Pd_{0.5}Ag_{0.5}$. The standard values for the heat of desorption, ΔH_{H_2}, and the entropy of desorption, ΔS_{H_2} (based on H_2) obtained by

$$\ln K' = -\frac{\Delta H_{H_2}}{2RT} + \frac{\Delta S_{H_2}}{2R} \qquad (13)$$

are also given in Table II (K' = Sieverts' constant, pressure unit atmospheres).

The heat of desorption increases with rising Ag content and has a maximum between $X_{Ag} = 0.4$ and $X_{Ag} = 0.5$, whereas the entropy of desorption changes little. Figure 8 shows the change in total hydrogen flux as a function of membrane composition and temperature. As a consequence of the changes in D and K reported above, there is a maximum hydrogen permeability for a membrane of an approximate composition $Pd_{0.76}Ag_{0.24}$. This is in keeping with prior findings.[25]

Discussion

It should be recalled that Ag forms random substitutional alloys with Pd, in which hydrogen atoms are located in the octahedral interstices of the fcc lattice.[26,27]

(25) J. B. Hunter, *Platinum Metals Rev.*, **4**, 130 (1960).

(26) J. Bergsma and J. A. Goedkoop, *Physica*, **26**, 744 (1960).

(27) J. E. Worsham, Jr., M. K. Wilkinson, and C. G. Shull, *J. Phys. Chem. Solids*, **3**, 303 (1957).

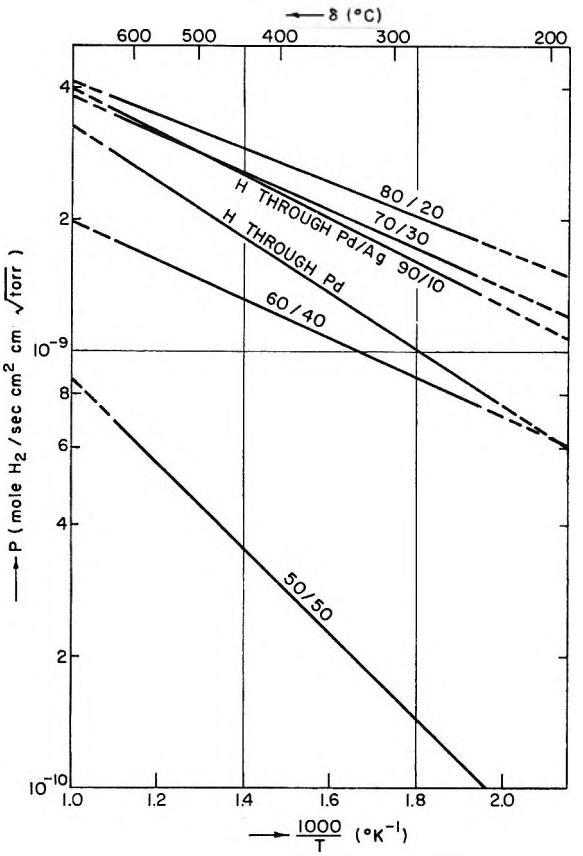

Figure 8. Temperature dependence of hydrogen permeation through membranes of Pd and Pd–Ag alloys.

Hydrogen Diffusion. The theory of hydrogen diffusion has been discussed several times,[14,15,23,28] and will not be repeated in detail here. As a result, one obtains for the frequency factor in eq 10

$$D_0 = a_0^2 \nu_0 \kappa_0 Z_p \frac{2\,kt}{h\nu_0} \sinh\left(\frac{h\nu_0}{2kT}\right) \exp\left(\frac{\Delta S^\circ}{R}\right) \quad (14)$$

where a_0 = lattice constant, ν_0 = vibrational frequency of H in the octahedral interstice, κ = transmission factor of the order of 1, and Z_p = number of exits for an H atom from its octahedral interstice (Z_p = 12 if the H atom jumps through in edge of the octahedron; Z_p = 8 if it leaves through a face of the octahedron—the latter is probably more favorable from an energetic point of view), k = Boltzmann constant, h = Planck constant, and ΔS° = entropy of activation.

For a_0 = 3.89 Å, a linear expansion coefficient of 11.76 × 10^{-6}, ν_0 = 12.3 × 10^{12} (estimated from equilibrium measurements[29]), κ = 1, and Z = 8, one obtains for ΔS° a value of −2.9 cal/deg g-atom at 400° (400° was chosen as a median value of the temperature range covered by the experiments). This result differs from the assumption of Zener that positive entropies of activation should be expected for interstitial diffusion. A similar negative value for ΔS° was also observed for H diffusion in Pd at low temperatures.[15]

As can be seen from Table II, D_0 decreases slightly with increasing Ag content, in spite of an increase in the lattice constant, a_0. There is probably not much change in the vibrational frequency, ν_0, in view of the nearly constant entropy of desorption. Thus, the remaining parameters Z_p and ΔS° would have to account for the decrease in D_0 in spite of an increase in a_0. Most likely, this is accomplished by an increasingly negative entropy of activation, possibly as a result of high vibrational frequencies perpendicular to the jump direction at the saddle point.

The activation energies for hydrogen diffusion show little change from Pd to $Pd_{0.8}Ag_{0.2}$, and a progressive increase at higher Ag concentrations. Hydrogen diffusion measurements[30] in pure Ag from 388 to 600° (D = 2.82 × 10^{-3} exp(−7500/RT),) suggest the presence of a maximum in E between $Pd_{0.5}Ag_{0.5}$ and pure Ag.

Earlier diffusion measurements of hydrogen in Pd in the temperature range of this investigation are summarized in Table III. Results obtained by permeation measurements in the intermediate temperature range[3,4] of 175 to 375° were recalculated[15] using newer equilibrium data obtained by interpolating the results of Nernst,[29] and those of Gillespie and Galstaun.[8] The permeation rates observed by Davis[12] are close to those reported here, as are his diffusion coefficients obtained by using Sieverts' solubility data. However, the activation energy is somewhat larger.

Table III: Diffusion of Hydrogen in Palladium at Low Concentrations above 200°

D_0, cm²/sec × 10^{-3}	E, kcal/g-atom		
5.4–8.4	5.72	190–400°	Jost and Widmann[1]
4.3	5.62	200–700°	Davis[2]
8.5	5.45	175–375°	Toda[3]
4.1	5.45	200–375°	Katz and Gulbransen[4]

Extrapolation of hydrogen diffusion coefficients for Pd from measurements between 0 and 100° to high temperatures results in values close to those reported here. For example, Bohmholdt and Wicke[15] found for Pd

$$D = (3.65 \pm 0.8) \times 10^{-3} \exp\left(-\frac{5600 \pm 100}{RT}\right)$$

It seems reasonable to assume that the activation energy for hydrogen diffusion changes with tempera-

(28) C. A. Wert and C. Zener, *Phys. Rev.*, **76**, 1169 (1949); C. A. Wert, *ibid.*, **79**, 601 (1950); C. Zener in "Imperfections in Nearly Perfect Crystals," W. Schockley, Ed., John Wiley and Sons, New York, N. Y., 1952.

(29) E. Wicke and H. G. Nernst, *Ber. Bunsenges. Phys. Chem.*, **68**, 224 (1964) (H. G. Nernst, Dissertation, Münster, 1963).

(30) W. Eichenauer, H. Künzig, and A. Pebler, *Z. Metallk.*, **49**, 220 (1958).

ture, as indicated by the experimental results. An approximate estimate of the magnitude of this effect can be made by following Jost[23] in representing the dependence of the activation energy on the lattice distance by

$$E_1 \approx E_2\left(\frac{a_2}{a_1}\right)^u \qquad (15)$$

where E_1 and a_1 are the activation energy and the lattice constant, respectively, at temperature 1; E_2 and a_2 are the corresponding quantities at temperature 2; and u is of the order of magnitude of 10. Using an average temperature of 400° for the results reported here and $\alpha = 11.76 \times 10^{-6}$ for the linear expansion coefficient of Pd, a value of $u \approx 14$ would be required to account for a decrease in activation energy from 5600 at 25° to 5260 at 400°. This seems to be reasonably in agreement with general experience.

There are no reports on hydrogen diffusion in Pd–Ag alloys which could be directly compared with the results presented here. Around room temperature (0 to 90°), however, a few contradictory data on hydrogen diffusion in Pd–Ag alloys at low hydrogen concentrations do exist.[14,15,17] Küssner,[17] for example, found a large decrease in values of D_0 at a constant activation energy of 5700 cal when the Ag content was increased from 25 to 50%. In comparison, Holleck and Wicke[14] reported at low hydrogen concentration only a small change in hydrogen diffusion coefficents for Pd and Pd-rich alloys, as suggested by the present investigation. It should be noted, however, that there seem to be significant differences in the hydrogen diffusion behavior at high hydrogen concentrations.[14,15]

In a recent publication, Bersier and Küssner[31] reported on the concentration dependence of hydrogen diffusion coefficients in $Pd_{0.77}Ag_{0.23}$ from 30 to 280°. Their results at very low hydrogen concentration were represented by $D = 5.1 \times 10^{-4} \exp(-4440/RT)$. This activation energy seems to be quite low compared with 5500 cal interpolated from results reported here. Furthermore, they found a very strong concentration dependence in D at very low hydrogen concentrations. In the present work, no indication of such behavior could be detected.

Hydrogen Solubility. Hydrogen solubility in Pd and Pd alloys has been the subject of many investigations,[32] and a model has been developed allowing a quantitatively satisfactory interpretation for the isotherms.[31,33–35] Here we will discuss only the hydrogen solubility at very small concentrations as reflected in Sieverts' constant K (see eq 13). Such values are given in Table IV. They were obtained by a least-squares fit of $\log K$ against $1/T$. In the case of Pd, they were calculated with and without the two measurements above 600°. The numbers of data points are, in all cases, quite small, however. If one disregards the measurements above 600°, there is a reasonably good agreement between Sieverts' values and the results given here. With the Pd–Ag alloys, the discrepancy is somewhat larger, showing, however, the same general trend.

Table IV: Heats and Entropies of Desorption for Hydrogen in Pd and Pd–Ag Alloys Calculated from Solubility Data

	ΔH_{H_2}, cal/g-atom	ΔS_{H_2}, cal/deg g-atom	T, °C	
Pd	3522	21.2	200–800	Sieverts[6]
	3912	23.1	200–600	
Pd	3328	22.4	300–800	Sieverts and Zapf[7]
	3790	23.1	300–600	
$Pd_{0.9}Ag_{0.1}$	5000	23.5	317–822	Sieverts[9]
$Pd_{0.6}Ag_{0.4}$	7700	25.1	221–621	
$Pd_{0.5}Ag_{0.5}$	6400	25.8	221–822	

Brodowsky and Poeschel[35] have reported on hydrogen in Pd–Ag alloys at temperatures of 0 to 175°. They find similarly increasing values for the heat of desorption from 4500 cal/mol of H_2 for Pd[29] to 11660 cal/mol of H_2 for $Pd_{0.6}Ag_{0.4}$ at $n \to 0$. Besides the fact that the values are generally higher, there seems to be a larger increase with rising Ag content. The ΔS_{H_2} values were found to rise from 25.1 for Pd[29] to 31.4 cal/deg mol of H_2 for $Pd_{0.6}Ag_{0.4}$, compared to only a slight change in the present investigation.

It is, however, reasonable to assume that the heat of hydrogen desorption from Pd will change with temperature. An estimate of the magnitude and direction of this effect can be obtained in the following way. The heat of desorption at temperature, T_2, is given by

$$\Delta H_{H_2}(T_2) = \Delta H_{H_2}(T_1) + \int_{T_1}^{T_2} \Delta c_p dT \qquad (16)$$

For Δc_p we will consider only hydrogen, since the heat capacity of Pd for pure Pd and for PdH ($n_H \to 0$) will not differ significantly. Therefore

$$\Delta c_p = c_{pH_2} - 2c_{pH\,abs} \qquad (17)$$

The heat capacity of hydrogen gas can be expressed by

$$c_{pH_2} = 6.947 - 0.2 \times 10^{-2}T + 4.8 \times 10^{-7}T^2 \qquad (18)$$

To arrive at a value for $c_{pH\,abs}$ we regard hydrogen in Pd as an Einstein oscillator with $\nu_H = 16.9 \times 10^{12}$ sec^{-1} (determined for the α phase by neutron scattering experiments). At relatively high temperatures, the heat capacity for a solid is

(31) J. Bersier, A. Küssner, 2es Journeés Internationales d'Etude des Piles a Combustible.

(32) F. A. Lewis, "The Palladium Hydrogen System," Academic Press, New York, N. Y., 1967.

(33) J. W. Simons and T. B. Flanagan, *Can. J. Chem.*, **43**, 1665 (1965).

(34) H. Brodowsky, *Z. Physik. Chem.*, (Frankfurt am Main), **44**, 129 (1965).

(35) H. Brodowsky and E. Poeschel, *ibid.*, **44**, 143 (1965) (E. Poeschel, Dissertation, Münster 1964).

$$c_{\mathrm{pH\ abs}} = 3R\left[1 - \frac{1}{12}\left(\frac{\theta}{T}\right)^2\right] \qquad (19)$$

From eq 17 through 19, and for $\theta = h\nu_H/k = 812$, $T_1 = 298°K$, and $T_2 = 673°C$, one obtains for the integral in eq 16 a value of -636 cal/mol of H_2. This compares favorably with a difference of -500 cal/mol of H_2 from heats of hydrogen desorption experimentally determined for an average temperature of 400° (4000 cal/mol H_2) and 25° (4500 cal/mol H_2).

It is interesting to note that the values for K calculated from hydrogen equilibrium measurements in Pd by Gillespie and Galstaun[8] (at 200 to 313°) fit exactly between the extrapolations from high and low temperatures. This suggests that there is a continuous decrease in the heat of desorption with increasing temperature, similar to the activation energy for hydrogen diffusion.

Inhibitions at the Membrane–Gas Interface. In a recent publication,[36] Wicke and Meyer discussed extensively the reactions occurring at the Pd–gas interface during hydrogen permeation. They showed that inhibition is present even at an interface activated by a cover of Pd black. The effect of such inhibition on the diffusion and solubility results reported above may be determined as follows. At the presence of an inhibition at the interface, the hydrogen pressure at the entering side, P_1, will be larger than the equilibrium pressure, P_{1e}: $P_1 = P_{1e} + \Delta P_1$. The hydrogen pressure at the exit side, P_2, will be smaller than the equilibrium pressure, P_{2e}: $P_2 = P_{2e} - \Delta P_2$. From eq 7 and 8, we obtain for the hydrogen flux through the membrane

$$J = \frac{D}{V_{\mathrm{Me}} s K}[(P_{1e})^{1/2} - (P_{2e})^{1/2}] \quad (\mathrm{mol\ of\ H/cm^2\ sec})$$

which can be written

$$\left(\frac{P_1}{J}\right)^{1/2}\left(1 - \frac{\Delta P_1}{P_1}\right)^{1/2} = \frac{K V_{\mathrm{Me}} s}{D} J^{1/2} + \left(\frac{P_2 + \Delta P_2}{J}\right)^{1/2} \qquad (20)$$

Plots of $(P_1/J)^{1/2}$ *vs.* $J^{1/2}$ at a given temperature showed a linear relationship, with an intercept $A = [(P_2 + \Delta P_2)/J]^{1/2}$. From values of A, the pressure difference due to the interface inhibition at the low-pressure side of the membrane, ΔP_2, can be easily obtained

$$\Delta P_2 = A^2 J - P_2$$

The actual values of A were dependent on the individual activation and ranged between 0.5×10^3 to 2×10^3, with a majority of samples yielding values of 0.6×10^3 to 1×10^3. At the same membrane, values of A decreased slightly with increasing temperature, often showing a minimum at approximately 400°. The slight increase at 600° could be due to sintering of the activating Pd black layer. Thus, values of ΔP_2 ranged approximately from 0 to 2 Torr, depending on sample activity and hydrogen flux. Assuming the same values for ΔP_1, it can easily be seen that the factor $\Delta P_1/P_1$ in eq 20 becomes small compared with 1 at larger values of P_1, and can then be neglected. If we take into account the inhibition at the interface, we find values of D which are approximately up to 5% higher than those reported above. However, this is still within the limits of experimental error. There is practically no change in the energy of activation for hydrogen diffusion, since the slight decrease in values of A is compensated by an increase in J. Also, there will be practically no change in values of K (eq 9), since the increase in values of D is nearly compensated by a decrease in the values of the term $[(P_{1e})^{1/2} - (P_{2e})^{1/2}]$.

Acknowledgment. The author is grateful to Dr. A. C. Makrides for initiating this research. The author wishes to thank Mr. S. Michalik for preparing the Pd–Ag alloys.

(36) E. Wicke and K. Meyer, *Z. Phys. Chem.*, (Frankfurt am Main), **64**, 225 (1969).

The Crystal Structure of *cis*-1,2-Cyclohexanedicarboxylic Acid

by Ettore Benedetti,[1a] Carlo Pedone,[1a] and Giuseppe Allegra[1b]

Chemistry Department and the Polymer Research Institute of the Polytechnic Institute of Brooklyn, Brooklyn, New York 11201 *(Received July 7, 1969)*

cis-1,2-Cyclohexanedicarboxylic acid, $C_8H_{12}O_4$, crystallizes in the triclinic system, space group $P\bar{1}$, with a = 6.93, b = 10.95, c = 6.38 Å and α = 108°3′, β = 114°51′, γ = 90°16′ and two molecules per unit cell. The structure has been solved by joint application of the symbolic addition procedure and the method based on the maximum probability described by Allegra and Valle, which maximizes the $\Pi(s_1, s_2, s_3, \ldots)$ function. The structure has been refined to an R factor of 0.056 for 1505 independent reflections measured by counter techniques (Cu Kα). One of the two carboxyl groups is in the axial, the other in the equatorial position relative to the cyclohexane ring. The observed conformation of this molecule is compared with that recently given for the *trans* isomer.

Introduction

Contrary to the case of *trans*-1,2-cyclohexanedicarboxylic acid [2a,b] (TCDA), the molecule of the *cis*-1,2-isomer (CCDA) does not possess intrinsic chirality.[3,4] Assuming the cyclohexane ring to be in the usual chair form, two equivalent molecular conformations are possible, mutually mirror images which bear one group in the axial and the other in the equatorial position.

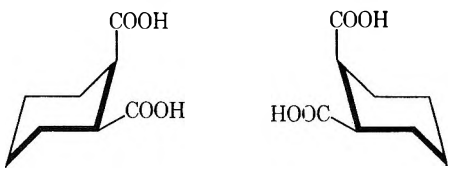

The investigation of the effect of the axial carboxylic group on the conformation of the ring seems particularly interesting to us, especially in view of the possibility of comparing the results with the accurate structural data recently obtained by some of us for both the racemic and the optically active *trans* forms.[2] It is for these reasons that, in the context of our structural studies on dicarboxylic acids,[5-8] we have undertaken a detailed single crystal X-ray investigation on CCDA.

Experimental Section

Single crystals of *cis*-1,2-cyclohexanedicarboxylic acid, $C_8H_{12}O_4$ (water, mp 193–196° dec), suitable for X-ray diffraction analysis were kindly prepared for us by T. Furujama. Preliminary Weissenberg photographs taken with Cu Kα radiation indicate the triclinic system. The crystal chosen for the investigation was centered on a Picker four-circle automated diffractometer equipped with a PDP-8 digital computer. The unit cell parameters were determined from a least-squares fitting of the setting angles (2θ, ω, χ) of twelve high angle reflections ($2\theta > 90°$). The parameters obtained are reported in Table I. The density calculated on the basis of two molecules per unit cell (mol wt = 172.18) is 1.38 g/cm³.

Table I: Unit Cell Dimensions

cis-1,2-Cyclohexanedicarboxylic Acid, $C_8H_{12}O_4$, Mol wt = 172.18
Triclinic, space group $P\bar{1}$, Z = 2, $F(000)$ = 184

a = 6.930 ± 0.003 Å	α = 108°3′ ± 10′
b = 10.947 ± 0.005 Å	β = 114°51′ ± 10′
c = 6.377 ± 0.002 Å	γ = 90°16′ ± 10′
d_{calcd} = 1.38 g/cm³	

Integrated intensities were measured with the θ–2θ scan mode using Ni-filtered Cu Kα radiation (λ 1.5418 Å), pulse height analysis to reduce unwanted background, and a scintillation counter. A scan range of 2.0° was found to be sufficient in the range of 2θ examined (0–130°) with a scan speed of 1°/min. The take-off angle of the tube was 3.0° and a counter aperture, 4.0 × 4.0 mm, was placed 30 cm from the crystal. Two stationary crystal, stationary counter background counts of 10 sec were taken at the two ends of each scan. A total of 1505 nonzero independent reflections was collected. One standard reflection was measured every 20 reflections (every 50 min) during data collection in order to check the electronic stability of the instrument and any deterioration of the crystal.

(1) (a) Universita' di Napoli, Istituto Chimico, Napoli, Italy. (b) Visiting Professor from the Istituto di Chimica Industriale del Politecnico di Milano, Milano, Italy.

(2) (a) E. Benedetti, P. Corradini, C. Pedone, and B. Post, *Chem. Comm.*, 1626 (1968); (b) E. Benedetti, P. Corradini, and C. Pedone, *J. Amer. Chem. Soc.*, **81**, 4075 (1969).

(3) R. S. Cahn, C. K. Ingold, and V. Prelog, *Experientia*, **12**, 81, (1956).

(4) R. S. Cahn, C. K. Ingold, and V. Prelog, *Angew. Chem. Int. Ed.*, **5**, 385 (1966).

(5) P. Corradini, P. Ganis, C. Pedone, and G. Diana, *Makromol. Chem.*, **61**, 242 (1963).

(6) E. Martuscelli, E. Benedetti, P. Ganis, and C. Pedone, *Acta Cryst.*, **23**, 747 (1967).

(7) P. Ganis, A. Panunzi, and C. Pedone, *Ric. Sci.*, **28**, 801(1968).

(8) G. Allegra, E. Benedetti, and C. Pedone, *Acta Cryst.*, **A25**, Part S3, S136 (1969).

Table II: Final Atomic Parameters

A. Positional Parameters

Atom	*x/a*	*y/b*	*z/c*
C1	0.0645 (4)	0.1565 (2)	−0.5489 (5)
C2	0.0873 (4)	0.2418 (2)	−0.2938 (5)
C3	−0.1276 (4)	0.2893 (3)	−0.3192 (5)
C4	−0.2061 (5)	0.3592 (3)	−0.5042 (5)
C5	−0.2271 (5)	0.2722 (3)	−0.7550 (5)
C6	−0.0149 (4)	0.2254 (3)	−0.7375 (5)
C7	0.2703 (4)	0.3539 (2)	−0.1698 (5)
C8	0.2644 (4)	0.0955 (2)	−0.5255 (5)
O1	0.2900 (3)	0.4291 (2)	0.0458 (4)
O2	0.3899 (3)	0.3716 (2)	−0.2557 (3)
O3	0.3036 (5)	0.0683 (3)	−0.7156 (4)
O4	0.3730 (4)	0.0678 (3)	−0.3412 (4)
H1(C1)[a]	−0.053 (5)	0.066 (3)	−0.619 (6)
H1(C2)	0.128 (5)	0.192 (3)	−0.167 (6)
H1(C3)	−0.112 (5)	0.341 (3)	−0.159 (7)
H2(C3)	−0.258 (5)	0.198 (3)	−0.396 (6)
H1(C4)	−0.095 (5)	0.442 (3)	−0.444 (6)
H2(C4)	−0.363 (5)	0.381 (3)	−0.532 (6)
H1(C5)	−0.254 (6)	0.326 (4)	−0.868 (7)
H2(C5)	−0.351 (6)	0.180 (4)	−0.828 (7)
H1(C6)	0.103 (5)	0.303 (3)	−0.686 (6)
H2(C6)	−0.036 (5)	0.163 (3)	−0.898 (7)
H1(O1)	0.421 (6)	0.030 (4)	−0.693 (7)
H1(O3)	0.385 (6)	0.489 (4)	0.098 (7)

B. Anisotropic Thermal Parameters[b] × 10^4

Atom	β_{11}	β_{22}	β_{33}	β_{12}	β_{13}	β_{23}
C1	164 (7)	54 (2)	237 (9)	19 (3)	97 (6)	17 (4)
C2	164 (7)	57 (2)	225 (9)	18 (3)	96 (6)	25 (4)
C3	182 (7)	77 (3)	281 (11)	36 (3)	129 (7)	40 (4)
C4	224 (8)	97 (3)	338 (12)	69 (4)	138 (8)	70 (5)
C5	217 (9)	129 (4)	292 (12)	78 (5)	106 (8)	81 (5)
C6	198 (7)	86 (3)	238 (11)	36 (4)	100 (7)	41 (5)
C7	166 (7)	57 (2)	213 (9)	27 (3)	68 (7)	19 (4)
C8	175 (7)	46 (2)	265 (11)	5 (3)	105 (7)	5 (4)
O1	254 (6)	91 (2)	286 (8)	−15 (3)	150 (6)	−28 (3)
O2	207 (6)	81 (2)	275 (8)	−15 (2)	129 (6)	1 (3)
O3	264 (7)	120 (2)	339 (8)	81 (3)	183 (6)	54 (4)
O4	247 (6)	98 (2)	316 (8)	73 (4)	138 (6)	62 (4)

[a] H*n*(X*m*) stands for hydrogen number (*n*) bonded to X(*m*). [b] Temperature factor in the form $T = \exp[-(\beta_{11}h^2 + \beta_{22}k^2 + \beta_{33}l^2 + 2\beta_{12}hk + 2\beta_{13}hl + 2\beta_{23}kl)]$. The esd are given in parentheses in units of the last significant digit.

The fluctuation in the intensity of this reflection was within 3% over the data collection time (62 hr). The integrated intensities from which the background counts were subtracted were then corrected for Lorentz and polarization effects in the usual way.

Structure Determination and Refinement

Assuming the triclinic space group to be the centrosymmetric $P\bar{1}$, the structure of CCDA has been solved *via* joint application of two different direct methods: the symbolic addition procedure[9] and the maximum probability method based on the maximization of the Π (s_1, s_2, s_3, . . .) function[10,11] derived from an expression of the sign probability distribution proposed by one of us.[12] The symbolic addition procedure was applied to all the reflections with $|E| > 1.5$, starting with the attribution of 7 basic symbols to some of the strongest reflections; four most probable sign combinations were obtained. The maximization of the Π (s_1, s_2, s_3, . . .) function, taking 24 basic signs, three of which were fixed in order to fix the origin of the unit cell, gave 16 sign combinations having the same (maximum) Π value. They could be grouped into four sets, each made up of four similar combinations, *i.e.*, differing only in few signs (3–5). We took into consideration only the signs in common to the four combinations of each

(9) I. L. Karle and J. Karle, *Acta Cryst.*, **17**, 1356 (1964).

(10) G. Allegra and S. Valle, *ibid.*, **B25**, 107 (1969).

(11) A. Braibanti, A. M. Manotti Lanfredi, A. Tiripicchio, and F. Logiudice, *ibid.*, **B25**, 93, (1969).

(12) G. Allegra, *ibid.*, **19**, 949, (1965).

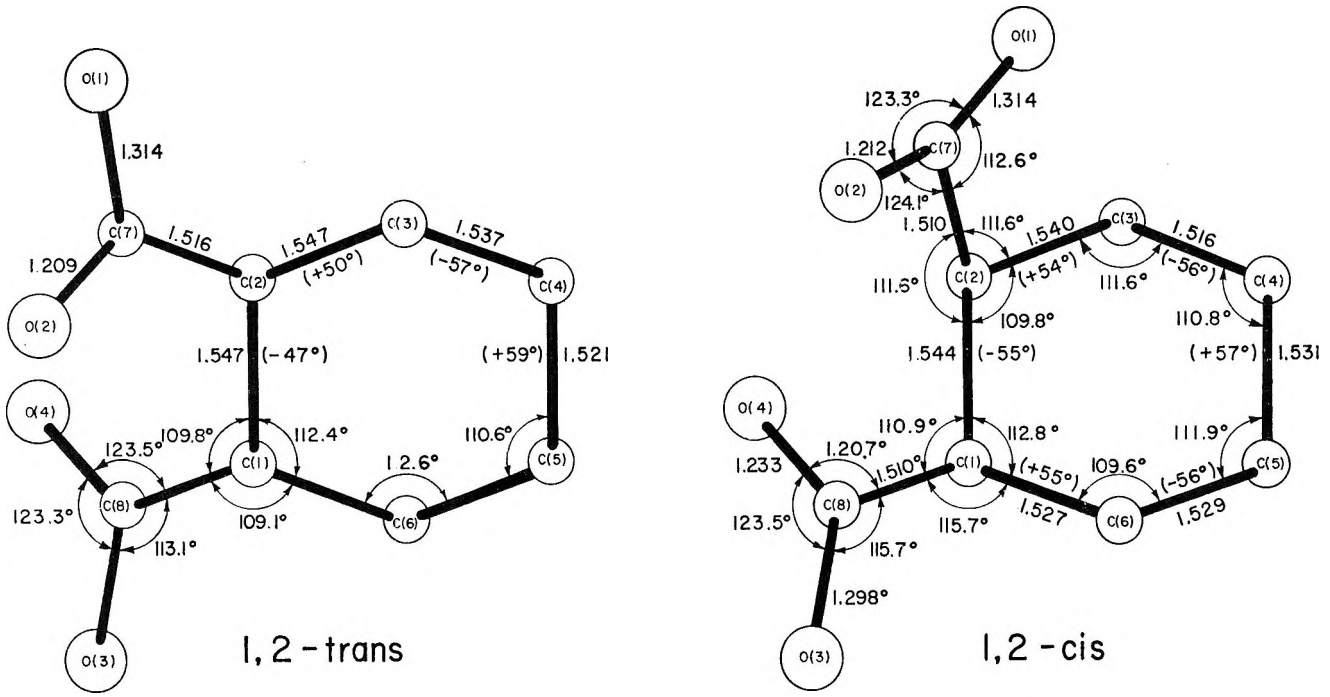

Figure 1. Comparison of the molecular models of the 1,2-*trans* and 1,2-*cis*-cyclohexanedicarboxylic acids. Bond lengths and bond angles of both molecules are indicated; their average estimated standard deviations are 0.004 Å and 0.3°, respectively. The internal rotation angles which define the ring conformation are also reported in parentheses. In the *cis* isomer the C(7)O(1)O(2) carboxyl group is in axial position.

set. The four resulting sets of signs were found to correspond to the four solutions obtained by the symbolic addition procedure. One of these sets contained only positive signs and was therefore discarded; three Fourier syntheses were then evaluated in correspondence of the other sets. Twelve well resolved peaks of approximately equal weights were obtained only with one of the three sets of signs; accordingly, a reasonable molecular conformation could be easily derived and the expected hydrogen-bond system between facing carboxyl groups across symmetry centers was clearly recognized. The structure was then refined through a total of 12 least-squares cycles;[13a] anisotropic thermal factors were assigned to all nonhydrogen atoms only after the sixth cycle, when the R disagreement factor ($= \Sigma||F_c| - |F_o||/\Sigma|F_o|$) was 0.16. All the hydrogen atoms were clearly detected from a difference Fourier synthesis and introduced in the last two cycles, where their positional parameters were allowed to vary, assuming isotropic thermal factors equal to the average of the B_{ii}'s of the carrier atom. The final value of the R factor is 0.056 for the 1505 observed reflection with unit weight. The list of the resulting fractional coordinates and thermal factors is given in Table II.[13b]

Discussion of the Structure

The bond lengths and angles for the nonhydrogen atoms are reported in Figure 1, where, for sake of comparison, the corresponding data for the *trans*-1,2 isomer (racemic form)[1] are also given. The range of 10 independent C–H bond lengths is 1.05 ± 0.10 Å, while that of the O–H bond lengths is 0.87 ± 0.05 Å. Ranges of the C–O–H, H–C–H, and H–C–C bond angles are 109 ± 2°, 111 ± 5°, and 108 ± 4°, from 2, 4, and 22 independent measurements, respectively.

The internal rotation angles which define the ring conformation are also given, in parentheses, in Figure 1. The two isomers show a significant difference in the ring rotation angle around C1–C2, which is larger for the *cis* compound (55.1 ± 0.3° *vs.* 47.0 ± 0.3°). In our opinion, this reflects the tendency to keep the two carboxyl groups as far apart as possible; in the *trans* isomer this is obtained through a decrease of the rotation angle around C1–C2, with respect to the average value (54.3° for the two forms). In the *cis* isomer, for the same reason we should expect an increase of the same rotation angle; this is not observed, however, and the reason is probably due to the tendency to keep in a proper balance the (carboxyl$_{axial}$–carboxyl$_{equatorial}$) and the (carboxy$_{axial}$–ring) nonbonded interactions. As a result, the geometry of the ring is more uniform in the *cis* isomer.

(13) (a) A complete set of crystallographic FORTRAN IV programs written by A. Immirzi (*Ric. Sci.*, 37, 846, 850, 743 (1967)), was used. All the computations were carried out at the Computer Center of the Polytechnic Institute of Brooklyn (IBM 360/50). (b) A list of the observed and calculated structure factors has been deposited as document number NAPS-00530 with the ASIS National Auxiliary Publication Service, c/o CCM Information Corp., 909 3rd Ave., New York, N.Y., 10022. A copy may be obtained by citing the document number and by remitting $1.00 for microfiche or $3.00 for photocopies. Advance payment is required. Make checks or money orders payable to ASIS–NAPS.

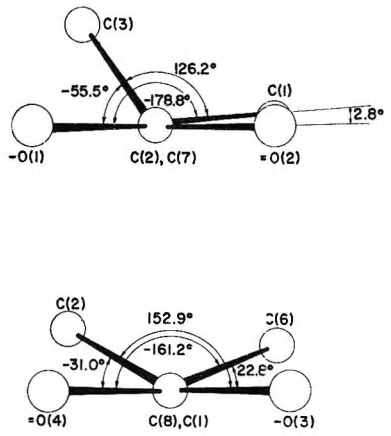

Figure 2. Conformations of the carboxyl groups: top, $-C\begin{smallmatrix}01\\ \diagup\\ \\ \diagdown\\ 03\end{smallmatrix}$ (axial), bottom, $-C\begin{smallmatrix}03\\ \diagup\\ \\ \diagdown\\ 04\end{smallmatrix}$ (equatorial). The average estimated standard deviation of the internal rotation angles reported is 1°.

As shown in Figure 2, only the C=O bond of the axial carboxyl group is found to be in the preferred *syn*-planar conformation with respect to a C_α–C_β bond,[14] while the equatorial group adopts a quasi-symmetrical orientation. It is interesting to observe that a rather analogous orientation for both carboxyl groups has been found by Burgi and Dunitz[15] in the case of *cis*-1,2-cyclooctanedicarboxylic acid. In our case, the deviation of one carboxyl group from the *syn*-planar conformation can be attributed to the need of relaxing the O(2)···O(4) intramolecular contact (exptl, 3.19 Å).

In Table III the parameters concerning the intermolecular hydrogen bonds are reported, while Table IV is a summary of the internal rotation angles. Of the two crystallographically independent pairs of facing carboxyl groups, the atoms belonging to the axial one are very closely coplanar. The equation

Table III: Hydrogen Bond Parameters[a]

O1...O2*	2.669 (3) Å	
H1(O1)...O2*	1.86 (4) Å	
O3...O4*	2.656 (3) Å	
H1O3...O4*	1.77 (4) Å	
C7–O2...H1O1*		122.8°
C7–O2...O1*		124.9° (0.5°)
O1–H1(O1)...O2*		173.3°
H1(O1)–O1...O2*		4.6°
C8–O4...H1(O3)*		126.7°
C8–O4...O3*		126.1° (0.5°)
O3–H1(O3)...O4*		173.8°
H1(O3)–O3...O4*		4.1°

[a] The atoms labeled with an asterisk are symmetry related to those of the independent structural unit.

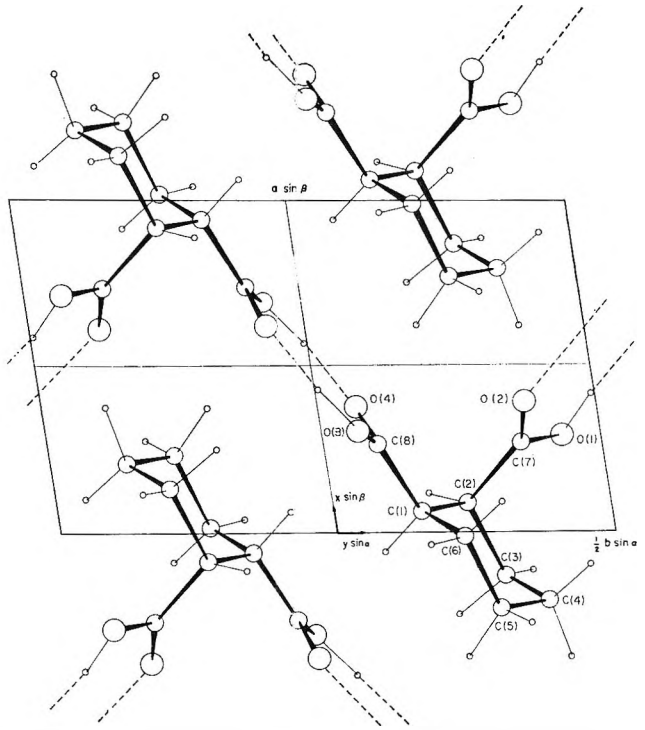

Figure 3. Molecular packing of *cis*-1,2-cyclohexanedicarboxylic acid as viewed along [001]. The labeling of the hydrogen atoms may be easily derived from Table II.

Table IV: Internal Rotation Angle[a]

C1–C2–C3–C4	+54.9° (3)
C2–C3–C4–C5	−56.3° (3)
C3–C4–C5–C6	+56.9° (4)
C4–C5–C6–C1	−55.6° (3)
C5–C6–C1–C2	+55.4° (3)
C6–C1–C2–C3	−55.1° (3)
C8–C1–C2–C7	−62.4° (3)
C8–C1–C6–C5	+175.4° (3)
C8–C1–C2–C3	−173.2° (2)
C7–C2–C3–C4	−69.4° (2)
C7–C2–C1–C6	+69.2° (3)
O1–C7–C2–C1	−178.8° (5)
O1–C7–C2–C3	−55.5° (3)
O2–C7–C2–C1	+2.8° (5)
O2–C7–C2–C3	+126.2° (3)
O3–C8–C1–C2	+152.9° (2)
O3–C8–C1–C6	+22.8° (3)
O4–C8–C1–C2	−31.0° (3)
O4–C8–C1–C6	−161.2° (2)

[a] Defined as the dihedral angles between the planes containing the first three and the last three atoms of the sequence. We assume the *trans* conformation equal to 180°.

of the corresponding least-squares plane through (C–C$\begin{smallmatrix}O\\ \diagup\\ \\ \diagdown\\ O\end{smallmatrix}$) and the centrosymmetrical atoms is

(14) J. D. Dunitz and P. Strickler, *Helv. Chim. Acta*, **49**, 2505 (1966); "Structural Chemistry and Molecular Biology," A. Rich and N. Davidson, Ed., W. H. Freeman and Co., San Francisco, Calif., 1968, p 595.

(15) H. B. Burgi and J. D. Dunitz, *Helv. Chim. Acta*, **51**, 1514 (1968).

$$-0.4773x + 0.7567y - 0.4187z - 2.4880 = 0$$

referred to the crystallographic axes (x, y, and z in Å), the root-mean-square displacement of the atoms from this plane being 0.016 Å. The symmetry related equatorial carboxyl groups deviate appreciably from planarity (rms distance 0.080 Å); the equation of the corresponding least-squares plane is

$$0.4740x + 0.7746y - 0.0883z - 1.9238 = 0$$

However, the rms displacement of the four atoms of the equatorial carboxyl group from their average plane is much lower (0.011 Å). Figure 3 shows a view of the molecular packing along (001); the rows of hydrogen-bonded molecules extend along the b direction (*ti* symmetry[16]). The shortest intermolecular contacts between nonhydrogen atoms are 3.38 and 3.86 Å for C··O and C··C, respectively, to be compared with the corresponding sums of the van der Waalss radii of the oxygen (1.4 Å) and of the hydrogen-screened carbon atom (2.0 A).[17]

Acknowledgment. We wish to thank Professors M. Goodman and C. Overberger for their constant interest in this work and Dr. T. Furujama, who kindly prepared the compound. We also gratefully acknowledge the support of research grants from the National Science Foundation (GB 7558) and the National Institutes of Health (GM 08974).

(16) P. Corradini, *Acc. Natl. Lincei*, **24**, 8 (1960).

(17) L. Pauling, "The Nature of the Chemical Bond," Cornell University Press, Ithaca, N. Y., 1960, Chapter 7.

Antagonistic Interactions between Copper Sulfate and Tetra-*n*-butylammonium Salts in Water at 25°

by Joseph Steigman[1] and Mario Della Monica

Department of Chemistry, Polytechnic Institute of Brooklyn, Brooklyn, New York 11201 *(Received July 22, 1969)*

The absorbance at 250 mμ of 0.02 *M* copper sulfate in water at 25°, which is largely due to ion pairs, decreases steadily in increasingly concentrated solutions of sodium ethanesulfonate. With tetra-*n*-butylammonium ethanesulfonate, the absorbance of 0.02 *M* $CuSO_4$ decreases slightly with increasing ethanesulfonate concentration, passes through a shallow minimum near 0.2 *M*, and then increases, exceeding in 0.4 *M* sulfonate the value in water alone. A conductivity study showed that the effect of the quaternary ammonium salt was not due to its own extensive ion-pair formation. A spectrophotometric study of the spectrum of the mixed solution from 350 to 250 mμ, compared with that of copper sulfate alone, indicated that there was no large medium effect of the quaternary ammonium salt on the $CuSO_4$ ion-pair spectrum. It was concluded that the effect was caused by the antagonism between the structure of the hydrogen-bonded water cages surrounding the organic cations and that of the charge-oriented water dipoles surrounding the sulfate ions. There was an increased escaping tendency on the part of each electrolyte, resulting in an increased yield of $CuSO_4$ ion pairs. Calculations of the mean activity coefficient of $CuSO_4$ in the various solutions supported this hypothesis. It was found that sodium chlorate and tetra-*n*-butylammonium chlorate behaved like the corresponding ethanesulfonates toward $CuSO_4$. Similar effects noted with the two bromides were partially obscured by interference of the $CuBr^+$ complex.

Introduction

The concept of antagonistic and cooperative electrolytes was developed in a previous article.[2] There it was reported that the solubility of $CaSO_4$ at 25° decreased below the value in water in the presence of moderately concentrated tetra-*n*-butylammonium bromide. The same effect was found for tetra-*n*-butylammonium perchlorate in the presence of added sodium sulfate. It was attributed to the mutually incompatible or antagonistic water structures surrounding the organic cation and the sulfate ion. Hydrogen-bonded water cages are believed to be stabilized around the larger quaternary ammonium ions.[3] There is a different and incompatible dipole orientation in the water molecules surrounding a water-structure former such as sulfate ion. In a mixture of antagonistic salts, each electrolyte

(1) To whom inquiries should be addressed.

(2) J. Steigman and J. Dobrow, *J. Phys. Chem.*, **72**, 3424 (1968).

(3) H. S. Frank and W. Y. Wen, *Discussions Faraday Soc.*, **24**, 133 (1957).

raises the escaping tendency of the other, producing an observable decrease in solubility for the less soluble salt of the pair.

The present paper describes a study of a similar effect in homogeneous aqueous solution. The absorptivity coefficient in the uv of ion pairs of copper sulfate is considerably greater than that of hydrated copper(II).[4] Spectrophotometric measurements were made on aqueous $CuSO_4$ solutions containing tetra-*n*-butylammonium ethanesulfonate ($(n\text{-}C_4H_9)_4NC_2H_5SO_3$, referred to as Bu_4NETS), tetra-*n*-butylammonium chlorate (Bu_4NClO_3), and tetra-*n*-butylammonium bromide (Bu_4NBr). The results were compared with those of solutions containing $CuSO_4$ and the corresponding sodium salts.

Experimental Section

A. Chemicals. $CuSO_4$ was a Baker and Adamson high-purity material which was recrystallized twice from water. A concentrated stock solution was analyzed by electrogravimetry. NaBr, Baker and Adamson reagent greade, was recrystallized twice from water and dried in a vacuum oven at 100°. Bu_4NBr, Southwestern Analytical Chemicals, polarographic grade, was recrystallized twice from ethyl acetate–diethyl ether and dried *in vacuo*. NaETS was prepared by potentiometric titration of aqueous ethanesulfonic acid (Eastman Kodak) with NaOH, removing water *in vacuo*, recrystallizing three times from methanol, and drying *in vacuo* at 60°. Bu_4NETS was similarly prepared with tetra-*n*-butylammonium hydroxide (1 *M*, Southwestern Analytical Chemicals, polarographic grade), removing water *in vacuo*, recrystallizing twice from ethanol–diethyl ether, and drying *in vacuo*. $NaClO_3$, Baker and Adamson reagent grade, was recrystallized from water and vacuum-dried at 80°. Bu_4NClO_3 was prepared in concentrated aqueous solution by neutralizing aqueous chloric acid with Bu_4NOH. In turn, the chloric acid was prepared by passing $NaClO_3$ solution through an Amberlite IR-120 column in the acid form. The concentrated Bu_4NClO_3 solution (1 *M*) was used as the stock for more dilute solutions. $Cu(ClO_4)_2$ was a purified sample for which we thank Professor S. Petrucci of this department.

B. Equipment and Experimental Procedures. Spectrophotometric measurements were made at 25° on a Beckman DU spectrophotometer, usually at 250 mμ, with a 0.4-mm slit opening, in 1- or 5-cm quartz cells. Samples were prepared by dilution from stock solutions and were run against water. Those which contained 0.1 *M* added salt or higher concentrations were measured against salt solutions of the same concentration as reference. Sufficient concentrated acid (either HETS or $HClO_3$) was added from a Digi-pet to all solutions to repress hydrolysis of Cu(II). Solution resistances were measured to ±0.1% with an Industrial Instruments conductance bridge (RC18) in a Daggett–Kraus cell,[5] which was maintained at 25.000 ± 0.005° in a thermostated oil bath. The cell constant was 0.27985. Measurements were made at 3000 cps. No effect of frequency change was observable down to 1000 cps. A stock solution of salt was prepared by weighing both salt and water. Successive dilutions were carried out by adding known weights of the preceding solution to a known weight of water. The conductivity of the distilled water (7×10^{-7} ohm^{-1} cm^{-1}) was subtracted from the conductivity of each solution. In calculations of Λ, the equivalent conductivity, it was assumed that the densities of the various solutions were the same as that of pure water at 25°, since they were quite dilute.

Results and Discussion

Figure 1 shows the absorbance at 250 mμ of 0.02 *M* $CuSO_4$ solutions containing different concentrations of NaETS and of Bu_4NETS plotted against the concentration of added salt. It is not possible to find a uv absorption band in $CuSO_4$ solutions of this concentration, and previous workers have measured solution absorbances at a fixed wavelength, near or at 250 mμ.[4,6-8] The ethanesulfonate salts were used in the present work because they are transparent in the uv region of interest, and the anion most probably does not complex with Cu(II). Perchlorates could not be used because the tetra-*n*-butylammonium salt has a limited solubility (0.01 *M*) at 25°.[2] Nitrate ion absorbs in the uv, fluoride ion in acid solution may attack the quartz cells, and chloride and bromide form complexes with Cu(II) which absorb strongly near 250 mμ.

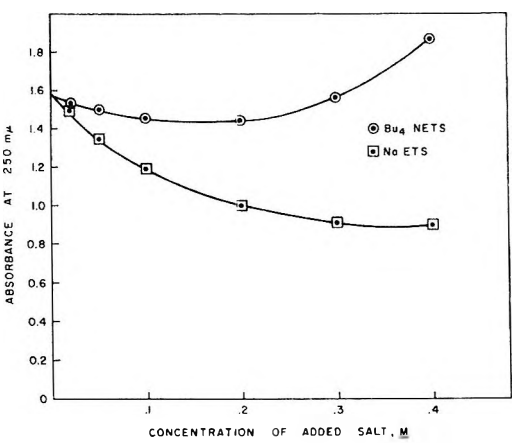

Figure 1. Absorbance of 0.02 *M* $CuSO_4$ at 250 mμ in solutions of NaETS and of Bu_4NETS, plotted against the molar concentration of added salt.

(4) W. D. Dale, E. W. Davis, and C. B. Monk, *Trans. Faraday Soc.*, **52**, 816 (1956).

(5) H. M. Daggett, E. J. Blair, and C. A. Kraus, *J. Amer. Chem. Soc.*, **73**, 799 (1951).

(6) W. G. Davies, R. J. Otter, and J. E. Prue, *Discussions Faraday Soc.*, **24**, 103 (1957).

(7) R. A. Matheson, *J. Phys. Chem.*, **69**, 1537 (1965).

(8) P. Hemmes and S. Petrucci, *ibid.*, **72**, 3986 (1968).

Chlorate was a possible counterion for extended studies. However, in spite of the fact that Bu_4NClO_3 is soluble in 1 *M* aqueous solution, 0.02 *M* $CuSO_4$ produced a faint opalescence in 0.3 *M* Bu_4NClO_3, and in 0.4 *M* Bu_4NClO_3 a precipitate appeared. The use of chlorate was therefore limited to 0.1 *M* solutions, and the larger part of this investigation was carried out with the ethanesulfonate salts.

It can be seen from the figure that the addition of 0.4 *M* NaETS produces a marked decrease in the absorbance of 0.02 *M* $CuSO_4$, from 1.591 to 0.900. This is caused by the decrease in activity coefficient of Cu(II) and SO_4^{2-} ions, and the dissociation of $CuSO_4$ ion pairs. On the other hand, the absorbance decreases only slightly in the more dilute Bu_4NETS solutions, passing through a minimum near 0.2 *M*, and increasing to 1.843 in 0.4 *M* added salt. This could be due to three factors: a medium effect of the Bu_4N^+ ion on the spectrum of the $CuSO_4$ ion pairs, extensive ion-pair formation of Bu_4NETS (requiring a stoichiometric formation constant greater than 300 in the most concentrated solutions), or the antagonistic interactions between Bu_4N^+ and SO_4^{2-} ions which were described earlier.

If there were a medium effect of the quaternary ammonium ions on the spectrum of the $CuSO_4$ ion pairs, one would expect that there would be changes in the absorptivity coefficients at different wavelengths. The absorbance of an approximately 0.02 *M* $CuSO_4$ solution was measured at 10-mμ intervals from 350 to 240 mμ with a 0.4-mm slit. A solution of 0.02 *M* $CuSO_4$ in 0.3 *M* Bu_4NETS (measured against 0.3 *M* Bu_4NETS) was adjusted in $CuSO_4$ concentration so that the two $CuSO_4$ solutions had identical absorbances (1.700) at 250 mμ. This solution was also measured from 350 to 240 mμ. Above 250 mμ the largest difference in absorbance between the two solutions was 0.005 absorbance unit. At 240 mμ with a wider slit, the difference was 0.050 unit for a value of 2.400. This is not a definite proof of the absence of a medium effect, but shows that the band shape is essentially the same in the two solutions over the spectral range of interest. It is concluded tentatively that if there is such a medium effect, it is small.

The resistances of NaETS and of Bu_4NETS were measured in the approximate concentration ranges 6×10^{-5} to 2.5×10^{-3} *N* and 10^{-4} to 3×10^{-3} *N*, respectively. Successive approximations were used to arrive at the final values of Λ′ in the Fuoss–Onsager equation[9]

$$\Lambda' = \Lambda + Sc^{1/2} - Ec \ln c = \Lambda_0 + J_1 c \qquad (1)$$

In this equation, *c* is the normality of the electrolyte; *S* and *E* are constants; Λ is the experimental equivalent conductivity at concentration *c*; Λ_0 is the limiting equivalent conductivity; and Λ′ is an approximation to it which varies with concentration. It is assumed that the effect of viscosity on the conductivity is unimportant in these solutions, and that there is no ion-pair formation. Table I shows the concentrations and the equivalent conductances of the various solutions. *E* has the values 65.946 and 49.628 for NaETS and Bu_4NETS, respectively; *S* = 80.031 and 72.951.

Table I: Conductance Data for NaETS and Bu_4NETS in H_2O at 25°

$N \times 10^5$	Λ
NaETS	
6.3884	85.779
29.2606	85.131
57.3382	84.558
92.4114	84.058
127.702	83.703
159.056	83.359
183.733	83.125
219.522	82.846
251.038	82.672
Bu_4NETS	
9.6214	54.806
43.9860	53.996
83.3907	53.433
132.642	52.922
184.376	52.465
227.280	52.134
310.191	51.596

Figure 2 shows Λ′ plotted against the normality of the solution for both NaETS and Bu_4NETS. Least-squares calculations gave $\Lambda_0 = 86.45$ for NaETS and $\Lambda_0 = 55.53$ for Bu_4NETS for the two intercepts. The slopes are 254.6 and 168.7 for the respective J_1 values, equivalent to 6 Å and 4.4 Å for the distances of closest approach. The distance value for the quaternary ammonium salt is undoubtedly much too low, but this is probably due to the neglect of viscosity effects.[10] The main conclusion which is drawn from these figures is that there is no evidence for extensive ion-pair formation by Bu_4NETS in water. The conductivity measurements, while they are certainly precise enough to rule out appreciable ion-pair formation, cannot be used to decide whether or not there is a small association constant for Bu_4NETS in water.

It is concluded, therefore, that the effect of Bu_4NETS on the absorbance of 0.02 *M* $CuSO_4$ shown in Figure 1 is due mainly to the antagonistic interactions between the organic cations and SO_4^{2-} anions in water. The incompatibility of the two different types of organized water atmospheres forces each ion to associate with a more compatible counterion. There is thus a demixing

(9) R. M. Fuoss and L. Onsager, *J. Phys. Chem.*, **61**, 668 (1957).

(10) H. S. Harned and B. B. Owen, "The Physical Chemistry of Electrolytic Solutions," Reinhold Publishing Corp., New York, N. Y., 1959, pp 272, 277.

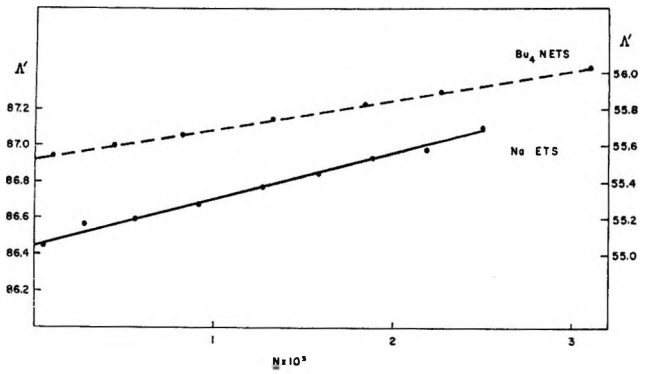

Figure 2. The term A′ for NaETS of the Fuoss–Onsager equation plotted against the normality of NaETS (——) and against that of Bu_4NETS (– – –). Left-hand ordinates are for the sodium salt, and right-hand ordinates are for Bu_4NETS.

of the four ions in solution, as in a liquid ion exchanger. There are two opposing effects here. Any electrolyte, including the quaternary ammonium salt, will tend to decrease the activity coefficients of Cu(II) and SO_4^{2-} ions. The antagonistic effect will increase these coefficients. In more dilute Bu_4NETS solution, there is a net decrease in ion-pair formation; in the more concentrated solutions, the yield goes up, and the demixing effect is clearly predominant. In this connection, in 0.002 *M* $CuSO_4$ solution the difference between the two added salts is still evident, but it is much smaller. In the sulfonate concentration interval 0.002–0.01 *M*, the $CuSO_4$ absorbance at 250 mμ decreases by 6% in the sodium salt solution and by 3% in the quaternary ammonium salt solution.

$CaSO_4$ in the presence of Bu_4NBr in water shows a decreased solubility and hence an increased escaping tendency and an increased activity coefficient.[2] In the present case, the antagonistic interaction between $CuSO_4$ and Bu_4NETS shows itself in an increase in the concentration of $CuSO_4$ ion pairs. This also requires an increased activity coefficient for the Cu(II) and SO_4^{2-} ions (assuming that the ion pairs have a coefficient of unity) with increasing Bu_4NETS concentration. In calculating these activity coefficients, it was assumed that the difference in molar absorptivity coefficients between $CuSO_4$ ion pairs and Cu(II) ions ($a_{CuSO_4} - a_{Cu^{2+}}$) was a constant, independent of salt type or salt concentration, and had the value 240 cm²/mol, which is the average for different (dilute) solutions from different sources.[11] The stoichiometric ion-pair formation constant is given by[8]

$$K = \frac{x}{(c - x)^2} \tag{2}$$

Here x is the molar concentration of ion pairs and c is the stoichiometric concentration of $CuSO_4$. Equation 3 follows

$$A - A' = x(a_{CuSO_4} - a_{Cu^{2+}}) \tag{3}$$

The absorbance of a $CuSO_4$ solution is A, and that of an equal concentration of $Cu(ClO_4)_2$ is A', both normalized for a 1-cm path length. The thermodynamic ion-pair formation constant of $CuSO_4$, K_0, is defined by

$$K_0 = \frac{K}{f_{\pm}^2} \tag{4}$$

in which $f_{\pm}^2$ is the square of the mean (molar) activity coefficient of Cu(II) and SO_4^{2-}. The value of K_0 at 25° was taken as 225 M^{-1}.[8] The results for the two salts are given in Table II.

The expected increase in the activity coefficient of $CuSO_4$ in the more concentrated solutions of Bu_4NETS is evident.

Figure 3 shows the absorbance at 250 mμ of 0.02 *M*

Table II: Activity Coefficients of 0.02 *M* $CuSO_4$ in NaETS and in Bu_4NETS Solutions in Water at 25°

Added salt, *M*	$A - A'$	10^3x, *M*	K, M^{-1}	$f_{\pm}^2$
		NaETS		
0.00	1.355	5.56	26.7	0.1186
0.02	1.243	5.18	23.6	0.1068
0.05	1.097	4.57	19.2	0.0853
0.1	0.940	3.92	15.2	0.0673
0.2	0.745	3.10	10.9	0.0483
0.3	0.660	2.75	9.2	0.0411
0.4	0.645	2.69	9.0	0.0399
		Bu_4NETS		
0.02	1.270	5.29	24.5	0.1087
0.05	1.250	5.21	23.8	0.1058
0.1	1.105	4.60	19.4	0.0863
0.2	1.069	4.45	18.4	0.0819
0.3	1.305	5.44	25.7	0.1140
0.4	1.607	6.70	37.9	0.1682

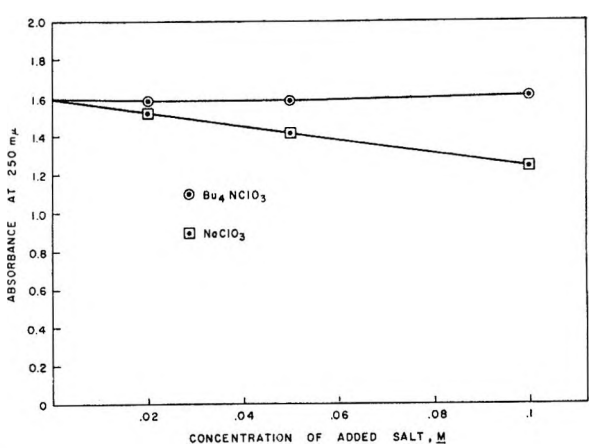

Figure 3. Absorbance of 0.02 *M* $CuSO_4$ at 250 mμ in solutions of $NaClO_3$ and of Bu_4NClO_3 plotted against the molar concentration of added salt.

(11) This represents an average of published and as yet unpublished data. The latter are from the laboratory of S. Petrucci.

$CuSO_4$ in solutions of $NaClO_3$ and Bu_4NClO_3 plotted against the molar concentrations of the added salts. It can be seen that the curves essentially duplicate those of Figure 1. If anything, assuming constant absorptivity coefficients for $CuSO_4$ ion pairs, the demixing effect of Bu_4NClO_3 may be greater than that of Bu_4-NETS.

Spectra were run in 0.02 *M* $CuSO_4$ containing 0.1 *M* NaBr and 0.1 *M* Bu_4NBr. After rough empirical corrections for absorption by the $CuBr^+$ complex, at 250 mμ, the residual absorbance in NaBr was 0.95 and in Bu_4NBr was 1.35. The same demixing effect is qualitatively evident in this latter system.

Up to this point, it has been assumed that the only significant antagonistic interaction is that between the organic cations and the sulfate anions. However, the remaining ions must also play some part, although it is probably less important in the present cases. The anions chlorate and bromide are water structure-breakers, with negative viscosity-*B* coefficients.[12] The ethanesulfonate ion may also be a structure-breaker, or a weak structure-former of the organic type. A structure-breaking anion would exert a cooperative effect in the sense that it can provide loose water molecules to be organized around the quaternary ammoninm ion.[2] The small differences between the ethanesulfonate and chlorate solutions may reflect differences in their compatibilities with the quaternary ammonium ion. One consequence of this hypothesis is that the demixing effect would be very much smaller in solutions of $CuSO_4$ and Bu_4NF, since both sulfate and fluoride ions are strong water-structure formers of the charge-oriented type.

Acknowledgment. We thank Professor S. Petrucci of this department for assistance and helpful suggestions.

(12) Reference 10, p 241.

Study of Ionic Surfactants by Membrane Osmometry

by H. Coll

Shell Development Company, Emeryville, California 94608 *(Received May 26, 1969)*

The micellar weight of well-purified sodium dodecyl sulfate (NaDDS) was determined by means of an automatic osmometer in 0.03, 0.1, and 0.342 *M* aqueous sodium chloride solution at 36.5°. The respective average numbers of monomer molecules in the micelles, *N*, were 58.9, 82.9, and 115; in 0.03 *M* NaCl at 21°, $N = 63.1$. The solvent contained a specified amount of NaDDS in order to repress dissociation of the micelles and to minimize the monomer contribution to the osmotic pressure. The dialytic behavior of NaDDS is discussed, and the magnitude of the Staverman reflection coefficient is estimated. Saturation of the aqueous solution with benzene was found to increase *N*.

Introduction

Determination of micellar weights of ionic surfactants in aqueous solutions by conventional absolute methods encounters considerable difficulties. Because of the ionic character, one can hardly obtain meaningful micellar weights from measurements of colligative properties such as vapor pressure lowering. Light scattering[1,2] has been used extensively for estimating micellar size. The theoretical difficulty lies in accounting for the extent of interaction between the charged micelle and diffusible ions in solution (counterions, added electrolyte). In all cases certain assumptions have to be made with respect to the (negative) adsorption of diffusible ions on the macro-ion. Assumptions which use the concept of "effective charge" to account for this adsorption have been criticized.[3] Huisman,[4] in his studies on sodium alkyl sulfates by light scattering, has overcome this problem by measuring apparent micellar weights in the presence of dissolved sodium fluoride, chloride, bromide, and iodide, respectively, and extrapolating the result to zero refractive index increment for the added electrolyte which makes the interaction term vanish.[3] This approach appears to be less controversial than earlier ones. It only contains the

(1) W. Prins and J. J. Hermans, *Proc. Kon. Ned. Akad. Wetensch.*, **B59**, 298 (1956).

(2) K. J. Mysels and L. H. Princen, *J. Phys. Chem.*, **63**, 1699 (1959).

(3) A. Vrij and J. Th. G. Overbeek, *J. Colloid Sci.*, **17**, 570 (1962).

(4) H. F. Huisman, *Proc. Kon. Ned. Akad. Wetensch.*, **B67**, 367 (1964).

assumption that the nature of the co-ion has no effect on the micelle.

Determinations of micellar weights of ionic detergents by osmometry have not come to our attention. We hope to show in the following that this method holds considerable promise provided certain precautions are taken. Here the main problem arises from the condition of nonequilibrium in the osmometer because of the dissociation of micelles into lower association products and monomer, which are not retained by the membrane.

Generally, this problem will be most severe with rapidly dissociating micelles and whenever the critical micelle concentration (cmc) is high. Osmometric determination of micellar weights of nonionic detergents in benzene have been reported by McBain and Working[5] on aluminum dilaurate and by Singleterry and Weinberger[6] on calcium xenylstearate. Singleterry's results agreed well with micellar weights determined by other methods. These measurements, however, were favored by the great stability of the micelles (very low cmc).[7] Similarly, measurements in our laboratory on Aerosol OT (Union Carbide) in toluene by means of a quick-responding automatic osmometer gave pressures which slowly declined with time. Extrapolation of the osmotic pressure to zero time resulted in an apparent micellar weight between 5000 and 6000. This result is in good agreement with the value reported by Corkill, *et al.*,[8] from vapor pressure osmometry, although some doubts about the magnitude of the Staverman effect[9,10] and contributions from nonmicellar solution components remain.

Yet, the same easy procedure could not be followed in the case of sodium dodecyl sulfate (NaDDS) in water. First, in order to suppress the very large second virial coefficient in pure aqueous solution, electrolyte (sodium chloride) had to be added to the solution. But, more seriously, the micelles appeared to be too unstable (cmc too high) for the experimental osmotic pressure to be a reliable measure for the micellar weight. The experimental pressures (P) decreased rapidly with time, and more so at lower concentrations of surfactant. Extrapolation of P to zero time, and subsequent extrapolation of the reduced osmotic pressures to $c \rightarrow$ cmc could not be carried out with any confidence. Moreover, the contribution of monomeric NaDDS to the osmotic pressure was appreciable and could not be accurately assessed. All these complications could be reduced to tolerable proportions by measuring the osmotic pressure against a more dilute solution of NaDDS with a concentration above the cmc rather than measuring against pure solvent (aqueous sodium chloride). The resulting micellar weights agreed well with Huisman's results.[4]

In addition, experiments such as those to be described below give some information about the dialysis of micellar substances through membranes.

Experimental Section

The osmometer used was an automatic recording instrument of Shell design[11] manufactured by Hallikainen Instrument Company (Richmond, California). One series of osmotic pressure determinations was made at 21°. Because of the positive temperature control of the instrument, an ambient temperature below 16° was required. Most measurements were, therefore, carried out at the more convenient cell temperature of 36.5°.

The osmometer membranes were supplied by Schleicher and Schuell (Keene, N. H.). For some of the preliminary measurements we used the less retentive membrane B 19, but all further results were obtained with B 20 which is the most retentive membrane of this series made of cellulose acetate. This type is recommended for use with aqueous solutions. The membranes had been stored in 20% ethanol solution. They were thoroughly rinsed with distilled water before being installed in the osmometer.

Materials. The sodium dodecyl sulfate was of very high purity. Preparation and measurements of cmc under various conditions on this particular sample of surfactant have been discussed by Rehfeld.[12] Sodium chloride and benzene (the latter used as an additive in one series of measurements) were of reagent grade. To avoid the formation of air bubbles in the osmometer cell, all solutions were briefly stirred under reduced pressure before being introduced in the osmometer.

Procedure. Because of the more or less extensive diffusion of surfactant into and across the membrane, each determination of osmotic pressure was preceded by rinsing both sides of the membrane (sample as well as solvent cell of the osmometer) with several portions of solvent, followed by one or more blank runs (solvent on both sides of the membrane). Such runs lasted between 1 and 2 hr, until the constancy of pressure had been ascertained. About 8–10 ml of sample solution was then transferred to the filling funnel, and the sample valves were opened. This time was taken as $t = 0$. The larger first portion of the solution drained through the osmometer flushing out the previous contents of the sample cell. Only the last portion (approximately 2 ml) was retained in the sample cell by closing of the sample inlet valve. Temperature equilibrium was reached within 1–2 min after which the sample outlet

(5) J. W. McBain and E. B. Working, *J. Phys. Colloid Chem.*, **51**, 974 (1947).

(6) C. R. Singleterry and L. A. Weinberger, *J. Amer. Chem. Soc.*, **73**, 4574 (1951).

(7) C. R. Singleterry, *J. Amer. Oil Chem. Soc.*, **32**, 446 (1955).

(8) J. M. Corkill, J. F. Goodman and T. Walker, *Trans. Faraday Soc.*, **61**, 589 (1965).

(9) A. J. Staverman, *Rec. Trav. Chim. Pays-Bas*, **70**, 344 (1951).

(10) A. J. Staverman, D. T. F. Pals, and Ch. A. Kruissink, *J. Polymer Sci.*, **23**, 57 (1957).

(11) F. B. Rolfson and H. Coll, *Anal. Chem.*, **36**, 888 (1964).

(12) S. J. Rehfeld, *J. Phys. Chem.*, **71**, 738 (1967); **74**, 117 (1970).

valve was closed. The contents of the cell at this point were under a small negative pressure, so that in all cases the pressure balanced by an approach "from below." This is the procedure which is generally followed with instruments of this kind. But previous experiments had indicated that the exchange of liquid in the cell is not complete. Thus, the pressure reading on a polymer solution preceded by a blank was generally lower by about 4% than subsequent repeat measurements on the same solution.[11] Since this effect cannot be studied with membrane-permeating solutes such as NaDDS, we made a series of measurements on aqueous solutions of a dextran fraction of sufficiently high molecular weight. Again, a pressure deficiency of about 4% was observed. Hence, all measurements of experimental osmotic pressure in the present work were corrected by adding 4%.

The osmotic pressure was recorded over periods of many hours. The logarithms of the pressures were plotted against time and extrapolated to $t = 0$ by linear least-square fits. The resulting pressures, P_0, were then subjected to least-square fits of the form $P_0 = a_1c + a_2c^2$, c being the concentration in g/l. The micellar weight was calculated from a_1, the second viral coefficient from a_2 (see below).

In one series of measurements, the solutions of NaDDS were saturated with benzene in order to see whether this additive had a measurable effect on the micellar weight. The influence of benzene on the cmc has been demonstrated by Rehfeld.[12] For this purpose, sample as well as blanks were gently stirred for several hours at room temperature with a layer of benzene on top. Great care was taken to avoid emulsification. Turbid solutions were discarded. The greater portion of the aqueous phase was subsequently withdrawn by means of a hypodermic syringe and transferred to to osmometer.

The majority of the osmotic pressure measurements were carried out with 2 g/l. of NaDDS present in the solvent. We shall refer to this as "background NaDDS."

Results and Discussion

Figure 1 compares osmotic pressure–time curves at different concentrations of sodium chloride. The large deviation from ideality in pure water is evident as the extrapolated pressure at $t = 0$ is about 10 times as high as the corresponding value in 1% sodium chloride solution. The pressure level at 0.1% sodium chloride lies between the two. The nonlinearity of this particular plot is explained by the monomer–micelle equilibrium. This will be discussed in more detail later on. Sodium chloride was added to the solutions in all subsequent measurements. Effects due to an initial difference of chemical potential of sodium chloride between the osmometer cells were not noticeable because of the relatively rapid diffusion of the salt through the membrane.

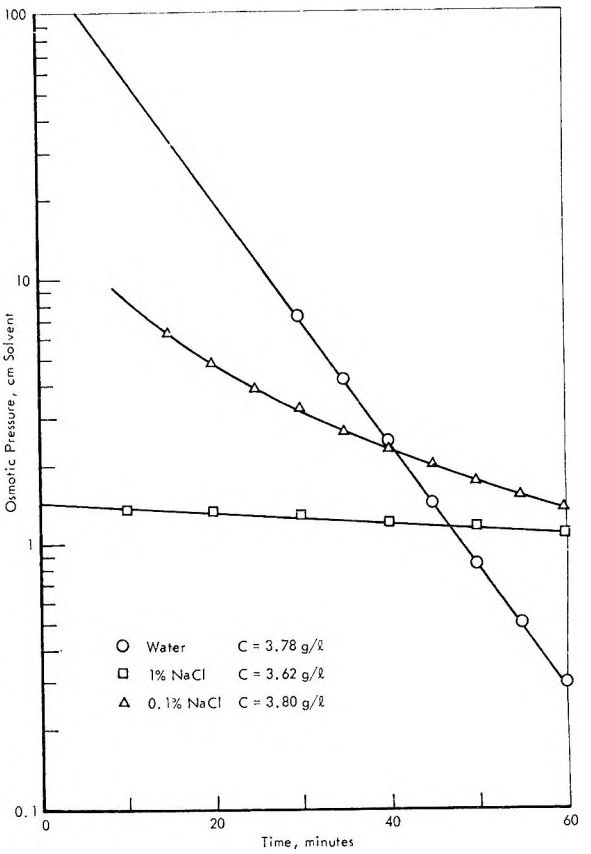

Figure 1. Sodium dodecyl sulfate osmotic pressure at different sodium chloride concentrations.

Critical Micelle Concentration (cmc). The cmc depends on the ionic strength, on the level of impurities, and on temperature. The data of Flockhart[13] indicate that raising the temperature from 21 to 36.5° should increase the cmc of NaDDS in water by approximately 3%. Then, with reference to Huisman's cmc values[4] for varying ionic strength (21°) we obtained the cmc shown in column 3 of Table I. Surface tension measurements gave a cmc of 0.96 ± 0.03 g/l. for 0.03 *M* sodium chloride at 36.5°. We note that an accurate knowledge of the cmc is in no way necessary for the purpose of determining the micellar weight by the present method.

Osmotic Pressure–Time Curves in the Presence of Background NaDDS. The rapid decrease of osmotic pressure with time (*cf.* Figure 1) is no longer observed if NaDDS, at concentrations above the cmc, is made a component of the solvent, and hence, at all times is present on both sides of the osmometer membrane. We chose a background concentration of 2 g/l. for most measurements. The observed decline of osmotic pressure was found to be exponential within experimental error (see eq 1).

(13) B. D. Flockhart, *J. Colloid Sci.*, 16, 484 (1961).

Table I: Association of Sodium Dodecyl Sulfate in Aqueous Sodium Chloride Solutions

Salt concn, mol/l.	T, °C	cmc,[a] g/l.	M[b]	N[b]	$B \times 10^6$,[b] l./g	Standard error, % M
0.03	21	0.90	18,200	63.1	1.1	2.7
0.03	36.5	(0.93)	17,000	58.9	1.5[c]	2.5
0.10	36.5	(0.43)	23,900	82.9	0.52	2.7
0.342	36.5	(0.18)	33,300	115	0.29	2.0

[a] Based on ref 4; corrected for 36.5° by adding 3% (*cf.* ref 13). [b] M, micellar weight; N, number of monomer molecules in micelle; B, second virial coefficient. [c] Average of two determinations.

$$P = P_0 \exp(-\alpha t) \quad (1)$$

Figures 2 and 3 show plots of α (in reciprocal minutes) as a function of excess concentration (c) of NaDDS in the sample cell. The rate constant α decreases with increasing salt concentration and background concentration. An increase of NaDDS concentration also lowers α. This can be explained by the fact that beyond the cmc the micellar concentration rises much faster than the monomer concentration; P_0 is primarily determined by the excess concentration of micelles in the sample cell while $-dP/dt$ is governed by the difference of monomer concentration in the two cells. This interpretation, at the same time, suggests that the exponential decline given by eq 1 is not strictly correct.

Under the assumption of unchanged transport characteristics of the membrane, a comparison of α, at the same P_0 and background concentration in the solvent cell, may serve as an indicator for the relative

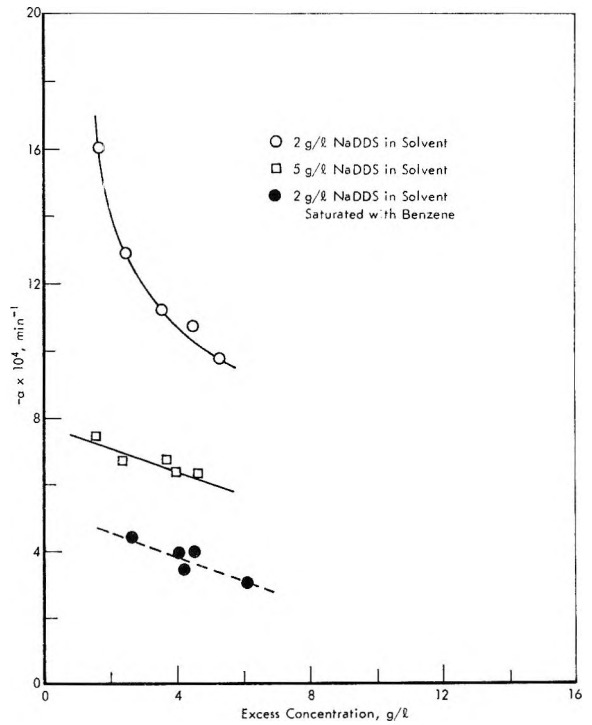

Figure 2. Rate constants of pressure decline, NaDDS, 0.03 M NaCl at 36.5°.

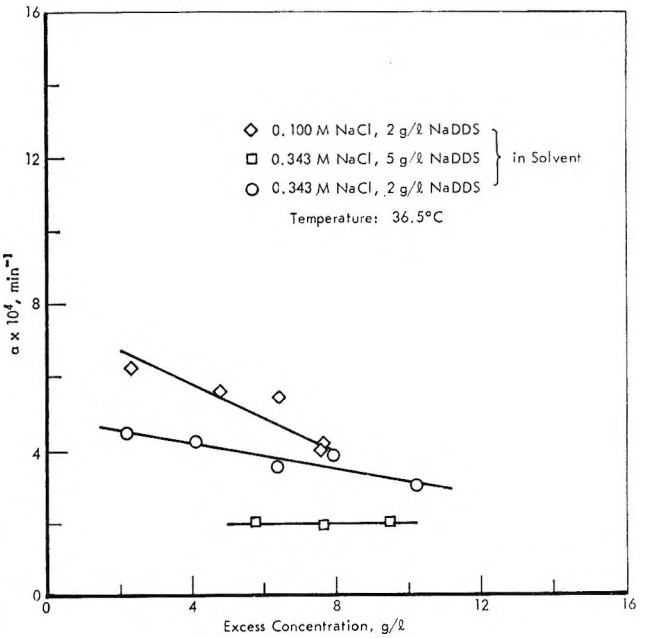

Figure 3. Rate constants of pressure decline, NaDDS.

stability of the micelles. (In this context "stability" is to be understood entirely in terms of a thermodynamic equilibrium constant. It does not refer to dissociation rates of micelles.) This is illustrated by the decrease of α with increasing concentration of sodium chloride (Figures 2 and 3).

In the absence of background NaDDS eq 1 does not hold and the plots of log P *vs.* time deviate markedly from straight lines; the rate constants α at the beginning of the run are also considerably larger than those shown in Figures 2 and 3.

Micellar Weight. The experimental osmotic pressure, P, between sample (containing $c + c_0$ g/l. of NaDDS) and solvent (containing c_0 g/l. of NaDDS) can be expressed as

$$P = s_1RT(c_1'' - c_1')/M_1 + sRT[(c + c_0 - c_1'') - (c_0 - c_1')]/M + sRBT[(c + c_0 - c_1'')^2 - (c_0 - c_1')^2] \quad (2)$$

M_1 is the monomer weight (formula weight = 288.4), M the micellar weight; c is the excess solute added to the sample solution, c_0 the background concentration of

NaDDS, c_1 the monomer concentration. The single prime refers to the contents of the solvent cell, the double prime to the contents of the sample cell. The symbols s_1 and s designates the effective Staverman coefficient to account for the pressure deficiency as a result of the solute permeation through the membrane. RT has the conventional meaning, B is the second virial coefficient. The first term in eq 2 expresses the contribution to the osmotic pressure from the difference of monomer concentration in the two cells. The difference is small, however ($c_1'' \cong c_1' \cong$ cmc). In the present case, s_1 was estimated as approximately equal to 0.06 (from measurements on NaDDS solutions below the cmc), and the contribution from the first term should not amount to more than 2% of P (strictly speaking, a factor approaching 2 should appear in front of the monomer term to account for ionic dissociation; then $s_1 \simeq 0.03$). The difference between c_1'' and c_1' is even less significant in the further terms of eq 2. We can therefore write

$$P = sRTc/M + sRTB[c^2 + 2c(c_0 - \text{cmc})] \quad (3)$$

Next, we assume that for the present case $s = 1$. This will be justified later on. Then, in a conventional plot of reduced osmotic pressure, P/c, *vs.* c we obtain as intercept at $c = 0$

$$(P/c)_{c=0} = RT/M + 2RTB(c_0 - \text{cmc}) \quad (4)$$

Since B is obtained from the slope of the plot of reduced osmotic pressure, and the cmc is assumed as approximately known, M can be calculated. Figure 4 shows plots of reduced osmotic pressure obtained under different experimental conditions. The results are summarized in Table I. The constant RT was calculated for the appropriate cell temperature and solvent density, the osmotic pressures being expressed as cm of solvent head.

At this point, we shall review the approximations and corrections made in the calculation of the micellar weights. (1) The use of concentrations expressed as g/l. instead of molalities introduces a small error (<0.7%) with respect to $(P/c)_0$ which was ignored. (2) The assumption of the monomer concentration to be equal to the cmc, under the present experimental condition introduces an error no greater than −2% with respect to M. No correction was applied. (3) The assumption was made that $s = 1$. We will try to show in a later section that $s > 0.96$, and the resulting error should be less than 4% (M too high). The errors from (2) and (3) will at least partially cancel. (4) A correction of +4% was applied to all pressure readings. This has been discussed in the Experimental Section. (5) Finally, as discussed, the term $2RTB$ (c_0 − cmc) has to be subtracted from $(P/c)_{c=0}$ to allow calculation of M. This correction term is small, so that an accurate knowledge of B and the cmc is not important.

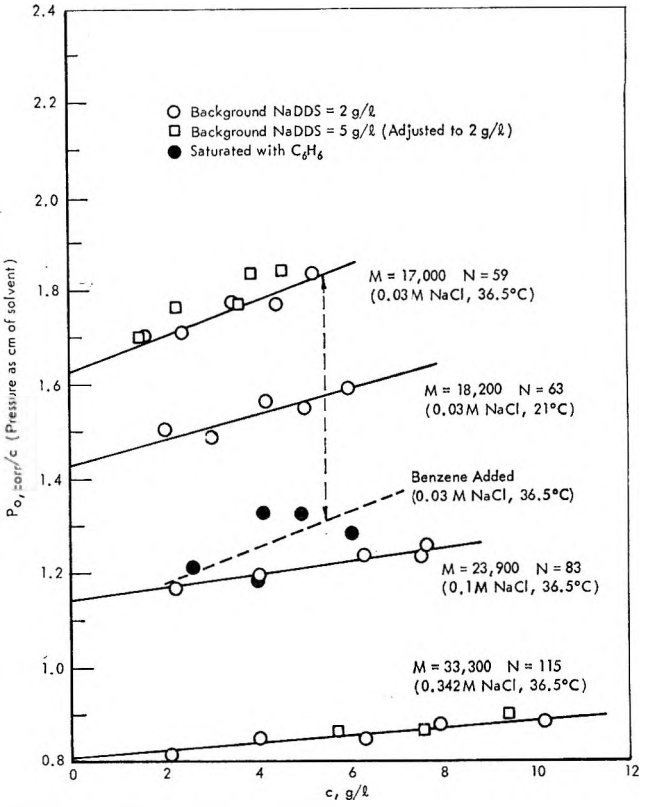

Figure 4. Sodium dodecyl sulfate (NaDDS) reduced osmotic pressure *vs.* concentration.

Figure 5 compares the present results with those of Huisman obtained by light scattering.[4] The two sets differ by 10 to 20%, the difference being larger at low salt concentrations. From our value for 0.03 M sodium chloride solution at 21° and 36.5° it appears that the temperature effect on M is small, although the low value for B (*cf.* Figure 6) suggests that the result for 21° may be somewhat low. The closeness of weight-average and number-average micellar weights indicates that in the present case polydispersity of the micelles is not very pronounced, if it exists at all.

Measurements with 5 g/l. NaDDS as Background. At two instances 5 instead of 2 g/l. of NaDDS was added to the solvent. The resulting osmotic pressures were corrected for the now larger contributions from the term containing the second virial coefficient to allow a comparison with the data for 2 g/l. background. In the case of 0.342 M sodium chloride the agreement is excellent, while at 0.03 M sodium chloride, on the average, the pressures are higher by approximately 1.7% (the scatter of the points, however, is such that least-square extrapolation yields the same intercept as for 2 g/l. background). As already mentioned, the rate constants, α, were lowered by an increase of background NaDDS.

Second Virial Coefficients. Figure 6 shows a comparison of second virial coefficients with the results of Huisman.[4] Because of the limited number of experi-

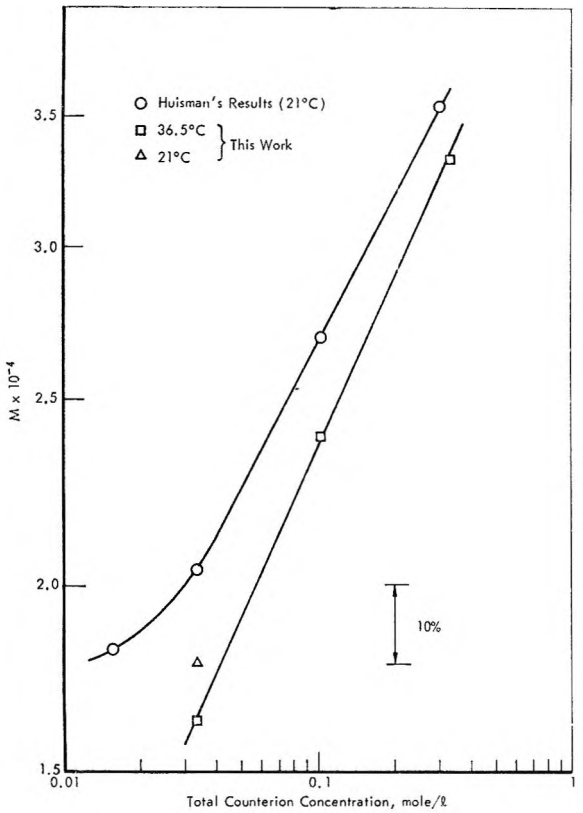

Figure 5. Comparison with Huisman's light-scattering results.

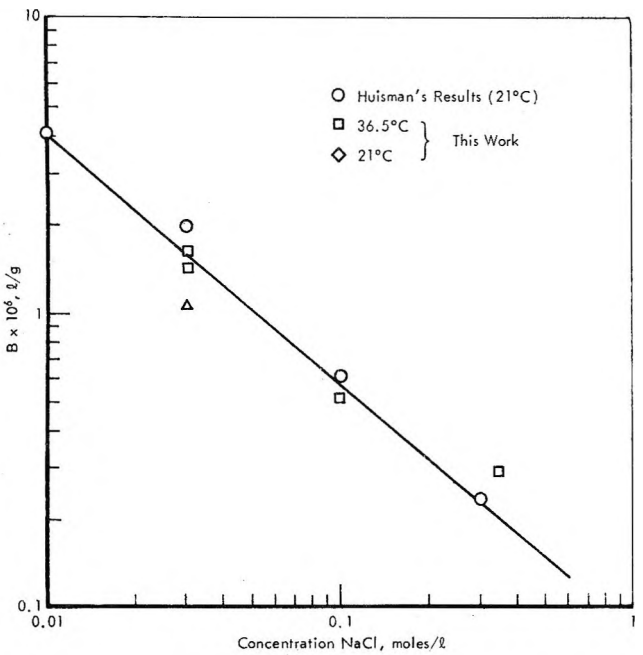

Figure 6. Sodium dodecyl sulfate; second virial coefficients.

mental points, an appreciable error in our results is quite possible. A significant effect due to the temperature difference of 15.5° is not likely, and the solid line in Figure 6, equal to $B = 8.3 \times 10^{-8} m^{-0.84}$ (l./g), where m is the molar concentration of sodium chloride, may be taken as a representation of the combined results.

Effect of Benzene. Additives and impurities in surfactants often have a pronounced effect on the cmc and on micellar size. The effect of benzene on the cmc of sodium dodecyl sulfate has been reported by Rehfeld.[12] We were interested to find out whether osmometry would reveal a corresponding effect on the number of monomer molecules associated in the micelle. For this purpose all solutions (blanks included) were saturated with benzene (see Experimental Section). As shown in Figure 4, appreciably lower osmotic pressures were observed from which can be concluded that the average number of monomers in the micelle increased by roughly 25–30% (0.03 *M* sodium chloride, 36.5°). The results are somewhat erratic, however; they would, in our opinion, be improved by saturating the surfactant solutions with benzene under better controlled conditions (thermostating, saturation *via* the vapor phase). It is interesting that the rate constants, α, are also appreciably lowered by the presence of benzene (Figure 2), which can again be interpreted in terms of enhanced micellar stability, as this is also indicated by lowering of the in cmc the presence of benzene.[12]

Staverman Coefficient. Staverman[9,10] has shown by arguments of irreversible thermodynamics that a deficiency of osmotic pressure has to be expected whenever the membrane is permeable to the solute. It may be assumed that in the present case the intact micelles are too large for passing through the membrane. Yet, the micelles are in equilibrium with monomer which is capable of diffusing through the membrane. Monomer which has diffused out of the sample cell is replenished by dissociation of micelles, while association to form micelles occurs in the solvent cell once the total concentration there is equal to or higher than the cmc. Thus, from a phenomenological standpoint, a transport of micelles across the membrane takes place. The condition of thermodynamic equilibrium no longer prevails, and we may, therefore, expect the experimental osmotic pressure, P, to be lower than the theoretical equilibrium pressure, Π, *i.e.*, $s = P/\Pi < 1$. It may appear desirable to use a very retentive membrane which also holds back the monomer while allowing comparatively easy passage for water and supporting electrolyte. In the first place, such a membrane is not likely to exist. Secondly, a great disadvantage would be the very extensive contribution of monomer to the total osmotic pressure, which may be many times larger than the contribution from the micelles. In order to calculate the micellar weight, a very accurate knowledge of monomer concentration would be required. It would be inadequate to assume the latter to be equal to the cmc. The "leakiness" of the membrane with respect to monomer should therefore rather be

considered an advantage, although it makes the addition of background surfactant to the solvent necessary.

Several attempts have been made to predict theoretically the magnitude of the Staverman coefficient. An example is the equation derived by Vink[14]

$$P = [1 - (\beta + v_2/v_1)L_{22}/L_{11}][\exp(-\alpha t) - \exp(-\alpha_1 t)]RTc/M(1 - \alpha/\alpha_1) \quad (5)$$

$$\alpha = A'L_{22}v_1RT/M \quad (6)$$

where L_{11} is the permeation constant of solvent, L_{22} is the permeation constant of solute, β is the "drag" (co-transport) coefficient to account for the number of solvent molecules carried along by the permeating solute, v_1 and v_2 are (partial) specific volumes of solvent and solute, respectively, α_1 and α are rate constants for solvent and solute flow, respectively, c is concentration, M, is the molecular weight of the solute, and A' is an apparatus constant.

If $\alpha \ll \alpha_1$, after substitution of (6) in (5) we may write

$$P = [1 - (\beta + v_2/v_1)M\alpha/A]RTc \exp(-\alpha t/M) \quad (7a)$$

once t is sufficiently large for the second exponential to be insignificant. Here $A = A'L_{11}v_1RT$ and is a constant independent of the solute. The factor in brackets can be identified with s, the Staverman coefficient

$$s = 1 - (\beta + v_2/v_1)M\alpha/A \quad (7b)$$

Simultaneous application of (7b) to the unknown solute as well as to a reference solute of known molecular weight under the same experimental conditions, and elimination of A between the two equations, suggests itself as an approach for calculating s of the unknown. However, there does not seem to be a reliable method for evaluating β which can be expected to depend on the solute. Furthermore, the solute may interact with the membrane to a different extent;[15] difficulties may also arise with unstirred solutions[15,16] because of nonuniform concentration in the osmometer cells. Complications of this kind have not been accounted for in the derivation of eq 5. These objections, on the other hand, lose most of their force if, for instance, the results obtained with 2 g/l. and 5 g/l. of NaDDS as background are compared. The solutes are identical and by applying (7b) to the respective experimental conditions, one obtains

$$\frac{1 - s}{1 - s^*} = \frac{\alpha}{\alpha^*} \quad (8)$$

since $M = M^*$, $v_2 = v_2^*$, and $\beta = \beta^*$.

In the case of the measurements at 0.03 M sodium chloride, the experimental pressures were, on the average, increased by approximately 1.7% if 5 instead of 2 g/l. of NaDDS was added to the solvent. Thus, $s^* = 1.017s$. Correspondingly, a value of 1.8 may be taken as typical for the ratio of rate constants, α/α^* (Figure 2). Then, from eq 8, $s = 0.965$.

Applying the same argument to the results obtained for 0.342 M sodium chloride solutions where the experimental pressures appeared to be identical, we conclude that $s^* = s = 1$. It should be noted that eq 7 describes an exponential decline of P. This, in a strict sense, cannot be the correct function for the present situation where nonpermeating micelles are in equilibrium with permeating monomer. Here, then, may be a further objection against the use of eq 7. Deviations from an exponential decline were not evident within experimental error, however, whenever the solvent contained background NaDDS.

It should be borne in mind that the present application of Vink's equation only concerns a limiting case; the purpose is to demonstrate that the Staverman coefficient, under the present experimental conditions, is close to unity. In this special case, we believe the foregoing approach to be fully justified.

Dialysis in the Osmometer. The process that takes place in the osmometer during the experiments described in the preceding sections can be considered as the dialysis of NaDDS through the osmometer membrane. If the solvent cell initially does not contain any surfactant, the experimental pressure–time curves resemble the dialysis plot of Mysels and coworkers.[17] This is not surprising since the osmotic pressure is a measure for the concentration difference across the membrane.

Figure 7 compares plots of log P *vs.* time for NaDDS at different initial concentrations with and without background NaDDS. In the absence of background NaDDS decrease of pressure is rapid, particularly if the concentrations are low. The decline of osmotic pressure is not exponential because of the equilibrium between micelles and monomer. The rate of pressure decrease is markedly reduced if background NaDDS is present, and the plots appear to be linear (curves D and E in Figure 7), as this has already been expressed by eq 1.

The rate of monomer transport through the membrane can be written as

$$-dc_1/dt = k(c_1'' - c_1') \quad (9)$$

$c_1'' - c_1'$ being the difference of monomer concentration between the two cells (both cells have the same geometry).

The rate constant k can be determined from the decline of osmotic pressure at surfactant concentrations below the cmc, the rate of pressure decline being $2k$.

(14) H. Vink, *Arkiv Kemi*, **15**, 149 (1960).

(15) H. Vink, *ibid.*, **19**, 15 (1962).

(16) W. H. Kuhn and G. V. Schulz, *Makromol. Chem.*, **50**, 52 (1961).

(17) K. J. Mysels, P. Mukerjee, and M. Abu-Hamdiyyah, *J. Phys. Chem.*, **67**, 1943 (1963).

Then, if one expresses the equilibrium between monomer and micelles in terms of an association constant, K, it should in principle be possible to derive theoretical expressions for the curves shown in Figure 7, if one assumes that the surfactant is transported across the membrane as monomer only. An additional assumption is that equilibration between monomer and micelles is very rapid compared with the rate of transport through the membrane. The functional relationship between osmotic pressure and time in Figure 7 then depends on k, K, and on the total initial surfactant concentration in the cells.

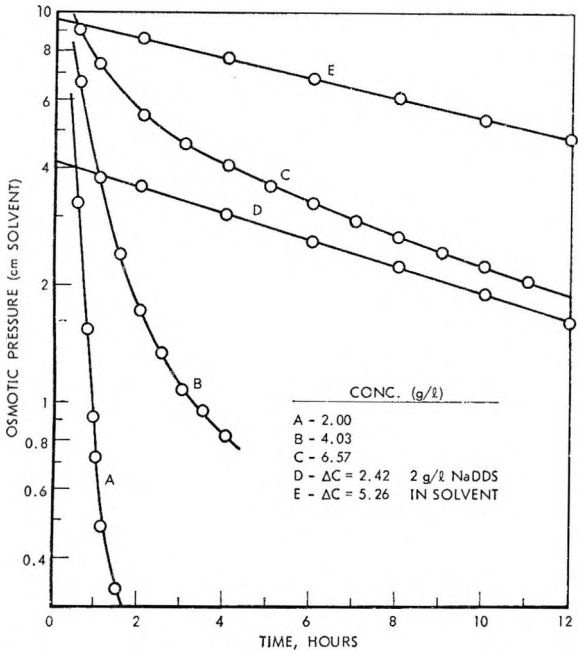

Figure 7. Sodium dodecyl sulfate; decrease of osmotic pressure with time.

Preliminary calculations in which the equilibrium between micelles and monomer was expressed by means of the equations of Phillips[18] gave results that did not agree with the experimental curves. Apparently, permeation of surfactant through the membrane was more than 3 times as fast as could be accounted for by theory. The difference was too large to be explained by shortcomings of the theory of Phillips,[18] as these have been pointed out by Matijevic and Pethica.[19]

The most obvious explanation for the disagreement of results is that transport through the membrane is not restricted to monomers, and that some permeation of intact micelles, or fragments of micelles, is taking place. This conclusion, however, could not be drawn directly because of some evidence for nonuniformity of concentration in the respective osmometer cells, an effect not accounted for by the theoretical treatment. Although a quantitative evaluation of this effect is not possible, some further comment on nonuniform concentration (diffusion layers) is called for.

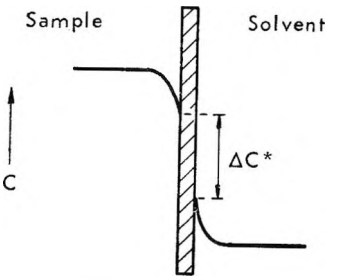

Figure 8. Concentration profile in osmometer.

Diffusion Layers

Nonuniform concentrations are likely to occur in the case of rapid solute permeation through the membrane if the liquids in the osmometer cells are not stirred.[15,16] Design and geometry of the osmometer cells are factors determining the extent of this generally undersirable effect. Some evidence for its occurrence in the present case can be furnished. The experimental curve C in Figure 7 may serve as an illustration.

The initial concentration in the sample cell was 6.57 g/l. of NaDDS. The solvent cell initially contained no surfactant. As the surfactant diffuses through the membrane a point must be reached when the concentration in the solvent cell becomes exactly 2 g/l. with 4.57 g/l. remaining in the sample cell (the cell volumes are equal). In the case of uniform concentrations in the cells, at this point, the same situation should prevail as in the earlier experiment with 2 g/l. of NaDDS as background concentration in the solvent, and an excess concentration of 2.57 in the sample cell. From Figure 4 we calculate the osmotic pressure corresponding to this excess concentration as 4.43 cm of solvent. The corresponding rate constant, 1.27×10^{-3} min^{-1}, is read from Figure 2. According to curve C in Figure 7, the osmotic pressure of 4.43 is reached after 3.3 hr; the tangent drawn through the point (3.3, 4.43), however, has a slope $2.2. \times 10^{-3}$ min^{-1} which is about 1.7 times as large as the rate constant read from Figure 3. This disagreement then strongly suggests that the concentration profile in the osmometer cells is not the same in the two instances. Apparently, at $t = 3.3$ hr the condition of a uniform concentration equal to 2 g/l. in the solvent cell has not been attained; as shown in Figure 8, the concentration drop of 2.57 only pertains to the surfaces of the membrane while the difference between the average concentrations in the two cells is larger.

The occurrence of diffusion layers in the osmometer cells should cause an initial rapid drop of osmotic pressure with time. Later, the rate of pressure decreases should be less than in an ideal osmometer where uniform concentrations prevail. Diffusion layers

(18) J. N. Phillips, *Trans. Faraday Soc.*, **51**, 561 (1955).
(19) E. Matijevic and B. A. Pethica, *ibid.*, **54**, 587 (1958).

should be particularly noticeable in the case of rapidly permeating solute, and it can then be argued that k in eq 9, determined by osmotic pressure measurements on rapidly diffusing monomer, has been too low, the initial pressure drop being obscured by the balancing of the osmometer. This may at least partially explain the disagreement of the dialysis results mentioned in the previous section.

The question then arises whether the effect of diffusion layers will invalidate the determinations of micellar weight as described in this investigation. It is not certain that extrapolation of the pressure–time curves to zero time will eliminate the effect. Then, instead of the Staverman coefficient, s, one should more correctly introduce an empirical factor $s' < s$. This inequality, however, becomes smaller with increasing s, and in the limit of full solute retention $s' = s = 1$. The earlier argument that in the present case, at 2 g/l. background NaDDS, the extrapolated experimental osmotic pressure is near the equilibrium pressure, can therefore be expected to hold. Because of its proximity to unity it is of no particular importance whether the value of 0.96, as previously calculated by means of the equations of Vink (5 and 6), refers to s or to s'. Furthermore, the very low rate of solute permeation in the presence of background NaDDS is, by itself, an argument against the likelihood of significant diffusion layers.

Conclusion

The determination of micellar weight by means of membrane osmometry has been shown to be feasible in the case of an ionic surfactant with a cmc as high as 0.9 g/l. The present technique appears to be applicable to the determination of micellar weight in general. If the cmc is very low and the micelles exhibit great stability, it may be unnecessary to add surfactant to the solvent in order to repress the transport of monomer across the membrane.

While difficulties in the determination of micellar weight of ionic detergents by means of light scattering arise from the interaction between macro-ion and counter-ions, the problematic feature of osmometry is the inherent condition of nonequilibrium. This may lead to $P < RTc/M$, and hence to micellar weights which are too high. We have shown, however, that at least in the present case the pressure deficiency is small, and how, if necessary, a correction can be applied.

On the other hand, the decrease of osmotic pressure with time appears to be useful for the study of the dialytic behavior of micelles. The rate of diffusion across a given membrane can serve as a relative measure for the thermodynamic stability of the micelles. The effect of increased salt concentration and of benzene has been demonstrated. A more rigorous quantitative interpretation of the results from dialysis in the osmometer can be envisaged. The condition for this is the absence of concentration gradients in the osmometer cells.

Acknowledgment. The author wishes to thank Hallikainen Instrument Company for the loan of the automatic osmometer, and S. J. Rehfeld for having supplied the highly purified surfactant.

The Time Dependence of Effusion Cell Steady-State Pressures of Carbon Monoxide and Calcium Vapors Generated by the Interaction of Calcium Oxide and Graphite

by Juey Hong Rai and N. W. Gregory

Department of Chemistry, University of Washington, Seattle, Washington 98105 *(Received July 11, 1969)*

Torsion effusion steady-state pressures of Ca(g) and CO(g), generated by the reaction CaO(s) + C(s) = Ca(g) + CO(g), are found to decrease with time at a rate dependent on effusion cell parameters and area of contact of the reacting solids. A method of deriving equilibrium pressures by extrapolation to time zero is presented and discussed along with thermodynamic and kinetic properties of the reaction. Addition of a few per cent of CaF_2 is shown to decrease the rate at which steady-state pressures fall with time.

Numerous problems associated with effusion experiments have been discussed by a number of authors;[1] yet, because of its convenience, the method is still widely used for the study of vaporization processes and, with proper cell design and for suitable systems, has been shown to give excellent results. As usually applied, the Knudsen method gives the average rate of effusion over a long time interval and will yield a close approximation to the equilibrium pressure only when the rates of vaporization and condensation are rapid relative to the rate of effusion over the entire period of the experiment. For complex vaporization processes, such as the formation of gases by interaction of a heterogeneous mixture of solids, one has no assurance that this condition will be met. By use of the torsion effusion method, however, the rate of effusion may be observed as a function of time. Such studies have shown, for example, that the steady-state effusion pressure of CO, produced (along with a solid zirconium carbide phase) by reaction of ZrO_2 with graphite, falls off with time.[2] Some reactions which appear simpler, such as the decomposition of Mg_3N_2, have also been found to give steady-state effusion pressures well below expected equilibrium values.[3]

In the present paper we report results of a systematic study of the time dependence of the effusion steady-state pressures of calcium and carbon monoxide generated by the reaction

$$CaO(s) + C(\text{graphite}) = Ca(g) + CO(g) \quad (1)$$

in the temperature interval 1429 to 1525°K. The effusion pressures were observed to fall with time at a rate which varied with sample size and cell orifice area. Values observed immediately following a degassing period were close to those expected at equilibrium. It is found that extrapolation of the pressure–time curve, as observed for periods of time between 1 and 9 hr after initiation of the reaction, back to zero time leads to similar "initial pressures" for the various samples and cells, and these pressures may be taken as equilibrium values for the reaction. It has also been shown that 1–2% CaF_2 reduces the time dependence of the effusion cell steady-state pressures.

Experimental Section

The details of the torsion effusion apparatus and vacuum furnace have been described previously.[2,4] A cell constant for each graphite effusion cell and its suspension fiber (a 2-mil tungsten wire) was determined by use of the vapor pressure of silver (99.99%, Koch Light Laboratories, Ltd., Colnbrook, Buckinghamshire, England) as standard. Nesmeyanov, *et al.*,[5] have reviewed vapor pressure data for silver; the work of Alcock, *et al.*,[6] covers a broad temperature range and agrees closely with results of most other workers; we have used their data as a basis for the calibration (Table I). Cells with uniform $^1/_8$-in. wall thickness were formed from high-density graphite.[2] The orifice holes were drilled (cylindrical in shape) and the wall thickness at the orifice reduced with a taper which flared the outer opening to approximate a hemispherical shape of 5-mm diameter. The l/r values of the orifices were all nearly the same, *ca.* 0.09. The Clausing–

(1) See, for example, J. W. Ward, R. N. R. Mulford, and M. Kahn, *J. Chem. Phys.*, **47**, 1710 (1967); "The Characterization of High Temperature Vapors," J. L. Margrave, Ed., John Wiley and Sons, Inc., New York, N. Y., 1967; G. M. Rosenblatt, *J. Electrochem. Soc.*, **110**, 563 (1963).

(2) J. R. Hollahan and N. W. Gregory, *J. Phys. Chem.*, **58**, 2346 (1964).

(3) B. A. H. Blank and A. W. Searcy, *ibid.*, **72**, 2241 (1968).

(4) J. H. Rai, Ph.D. Thesis, University of Washington, Seattle, Wash. 98105, 1969.

(5) An. N. Nesmeyanov, "Vapor Pressures of the Elements," Academic Press, New York, N. Y., 1961.

(6) P. Grieveson, G. W. Hooper, and C. B. Alcock, "Physical Chemistry of Process Metallurgy," Interscience Publishers, New York, N. Y., 1961, pp 341–352.

Table I: Torsion Cell Constants

Cell	Total orifice area, a, cm^2 × 10^3	Suspension wire length, cm	Torsion-cell constant × 10^4 atm radian^{-1}
1	3.47	60	7.36
2	5.91	58	4.77
3	6.51	55	5.27
3	6.51	59.2	3.07
4	13.16	40.7	3.40
4	13.16	55	2.42

Freeman–Searcy orifice correction for the measured pressures is included in the experimentally derived cell-torsion constant.

Temperatures were measured with an optical pyrometer. The pyrometer had been calibrated with a standard lamp and was checked by comparison with temperatures indicated by a Pt—Pt–10% Rh thermocouple placed inside a cell suspended as in the actual torsion effusion experiments. The melting points of tin, zinc, copper, and gold were used as reference points. Optical pyrometer temperatures reported in the following discussion are believed within ±4° of true values.

When the empty cells were suspended and heated, a small reproducible temperature dependent displacement was observed. This effect has been observed by others although a satisfactory explanation of its origin has not been given.[2,7,8] The same displacement was assumed to occur during actual effusion runs and its contribution was subtracted from the total displacements observed. The correction was generally less than 10%; even for the lowest pressure (at the end of the P–t runs at the lower temperatures) the correction did not exceed 20% (see ref 4).

The calibration of the torsion systems was checked by measurement of the vapor pressure of copper (99.9%, Baker's Analyzed Reagent). The results, Figure 1, are seen to agree closely with those of Alcock, *et al.*,[6] Krupkowskii and Golonka,[9] and Morris and Zellars,[10] but are slightly higher than those of Hersch[11a] and McCormack, *et al.*[12] This method of calibration is subject to error if the torsion angle is influenced significantly by diffusion of vapors through graphite and if the rates of diffusion of silver and copper are sufficiently similar to mask the effect in this comparison. We have attempted to minimize diffusion effects by use of high-density graphite with uniform cell wall thickness. Because of uncertainty in locating the center of gravity of the cell and connecting arm in the suspension system, we have preferred to use the calibration constants based on the vapor pressure of silver rather than those based on moment of inertia measurements.

CaO powder (Allied Chemical, Morristown, N. J., Code 1529, 98%), heated first under vacuum at 300° for 5 to 12 hr, was mechanically ground together with graphite (National Carbon Co., San Francisco, Calif.,

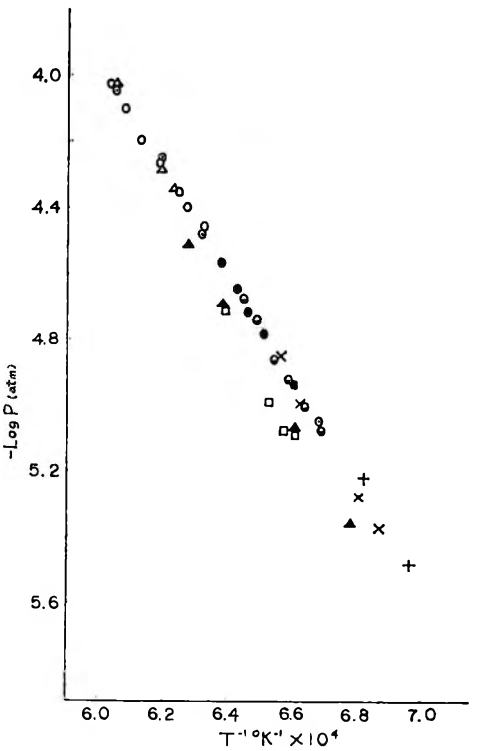

Figure 1. Test of cell-torsion constants. Vapor pressure of copper in comparison with results of other workers: ○, cell 1; ●, cell 3; ◒, cell 4; △, Morris and Zellars;[10] □, Hersch;[11a] +, Marshall and Norton;[11b] ×, Krupkowskii and Golonka;[9] ▲, McCormack, *et al.*;[12] ⊙, Alcock, *et al.*[6]

Code Sp-1-C, 98.5%, spectroscopic grade) and the mixture pressed (1500 psi) into pellets. The pellets were then broken into small particles which were placed in the cells. Reactant mixtures of composition 1:6, 1:1, 2:1, and 3:1 (mol of CaO to mol of graphite) were studied.

In preliminary experiments, it became clear that steady-state pressures were dependent on the amount of the sample and the cell orifice, and in a given experiment, decreased with time when the cell was held at a fixed temperature. If, after an extended period, samples were cooled, reground and repressed, and reheated in the cells, the time dependence of the pressure was again virtually the same as that observed during the first heating period. To obtain comparable results, data presented in the following section were obtained in the following way (except for special experiments): 2.3 g of the reactant mixture (as large a quantity as the

(7) D. A. Schulz and A. W. Searcy, *J. Phys. Chem.*, **67**, 103 (1963).

(8) R. D. Freeman and P. D. Gwinup, *Rev. Sci. Instrum.*, **37**, 773 (1966).

(9) A. Krupkowskii and J. Golonka, *Bull. Acad. Polon. Sci., Ser. Sci. Tech.*, **12** (1), 69 (1964).

(10) J. P. Morris and G. R. Zellars, *J. Metals*, **8**, 1086 (1956).

(11) (a) H. N. Hersch, *J. Amer. Chem. Soc.*, **75**, 1529 (1953); (b) A. L. Marshall and F. J. Norton, *ibid.*, **59**, 1161 (1937).

(12) J. M. McCormack, J. R. Myers, and R. K. Sayer, *J. Chem. Eng. Data*, **10**, 319 (1965).

cell could reasonably accommodate) with a 2:1 mole ratio (CaO/C) was placed in the cell. The latter was brought slowly (over a period of 2–3 hr, under high vacuum) to around 1000° and then quickly (in a few minutes) to the temperature of interest. During the early period at the reaction temperature, pressures were high due to degassing and some time was required to reduce the background pressure in the system. As indicated on the graphs, effusion steady-state pressures were not considered meaningful relative to reaction 1 until *ca.* 1 hr after the reaction temperature was reached. The displacement of the cell was then observed intermittently for periods of 4–8 hr.

Results

The reaction of CaO with graphite has been the subject of several studies.[13–16] Most have been concerned with the formation of CaC_2; it is generally agreed by these authors, and is consistent with thermodynamic predictions based on data tabulated by Kelley,[17,18] that $CaC_2(s)$ is not formed under the conditions of our experiments. We also found no evidence for formation of carbide. After the effusion experiments X-ray powder patterns of the residual solid showed only lines of CaO and graphite; the odor of acetylene was not detected when samples were moistened. Hence we have assumed that our results characterize reaction 1.

Torsion effusion experiments give the total pressure within the cell; hence for reaction 1 we obtain the sum of the partial pressures of calcium and carbon monoxide. Since the stoichiometry of the reaction requires the two to effuse at equal rates, by kinetic theory, their partial pressures within the cell must be in the ratio $(40/28)^{1/2}$. During effusion near equilibrium conditions, the equilibrium constant K is expected to have the following relationship to the total effusion pressure, P: $K = P_{Ca}P_{CO} = 0.248P^2$.

The variation of P with time was most pronounced with cell 4, which has the largest orifice. The behavior is shown in Figure 2; a similar, though smaller fall-off was observed with the other cells. In all cases, the curvature of the pressure–time (P–t) line seemed close to exponential, *i.e.*, a log P *vs.* t plot was nearly linear, with different slopes for each cell. Data from cells 1, 2, and 4 are shown plotted in this way in Figure 2. When these lines were extrapolated to time zero, the "initial pressures," P_i (pressures one would expect at time zero if general degassing did not occur and if the line shape remained the same), were found to be virtually equal for the various cells and samples at comparable temperatures. A plot of the various log P_i values *vs.* $1/T$ is shown in Figure 3 (the solid line represents equilibrium values of P predicted from independent thermodynamic data and will be discussed later). Hence it appears that these extrapolated lines lead to

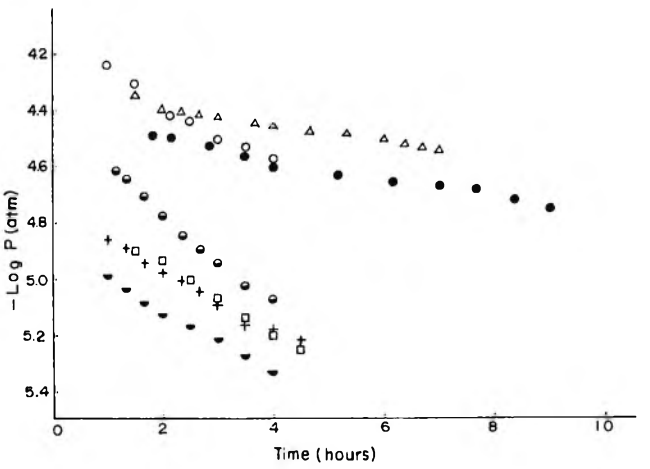

Figure 2. Log P(atm) *vs.* time for various cells: ○, 1525 °K, cell 1; △, 1505°K, cell 2; ●, 1487°K, cell 2; ◒, 1484°K, cell 4; □, 1457°K, cell 4; +, 1452°K, cell 4; and ●, 1429°K, cell 4.

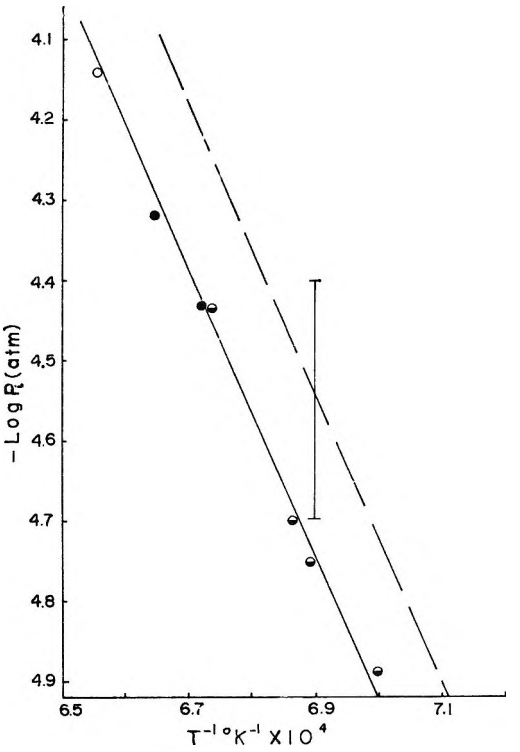

Figure 3. Log P_i(atm) *vs.* $1/T$: ○, cell 1; ●, cell 2, ◒, cell 4. Dashed line represents prediction based on independent thermodynamic data. Solid line represents correlation of present results based on free energy function treatment.

(13) W. J. Thoburn and L. M. Pidgeon, *Can. Metal. Quart.*, **4**, (3), 205 (1965).

(14) H. Frank, *Z. Anorg. Chem.*, **232**, 75 (1937).

(15) T. Mukaibo and Y. Yamanaka, *J. Chem. Soc., Jap., Ind. Chem. Sec.*, **56**, 73 (1953).

(16) H. Tagawa and H. Sugowara, *Bull. Chem. Soc., Jap.*, **35**, 1276 (1962).

(17) K. K. Kelley, U. S. Bureau of Mines Bull., 584, U. S. Government Printing Office, Washington, D. C., 1954.

(18) K. K. Kelley, *Ind. Eng. Chem.*, **33**, 1314 (1941).

what may be taken as equilibrium pressures for reaction 1.

To provide partial verification of the composition of the effusing vapors, two Knudsen experiments were carried out at 1459°K. In these experiments, the calcium vapor was quantitatively condensed on an Mo liner, which extended outside the quartz tube holding the effusion cell (such a collection was not practical in the torsion apparatus). After a 3-hr effusion period, the quantity of calcium was determined by solution of the sample in dilute HCl solution and titration with 0.01 *M* EDTA solution. It is clear that when the effusion pressure varies with time, the apparent pressure derived from the quantity collected will represent an average of the changing value over the period of the experiment. The partial pressures of calcium derived from the two Knudsen experiments were found to be the same (within experimental error) as those deduced from averaging the results of the torsion experiments over a similar time interval (*ca.* one-half the total pressure).

CaF_2 has been reported to act as a catalyst for certain solid–solid reactions, *e.g.*, Khazanov, *et al.*,[19] (MgO + Al_4C_3) and Mack[20] (MgO + C). We have observed that addition of from 1–2% CaF_2 to the CaO–graphite mixtures, before pressing, results in a pronounced decrease in the rate of fall-off of the effusion steady-state pressures. Figure 4 shows the behavior of such a sample in cell 3. The decrease in pressure is only a few per cent over a 5-hr period. In Figure 5 the behavior of this sample at 1486°K is compared with similar data from cell 2, which has nearly the same orifice area as cell 3, and cell 4; the cell 2 and cell 4 samples did not contain CaF_2. The results of Schulz and Searcy[7] and of Margrave, *et al.*,[21] may be used to calculate the partial pressures of CaF (formed by interaction of Ca(g) and CaF_2) and CaF_2 expected in the cell when CaF_2(s) is present at unit activity. While their predicted total contribution is less than 10% of the total pressure, a correction is necessary and the ratio P_{Ca}/P_{CO} is also affected by the equilibrium between CaF_2(s), Ca(g), and CaF(g). The data, Figure 4, were extrapolated to time zero as described for the other experiments, and with allowance for the presence of CaF(g) and CaF_2(g), values of $P_{Ca}P_{CO}$, the apparent equilibrium constant for (1), derived. These values were found to agree within experimental error with those based on experiments in which CaF_2 was not present.

Discussion

General Consideration of the Steady-State in the Effusion Cell. A quantitative explanation of the *P–t* dependence of the effusion steady-state pressures has not been found. However, we make the following observations. The steady-state pressure is determined by the condition

rate of forward reaction =

rate of reverse reaction + rate of effusion (2)

The rate of the forward reaction may be considered to depend on a rate constant k_f (molecules cm^{-2} sec^{-1}) and the interfacial contact area, A, between the solid

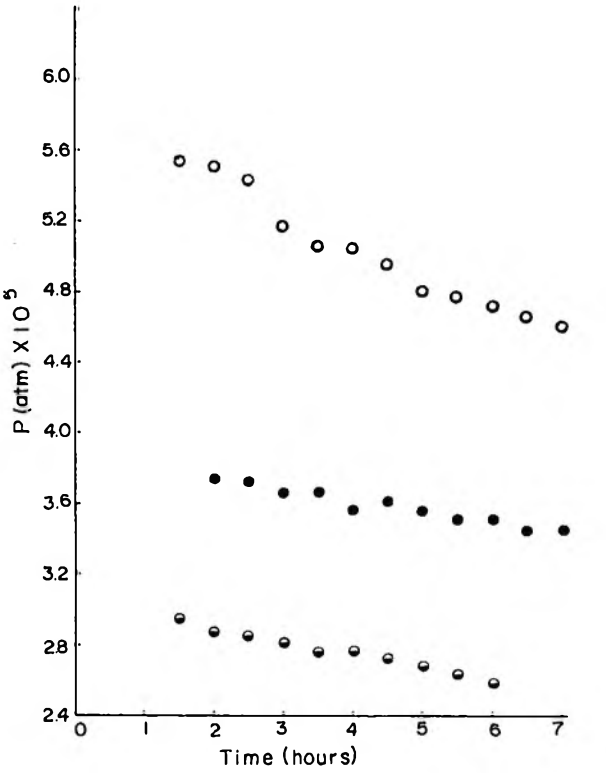

Figure 4. Time dependence of effusion steady-state pressures (cell 3) when 2% CaF_2 has been added to the reaction mixture; (symbol, T°K): ○, 1505°K; ●, 1486°K and ◒, 1466°K.

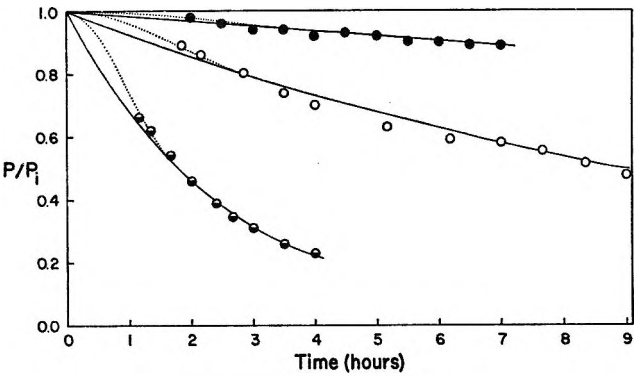

Figure 5. Comparison of steady-state effusion pressures at 1486°K: ●, cell 3 (with 2% CaF_2 added); ○, cell 2; ◒, cell 4. The solid line represents a curve of the form $P/P_i = e^{-st}$, fitted to the data by a least-squares treatment. The dotted curve is proposed as the real behavior near time zero.

(19) E. I. Khazanov, E. G. Saforova, S. A. Stakheeva, and G. V. Kuzmina, *Zh. Prikl. Khim.*, **36**, 251 (1963).

(20) M. Mack, *Radex Rundschau*, **1**, 13 (1951).

(21) G. D. Blue, J. W. Green, R. G. Bautista, and J. L. Margrave, *J. Phys. Chem.*, **67**, 877 (1963).

reactants CaO and graphite. By the kinetic theory of gases, the rate of effusion for each vapor species is $fP_x(2\pi m_x kT)^{-1/2}a_0$, where f is the orifice transmission (Clausing) factor, a_0 is the orifice area, and P_x the partial pressure of species x; in our case P_x is proportional to P, the total effusion pressure. Hence, at each temperature the effusion rate may be given the form $k_e f a_0 P$. The pressure will be assumed uniform throughout the cell. By microscopic reversibility, the rate of the reverse reaction must also depend on A, as well as the frequency of collision of gas molecules with reaction sites. If simultaneous collision of Ca and CO molecules with the surface is required, the collision frequency is expected to depend on P^2; a more likely mechanism may be one which assumes that CaO and graphite are re-formed whenever a Ca atom, or, alternatively a CO molecule, strikes a special interface site, formed through previous collisions or by surface diffusion, with the proper orientation and composition to lead to re-formation of CaO and graphite. If this is the case, we may write (2) in the form

$$k_f A = k_r A P + f k_e a_0 P \qquad (3)$$

It is to be expected that both k_f and k_r may not be simple rate constants, *i.e.*, their magnitudes may differ for different kinds of interfacial contact sites; similarly A also may be a composite of areas of contact of these different sites. We may assume, however, that when $a_0 = 0$, P becomes equal to P_e (the equilibrium total pressure); hence, from (3), $k_f = k_r P_e$ for each kind of site and (3) becomes

$$P_e = P\left(1 + \frac{f a_0 k_e}{k_r A}\right) \qquad (4)$$

Equation 4 suggests that when $f a_0 k_e / k_r A \ll 1$, $P \approx P_e$. Our observations for reaction 1 indicate that this condition is met at time zero in all of our effusion experiments, but that $f a_0 k_e / k_r A$ rapidly becomes significant relative to unity and increases continuously as effusion is allowed to continue. For a given cell this variation is attributed to a change in $k_r A$, since the numerator is fixed by the cell geometry. Since there is a continuous loss of Ca and CO from the cell, it is clear that the area of interfacial contact will diminish as time progresses.

Equation 4 provides a basis for a qualitative explanation of the observed behavior. When $k_r A$ and its time dependence is presumed fixed, by duplicating conditions of preparation and quantity of reactant mixture, the rate of fall-off of P is found to increase as cells with larger a_0 values are used. In experiments in which a_0 (the cell) was kept constant but $k_r A$ varied by changing the amount of sample or the ratio of reactants, an increase in the fall-off was observed when the amount of sample was reduced. We suggest that the effect of CaF_2 may be due to an effective increase (catalytic) in k_r (and k_f), possibly by an increase in the reactivity of the surface sites by formation of defects or vacancies, and/or an influence on the rate of surface diffusion. If $k_r A$ is effectively increased in this way, the ratio $f a_0 k_e / k_r A$ would then remain small for a longer period, effectively reducing the rate of fall-off. The action of CaF_2 appears catalytic, although by formation of CaF, it may also be said to interact with components of the system. Our reaction temperatures are more than 100° below the eutectic temperature reported for the CaO–CaF_2 system (1362°).[22]

The close approximation of the P–t curve to an exponential relationship is surprising in that it holds even when P closely approximates P_i, for example up to $P/P_i = 0.96$ in cell 3 (with catalyst), 0.9 in cell 2 and 0.7, in cell 4, albeit with different slopes, for the data shown in Figure 5. If the rate of the reverse reaction were virtually zero, such a relationship is to be expected if the forward reaction follows first-order kinetics in [A]. However, in such a case, substantially different P_i values should be derived from data for different cells and samples, rather than the observed convergence on what appears to be a close approach to the equilibrium pressure. We suggest that the real P–t behavior in the near-equilibrium range may be something like that indicated by the dotted lines in Figure 5. One expects that near equilibrium, dP/dt, and hence $d \ln P/dt$, should be near zero. If so, this condition appears to exist for reaction 1 for only a very short time and is lost experimentally in the degassing period. If the line shape is similar to that suggested, it is possible for the extrapolation based on the apparent exponential form (the solid lines, Figure 5, derived by a least-squares treatment) to give a good approximation to the equilibrium value even though the exponential relationship may not hold strictly all the way to time zero. A test of the validity of the extrapolation is given by comparison of the results for cells with significantly different orifice areas and with different samples. If the rate of the reverse reaction were not significant, one would expect the P_i values to be proportional to the ratio $k_f A/a_0$. It is likely that other systems would show a variation of P_i with a_0. In such a case, after derivation of P_i by extrapolation of P–t curves for each orifice to zero time, a further plot of P_i *vs.* a_0 and extrapolation to zero orifice area would be necessary to derive equilibrium data. However, it seems unlikely that the method would be feasible unless initial pressures are close to equilibrium values.

According to (4), the variation of P with time should reflect the variation of $k_r A$ with time. In a simple view, neglecting such things as surface diffusion, the variation of interfacial area with time should be proportional to the amount of material leaving the cell, *i.e.*, $dA/dt = -kP$; however, this relationship is not consistent with (4) if P is set equal to $P_i e^{-st}$ and k_r is assumed independent of time. We suggest that varia-

(22) W. Eitel, *Zement*, **27**, 455, 469 (1938).

tion of k_r may also be an important factor. A certain limited number of contact sites, between CaO and graphite in the mixture as first formed, may be very reactive, *i.e.*, have large values of k_r (and k_f) and permit the system to maintain equilibrium pressures for a short time interval. As these more favorable sites are depleted by loss of Ca and CO from the orifice, those remaining are less favorable for reaction [have smaller values of k_r (and k_f)] and the rates of reaction quickly become comparable to the rate of effusion; the steady-state pressures diminish accordingly. Consideration of the combined effects of changing A and k_r, would then be necessary to account for the observed P–t behavior.

Thermodynamic Analysis. P_i values were derived for each set of effusion data by a least-squares evaluation of the intercept, assuming a linear relationship between log P and time, Figure 4. For evaluation of the enthalpy of reaction, free energy functions for Ca(g) and CaO(s) were obtained from high-temperature heat content and entropy data given by Kelley;[17] for CO(g) and graphite, data in the JANAF tables were used.[23] $\bar{S}°_{298°K}$ values for CaO(s) and for Ca(g) are given by Kelley and King.[24] If we assume $P_i \approx P_e$ and use the relationship between P_e and K, the equilibrium constant for (1), cited earlier, we may write

$$\Delta H°_{298} = 2.771T - 9.152T \log P_i(\text{atm}) - T\Delta \frac{\bar{F}°_T - \bar{H}°_{298}}{T} \quad (5)$$

Results of this calculation are shown in Table II. Values marked with an asterisk are those derived from experiments in which CaF_2 was present. Equation 5 does not apply in this case as the relative pressures of Ca and CO are changed by the presence of CaF(g).

Table II: Values Derived for $\Delta H°_{298}$ for (1)

°K	$-\log P_i$, atm	$\frac{-\Delta\bar{F}°_T - \bar{H}°_{298}}{T}$, cal deg^{-1} mol^{-1}	$\Delta H°_{298}$, kcal mol^{-1}
1525	4.1416	70.86	170.1
1505	4.3208	70.90	170.0
1505	...	70.90	169.9*
1487	4.4314	70.93	169.9
1486	...	70.93	170.2*
1484	4.4368	70.94	169.7
1466	...	70.99	169.5*
1457	4.7008	71.01	170.2
1452	4.7508	71.02	170.3
1429	4.8862	71.09	169.4
			169.9 (average)

The equilibrium constants calculated from data from these runs were used directly with the relative free energy function to evaluate $\Delta H°_{298}$.

The standard deviation of the values of $\Delta H°_{298}$ is only 0.3 kcal mol^{-1}, and no temperature-dependent trend is observed. However, in view of the uncertainties in the extrapolation and in temperature, the absolute uncertainty is estimated at ±3 kcal mol^{-1}. A van't Hoff treatment of the slope (Figure 4) yields a value of $\Delta H°$ of 159 ± 6 kcal mol^{-1}, in satisfactory agreement with that derived from the free energy function treatment. The predicted value of $\Delta H°_{298}$ using the enthalpy of formation of CaO(s) as −151.8 kcal mol^{-1}, derived by Huber and Holley from heat of combustion data,[25] and values for Ca(g) and CO(g) of 42.2 and −26.4 kcal mol^{-1}, respectively,[17] is 167.6 kcal mol^{-1}, which compares favorably with our result. If the literature data cited are used to predict values of P_e at the temperatures of our experiments, the result shown as a line on Figure 3 is obtained. The uncertainties in the values cited lead to an uncertainty in the predicted pressures of a magnitude indicated by the vertical line terminated by bars (Figure 3).

No other report of a direct study of reaction 1 has been found in the literature. Our derived equilibrium pressures are slightly below those based on independent thermodynamic measurements, but considering the overall uncertainties and the large temperature difference between the calorimetric and effusion measurements, we are quite satisfied with the general agreement.

In general, our results suggest that the usefulness of the effusion method for the study of vaporization processes involving the interaction of solids may be considerably enhanced by following the variation of steady-state pressures with time. In cases where a fall-off with time is observed, extrapolation back to time zero may lead to near equilibrium pressures. A variety of cell orifice and sample sizes must be used to make certain that a valid extrapolation procedure has been used.

Acknowledgments. This work was supported in part by National Aeronautics and Space Administration Grant Number NGL 48-002-004 for "Interdisciplinary Research on the Nature and Properties of Ceramic Materials" and in part by the National Science Foundation Grant GP-6608X for the study of "Vaporization Reactions."

(23) "JANAF Thermochemical Data," Dow Chemical Co., Midland, Mich.

(24) K. K. Kelley and E. G. King, U. S. Bureau of Mines Bull. 592, U. S. Government Printing Office, Washington, D. C., 1961.

(25) E. J. Huber and C. E. Holley, *J. Phys. Chem.*, **60**, 498 (1956).

Spectroscopic Studies of Ionic Solvation in Pyridine Solutions[1]

by William J. McKinney and Alexander I. Popov[2]

Department of Chemistry, Michigan State University, East Lansing, Michigan 48823 *(Received July 31, 1969)*

Infrared spectra of a number of lithium, ammonium, and sodium salts were obtained in the 2000–100-cm^{-1} spectral region in pyridine solutions. In all cases a low-frequency band was observed whose position was dependent on the nature of the cation but, with the exception of NaI, not of the anion. The band maxima fall at ~418, 199, and 180 cm^{-1} for Li, NH_4, and Na salts, respectively. Substitution of ND_4^+ for NH_4^+ ion shifts the band by ~17 cm^{-1}. Examination of the skeletal vibrations of pyridine upon addition of alkali metal salts produces a shift to higher frequencies. The evidence indicates that the alkali cations are solvated in pyridine solutions and that the far-infrared bands can be assigned to the vibrations of the cations in the solvent cage.

Introduction

During the past few years, several investigators have reported far-infrared studies of alkali metal or tetraalkylammonium salts in various solvents.[3-6] In all cases a band was observed whose frequency was dependent on the mass of the cation. In polar solvents, such as dimethyl sulfoxide[5c] or 1-methyl-2-pyrrolidone,[5d] the frequency was independent of the anion and the bands were ascribed to the vibration of cations in a solvent cage. In nonpolar solvents such as benzene[3] or tetrahydrofuran[4] the band frequencies were anion dependent. These bands are probably due either to the vibration of unsolvated ion pair[3] or at least to the vibration of the cation in a cage consisting of both the solvent molecules and the anion.

French and Wood[6] recently measured the far-infrared spectra of sodium tetraphenylborate in pyridine, 1,4-dioxane, piperidine, and tetrahydrofuran solutions. They report a band at 175 cm^{-1} in all four solvents and assign the band to the interionic vibration of an unsolvated ion pair. They claim that the isotope shift of the 198-cm^{-1} band for $NH_4^+BPh_4^-$ solution to 183 cm^{-1} for $ND_4^+BPh_4^-$ also fits a bare ion model. It should be noted that no mention was made of the influence of anion substitution on the frequency of the observed bands.

Present work represents a part of a detailed spectroscopic study of ionic solvation carried out in this laboratory.

Experimental Part

All alkali metal salts were analytical grade reagents dried by standard procedures except for the ammonium and potassium tetraphenylborates which were prepared by adding a slight excess of an aqueous solution of ammonium or potassium chloride to an aqueous solution of sodium tetraphenylborate. The precipitate was then washed with water and dried under vacuum. Purification of pyridine has been described previously.[7] The purified pyridine was stored in an amber glass bottle over molecular sieves (Fisher Type 4A). The water content of the pyridine was approximately 3 m*M* as determined by a Karl Fisher titration. Tetrahydrofuran and 1,4-dioxane were reagent grade chemicals dried over calcium sulfate. Piperidine was fractionally distilled from granulated barium oxide. Since both the solvents and the salts were hydroscopic, care was taken to prepare them in as nearly anhydrous conditions as possible. Exposure of the solvents and solutions to the atmosphere during preparation or transfer was minimized by performing these operations with syringes.

Attempts to obtain the far-infrared spectra of potassium, rubidium, and cesium salts were unsuccessful owing to their low solubility in pyridine.

Infrared spectra were obtained on two instruments, a Perkin-Elmer Model 225 spectrometer with a range of 4000–200 cm^{-1} and Perkin-Elmer Model 301 spectrometer with a range of 666–20 cm^{-1}. Normally the Model 225 instrument was used for spectra at 4000–600 cm^{-1} and the Model 301 was used in the 666–50-cm^{-1} region. In cases in which duplicate measurements were made, they always agreed within experimental error. The frequency scale of the 301 spectrometer was calibrated using the rotational spectrum of water vapor. Standard infrared solution cells with NaCl windows were used from 4000 to 600 cm^{-1}, and polyethylene cells with 0.1 or 0.2-mm path lengths, purchased from Barnes Engineering Co., were used below 600 cm^{-1}. Concentration of solutions varied

(1) Abstracted in part from the Ph.D. Thesis of W. J. McKinney Michigan State University, 1969.

(2) To whom correspondence should be addressed.

(3) J. C. Evans and R. Y. Lo, *J. Phys. Chem.*, 69, 3223 (1965).

(4) (a) W. F. Edgell, J. Lyford, R. Wright, and W. Risen, *J. Amer. Chem. Soc.*, 88, 181 (1966); b) personal communication, in press.

(5) (a) B. W. Maxey and A. I. Popov, *J. Amer. Chem. Soc.*, 89, 3223 (1967); (b) *ibid.*, 90, 4470 (1968); (c) *ibid.*, 91, 20 (1969); (d) J. L. Wuepper and A. I. Popov, *ibid.*, 91, 4352 (1969).

(6) M. J. French and J. L. Wood, *J. Chem. Phys.*, 49, 2358 (1968).

(7) W. J. McKinney, M. K. Wong, and A. I. Popov, *Inorg. Chem.*, 7, 1001 (1968).

between 0.05 and 1.5 M. In general the band intensities were proportional to concentrations.

Results and Discussion

The frequencies of the infrared bands of lithium, ammonium, and sodium salts in pyridine are shown in Table I. These bands are similar in shape and are found in approximately the same spectral region as those reported for these salts in dimethyl sulfoxide,[5c] tetrahydrofuran,[4] and 1-methyl-2-pyrrolidone.[5d] It is seen that within experimental error the frequencies of the bands for lithium and ammonium salts are independent of the anion. With sodium salts the perchlorate, thiocyanate, and tetraphenylborate bands show approximately the same frequency at 180 cm^{-1} but the band for sodium iodide is 10 wave numbers lower in frequency. If the vibrations were due to unsolvated ion pairs, much greater dependence on the mass of the anion would be observed. The position of the band for the d_4-ammonium iodide salt in solution is shifted to lower energy by approximately 17 cm^{-1}. A simple calculation, based on a NH_4^+-pyridine "diatomic" model predicts a shift of 15 cm^{-1}. The good agreement between theory and experiment can be used as evidence that a cation–solvent vibration is involved in the appearance of these bands; however, it must be noted that in a calculation of this type in which molecules and ions are being treated as point masses, the predicted shift is a result of the change of mass of the ammonium ion. It is not sensitive to the mass of the solvent or anion as can be seen in the following equation

$$\nu_{ND_4^+} = \nu_{NH_4^+}\sqrt{\left(\frac{18 \times S}{18 + S}\right)\left(\frac{22 + S}{22 \times S}\right)}$$

In this equation, $\nu_{ND_4^+}$ and $\nu_{NH_4^+}$ are the frequencies of the vibration of the ammonium ions with the interacting species,[5] 18 is the mass of the ammonium ion, 22 is the mass of the d_4-ammonium ion, and S is the mass of the solvent molecule or anion interacting with the ammonium ion. For most values of S the term under the radical reduces to 18/22. It is significantly different from this value only for very small values of S. French and Wood[6] also carried out measurements of band shifts upon substitution of the ND_4^+ cation for the NH_4^+ cation. Their value of 183 ± 3 cm^{-1} for the d_4-ammonium tetraphenylborate band in pyridine agrees with the value obtained in this investigation for the d_4-ammonium iodide. The above authors, however, interpreted their results as an added evidence for their assignment of the band to an inner ion-pair vibration. It is seen that an equally plausible assignment of the band to a cation–solvent vibration can be made.

Table I: Frequencies of the Vibrational Bands of Alkali Metal Salts in Pyridine

Compound	ν_{max}, cm^{-1}
LiCl	416 ± 4
LiBr	418 ± 4
LiI	419 ± 4
$LiClO_4$	419 ± 4
$LiNO_3$	420 ± 4
NH_4I	196 ± 3
NH_4ClO_4	197 ± 3
NH_4NO_3	201 ± 3
NH_4SCN	199 ± 3
NH_4BF_4	198 ± 3
NH_4BPh_4	199 ± 3
ND_4I	183 ± 3
NaI	170 ± 3
$NaClO_4$	182 ± 3
NaSCN	180 ± 3
$NaBPh_4$	179 ± 3

Following the example of French and Wood,[6] an attempt was also made to obtain the infrared spectra of sodium tetraphenylborate in 1,4-dioxane, tetrahydrofuran, and piperidine. In the last solvent as well as in pyridine our results agree with the above authors (176 ± 4 cm^{-1} and 179 ± 3 cm^{-1}). We were unsuccessful with 1,4-dioxane solutions since the concentrations of the saturated solutions were too low for measurements. In tetrahydrofuran, however, the band was observed at 194 ± 4 cm^{-1} instead of 179 cm^{-1} as reported by French and Wood. Our results, however, agree with those of Edgell, *et al.*,[4b] who report a band at 198 ± 3 cm^{-1} for sodium tetraphenylborate solutions in tetrahydrofuran.

Additional evidence for the solvation of alkali metal ions by pyridine comes from the study of the shifts of the pyridine skeletal vibrations in the presence of alkali salts. Takahashi, *et al.*,[8] have shown that in the presence of hydrogen-bonding solvents such as H_2O, CH_3OH, C_2H_5OH, and $CHCl_3$ these bandss hift to higher frequencies, instead of lower frequencies as expected from the increase in mass. The observed shifts indicate that pyridine–hydrogen bonding solvent interactions change the electron distribution of the pyridine ring and strengthen the chemical bonds within the ring. Similar shifts have been observed by us upon addition of alkali metal salts to pyridine. The results are shown in Table II. Spectral shifts are in the same direction and of the same magnitude as those reported by Takahashi, *et al.*[9] For example, these authors observe a shift of +11–12 cm^{-1} for ν_{8a} band, +9–10 cm^{-1} for ν_1 and +11 cm^{-1} for ν_{6a}. It seems reasonable to assume that in this work the shifts of the skeletal vibrations are due to the same phenomena as in the work of Takahashi, *et al.*, namely to the interactions of pyridine with the alkali metal cations. At least four

(8) H. Takahashi, K. Mamola, and E. K. Plyler, *J. Mol. Spectrosc.*, 21, 217 (1966).

(9) Reference 8, Table I.

salts of each cation were examined and no anion effect was observed. Infrared spectra of the tetraalkylammonium perchlorate likewise did not indicate any shift for the three bands. The magnitude of the shift is low conductances of alkali metal salts in pyridine have been explained as being due to an interaction between the alkali metal ions and pyridine.[11]

On the basis of the above evidence it seems reasonable to conclude that the alkali metal cations are solvated in pyridine solutions and that the infrared bands listed in Table I are due to the vibrations of the cations in the solvent cage. This observation does not preclude the formation of solvent-separated ion pairs in pyridine solutions as demonstrated by conductometric measurements.[11,12] In most cases, however, electrostatic interaction between solvated ions does not seem to influence noticeably the frequencies of the solvent–metal ion vibrations. It is possible that in the case of sodium iodide, the anion may enter into the primary solvation shell of the cation.

Acknowledgment. The authors gratefully acknowledge the support of this work by a grant from the National Science Foundation.

Table II: Frequency Shifts of Three Pyridine Skeletal Vibrations Produced by Alkali Metal Salts

	ν_{max}, cm^{-1}					
	ν_{8a}[a]	$\Delta\nu$	ν_1	$\Delta\nu$	ν_{6a}	$\Delta\nu$
Pyridine	1581	...	992	...	603	...
Na^+ solutions	1590	+9	996	+4	611	+8
NH_4^+ solution	1592	+11	999	+7	614	+11
Li^+ solution	1597[b]	>+12	1003	+11	620	+17

[a] Assignments of L. Corrsin, B. J. Fax, and R. C. Lord, *J. Chem. Phys.*, **21**, 1170 (1953). [b] The shifted 1581-cm^{-1} band lies too close to the 1598-cm^{-1} pyridine band to be resolved; consequently, only a single band at 1597 cm^{-1} is observed.

$Na^+ < NH_4^+ < Li^+$ and should give an indication of the relative bond strength of the three ions with the pyridine molecules.

Finally, the interaction of pyridine with alkali metal salts has also been demonstrated by the formation of solid solvates with lithium chloride.[10] Likewise, the

(10) H. Brusset and S. Halut-Desportes, *Bull. Soc. Chim. Fr.*, 459 (1967).

(11) D. S. Burgess and C. A. Kraus, *J. Amer. Chem. Soc.*, **70**, 706 (1948).

(12) H. C. Mandel, W. M. McNabb, and J. F. Hazel, *J. Electrochem. Soc.*, **102**, 263 (1955).

Infrared Matrix Isolation Spectrum of the Methyl Radical Produced by Pyrolysis of Methyl Iodide and Dimethyl Mercury

by Alan Snelson

IIT Research Institute, Chicago, Illinois 60616 *(Received March 12, 1969)*

The matrix isolation technique has been used to trap methyl radicals formed by the gas-phase pyrolysis of methyl iodide, d_3-methyl iodide, and dimethyl mercury. The three observed infrared-active vibration frequencies of the CH_3 radical assuming a planar structure, point group D_{3h}, are $\nu_2 = 617$ cm^{-1}, $\nu_3 = 3162$ cm^{-1}, and $\nu_4 = 1396$ cm^{-1}. The corresponding frequencies for CD_3 are $\nu_2 = 463$ cm^{-1}, $\nu_3 = 2381$ cm^{-1}, and $\nu_4 = 1026$ cm^{-1}. The infrared-inactive frequency ν_1 is calculated at 3044 and 2153 cm^{-1} for CH_3 and CD_3, respectively, using the UBFF potential for an analysis of the vibrational modes. Some observations on the mechanisms of decomposition of methyl iodide and dimethyl mercury under the present experimental conditions are made, and a tentative vibrational assignment for the radical $HgCH_3$ is given.

Introduction

The results of three investigations aimed at trapping methyl radicals in rare gas matrices have recently been published. In the first of these, Pimentel and Andrews[1] attempted to form methyl radicals by reaction of either methyl iodide or bromide with lithium atoms during the deposition of the matrix.[2] Two absorption bands were observed in an argon matrix at 730.3 and 1383 cm^{-1} which were assigned to the

(1) L. Andrews and G. C. Pimentel, *J. Chem. Phys.*, **47**, 3637 (1967).

(2) W. L. S. Andrews and G. C. Pimentel, *ibid.*, **44**, 2527 (1966).

methyl radical with D_{3h} symmetry. The lower frequency was assigned to the out-of-plane bending mode from observations of the isotopic frequency shifts using deuterium and carbon-13 substituted species. The agreement between the observed and calculated frequency shifts was excellent. In the second investigation, Milligan and Jacox[3] attempted to form methyl radicals by the vacuum-ultraviolet photolysis of methane in argon and nitrogen matrices. From the ultraviolet spectrum of the photolyzed methane, absorption features were observed at about 1500 Å in excellent agreement with Herzberg's[4] assignment for one of the CH_3 radical's electronic transitions. An absorption band at 611 cm^{-1} in the argon matrix was assigned to the out-of-plane bending mode of the CH_3 radical, and again, frequency shifts due to isotopic substitution with deuterium and carbon-13 supported this assignment. The obvious disagreement between the two reported values for the out-of-plane bending mode of the CH_3 radical prompted Pimentel and Tan[5] to reinvestigate their alkyl halide plus alkali metal system. This time sodium and potassium were used in addition to lithium atoms to reduce the methyl halides during entrapment in the inert gas matrices. This study indicated that the band at 730 cm^{-1} previously assigned to the methyl radical could be best assigned to a new molecular species, a methyl alkali halide. This interpretation throws some doubt on the value of the higher frequency at 1383 cm^{-1} previously assigned to a doubly degenerate in-plane bending mode of the methyl radical.[2] Milligan and Jacox attributed their inability to locate the frequencies for the two infrared-active in-plane bending and stretching modes to low extinction coefficients.

In an effort to observe the three infrared-active vibration frequencies of the methyl radical an attempt was made to adapt the matrix isolation technique to the trapping of radicals produced by the low-pressure pyrolysis of suitable organic compounds. Although this type of experiment has been tried by several workers before[2] without success, the results of some recent studies on the matrix isolation spectrum of lithium fluoride in this laboratory[6] suggest that this is now possible. In the earlier attempts, matrix dilutions of several hundred parts of inert gas to one of the trapped species were used. The study on lithium fluoride demonstrated that efficient isolation of a reactive material in a molecular beam can only be achieved at dilution ratios of about 80,000 parts of matrix to one of the reactive molecule. There is little doubt that the primary cause of failure in the earlier studies was that of poor isolation.

Experimental Section

The matrix isolation cryostat used in this study has been described elsewhere,[6] and only the modifications new to the present arrangement are described.

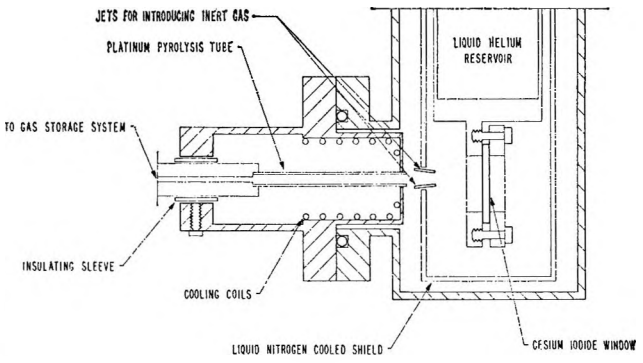

Figure 1. Pyrolysis attachment to matrix isolation cryostat.

The original Knudsen cell furnace was removed from the cryostat. In its place an attachment for the pyrolysis of suitable organic vapors was added. This is shown in Figure 1. The pyrolysis reactor consisted of a platinum tube about 1.8 in. long with an id of about 0.090 in. It was heated resistively. No attempt was made to achieve temperature uniformity along the length of the pyrolysis zone. The temperature was measured at the center of the pyrolysis zone with an optical pyrometer. To achieve better heat transfer between the reactor and the reactant, the pyrolysis zone was packed with a small amount of platinum gauze. One end of the tube was mounted in a water-cooled copper plate and was placed about 1.5 in. from the matrix isolation window in the cryostat. The other end was attached to a gas inlet system. The material to be pyrolyzed was fed into the reactor, usually at a rate of about $1-5 \times 10^{-5}$ mol/hr. The amount of material which is described as being deposited on the window in Figures 1, 2, and 3 is simply the number of moles of the given species which were bled into system *via* the pyrolysis tube during the course of the experiment. This rate was controlled by interposing a slow fixed leak between the gas storage system and the pyrolysis reactor and maintaining a suitable pressure differential across the leak. The matrix gas flow rate was controlled by a needle valve and monitored by measuring the pressure differential on a dibutyl phthalate manometer. In all experiments flow rates of about 0.05 mol/hr were used, and neon was used as the matrix material since experience has shown that this gas produces the most transparent matrices. Liquid helium was used as the refrigerant. Although the experimental conditions used in the present study were sufficient to obtain fairly good isolation of the reactive species, they were definitely not good enough to prevent a small amount of reaction occurring in the trapping process.

(3) D. E. Milligan and M. E. Jacox, *J. Chem. Phys.*, **47**, 5146 (1967).
(4) G. Herzberg, *Proc. Roy. Soc.*, **A262**, 291 (1961).
(5) L. Y. Tan and G. C. Pimentel, *J. Chem. Phys.*, **48**, 5202 (1968).
(6) A. Snelson, *J. Phys. Chem.*, **74**, 1919 (1969).

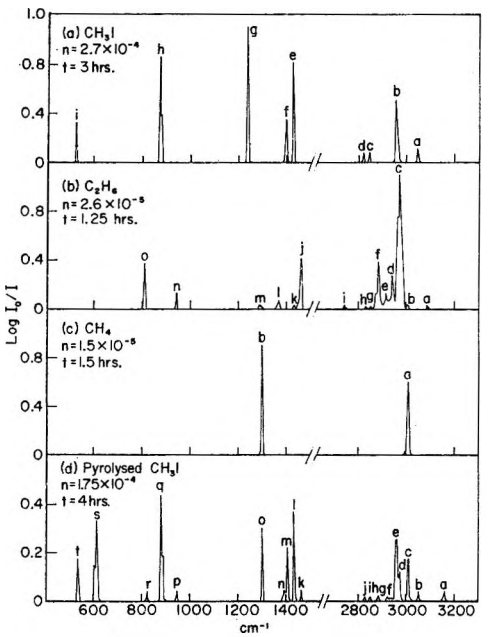

Figure 2. Matrix isolation spectra in neon of (a) pure CH_3I, 2.7×10^{-4} mol; (b) pure C_2H_6, 2.6×10^{-5} mol; (c) pure CH_4, 1.5×10^{-5} mol; and (d) pyrolyzed CH_3I, 1.75×10^{-4} mol. Approximate fraction decomposed 0.25.

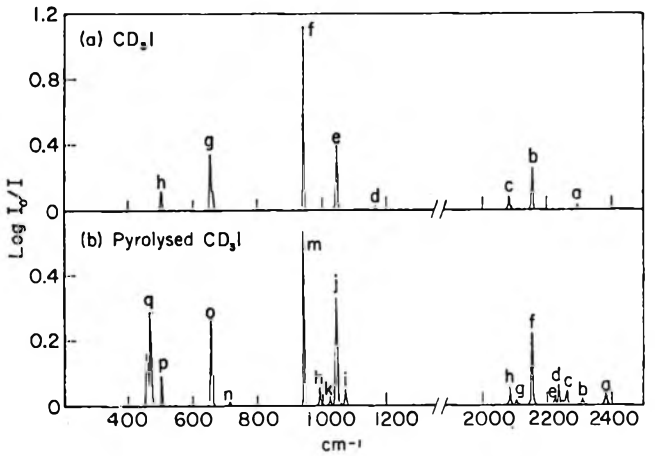

Figure 3. Matrix isolation spectra in neon of (a) pure CD_4I, 8.8×10^{-5} moles deposited in 3 hr, and (b) pyrolyzed CD_3I, 1.1×10^{-4} mol deposited in 6 hr. Approximate fraction decomposed, 0.20.

Methyl iodide (Matheson Coleman and Bell) reagent grade was distilled once prior to introduction to the gas storage system. It was out-gassed thoroughly using standard vacuum line techniques. The d_3-methyl iodide (Volk Radiochemical Company) was used directly after thorough out-gassing. Dimethyl mercury (Alpha Inorganics) was thoroughly out-gassed and distilled under high vacuum using liquid nitrogen as a coolant. The initial condensate was discarded, and the middle fraction retained for use. Methane (Matheson Co. research grade) with a stated purity of 99.99% was used without any pretreatment. Ethane (Matheson Co. technical grade) was used without any pretreatment. The maximum stated hydrocarbon impurities in the sample on a volumetric basis were ethylene 5%, methane 1%, and propane plus propylene 2%. Research grade neon (Matheson Co.) was used for the matrix gas and was passed through a liquid nitrogen cooled trap prior to injection into the matrix isolation cryostat. Infrared spectra were recorded on a Perkin-Elmer 621 spectrophotometer. The calibration of the instrument was checked against atmospheric water and carbon dioxide bands. Reported frequencies are believed accurate to ± 1 cm^{-1}.

Infrared Spectra. Results

The pyrolysis of methyl iodide is known to occur by schism of the carbon–iodine bond.[7] At the pressures existing in the pyrolysis reactor used in this study of approximately 10^{-6} atm, some of the radicals undergo reaction through gas-phase collision before escaping from the reactor and being trapped in the matrix. These reactions can lead to the formation of stable products methane and ethane, etc. For this reason, it was deemed advisable to examine the matrix isolation spectra not only of pure methyl iodide and its deuterated derivatives before pyrolysis, but also that of methane and ethane. In this way the effect of the matrix environment on the spectra of the various compounds could be observed, allowing more positive identification of the products of the pyrolysis reaction.

The important regions in the spectra of CH_3I, CD_3I, $Hg(CH_3)_2$, CH_4, and C_2H_6, are shown in Figures 2, 3, and 4. Frequencies are listed in Table I. Absorbance values were calculated for all lines so that relative intensity considerations in addition to frequency values could be used in making assignments for the pyrolysis products. With the exception of five bands in the spectrum of CH_3I, all the matrix frequencies were found to correspond with the previously reported gas phase values.[8–16]

It was found possible to assign these five "excepted" bands in the CH_3I spectrum to combination modes rather than to impurity bands. In general, the matrix frequencies were lower than the reported gas-phase

(7) S. W. Benson, "The Foundations of Chemical Kinetics," McGraw-Hill Book Co., Inc., New York, N. Y., 1960.

(8) W. T. King, I. M. Mills, and B. Crawford, *J. Chem. Phys.*, 27, 455 (1957).

(9) F. D. Verderame and E. R. Nixon, *ibid.*, 45, 3476 (1966).

(10) G. Herzberg, "Infrared and Raman Spectra of Polyatomic Molecules," D. Von Nostrand Co., Inc., Princeton, N. J., 1960.

(11) L. G. Smith, *J. Chem. Phys.*, 17, 139 (1949).

(12) A. Cabana, G. B. Savitsky, and D. F. Hornig, *ibid.*, 39, 2942 (1963).

(13) F. H. Fraver and G. E. Ewing, *ibid.*, 48, 781 (1968).

(14) H. S. Gutowsky, *ibid.*, 17, 128 (1949).

(15) A. B. Kittila, Ph.D. Thesis, University Microfilms Inc., Ann Arbor, Mich., No. 66-7056.

(16) D. R. J. Boyd, H. W. Thompson, and R. L. Williams, *Discussions Faraday Soc.*, 9, 154 (1950).

Table I: Observed Frequencies (cm^{-1}) for CH_3I, CD_3I, CH_4, C_2H_4, C_2H_6, and $Hg(CH_3)_2$ Trapped in a Neon Matrix

CH_3I		CD_3I		C_2H_6		C_2H_4		$Hg(CH_3)_2$			
a	3055	a	2267	c	2979	a	3099	a	2988	f	1442
b	2965	b	2154	d	2947	k	1437	b	2943	g	1430
c	2855	c	2080	e	2921	n	948	c	2906	h	1375
d	2830[b]	d	1045	f	2888			d	2828	i	1337
e	1435	e	1169	g	2857		CH_4[c]	x	2380	j	1199
f	1409[b]	f	945	h	2839	b	3015	x	1720	k	784
g	1249	g	655	i	2747	m	1305	e	1472	l	549
h	883	h	499	j	1467						
i	532			l	1372						
x[a]	2496[b]		CH_4	o	819						
x[a]	2320[b]	a	3015								
x[a]	2135[b]	b	1305								

[a] The frequencies designated with an x are not shown in Figures 1, 2, and 3. [b] These frequencies were not included in Crawford's assignment for CH_3I. [c] These frequencies result from C_2H_4 and CH_4 impurities in the C_2H_6.

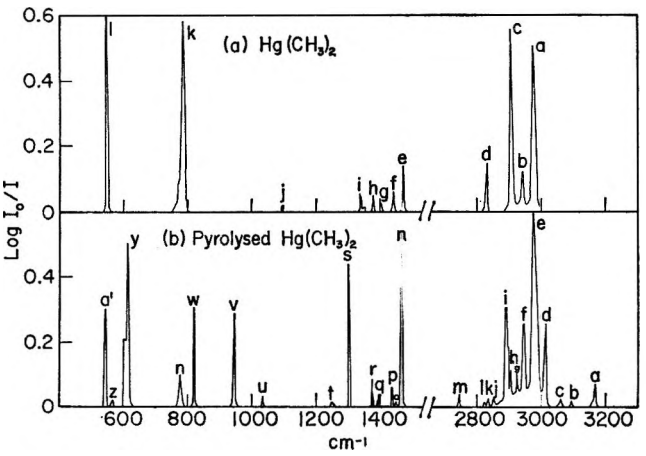

Figure 4. Matrix isolation spectra in neon of (a) pure $Hg(CH_3)_2$, 4.7×10^{-5} mol deposited in 2.5 hr, and (b) pyrolyzed $Hg(CH_3)_2$, 8.3×10^{-5} mol deposited in 4 hr. Approximate fraction decomposed, 0.83.

values by about 5 cm^{-1}, and there was little evidence of the matrix environment causing splitting of absorption bands due to the trapped molecule occupying different sites in the matrix lattice. The only previous matrix studies involving any of these species involved the trapping of CH_4 in matrices of argon, krypton, and xenon.[12,13] In these matrices, both CH_4 infrared absorption bands showed considerable structure which was satisfactorily interpreted as being due to hindered rotation of CH_4 in the matrix cage. The lack of any structure for these same bands in a neon matrix suggests that hindered rotation is not occurring in this matrix.

Pyrolyzed CH_3I, CD_3I, and $Hg(CH_3)_2$. Methyl iodide and d_3-methyl iodide were pyrolyzed at temperatures between 1200 and 1400°. The spectra are shown in Figures 2d and 3b, and the frequencies listed in Tables II and III. Five experiments were made with methyl iodide using somewhat different flow rates through the pyrolyzing zone. In this way it was

Table II: Frequency Assignment for the Pyrolysis Products[a] of Methyl Iodide (cm^{-1})

	Frequency, cm^{-1}	Species		Frequency, cm^{-1}	Species
a	3162	CH_3	k	1467	C_2H_6
b	3055	CH_3I	l	1435	CH_3I
c	3015	CH_4	m	1409	CH_3I
d	2979	C_2H_6	n	1398	CH_3
e	2965	CH_3I	o	1305	CH_4
f	2948	C_2H_6	p	948	C_2H_4
g	2921	C_2H_6	q	883	CH_3I
h	2888	C_2H_6	r	819	C_2H_6
i	2855	CH_3I	s	614	CH_3
j	2830	CH_3I	t	532	CH_3I

[a] Pyrolysis temperature of 1300° and a neon matrix.

Table III: Frequency Assignment for the Pyrolysis Products[a] of d_3-Methyl Iodide (cm^{-1})

	Frequency, cm^{-1}	Species		Frequency, cm^{-1}	Species
a	2381	CD_3	j	1045	CD_3I
b	2297	CD_3I	k	1026	CD_3
c	2258	CD_4	l	996	CD_4
d	2236	C_2D_6	m	945	CD_3I
e	2225	C_2D_6	n	717	C_2D_4
f	2154	CD_3I	o	655	CD_3I
g	2005	C_2D_6	p	499	CD_3I
h	2080	CD_3I	q	463	CD_3
i	993	C_2D_4			

[a] Pyrolysis temperature of 1350° and a neon matrix.

possible to use absorption intensity considerations to identify bands belonging to the same molecular species. For methyl iodide it was found possible to account for all absorption bands, with the exception of three, in terms of the species CH_3I, CH_4, C_2H_6, and C_2H_4. Relative absorption intensities of bands assigned to these species were in agreement with those

observed previously in the spectra of the pure compounds. The most intense of the three unassigned bands occurred at 617 cm^{-1}, with two much weaker features at 1395 and 3162 cm^{-1}. The band at 617 was split into two components with a separation of 6 cm^{-1}. It was difficult to discriminate if splitting occurred in the band at 1398 cm^{-1} due to the close proximity of a methyl iodide band at 1409 cm^{-1}. No splitting occurred in the band at 3162 cm^{-1}. Four pyrolysis experiments were made on d_3-methyl iodide. Absorption bands assigned to CD_4, C_2D_6, and C_2D_4 were made using the gas-phase frequencies listed by Herzberg[10] and comparison with the comparable spectra of the hydrogenated species. Again three absorption bands were observed which could not be assigned to the above stable hydrocarbons; these occurred at 2381, 1026, and 463 cm^{-1}. The low-frequency band at 463 cm^{-1} exhibited a splitting of 7 cm^{-1}, but the two higher frequencies appeared as singlets.

Dimethyl mercury was pyrolyzed at temperatures between 1200 and 1400°. A typical spectrum is shown in Figure 3b and the frequencies listed in Table IV. Of twenty-seven absorption bands, nineteen can be assigned between the species $Hg(CH_3)_2$, CH_4, C_2H_6, and C_2H_4. Of the remaining eight, three at 617, 1396, and 3162 cm^{-1} had similar relative intensities as bands with the same frequencies in the spectrum of pyrolyzed CH_3I. The band at 617 cm^{-1} showed splitting of 6 cm^{-1}. The two higher frequencies appeared as singlets.

Table IV: Frequency Assignment for the Pyrolysis Products[a] of $Hg(CH_3)_2$

	Frequency, cm^{-1}	Species		Frequency, cm^{-1}	Species
a	3162	CH_3	o	1450	$HgCH_3$
b	3099	C_2H_4	p	1437	C_2H_4
c	3062	$HgCH_3$	q	1396	CH_3
d	3015	CH_4	r	1372	C_2H_6
e	2979	C_2H_6	s	1305	CH_4
f	2947	C_2H_6	t	1245	$HgCH_3$
g	2921	C_2H_6	u	1030	$HgCH_3$
h	2906	$Hg(CH_3)_2$	v	948	C_2H_4
i	2888	C_2H_6	w	819	C_2H_6
j	2857	C_2H_6	x	784	$Hg(CH_3)_2$
k	2839	C_2H_6	y	614	CH_3
l	2828	$Hg(CH_3)_2$	z	570	$HgCH_3$
m	2747	C_2H_6	a′	549	$Hg(CH_3)_2$
n	1467	C_2H_6			

[a] Pyrolysis temperature of 1300° and a neon matrix.

In Table V, the intensities of the absorption bands at 617, 1396, 3162, 463, 1023, and 2381 cm^{-1} obtained from the various pyrolysis experiments are shown. Because of the relatively large difference in absorption intensity between the low- and two higher-frequency bands in the three sets of pyrolysis experiments, accurate intensity measurements were difficult. For the data quoted in Table V, the automatic slit programmer of the spectrometer was disengaged and the slit opening maintained at a fixed setting during the intensity measurements. No intensities for the band at 1396 cm^{-1} in the pyrolysis of CH_3I are listed since the close proximity of a methyl iodide band precluded meaningful measurements. The precision of the intensity measurements is believed to be about ±5% for the high-frequency low-intensity bands and somewhat better for the more intense low-frequency bands. The values for the ratios of band intensities listed in Table V are consistent, within the precision of the measurements, with an assignment for the bands at 617, 1396, and 3162 cm^{-1} to a single molecular species and those at 463, 1023, and 2381 cm^{-1} likewise to a single molecular species.

Discussion

Methyl Radical. In the spectra of both pyrolyzed methyl iodide and d_3-methyl iodide, two sets of absorption bands are observed at 617, 1398, and 3162 cm^{-1}, and 463, 1026, and 2381 cm^{-1}, respectively, which cannot be assigned to any of the expected stable pyrolysis products of the reactants. The appearance of three absorption bands in the spectra of pyrolyzed dimethyl mercury with similar frequencies and relative intensities as those observed in the pyrolysis of methyl iodide is evidence that the same compound is responsible for both sets of absorption bands and that it consists of carbon and hydrogen only. The frequencies of the most intense absorption bands at 617 cm^{-1} (pyrolyzed CH_3I) and 463 cm^{-1} (pyrolyzed CD_3I) are in close agreement with those assigned by Milligan and Jacox[3] to the out-of-plane bending modes of CH_3, 611 cm^{-1} and CD_3, 463 cm^{-1}. The latter frequencies were recorded for the radicals trapped in a nitrogen matrix and hence exact agreement cannot be expected with those obtained in the present investigation for which a neon matrix was used. Milligan and Jacox have concluded from the existing data on the methyl radical and from their own experiments that the methyl radical is most probably planar, belonging to the point group D_{3h}. Such a molecule has, in addition to the out-of-plane bending mode, two infrared-active in-plane vibration modes. If the interpretation of the present experimental data is correct, these modes should correspond to the two higher frequencies observed at 1398 and 3162 cm^{-1} and 1026 and 2381 cm^{-1} in the CH_3I and CD_3I pyrolysis studies. Evidence in favor of this assignment may be obtained from a comparison of the observed and calculated isotopic shifts of these lines. Using the nomenclature of Herzberg, the ratio $\nu_3^{H_2}\nu_4^{H_2}/\nu_3^{D_2}\nu_4^{D_2}$ based on the atomic masses is calculated at 1.824. The H_2 and

Table V: Experimental Absorption Intensities and Intensity Ratios for Absorption Bands Assigned to the CH_3 and CD_3 Radicals

Expt no.[a]	Log I_0/I for peak at: 617 cm^{-1}	1396 cm^{-1}	3162 cm^{-1}	Intensity ratios[b] A^{617}/A^{1396}	A^{617}/A^{3162}	A^{3162}/A^{1396}
1	0.379	0.039	0.043	9.72	8.81	1.10
2	1.192	0.121	0.131	9.85	9.10	1.08
3	0.627	0.066	0.075	9.50	8.36	1.14
4	0.525	...	0.062	...	8.47	...
5	0.431	...	0.050	...	8.63	...
	Log I_0/I for peaks at: 463 cm^{-1}	1026 cm^{-1}	2381 cm^{-1}	Intensity ratios A^{463}/A^{1026}	A^{463}/A^{2381}	A^{2381}/A^{1026}
6	0.203	0.024	0.033	8.44	5.78	1.37
7	0.226	0.026	0.038	8.64	6.00	1.44
8	0.187	0.021	0.031	9.04	6.11	1.48

[a] Expt no. 1, 2, and 3 apply to CH_3 from the pyrolysis of $Hg(CH_3)_2$, and no. 4 and 5, to CH_3 from the pyrolysis of CH_3I. [b] A^N = log I_0/I for the absorption band at N cm^{-1}.

D_2 superscripts indicate the frequencies of the hydrogenated and deuterated samples, respectively. The observed value for this ratio is 1.810 in good agreement with the calculated value considering that no anharmonic corrections have been applied to be observed frequencies. In calculating this observed ratio of the frequencies, the value of $\nu_4^{H_2}$ = 1396 cm^{-1} was used, derived from the pyrolysis of dimethyl mercury. The value obtained from the methyl iodide pyrolysis was complicated by the proximity of the $\nu_3 + \nu_6$ combination band of CH_3I and was believed to be less reliable.

Further support for the present assignment might be obtained by attempting to observe the spectra of the species CH_2D and CHD_2, since for these radicals all six fundamental vibration modes are ir active. Unfortunately, at the time of the investigation, this was not possible. The author believes that such a study would probably encounter difficulties with low absorption intensities of some of the in-plane vibration modes. Although, in principle, weak absorption bands can be observed by performing experiments with long deposition times, practical experience shows that at the high matrix dilutions used in these experiments, the optical transparency of the matrix becomes severely reduced after about 8 hr of deposition.

In Table VI the results of applying the Urey–Bradley force field to the in-plane vibrations of CH_3 and CD_3 are given. To simplify the calculations, the approximation for the interaction constants given by Shimanouchi,[17] $F' = 0.1F$, was used and values of K, H, and F, the in-plane bond stretching, bond bending, and nonbonded interaction constants calculated. Shimanouchi,[17] after applying the UBFF to a variety of molecules containing carbon–hydrogen bonds found that K ranged between 3.9 and 4.8 $\times 10^{-5}$ dyn cm^{-1}. The value of $K = 5.2 \times 10^{-5}$ dyn cm^{-1} obtained for the CH_3 radical is somewhat larger than Shimanouchi's typical values, but is not unreasonable considering the the bond length given by Herzberg,[4] from an analysis of the rotational

Table VI: Force Constants and Frequencies for CH_3 and CD_3[a]

	CH_3 Frequencies, cm^{-1} Obsd	Calcd	CD_3 Frequencies, cm^{-1} Obsd	Calcd
ν_1		3044		2153
ν_2	617	617	463	476
ν_3	3162	3161	2381	2362
ν_4	1396	1398	1026	1025

[a] $K = 5.2 \times 10^5$ dyn cm^{-1}, $H = 0.315 \times 10^6$ dyn cm^{-1}, $F = 0.100$ dyn cm^{-1}, and $F' = 0.1F$ and $F_\gamma = 0.179 \times 10^5$ dyn cm^{-1}.

spectrum of CD_3, at 1.079 Å, is shorter than that found in methane, 1.091 Å, and ethylene, 1.086 Å. The in-plane bending constant $H = 0.315 \times 10^5$ dyn cm^{-1} and the interaction constant $F_\gamma = 0.1 \times 10^5$ dyn cm^{-1} are in the same range as for other carbon–hydrogen molecules. The effect of varying F' by $\pm 100\%$ in terms of F was found to have a negligible effect on the calculated values of K, H, and F. Considering that anharmonic effects were not taken into account, the agreement between the observed and calculated values of ν_3 and ν_4 for CH_3 and CD_3 is satisfactory. The out-of-plane bending constant $F_\gamma = 0.179 \times 10^5$ dyn cm^{-1} was calculated from the observed frequency for CH_3. The rather poor agreement between the observed and calculated values of this frequency for CD_3 using the above value of F_γ can probably be attributed to anharmonic effects. The ratio of the in-plane to out-of-plane bonding force constants of CH_3, $K/F_\gamma = 29$, is considerably larger than the same ratios for other XY_3 ions and molecules which have been studied, values of latter ranging from 3.7 to 9.8.[18] This relatively low out-of-plane bending frequency is almost certainly a reflection of the small amount of energy required for the CH_3 radical to assume a nonplanar configuration.

(17) T. Shimanouchi, *J. Phys. Chem.*, 17, 849 (1949).
(18) G. J. Janz and Y. Mikawa, *J. Mol. Spectrosc.*, 1, 92, 1960.

Pimentel, *et al.*,[1] have reported a value of $\nu_4 = 1383$ cm^{-1} for the methyl radical. However, in a later publication they showed that the absorption bands previously assigned to the methyl radical were almost certainly due to a compound of the type CH_3MX where M is an alkali metal and X a halogen atom. Comparison of this assignment for ν_4 with that derived from this study is therefore not valid.

Pyrolysis Reactions. In the pyrolysis of methyl iodide (Figure 2d) the only products formed based on the infrared spectroscopic analyses were CH_4, C_2H_4, C_2H_6, and CH_3. No absorption bands were observed which could not be assigned to these species. Although no detailed pyrolysis study of methyl iodide has been made, Benson[19] has predicted the products to be CH_4, C_2H_4, and I_2, methane being formed in the reaction $CH_3 + CH_3I = CH_4 + CH_2I$ and ethylene from $2CH_2I = (C_2H_4I_2)^* = C_2H_4 + I_2$. If Benson's predictions are correct, the presence of ethane in the reaction products of pyrolysis in this study must be assigned to polymerization of CH_3 radicals occurring in the matrix. However, estimates of the amount of ethane formed by polymerization in the matrix under the conditions of these experiments are lower by a factor of 5 than those actually observed. There appears to be a possibility in the methyl iodide pyrolysis that reactions of the type $CH_3 + CH_3I = C_2H_6 + I$ or $CH_3 + CH_3 + M = C_2H_6 + M$ are occurring. Two pyrolysis experiments were made in which both the matrix gas and methyl iodide were passed through the reactor at about 1300° and then frozen on the matrix window. In these experiments the amount of methane formed was smaller by a factor of five compared to when methyl iodide alone was passed through the pyrolysis zone. No ethylene was observed at all. This observation is consistent with the reaction steps proposed by Benson for the formation of methane and ethylene. The fact that no absorption bands were observed which could be assigned to the intermediate CH_2I suggests that either its concentration is too low, thus precluding its observation spectroscopically, or that its lifetime under the experimental conditions is too short. The former possibility is not likely, since if sufficient CH_2I is formed to yield a measurable quantity of ethylene by bimolecular collision, it would be expected that enough would fail to react to permit trapping and observation.

The pyrolysis of dimethyl mercury (DMM) in this investigation gives the products CH_4, C_2H_4, C_2H_6, and CH_3 and some other specie or species. This products distribution is based on analysis of the infrared spectra of the pyrolysis reaction. Reference to previous studies on the pyrolysis of DMM shows that at moderate pressures, and temperatures of 300–400°, a typical product distribution might be CH_4, 50%; C_2H_4, 7%; C_2H_6, 30%; C_3H_8, 12%, with the remaining 1% consisting of other hydrocarbons.[20] In the present study, the ratio of C_2H_6:CH_4 is about 2:1. This is markedly different from the "typical product distribution" at 300–400° but the observation has been made that at higher temperatures the ethane production is enhanced. In this study it was not possible to estimate the relative amount of ethylene to methane or ethane, since no calibration experiments were performed with pure ethylene. According to Kallend, *et al.*,[20] the major reactions leading to methane and ethane formation at moderate pressures are $CH_3 + CH_3HgCH_3 = CH_4 + CH_2HgCH_3$, and $CH_3 + CH_2HgCH_3 = C_2H_5 + Hg + CH_3$ followed by $C_2H_5 + CH_3HgCH_3 = C_2H_6 + CH_2HgCH_3$. This scheme accounts for the formation of larger quantities of methane than ethane, but in the present study more ethane than methane was produced. Thus at the low pressure and the high temperatures used in this study ethane must be formed by some additional process, possibly from the recombination of methyl radicals, $2CH_3 = C_2H_6$, or by a radical abstraction reaction, $CH_3 + CH_3HgCH_3 = C_2H_6 + HgCH_3$. Kallend, *et al.*,[20] have reviewed the available data of the DMM pyrolysis and conclude the initial reaction can be represented by $CH_3HgCH_3 = 2CH_3 + Hg$, but suggest that it probably occurs in two steps, $CH_3HgCH_3 = HgCH_3 + CH_3$ and $HgCH_3 = Hg + CH_3$. They have inferred from kinetic data that the decomposition of $HgCH_3$ occurs with zero activation energy and hence its lifetime is short. That no absorption bands with similar intensity as the strongest of the methyl radical bands occur which can be assigned to $HgCH_3$ is evidence in favor of short lifetime for $HgCH_3$; alternatively, it could indicate that $HgCH_3$ does not exist, and that the initial decomposition reaction is not a two-step process.

In the analysis of the infrared spectrum of pyrolyzed DMM, five weak absorption bands were observed which could not be assigned to an expected hydrocarbon species. Tentatively, these bands are assigned to the radical $HgCH_3$, which, assuming the same structure as methyl iodide, will have six infrared active absorption bands. Comparison of the frequencies listed in Table IV for $HgCH_3$ with those of methyl iodide given in Table I indicate the following assignment to be reasonable: $\nu_1 = 3062$ cm^{-1}, $\nu_5 = 1450$ cm^{-1}, $\nu_2 = 1245$ cm^{-1}, $\nu_6 = 1030$ cm^{-1}, and $\nu_3 = 570$ cm^{-1}. The unobserved frequency would be expected in the region of the ethane and methane intense absorption bands at 3000 cm^{-1}. The origin of the $HgCH_3$ radicals, in view of the low intensity of the absorption bands assigned to the species, can most likely be attributed to reaction of methyl radicals and mercury atoms during the trapping process, with possibly some contribution from a short-lived radical CH_3Hg.

Conclusion

The matrix isolation technique can be used to trap

(19) S. W. Benson, *J. Chem. Phys.*, **38**, 1945 (1963).

(20) A. S. Kallend and J. H. Purnell, *Trans. Faraday Soc.*, **60**, 93 (1966).

free radicals formed by the pyrolysis of suitable chemical compounds. This has been demonstrated in an investigation of the pyrolysis of methyl iodide and dimethyl mercury resulting in the infrared spectrum of the methyl radical being characterized. This type of experiment should be of great use, not only as a means of observing the spectra of free radicals but also to obtain data on the primary reaction products in thermal decomposition reactions. It should be emphasized that the primary object of this study was to demonstrate the feasibility of trapping free radicals formed in pyrolysis reactions using the matrix isolation technique. In the present study, the pyrolysis reactor, although effective, was rather crude in design since the true pyrolysis temperature and surface area of the reactor were ill defined. If this reactor were replaced by the "very low pressure pyrolysis reactor" as described by Benson, *et al.*,[21] and the matrix isolation technique used in a quantitative mode as has been recently demonstrated,[6] kinetic data on the primary dissociation reactions could be obtained. In some cases the matrix isolation method has advantages over the mass spectrometer as a means of analysis, since with the latter the detection and quantitative measurement of free radicals is fraught with difficulties.[22] Another area where the pyrolysis method in conjunction with the matrix isolation technique could be useful would be in the study of reactions occurring between free radicals and neutral molecular species. This could be achieved as described by Benson, *et al.*,[22] by allowing the radical source in addition to a second molecular species to pass through the pyrolysis zone. Alternatively, the molecular species could be added to the matrix gas and reaction allowed to proceed during the trapping of the radical species.

Acknowledgment. The author gratefully acknowledges the support of the Air Force Office of Scientific Research in funding this study.

(21) S. W. Benson and G. N. Spokes, *J. Amer. Chem. Soc.*, **89**, 2525 (1967).

(22) F. P. Lossing, "Mass Spectrometry," C. A. McDowell, Ed., McGraw-Hill Book Co., Inc., New York, N. Y., 1963, p 442.

Structure and Conformations of Free Radicals. II. Radical Ions from Nitrophenyl Aromatic Hydrocarbons[1]

by Graham R. Underwood, Don Jurkowitz, and S. Carlton Dickerman

Department of Chemistry, New York University, University Heights, Bronx, New York 10453
(Received July 11, 1969)

The radical anions and cations of a large number of nitrophenylbenzenes, -naphthalenes, and -anthracenes have been studied by epr spectroscopy. The experimental data were compared with McLachlan SCF spin densities calculated by assuming various angles between the nitrophenyl ring and the remaining planar part of the molecule. It was found that the *p*-nitrophenyl derivatives were the only ones which could be expected to give meaningful results, and the apparent angles obtained appear reasonable in comparison with other techniques.

Recent interest in studies concerned with the nonplanarity of phenyl-substituted anthracenes and related compounds[2-9] has stimulated us to examine the radical anions and cations derived from nitrophenyl-substituted benzene, naphthalene, anthracene, and ferrocene. The reason for this interest has been severalfold. Basically, however, the work has been centered around the fact that even in the simplest system—biphenyl—there is expected to be some degree of nonplanarity between the two aromatic rings due to steric repulsion between the two pairs of *ortho* hydrogens. This nonplanarity is reflected in those physical and chemical properties which are dependent on the distribution and molecular orbital energy levels of the π-electron cloud. Thus, for

(1) For paper I, see G. R. Underwood and R. S. Givens, *J. Amer. Chem. Soc.*, **90**, 3713 (1968).

(2) L. O. Wheeler, K. S. V. Santhanam, and A. J. Bard, *J. Phys. Chem.*, **73**, 2223 (1967).

(3) A. J. Bard, K. S. V. Santhanam, J. T. Maloy, J. Phelps, and L. O. Wheeler, *Discussions Faraday Soc.*, 167 (1968).

(4) H. Suzuki, *Bull. Chem. Soc. Jap.*, **32**, 1340, 1350 (1959), and references cited therein.

(5) J. N. Murrell and H. C. Longuet-Higgins, *Proc. Phys. Soc.*, **A68**, 601 (1955).

(6) J. N. Murrell, *J. Chem. Soc.*, 3779 (1955).

Table I: Experimental Hfsc's for All Radical Anions in This Study[a]

Compound	Hyperfine splitting constants, G[b]			
	a^N	a^{o} [c]	a^{m} [c]	a^{p} [c]
2-Nitrobiphenyl	8.8	−3.0[d] (1)	0.9 (2)	−4.0 (1)
3-Nitrobiphenyl	9.6	−3.35 (2)	1.2 (1)	−4.3 (1)
4-Nitrobiphenyl	8.3	−2.9 (2)	0.75 (2)	...
1-*m*-Nitrophenylnaphthalene	9.4	−3.35 (2)	1.2 (1)	−4.2 (1)
1-*p*-Nitrophenylnaphthalene	7.0	−2.4 (2)	0.7 (2)	...
2-*m*-Nitrophenylnaphthalene	9.7	−3.35 (2)	1.2 (1)	−4.2 (1)
2-*p*-Nitrophenylnaphthalene	7.0	−3.1 (2)	0.8 (2)	...
1-*o*-Nitrophenylanthracene	7.5	−3.2 (1)	0.5 (2)	−2.4 (1)
1-*p*-Nitrophenylanthracene	5.3	−2.0 (2)	0.3 (2)	...
2-*o*-Nitrophenylanthracene	6.3	−3.1 (1)	0.6 (2)	−2.4 (1)
2-*p*-Nitrophenylanthracene	5.7	−1.9 (2)	0.3 (2)	...
9-*o*-Nitrophenylanthracene	9.8	−3.3 (1)	1.2 (2)	−4.1 (1)
9-*m*-Nitrophenylanthracene	9.5	−3.0 (2)	1.1 (1)	−3.9 (1)
9-*p*-Nitrophenylanthracene	9.6	−3.2 (2)	1.1 (2)	...
p-Nitrophenylferrocene	9.3	−3.15 (2)	1.08 (2)	...
m-Nitrophenylferrocene	9.52	−3.25 (2)	0.98 (1)	−3.86 (1)

[a] The solvent was dimethylformamide which was thoroughly dried in all cases except for the nitrophenylferrocenes. The numbers in parentheses refer to the number of hydrogens giving rise to the assigned hfsc. [b] All values have an approximate uncertainty of ±0.1 G. [c] a^{o}, a^{m}, and a^{p} refer to hydrogens *ortho*, *meta*, and *para*, respectively, to the nitro group. [d] The signs of a^{o} and a^{p} are assumed negative; a^{m} is assumed positive.

example, ultraviolet absorption,[4] epr spectra,[9] reduction and oxidation potentials,[3] and nmr spectroscopy[10] have been used in investigating this phenomenon as well as the more direct techniques of X-ray crystallography[8] and electron diffraction.[7]

For biphenyl the angle between the two phenyl rings has been determined as varying from 0°[8] to 45° ± 10°[7] depending on the technique used and state of the compound under examination. Phenyl-substituted anthracenes and particularly 9-phenyl- and 9,10-diphenylanthracenes have been closely studied[2,3] because in these compounds there can exist extreme degrees of steric interaction. Bard and coworkers[3] have found, for example, using both electrochemical and epr measurements that the angle between the phenyl ring and the anthracene ring in phenylanthracenes was dependent on the position of substitution and increased from 25° at the 2 position to 53° at the 1 position and 68° at the 9 position. The compounds studied in this investigation are listed in Table I. The examination of these particular compounds resulted from our own interest in crowded anthracenes[11] and by earlier studies of nitrophenylation reactions[12] which have made available a wide range of nitrophenyl-substituted aromatic hydrocarbons. We were also encouraged early in this work by molecular orbital calculations which indicated that the epr spectra of these compounds should, in certain cases, be quite sensitive to conformational differences and by the fact that a study of the epr spectra of the anions and cations of these systems would provide unequivocal confirmation of the structure of these compounds—information which had only previously been obtainable by laborious degradations.

The nitrophenyl aromatics provide a particularly interesting set of compounds for epr study because from them it is possible to generate easily both radical cations and radical anions. Furthermore, in the case of the radical anions, the unpaired electron should be localized primarily in the nitrophenyl residue, while in the radical cations, the unpaired electron (and the charge) should be confined mainly to, for example, the anthracene moiety.

Experimental Section

Sources of Compounds Studied. The following compounds were obtained from Aldrich Chemical Co. and were used without further purification: 2-nitrobiphenyl, 3-nitrobiphenyl, and 4-nitrobiphenyl. The following compounds were prepared by the method cited in the corresponding references; the literature melting points (if reported) and the observed melting points,[13] respectively, are given in parentheses after the name of the compound: 1-*m*-nitrophenylnaphthalene[14] (67.5–8.5°, 68.0–69.5°); 2-*m*-nitrophenylnaphthalene[14]

(7) O. Bastiansen, *Acta Chem. Scand.*, **3**, 408 (1949).

(8) J. Dhar, *Indian J. Phys.*, **7**, 43 (194); *Proc. Nat. Inst. Sci. India*, **15**, 11 (1949).

(9) K. Möbius, *Z. Naturforsch. A*, **20**, 1117 (1965).

(10) P. C. Lauterbur, *J. Chem. Phys.*, **38**, 1432 (1963).

(11) (a) S. C. Dickerman, J. H. Berg, J. R. Haase, and R. Varma, *J. Amer. Chem. Soc.*, **89**, 5457 (1967); (b) S. C. Dickerman and J. R. Haase, *ibid.*, **89**, 5458 (1967); (c) S. C. Dickerman, A. M. Felix, and L. B. Levy, *J. Org. Chem.*, **29**, 26 (1964).

(12) S. C. Dickerman, M. Klein, and G. B. Vermont, *ibid.*, **29**, 3695 (1964), and preceding papers.

(13) All melting points were recorded on a Meltemp melting point apparatus and are uncorrected.

(14) P. S. Johnson and W. A. Waters, *J. Chem. Soc.*, 4652 (1962).

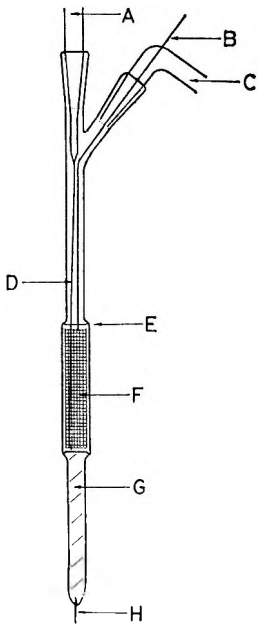

Figure 1. Schematic representation of the electrolytic cell used for the generation and study of the radical anions: A, nitrogen inlet; B, platinum wire electrode; C, nitrogen outlet; D, capillary tube; E, solvent level; F, fine platinum grid acting as cathode; G, mercury pool; H, tungsten wire.

(130–131°, 131–132°); 1-*p*-nitrophenylnaphthalene[15] (132–133°, 132–133°); 2-*p*-nitrophenylnaphthalene[15] (174°, 183–184°); *p*-nitrophenylferrocene[16] (169–170°, 167–169°); *m*-nitrophenylferrocene[17] (84–85°, 85.5–86.0°); 9-*o*-nitrophenylanthracene[11c] (150–151°, 150–151°); 9-*m*-nitrophenylanthracene[11c] (158–159°, 158–159°); and 9-*p*-nitrophenylanthracene[11c] (229–230°, 229–230°). The following new compounds were prepared by modification of earlier methods:[11c,18] 1-*o*-nitrophenylanthracene; 1-*p*-nitrophenylanthracene; 2-*o*-nitrophenylanthracene; and 2-*p*-nitrophenylanthracene.

Generation of Radicals. A Varian Associates V-4502 spectrometer employing 100-kHz field modulation was used. Samples were contained in a modified Varian aqueous sample cell.

For convenience, the anion radicals were generated by a crude controlled potential electrolysis using the assembly shown in Figure 1. The solvent was carefully dried dimethylformamide (DMF) and tetra-*n*-butylammonium chloride was used as the electrolyte. The solution was degassed thoroughly using nitrogen which was prepurified by bubbling through a blue solution of potassium benzophenone followed by an efficient drying train. Before the epr spectra were measured it was necessary to stop the nitrogen gas flow. Under these conditions the radical anions could rapidly be generated in quite high concentrations. However, presumably owing to the reaction of the radical anions with the mercuric ion, the radicals were stable for only a few minutes under these conditions, but no difficulty was experienced in measuring the epr spectra.

The cation radicals were prepared by dissolving the solid compound in about 10 ml of concentrated sulfuric acid in an inverted U mixing cell which has been described previously.[19]

The HMO calculations modified according to McLachlan[20] were performed on an IBM 360/30 computer. The spectra obtained were sufficiently simple to be analyzable on a first-order basis, and computation of theoretical spectra was considered unjustified. The line widths of the spectra were generally of the order of 0.1 G, and we have set an upper limit on the uncertainty of our epr measurements also as 0.1 G.

Previous workers have made epr studies of nitrobenzene[21] where the conclusion has been unanimous that the nitro group lies in the plane of the benzene ring. Nitrobiphenyls have been studied by Nakai, *et al.*,[22] who concluded that there is little effect on the spin density distribution in the nitrophenyl ring upon introduction of the substituent. This conclusion essentially confirms our own findings.

Results and Discussion

The epr hyperfine splitting constants (hfsc's) for hydrogen and nitrogen are summarized in Tables I and II for the radical anions and cations, respectively. HMO spin densities were determined by solving the appropriate secular determinants for each radical. Such calculations require the use of certain parameters associated with the nitro group and also a particular value of β to describe the resonance integral between the phenyl ring and the remainder of the molecule. The parameters chosen for the nitro group were those suggested by Rieger and Fraenkel[23] as being most appropriate. These values are $h_N = 2.2$, $h_O = 1.4$, $k_{NO} = 1.67$, $K_{CN} = 1.2$. The value for the resonance integral was chosen by assuming that the angle between the phenyl substituent and the anthracene nucleus, θ, varies between 0 and 90° and that the resonance integral β_θ for the resonance integral for that bond is given by $\beta_\theta = \beta_0 \cos\theta$[24] where β_0 is the resonance integral for the carbon–carbon bond in planar systems. Possibly, since it is anticipated that this bond is nearer to

(15) B. A. Marshall and W. A. Waters, *J. Chem. Soc.*, 381 (1959).

(16) G. D. Broadhead and P. L. Pauson, *ibid.*, 367 (1955).

(17) A. N. Nesmetanov, E. G. Perevalova, R. V. Golovnya, and L. S. Shilovtseva, *Dokl. Akad. Nauk SSSR*, **102**, 535 (1955); *Chem. Abstr.*, **50**, 4925*h* (1956).

(18) S. C. Dickerman and M. Klein, to be published.

(19) G. A. Russell, E. G. Janzen, and E. T. Strom, *J. Amer. Chem. Soc.*, **86**, 1807 (1964).

(20) A. D. McLachlan, *Mol. Phys.*, **3**, 233 (1960).

(21) See, for example, D. H. Geske, *Progr. Phys. Org. Chem.*, **4**, 125 (1967).

(22) Y. Nakai, K. Kawamura, K. Ishizu, Y. Deguchi, and H. Takaki, *Bull. Chem. Soc. Jap.*, **39**, 847 (1966).

(23) P. H. Rieger and G. K. Fraenkel, *J. Chem. Phys.*, **39**, 609 (1963).

(24) R. S. Mulliken, C. A. Rieke, and W. G. Brown, *J. Amer. Chem. Soc.*, **63**, 41 (1941).

Table II: Experimental Hfsc's for All Radical Cations in This Study[a]

Compound	Hydrogen hyperfine splitting constants[b] for position 1[c]	2[c]	9[c]
1-*m*-Nitrophenylnaphthalene	−4.8[d] (3)	−1.8 (4)	...
1-*p*-Nitrophenylnaphthalene	−4.8 (3)	−1.8 (4)	...
2-*m*-Nitrophenylnaphthalene	−4.7 (4)	−1.8 (3)	...
2-*p*-Nitrophenylnaphthalene	−4.7 (4)	−1.8 (3)	...
1-*o*-Nitrophenylanthracene	−2.7 (3)	−1.2 (4)	−6.4 (2)
1-*p*-Nitrophenylanthracene	−2.7 (3)	−1.2 (4)	−6.5 (2)
2-*o*-Nitrophenylanthracene	−2.6 (4)	−1.2 (3)	−6.5 (2)
2-*p*-Nitrophenylanthracene	−2.7 (4)	−1.2 (3)	−6.6 (2)
9-*o*-Nitrophenylanthracene	−2.5 (4)	−1.1 (4)	−7.0 (1)
9-*m*-Nitrophenylanthracene	−2.4 (4)	−1.1 (4)	−7.0 (1)
9-*p*-Nitrophenylanthracene	−2.4 (4)	−1.1 (4)	−7.0 (1)

[a] The solvent was concentrated sulfuric acid. The numbers in parentheses refer to the number of hydrogens giving rise to the assigned hfsc's. [b] All values measured in gauss to an accuracy of ±0.1 G. [c] The numbers refer to the position on the naphthalene or anthracene ring. [d] The signs are all assumed to be negative.

Table III: The Apparent Angles between the Nitrophenyl Ring and the Remaining Aromatic Ring in the Radical Anions as Estimated from the Hfsc Listed at the Head of Each Column[a]

Compound	Angles[b] estimated from a^N[c]	a^o[c]	a^m[c]	a^p[c]	All data[d]
2-Nitrobiphenyl	60–64	52–64	0–45	70–80	45–70
3-Nitrobiphenyl	55–90	9–90	0–90	45–55	55
4-Nitrobiphenyl	42–48	25–45	0–40	...	40–42
1-*m*-Nitrophenylnaphthalene	38–55	0–90	0–90	64–72	55–64
1-*p*-Nitrophenylnaphthalene	48–50	32–44	45–55	...	44–48
2-*m*-Nitrophenylnaphthalene	50–90	0–90	0–90	40–90	50–90
2-*p*-Nitrophenylnaphthalene	30–36	55–70	38–54	...	36–55
1-*o*-Nitrophenylanthracene	82–84	62–64	66–68	68–72	64–82
1-*p*-Nitrophenylanthracene	71–73	70–72	68–70	...	70–71
2-*o*-Nitrophenylanthracene	68–70	84–86	72–74	50–54	54–84
2-*p*-Nitrophenylanthracene	65–67	60–64	32–34	...	34–65
9-*o*-Nitrophenylanthracene	90[e]	90	90[e]	90	90
9-*m*-Nitrophenylanthracene	88	80–81	80–84	80–81	80–88
9-*n*-Nitrophenylanthracene	88	88	88	...	88

[a] The ranges given are those corresponding to the hfsc's recorded in Table I, with a range of ±0.1 G. The ranges in the last column are those values which are necessary to accommodate all the values in the preceding columns and probably give some indication of the accuracy of the estimate. [b] All values given in degrees. [c] These symbols refer to the same quantities as in Table I. [d] The values listed in this column are the minimum ranges necessary to accommodate all data, and in no way are they meant to indicate confidence limits. [e] The experimental hfsc is greater than any calculable by the methods described in the text but is in closest agreement with the value recorded here.

the length of a normal carbon–carbon single bond,[25] this value of β_θ is somewhat too large. In the absence of a more definitive estimate of the bond length, we retain this approximation and note that this introduces a limit to the accuracy of our results.[26]

For the radical anions where negative spin densities were anticipated (and in fact, assumed) the HMO spin densities were modified according to the method of McLachlan[20] whereby negative spin densities are introduced as a natural consequence of the consideration of spin polarization.

The spin densities, ρ_C, thus obtained for the various angles of θ were converted into calculated hfsc's in the following way. For the hydrogen hfsc's the McConnell relationship[27] $a^H = Q_{CH}{}^H \cdot \rho_C$ was assumed to adequately describe the dependence of a^H on ρ_C. $Q_{CH}{}^H$ was taken to be −23.7 G as this value gave best agreement for many substituted nitrobenzenes. Several refinements of this equation have been suggested,[28,29] but the

(25) There is considerable evidence, however, that the shortening of double bonds may be largely due to the overlap of the sp^2–sp^2 σ bonds and that the π bonding may have little effect on the bond length. If this is the case, then the error introduced at this stage would be small. See, for example, M. J. S. Dewar and H. N. Schmeising, *Tetrahedron*, **11**, 96 (1960).

(26) For an estimate of the variation of resonance integral with bond length, see R. S. Mulliken, C. A. Rieke, D. Orloff, and H. Orloff, *J. Chem. Phys.*, **17**, 1248 (1949).

(27) H. M. McConnell, *ibid.*, **24**, 632 (1956).

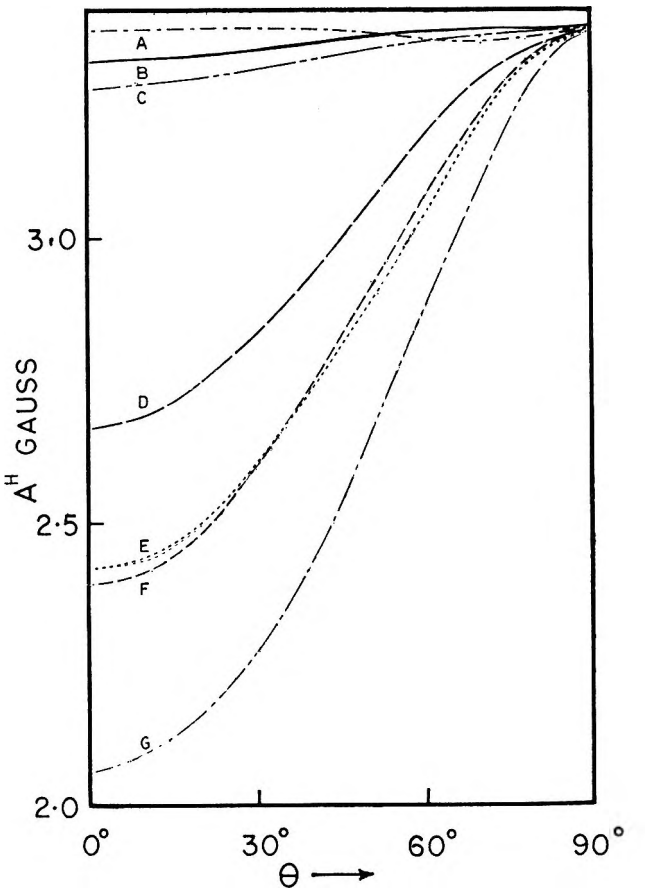

Figure 2. The effect of θ, the angle between the the aromatic ring systems, on the hfsc's of hydrogens *ortho* to the nitro group in the radical anions derived from: A, 3-nitrobiphenyl; B, 2-*m*-nitrophenylnaphthalene; C, 1-*m*-nitrophenylnaphthalene; D, 4-nitrobiphenyl; E, 2-*p*-nitrophenylnaphthalene; F, 2-nitrobiphenyl; G, 1-*p*-nitrophenylnaphthalene.

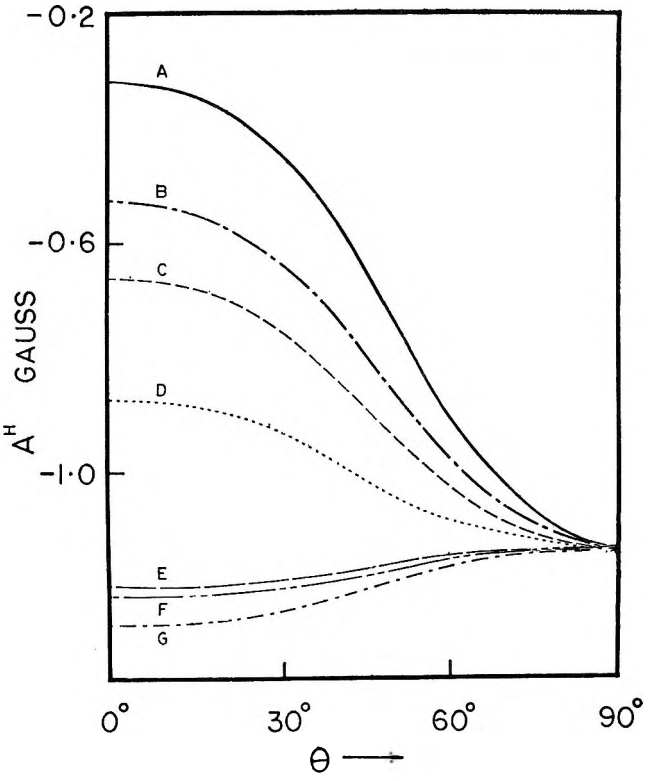

Figure 3. The effect of θ, the angle between the aromatic ring systems, on the hfsc's of hydrogens *meta* to the nitro group in the radical anions derived from: A, 1-*p*-nitrophenylnaphthalene; B, 2-*p*-nitrophenylnaphthalene; C, 4-nitrobiphenyl; D, 2-nitrobiphenyl; E, 3-nitrobiphenyl; F, 2-*m*-nitrophenylnaphthalene; G, 1-*m*-nitrophenylnaphthalene.

accuracy of this work does not warrant such sophistication; in any event the value of such modifications is in doubt.[30]

The nitrogen hfsc's were estimated according to the theory of Karplus and Fraenkel[31] where

$$a^N = Q_N{}^N\rho_N + 2Q_{ON}{}^N\rho_O + Q_{CN}{}^N\rho_C$$

The values assumed were $Q_N{}^N = 100.0$ G, $Q_{ON}{}^N = 71.0$ G, and $Q_{CN}{}^N = 0.0$ G. These are in very close agreement with the values of Rieger and Fraenkel[23] and have been only slightly modified to give an exact agreement with epr spectrum of nitrobenzene in DMF.[32] This agreement is not attained by using the original parameters which were deduced for a wide range of substituted nitrobenzenes.

Figures 2–4 show typical results for the effect upon the calculated hfsc's of the angle, θ, between the nitrophenyl and the other aromatic ring. In each of the radical anions studied there are three or four experimental hfsc's which may be compared with their theoretical counterparts. It will be noted that in some cases, *e.g.*, the *m*-nitrophenyl derivatives, equivalence is assumed for hydrogens which are in fact not exactly equivalent. The coupling constants calculated from the spin densities in these cases were within 0.1 G of each other, and the line intensities in the experimental spectra were in such good agreement with those predicted that differences of less than 0.03 G were estimated. Table III shows the range of values of θ obtained by each comparison and the most appropriate apparent angles to account for the observed hfsc's.

The apparent angles determined by this study should not be confused with an exact or static geometry, but rather it should be borne in mind that these are, at the best, only weighted time-average values. This fact is

(28) (a) J. P. Colpa and J. R. Bolton, *Mol. Phys.*, **6**, 273 (1963); (b) J. R. Bolton, *J. Chem. Phys.*, **43**, 309 (1965).

(29) G. Giacometti, C. L. Nordio, and M. V. Pavan, *Theoret. Chim. Chim. Acta*, **1**, 404 (1963).

(30) J. E. Bloor, B. R. Gilson, and P. N. Daykin, *J. Phys. Chem.*, **70**, 1457 (1966).

(31) M. Karplus and G. K. Fraenkel, *J. Chem. Phys.*, **35**, 1313 (1961).

(32) Perhaps a better model compound would have been the corresponding methyl- or *t*-butylnitrobenzene as there may be some effect due to the substituent. However, the further empiricism necessary to accommodate the *ortho*, *meta*, and *para* substituents and the lack of knowledge of the inductive effect of the various nitrophenyl substituents decided us against this alternative. This factor may partly account for the anomalous results for 9-*o*-nitrophenylanthracene.

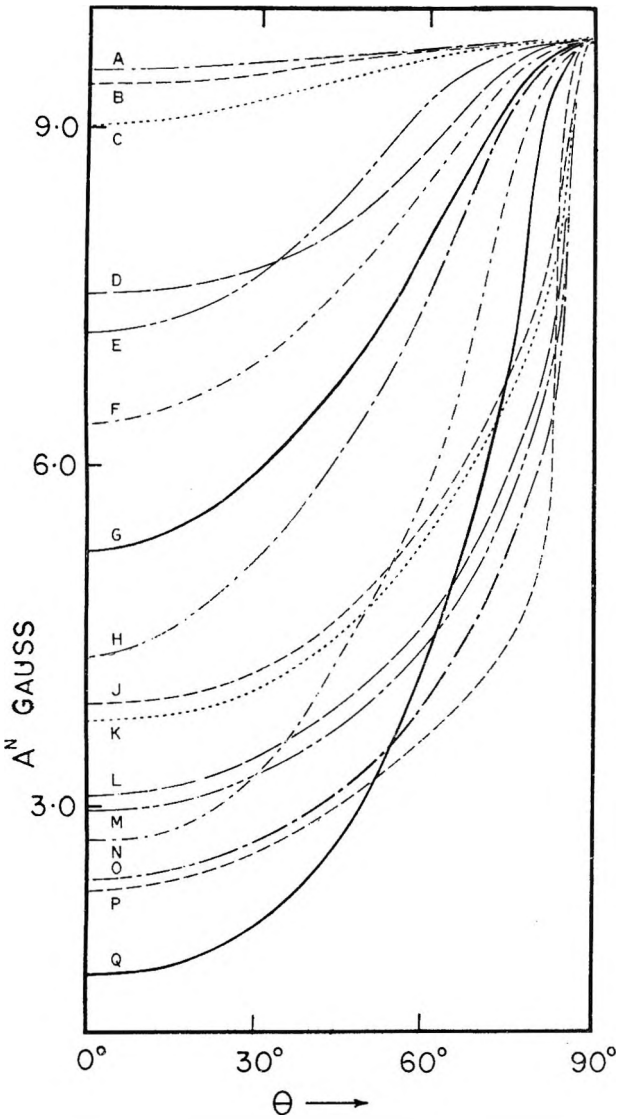

Figure 4. The effect of θ, the angle between the aromatic ring systems, on the hfsc's of the nitrogens in the radical anions derived from: A, 3-nitrobiphenyl; B, 2-*m*-nitrophenylnaphthalene; C, 1-*m*-nitrophenylnaphthalene; D, 2-nitrobiphenyl; E, 4-nitrobiphenyl; F, 2-*p*-nitrophenylnaphthalene; G, 1-*p*-nitrophenylnaphthalene; H, 2-*m*-nitrophenylanthracene; J, 2-*o*-nitrophenylanthracene; K, 2-*p*-nitrophenylanthracene; L, 1-*o*-nitrophenylanthracene; M, 1-*p*-nitrophenylanthracene; N, 1-*m*-nitrophenylanthracene; O, 9-*o*-nitrophenylanthracene; P, 9-*p*-nitrophenylanthracene; Q, 9-*m*-nitrophenylanthracene.

often overlooked in problems of conformational analysis although it has been suitably emphasized by Stone and Maki.[33]

Radical cations do not appear to have been generated from nitroaromatic hydrocarbons prior to this study. In these particular cases, however, it was correctly anticipated that the one-electron oxidation would present no difficulty as the highest occupied molecular orbital (HOMO) in each case was very similar to that of anthracene. This is demonstrated by the similarity of the spin density distribution in the nitrophenyl-substituted radical cations and in the anthracene cation.

From Table II, it is obvious that there is little change in the unpaired electron density in the radical cations as the position of substitution is varied. As a consequence, no attempt was made to perform McLachlan SCF calculations to determine the spin densities.

Some interesting observations can be made regarding the utility of this method for determining the conformations of potentially nonplanar aromatic systems. Three points are immediately obvious. First, the radical cations are not suitable for such studies as, even between the extreme limits of 0 and 90°, insufficient difference is predicted for the hydrogen hfsc's due to the fact that the unpaired electron (and the positive charge) is not significantly delocalized into the nitrophenyl group even when the two aromatic systems are completely planar. This limitation of course is only existent if nitrophenyl substituents are used and more satisfying results have been obtained by using phenyl substituents.[3] Secondly, this method is equally inapplicable to the anion radicals of *m*-nitrophenyl-substituted radicals, because in this case, even if the two rings are completely planar, there is insufficient conjugation between the nitro group and the other aromatic ring *meta* to it. Thirdly, we note that the technique of epr spectroscopy can be uniquely valuable in determining the structure of complex aromatic structures such as these. This is particularly notable when it is recalled how complex and uninformative the nmr, ir, and uv spectra[18] of these molecules may be expected to be.

Other more subtle features emerge from the data given in Table III. While HMO calculations indicate that the *ortho*-substituted compounds should be as sensitive to conformational change as are the *para*-substituted ones, it is obvious from the results that the *ortho*-substituted compounds are generally quite unsuitable. This is probably due to the crowding between the nitro group and the relatively bulky substituent *ortho* to it. It is known[21] that such crowding can cause twisting of the nitro group out of the plane of the benzene ring necessitating different values for the carbon–nitrogen resonance integral. It is equally probable that there is a restriction to solvation of the nitro group in such cases, a phenomenon which would manifest itself as a change in the Coulomb integral necessary to describe the oxygen atoms. A combination of these effects would help to explain the apparent anomaly in the results for 9-nitrophenylanthracene. We find also that the angle between the two aromatic rings appears to be greatest when the nitrophenyl substituent is in the 9 position of anthracene. Similar results were obtained by Bard and coworkers.[3] We find, however, that there appears to be little difference in the steric requirements of the 1 and the 2 position of anthracene, but the accuracy of our results could well accommodate

(33) E. W. Stone and A. H. Maki, *J. Chem. Phys.*, **37**, 1326 (1962).

the expected preferences. Similarly, we find little difference between the steric requirements of the benzene ring and the 1 and 2 positions on the naphthalene ring. Our results here are in good agreement with the studies on biphenyl by Möbius[9] and by Bastiansen.[7]

The HMO calculations also indicate that a study of the polarographic data for these compounds should provide useful information regarding the conformations of the neutral molecules. This possibility is being investigated further, and the results of this work will be reported at a later date.

Reactions of Electrons Photoejected from Aromatic Amino Acids in Frozen Aqueous Solutions of Divalent Metal Salts

by René Santus,[1] Annie Hélène, Claude Hélène, and Marius Ptak

Centre de Biophysique Moléculaire, Orleans, France *(Received April 1, 1969)*

Aromatic amino acids (tryptophan, tyrosine) are ionized by ultraviolet radiation in frozen aqueous solutions containing various divalent salts. Their triplet → triplet and radical cation absorption spectra have been recorded at 77°K. According to electron spin resonance studies, electron photoejection occurs *via* a triplet–triplet absorption process. Photoejected electrons react with M^{2+} ions to give M^{+} ions or with H^{+} to give H atoms. The nature and number of electron traps depend on the salt, as deduced from temperature and light effects. In the presence of $CdCl_2$, photoejected electrons are trapped in many heterogeneous sites producing a broad esr resonance. Cl_2^- radical-ions are also produced when chloride is present. There are great similarities in the effects of γ and uv radiations. When uv-irradiated frozen aqueous solutions of tryptophan containing $CdSO_4$ are further irradiated at longer wavelengths, translocation of trapped electrons is observed. Photobleaching with various wavelengths detects electrons trapped in wells of different depths.

Introduction

Flash photolysis in fluid solutions,[2a] luminescence, and esr measurements[2b] at low temperature demonstrate that photoionization is the main primary photochemical process in the photolysis of aromatic amino acids or related compounds. From a biological point of view, studies of these primary processes can help to elucidate some aspects of enzyme inactivation which occurs after absorption of uv light by aromatic and sulfur-containing amino acid residues. Photoejected electrons could react with amino acid residues or electrophilic agents far from the photoejection center. Many enzyme systems contain metal cations which are required for activity. These cations could also be involved in the photoinactivation processes. It is thus of great interest to study the behavior of electrons photoejected by aromatic amino acids in frozen aqueous solutions of various divalent cations. Moorthy and Weiss[3] have already reported the formation of M^{+} cations by γ irradiation of frozen aqueous solutions of M^{2+} divalent cations in which electrons are also produced. In the present studies, we show that aromatic amino acids or related compounds, dissolved in such solutions of divalent cations and irradiated with ultraviolet light at low temperature, are a good source of electrons which may diffuse in the solid medium. Different possibilities of reaction and trapping are offered and we present results concerning identification and stability of different photochemical species formed under these conditions. At 77°K, most of the photoejected electrons are stabilized by chemical and physical traps of the glassy or polycrystalline medium. Environment, temperature, and light effects on the recombination processes can be conveniently studied with such samples. We also confirm that the triplet state of aromatic amino acids is involved in the photoionization process at low temperature.

Experimental Section

The esr spectra were recorded with a Varian V. 450I A spectrometer, equipped with a 100-kc modula-

(1) Laboratoire de Biophysique—Museum National d'Histoire Naturelle, 61, rue Buffon, 75-Paris-5ème.

(2) (a) L. I. Grossweiner, G. Swenson, and E. Zwicker, *Science*, **141**, 805 (1963). (b) R. Santus, C. Hélène, and M. Ptak, *Photochem. Photobiol.*, **7**, 341 (1968).

(3) P. M. Moorthy and J. J. Weiss, "Solvated Electron," Advances in Chemistry Series, No. 50, American Chemical Society, Washington, D. C., 1965, p 180.

tion. The magnetic field strength was calibrated by means of a Varian F_8 proton resonance fluxmeter, the frequency of which was monitored by a Hewlett-Packard frequency counter. The microwave frequency was measured with the Hewlett-Packard frequency counter. For all experiments, we used the Varian optical transmission cavity equipped with a low-temperature gas-flow system, the temperature of which was regulated by the Varian temperature regulating system. The light of an OSRAM HBO or XBO W 450 lamp (see text for further details) was filtered with appropriate filters. In order to determine the thermal stability of paramagnetic species produced upon uv irradiation, the frozen solutions were heated and maintained for 3 min at the desired temperature and cooled once again to 77°K and the esr spectra were recorded at this temperature.

Optical measurements were performed with a Cary 14 spectrophotometer and a Jobin Yvon spectrofluorophosphorimeter. Triplet–triplet absorption spectra[4] were measured using cross-irradiation in the Cary 14 spectrophotometer as described by Henry and Kasha.[5] Because of photolytic reactions, the absorption intensities were measured at different wavelengths with the exciting light on and off. Amino acids, peptides, and proteins were purchased from Mann Research and Calbiochem. Salts were purchased from Merck and all these products were used without further purification. All solutions were prepared with water that was first deionized and then doubly distilled.

Results

I. Esr of Photochemically Produced Species at 77°K. *(1) Solutions Containing Sulfate.* The esr spectrum of frozen aqueous solution of tryptophan (5×10^{-4} *M*) containing 1 M $CdSO_4$ irradiated with uv light of wavelengths longer than 245 nm (optical filter F_0: Figure 2) is shown in Figure 1. The most important features of this spectrum are the presence of a complex central signal (A and B) and also the presence of two lines C and D, separated by 139 G. In addition, we observe H· atom resonances as two hyperfine lines separated by 504 G and centered on $g = 2$.

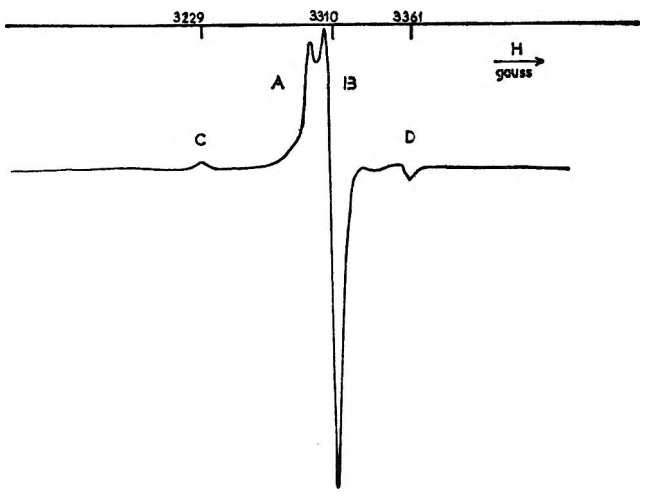

Figure 1. Esr spectrum of a 1 *M* $CdSO_4$ containing frozen aqueous solution of tryptophan, uv irradiated at 77°K. Concentration of tryptophan, 5×10^{-4} *M*; time of irradiation, 30 sec; microwave frequency, 9230 MHz.

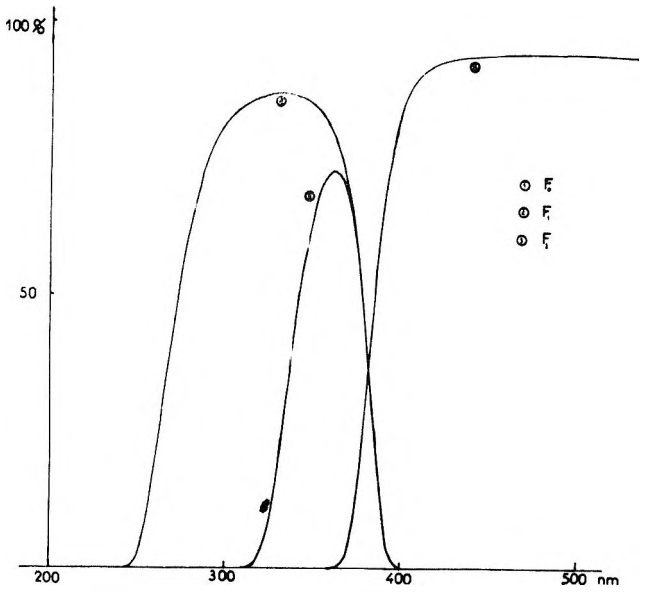

Figure 2. Optical transmission of the optical filters used for uv or visible irradiation of the frozen samples at 77°K: F_0, M.T.O. uv 10A optical filter; F_1, PMMA glass plate (thickness 1 cm); F_2F_0 + Pyrex glass plate.

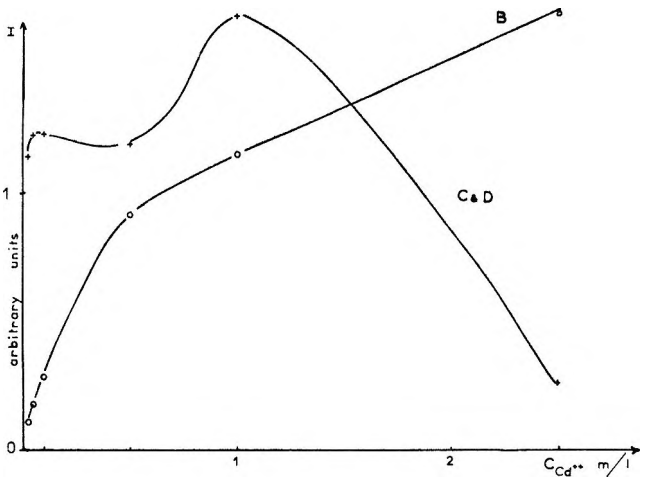

Figure 3. Relative intensity of B, C, and D resonances (see text) *vs.* Cd^{2+} concentration (tryptophan concentration 5×10^{-4} *M* in all samples) under the same conditions of uv irradiation. C intensity is normalized to D intensity; D and B intensity scales are different.

The central signal gives a different pattern when O_2 saturated solutions are uv irradiated at higher temperature (see below); A is shifted toward a higher *g* value, and the position of B is not affected. Thus, it

(4) R. Santus, Thesis, Paris (1968) No. CNRS AO 1946.

(5) B. R. Henry and M. Kasha, *J. Chem. Phys.*, **47**, 3319 (1967).

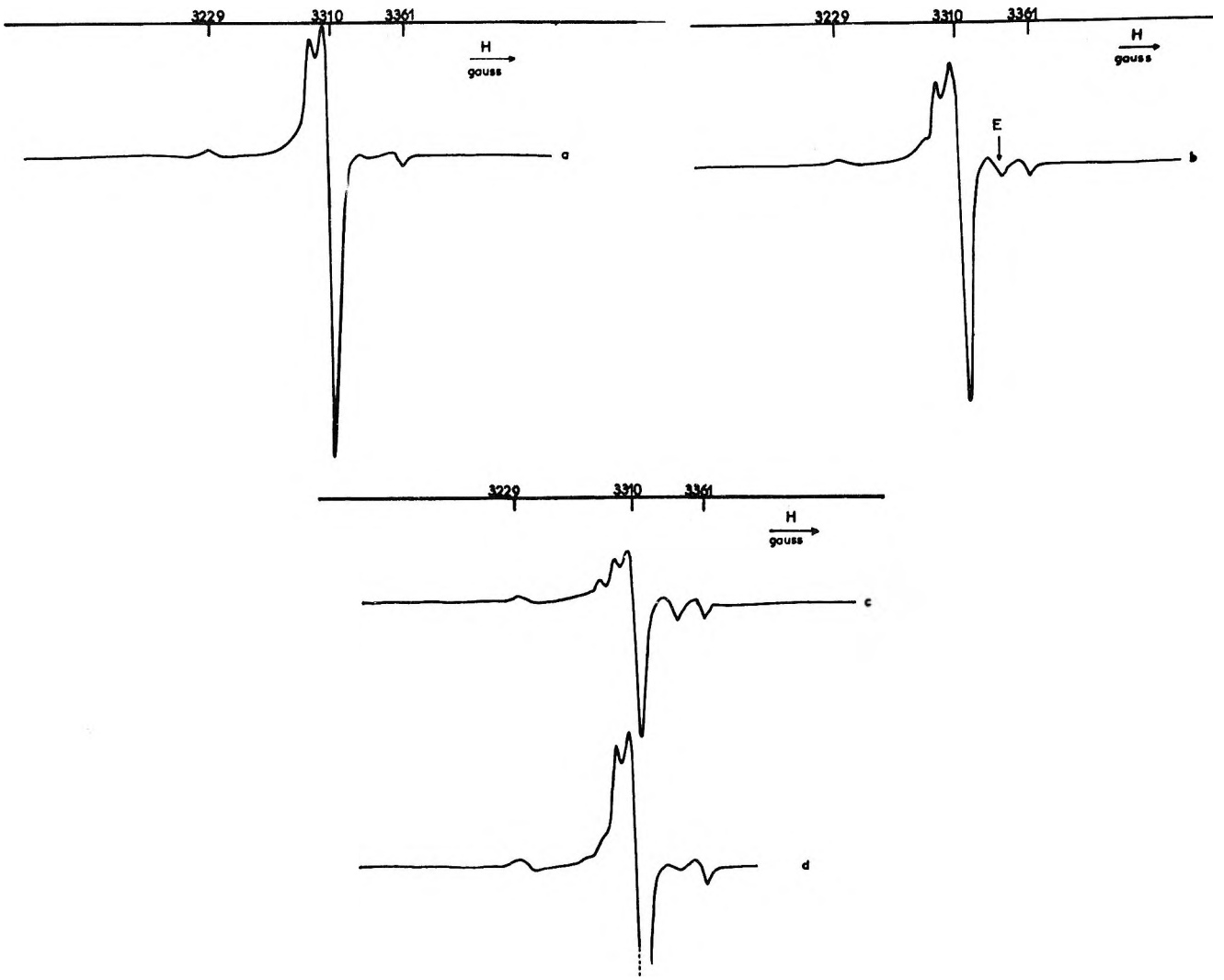

Figure 4. Esr spectrum of 1 M $CdSO_4$ containing frozen solution of tryptophan irradiated at 77°K, tryptophan concentration 3×10^{-4} M: a, after uv irradiation (30 sec); b, further irradiation with F_1 optical filter (3 min); c, further irradiation with F_2 optical filter (3 min); d, further irradiation with F_0 optical filter (30 sec).

seems reasonable to attribute the line A to an organic free radical as such radicals are known to be sensitive to peroxidation. Since uv irradiation of phosphorescent amino acids in frozen aqueous solutions leads to their photoionization,[2b] we attribute A resonance to the amino acid positive radical ion. The intensity of line B increases with the concentration of $CdSO_4$ (Figure 3), and B is not observed when $CdSO_4$ concentration is less than 10^{-2} M. Furthermore, the g values of line B, calculated according to Kneubuhl's analysis,[6] are in good agreement with those given by Moorthy and Weiss[7] and attributed to Cd^+ ion.

Increasing the concentration of $CdSO_4$ markedly affects the intensity of lines C and B (Figure 3).

For $CdSO_4$-saturated aqueous solutions of tryptophan (5×10^{-4} M) which form glasses at low temperature, C and D peaks are visible at only high sensitivity. At $CdSO_4$ concentrations higher than 1 M, a new line (E) appears (Figure 4) in addition to lines A, B, C, and D at high field ($g = 1.9710$) after uv irradiation at 77°K. Long exposure to uv light (optical filter F_0: Figure 2) of frozen concentrated aqueous solutions of $CdSO_4$ (concentration up to 2 M) without tryptophan produces a weak esr spectrum and only lines B, C, and D are observed; as expected line A is not visible. Oxygenation does not produce any shift in the g values of the different signals after irradiation at higher temperature. The study of saturation properties of the signals A, B, C, and D gives us information about the coupling of the different species with respect to their environment and also gives added support to hypothesis that the resonances arise from different species. Comparison of A, B, C, and D peak intensities, using the same range of microwave power for all measurements, shows that the C and D resonances do not saturate, whereas the B resonance saturates more rapidly.

Quite similar spectra are obtained with frozen aqueous

(6) F. K. Kneubuhl, 33, *J. Chem. Phys.*, 1074 (1960).
(7) P. N. Moorthy and J. J. Weiss, *Nature*, 201, 1317, (1964).

Table I: Effect of Various Electron Scavengers on the Intensity of Esr lines C, D, E[a]

Relative intensity of paramagnetic resonance signals	Salt				
	$CdSO_4$, 0.2 M			$ZnSO_4$, 0.1 M	
	77°K		130°K	130°K	
E	Nil		1		
	HCl (0.05 M)		0		
	H_2SO_4 (0.05 M)		0		
	Ethanol (0.05 M)		0		
	N_2O (saturated)		0.5		
	Cysteamine (0.05 M)		0		
C	Nil	1	1	Nil	1
	HCl (0.05 M)	0.7	0.4	HCl (0.05 M)	0.25
	H_2SO_4 (0.05 M)	0.6	0.4	H_2SO_4 (0.05 M)	0.3
	Ethanol (0.05 M)	0.3	0.5	Ethanol (0.05 M)	0.1
	N_2O (saturated)	0.7	0.3		
	Cysteamine (0.05 M)	0	0		
D	Nil	1	1	Nil	1
	HCl (0.05 M)	0.6	0.4	HCl (0.05 M)	0.25
	H_2SO_4 (0.05 M)	0.6	0.5	H_2SO_4 (0.05 M)	0.3
	Ethanol (0.05 M)	0.2	0.5	Ethanol (0.05 M)	0.1
	N_2O (saturated)	0.7	0.3		
	Cysteamine (0.05 M)	0	0		

[a] See text. Tryptophan concentration: 5×10^{-4} M.

solutions of tryptophan or any phosphorescent aromatic amino acid or purine base containing $ZnSO_4$ or $MgSO_4$ although $MgSO_4$ solutions give weaker signals. In saturated solutions of $ZnSO_4$ or $MgSO_4$, H atoms are produced in much higher yield than in $CdSO_4$ solutions.

In order to determine which paramagnetic species are due to reaction with photoproduced electrons, frozen aqueous solutions of tryptophan containing salts and different electron scavengers,[8,9] *i.e.*, N_2O, alcohols, acids, or cysteamine were irradiated with uv light. The results are presented in Table I. These electron scavengers have a marked effect on the C, D, E resonance intensities at different temperatures. Obviously, electrons are involved in the formation of the C, D, and E resonances. However, it must be noticed that alcohols, acids, or cysteamine may also modify the medium structure and the solute molecule environment.[10] Uv irradiation of a frozen aqueous solution of tryptophan containing 1 M $CdSO_4$ and 0.5 M cysteamine does not produce signals C, D, and E and we observe the formation of an unresolved esr signal at $g \sim 2$ similar in shape with that obtained by uv photolysis of cysteine powder at 77°K[11] or by sensitized photolysis of cysteine by tryptophan in aqueous frozen solutions.[12]

Trapped electrons generated by γ radiolysis[13,14] or by uv irradiation[2,15] have been detected by optical and esr spectroscopies, in frozen solutions of alkali or neutral salts[2,16] and revealed by optical bleaching experiments. Further irradiation of the uv-irradiated frozen aqueous solutions of tryptophan containing $CdSO_4$ (Figure 4a) with wavelengths longer than 400 nm (optical filter F_1) decreases the intensity of lines A and B of the esr spectrum and the line (E) ($g_\perp$ = 1.9710, $g_\parallel$ = 1.9764) appears at higher field (Figure 4b). The g factors of line E indicate that the species responsible for this line is an electron excess center[17] with small spin–orbit coupling since resonance (E) saturates rapidly. C and D resonances are practically unaffected. Irradiation with wavelengths between 315 and 370 nm (optical filter F_2) produces an increase in signals C, D, E and markedly affects line B (Figure 4c). As pointed out by Moorthy and Weiss,[7] the unpaired electron in Cd^+ occupies an s orbital with a relatively weak binding. Furthermore, the spectrum of Cd^+ in solution was considered[18] to be of charge-transfer character. Photobleaching with light of appropriate wavelengths (optical filter F_1) of frozen aqueous solutions of tryptophan containing $ZnSO_4$ or $MgSO_4$ uv irradiated at 77°K produces a slight decrease in the central resonance and an increase

(8) J. P. Keene, *Radiat. Res.*, **22**, 1 (1964).

(9) J. Jortner, M. Ottolenghi, J. Rabani, and G. Stein, *J. Chem. Phys.*, **37**, 2488 (1962).

(10) C. Hélène, R. Santus, and M. Ptak, *Compt. Rend.*, **262D**, 1349 (1966).

(11) M. Ptak, Thesis, Paris, 1965.

(12) R. Santus, C. Hélène, and M. Ptak, *Compt. Rend.*, **262D**, 2077 (1966).

(13) D. Schulte Frohlinde and K. Eiben, *Z. Naturforsch.*, **17a**, 445 (1962).

(14) T. Henriksen, *Radiat. Res.*, **23**, 63, (1964).

(15) J. Jortner and B. Scharf, *J. Chem. Phys.*, **37**, 2506 (1962).

(16) V. N. Belevskii and L. T. Bugaenko, *Zh. Fiz. Khim.*, **39**, 2958, (1965).

(17) D. J. E. Ingram, "Free Radicals as Studied by Electron Spin Resonance," Butterworth and Co., Ltd., London, 1958, p 190.

(18) G. E. Adams, J. H. Baxendale, and J. W. Boag, *Proc. Chem. Soc.*, **241**, (1963).

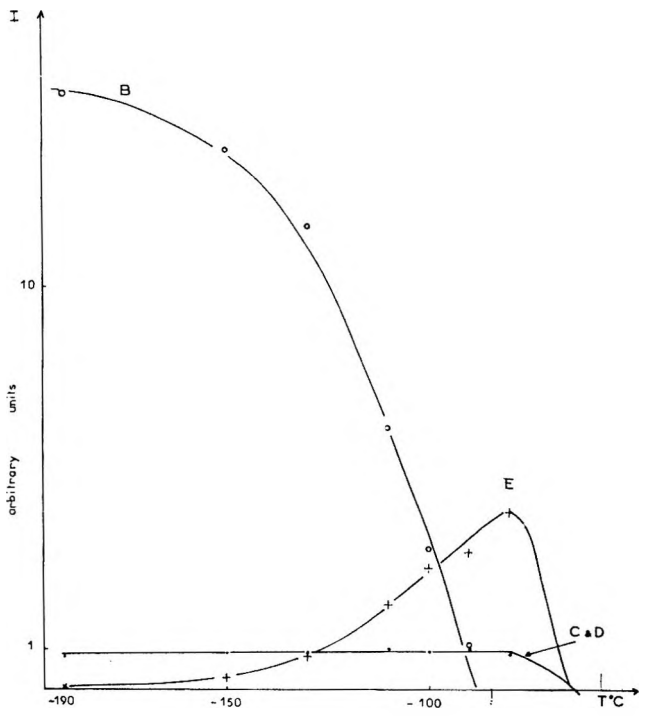

Figure 5. Effect of thermal annealing on the intensity of lines B, C, D, E (see text).

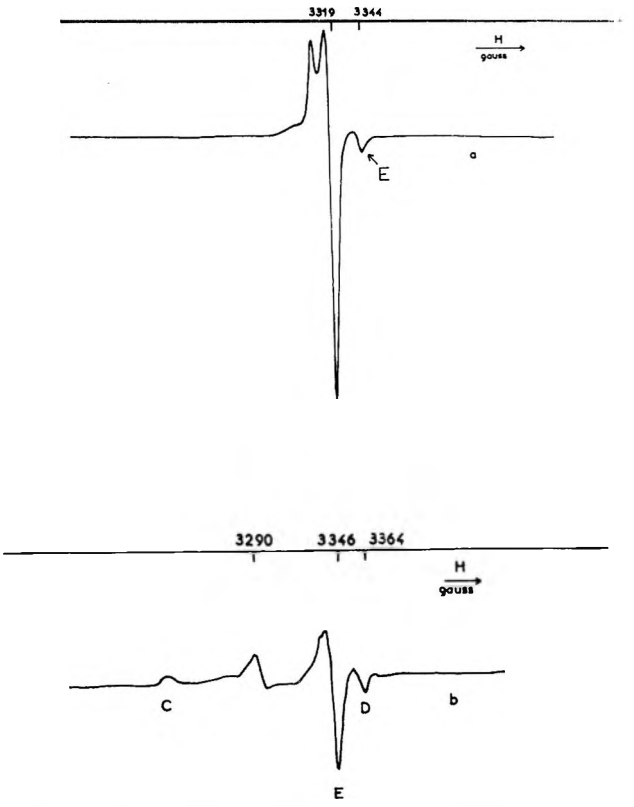

Figure 6. (a) Esr spectrum of uv-irradiated $CdSO_4$ containing frozen aqueous solution of tryptophan at 130°K. $CdSO_4$ concentration, 1*M*; tryptophan concn, 5×10^{-4}; time of irradiation, 30 sec. (b) Esr spectrum obtained after uv irradiation at 190°K.

in signals C and D. New resonances (such as E in $CdSO_4$ case) are not observed.

The intensity of the different signals *vs.* absolute temperature is plotted in Figure 5 in the case of $CdSO_4$ solutions. C and D signals decrease at the same rate when the temperature increases. This fact confirms that C and D belong to the same paramagnetic species.

As the temperature increases, resonance (E) increases, while lines A and B decrease. Thus, heating has the same effect on resonance (E) as bleaching; furthermore, at a given temperature between 77 and 170°K, it is possible to increase intensity of line E by photobleaching of the sample. Then signal E is closely related to a species produced by reaction with mobile electrons.[18] With air-saturated samples, the disappearance of the A resonance signal is accompanied by an increase in the resonance signal attributed to the oxidized R^+ radical ion (g = 2.0071) (see above). Oxygen diffusion occurs at about 170°K; a similar phenomenon in frozen aqueous solutions of amino acids has been reported by Azizova, *et al.*[19]

Uv irradiation of frozen aqueous solutions of tryptophan containing $CdSO_4$ at temperatures higher than 77°K produces the same stable paramagnetic species as uv irradiation at 77°K. In addition the E resonance is easily detected before bleaching. For example, we have reproduced in Figure 6a the esr spectrum of a frozen solution of tryptophan containing 1 *M* $CdSO_4$, uv irradiated at 130°K. At 190°K, the Cd^+ resonance disappears and the E resonance intensity reaches a maximum (Figure 6b). At any temperature between

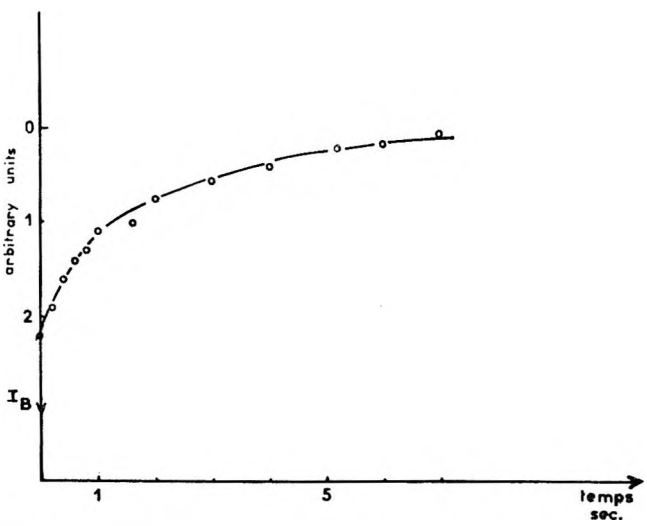

Figure 7. Variation of the intensity of line B (I_B) with time following irradiation with photobleaching wavelengths. Cd^{2+} concn, 1 *M*; tryptophan concn, 5×10^{-3} *M*; 140K°. The photobleaching irradiation has been stopped at time t = 0.

77 and 190°K it is possible to increase the intensity of (E) resonance after uv irradiation by bleaching with optical filter F_2. The intensity of (E) resonance in-

(19) O. A. Azizova, Z. P. Gribova, L. D. Kayushin, and M. K. Pulatova, *Photochem. Photobiol.*, 5, 763 (1966).

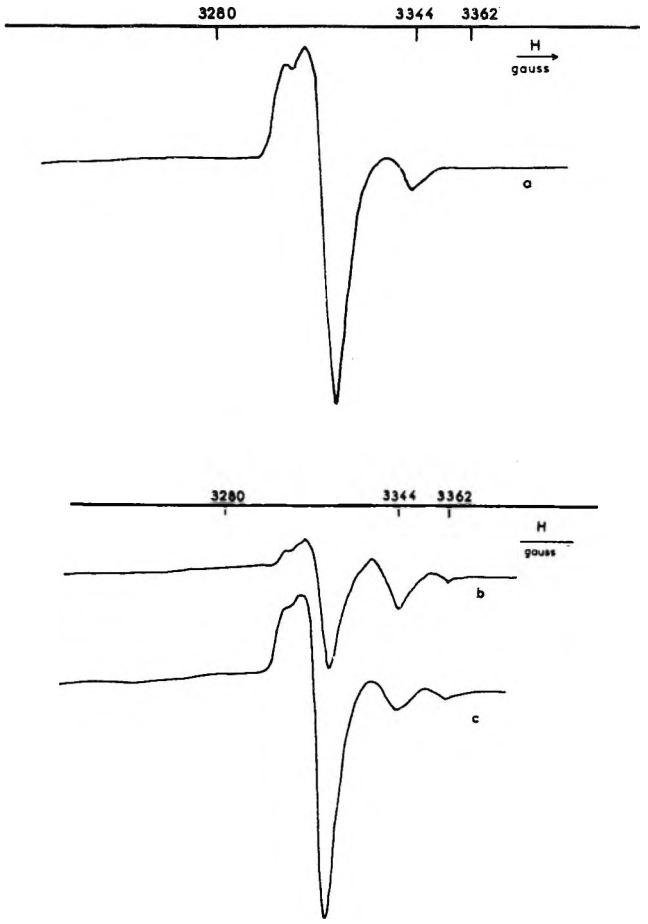

Figure 8. a, Esr spectrum of uv-irradiated $CdSO_4$ containing frozen aqueous solution of tryptophan at 130°K. $CdSO_4$ concn, 1 *M*; tryptophan concn, 5×10^{-4} *M*; time of irradiation, 15 sec; b, a after optical bleaching; c, b after uv irradiation with F_0 optical filter, time of uv irradiation = 30 sec.

creases, while that of B resonance decreases even after irradiation with bleaching light has been stopped (Figure 7). This experiment demonstrates that electrons ejected from their traps by photobleaching are able to diffuse slowly in the medium toward other trapping centers giving rise to signal E. Another interesting property of the (E) resonance is the marked decrease of its intensity under uv irradiation. Uv irradiation of frozen solution of tryptophan containing 1 *M* $CdSO_4$ at 130°K produces the expected spectrum (Figure 8a). Photobleaching with F_2 optical filter leads to an increase in the E resonance and a decrease in the B resonance intensity (Figure 8b). Further illumination with uv light (optical filter F_0) produces a decrease in the intensity of (E) (Figure 8c). It is possible to observe the same result at 77°K (Figure 4d) and also with γ-irradiated frozen aqueous solutions of $CdSO_4$. In the latter solutions, thermal annealing at 190°K leads to the disappearance of the Cd^+ resonance. Irradiation with optical filter F_0 at 77°K produces a decrease in the E resonance and reappearance of the Cd^+ resonance. This cycle can be repeated again and again, so that resonance (E) comes from trapped electrons which have moved under bleaching effect from a Cd^+ center to a solvated Cd^{2+} ion, whose ground-state energy has been lowered by specific phenomena, in the rapid cooling process, such as aggregation of hydrated Cd^{2+} ions or metastable coordination of Cd^{2+} ions with water molecules. This is similar to Walker's model[20] which suggests that electrons are trapped in preexisting potential wells of different depths and able to move among these wells by jumping or tunneling.

2. Solutions Containing Chloride. In Figure 9a are shown the esr spectra of a frozen aqueous solutions of tryptophan containing 0.5 *M* $CdCl_2$, after uv irradiation, at 77°K, with an optical filter type F_0. A broad, intense resonance (about 250 G) appears at about $g \sim 2$ in addition to signal A (tryptophan positive radical-ion) described above. Lines C and D are present as in the esr spectrum shown in Figure 1a. An increase in temperature produces a general decrease in the broad resonance signal, but this broad signal is still detected at temperature higher than 220°K. This corresponds to a remarkably stable paramagnetic species in this system. Another resonance appears at lower field and its occurrence in other chlorinated systems (aqueous solutions containing $BaCl_2$, $MgCl_2$, $ZnCl_2$, $CaCl_2$) allows us to attribute this signal to a paramagnetic chlorinated species G (see Discussion).

With $CdCl_2$-saturated frozen solutions of tryptophan (Figure $9b_1$) we obtain the same broad and intense resonance and we note that a high concentration of $CdCl_2$ markedly depresses C and D resonances intensities as reported above for $CdSO_4$. Photobleaching with filter F_1 and F_2, leads to a decrease of the broad line intensity. A weak signal appears at the same field as signal E described above (Figure $9a_2$). The case of saturated solution (Figure $9b_2$) does not require special comments. However, the intensity of the G resonance is markedly affected by photobleaching.

Uv irradiation of frozen solutions of tryptophan containing $ZnCl_2$, $CaCl_2$, or $BaCl_2$ does not give the broad esr line even at high salt concentration (Figure 9c). Bleaching experiments carried out with optical filter F_2 produce a small decrease in the intensity of the central resonance. With $MgCl_2$ (Figure $9c_2$) the bleaching effect is more pronounced. In all cases, the intensity of C and D signals increases. Photobleaching has no important effect on the intensity or shape of the G resonance. It is possible that M^+ ions are also formed in frozen aqueous solutions containing chloride. These resonances appear as shoulders more or less resolved in the esr spectra at about the same resonance fields given for Cd^+, Zn^+, Mg^+ in the sulfate case. H atom signals are easily observed in $ZnCl_2$- or $MgCl_2$- containing solutions.

(20) D. C. Walker, *Quart. Rev.* (London), **21**, 79, (1967).

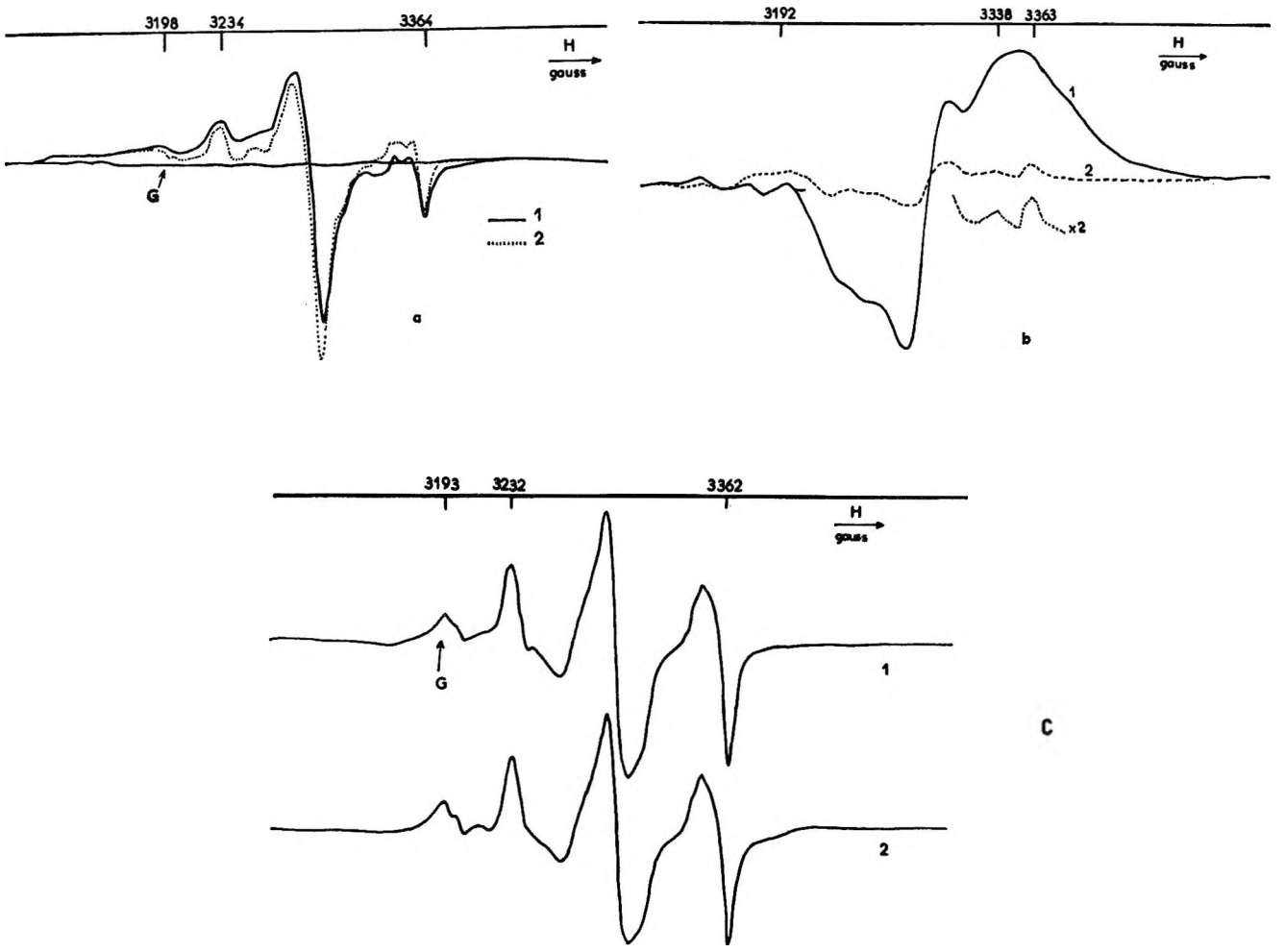

Figure 9. Esr spectra of uv irradiated frozen aqueous solution of tryptophan 5×10^{-4} *M* containing divalent chlorides; microwave frequency, 9230 Mhz: a_1, Esr spectrum of a sample containing $CdCl_2$ (0.5 *M*) time of irradiation, 30 sec; a_2, a_1 after photobleaching (see text); b_1, esr spectrum of $CdCl_2$ saturated sample after 30-sec irradiation; b_2, b_1 after photobleaching (see text); c_1, esr spectrum of a sample containing $MgCl_2$ (2 *M*); c_2, c_1 after bleaching.

II. γ-Radiolysis Results: Comparison with Ultraviolet Photolysis Results. γ-Irradiation of frozen aqueous solutions containing $CdSO_4$ or $ZnSO_4$ has been extensively studied by Moorthy and Weiss[7] at 77°K. Nevertheless, we have reexamined the esr spectrum of γ-irradiated frozen 0.2 *M* $CdSO_4$ solutions (dose; 0.7 Mrad). Our spectrum is shown in Figure 10a and is in total agreement with that reported in ref 7. However, at higher sensitivity, it is possible to detect the same (E) resonance that we have obtained after optical bleaching of uv-irradiated frozen tryptophan solutions. Furthermore, irradiation with optical filter F_2 and thermal annealing at 110°K (Figure 10b) give rise to the C and D resonances and increase (E) resonance intensity. But the former disappear when $CdSO_4$ concentration is raised to 2 *M*. Therefore, there is no important qualitative difference between most paramagnetic species produced by γ radiolysis and by uv photolysis.

γ Irradiation (dose, 0.7 Mrad) of frozen aqueous solutions containing $CdCl_2$, at 77°K, produces a broad intense esr spectrum (Figure 11a) which is identical with that obtained by uv photolysis of $CdCl_2$-containing tryptophan solutions (Figure 9). In addition, we observe the resonance of OH· radicals (which disappears after thermal annealing at 110°K) and the resonance line of the chlorinated species (G) described in the former section. Photobleaching with F_2 and F_1 optical filters at 110°K (Figure 11c) markedly depresses the broad line and allows the appearance of the underlying Cd^+ ion resonance. By heating the sample, we observe that resonances G and J decrease at the same rate. Furthermore, G and J signals have the same microwave power saturation properties, so that they belong to the same species.

III. Optical Absorption Spectroscopy at 77°K of Irradiated Frozen Aqueous Solutions Containing Divalent Cations. Concentrated solutions (4 *M*) of $CaCl_2$ or $MgCl_2$, saturated solutions of $CdCl_2$ or $CdSO_4$ give transparent glasses at 77°K. These glasses do not absorb uv light able to excite aromatic amino acids. It was of great interest to compare the optical absorption spectra of

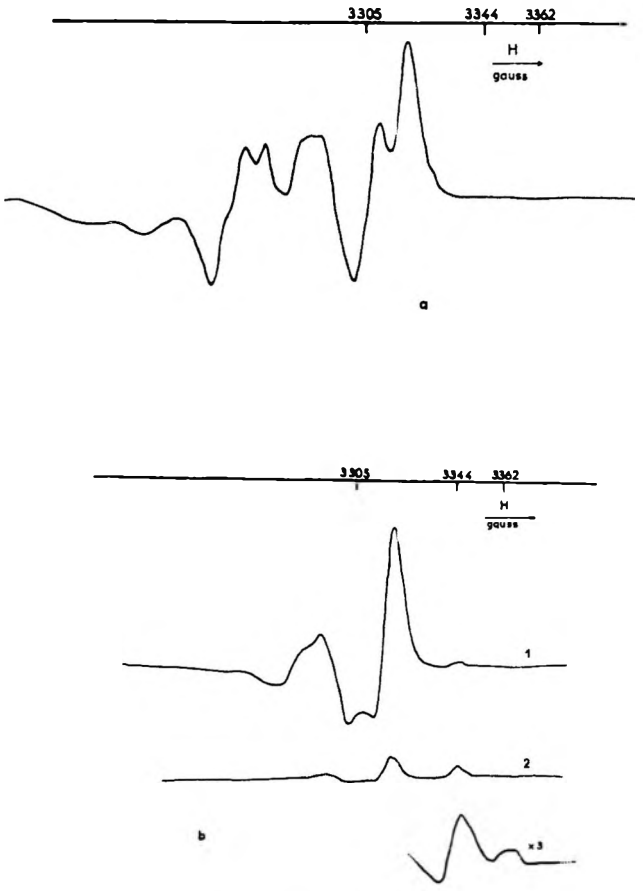

Figure 10. a, Esr spectrum of a γ-irradiated frozen aqueous solution of $CdSO_4$ (0.2 *M*) at 77°K, microwave frequency, 9230 MHz; b_1 after thermal annealing at 110°K; b_2, b_1 after photobleaching and at two different gain settings.

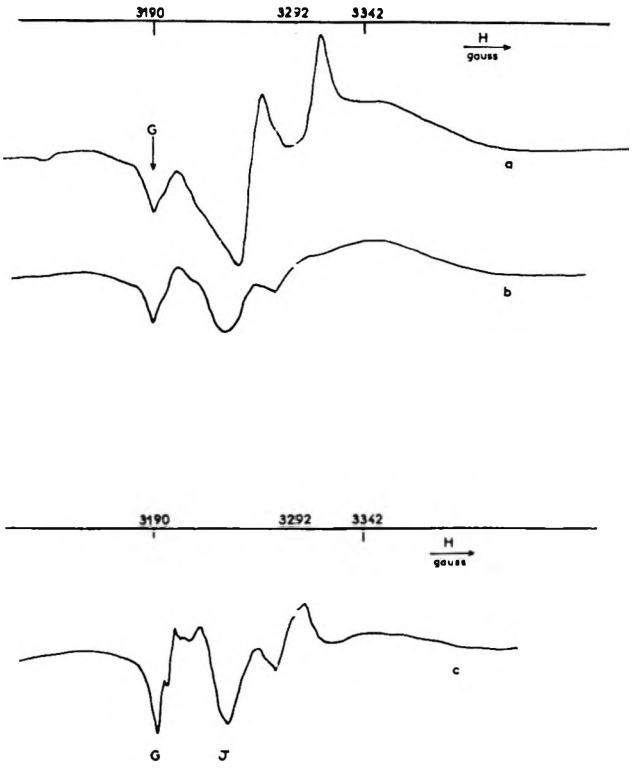

Figure 11. a, Esr spectrum of a γ-irradiated frozen aqueous solution of $CdCl_2$ (2 *M*) at 77° K, microwave frequency 9230 MHz; b, after thermal annealing at 110°K; c, b after photobleaching.

tryptophan photoproducts at low temperature in $CaCl_2$ solutions ($CaCl_2$ concentration is 4 *M*) in which photobleaching has a rather small effect on the esr spectrum, with those in $CdCl_2$ saturated solutions in which photobleaching induces marked effects. The optical absorption spectra of solutions are shown in Figure 12 (a and b). At 77°K the absorption spectrum (Figure 12a) of tryptophan solution containing $CaCl_2$, irradiated with optical filter F_0 shows that the major component is the positive radical ion of tryptophan.[2,21] Bleaching using optical filter F_2 does not produce any important modification in the intensity and position of the different absorption bands. On the other hand, uv irradiation of $CdCl_2$ saturated solution of tryptophan produces (Figure 12b) broader absorption bands in the range of 310–720 nm. When compared with Figure 12a it can be seen that another absorption band (attributed to trapped electrons) is superimposed on the tryptophan positive radical ion absorption band at about 310–500 nm. Bleaching with F_1 and F_2 filters produces a general decrease of the various absorption bands (Figure $12b_2$).

The photochemical reaction taking place during bleaching is

$$R^+ + \bar{e} \longrightarrow R$$

where R is the aromatic amino acid molecule and R^+ its positive radical ion. The general decrease which is observed after photobleaching in the esr spectrum of $CdCl_2$- saturated frozen solutions of tryptophan is due to the same reaction and the broad esr resonance (Figure 9b) can be attributed to trapped electrons (see Discussion).

IV. Electron Photoejection Mechanism. Triplet–Triplet Absorption Process. Former studies have shown that the triplet state of aromatic amino acids is involved in the photoionization process of these molecules in frozen aqueous solutions.[2,22] We now present some evidence that this triplet state is an intermediate state in the photoejection of electron from aromatic amino acids in frozen aqueous solutions containing divalent cations.

While phosphorescence spectroscopy can be used to study the radiative deactivation process of the triplet state, the esr intensity of the so-called "$\Delta m = 2$" transition is closely related to the triplet state population. The triplet state of aromatic amino acids (*i.e.*, tryptophan or tyrosine; free or included in peptides or proteins) is easily detected in frozen aqueous solution containing $CdSO_4$ or $CdCl_2$. A remarkable fact is the possibility to detect "$\Delta m = 2$" transition at relatively

(21) R. Santus, R. Guermonprez, and M. Ptak, *Compt. Rend.*, **261**, 117 (1965).

(22) E. E. Fessenko, E. A. Burstein, and J. A. Vladimirov, *Biofizika*, **12**, 616 (1967).

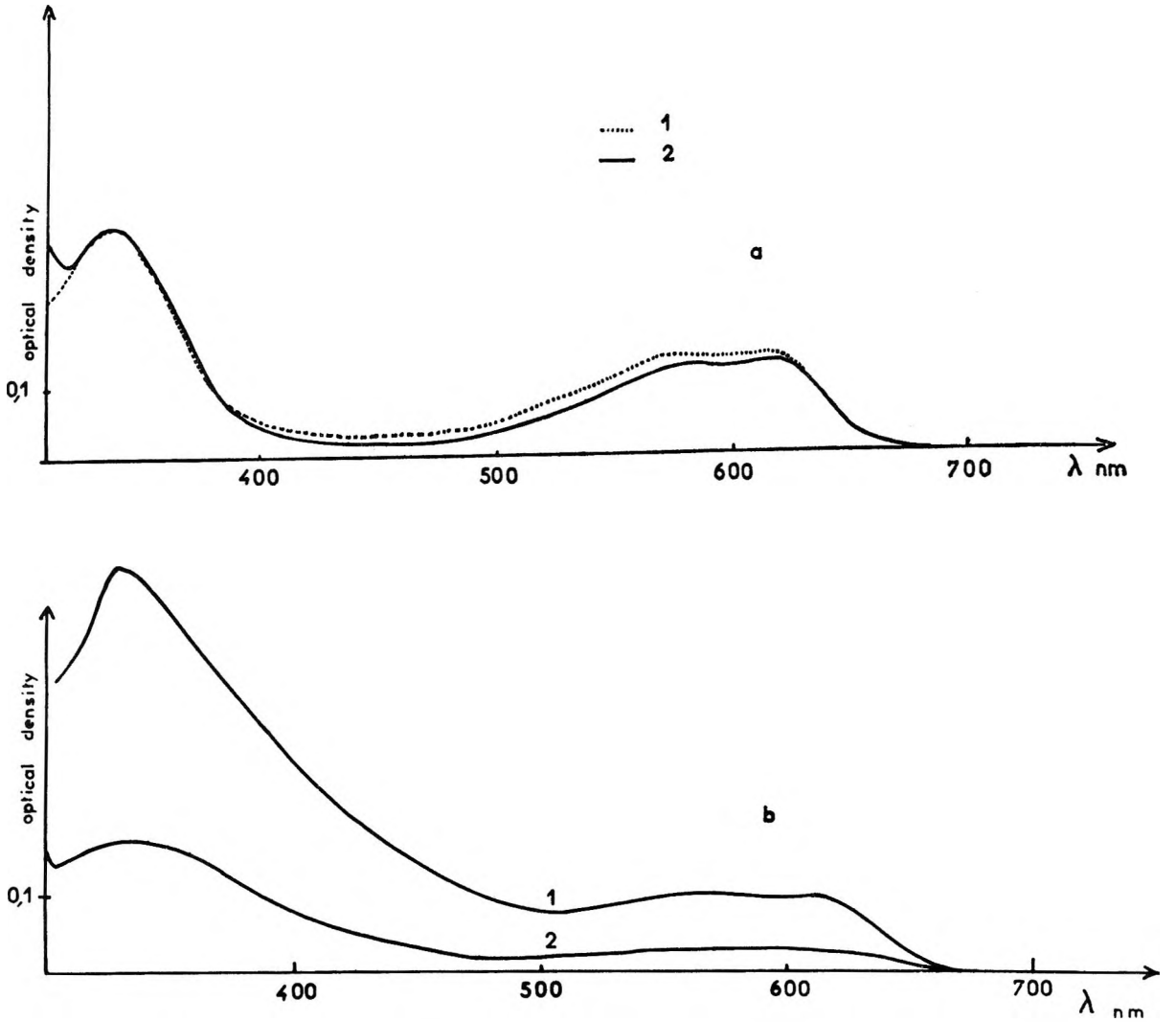

Figure 12. a, Optical absorption spectrum at 77°K of a uv-irradiated glassy sample of tryptophan in $CaCl_2$ frozen aqueous solution. Tryptophan concentration, 5×10^{-4} *M*; 1, after uv irradiation (2 min) with F_0 filter; 2, after photobleaching with F_2 optical filter; b, optical absorption spectrum at 77°K of a uv-irradiated $CdCl_2$ saturated frozen aqueous solution of tryptophan (tryptophan concentration 5×10^{-4} *M*): 1, after uv irradiation with filter F_0; 2, after photobleaching with F_2 optical filter.

high temperatures in such media. In Figure 13 is plotted the intensity of the "$\Delta m = 2$" esr transition as a function of the temperature; esr detection of the triplet state is possible at temperatures higher than 170°K and consequently the steady-state population of the triplet is still important at these temperatures.

The high steady-state concentration of these molecules in the triplet state makes it possible to obtain their triplet–triplet absorption spectra at low temperature (Figure 14). All experiments were performed at 77°K on transparent glassy $CaCl_2$ solutions of tryptophan or tyrosine. Triplet–triplet absorption spectra have already been reported by Vladimirov[23] in glycerol at 80°K in the wavelength range 400–700 nm. We have extended these measurements to 300 nm. The decay times of the triplet–triplet absorption when irradiation is switched off are in good agreement with those measured on the same samples from phosphorescence decay curves.

To show that this triplet–triplet absorption can lead to photoejection of electrons, we have irradiated the tryptophan samples with two light beams, using the optical window of the Varian esr optical cavity (Figure 15a). Wavelengths which are absorbed by the chromophore are selected by a Schott optical filter no. uv-R-280 (R_1 radiation in Figure 15a). Wavelengths which do not excite the chromophore, but are efficient for the triplet–triplet absorption, are selected by convenient chemical filters, in the range of 310–600 nm (R_2 radiation in Figure 15a); the bandwidths are of the order of 100 Å. A typical result is given in Figure 15b. When a $CdSO_4$-saturated frozen aqueous solution of tryptophan is irradiated with R_1 and R_2 simultaneously at 77°K, the intensity of the Cd^+ resonance (Figure 15b$_1$) is higher than that obtained when R_1 is applied alone.

(23) S. L. Aksencev, J. Vladimirov, V. Olenev, and E. Iesenko, *Biofizika*, **12**, 63 (1967).

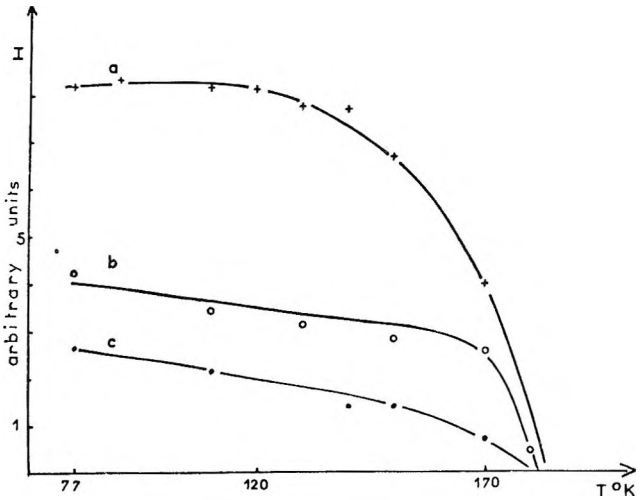

Figure 13. Relative intensity of "$\Delta m = 2$" transitions of tryptophan triplet state molecules *vs.* absolute temperature in different media. a, tryptophan (10^{-2} *M*) in saturated frozen aqueous solution of $CdCl_2$; b, tryptophan (10^{-2} *M*) in frozen aqueous solutions of $CdSO_4$ (0.5 *M*); c, bovine serum albumin in saturated frozen aqueous solution of $CdSO_4$; tryptophan concn 5×10^{-3} *M* (obtained by measurement of the optical absorption of serum albumin solution at 282 nm).

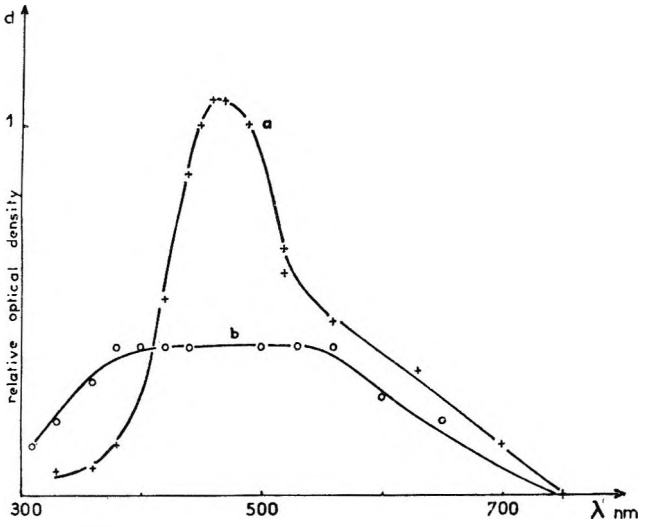

Figure 14. Triplet–triplet absorption spectrum in glassy frozen aqueous solution of 4 *M* $CaCl_2$: a, 5×10^{-4} *M* tryptophan; b, 5×10^{-4} *M* tyrosine.

However, the wavelength of the R_2 radiation must be shorter than 390 nm. Therefore, molecules which have reached the triplet state (after uv irradiation and intersystem crossing) undergo photoionization by irradiation with wavelengths shorter than 390 nm. An energy of about 6.5 eV is therefore needed to produce photoionization of tryptophan molecules in frozen aqueous solutions at 77°K. The same phenomenon can take place at higher temperature, as the triplet state remains highly populated, but in fluid medium direct ionization from the lowest singlet or triplet state could be allowed *via* charge transfer with the solvent

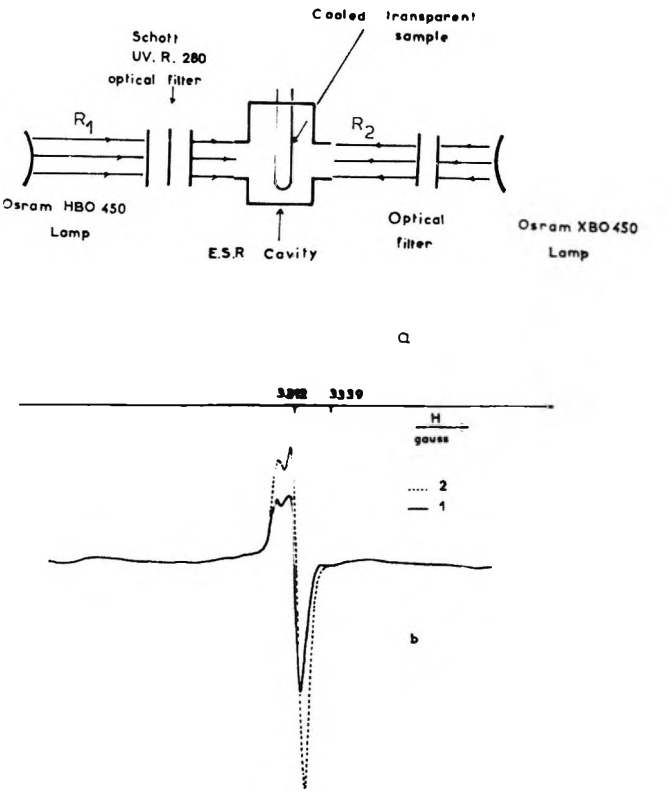

Figure 15. a, Schematic diagram of the experimental procedure used to observe triplet–triplet absorption in the esr cavity. b, esr spectrum obtained by irradiation of a 5×10^{-4} *M* frozen aqueous solution of tryptophan saturated with $CdSO_4$. 1, uv irradiation (R_1 radiations alone), time of exposure, 15 sec; 2, (R_1) + (R_2) radiations, time of exposure, 15 sec.

Discussion

Ultraviolet irradiation of frozen aqueous solutions of aromatic amino acids containing various divalent salts leads to photoionization of the phosphorescent chromophore, *via* a triplet–triplet absorption process. The complexing of a part of the divalent cations by the aromatic amino acids which probably occurs in these solutions[24] does not greatly modify the spectroscopic properties of the chromophore. Absorption and esr spectroscopies have allowed us to characterize the positive radical ions of aromatic amino acids and the trapped electrons. The investigation of the properties of the trapped electrons shows that the nature of traps depends on medium and temperature. As already pointed out by several authors,[25–27] there are two kinds of electron traps—chemical and physical.

In frozen aqueous solutions of aromatic amino acids containing divalent cations, the major chemical traps

(24) M. M. Ramel and M. R. Paris, *Bull. Soc. Chim.*, 1359 (1967).

(25) See, for example, M. Burton, M. Dillon, and R. Rein, *J. Chem. Phys.*, **41**, 2228 (1964), or ref 26 and 27.

(26) W. M. McClain and A. C. Albrecht, *J. Chem. Phys.*, **43**, 465 (1965).

(27) J. B. Guarino and W. H. Hamill, *ibid.*, **44**, 1279 (1966).

are H^+ ions and the metal cations themselves. H atoms are produced in good yield with $ZnSO_4$, $ZnCl_2$, $MgCl_2$, and $MgSO_4$ as added salts. (The pH of these solutions is less than 5 at room temperature.) The presence of H atoms, revealed by their esr spectrum at 77°K, prevents the photobleaching reaction. More interesting is the trapping of electrons by divalent cations. This electron capture is the main primary process in uv irradiated frozen aqueous solutions of amino acids containing Zn^{2+}, Mg^{2+}, Cd^{2+} (see section 1).

Likewise, the esr study of uv irradiated samples of tryptophan in the presence of Ca^{2+} or Ba^{2+} strongly suggests that these cations are also able to trap photoejected electrons at low temperature although Ca^{2+}, Ba^{2+} have been found to be unreactive toward solvated electrons at room temperature.[28] On the other hand, paramagnetic signals such as E, C, D, are probably related to physical traps. The difference in the effects of photo bleaching and thermal annealing on lines B, E, C, and D indicate that these resonances belong to physical traps of different depths. This phenomenon has been very recently reported by several authors.[29-31] C and D resonances are present in a variety of uv-irradiated frozen aqueous solutions of various sensitizers containing alkali or alkaline earth metal ions; they are also produced by thermal annealing or photobleaching of γ-irradiated samples but in a very low yield. The intensity of lines C and D is affected by electron scavengers, but deuteration does not produce any change in their esr spectrum. It must be noted that g factors slightly depend on the cation so that the paramagnetic species interact with the metal ion which is present in the frozen solution. At this stage of the study, we cannot say anything definite about the type of traps which are responsible for C and D resonances; further studies are necessary for accurate assignment.

Examination of the bleaching effects on the esr spectrum of uv irradiated frozen aqueous solutions of aromatic amino acids containing $CdCl_2$ or of γ-irradiated frozen aqueous solutions of $CdCl_2$ shows that ejected electrons are trapped in many heterogeneous sites probably produced in a random way during the rapid cooling process. The lines G and J (Figures 9 and 11) common to other chlorinated systems (NaCl,[2] $CaCl_2$, $BaCl_2$, $MgCl_2$, HCl) are probably a part of the Cl_2^- radical ion esr spectrum which has just been extensively studied by Roncin[32] in different media. Upon uv irradiation, the formation of Cl_2^- radical ion can be explained by the photosensitized decomposition of Cl^- induced by the phosphorescent molecule, *i.e.*, an energy transfer[2] between an upper excited triplet state of the phosphorescent molecule (reached by triplet–triplet absorption) and the anion in its ground state, then followed by a charge-transfer process[33,34] toward the solvent according to the scheme

$$R \xrightarrow{h\nu_1} {}^1R_1^* \xrightarrow{\text{I.S.C.}} {}^3R_1^* \xrightarrow{h\nu_2} {}^3R_2^* \dashrightarrow {}^3R_n^*$$

$$T \longrightarrow T \text{ absorption}$$

$${}^3R_n^* + Cl^- \longrightarrow {}^3(Cl^-)^* + R$$

$$\longrightarrow Cl^{\cdot} \ldots . e^-$$

R is the aromatic amino acid in its ground state ${}^1R_1^*$ in its first excited singlet state, ${}^3R_1^*$ in its first triplet state, ${}^3R_n^*$ in the nth excited triplet state.

I.S.C. represents intersystem-crossing (singlet-triplet conversion). Then the rapid recombination of $Cl^{\cdot}$[32] with a Cl^- anion which occurs at 77°K produces the Cl_2^- radical anion.

In this case, a portion of the trapped electrons is produced by sensitized photolysis of the anion. Such a phenomenon has been recently reported by Devonshire and Weiss[33] in the direct uv photolysis of various anions (Cl^-, I^-, Br^-, SO_4^{2-}, HPO_4^{2-}) in aqueous solutions at room temperature. This sensitized photolysis of the anions is also likely for frozen aqueous solutions of aromatic amino acids containing sulfate at low temperature, but the SO_4^- radical signal is superimposed on that of the positive radical ion of the aromatic amino acid. The small effect of photobleaching light on the intensity of G resonance (see section I-2) indicates that photolysis of Cl_2^- may occur. Based on the generally accepted polaron theory,[35,36] electrons in frozen chlorinated media in which water dipoles are frozen in their liquid-phase orientation around Cl^- ions may also be trapped at sites corresponding to anion vacancies after the reaction $Cl^- + Cl^{\cdot} \rightarrow Cl_2^-$. Such a mechanism has been put forward to explain the formation of solvated electrons in alkaline ice.[37] The heterogeneous distribution of water dipoles before cooling may explain the broad esr resonance attributed to trapped electrons. The resultant line shape is probably due to the addition of the individual line shapes of different trapping site resonances, each characterized by two or three principal g factors[6] according to their magnetic symmetry. The unusual broadening of the trapped electron esr resonance cannot be explained by dipolar broadening. Photobleaching affects the esr spectrum of a uv-irradiated frozen aqueous

(28) M. Anbar and E. J. Hart, *J. Phys. Chem.*, 69, 1244 (1965).
(29) M. Irie, K. Hayashi, and S. Okamura. *J. Chem. Phys.*, 48, 922 (1968).
(30) F. S. Dainton, G. S. Salmon, and U. F. Zucker, *Chem. Commun.*, 1172 (1968).
(31) R. Guermonprez, C. Hélène, and M. Ptak, *J. Chim. Phys.*, 64, 1376 (1967).
(32) J. Roncin, *J. Chem. Phys.*, 49, 2876 (1968), and personal communication.
(33) R. Devonshire and J. J. Weiss, *J. Phys. Chem.*, 72, 3815 (1968).
(34) P. N. Moorthy and J. J. Weiss, *J. Chem. Phys.*, 42, 3121 (1965).
(35) J. Jorther, *Radiat. Res. Suppl.*, 4, 24 (1964).
(36) R. L. Platzman and J. Franck, *Z. Physik.*, 138, 411 (1965).
(37) J. Zimbrick and L. Kevan, *J. Amer. Chem. Soc.*, 88, 3678 (1966).

solution of tryptophan containing $CdCl_2$, whatever the concentration of $CdCl_2$. With a $CdCl_2$-saturated frozen aqueous solution of tryptophan, the esr resonance is independent of the uv irradiation time.

All the results reported here have been obtained in frozen solutions. However, flash-photolysis studies have already shown that photoionization is the main primary photochemical reaction of aromatic amino acids in aqueous solutions. From a biological point of view, this ejection process could be of great importance in the ultraviolet inactivation of enzymes. Photoejected electrons could react with amino acid residues which are far apart from the ejection center. Such reactions have already been demonstrated in frozen solutions; this includes breakage of disulfide bonds and deamination reactions.[12] They have also been shown to occur in the direct electron irradiation of aqueous amino acid solutions.[38]

The results reported above show that the ejected electrons are easily trapped in metal ions such as Cd^{2+} Zn^{2+}, etc.; these reactions could be important in the photoinactivation of metalloenzymes. More work is clearly needed to elucidate these points, but the methods presented here appear to be very convenient to understand some of the primary photochemical processes in biological molecules.

Acknowledgments. We wish to thank Professor C. Sadron for his interest in this work. We are indebted to Doctors F. Kieffer, A. Deroulede, and J. Roncin, (Laboratoire de Physico-chimie des Rayonnements de la Faculté des Sciences d'Orsay) both for providing a γ-ray source and helpful discussions. Helpful criticism by the referees is gratefully acknowledged.

(38) R. Braams, *Radiat. Res.*, 27 319 (1966).

The Single Crystal Spectra of Dichlorotetrapyrazolenickel(II), Dibromotetrapyrazolenickel(II), and Hexapyrazolenickel(II) Nitrate

by Curt W. Reimann

National Bureau of Standards, Washington, D. C. 20234 *(Received June 30, 1969)*

The single crystal spectra of hexapyrazolenickel(II) nitrate, dichlorotetrapyrazolenickel(II), and dibromotetrapyrazolenickel(II) from 6000 to 30,000 cm^{-1} have been measured. The spectra of the halide complexes have been assigned on the basis of tetragonal molecular symmetry using the spectrum of hexapyrazolenickel(II) nitrate as a comparison. The tetragonal splittings in the first octahedral bands are considerably larger than observed in related complexes. These large splittings are related to low values of the effective Dq of the halide ions. Detailed crystallographic data are presented which show that the low effective field of the halide ions arises through an internal hydrogen bond interaction with the coordinated pyrazole molecules.

Introduction

The spectrochemical series has been widely used to interpret the spectra of octahedral complexes of transition metal ions. The spectra of ions in lower symmetry environments, however, have been less extensively studied and relatively few data are available to serve as a guide in the interpretation of the spectrum of a given ion in a variety of environments. One method for investigating the influence of changing environments utilizes crystallographic and spectroscopic data obtained from octahedral species and their substitution products. The primary advantage of this method is that the energy levels of the substitution products can be traced to those of the parent octahedral species. Moreover, the most conspicuous spectroscopic changes which occur upon substitution can be interpreted in terms of descent in symmetry.

In an effort to obtain a series of complexes suitable for detailed study, two pyrazole (I) complexes of nickel(II) were prepared—hexapyrazolenickel(II) ni-

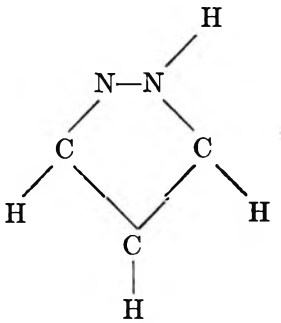

I

trate [Ni(pyrazole)$_6$(NO$_3$)$_2$] and dichlorotetrapyrazolenickel(II) [Ni(pyrazole)$_4$Cl$_2$]. Preliminary spectroscopic measurements show that the band system in Ni(pyrazole)$_6$(NO$_3$)$_2$ contains three broad bands while that of Ni(pyrazole)$_4$Cl$_2$ has five broad bands which are distributed over a wider energy region. A comparison of these spectra indicates that large low symmetry splittings exist in the spectrum of Ni(pyrazole)$_4$Cl$_2$. The structures of the above complexes were then determined to provide a structural basis for an analysis of their spectra. This analysis shows that the spectrum of the chloride complex can be interpreted on the basis of tetragonal symmetry but that the magnitude of the tetragonal splittings can be accounted for only if the spectrochemical *Dq* for the Cl$^-$ ion is greatly reduced from its typical value. As the *Dq* values for Cl$^-$ and Br$^-$ in the related pyridine complexes [Ni(pyridine)$_4$Cl$_2$ and Ni(pyridine)$_4$Br$_2$] were found to be normal,[1] the complex Ni(pyrazole)$_4$Br$_2$ was prepared for comparison. The structure of Ni(pyrazole)$_4$Br$_2$ has recently been completed. In this paper the single crystal spectra of Ni(pyrazole)$_4$Cl$_2$ and Ni(pyrazole)$_4$Br$_2$ are reported and assignments are made on the basis of tetragonal symmetry with the aid of the Ni(pyrazole)$_6$(NO$_3$)$_2$ comparison spectrum. An analysis of these spectra is presented which shows that the magnitude of the tetragonality is considerably larger than could have been anticipated from spectrochemical series data. Finally, the unexpectedly large tetragonality is interpreted in terms of specific structural features of the pyrazole complexes.

Crystal Data

Crystals of Ni(pyrazole)$_6$(NO$_3$)$_2$[2] are hexagonal (space group P$\bar{3}$) with one molecule per unit cell of dimensions a = 9.958 and c = 7.278 Å. The structure of the Ni(pyrazole)$_6^{2+}$ cation viewed along the threefold axis is shown in Figure 1. The coordinating nitrogen atoms in this cation describe a polyhedron which is very nearly a regular octahedron. Figure 1 shows that the deviation from a regular octahedral configuration is small and that the observed polyhedron may be described as a trigonally compressed octahedron.

Crystals of Ni(pyrazole)$_4$Cl$_2$[3] and Ni(pyrazole)$_4$Br$_2$[4] are monoclinic (space group C2/c with four molecules

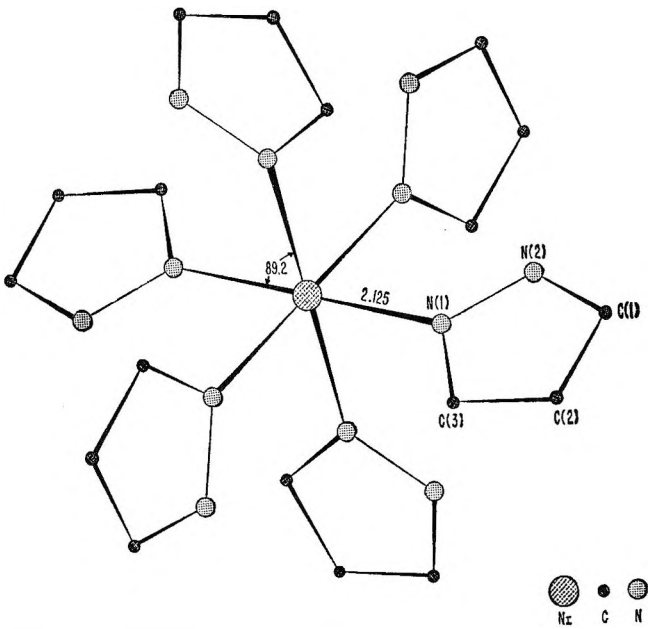

Figure 1. Structure of the Ni(pyrazole)$_6^{2+}$ cation.

per unit cell of dimensions a = 13.876, b = 9.263, c = 14.451 Å, β = 116.83° for the chloride complex and a = 14.127, b = 9.334, c = 14.702 Å, β = 118.62° for the bromide complex. The molecular structure of Ni(pyrazole)$_4$Cl$_2$ is shown in Figure 2 and that of Ni(pyrazole)$_4$Br$_2$ is shown in Figure 3. In both of these structures the planar pyrazole molecules are virtually normal to the plane defined by the coordinating nitrogen atoms. The only rigorous symmetry element in these molecules is a center of symmetry ($\bar{1}$ site symmetry at the nickel ion). If the geometry of only the coordination polyhedra is considered, however, the symmetry is approximately tetragonal (D_{4h}). The details of the coordination polyhedron in the chloride complex are shown in Figure 4 and the projection of these polyhedra down the crystallographic b axis is shown in Figure 5.

Experimental Section

Crystals of Ni(pyrazole)$_6$(NO$_3$)$_2$, Ni(pyrazole)$_4$Cl$_2$, and Ni(pyrazole)$_4$Br$_2$ were grown from stoichiometric aqueous solutions of pyrazole and nickel(II) nitrate, nickel(II) chloride, and nickel(II) bromide, respectively. For spectroscopic measurements crystals ~3 × 3 × 1 mm were polished to a thickness of about 0.5 mm. Crystal thicknesses for measurements reported here were determined with a micrometer. Spectroscopic measurements were carried out on a recording spectrophotometer (Cary 14). Glan-Thompson polarizers

(1) D. A. Rowley and R. S. Drago, *Inorg. Chem.*, **6**, 1092 (1967).

(2) C. W. Reimann, A. Santoro, and A. D. Mighell, *Acta Cryst.*, in press.

(3) C. W. Reimann, A. D. Mighell, and F. A. Mauer, *ibid.*, **23**, 135 (1967).

(4) A. D. Mighell, C. W. Reimann, and A. Santoro, *ibid.*, **B25**, 595 (1969).

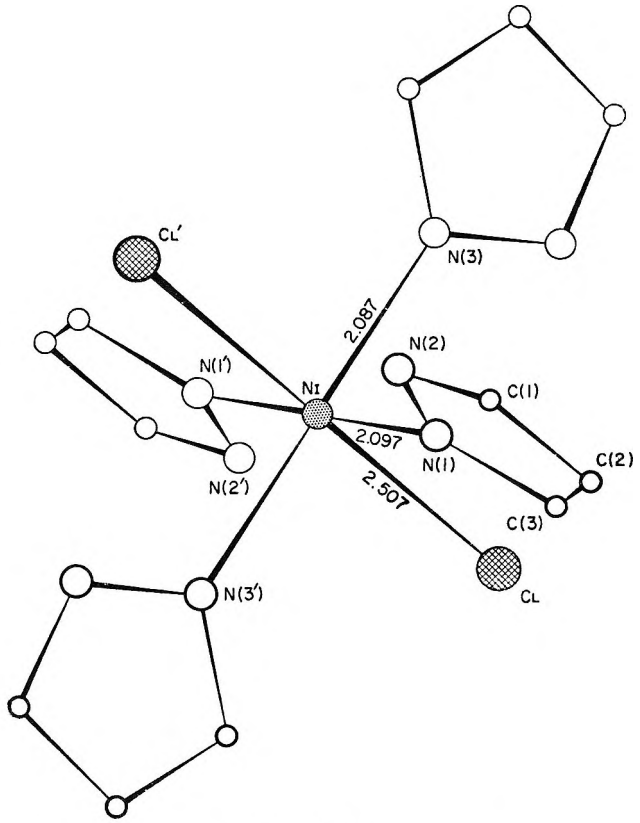

Figure 2. Molecular structure of Ni(pyrazole)$_4$Cl$_2$.

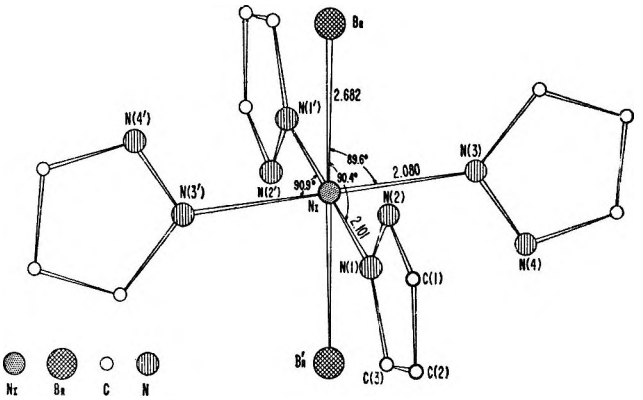

Figure 3. Molecular structure of Ni(pyrazole)$_4$Br$_2$.

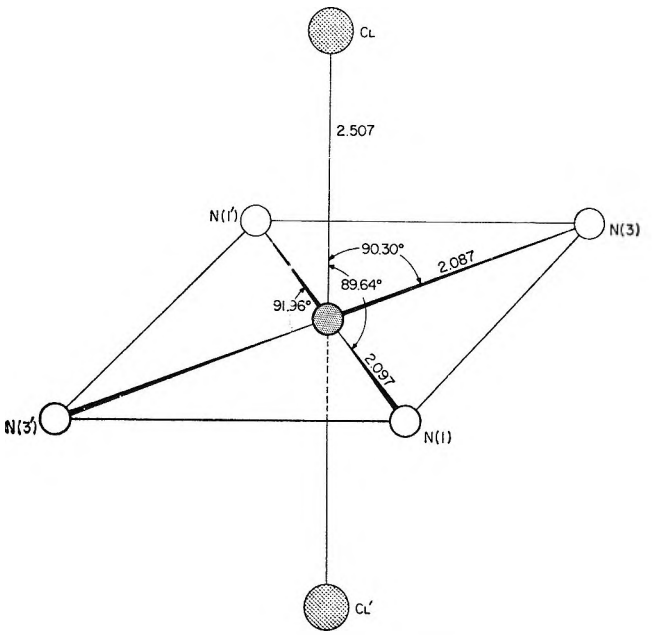

Figure 4. Detailed geometry of the coordination sphere in Ni(pyrazole)$_4$Cl$_2$.

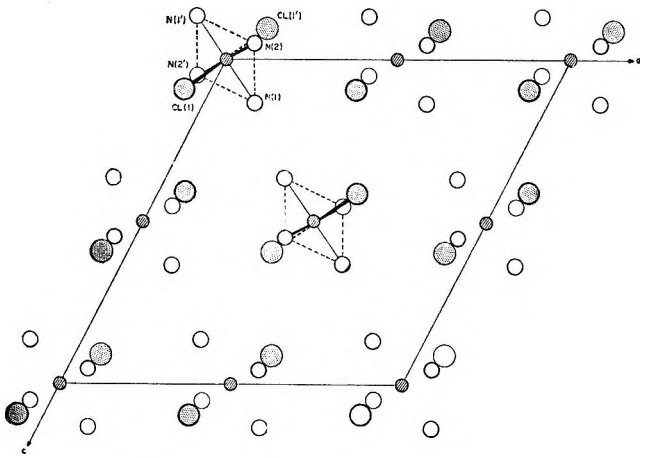

Figure 5. Projection of the coordination polyhedra in Ni-(pyrazole)$_4$Cl$_2$ down the crystallographic *b* axis.

were used to obtain polarized light. Liquid nitrogen temperature spectra were recorded with the crystal in contact with a brass cold finger inside a simple silica dewar. Extinction coefficients were calculated from the observed optical densities and measured crystal thicknesses.

The single crystal spectrum of Ni(pyrazole)$_6$(NO$_3$)$_2$ at room temperature and at liquid nitrogen temperature is shown in Figure 6. The principal changes which accompany the reduction in temperature are the blue shift in the three main bands, the appearance of a weak narrow band near 22,500 cm^{-1}, and the appearance of structure in the weak band near 13,400 cm^{-1}.

The single crystal spectra of Ni(pyrazole)$_4$Cl$_2$ at liquid nitrogen temperature with light incident upon the (010) face are shown in Figure 7. Spectra were measured with light polarized with the electric vector approximately parallel and perpendicular to the [101] direction. The absorption near 13,300 cm^{-1} consists of a broad band with narrower bands superimposed upon it. This feature is particularly evident along the [101] direction. For purposes of comparison, the room temperature unpolarized spectrum was also recorded.

The single crystal spectrum of Ni(pyrazole)$_4$Br$_2$ is shown in Figure 8. A summary of the bands observed in the room temperature spectra of Ni(pyrazole)$_6$-(NO$_3$)$_2$, Ni(pyrazole)$_4$Cl$_2$, and Ni(pyrazole)$_4$Br$_2$ is given in Table I.

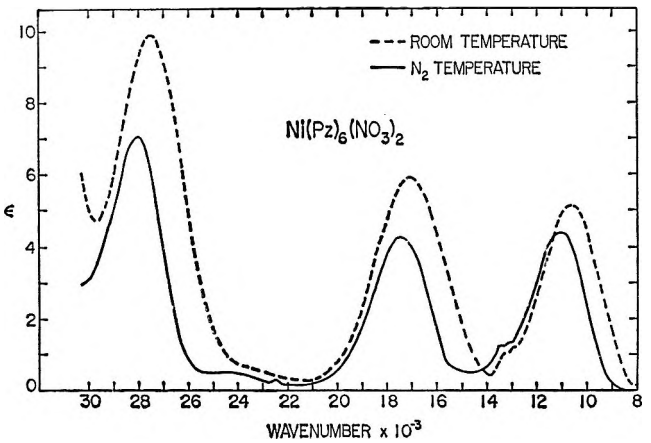

Figure 6. The electronic spectrum of Ni(pyrazole$_6$(NO$_3$)$_2$ from 8000 to 30,000 cm^{-1}.

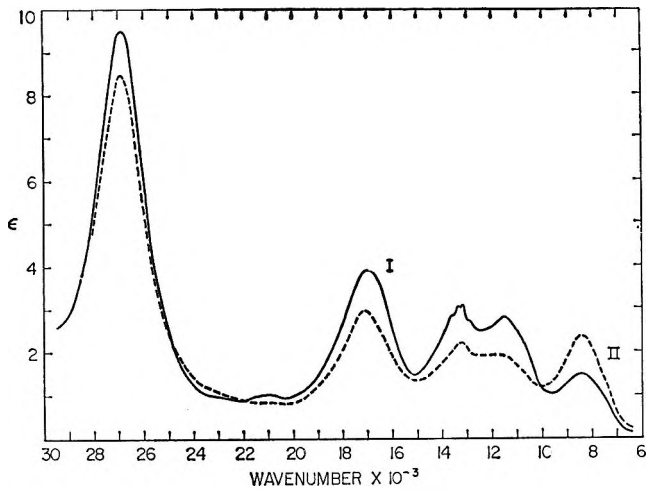

Figure 7. Polarized electronic spectra of Ni(pyrazole)$_4$Cl$_2$ at liquid nitrogen temperature. Spectrum I was measured in the (010) face with light polarized along one extinction direction (approximately [101]). Spectrum II was measured 90° to the [101] direction.

Table I: Absorption Bands (in cm^{-1}) Observed in Three Pyrazole Complexes at Room Temperature

Ni(pyrazole)$_6$(NO$_3$)$_2$	Ni(pyrazole)$_4$Cl$_2$	Ni(pyrazole)$_4$Br$_2$
10,650	8,000	7,240
13,500	10,950	10,900
17,100	13,100	12,000
27,500	13,500	15,900
	16,400	25,800
	26,500	

Assignments of Spectra

1. Ni(pyrazole)$_6$(NO$_3$)$_2$. The structural data given above show that the coordination sphere in the Ni(pyrazole)$_6^{2+}$ cation is a very slightly distorted octahedron. The three most prominent bands in the spectrum of Ni(pyrazole)$_6$(NO$_3$)$_2$ at room temperature show no evidence for band splitting, nor does any evidence

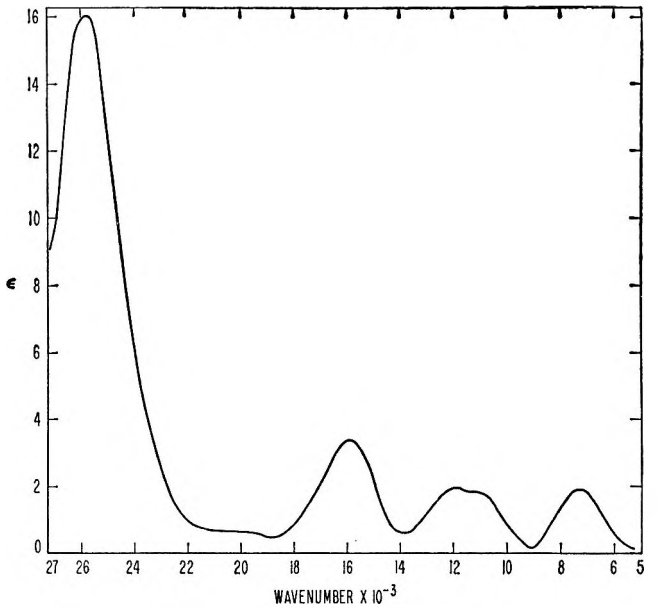

Figure 8. Single crystal spectrum of Ni(pyrazole)$_4$Br$_2$ at room temperature.

for such splittings appear in the liquid nitrogen temperature spectrum. Consequently, the approximation of octahedral symmetry should provide a valid basis to make the assignments of the bands in the spectrum of Ni(pyrazole)$_6$(NO$_3$)$_2$.

The nickel(II) ion has eight 3d electrons which permit the free ion terms ^{3}F, ^{3}P, ^{1}D, ^{1}G, and ^{1}S. In crystalline fields of octahedral symmetry the sevenfold degeneracy of the ^{3}F free ion ground term is partially removed, and the ^{3}A$_2$g(F), ^{3}T$_2$g(F), and ^{3}T$_1$g(F) crystal field states arise. The ^{3}P free ion term remains unsplit in an octahedral field (^{3}T$_1$g(P)). The remaining free ion terms, ^{1}D, ^{1}G, and ^{1}S, become the crystal field states ^{1}Eg(D), ^{1}T$_2$g(D), ^{1}A$_1$g(G) + ^{1}T$_1$g(G) + ^{1}E$_1$g(G) + ^{1}T$_2$g(G), and ^{1}A$_1$g(S), respectively.

The three broad bands observed in the room temperature spectrum of Ni(pyrazole)$_6$(NO$_3$)$_2$ at 10,650, 17,100, and 27,500 cm^{-1} are readily identified with the three spin-allowed transitions. The 10,650-cm^{-1} band corresponds to the ^{3}A$_2$g(F) → ^{3}T$_2$g(F) transition while the 17,100- and 27,500-cm^{-1} bands are assigned to the ^{3}A$_2$g(F) → ^{3}T$_1$g(F) and ^{3}A$_2$g(F) → ^{3}T$_1$g(P) transitions, respectively. The separation between the ^{3}A$_2$g(F) and ^{3}T$_2$g(F) states is equal to 10 Dq, where Dq is the spectrochemical series parameter which is a measure of the ligand field strength. Thus, Dq for Ni(pyrazole)$_6$(NO$_3$)$_2$ is 1065 cm^{-1}. The interelectronic repulsion parameter, B, can be computed[5] from the energies of the ^{3}A$_2$g(F) → ^{3}T$_1$g(F) and ^{3}A$_2$g(F) → ^{3}T$_1$g(P) transitions using this value of Dq. The computed value of B for this case, 735 cm^{-1}, represents ~25% reduction from the free ion value.

(5) O. Bostrup and C. K. Jorgensen, *Acta Chem. Scand.*, 11, 1223 (1957).

The assignments of the spin-forbidden bands, which are particularly evident in the liquid nitrogen temperature spectrum, can be made with the aid of the Liehr–Ballhausen[6] energy level diagram for the $3d^8$ system. The low-intensity shoulder near 13,400 cm^{-1} is assigned to the $^3A_2g(F) \rightarrow {}^1Eg(D)$ transition. A relatively sharp, weak band at 22,500 cm^{-1} is assigned to the $^3A_2g(F) \rightarrow {}^1A_1g(G)$ transition, and a much broader weak band observed at ~24,000 cm^{-1} is assigned to the $^3A_2g(F) \rightarrow {}^1T_2g(D)$ transition. The last two assignments are supported by the breadth of the bands as well as by their energies. The breadths differ as a consequence of the fact that the upper states have different dependencies upon Dq. Thus the $^1A_1g(G)$ level, which is less sensitive to changes in Dq, is considerably less vibrationally broadened. The remaining possible band in the spectral region studied, $^3A_2g(F) \rightarrow {}^1T_1g(G)$, is expected to be just below the more intense and broader $^3A_2g(F) \rightarrow {}^3T_1g(P)$ band. It was not observed. A summary of these assignments is presented in Table II.

Table II: Assignments of Observed Bands in $Ni(pyrazole)_6(NO_3)_2$

Band, cm^{-1} ~300°K	Band, cm^{-1} ~77°K	Assignment
10,650	11,100	$^3A_{2g}(F) \rightarrow {}^3T_{2g}(F)$
13,500	13,500	$\rightarrow {}^1E_g(D)$
17,100	17,500	$\rightarrow {}^3T_{1g}(F)$
	22,500	$\rightarrow {}^1A_{1g}(G)$
	24,000	$\rightarrow {}^1T_{2g}(D)$
27,500	28,100	$\rightarrow {}^3T_{1g}(P)$

2. $Ni(pyrazole)_4Cl_2$ and $Ni(pyrazole)_4Br_2$. The structural data given above show that the halide complexes may be regarded as *trans* substitution products of the $Ni(pyrazole)_6^{2+}$ cation. This interchange reduces the coordination symmetry about the nickel ion from octahedral (~O_h) to tetragonal (~D_{4h}) and each of the ^3T octahedral states splits into two tetragonal states as shown in Figure 9. The degree of splitting and relative order of the two tetragonal states which arise from each ^3T octahedral state depend on the nature of the tetragonal perturbation. This perturbation may be represented by two tetragonal splitting parameters Ds and Dt[7] which describe the splittings in all three octahedral ^3T states. The derived[8] splittings for the three octahedral bands are $-{}^{35}/_4Dt$, $6Ds - {}^5/_4Dt$, and $-3Ds + 5Dt$. The splittings in the second and third bands become $4.9Ds - 0.5Dt$ and $-1.9Ds + 4.35Dt$ when configuration interaction between the two ^3T_1g octahedral states is taken into account. Thus, the interpretation of the spectrum of a tetragonal nickel(II) complex requires a band assignment and the description of the observed splittings in the three ^3T octahedral levels in terms of Ds and Dt. In principle, the assignment could be carried out by determining the symmetry type of each level using the selection rules and the observed polarization properties of each transition. However, the halide complexes under investigation are rigorously centrosymmetric and the d–d transitions are Laporte forbidden. In such cases the vibronic[9] intensity mechanism must be invoked, and the symmetry of each coupling vibrational mode must be included. This analysis for the halide complexes (Table III) shows that only the $^3B_{1g} \rightarrow {}^3A_{2g}$ and $^3B_{1g} \rightarrow {}^3B_{2g}$ transitions have restrictive selection rules. These restrictions, though useful, do not provide a basis for an unambiguous assignment of the entire set of observed bands. In practice assignments will be made using the spectrum of $Ni(pyrazole)_6(NO_3)_2$ as a comparison and reinforced by the available polarization data.

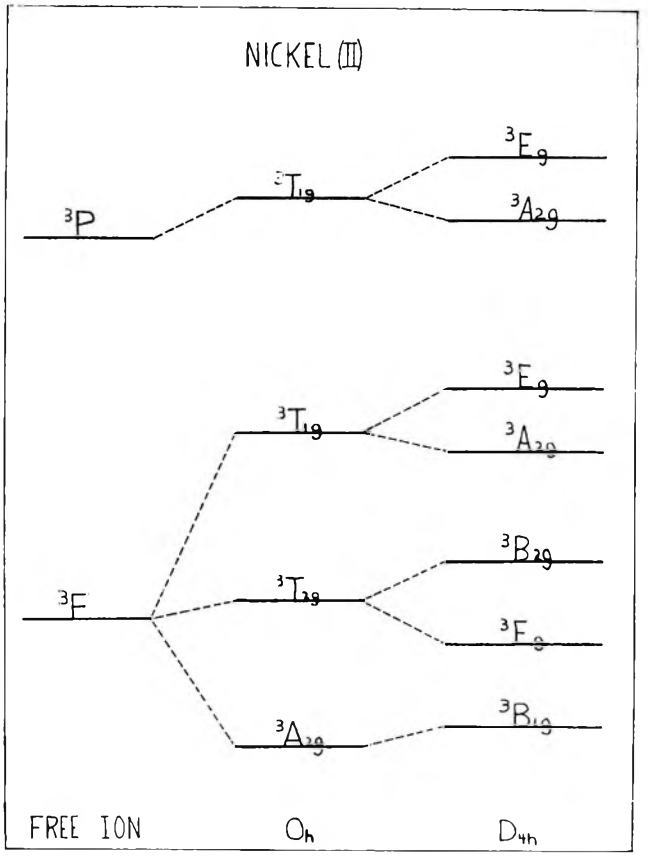

Figure 9. Schematic correlation diagram of the nickel(II) energy levels from the terms of the free ion into fields of octahedral and tetragonal symmetry.

To utilize the spectrum of $Ni(pyrazole)_6(NO_3)_2$ as a basis for specific assignments of the spectra of the derivative halide complexes, it is helpful to characterize the behavior of the octahedral ground state and first

(6) A. D. Liehr and C. J. Ballhausen, *Ann. Phys.* (N. Y.), **6**, 134 (1959).

(7) C. J. Ballhausen, "Introduction to Ligand Field Theory," McGraw-Hill Book Co., Inc., New York, N. Y., 1962.

(8) C. R. Hare and C. J. Ballhausen, *J. Chem. Phys.*, **40**, 792 (1964).

(9) A. D. Liehr, *Ann. Phys.* (N. Y.), **1**, 221 (1957).

Table III: Vibronic Selection Rules for Ni(pyrazole)$_4$Cl$_2$ and for Ni(pyrazole)$_4$Br$_2$

Transition	Polarization direction	Coupling vibration
$^3B_{1g}$—^3E_g	∥	ϵ_u
	⊥	α_{2u}, β_{2u}
$^3B_{1g}$—$^3A_{2g}$	⊥	ϵ_u
$^3B_{1g}$—$^3B_{2g}$	⊥	ϵ_u

excited state under the action of a tetragonal perturbation. The tetragonal ground state (^3B_1g) is raised $7Dt$ relative to the octahedral ground state (^3A_2g) by a tetragonal potential. The splitting in the first octahedral state gives a ^3B_2g state which is raised $7Dt$ relative to ^3T_2g and ^3Eg which is $^7/_4Dt$ below ^3T_2g. As both ^3B_1g and ^3B_2g have been raised $7Dt$ relative to their parent octahedral states, the $^3B_1g \rightarrow {}^3B_2g$ transition should occur at approximately the same energy as the $^3A_2g(F) \rightarrow {}^3T_2g(F)$ octahedral field transition. Moreover, because the splitting in $^3T_2g(F)$ depends only on Dt, the identification of the split components of $^3T_2g(F)$ allows a determination of Dt. This value of Dt can, in turn, be used to interpret the remainder of the spectrum.

According to the above analysis, both the ^3B_1g and ^3B_2g levels are raised $7Dt$ relative to their parent octahedral states. Therefore, the $^3B_1g \rightarrow {}^3B_1g$ transition should occur with approximately the same energy as the first octahedral band in Ni(pyrazole)$_6$(NO$_3$)$_2$ (10,650 cm^{-1}). On this basis the bands at 10,950 cm^{-1} in Ni(pyrazole)$_4$Cl$_2$ and 10,900 cm^{-1} in Ni(pyrazole)$_4$Br$_2$ represent the most reasonable choices for the $^3B_1g \rightarrow {}^3B_2g$ transition. This suggests that the band at 8000 cm^{-1} in Ni(pyrazole)$_4$Cl$_2$ and 7240 cm^{-1} in Ni(pyrazole)$_4$Br$_2$ are the second components of the ^3T_2g octahedral band and correspond to $^3B_1g \rightarrow {}^3Eg$ transitions. Table III shows that the vibronic selection rules are consistent with the assignments of the two lowest energy bands in the polarized spectrum of Ni(pyrazole)$_4$Cl$_2$. More importantly, the observed polarizations rule out the choice of the lowest energy band as the $^3B_1g \rightarrow {}^3B_2g$ transition. This conclusion follows from the fact that the first tetragonal band has greater intensity parallel to the fourfold molecular axis than perpendicular to it. This should not be observed for a band with no allowed parallel component ($^3B_1g \rightarrow {}^3B_2g$). From these assignments Dt is found to be 337 cm^{-1} in the chloride complex and 418 cm^{-1} in the bromide complex.

To assign the remaining bands in the halide complexes and to determine Ds, it is once again helpful to compare the spectra of the halide complexes with that of Ni(pyrazole)$_6$(NO$_3$)$_2$. The most conspicuous difference in the region above 12,000 cm^{-1} is the large intensity increase near 13,400 cm^{-1}. The band at 13,500 cm^{-1} in the spectrum of Ni(pyrazole)$_6$(NO$_3$)$_2$ has been assigned to the spin-forbidden $^3A_2g(F) \rightarrow {}^1Eg(D)$ transition. The intensity near 13,500 cm^{-1} in the halide complexes appears to be too large to attribute to differences in percentage triplet character. If this view is correct, the intensity at 13,400 cm^{-1} must be attributed primarily to a spin-allowed transition as well as to the spin-forbidden transition. This view is supported by the appearance of narrower bands superimposed upon the broad band in the spectrum of Ni(pyrazole)$_4$Cl$_2$. These narrower bands resemble those observed in the spectrum of Ni(pyrazole)$_6$(NO$_3$)$_2$ which have been assigned to the $^3A_2g(F) \rightarrow {}^1Eg(D)$ transition. According to Figure 9 two possible assignments can be made for the band which occurs at 13,100 cm^{-1} in the spectrum of Ni(pyrazole)$_4$Cl$_2$ and at 12,000 cm^{-1} in the spectrum of Ni(pyrazole)$_4$Br$_2$. If these bands are assigned to the $^3B_1g \rightarrow {}^3Eg$ transition, the computed values of Ds (assuming configuration interaction) would be (708), for Cl and (839) for Br. If these bands are assigned to the $^3B_1g \rightarrow {}^3A_2g$ transition, Ds would be -640 cm^{-1} in the chloride complex and -753 cm^{-1} in the bromide complex. The expression for the tetragonal splitting in the $^3A_2g(F) \rightarrow {}^3T_1g(P)$ band shows that a large negative value of Ds would manifest itself in a large splitting because negative Ds and positive Dt act together to split this band. No noticeable splitting occurs in the $^3A_2g(F) \rightarrow {}^3T_1g(P)$ transitions which indicates that the negative values of Ds do not lead to a consistent interpretation. Taking the positive values of Ds, the predicted splitting in the $^3A_2g(F) \rightarrow {}^3T_1g(P)$ bands are only 121 and 224 cm^{-1} for the chloride and bromide complex, respectively. A summary of the assignments for the halide complexes is given in Table IV.

Table IV: Assignment of Spin-Allowed Transitions (cm^{-1}) in Ni(pyrazole)$_4$Cl$_2$ and Ni(pyrazole)$_4$Br$_2$ at Room Temperature

Transition	Ni(pyrazole)$_4$Cl$_2$	Ni(pyrazole)$_4$Br$_2$
$^3B_{1g} \rightarrow {}^3E_g$	8,000	7,240
$\rightarrow {}^3B_{2g}$	10,950	10,900
$\rightarrow {}^3A_{2g}$	13,100	12,000
$\rightarrow {}^3E_g$	16,400	15,900
$\rightarrow {}^3E_g$, $^3A_{2g}$	26,500	25,800

Discussion

The foregoing analysis shows that the tetragonal splitting in the first octahedral band ($^3A_2g(F) \rightarrow {}^3T_2g(F)$) is larger in Ni(pyrazole)$_4$Br$_2$ than in Ni(pyrazole)$_4$Cl$_2$. The lower component of the split $^3T_2g(F)$ level is found to be particularly sensitive to the difference between Cl and Br. The upper component, however, is almost identical in both complexes and lies ~250 cm^{-1} above the $^3A_2g(F) \rightarrow {}^3T_2g(F)$ transition in the octahedral com-

plex $Ni(pyrazole)_6(NO_3)_2$. As detailed structural data are available for all three complexes, the behavior of these related energy levels may be considered in terms of structural differences. Also, the qualitative and quantitative features of the tetragonal splittings may be compared with expectations based on spectrochemical series data.

The tetragonality parameters are defined so that a positive sign corresponds to axial elongation or to a weaker ligand on the fourfold axis (z) than in the plane (x,y). Wentworth and Piper[10] have given an expression (shown here as eq 1) which relates the splitting

$$Dt = {}^4/_7[Dq(x,y) - Dq(z)] \quad (1)$$

parameter Dt to the spectrochemical series parameters for the in-plane and axial ligands. The Dq values for the ligands on the z axis [Cl (680 cm^{-1}), Br (600 cm^{-1})][11] are both less than Dq(pyrazole) (1065 cm^{-1}) and the positive signs for Dt determined from the spectra are qualitatively consistent with spectrochemical series data. Equation 1 also shows that Dt should be greater in the bromide complex than in the chloride complex. Therefore, the observation that the separation between the $^3B_{1g} \rightarrow {}^3E_g$ and $^3B_{1g} \rightarrow {}^3B_{2g}$ transitions increases with the substitution of Cl by Br is consistent with an increase in tetragonality which is proportional to the disparity between the field strengths associated with axial and in-plane ligands. The entire increase in splitting brought about by the substitution of Cl by Br occurs through the reduction in the $^3B_{1g} \rightarrow {}^3E_g$ level. In both halide complexes, however, part of the splitting in the first octahedral band occurs through a $\sim$250 cm^{-1} rise in the $^3B_{1g} \rightarrow {}^3B_{2g}$ relative to the $^3A_{2g} \rightarrow {}^3T_{2g}$ octahedral transition. In making the assignment of the $^3B_{1g} \rightarrow {}^3B_{2g}$ transitions it was mentioned above that these transitions should occur at the same energy as the first octahedral bond in $Ni(pyrazole)_6(NO_3)_2$ because the in-plane ligand is the same in all three complexes. This small ($\sim$250 cm^{-1}) upward shift of $^3B_{1g} \rightarrow {}^3B_{2g}$ relative to $^3A_{2g}(F) \rightarrow {}^3T_{2g}(F)$ is undoubtedly a consequence of the fact that, in the halogen-substituted complexes, the four pyrazole molecules lie closer to the nickel ion than in the unsubstituted complex (see Figures 1–3). The effective field of pyrazole increases by about 3% in the substituted complexes. Thus, the two tetragonal components of the split $^3T_{2g}$ octahedral state behave in accord with expectations based upon reduction in symmetry.

The absence of ambiguity in these assignments notwithstanding, the quantitative agreement between the values of Dt derived from the observed spectra and those calculated from the spectrochemical series values of Dq is very poor. In both cases, Dt derived from the spectra is considerably larger than Dt computed using eq 1. This indicates that the disparity between Dq(pyrazole) and Dq(halogen) is larger than could be anticipated from spectrochemical series data. As Dq(pyrazole) in the tetragonal complexes is determined directly from the energies of the $^3B_{1g} \rightarrow {}^3B_{2g}$ transitions, the large values of Dt must be associated with a reduction in the effective field of the halide ions. Using the observed values of Dt and of Dq(pyrazole), the effective Dq's for Cl^- and Br^- are found to be 505 and 358 cm^{-1}, respectively. The 26% reduction in $Dq(Cl^-)$ and 40% reduction in $Dq(Br^-)$ represent substantial deviations from the range of typical values for such parameters. For example, in the closely related pyridine[1] complexes, $Ni(pyridine)_4Cl_2$ and $Ni(pyridine)_4Br_2$, the effective field of each halide ion agrees closely with the spectrochemical series value. Consequently, the behavior of the halide ions in the pyrazole complexes must be interpreted in terms of specific properties of these complexes.

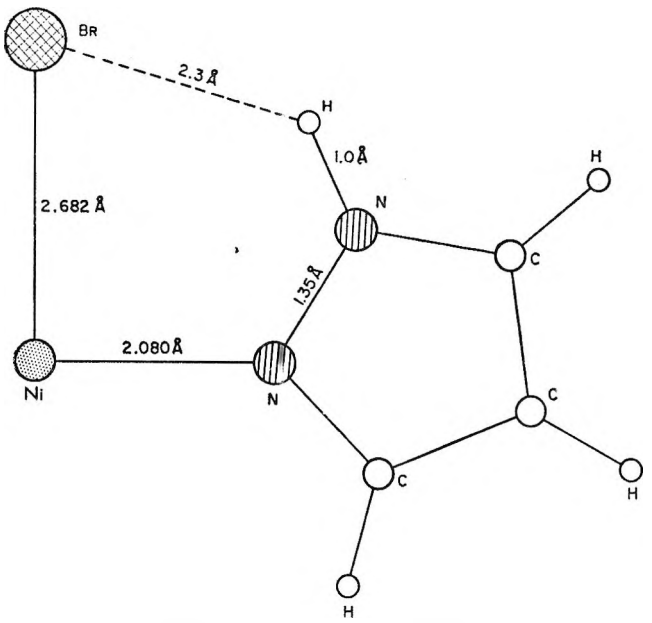

Figure 10. Detailed configuration of one pyrazole molecule in relation to adjacent Ni–Br group.

The specific property of the pyrazole complexes which is related directly to the large tetragonal splitting can be identified by comparing the structures of pyrazole complexes and those involving related ligands. Pyrazole and other ligands which contain $\geq$N and >N–H groups may utilize them in coordination ($\geq$N) and in hydrogen bonding (>N–H). In pyrazole (I) these bonding groups are adjacent and the angle between the coordinate bond and the N–H direction is only $\sim$72°. In the structure of the tetragonal pyrazole complexes (Figures 2 and 3) each pyrazole ring is nearly coplanar with the Cl–Ni–Cl and Br–Ni–Br groups.

(10) R. A. D. Wentworth and T. S. Piper, *Inorg. Chem.*, 4, 709 (1965).

(11) B. N. Figgis, "Introduction to Ligand Field," Interscience Publishers, New York, N. Y., 1966.

This orientation permits the 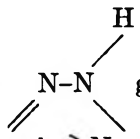 group to coordinate to the nickel ion through $\geqslant$N with the N–H groups pointing toward the coordinated halide ions. The steric relationship between one pyrazole ring and an Ni–Br group is shown in Figure 10. The same relative relationship exists in the chloride complex with an Ni–Cl bond distance of 2.507 Å. In the corresponding dibromotetrapyridinenickel(II)[12] and dichlorotetrapyridinenickel(II)[13] complexes the pyridine rings are inclined ~45° away from the Br–Ni–Br and Cl–Ni–Cl directions, the Ni–Br distance is 2.58 Å, and the Ni–Cl distance is 2.38 Å. These data suggest that the pyridine rings assume positions which compromise the mutual repulsion between the pyridine rings (which is a minimum when the rings are aligned with the Ni–X direction) and the repulsion between the halide ions and the pyridine rings. In the pyrazole complexes, however, the interaction between pyrazole and the halogen ions is a net attraction which stabilizes the configuration shown in Figure 10. The hydrogen bond interactions (two interactions per halide ion) reduce the effective field of the halide ions, and this reduction manifests itself directly in the longer Ni–X bond lengths and indirectly in the unusually large tetragonal distortion in the ligand field of the Ni(II) ion.

(12) A. S. Antsishkina and M. A. Porai-Koshits, *Kristallografiya*, 3, 684 (1958).
(13) M. A. Porai-Koshits, *Dokl. Akad. Nauk SSSR*, 10, 117 (1954).

The Photochemistry of N_3^- in Aqueous Solution at 2288 and 2139 Å

by I. Burak, D. Shapira, and A. Treinin

Department of Physical Chemistry, Hebrew University, Jerusalem, Israel *(Received June 2, 1969)*

The photolysis of N_3^- at 2288 Å hardly differs from that at 2537 Å; both probably involve the n,π^* state of N_3^-. On the other hand, new features are shown by the photolysis at 2139 Å, which is within the charge-transfer-to-solvent (CTTS) absorption band. About 10% of the excited ions undergo ionization and ~30% produce NH_2OH, probably by first being internally converted to the n,π^* state. Ammonia is produced from the reduction of hydroxylamine by solvated electrons. This is indicated by the effect of electron scavengers The azide radical appears to abstract H atom from alcohols and, more readily, from acetone and NH_2OH. A full mechanism is proposed for the photolysis.

The thermal and photochemical decomposition of heavy metal azides is usually considered to involve the formation of the azide radical as the primary chemical process.[1] For azides with relatively high exciton levels (*e.g.*, KN_3 and $Ba(N_3)_2$) some internally excited states of N_3^- appear to play an important role.[1] This is also the case for N_3^- in solution, which has an n,π^* ($^1\Delta_u$–$^1B_2$) state below a charge-transfer-to-solvent (CTTS) state (the latter may be considered as an exciton of low mobility);[2] indeed, the photolysis of N_3^- in aqueous solution is highly governed by the n,π^* state. There is no indication of photoionization of N_3^- at 2537 Å, a wavelength lying well within the n$\rightarrow\pi^*$ absorption band.[3] On the other hand, recent flash photolysis studies have indicated that excitation within the CTTS band (below 230 mμ) yields solvated electrons[4] and azide radicals;[5] still other processes may compete with ionization. The present work provides information on the efficiency of the photoionization process and its subsequent chemical effects. It leads to conclusions concerning the chemical properties of some important nitrogen containing radicals in aqueous solution, in particular N_3 and NH_2.

Experimental Section

Light sources. Irradiation at 2139 Å was conducted with a 25-W Philips zinc spectral lamp No. 93106. To reach stable intensity, the lamp was warmed 20 min before irradiation. The stability of the lamp was checked by measuring the azide depletion in a 10^{-3} *M* NaN_3 solution containing air, and this was carried out just before and after irradiation of the given sample. To minimize the effect of photolysis by light at wave-

(1) P. Gray, *Quart. Rev.*, (London), 17, 441 (1963).
(2) I. Burak and A. Treinin, *J. Chem. Phys.*, 39, 189 (1963).
(3) I. Burak and A. Treinin, *J. Amer. Chem. Soc.*, 87, 4031 (1965).
(4) D. Behar, D. Shapira, and A. Treinin, to be published.
(5) A. Treinin and E. Hayon, *J. Chem. Phys.*, 50, 538 (1969).

lengths greater than 2139 Å the concentration of N_3^- was not raised above 10^{-3} *M;* under these conditions, absorption at 2139 Å was complete. Irradiation at 2288 Å was conducted with a 25-W Philips cadmium spectral lamp No. 93107. Under the conditions employed the only line absorbed, of significant intensity, was at 2288 Å.

The light output was determined by differential actinometry with uranyl oxalate.[6] The quantum yields of the oxalate loss were taken to be $\phi_{2139} = 0.49$ and $\phi_{2288} = 0.55$ (interpolated from data given in ref 7). The intensities of light absorbed were about 5×10^{-7} and 5×10^{-6} einstein $l.^{-1}$ sec^{-1}, respectively.

Materials. NaN_3 (CP) was twice recrystallized from water–ethanol solutions (further recrystallization proved to have no effect on the yields of the photolysis). Ethanol and acetone (Spectrograde) and other materials of Analar grade were used without further purification. NH_2OH was introduced as $(NH_2OH)_2$-H_2SO_4, neutralized by equivalent amounts of NaOH. The water was redistilled from alkaline permanganate and then from dilute phosphoric acid in an all-glass still. N_2O (analytical grade, Standard Air Co., New Jersey) was triply distilled in the vacuum system to remove O_2. Oxygen (analytical grade, Matheson) was not further purified. The solution was equilibrated with the gas by stirring for 3–4 hr.

Solutions and Procedure. The reaction vessels and procedure were as described elsewhere.[3] A borate buffer was used to fix the pH within ±0.05. Unless otherwise stated the temperature was kept as 23 ± 1° and the pH at 7.7.

Analytical Methods. The solutions were analyzed immediately after the photolysis, in order to minimize decomposition reactions. In alkaline solutions, NH_2-OH undergoes thermal decomposition to yield NH_3. This reaction should be carefully considered, especially when no buffer is present to prevent the rise of pH during photolysis. It appears that such precautions were not taken in a recent work[8] where it was claimed that the photolysis of N_3^- at 2537 Å yields NH_3 but not NH_2OH. Endres' method,[9] the phenol hypochlorite method,[10] and the ferric nitrate method[11] were used, with some modifications, to determine NH_2OH, NH_3, and N_3^-, respectively. Great precautions were taken in standardization and calibration of these methods. Fresh reagents were always used and the results were immediately checked against blanks with the same compositions, including all other components. Samples of 1 or 2 ml of the irradiated solutions were analyzed as follows.

NH_2OH. To expel the azide (which seriously interferes with the method), 3 ml of 1 *N* H_2SO_4 was added and the solution was evaporated under low pressure until its volume was reduced to less than 1 ml; 3 ml of 6.5×10^{-2} *M* sulfanilic acid (dissolved in 20% acetic acid), 4.5 ml of 1 *N* NaOH, and 0.3 ml of glacial acetic acid saturated with I_2 were then added and the mixture was kept for 10 min. A few drops of saturated $Na_2S_2O_3$ solution were added to remove I_2 and 4 ml of 1 *N* H_2SO_4 to keep the pH below 2; 2 ml of 4×10^{-3} *M* N-1-naphthylethylenediamine dihydrochloride was immediately added and the mixture was kept for 5 min. After proper dilution, the absorbance was measured at 540 mμ ($\epsilon \sim 47500$ M^{-1} cm^{-1}). Acetone does not interfere with the method since the oxime is completely hydrolyzed and NH_2OH is released by subjecting the solution to the prescribed treatment.

NH_3. The phenol hypochlorite method[10] was employed without adding $MnCl_2$ as a catalyst. Hydroxylamine (but not N_3^- at 10^{-3} *M*) interferes with the method. A blank containing the known concentration of NH_2OH was used to correct for the additive contribution of NH_2OH to the color. With proper blanks the method could also be extended to ethanol containing solutions. Acetone interfered with the method.

The ferric nitrate method[11] could not be applied to determine N_3^- in phosphate containing solutions.

Results

There is little difference between photolysis at 2537 Å and 2288 Å (Figure 1); what difference exists is probably attributable to errors in actinometry at 2288 Å. Improved actinometry for 2537 Å has led to quantum yields 7% higher than that previously recorded.[3] In particular, for both wavelengths at 10^{-3} *M* NaN_3, the quantum yields $-\varphi_{N_3^-}$, ϕ_{NH_2OH}, and ϕ_{N_2} were found to be almost equal (within 10%). Thus, under these conditions the reaction is essentially

$$N_3^- + 2H_2O \xrightarrow{h\nu} NH_2OH + N_2 + OH^- \quad (1)$$

On the other hand, new features are revealed at 2139 Å. The results for air-free solutions of 10^{-3} *M* NaN_3 are summarized in Figure 2. NH_3 becomes a significant product and together with N_2 and NH_2OH they account for the nitrogen balance (Table I). The quantum yield of N_3^- depletion is ~0.31. Mass spectrometric analysis of the gas evolved showed no evidence for H_2 or oxides of nitrogen. At pH 7.7 the quantum yields ϕ_{NH_2OH} and ϕ_{NH_3} decrease and increase, respectively, with irradiation time, finally tending to limiting values. These limiting quantum yields could be obtained from the beginning of irradiation by conducting the photolysis of N_3^- in presence of NH_2OH at 3×10^4 *M* (Figure 3) or higher concentrations. (This was checked up to 10^{-3} *M* NH_2OH). The same effect

(6) J. Jortner, M. Ottolenghi, and G. Stein, *J. Amer. Chem. Soc.*, **85**, 2712 (1963).

(7) F. P. Brackett and G. S. Forbes, *ibid.*, **55**, 4459 (1933).

(8) V. R. Pai Verneker and M Blais, *J. Phys. Chem.*, **72**, 774 (1968).

(9) G. Endres, *Ann.*, **518**, 109 (1935).

(10) F. D. Snell and C. T. Snell, "Colorimetric Methods of Analysis," D. Van Nostrand, New York, N. Y., 1949, p 818.

(11) P. Kelly and M. Smith, *J. Chem. Soc.*, 1479, (1961).

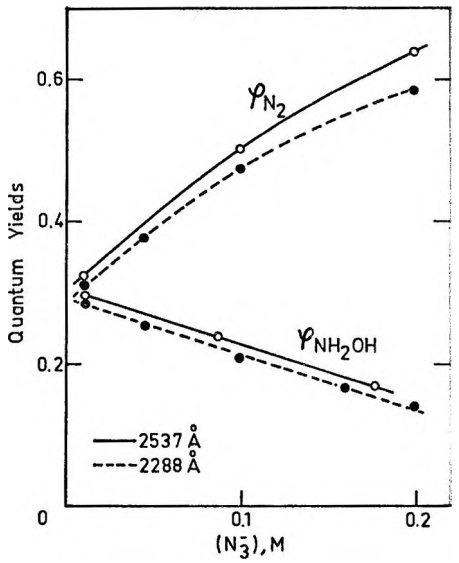

Figure 1. Quantum yields for the photolysis of air-free, aqueous solutions of N_3^- at 2288 and 2537 Å as a function of the azide concentration.

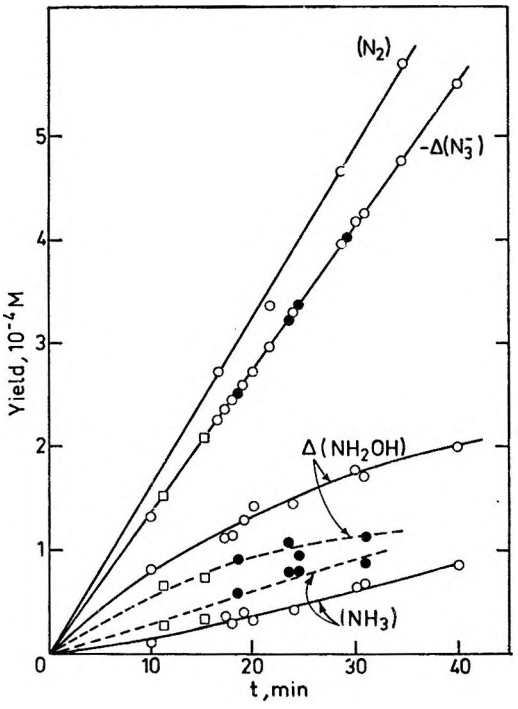

Figure 2. The 2139-Å photolysis of 10^{-3} M N_3^- in air-free aqueous solutions at pH 7.7 (open symbols) and pH 6.9 (dark symbols); squares, 55°.

on ϕ_{NH_3} is achieved by lowering the pH to 6.9; simultaneously, ϕ_{NH_2OH} decreases but being still above its limiting value, further accumulation of NH_2OH is required before the limiting value is approached (Figure 2). An increase of temperature also brings ϕ_{NH_2OH} and ϕ_{NH_3} closer to the limiting yields (Figure 2).

It appears that at 2139 Å there is some mechanism by which NH_2OH is consumed and NH_3 is produced. Apparently, this mechanism does not operate in the

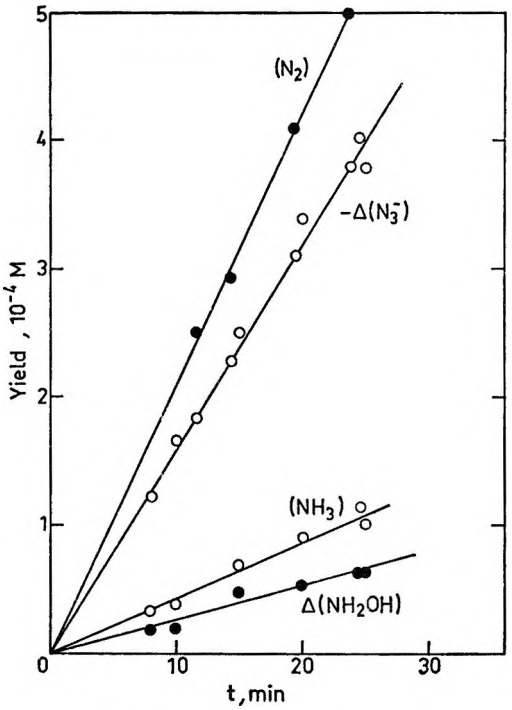

Figure 3. The 2139-Å photolysis of 10^{-3} M N_3^- in air-free aqueous solutions, with 3×10^{-4} M NH_2OH initially added.

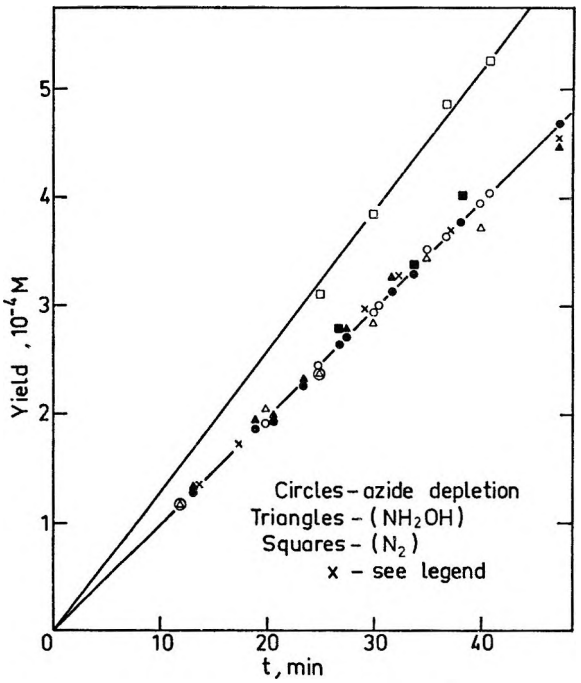

Figure 4. The 2139-Å photolysis of 10^{-3} M N_3^- in air-free aqueous solutions in presence of 10^{-3} M acetone (dark symbols) and 1.5×10^{-2} M N_2O + 1 M ethanol (open symbols); ×, the azide depletion in absence of foreign scavenger.

presence of acetone or N_2O + ethanol (Figure 4). With acetone $-\phi_{N_3^-} = \phi_{NH_2OH} = \phi_{N_2}$, *i.e.*, no ammonia is produced. Similar results were obtained with N_2O + ethanol, but now ϕ_{N_2} increased by ~30%. Other systems which inhibit the formation of ammonia include

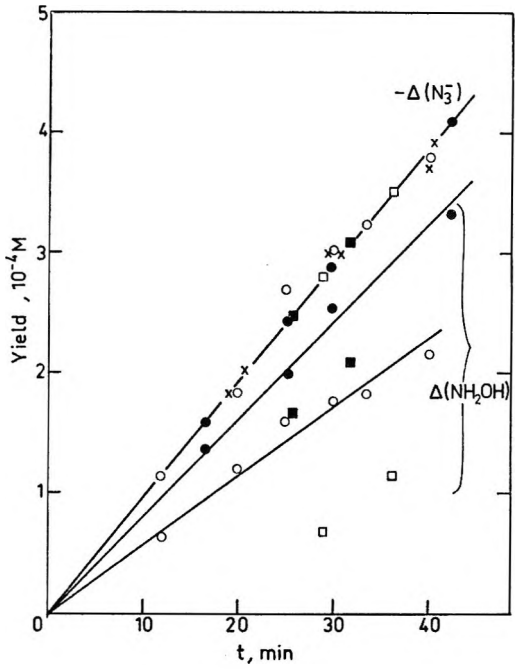

Figure 5. The 2139-Å photolysis of 10^{-3} *M* N_3^- in aqueous solutions, in presence of 1.2×10^{-3} *M* O_2 (dark symbols) and 1.5×10^{-2} *M* N_2O (open symbols); squares, with 2.9×10^{-4} *M* NH_2OH initially added; ×, azide depletion in absence of foreign scavenger.

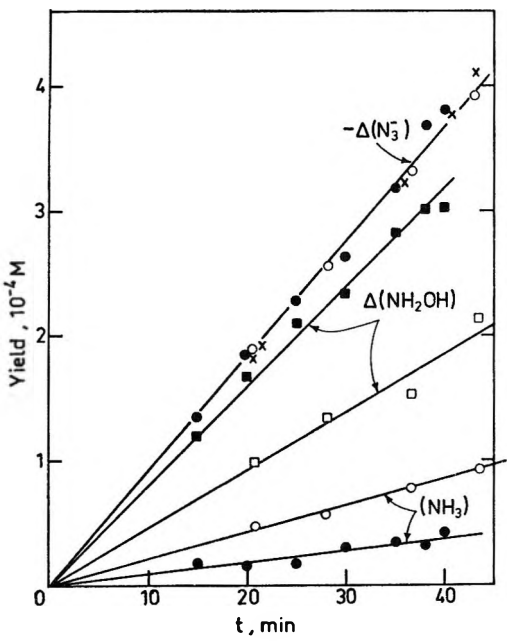

Figure 6. The 2139-Å photolysis of 10^{-3} *M* N_3^- in air-free aqueous solutions, in presence of 1 *M* ethanol (dark symbols) and 1 *M* ethanol + 10^{-3} *M* NH_2OH initially added (open symbols); ×, azide depletion in absence of foreign scavenger.

O_2, N_2O (without ethanol), and phosphate–ethanol mixture (0.4 *M* Na_2HPO_4 + 0.1 *M* KH_2PO_4 + 1 *M* ethanol). In the first two cases ϕ_{NH_2OH} was lower than $-\phi_{N_3^-}$ but still higher than with N_3^- alone (Figure 5). In the case of the phosphate–alcohol system, we could not determine (N_3^-). Moreover, $H_2PO_4^-$ also undergoes photolysis. Thus, the ammonia inhibitors protect the hydroxylamine, either fully (acetone or N_2O + ethanol) or partially (O_2 or N_2O).

Ethanol alone considerably increases ϕ_{NH_2OH} but does not inhibit the formation of NH_3. With increasing time of irradiation ϕ_{NH_2OH} and ϕ_{NH_3} were found to decrease and increase, respectively. For this reason the photolysis was carried out in the presence of 10^{-3} NH_2OH; the results are shown in Figure 6.

Variation in light intensity by a factor of 2 did not affect the quantum yields.

Discussion

The onset of the CTTS band of N_3^- is at ~235 mμ, but owing to overlap with the n,π* band, its contribution to the total light adsorption becomes significant only at $\lambda \lesssim 225$ mμ.[2] Thus, 2537 and 2288 Å fall, in effect, within the same n,π* band. The fact that their photochemical effects are nearly the same supports the view[3] that N_3^{-*} (n,π*) does not first predissociate, but reacts with water after undergoing vibrational equilibration. The wavelength 2139 Å lies well within the CTTS and this explains the change in photochemistry. Our following results indicate that the production of NH_3 is initiated by a reaction of solvated electrons with hydroxylamine. (a) Electrons scavengers (N_2O, acetone, $H_2PO_4^-$, and O_2) inhibit the formation of NH_3. Scavenging of N_3 alone by alcohol does not lead to this effect. (b) At low NH_2OH concentration (short irradiation times) impurities (*e.g.*, O_2) probably compete on e_{aq}^- and this leads to higher ϕ_{NH_2OH} and lower ϕ_{NH_3}. Flash photolysis work[4] showed a first-order decay of e_{aq}^- which was not influenced by varying (N_3^-) in the range 10^{-4} to 10^{-3} *M*; so the reaction between e_{aq}^- and N_3^- can be ruled out. But our results show that [NH_2OH] > 3×10^{-4} *M* is sufficient to scavenge effectively all the electrons and further increase in [NH_2OH] has no effect on ϕ_{NH_3}. (c) Some preliminary results concerning the reaction of e_{aq}^- with NH_2OH[4] show for pH <7 rate constants considerably higher than that previously recorded.[12] The discrepancy is probably due to a pH effect, since NH_3OH^+ has p*K* ~ 6[13] and it is expected to react much faster than NH_2OH. On changing the pH from 7.7 to 6.9 the rate constant of this reaction may increase by a factor of 5, and so total scavenging of e_{aq}^- by hydroxylamine could now be attained at [NH_2OH] < 10^{-4} *M* (Figure 2). This is also reflected in the simultaneous drop in ϕ_{NH_2OH}, but here the effect is not complete unless [NH_2OH] $\gtrsim 2 \times 10^{-4}$ *M* (Figure 2). This suggests the presence of another intermediate which attacks NH_2OH through a reaction which is not so enhanced by decrease of pH. We believe that this is the azide radical. N_3

(12) M. Anbar and P. Neta, *Int. J. Appl. Radiat.*, **18**, 493 (1967).

(13) P. Lumme, P. Lahenmo, and J. Tummavouri, *Acta Chem. Scand.*, **19**, 2175 (1965).

is known to have high chemical reactivity.[5] Its apparent yield from N_3^- and its decay rate is sensitive to impurities. Its reaction with NH_2OH could be directly followed. (The reactions of e_{aq}^- and N_3 with NH_2OH are being further studied in our laboratory.)

When ϕ_{NH_2OH} reaches its limiting yield (Figure 3), both e_{aq}^- and N_3 radicals should be totally scavenged by NH_2OH. For these conditions we propose the following mechanism of photolysis

$$N_3^- \xrightarrow{h\nu} N_3^{-*} \quad (2)$$

$$N_3^{-*} + H_2O \xrightarrow{(1-\alpha)} NH + OH^- + N_2 \quad (3)$$

$$N_3^{-*} \xrightarrow{\alpha} N_3 + e_{aq}^- \quad (4)$$

$$NH + H_2O \longrightarrow NH_2OH \quad (5)$$

$$e_{aq}^- + NH_2OH \longrightarrow NH_2 + OH^- \quad (6)$$

$$NH_2 + NH_2OH \longrightarrow NH_3 + NHOH \quad (7)$$

$$N_3 + NH_2OH \longrightarrow N_3^- + H^+ + NHOH \quad (8)$$

$$2NHOH \longrightarrow N_2 + 2H_2O \quad (9)$$

(The acidic forms of NH_2OH, NH_2, etc., may play a prominent role in some of these reactions.) According to the proposed mechanism, the excited azide ions undergo two chemical reactions: a reaction with water to yield NH with quantum yield $\phi\ (1 - \alpha)$ and ionization with quantum yield $\phi\ \alpha$. Reactions 3 and 5 are identical with that proposed for the n,π^* state[3] and may actually involve this state. In this case, the competing reactions on the CTTS state of N_3^- are internal conversion to the n,π^* state and ionization (reaction 4). Reactions 7 and 9 were proposed for the radiolysis of NH_2OH in aqueous solution[14] (with some species in their acidic forms), and for the photolysis of NH_2OH in the gas phase.[15] The N–H bond of hydroxlamine is relatively weak[15] and so H abstraction by N_3 (reaction 8) and especially by NH_2 (reaction 7) should be exothermic processes. The absence of an effect of light intensity indicates that reactions 7 and 8 proceed much faster than the $NH_2 + NH_2$ or $N_3 + N_3$ reactions.

A stoichiometric summation of reactions 2–9 gives

$$(1 - \alpha)N_3^- + (2 - 5\alpha)H_2O \xrightarrow{h\nu} (1 - 4\alpha)NH_2OH + \alpha NH_3 + N_2 + (1 - \alpha)OH^-$$

According to this overall reaction the experimentally measured quantum yield of azide depletion $-\phi_{N_3^-}$ equals $\phi(1 - \alpha)$, the quantum yield of reaction 3. The quantum yields of the nitrogen containing products are related to $-\phi_{N_3^-}$ as follows

$$\phi_{NH_3}/-\phi_{N_3^-} = \alpha/(1 - \alpha) \quad (10)$$

$$\phi_{NH_2OH}/-\phi_{N_3^-} = (1 - 4\alpha)/(1 - \alpha) \quad (11)$$

$$\phi_{N_2}/-\phi_{N_3^-} = 1/(1 - \alpha) \quad (12)$$

The photoionization process (reaction 4) is responsible for the formation of NH_3 and for ϕ_{NH_2OH} being lower than $-\phi_{N_3^-}$. The ratio between the amount of ammonia produced and the amount of hydroxylamine consumed as a result of this process

$$\beta = \frac{(NH_3)}{-\Delta(N_3^-) - (NH_2OH)}$$

should equal $^1/_3$ independent of α (see overall reaction). This is because when all the solvated electrons and azide radicals are scavenged by NH_2OH, each e_{aq}^-–N_3 pair ultimately produces one molecule of NH_3 and consumes three molecules of NH_2OH.

Our results for the systems containing $(NH_2OH) \geq 3 \times 10^{-4}\ M$ are in agreement with the proposed mechanism (Figure 3). The experimental value of β is 0.31. By applying eq 10, 11, and 12 to our results we obtain for α the values 0.21, 0.22, and 0.24, respectively. Thus we conclude that only *ca.* 23% of the azide ions which react undergo ionization. Scavenging of N_3 by impurities may still involve H abstraction and lead to regeneration of N_3^-; and indeed $-\phi_{N_3^-}$ does not vary with irradiation time (Figure 2). On the other hand, NH_3 is formed only by reactions 6 and 7. The effect of impurities on β will depend on their relative efficiency in competing with reactions 6 and 8. The former competition is probably more efficient at pH 7.7, and so β tends to be lower than $^1/_3$ (Table I). At pH 6.9 the competition with reaction 8 predominates, and this is reflected in the values of β which were found to be higher than $^1/_3$.

The proposed mechanism is substantiated by the results obtained with foreign scavengers.

a. $N_3 + e_{aq}^-$ *Scavengers.* Scavengers which completely remove e_{aq}^- and convert N_3 to N_3^- (both reactions through intermediates which do not interfere with the photolysis of N_3^-) should lead to the overall conversion of N_3^- to NH_2OH and N_2 (reaction 1) with yield $\phi(1 - \alpha) = \phi_0$, where ϕ_0 is $-\phi_{N_3^-}$ in the absence of foreign scavengers. This is apparently the case for the systems shown in Figure 4. Ethanol scavenges OH radicals produced by the reaction of e_{aq}^- with N_2O. The reaction of N_3 with ethanol[5] probably involves H-abstraction

$$N_3 + CH_3CH_2OH \longrightarrow N_3^- + H^+ + CH_3CHOH \quad (13)$$

The behavior of the N_2O + ethanol system indicates that (a) the α hydroxyethyl radical does not react with NH_2OH and (b) $k_8/k_{13} \lesssim 2 \times 10^3$, so that in presence of 1 M ethanol and $4 \times 10^{-4}\ M$ NH_2OH, reaction 13 will predominate. A direct measure of α should be given by the yield of N_2 from N_2O. In principle this can be directly determined by using

(14) M. Lefort and X. Tarrago, *J. Inorg. Nucl. Chem.*, **16**, 169 (1961).

(15) J. Betts and R. A. Back, *J. Can. Chem.*, **43**, 2678 (1965).

Table I: Nitrogen Balance and Conversion Ratio for the Photolysis of 10^{-3} *M* NaN_3 (Air Free) at 2139 Å, 23°, and pH 7.7

$-\Delta(N_3^-)$, 10^{-5} *M*	(NH_2OH), 10^{-5} *M*	(NH_3), 10^{-5} *M*	(N_2),[a] 10^{-5} *M*	$-3\Delta(N_3^-)$, 10^{-5} *M*	$2(N_2) + (NH_2OH) + (NH_3)$, 10^{-5} *M*	$(NH_3)/[-\Delta(N_3^-) - (NH_2OH)]$
13.3	8.3	1.2	16.4	39.9	42.3	0.24
23.7	11.1	3.7	28.2	71.0	71.3	0.30
26.0	13.0	4.1	30.8	78.0	78.8	0.32
27.2	14.3	3.3	32.7	81.7	83.0	0.26
33.0	14.5	4.8	39.2	99.1	97.7	0.26
41.8	17.8	6.5	49.2	125.5	122.7	0.27
42.6	17.0	6.9	50.7	127.9	125.4	0.27

[a] Some of the N_2 yields were obtained by interpolation from Figure 2.

labeled N_2O; even so, from the observation that in contrast to the acetone system the N_2O + ethanol system gives $\phi_{N_2} > -\phi_{N_3^-}$, it follows that the 30% excess of N_2 results from reaction 14 (see below). In this case $\phi_{N_2}/-\phi_{N_3^-} = 1/(1-\alpha)$, from which we obtain $\alpha = 23\%$.

Nothing is known on the reaction of acetone with N_3 but it appears to be faster than reaction 8 and to affect the mechanism only by regenerating N_3^-.

b. e_{aq}^- Scavengers. O_2 and N_2O can only scavenge e_{aq}^-, but in the latter case the resulting OH radical should react with NH_2OH, or with N_3^-

$$e_{aq}^- + N_2O \longrightarrow N_2 + O^-(O^- + H_2O \longrightarrow OH + OH^-) \quad (14)$$

$$OH + NH_2OH \longrightarrow NHOH + H_2O \quad (15)$$

$$OH + N_3^- \longrightarrow OH^- + N_3 \quad (16)$$

$k_{16} = 6.5 \times 10^9\ M^{-1}\ \text{sec}^{-1}$, [12] and k_{15} cannot be much higher; so at 10^{-3} *M* N_3^- reaction 16 should occur. However, reaction 8 should follow and so the overall effect is the same as reaction 15. Therefore in presence of N_2O the mechanism of photolysis will consist of reactions 2–5, 14, 15, 8, 9. This leads to $-\varphi_{N_3^-} = \phi(1-\alpha) = \phi_0$ and $\phi_{NH_2OH}/-\phi_{N_3^-} = (1-3\alpha)/(1-\alpha)$. From our results (Figure 5) we obtain $\alpha \sim 17\%$. A similar value of α was derived from the analysis of the O_2 containing system (Figure 5). Here only the azide radicals attack NH_2OH to regenerate N_3^-. Considering reactions 2–5, 8, 9 we obtain $-\phi_{N_3^-} = \phi(1-\alpha) = \phi_0$ and $\phi_{NH_2OH}/-\phi_{N_3^-} = (1-2\alpha)/(1-\alpha)$. Applying the latter relation to our results it leads to $\alpha \sim 15\%$. Now these results support the view that reaction 8 is not very fast and so it has to compete with impurities, and indeed in presence of 3×10^{-4} *M* NH_2OH considerable decrease in ϕ_{NH_2OH} was detected (Figure 5) and the values for α came close to 25%.

c. N_3 Scavenger. With ethanol alone, reaction 6 is expected to be followed by

$$NH_2 + CH_3CH_2OH \longrightarrow NH_3 + CH_3CHOH \quad (17)$$

and N_3 undergoes reaction 13. Altogether $-\phi_{N_3^-}$ and ϕ_{NH_3} should not be affected by ethanol but NH_2OH should be protected, the conversion ratio β rising to 1. The latter prediction is in agreement with our results up to $(NH_2OH) \sim 3 \times 10^{-4}\ M$ (Figure 6). However, the ethanol brings about a large reduction in ϕ_{NH_3} and a corresponding increase in ϕ_{NH_2OH}. This can be explained on the basis of partial scavenging of e_{aq}^- by impurities and in particular by the acetaldehyde which results from the disproportionation of α-hydroxyethyl radicals. And again, by initially adding 10^{-3} *M* NH_2OH to the system the yield of ammonia comes close to the expected value ($\alpha = 0.20$). However, now β drops to $^1/_2$ (Figure 6; it also shows that at $(NH_2OH) \sim 3 \times 10^{-4}\ M$ β starts to drop). This suggests a switch over from reaction 13 to reaction 8 with $k_8/k_{13} \sim 2 \times 10^3$. The flash photolysis work[5] does show that NH_2OH reacts with N_3 faster than ethanol. The C–H and N–H bonds in ethanol and HN_3, respectively, are of comparable strengths (97 ± 4 kcal and <88 kcal, respectively[16]). The N–H bond in hydroxylamine appears to be considerably weaker. However, in the case of NH_2 the concentration of the scavenger should be a more decisive factor, since the bond energy $H-NH_2$ is 105 ± 2 kcal.[16] Therefore, as long as ethanol is in large excess, it will effectively scavenge the NH_2 radicals. In conclusion, with enough NH_2OH the results can be explained by a mechanism consisting of reactions 2–6, 8 and 17.

Finally, from the measured quantum yield of the azide depletion 0.31 and $\alpha = 0.23$, we obtain $\phi = 0.4$. Thus about 9% of the excited azide ions undergo ionization and 31% (*i.e.*, 34% of the rest) attack water. The latter figure is close to the quantum yield found at λ 2537 Å, which adds support to the internal conversion mechanism previously outlined.

Acknowledgment. We are indebted to Mr. M. Mautner for his help during the early stages of this work and gratefully acknowledge the support of this research by the U. S. Army (Contract DAJA 37-67-C-0767).

(16) V. I. Vedeneyev, L. V. Gurvich, V. N. Kondratyev, V. A. Medvedev, and Ye. L. Frankevich, "Bond Energies, Ionization Potentials and Electron Affinities," Edward Arnold, London, 1966

Photochemistry of Methylfurans. Selectivities of Ring Contraction Reactions

by H. Hiraoka

IBM Watson Research Center, Yorktown Heights, New York 10598 *(Received July 11, 1969)*

Vapor phase Hg($^3P_1$) photosensitizations of 2-methylfuran, 3-methylfuran, and 2,4-dimethylfuran resulted mainly in the formation of, respectively, 3-methylcyclopropene, 1-methylcyclopropene, and 1,3-dimethylcyclopropene upon decarbonylation. 3-Methylfuran was also formed from 2-methylfuran. The vapor phase direct photolysis of 2-methylfuran and 3-methylfuran gave mainly the ring open isomers of the methyl cyclopropenes, although small amounts of the cyclic products were found as well. The direct irradiation also mutually transformed 2-methylfuran and 3-methylfuran in low yield. The primary reactions in the Hg($^3P_1$) photosensitizations are the ring contraction to methyl-substituted cyclopropene carboxyaldehydes which subsequently dissociate to methyl-substituted cyclopropenes and carbon monoxide. Selective ring contraction to one of two possible cyclopropene carbonyl compounds in the mercury-sensitized reactions can be explained by assuming that it is directed by initial breakage of the weakest bond in the lowest excited state. Hückel molecular orbitals have been successfully used to predict these weakest bonds.

Introduction

In our earlier communication[1] we reported that the vapor phase direct photolysis and the Hg($^3P_1$) sensitization of 2-methylfuran resulted in the formation of 3-methylfuran in addition to carbon monoxide, 3-methylcyclopropene, and 1,3-butadiene. We also reported that the Hg($^3P_1$) sensitization of 3-methylfuran resulted in the formation of carbon monoxide, 1-methylcyclopropene, and its ring open isomers, with no traces of 2-methylfuran and 3-methylcyclopropene present in the products. We later found that the valence isomerization of 3-methylfuran to 2-methylfuran takes place under direct irradiation from a medium-pressure mercury lamp. The Hg($^3P_1$)-sensitized reactions can be best explained by assuming one of two possible cyclopropene carbonyl compounds (*e.g.*, 3-methylcyclopropene-3-carboxyaldehyde from 3-methylfuran) as a transient species. It will be reported here that selective ring contraction also takes place in the Hg($^3P_1$) sensitization of 2,4-dimethylfuran. A correlation between the selectivities of the ring contractions and the bond orders calculated from Hückel molecular orbitals of the excited states will be discussed.

Cyclopropene carboxyaldehyde was first proposed as a transient species in the Hg($^3P_1$) sensitization of furan,[2] which gave carbon monoxide and cyclopropene as the principal products. The direct irradiation of furan[3] resulted in the formation of carbon monoxide, allene, and methylacetylene, with cyclopropene present in only trace amounts. A pressure dependence of the quantum yield for CO production was observed in the Hg($^3P_1$)-sensitized reaction, but was absent in direct photolysis. These results suggested that the triplet furan was a precursor of cyclopropene carboxyaldehyde.

The direct irradiation of methylfurans gave results quite different from the Hg($^3P_1$) sensitization, as will be reported in some detail.

Experimental Section

A 2-m diisodecyl phthalate column was used for purification of 2-methylfuran with a Perkin Elmer vapor fractometer. 3-Methylfuran was prepared from 3-methyl-2-furoic acid.[4] Drs. E. Payo and C. Rivas kindly supplied us with 2,4-dimethylfuran.

The light source and the photoreactor were almost the same as in the previous report.[3]

A 2-m column of Ucon Oil 550x was used in the separation of the products. However, this column could not separate 1-butyne, 1-methylcyclopropene and 1,2-butadiene, in which case a 3-m tetraisobutylene column was added to the Ucon oil column. The gas chromatographic analysis of the products from the monomethylfurans was performed at 24° and of the products from the dimethylfuran was carried out at temperatures from 30 to 100°.

2-Methylfuran in vapor phase has its maximum uv absorption at 2050 Å, $\epsilon_{2050\ Å} = 2.1 \times 10^3$ l. mol^{-1} cm^{-1}. Absorption sharply decreases with increase of wave length, $\epsilon_{2350\ Å} = 1.4$ l. mol^{-1} cm^{-1}. 3-Methylfuran has a uv absorption similar to 2-methylfuran, with a maximum at 2075 Å, $\epsilon_{2075\ Å} = 6.5 \times 10^3$ l mol^{-1} cm^{-1}.

Methylacetylene, 1,3-butadiene, 1,2-butadiene, 1-bu-

(1) H. Hiraoka and R. Srinivasan, *J. Amer. Chem. Soc.*, **90**, 2720 (1968).

(2) R. Srinivasan, *ibid.*, **89**, 1758, 4812 (1967).

(3) H. Hiraoka and R. Srinivasan, *J. Chem. Phys.*, **48**, 2185 (1968).

(4) D. M. Burness, "Organic Syntheses," Coll. Vol. IV, John Wiley & Sons, Inc., New York, N. Y., 1963, p 628.

Table I: Hg($^3P_1$)-Sensitized Reaction of 2-Methylfuran,[a] ~24°

Pressure of 2-methylfuran, cm	Initial moles of 2-MF × 10^{-4}	Period of irradiation min	Rate of formation, 10^{-6} mol/min: CO		$CH_3C{\equiv}CCH_3$	$C_2H_5C{\equiv}CH$ + $CH_2CH{=}C{=}CH_2$	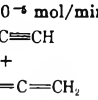	$CH_2CHCHCH_2$	Quantum yield of CO
0.85	5.61	1.0	5.12	0.50	none	1.48 + 0.25[d]	1.84	1.30	0.27
0.93	6.14	1.0	4.65	...[b]	...[b]	1.23	1.86	1.57	0.24
1.00	6.60	0.5	4.75	...[b]	...[b]	1.15	1.93	1.64	0.25
1.89	12.5	1.0	4.42	0.68	...[b]	0.96	1.75	1.51	0.23
2.00	13.2	0.5	4.38	0.79	0.04	0.93	1.70	1.55	0.23
2.06	13.6	1.0	4.35	...[b]	...[b]	1.00	1.74	1.42	0.23
2.40	15.8	1.0	4.20	0.62	...[b]	0.85	1.75	1.40	0.22
2.95	19.5	1.0	3.59	1.22	...[b]	0.73	1.65	1.35	0.19
3.00	19.8	1.0	3.80	...[b]	0.02	0.76	1.58	1.41	0.20
3.87	25.8	3.0	3.34	...[b]	0.02	0.57	1.30	1.16	0.18
1.01[c]	6.65	1.0	...[b]	1.88	...[b]	0.46	0.78	0.48	...[b]

[a] No formation of 1-methylcyclopropene has been confirmed. [b] Not measured. [c] 9.7 cm of N_2 was added. [d] A 2-m Ucon Oil column and a 3-m tetraisobutylene column were used in series.

Table II: Direct Photolysis of 2-Methylfuran. Whole Wavelength from Hanovia Type SH Except Mentioned, − 24°

Total pressure, cm	Initial moles of 2-MF × 10^{-4}	Period of irradiation min	Rate of formation, 10^{-8} mol/min: CO		$CH_3C{\equiv}CCH_3$	$C_2H_5C{\equiv}CH$ + $CH_3CH{=}C{=}CH_2$		$CH_2CHCHCH_2$	$CH_3C{\equiv}CH$	Note
2.11	2.27	4320	2.2 × 10^{-2}	...[c]	...[c]	1.6 × 10^{-2}	1.2 × 10^{-4}	1.6 × 10^{-3}	1.8 × 10^{-3}	2225 Å[a]
2.00	2.15	4305	7.4 × 10^{-2}	...[c]	...[c]	5.2 × 10^{-2}	7.7 × 10^{-4}	1.1 × 10^{-3}	6.8 × 10^{-3}	2380 Å[a,b]
0.95	1.02	90	5.6	0.45	0.25	4.25	0.054	0.58	0.46	
1.97	2.10	240	5.17	0.58	0.68	3.01	0.063	0.33	0.29	
3.87	4.14	130	3.64	...[c]	0.22	2.03	0.071	0.30	0.18	
7.87	8.35	152	2.30	...[c]	0.43	1.80	0.20	0.32	0.10	
1.92	1.07	120	4.14	0.51	1.0	2.36	0.048	0.36	0.22	0.85 cm of ether added
3.20	1.07	180	3.50	0.60	0.26	2.60	0.081	0.18	0.27	2.13 cm of ether added
6.00	1.07	180	2.80	0.88	<0.01	2.14	0.14	0.27	0.19	4.93 cm of ether added
10.30	1.07	165	1.74	1.6	<0.01	1.33	0.13	0.17	0.052	9.30 cm of ether added
10.40	1.07	120	...[c]	0.35	0.11	1.03	0.057	0.17	0.091	9.40 cm of O_2 added
4.94	1.00	88	...[c]	...[c]	0.14	2.12	0.010	0.31	0.22	4.00 cm of N_2 added
10.80	1.02	91	...[c]	1.2	0.065	1.06	0.049	0.15	0.12	9.84 cm of N_2 added
3.20[d]	3.44	123	1.42	0.66	0.12	0.71 + 0.23	0.028	0.17	0.11	

[a] A Bausch & Lomb monochromator with a dispersion of 16 Å/min was used. [b] Quantum yield of formation of CO was 0.57, based on the methyl ethyl ketone actionometry. [c] Not measured. [d] Same experimental conditions as the ones in Table IV.

tyne, 2-butyne, 3-methylfuran,[5] 2-methylfuran, isoprene, 2-pentyne, *cis* and *trans*-2,4-pentadiene were isolated from the products and confirmed by comparing with authentic samples their ir spectra, mass spectra, and retention times in gas chromatography. 1-Methylcyclopropene, 3-methylcyclopropene, and 1,3-dimethylcyclopropene were confirmed by comparing their ir, nmr, and mass spectra with those already published.[6]

Results

(*a*) *2-Methylfuran.* The direct photolysis with effective wavelength from 2300 to 2100 Å and the Hg($^3P_1$) photosensitization of 2-methylfuran resulted in the formation of carbon monoxide, methylacetylene, 3-methylcyclopropene, 1,3-butadiene, 1,2-butadiene, 1-butyne, and 3-methylfuran.

Table I shows the rates of formation of the products in the Hg($^3P_1$)-sensitized reaction as a function of pressure.

Although a small amount of methylacetylene was formed, this was a very minor product in the Hg($^3P_1$) sensitization. 2-Butyne was formed only in trace

(5) A sample prepared by E. Payo and C. Rivas of the Institute Venezolano de Investigaciones, Caracas, Venezuela.

(6) G. L. Closs, L. E. Closs, and W. A. Bell, *J. Amer. Chem. Soc.*, **85**, 3796 (1963); F. Fisher and D. E. Applequist, *J. Org. Chem.*, **30**, 2059 (1965).

Table III: Hg($^3P_1$)-Sensitized Reaction of 3-Methylfuran, ~ 24°, 1.0-min Irradiation

Pressure of 3-methylfuran, cm	Initial moles of 3-MF × 10^{-4}	Rate of formation, 10^{-5} mol/min						Quantum yield of CO
		CO	$CH_3C{\equiv}CCH_3$	$CH_3CH{=}C{=}CH_2$	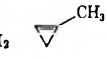	$C_2H_5C{\equiv}CH$	$CH_2CHCHCH_2$	
1.47	9.71	7.95	1.39	0.21	4.33	0.05	0.82	0.42
2.66	17.6	6.95	0.76	0.076	5.12	0.01	0.76	0.37
4.05	26.7	6.16	0.44	0.075	5.14	None	0.58	0.32
5.57	36.8	5.74	0.36	0.028	4.95	None	0.40	0.30
8.15	53.7	4.70	0.07	None	4.19	None	0.20	0.24
10.3	67.6	4.18	0.03	None	3.84	None	0.18	0.22

Table IV: Direct Photolysis of 3-Methylfuran,[a] 24°

Pressure of 3-methyl-furan, cm	Initial moles of 3-MF × 10^{-4}	Period of irradiation, min	Rate of formation, 10^{-5} mol/min									
			CO		$CH_3C{\equiv}CCH_3$	$CH_3CH{=}C{=}CH_2$		$C_2H_5C{\equiv}CH$		$CH_2CHCHCH_2$	$CH_3C{\equiv}CH$	$CH_2{=}C{=}CH_2$
1.93	2.08	70.0	3.36	Not measured	1.18	0.44	None	0.60	None	0.24	0.58	0.14
4.72	5.07	167	2.69	0.25	1.52	0.48	0.067	0.57	0.011	0.184	0.058	0.005
7.59	8.15	181	2.34	0.37	1.35	0.30	0.054	0.32	0.035	0.155	0.058	None
11.2	12.0	185	2.12	0.59	1.27	0.45	0.164	0.43	0.038	0.141	0.038	None

[a] Whole wave length from Hanovia type SH mercury lamp was used.

amounts, with no 1-methylcyclopropene present in the products. The material balance was generally good if the conversion was limited to a few per cent. Measurements of the light intensity in the Hg($^3P_1$)-sensitized reaction were performed with nitrous oxide in the presence of ethane.[7]

Table II shows the product yields in the direct photolysis as a function of pressure. The major differences from the Hg($^3P_1$)-sensitized reaction are that 3-methylcyclopropene became no longer a principal product but a minor one and that an appreciable amount of methylacetylene was formed. The formation of 3-methylcyclopropene became more important with an increase of pressure.

(*b*) *3-Methylfuran.* The mercury ($^3P_1$) sensitization of 3-methylfuran resulted in the formation of carbon monoxide, 1-methylcyclopropene, 2-butyne, 1,3-butadiene, 1,2-butadiene, and 1-butyne. Table III shows the rates of formation of the products in the Hg($^3P_1$) sensitization as a function of pressure. 3-Methylcyclopropene, which was a principal product from 2-methylfuran, was not found in the products even in a trace amount and a valence isomerization did not occur from 3-methylfuran to 2-methylfuran. The quantum yield for decarbonylation was found to be much higher than in the case of 2-methylfuran.

Table IV shows the rates of formation of the products in the direct photolysis of 3-methylfuran as a function of pressure. The major differences from the Hg($^3P_1$) sensitization are that small amounts of 1-methylcyclopropene as well as 3-methylcyclopropene were formed as minor photoproducts, and that the valence isomer, 2-methylfuran, now appeared.

(c) *2,4-Dimethylfuran.* The mercury ($^3P_1$) sensitization of 2,4-dimethylfuran yielded carbon monoxide and 1,3-dimethylcyclopropene as principal products, with small amounts of isoprene, *cis*- and *trans*- 1,3-pentadiene, 2-pentyne, 1-methylcyclopropenyl methyl ketone, and its further rearranged isomers. The sum of 1-methylcyclopropenyl methyl ketone and its further rearranged isomers amounted to less than ~20% of the total products. Table V shows the results.

Discussion

(*a*) *Mechanism of the Hg($^3P_1$)-Sensitized Reactions.* In the Hg($^3P_1$) sensitization of furan, cyclopropene 3-carboxyaldehyde was postulated as a transient species, followed by subsequent elimination of carbon monoxide and formation of vibrationally excited "hot" cyclopropene.[2] Because the direct photolysis of furan did not yield any trace of cyclopropene and since the pressure dependence of formation of carbon monoxide was absent in this case,[3] it has been argued that the triplet furan originating from collision with Hg($^3P_1$) atoms must be a necessary precursor for the ring contraction to cyclopropene 3-carboxyaldehyde. The

(7) In our previous communication, reference 1, we have carried out the actinometry with ethylene at its low pressure, 1 cm, which gave us erroneous results. The factor of 0.42 should be multiplied to the results obtained with ethylene in order to comply with the nitrous oxide + ethane actinometer at the same condition.

(i) 2-Methylfuran.

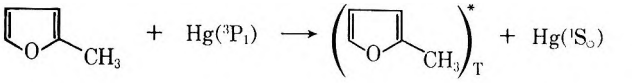

(1)

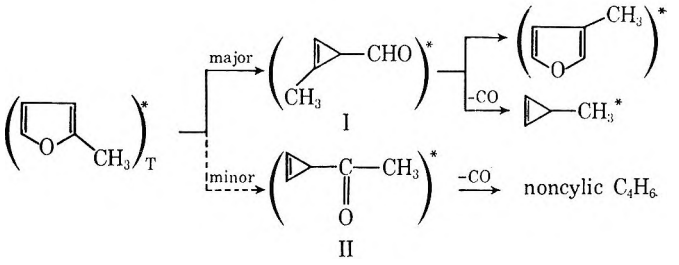

(2)

(3)

(4)

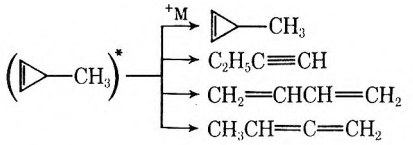

(5)

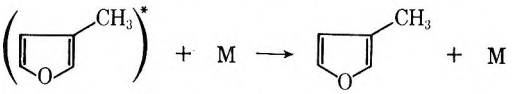

(6)

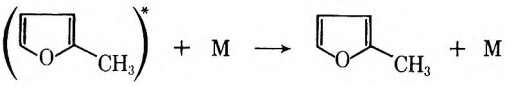

(7)

(ii) 3-Methylfuran.

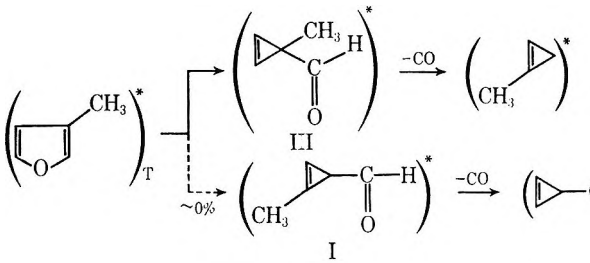

(8)

(9)

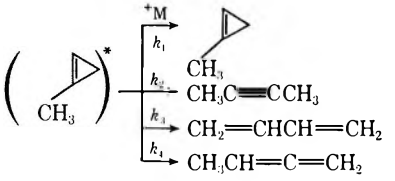

(10)

(iii) 2,4-Dimethylfuran.

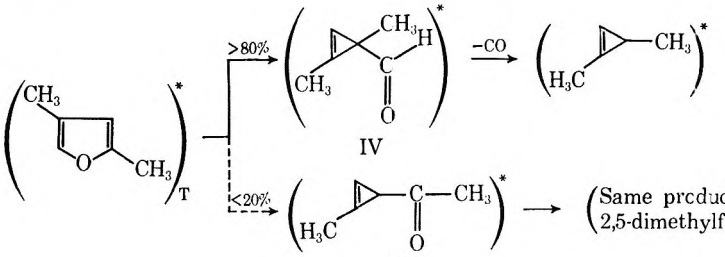

(11)

(12)

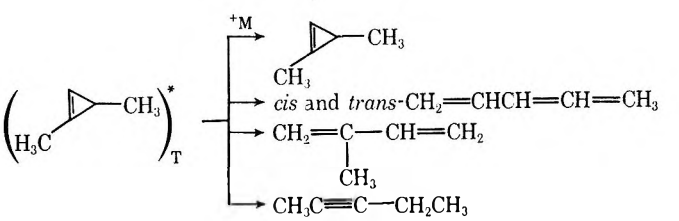

(13)

Table V: Hg($^3P_1$)-Sensitized Reaction of 2,4-Dimethylfuran, ~ 24°, 10.0-min Irradiation

Pressure of 2,4-dimethylfuran, cm	Initial Moles of 2,4-DMF × 10^{-4}	Rate of Formation, 10^{-8} moles/min: CO	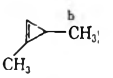	iso[b]-prene	*trans*-1,3-[b] pentadiene	*cis*-1,3,penta-[b] diene + 1,2-pentadiene	2-Pentyne[b]	Quantum yield of CO	Notes
1.25	8.25	1.72	0.95	0.088	0.20	0.32	0.17	0.184	
1.50	9.9	1.66	0.89	0.058	0.27	0.30 + 0.010	0.13	0.178	
1.50	9.9	1.46	0.93	0.10	0.16	0.19 + 0.017	0.067	0.148	3.07 cm of CO_2 added
1.50	9.9	1.26	0.79	0.080	0.12	0.20	0.066	0.135	4.67 cm of CO_2 added
1.50	9.9	1.23	0.82	0.074	0.11	0.17	0.054	0.126	5.48 cm of CO_2 added
1.67	11.0	1.13	...	...	...	...	...	0.115	7.71 cm of CO_2 added
1.47[a]	9.7	0.671						0.068	
1.40[a]	9.2	0.599	See ref 8.					0.060	2.41 cm of CO_2 added
1.49[a]	9.9	0.508						0.052	4.14 cm of CO_2 added

[a] These are the data for Hg($^3P_1$) sensitization of 2,5-dimethylfuran, observed under the same condition as employed for 2,4-dimethylfuran. [b] These values were calculated using the assumption that $\Sigma[C_5H_8] = [CO]$. Fragmentation was negligible in the case of 2,4-dimethylfuran.

valence isomerization from 2-methylfuran to 3-methylfuran and the formation of methylcyclopropenes which were found in this investigation strongly support the ring contraction mechanism to the cyclopropene carboxyaldehydes.

The reaction mechanism in eq 1–13 for the Hg($^3P_1$)-sensitized reactions would be most consistent with all the experimental results (T = triplet).

In Figure 1, the reciprocal of the quantum yield of CO formation is plotted against the total pressure. The slope of this curve should be approximately equal to the ratio of the rate constants for triplet quenching and for decomposition of the transient species. The formation of the stable ketones from 2,5-dimethylfuran[2] and 2-methyl-4,5-dihydrofuran[1] is consistent with strong pressure dependence of the quantum yields for their decarbonylation. The large differences in pressure dependence between 2,4-dimethylfuran and 2,5-dimethylfuran and between 2-methylfuran and 3-methylfuran indicate the quite different transient species proposed in the above reaction mechanisms.

The methylcyclopropenes formed by decarbonylation of the methylcyclopropene carboxyaldehydes have excess vibrational energy and isomerize to their ring open isomers, unless their excess energy is taken away in collisions. For the 1-methylcyclopropene formed in the Hg($^3P_1$) sensitization of 3-methylfuran, the following equation may be derived

$$\frac{\text{rate of formation of } \Sigma\ C_4H_6}{\text{rate of formation of } \cdot CH_3} = \frac{\Sigma[C_4H_6]}{[\cdot CH_3]} = \frac{k_2 + k_3 + k_4}{k_1 p} + 1 \quad (12)$$

where p is the total pressure. Similar equations are obtained for the formation of 3-methylcyclopropene and 1,3-dimethylcyclopropene. The ratio, $\Sigma[C_4H_6]/[\cdot CH_3]$, should approach unity with increasing pressure, and this was found to be the case in the formation of 1-methylcyclopropene from 3-methylfuran. However, the plots for 3-methylcyclopropene and for 1,3-dimethylcyclopropene do not converge to unity with an

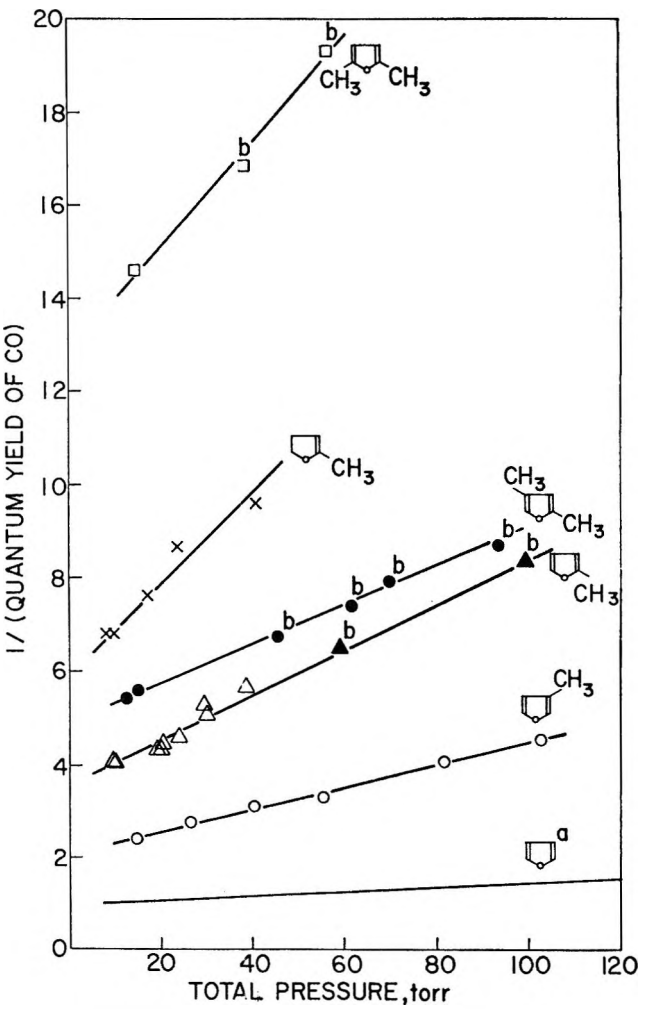

Figure 1. Quantum yields for decarbonylation in the Hg($^3P_1$) sensitizations of furans: a, R. Srinivasan, *J. Pure Appl. Chem.*, 18, 65 (1968); b, CO_2 added above a partial pressure of 15 Torr of the furans.

Table VI: π-Bond Orders (Hückel Type MO) of Furan Systems and Selectivities of Ring Contraction Reactions[a]

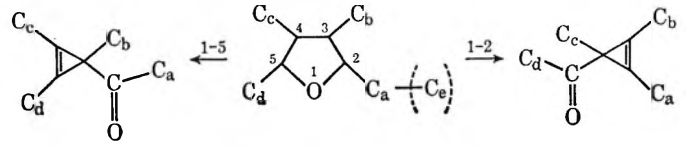

Systems		π-Bond Orders 1-2	1-5	2-3	3-4	4-5	2-C_a	2-C_b	4-C_c	5-C_d	C_a-C_e	Major transients in $Hg(^3P_1)$ sensitizations	Excitation energies
	G	0.308	0.308	0.839	0.511	0.839						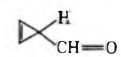	1.44β
	E_1	0.154	0.154	0.420	0.756	0.420							
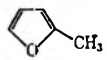	G	0.317	0.273	0.803	0.521	0.832	0.268					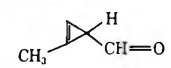	1.39β
	E_1	*0.147*	0.152	0.415	0.739	0.435	0.291						
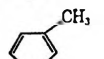	G	0.270	0.306	0.812	0.489	0.844		0.246					1.40β
	E_1	0.188	*0.112*	0.376	0.708	0.471		0.282					1.95β
	E_2	*0.207*	0.304	0.573	0.350	0.348		0.319					
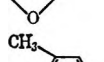	G	0.133	0.236	0.808	0.501	0.801	0.270		0.248			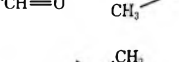	1.41β
	E_1	*0.128*	0.240	0.620	0.872	0.244	0.558		0.403				
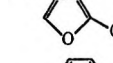	G	0.289	0.289	0.817	0.502	0.817	0.243			0.243		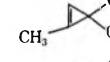	1.29β
	E_1	0.145	0.145	0.420	0.748	0.420	0.270			0.270			
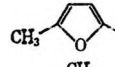	G	0.292	0.277	0.795	0.511	0.827	0.235	0.211				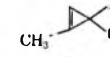	1.41β
	E_1	0.169	*0.120*	0.385	0.676	0.483	0.298	0.289					
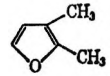	G	0.252	0.282	0.806	0.496	0.814	0.208	0.214		0.246		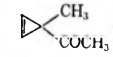	1.29β
	E_1	0.151	*0.112*	0.402	0.716	0.441	0.280	0.256		0.241			
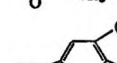	G	0.284	0.238	0.806	0.489	0.802	0.235	0.206	0.244			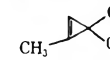	1.36β
	E_1	0.144	*0.118*	0.374	0.688	0.477	0.279	0.261	0.205				
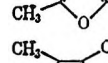	G	0.279	0.297	0.746	0.538	0.821	0.461				0.883	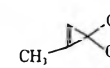	1.01β
	E_1	*0.157*	0.216	0.498	0.453	0.811	0.469				0.847		
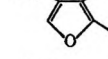	G	0.256	0.338	0.703	0.553	0.808	0.524				0.692	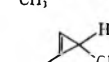	1.16β
	E_1	*0.214*	0.227	0.473	0.688	0.523	0.511				0.592		
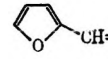	G	0.204	0	0.941	0	0	0.260					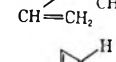	1.87β
	E_1	0.247	*0*	0.055	0	0	0.264						
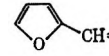	G	0.364	0.390	0.740	0.549	0.801	0.415					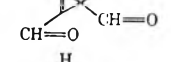	1.10β
	E_1	*0.209*	0.286	0.421	0.712	0.587	0.620						
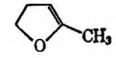	G	0.408	0.391	0.756	0.489	0.828		0.370				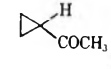	1.24β
	E_1	0.334	*0.180*	0.369	0.572	0.724		0.534					

?: Expected Product

[a] G: Ground electronic state; E_1: lowest electronic state; E_2: second lowest electronic state; β: resonance integral between carbon atoms.

increase of pressure, but they approach 1.2 ± 0.05 and 1.3 ± 0.05, respectively. This may indicate some contribution from alternative routes to the formation of the ring open isomers as indicated by eq 4 and eq 12. The different character of the transient species in the $Hg(^3P_1)$ sensitization of 2,4-dimethylfuran and of 2,5-dimethylfuran resulted in largely different values of

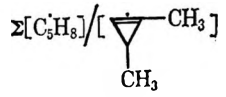

which was 1.65 for the former and 69 for the latter at 1.5 cm total pressure and room temperature.

(*b*) *Selectivity of the Ring Contraction Reactions.* One of the most interesting features of the substituted furan systems is the selectivity of the ring contraction in the $Hg(^3P_1)$-sensitized reactions. 3-Methylfuran isomerized to 3-methylcyclopropene 3-carboxyaldehyde III and yielded 1-methylcyclopropene with no trace of 3-methylcyclopropene derived from the alternative transient, 1-methylcyclopropene 3-carboxyaldehyde (I). The major reaction course of 2-methylfuran appears to be isomerization to 1-methylcyclopropene 3-carboxyaldehyde (I) and the principal reaction of 2,4-dimethylfuran was the isomerization to 1,3-dimethylcyclopropene 3-carboxyaldehyde (IV). This decomposed predominantly to 1,3-dimethylcyclopropene and carbon monoxide, leading thus to products quite different from the ones of 2,5-dimethylfuran.[8] The photochemistry of 2-furfuraldehyde[3] may also be explained by assuming a selective ring contraction to cyclopropene 1,3-dicarboxyaldehyde, as shall be discussed later.

The ring contraction reactions may first start with a bond breakage between the oxygen atom and one of the adjacent carbon atoms in the furan ring. Therefore, the specific direction of the ring contraction may be predicted if one knows which bond is the weakest in the excited state. The π-bond orders of the furan systems in Table VI have been calculated from the simple Hückel molecular orbitals for their ground and lowest excited states. The latter may be interpreted as an average of the triplet and the singlet states. The following parameters[9a-c] were used: $\alpha_{CH_3-} = \alpha + 3.0\beta$, $\alpha_{C-CH_3} = \alpha - 0.1\beta$, $\beta_{C-CH_3} = \beta$, $\alpha_{-O-} = \alpha + 2\beta$, $\alpha_{C-O} = \alpha + 0.2\beta$, $\beta_{C-O} = 0.6\beta$, $\alpha_{=O} = \alpha + 2\beta$, $\alpha_{C=O} = \alpha + 0.2\beta$, $\beta_{C=O} = \sqrt{2}\beta$, $\alpha_{-S-} = \alpha + 0.9\beta$, $\alpha_{C-S} = \alpha + 0.1\beta$, and $\beta_{C-S} = 0.5\beta$. Here, α and β stand for the coulomb and the resonance integrals of the conjugated carbon atom, respectively; α_{C-A} is the coulomb integral of the carbon atom adjacent to A, α_A is the coulomb integral of atom or radical A, and β_{C-A} is the resonance integral of the C–A bond.

In order to determine the bond strength, the σ bond order has to be added to the calculated π-bond order. Because the bond order is approximately inversely proportional to the bond length, it could be predicted from Table VI that the weakest bond in the lowest excited state of 3-methylfuran is the bond O_1–C_5. The ring contraction would therefore start with the breakage of that bond, leading to 3-methylcyclopropene 3-carboxyaldehyde (III).

All experimental results obtained so far are compatible with breakage of the predicted weakest bond of the excited state as shown in Table VI. In the case of 2-methylfuran, the difference of the bond orders between bond O_1–C_2 and bond O_1–C_5 is quite small. This may explain some contribution from cyclopropenyl methyl ketone (II), formed by breakage of the bond O_1–C_5, as has been discussed in the previous section.

The $Hg(^3P_1)$ sensitization and the direct photolysis of 2-furfuraldehyde[3] resulted in the formation of furan, cyclopropene, and carbon monoxide as principal products. The bond orders of its lowest excited state indicate the bond O_1–C_2 to be the weakest one, so that the following reaction scheme is indicated.

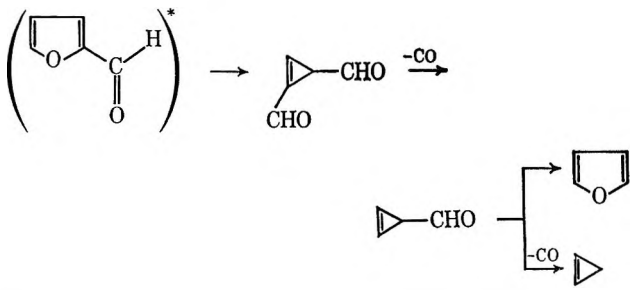

This possibility was discussed in our previous reports.[3]

The $Hg(^3P_1)$ sensitization of 2-vinylfuran gave cyclopentadiene as one of its major products,[10] which suggested the following reaction mechanism.

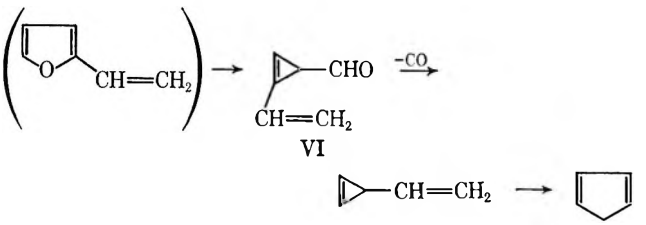

1-Vinylcyclopropene 3-carboxyaldehyde (VI) is again the predicted transient as shown in Table VI. Although there are no experimental results available on 2,3-dimethylfuran, 2,3,4-trimethylfuran, and 2,3,5-trimethylfuran, we may be able to predict the possible ring contraction products as shown in Table VI.

According to H. Wynberg and his coworkers,[11] 2-phenylthiophene rearranges *irreversibly* to 3-phenyl-

(8) A private communication with S. G. Boue and R. Srinivasan.

(9) (a) T. Yonezawa, *et al.*, "Introduction to Quantum Chemistry," Kagaku-Dojin, Kyoto, 1964, p 55; (b) A. Streitwieser, Jr., and P. M. Nair, "Conference of Hyperconjugation," Pergamon Press, London, 1959; (c) B. Pullman, and A. Pullman, *Rev. Mod. Phys.*, **32**, 428 (1960).

(10) H. Hiraoka and R. Srinivasan. Details of this study will be published later.

(11) Hans Wynberg, *et al.*, *J. Amer. Chem. Soc.*, **89**, 3501 (1967); see references in this paper.

thiophene under the influence of ultraviolet light. Assuming that the reaction mechanism of the thiophene photorearrangement parallels the one of the furan systems, the present scheme makes it possible to interpret the irreversible photorearrangement of 2-phenylthiophene to 3-phenylthiophene on the basis of the predicted transients

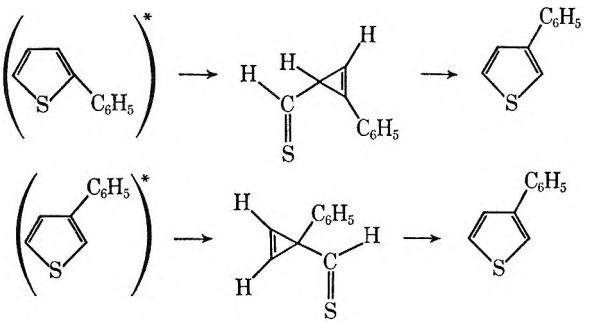

The theoretical considerations outlined here seem to be the only ones so far which can account for these specific rearrangements.

Besides the selectivity of the ring contraction, the specific hydrogen migration in the decarbonylation of the cyclopropene carboxyaldehydes is observed. In reaction 8, the aldehyde hydrogen migrates to one of the two double bond carbon atoms, not to the sp^3 carbon atom attached with a methyl group, probably from the energetic basis. In reactions 3 and 11, the aldehyde hydrogen migrates only to the double bond carbon atom attached with a methyl group, attracted by the higher electron density at that location.

Hückel molecular orbitals are admittedly a very crude approximation. The good agreement with the experimental results is therefore surprising to us, especially since the π-bond order of the excited triplet state was calculated from Hückel type wave functions. The bond order approach should be tested further with more refined molecular wave functions.

In the vapor phase direct photolysis of 3-methylfuran, the selective ring contraction to 3-methylcyclopropene 3-carboxyaldehyde disappeared and the ring contraction to 1-methylcyclopropene 3-carboxyaldehyde also occurs to give 2-methylfuran and 3-methylcyclopropene upon decarbonylation. The loss of selectivity in the direct photolysis may result from a partial contribution of the second lowest excited state, in which the bond O_1–C_2 is the weakest one.

Acknowledgments. The author wishes to thank Dr. R. Srinivasan for his initial suggestions of this work and for his encouragement, discussions, and comments throughout this work. He also thanks Dr. H. Hunziker for reading the manuscript and for his helpful comments.

Radiolysis of Water Vapor in a Wide Range Radiolysis Source of a Mass Spectrometer. I. Individual and Total Cross Sections for the Production of Positive Ions, Negative Ions, and Free Radicals by Electrons

by Charles E. Melton

Department of Chemistry, University of Georgia, Athens, Georgia 30601 *(Received July 14, 1969)*

The abundance of, and the total and individual cross sections for, primary products (positive ions, neutral species, and negative ions) resulting from elementary reactions induced by the absorption of energy by H_2O from ionizing radiation (100-eV electrons) have been measured. This was accomplished with the dual-beam and high transmission ion sources in a mass spectometer. Positive ions are produced in much greater abundance than free radicals, 67.2% *vs.* 32.1%. Negative ions, on the other hand, are about three orders of magnitude less abundant than the other primary products. Results for positive ions are in good agreement with those reported by other workers with the exception of that for H^+, which differs by a factor of 3. No valid reason for the discrepancy could be found. However, the present value for the total ionization cross section of 2.2×10^{-16} cm^2 molecule^{-1} is in good agreement with that reported by other workers. No previous values for radicals are available with which to make comparisons. The present results show that hydrogen radicals account for 54% of all neutral primary products while hydrogen molecules (produced by rearrangement) account for only 13%. On the basis of these results, hydrogen atoms play a dominant role in the radiolysis of water vapor.

Introduction

For over half a century investigators[1] have known that the excitation of water vapor by ionizing radiation produces many physical and chemical changes. Nevertheless, the elementary reactions by which these processes occur are almost completely unknown. This is true because of the vast amount of information necessary in order to establish a basis for understanding the system. For example, one must have an accurate knowledge of the various ions, excited species, and free radicals which are produced by each of the elementary steps in the mechanism. The most important elementary step is the initial step in which the primary products are formed. Primary products are defined as reactive species, positive and negative ions, excited molecules, and free radicals,[2] resulting from the excitation of the electronic system of the individual molecule by ionizing radiation. These primary products actually initiate all of the observed chemical and physical change. Consequently, little progress can be made in the interpretation of the reaction mechanism without a knowledge of the nature and abundance of the primary products. An experimental determination of these products is extremely difficult—particularly for free radicals and excited species. Because of these difficulties, no attempt has been made previously to measure and identify the primary neutral species. On the other hand, experimental determination of the primary ionic products by mass spectrometry is much less difficult; hence, data are available for these species, but various workers are in serious disagreement about the abundance of each species. For example, Schutten, *et al.*,[2] who have measured the primary positive ionic products formed by excitation with 100-eV electrons, report that H^+ accouts for 18.7% of the positively charged products. In sharp contrast, Mann, *et al.*,[3] report only 3.8% of H^+,a discrepancy of about a factor of 5. Such discrepancies are unusual in mass spectrometry even for ions of low mass wherein discrimination is troublesome. While it is true that the mass spectrometer does indeed discriminate against some types of ions, other experimental methods of attack do not appear feasible. Consequently, we have attempted to design an instrument to incorporate features which minimize ionic discrimination.

Theoretical approaches such as the Born–Bethe approximation[4] do not provide a suitable basis for evaluating the accuracy of the experimental results. Even if the individual cross sections for ionization (σ_i) could be calculated accurately from first principles, a new theoretical framework for dissociative ionization would have to be developed in order to calculate the abundance of

(1) W. Duane and O. Scheuer, *Radium* (Paris), **10**, 33 (1913).

(2) J. Schutten, F. J. DeHeer, H. R. Moustafa, A. J. H. Boerboom, and J. Kistemaker, *J. Chem. Phys.*, **44**, 3924 (1966).

(3) M. M. Mann, A. Hustrulid, and J. T. Tate, *Phys. Rev.*, **58**, 340 (1940).

(4) H. Bethe, *Ann. Phys.*, **5**, 325 (1930).

the ionic and neutral products. The theoretical approaches for the calculation of σ_i for large molecules are actually semiempirical approaches. Consider, for example, the theoretical relationship for σ_i of Miller and Platzman[5] based on the original Born–Bethe approximation

$$\sigma_i = (4\pi a_0^2 R/E_e) M_i^2 \ln (c_i E_e) \quad (1)$$

where a_0 is the first Bohr radius of atomic hydrogen, R is the Rydberg energy, E_e is the electron energy, and c_i is a constant. M_i^2 is related to the optical oscillator strength by the relationship

$$M_i^2 = \int_{E_i}^{\infty} \frac{df}{dE} \frac{R}{E} \eta(E)\, dE \quad (2)$$

where $\frac{df}{dE}$ is the optical oscillator strength, $\eta(E)$ is the ionization efficiency for a molecule of intrinsic energy E. Long-lived excited states having an energy greater than E_i, the ionization potential, can decay by ionization, thereby reducing $\eta(E)$ to less than unity. An approximate value for M_i^2 can be obtained from the relationship

$$M_i^2 = \frac{mcR}{\pi e 2h} \int_{E_i}^{\infty} \frac{\sigma_{ph}(E)}{E} dE \quad (3)$$

where σ_{ph} is the cross section for photoionization with photons of energy E. The precision in M_i^2 therefore is no better than the experimental value of σ_{ph}. Furthermore, the constant c_i must be determined by empirical means. In view of these facts, the experimental approach appears to be the better method to resolve the discrepancy.

The purpose of the present study was to obtain by experimental methods reliable values for the nature and abundance of all of the primary products produced in water vapor by 100-eV electrons. An upper limit can be placed on the abundance of a specific fragment ion from a knowledge of the abundance of all other primary products. For example, the production of H^+ is accompanied by either OH radicals or negative ions according to the mechanism

$$H_2O + e \longrightarrow H^+ + OH + 2e \quad (i)$$
$$\longrightarrow H^+ + OH^- + e \quad (ii)$$
$$\longrightarrow H^+ + H^- + O + e \quad (iii)$$
$$\longrightarrow H^+ + O^- + H + e \quad (iv)$$

The abundance of H^+ must therefore be given by the relationship

$$H^+ = \sum_{\text{All Processes}} (H_2O + e) \quad (3a)$$

Accordingly, results for all primary products should resolve the factor of 5 discrepancy in the reported abundance of H^+ from H_2O. This is true because eq 3a can then be summed over all possible reactions (i–iv).

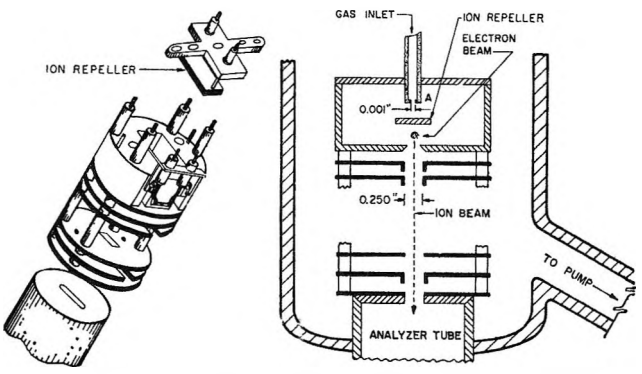

Figure 1. Schematic diagram of the high-transmission ion source. Dimensions of the defining slits are 0.25 × 0.50 in.

Experimental Section

Results were obtained with the Georgia research mass spectrometer. The instrument is a 6-in. radius, 60° sector type of mass spectrometer constructed in part from surplus components supplied by W. D. Harmon and W. Rice of the Y-12 Mass Spectrometer Laboratory, Oak Ridge, Tennessee. Specific features were added to minimize mass discrimination and thereby give high accuracy.

The gas handling system and spectrometer tube were constructed of borosilicate glass except for the copper magnetic analysis section. Base pressure in the gas handling system was about 1×10^{-7} Torr, whereas that in the source region and analyzer tube was over an order of magnitude lower. All stopcocks and standard taper joints in the sample handling system were lubricated with Apiezon N high-vacuum grease.

A glass pinhole leak 0.0001 in. diameter between the 3-l. sample reservoir and ionization chamber was used to maintain a constant pressure of the sample in the ionization chamber. Normal operating pressure in the ionization chamber was 1×10^{-7} Torr except for studies involving neutral species and negative ions. Reasonable signals from these species dictated that the operating pressures be increased to 6×10^{-6} Torr.

Absolute cross sections were obtained with the high-transmission ion source shown schematically in Figure 1. The performance has been fully discussed elsewhere;[6] hence, only the main features will be mentioned here. High transmission is achieved principally by the wide, 0.250 × 0.500-in., slits used throughout the source. These slits greatly reduce the resolution while enhancing the transmission. Normal accelerating potential in the source was 5–6 kV. However, the transmission was about constant for potentials greater than 4 kV.

Electrons incident on a system can be transmitted, scattered, captured, or degraded in energy depending

(5) W. F. Miller and R. L. Platzman, *Proc. Phys. Soc.*, **A70**, 299 (1957).

(6) C. E. Melton, *J. Sci. Instrum.*, **43**, 927 (1966).

upon the energy of the incident particles. The behavior of an electron beam can be expressed as

$$\frac{-dN_e}{N_e} = \sigma\, dx \qquad (4)$$

where N_e is the number of electrons, σ is the total cross section for all processes and x is the distance traversed. The total cross section σ is given by the relationship

$$\sigma = \sum_i \sigma_{ei} + \int_0^\epsilon \sigma_i\, d\epsilon \qquad (5)$$

The cross section σ_{ei} is the cross section for excitation of the ith state of the molecule and $\sigma_i\, d\epsilon$ is the cross section for an ionization reaction in which the energy of the ejected electron is between ϵ and $\epsilon + d\epsilon$. In this study, the high-transmission source was used to measure the absolute magnitude of the individual cross section σ_i for the production of a specific ion (positive or negative)

$$\sigma_i = \int_{E_i}^\epsilon \sigma\, d\epsilon \qquad (6)$$

by irradiating H_2O with 100-eV electrons. A solution of (4) and (6) leads to the first-order relationship for N^+ of

$$N^+ = \sigma_i N N_e x \qquad (7)$$

where N^+ represents the number of ions from a neutral species N, N_e is the current, and x is the distance traveled by the electrons. The accuracy of σ_i is a function of the error in each of the four variables in eq 7. The high-transmission ion source was designed to minimize the error in each of the variables.

The path length x of the electrons is not the linear distance across the ionization chamber, but rather the distance described by a helix of radius determined by the strength of the collimating magnet H and the initial direction at the electrons with respect to the magnetic field. If d is the diameter of the electron-defining aperture and E is the energy of the electrons in electron volts, the maximum path length of an electron is given by[7]

$$x = x_0(1 + 1.1 \times 10^{-4}\, d^2H^2/E) \qquad (8)$$

For our experimental conditions, $d = 1$ mm, $H = 400$ G, and $E = 100$ eV. The maximum path length of any of the electrons in the beam was only about 6% greater than the linear distance. The linear distance was used for the present calculations since the error involved would be much less than 6%. Equation 6 does not allow for an increase in the path of electrons caused by elastic scattering. It has been shown[7] that such an increase in path length, Δx, is given by the relationship

$$\Delta x = {}^1/_2\, N\sigma_s x_0^2(\ln\cos\theta + \cos\theta) + \frac{\lambda}{x_0} N\sigma_s \int_0^\infty (x_0 - x)\, dx \frac{x_0}{\lambda} \qquad (9)$$

In this relationship N is the number of molecules per cubic centimeter, σ_s is the cross section for elastic scattering of electrons by the gas, λ is the mean free path of the electrons, θ is the angle of deviation from the electron beam, and x is the distance traversed through the ionization chamber. Substituting parameters in eq 9 for our experimental conditions showed that the increase in path length (<1%) due to elastic scattering could be neglected in this study.

Free radicals and negative ions were studied with a dual electron beam ion source shown schematically in Figure 2. The operation of this type of source has been described elsewhere.[6,8] Cross sections for dissociation are given by the relationships[6]

$$N^+ = \sigma_* \sigma_i (N) N_e N_e' x_0 x_0' \frac{\eta}{v} \qquad (10)$$

Where N^+ is the ion current observed from a specific free radical, N, σ_* is the cross section for dissociation, N is the concentration of neutral molecules in chamber (1), N_e' is the number of electrons in chamber (2), x_0' is the distance the electrons travel in chamber (1), v is the average velocity of N, and η is the transmission coefficient from chamber (1) to chamber (2). The cross section for ionization of a specific free radical σ_i is usually unknown. Pending more accurate data, it was assumed that σ_i for a free radical was equal to σ_i for a similar stable molecule determined at an equal $(E-I)$, using the relationship obtained by assuming a linear energy dependence for σ_i of

$$\sigma_i = \sigma_0 (E - I) \qquad (11)$$

where σ_0 is a constant, E is the electron energy, and I is the corresponding ionization potential. For example,

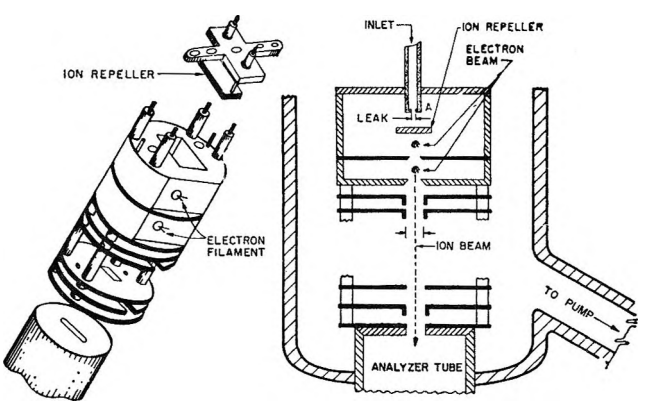

Figure 2. Schematic diagram of the dual electron beam ion source. The defining slit between the two chambers has dimensions of 0.005 × 0.500 in. All other defining slits have dimensions of 0.25 × 0.50 in.

(7) H. S. W. Massey and E. H. S. Burhop, "Electronic and Ionic Impact," Oxford University Press, Oxford, 1952, p 34.

(8) C. E. Melton, *J. Chem. Phys.*, **45**, 4414 (1966).

Table I: Individual Cross Sections for Initial Products Produced by the Irradiation of H_2O with 100-eV Electrons at a Pressure of 6×10^{-6} Torr

Positive Ions		Neutral Species			Negative Ions		
% of total products	$\sigma \times 10^{16}$ cm^2	Neutral	% of total products	$\sigma \times 10^{16}$ cm^2	Ion	% of total products	$\sigma \times 10^{16}$ cm^2
4.57	0.15	H	17.38	0.57	H^-	0.64	0.021
0.34	0.011	H_2	4.27	0.14			
1.62	0.053	O	2.87	0.094	O^-	0.034	0.0011
13.12	0.43	OH	7.57	0.248	OH^-	0.003	0.0001
47.58	1.56						
67.23	2.204	Total	32.09	1.052	Total	0.677	0.0222

σ_i for ionizing CH_3 (I = 9.8 eV)[9] by 13.8-eV electrons was assumed to be equal to σ_i for the ionization of CH_4 (I = 13.0 eV)[10] by 17-eV electrons. The use of this unavoidable assumption contributed to the uncertainty in the value of the individual cross sections for dissociation, σ_*.

The transmission coefficient η was obtained from the geometry of the dual beam ion source. We assumed transmission of all ions formed in the solid angle subtended by the slit separating the two chambers. This assumption was checked for validity by measuring the transmission of positive ions in the absence of an electric field. Such transmission was somewhat less than that calculated from the geometry of the source. This discrepancy was explained by the fact that the electron collimating magnet probably reduced the transmission of the ions.

Ions were normally detected by a 14-stage electron multiplier combined with a vibrating reed electrometer and strip chart recorder. Calibration (gain for positive *vs.* negative ions) of the detection circuit was accomplished by the use of a Faraday cup rather than the multiplier combined with the vibrating reed electrometer. The input resistors were calibrated for linearity by measuring the isotopic abundance of known (Ne) isotopic mixtures[11,12] over all operating ranges (5 to 1000 mV). Experimental error for the isotopic abundance of Ne was less than 0.05%. Ion focus controls were adjusted to maximize the intensity of each ion beam. No significant increase with focus adjustment was observed in the mass 16–18 range, but masses 1 and 2 were increased in intensity by about 20% by optimizing the ion repeller potential. All other electrode potentials remained constant for each determination. The increase in ion intensity for H^+ with increasing ion repeller field is consistent with that observed by Schutten, *et al.*[2]

The pressure in the ionization chamber was determined in part by methods previously discussed.[13] Because of adsorption on surfaces, the pressure of the water vapor was difficult to measure directly in the ionization chamber. A method was used in which water vapor was maintained at the normal vapor pressure in the expansion volume for the temperature of the experimental conditions. Thus, the pressure behind the leak could be both measured and calculated. The density of water vapor effusing from the leak was assumed to be equal to that for neon with equal pressures for the two gases behind the leak. Further details of the experimental procedure can be found elsewhere.[14]

Residual gases at pressures below 10^{-8} Torr contributed background ions at masses 1, 2, 16, 17, and 18 which interfered slightly with the interpretation of the results. The ion intensity at each of the mass positions under study was always at least two orders of magnitude greater than that of the background.

The sample of water was purified by the usual triple distillation method.[15] A mass spectral analysis indicated that the sample was greater than 99.99% pure.

Results and Discussion

The abundance of a specific primary product, for example H^+, produced in a given compound by ionizing radiation depends on a number of factors including excitation levels of the neutral molecule, energy of the ionizing radiation, and the rate constants for production of other products formed by competitive reactions. Usually the dependence must be expressed as a curve. Clearly, a large number of curves would be required to describe all of the primary products over the complete energy range of interest. Some data are available[2] for positive ionic products over a rather large energy range, but no data are available in the literature for primary neutral species. As a starting point, therefore, we have measured the abundance and cross sections for all of the primary products produced by electrons in water vapor at a specific energy, namely 100 eV. The pressure was maintained at a value low enough to preclude secondary reactions. Results given in Table I show that twelve different primary products are formed. The values for

(9) C. E. Melton and W. H. Hamill, *J. Chem. Phys.*, 41, 3464 (1964).
(10) C. E. Melton and W. H. Hamill, *ibid.*, 41, 546 (1964).
(11) J. R. Walton and A. E. Cameron, *Z. Naturforsch.*, 21a, 15 (1966).
(12) P. Eberhardt, O. Eugster, and K. Marti, *ibid.*, 20, 623 (1965).
(13) C. E. Melton in "Mass Spectra of Organic Ions," F. W. McLafferty, Ed., Academic Press, Inc., New York, N. Y., 1963, p 65.
(14) C. E. Melton, *Int. J. Mass Spectrom. Ion Phys.*, 1, 353 (1968).
(15) J. P. Chittum and V. K. Lamer, *J. Amer. Chem. Soc.*, 59, 2425 (1937).

the specific cross sections are actually sums of cross sections for all reactions that produce a specific product. As noted earlier, the cross sections for ionization of free radicals were necessary but not available in order to solve eq 10 to obtain the results for the neutral species given in Table I. The cross section for ionization of oxygen and hydrogen atoms was assumed to be one-half that for ionization of the corresponding neutral diatomic molecules for the same values of $(E - I)$. Results for the OH radical are perhaps more uncertain. The cross section was assumed to be equal to 70% of that for H_2O at equal values of $(E - I)$. This assumption probably gives the lower limit for the cross sections for ionization of OH.

Probable elementary reactions which lead to the observed primary products are listed in Table II. Although some of the observed products may be produced by means of a doubly charged intermediate complex, such reactions are not shown because of the relatively low excitation energy used in this study. When competing reactions are possible (*e.g.*, reactions 3 and 4), reactions which give the greatest change in energy and entropy are assumed to predominate. Thus, we postulate that reaction 4 has a much higher cross section than reaction 3.

Table II: Possible Reactions Leading to Primary Products in Water Vapor

Reactants	Products	
$H_2O + e \longrightarrow$	$H_2O^+ + 2e$	(1)
$\longrightarrow$	$OH^+ + H + 2e$	(2)
$\longrightarrow$	$O^+ + 2H + 2e$	(3)
$\longrightarrow$	$O^+ + H_2 + 2e$	(4)
$\longrightarrow$	$H^+ + OH + 2e$	(5)
$\longrightarrow$	$H^+ + O + H + 2e$	(6)
$\longrightarrow$	$H_2^+ + O + 2e$	(7)
$\longrightarrow$	$OH^- + H^+ + e$	(8)
$\longrightarrow$	$O^- + H^+ + H + e$	(9)
$\longrightarrow$	$O^- + H_2^+ + e$	(10)
$\longrightarrow$	$H^- + OH^+ + e$	(11)
$\longrightarrow$	$H^- + O^+ + H + e$	(12)
$\longrightarrow$	$H^- + O + H^+ + e$	(13)
$\longrightarrow$	$OH + H + e$	(14)
$\longrightarrow$	$O + 2H + e$	(15)
$\longrightarrow$	$O + H_2 + e$	(16)

A comparison of this work with previous results is restricted to the positive ions because no data are available for neutral species. In Table III, the relative abundance of positive ions measured in this study are shown together with those reported by others.[2,3] Mann, *et al.*,[3] reported a much lower abundance for all of the fragment ions that observed in the present study. Schutten, *et al.*,[2] also reported a lower abundance for all fragment ions except H^+, which is higher by a factor of 3.

On the other hand, the total cross section reported by Schutten, *et al.*,[2] agrees to within 5% with that measured in this study 2.1×10^{-16} *vs.* 2.2×10^{-16} cm^2 $molecule^{-1}$. Furthermore, individual cross sections reported by these workers agree with the present results to within about 25% for the fragment ions with the exception of that for H^+, which differs by a factor of 3. In an effort to resolve this discrepancy, we considered the cross sections for the other primary products which accompany the production of H^+. Reactions 5, 6, 8, 9, and 13 in Table II are involved in the production of H^+. Since reactions 8, 9, and 13 produce less than 0.05% of the total products (Tables I and II), reactions 5 and 6 are primarily responsible for the production of H^+. Reaction 6 is energetically much less favorable than reaction 5, hence we conclude that H^+ results chiefly from reaction 5. This conclusion enables us to check our results for self-consistency. The radical OH is a primary product in the production of H^+ by reaction 5. Thus, the cross section for the production of H^+ is equal to or less than that for the production of OH. Since OH is produced by reaction (14) as well as by reaction 5, the cross section for the production of H^+ should be much less than that for the production of OH. This conclusion is consistent with the present results in Table I. In contrast, the value reported by Schutten, *et al.*,[2] for the production of H^+ is greater than that observed in the present study for the production of OH (0.39 *vs.* 0.25×10^{-16} cm^2 $molecule^{-1}$). The present results are also consistent with the energetics. Ionization of a bonding orbital produces fragment ions from neutrals with the lower ionization potential (*IP*). For example, CH_3^+ is about 40 times more abundant than H^+ in the decomposition[16] of CH_4 ($IPCH_3 = 9.8$; $IP \cdot H = 13.5$ eV).[9] Therefore, ionization of an sp^2 electron in H_2O would be expected to produce a much higher abundance of OH^+ than of H^+ because the ionization potential of OH is less than that for H. We observe about a factor of 3 times more OH^+ than H^+, Table I. In contrast, Schutten, *et al.*,[2] report a greater abundance for H^+ than for OH^+.

In conclusion, we are unable to explain the discrepancy between the present results and those of Schutten, *et al.*[2] Because of the importance of these

Table III: Relative Abundance of Primary Positive Ions Produced by 100-eV Electrons in Water Vapor

Ion	Mann, *et al.*[a]	Schutten, *et al.*[b]	This work
H_2O^+	100	100	100.00
OH^+	23.2	25.8	27.29
O^+	2.0	2.65	3.38
H_2^+	0.07	0.30	0.72
H^+	5.0	29.6	9.48

[a] Reference 3. [b] Reference 2.

(16) C. E. Melton and P. S. Rudolph, *J. Chem. Phys.*, 47, 1771 (1967).

Table IV: Individual Cross Sections for the Production of Neutral Species by Unimolecular Decomposition of Excited H_2O

Species	Per cent of total products	Reaction	Cross section $\sigma \times 10^{16}$ cm^2 molecule^{-1}
OH	2.51	$H_2O + e \longrightarrow OH + H + e$	0.082
O	1.93	$H_2O + e \longrightarrow O + H_2 + e$	0.063
H	2.73	$H_2O + e \longrightarrow H + OH + e$	0.089
H_2	2.06	$H_2O + e \longrightarrow H_2 + O$	0.067
	9.23		0.30

results form both experimental and theoretical points of view, it is hoped that other workers will investigate the problem perhaps with other experimental methods.

Cross sections for decomposition of excited water into neutral fragments cannot be measured directly by the present techniques. However, such values can be calculated by correcting the total cross sections for neutrals produced by dissociative ionization. For example, OH is produced by reactions 5 and 14 of Table II. If one subtracts the cross section for reaction 5 from the total cross section, the residual is that for reaction 14. Results are shown in Table IV. These data show that less than 30% of the neutral products are formed by dissociation of neutral H_2O. Hence, most energy is absorbed in ionization processes.

Acknowledgment. This research was supported by the United States Atomic Energy Commission under Contract No. AT-(40-1) 3729.

Ionic Reactions in Gaseous Methylsilane

by P. Potzinger and F. W. Lampe

Department of Chemistry, The Pennsylvania State University, University Park, Pennsylvania 16802
(Received June 30, 1969)

Appearance potentials of the principal positive ions from methylsilane have been measured and from these data standard heats of formation of the various ions as well as that of the parent molecule itself have been derived. From the energetic onsets of some of the resonance-capture processes and pair-production processes thermochemical data for the Si^- and SiH^- and SiH_2^- ions are extracted. This was not possible for the other negative ions partly because their formation processes are dominated by the various dissociation channels of a common parent $CH_3SiH_3^{-*}$ ion. The only primary ions that react upon collision with CH_3SiH_3 are CH_3SiH^+ and SiH_2^+ and the principal reaction is that of abstraction of H^- from methylsilane with formation of $CH_3SiH_2^+$. The other ionic products of the major ion–molecule reactions are, in order of abundance, $(CH_3)_2SiH^+$, $Si_2CH_4^+$, $Si_2CH_5^+$, and $Si_2C_2H_8^+$. Reaction rate constants for thermal-energy ions have been determined.

Gaseous ion reactions in hydrocarbons and in their derivatives containing oxygen, nitrogen, sulfur, and halogens have been studied extensively and information obtained therefrom has been of great value to chemists interested in the energetics, reaction kinetics, and radiation chemistry of these substances.[1-6] A similar body of knowledge simply does not exist for compounds in which one or more carbon atoms of a hydrocarbon are replaced by another atom of group IV of the periodic table; yet such compounds, which are structurally similar to hydrocarbons and which are usually termed organometallics, are receiving ever increasing interest.

As part of a general program[7-13] concerned with the effects of ionizing radiation on silanes and organosilanes, we report in this paper results of mass spectrometric studies of ionic reactions in gaseous methylsilane.

(1) F. H. Field and J. L. Franklin, "Electron Impact Phenomena," Academic Press, New York, N. Y., 1957.

(2) J. H. Beynon, "Mass Spectrometry and Its Applications to Organic Chemistry," Elsevier Publishing Co., Amsterdam, The Netherlands, 1960.

(3) K. Biemann, "Mass Spectrometry: Organic Chemical Applications," McGraw-Hill Book Co., Inc., New York, N. Y., 1962.

(4) R. I. Reed, "Ion Production by Electron Impact," Academic Press, New York, N. Y., 1962.

(5) F. W. McLafferty, Ed., "Mass Spectrometry of Organic Ions," Academic Press, New York, N. Y., 1963.

(6) C. A. McDowell Ed., "Mass Spectrometry," McGraw-Hill Book Co., Inc., New York, N. Y., 1963.

(7) G. G. Hess and F. W. Lampe, *J. Chem. Phys.*, **44**, 2257 (1966).

(8) D. P. Beggs and F. W. Lampe, *ibid.*, **49**, 4230 (1968).

(9) J. F. Schmidt and F. W. Lampe, *J. Phys. Chem.*, **73**, 2706 (1969).

Table I: Positive Ion Formation by Electron Impact on Methylsilane

m/e	Relative abundance at 70 eV	Appearance potential, eV	Process assigned	$\Delta H_f°$ (ion), kcal/mol
45	89	11.80 ± 0.05	$CH_3SiH_3 + e \longrightarrow CH_3SiH_2^+ + H + 2e$	220 ± 3
44	100	11.45 ± 0.05	$CH_3SiH_3 + e \longrightarrow CH_3SiH^+ + H_2 + 2e$	264 ± 3
43	50	14.05 ± 0.05	$CH_3SiH_3 + e \longrightarrow CH_3Si^+ + H_2 + H + 2e$	272 ± 3
30	30	11.50 ± 0.05	$CH_3SiH_3 + e \longrightarrow SiH_2^+ + CH_4 + 2e$	283 ± 3[a]

[a] Calculated from studies of electron impact on SiH_4 and Si_2H_6 (ref 12 and 16).

Experimental Section

Ionization-efficiency curves and appearance potentials of the primary and secondary positive ions and the primary negative ions from methylsilane were obtained from studies utilizing a Nuclide Associates 12-90-G magnetic sector mass spectrometer. Studies of the secondary positive ions arising from ion–molecule reactions at elevated ion-source pressures were also conducted in a Bendix 14-101 time-of-flight mass spectrometer. The modifications to these instruments that are pertinent to the work reported in this paper have been described previously,[7,14] as also have the techniques employed in the determination of appearance potentials,[1,12] and in the elucidation and rate constant measurement of ion–molecule reactions.[7,8,10,11,13]

Methylsilane was purchased from the Peninsular Chemical Company. Each sample before use was thoroughly degassed at −160° (isopentane slush) and was then distilled on the vacuum line from a methanol slush (−98°). From gas chromatographic examination of the vapor collected we estimate the methylsilane admitted to the mass spectrometer to have a minimum purity of 99.5%.

Results and Discussion

1. Primary Positive Ions. The appearance potentials of the principal positive ions formed by electron impact on methylsilane are shown in Table I. Also shown in Table I are the relative abundancies of the ions at 70 eV ionizing energy, the processes assigned to the formation of the ions at their energetic thresholds, and their standard heats of formation computed from the appearance potentials and the assumption of zero excess energy in each process. The average deviation of replicate experiments was equal to or less than ±0.05 eV.

In order to calculate the standard heats of formation of the various ions it is necessary first to obtain a value for the standard heat of formation of methylsilane itself, a quantity that has not to our knowledge, been measured directly as yet. Gunn and Green[15] have reported a value of +7.3 kcal/mol for $\Delta H_f°(SiH_4)$, which is in good agreement with an earlier value of Brimm and Humphreys[16] of +7.8 kcal/mol, and, in addition, have reported that $\Delta H_f°(Si_2H_6)$ is +17.1 kcal/mol. We have found,[12] in agreement with Steele, Nichols, and Stone[17] and Steele and Stone[18] that values of $\Delta H_f°(SiH_2^+)$, calculated from the appearance potentials of SiH_2^+ from SiH_4 and Si_2H_6, assuming processes (1) and (2), agree within experimental error, giving $\Delta H_f°(SiH_2^+) = 283 \pm 2$ kcal/mol. This agreement attests to the internal consistency of the results of Gunn and Green.[15] Steele, Nichols, and Stone[17] have reported that the appearance potential of SiH_2^+ from methylsilane is 11.62 ± 0.10 eV, a value which is more than 1 eV lower than the appearance potential of SiH_3^+ and more than 3.5 eV lower than the appearance potential of CH_3^+ from the same compound. As pointed out by these authors, this suggests strongly that the neutral fragment formed simultaneously with SiH_2^+ is a molecule and, hence, the process can be hardly anything but

$$SiH_4 + e \longrightarrow SiH_2^+ + H_2 + 2e \quad (1)$$

$$Si_2H_6 + e \longrightarrow SiH_2^+ + SiH_4 + 2e \quad (2)$$

$$CH_3SiH_3 + e \longrightarrow SiH_2^+ + CH_4 + 2e \quad (3)$$

Our value of 11.50 ± 0.05 eV for the appearance potential of SiH_2^+ is in good agreement with the value reported by Steele, Nichols, and Stone[17] as is our observation that the ionization-efficiency curve shows no tail and is thus indicative of a simple process as (3) involving little or no excess energy.[1] We believe, therefore, that we may use our value, $\Delta H_f°(SiH_2^+) = 283 \pm 2$ kcal/mol, and the appearance potential of SiH_2^+ (as formed in (3)) to obtain a reasonably reliable value for the standard heat of formation of methylsilane. The value so obtained is $\Delta H_f°(CH_3SiH_3) = 0 \pm 2$ kcal/mol. With this value at hand we may

(10) D. P. Beggs and F. W. Lampe, *J. Phys. Chem.*, 73, 3307 (1969).
(11) D. P. Beggs and F. W. Lampe, *ibid.*, 73, 3315 (1969).
(12) P. Potzinger and F. W. Lampe, *ibid.*, 73, 3912 (1969).
(13) D. P. Beggs and F. W. Lampe, *ibid.*, 73, 4194 (1969).
(14) P. M. Becker and F. W. Lampe, *J. Chem. Phys.*, 42, 3857 (1965).
(15) S. R. Gunn and L. G. Green, *J. Phys. Chem.*, 65, 779 (1961).
(16) E. D. Brimm and H. M. Humphreys, *ibid.*, 61, 829 (1957).
(17) W. C. Steele, L. D. Nichols, and F. G. A. Stone, *J. Amer. Chem. Soc.*, 84, 4441 (1962).
(18) W. C. Steele and F. G. A. Stone, *ibid.*, 84, 3599 (1962).

compute the standard heats of formation of the principal ions at m/e 43, 44, and 45, as shown in Table I.

$CH_3SiH_2^+$ (m/e 45). We write this ion of m/e 45 as $CH_3SiH_2^+$ rather than as $SiH_3CH_2^+$ because the bond dissociation energies of Si–H bonds are generally less than corresponding C–H bonds and the ionization potentials of silyl radicals appear to be less than the corresponding alkyl radicals.[15,19] Hence, on energetic grounds $CH_3SiH_2^+$ is the more probable ion at the lowest energy onset of 11.80 eV. Reproducible breaks in the ionization-efficiency curve of m/e 45 were observed at 12.9 ± 0.1 eV and 14.7 ± 0.1 eV. The first break, lying 1.1 eV above onset, is probably to be attributed to onset of the process forming $SiH_3CH_2^+$, the basis of this conclusion being that the trend of differences between the ionization potentials of corresponding alkyl and silyl radicals[15,19] suggests ~1 eV as a plausible energy difference in the two dissociation processes. The cause of the second break at 14.7 eV cannot be ascertained but must represent the onset of a process that produces a different state of excitation of the $CH_3SiH_2^+$ and/or $SiH_3CH_2^+$ ions.

Hobrock and Kiser[20] have reported $\Delta H_f°(CH_3SiH_2^+)$ to be 216 kcal/mol which would seem to be in good agreement with our value of 220 ± 3 kcal/mol; we think, however, that this apparent agreement is only accidental. Their value[20] was obtained from the appearance potential of m/e 45 from trimethylsilane, an ion which can be formed only in a complex dissociative-rearrangement process, and their calculated heats of formation of ions formed in such processes from both trimethylsilane[20] and tetramethylsilane[21] are not in good agreement. Moreover, the $\Delta H_f°$ values calculated depend upon the values chosen for the standard heats of formation of trimethylsilane and tetramethylsilane; Kiser and Hobrock used values for these quantities[22] which, as we shall discuss in detail in a forthcoming paper,[23] appear to be too low by about 25 kcal/mol.

CH_3SiH^+ (m/e 44). Since the appearance potential of this ion is lower than that of m/e 45 it is most probable that at onset the neutral fragment is molecular hydrogen. Admittedly the argument is weak, but we choose CH_3SiH^+ as the favored structure because in its abundance in the mass spectrum and in its ion–molecule reactions its behavior resembles that of SiH_2^+ from SiH_4. Reproducible breaks in the ionization-efficiency curve of this ion were found at 12.4 ± 0.1 eV and 14.1 ± 0.1 eV. We believe the first break may be due to the formation of $CH_2SiH_2^+$, lying, as in the case of m/e 45, about 1 eV above onset, while we are unable to make an assignment of the second.

Hobrock and Kiser[20] have reported a value of $\Delta H_f°(CH_3SiH^+)$ drawn from electron impact studies on trimethylsilane. However, for reasons cited in the discussion of the m/e 45 ion, we do not think a comparison of this work with ours is meaningful.

CH_3Si^+ (m/e 43). We really do not have any basis for the assignment of structure to this ion but since m/e 43 is a major ion in the mass spectra of tetramethyl-, trimethyl-, and dimethylsilane we write it as above solely for convenience. A reproducible break was found at 15.5 ± 0.2 eV and may well be attributable to formation of an ion of different structure such as CH_2SiH^+. Hobrock and Kiser[21] have reported $\Delta H_f°(CH_3Si^+)$ to be 235 kcal/mol with an uncertainty that must be at least ±10 kcal/mol. In this case, the ion was formed by the impact of electrons on tetramethylsilane so that it could be formed in a simple consecutive methyl dissociation process. It is of interest that our values would agree within experimental error if the standard heat of formation of tetramethylsilane reported by Tannenbaum, Kaye, and Lewenz[22] were too low by 25 kcal/mol; this is the magnitude of the discrepancy in these thermochemical data[22] that we have found independently in our electron impact studies and shall report in a forthcoming publication.

2. Negative Primary Ions. Ionization-efficiency curves for the negative ions at m/e 28, 29, 30, 31, 43, 44, and 45 were obtained over the electron energy range 0–30 eV. The use of the retarding-potential-difference technique yielded curves that did not differ significantly from those using the full energy distribution of the electrons and therefore was not used in the negative ion studies.

For all ions except Si^- (m/e 28) the largest and sharpest resonance capture peak was found to have an onset of 7.1 ± 0.1 eV. This is quite analogous to the results found in our study[12] of negative ions from Si_2H_6 and must mean that capture of the electron in a Franck–Condon transition yields such a highly-excited $CH_3SiH_3^-$ ion that all dissociation channels are energetically possible and that the intensities of the various peaks are determined solely by the shape of the potential energy surface.

Two resonance-capture peaks are found for Si^-, the largest and sharpest having an onset of 8.2 ± 0.1 eV, while the second is a broad peak with an onset of 13.3 ± 0.1 eV. The energy difference in these two processes is probably to be attributed to different degrees of dissociation of the neutral fragments. If we take H_2 and CH_4 to be the neutral fragments of the lowest process we are led energetically to an improbably large *negative* electron affinity[12] of Si of −4.4 eV. It is more reasonable to assign as the process at the lowest energy onset of 8.2 eV

(19) G. G. Hess, F. W. Lampe, and L. H. Sommer, *J. Amer. Chem Soc.*, **87**, 5327 (1965).

(20) B. G. Hobrock and R. W. Kiser, *J. Phys. Chem.*, **66**, 155 (1962).

(21) B. G. Hobrock and R. W. Kiser, *ibid.*, **65**, 2186 (1961).

(22) S. Tannenbaum, S. Kaye, and G. F. Lewenz, *J. Amer. Chem. Soc.*, **75**, 3753 (1953).

(23) P. Potzinger and F. W. Lampe, *J. Phys. Chem.*, in press.

$$CH_3SiH_3 + e \longrightarrow Si^- + CH_4 + 2H \quad (4a)$$

or

$$CH_3SiH_3 + e \longrightarrow Si^- + H_2 + CH_3 + H \quad (4b)$$

The capture process having an onset of 13.3 eV is then to be attributed to

$$CH_3SiH_3 + e \longrightarrow Si^- + CH_3 + 3H \quad (5)$$

with the greater dissociation involved in (5) resulting in a broader peak. The energy difference would be expected to be ~4.5 eV and 5.1 eV is actually observed; the excess energy of 0.6 eV, which may well be kinetic energy of the fragments, is not unreasonable.

Pair-production processes having onsets of 21.9 ± 0.4 eV and 27.5 ± 0.5 eV are also observed for the Si^- ion. It is of interest that the energy difference between the lowest-energy resonance-capture process (4a,b) and the lowest-energy pair-production process is 13.7 eV, corresponding very closely to the ionization potential of the hydrogen atom. The same is approximately true of the difference between the onset of (5), namely 13.3 eV, and that of the higher-energy pair-production process. Therefore, for the two pair-production processes we suggest

$$CH_3SiH_3 + e \longrightarrow Si^- + CH_4 + H^+ + H \quad (6a)$$

or

$$CH_3SiH_3 + e \longrightarrow Si^- + H_2 + CH_3 + H^+;\ A = 21.9\ eV \quad (6b)$$

and

$$CH_3SiH_3 + e \longrightarrow Si^- + CH_3 + 2H + H^+;\ A = 27.5\ eV \quad (7)$$

Assuming no excess energy, one computes from the four processes the value $\Delta H_f^\circ(Si^-) = 115 \pm 10$ kcal/mol, which is in agreement with the value found previously from SiH_4.[12]

SiH^- (m/e 29). There is no indication of any process forming SiH^- below the aforementioned common resonance-capture peak at 7.1 eV. There are, however, three pair-production processes at 13.3 ± 0.2 eV, 18.1 ± 0.3 eV, and 22.2 ± 0.5 eV. Unless we are to attribute an improbably-large electron affinity to the SiH molecule (at least 1.1 eV greater than the electron affinity of either Si[24] or H[25]) the first of these energetic onsets can refer only to reaction 8, *viz.*

$$CH_3SiH_3 + e \longrightarrow SiH^- + CH_3^+ + H_2 \quad (8)$$

with the second being accounted for by

$$CH_3SiH_3 + e \longrightarrow SiH^- + CH_3^+ + 2H \quad (9)$$

We are unable to make any meaningful statement as to the process responsible for the onset at 22.2 eV. From the appearance potentials of (8) and (9) and the assumption of zero excess energy we may derive $\Delta H_f^\circ(SiH^-) = 48$ kcal/mol, in reasonable agreement with our earlier conclusion.[12] Combination of this value with $\Delta H_f^\circ(SiH)$[26] leads to the result that the electron affinity of SiH is 18 kcal/mol.

SiH_2^- (m/e 30). This ion exhibits a small resonance capture peak with an onset at 3.0 ± 0.3 eV which suggests strongly the process

$$CH_3SiH_3 + e \longrightarrow SiH_2^- + CH_4 \quad (10)$$

and yields an estimate of $\Delta H_f^\circ(SiH_2^-) = 51$ kcal/mol, a value in good agreement with the value obtained earlier from SiH_4.[12]

Pair-production processes are observed at 20.8 ± 0.4 eV and 22.7 ± 0.5 eV; in addition, there exists a process with an onset at 14.5 ± 0.3 eV which we are unable to assign to either pair-production or resonance capture.

The ionization-efficiency curves of the other negative ions from methylsilane exhibit some formation processes other than the common resonance capture peak at 7.1 eV but are so dominated by this peak that we feel a discussion of energetics based on them is not warranted.

3. Ion–Molecule Reactions. A. Effect of Pressure on Primary Ion Intensities. As can be seen from Figures 1 and 2, when the ion-source pressures are such that collision reactions of primary ions become of importance, the ion fraction $(I_i/\Sigma_i I_i)$ of CH_3SiH^+ (m/e 44) exhibits a sharp decrease with increasing pressure. This indicates that CH_3SiH^+ is the principal reactant ion in this system, which is analogous to the earlier finding that SiH_2^+ is the principal reactant ion in monosilane.[7] The ion fraction of $CH_3SiH_2^+$ (m/e 45) increases with source pressure to an extent (relative to the decrease in CH_3SiH^+) that indicates it to be a major product, if not the major product. Since the only primary ion showing a decrease large enough to account for the increase in $CH_3SiH_2^+$ is CH_3SiH^+, it is clear that the reaction involved is

$$CH_3SiH^+ + CH_3SiH_3 \longrightarrow CH_3SiH_2 + CH_3SiH_2^+ \quad (11)$$

which is most easily visualized as being a simple H^- transfer reaction such as is commonly observed in gas-phase collisions of ions and molecules.[5,6] Of course, the product ion may not be $CH_3SiH_2^+$ but rather may be $SiH_3CH_2^+$ or a mixture of both; however, on the basis of the relative strengths of C–H and Si–H bonds[15,19] we shall assume that the product is $CH_3SiH_2^+$.

Examination of Figure 2 indicates that SiH_3^+ (m/e 31) is neither a reactant ion nor a product ion. Thus, as in monosilane,[7] SiH_3^+ is inactive with respect to collision

(24) B. Edlén, *J. Chem. Phys.*, **33**, 98 (1960).
(25) C. L. Pekeris, *Phys. Rev.*, **112**, 1649 (1958).
(26) A. E. Douglas, *Can. J. Phys.*, **35**, 76 (1957).

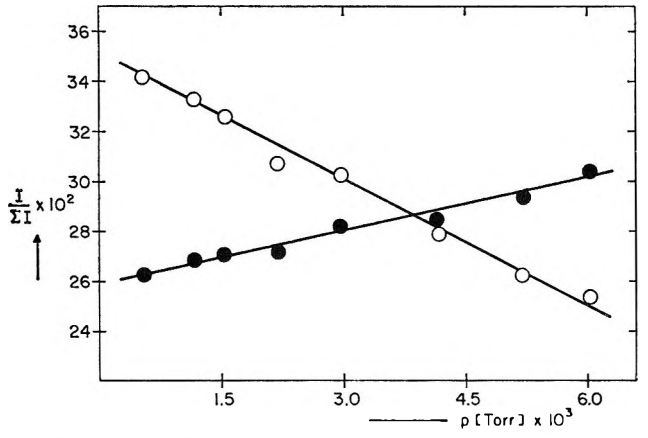

Figure 1. Ion fraction of primary ions as a function of ion-source pressure at 1.0-μsec delay time: ⊙, m/e 44; ●, m/e 45.

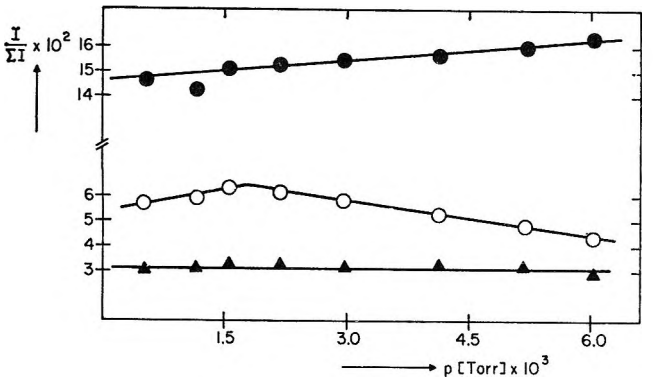

Figure 2. Ion fraction of primary ions as a function of ion-source pressure at 1.0-μsec delay time: ●, m/e 43; ⊙, m/e 30; ▲, m/e 31.

reactions even though some reactions are energetically feasible. Although not shown in Figures 1 and 2, the same is true of SiH^+ (m/e 29) and Si^+ (m/e 28). The behavior of m/e 43, which we have chosen to write as CH_3Si^+, points to it being formed by some ion–molecule reaction in the system, but we have not been able to identify the reaction involved. We can say, however, that if m/e 43 is the same ion as that formed by electron impact on CH_3SiH_3 (at threshold), there are no reactions of CH_3SiH^+ or SiH_2^+ ions in their ground states that can produce it that are energetically feasible.

The behavior of the ion fraction of SiH_2^+ (m/e 30), shown in Figure 2, is complex, at first increasing with source pressure but then reaching a maximum and thereafter decreasing with increasing source pressure. Since SiH_2^+ is the only reactant ion in SiH_4 we might expect it also to be reactive on collision with CH_3SiH_3. This is borne out by the decrease in ion fraction of SiH_2^+ (m/e 30) at pressures higher than $\sim 1.5 \times 10^{-3}$ Torr. The complex behavior, already noted, while not producing a sharp maximum, is real and is most easily attributed to SiH_2^+ being not only a reactant ion but also being produced by an ion–molecule reaction in the system. This can be shown (and some information concerning the relative values of the rate constants for the formation and destruction of SiH_2^+ derived) as follows.

Since the only reactant ion other than SiH_2^+ is CH_3SiH^+, we shall assume that SiH_2^+ is formed by reaction of CH_3SiH^+ with CH_3SiH_3. Thus, consider the sequence

$$CH_3SiH^+ + CH_3SiH_3 \longrightarrow SiH_2^+ + (CH_3)_2SiH_2 \quad (12)$$

$$SiH_2^+ + CH_3SiH_3 \longrightarrow \text{products} \quad (13)$$

In terms of ion fractions, X_{30} for SiH_2^+ and X_{44} for CH_3SiH^+, we may write the rate equations

$$\frac{dX_{30}}{dt} = (k_{12}X_{44} - k_{13}X_{30})[M] \quad (14)$$

$$\frac{dX_{44}}{dt} = -k_tX_{44}[M] \quad (15)$$

where $[M]$ is the number density of CH_3SiH_3 molecules, k_t is the sum of the rate constants for CH_3SiH^+ disappearance, k_{12} and k_{13} are the specific reaction rates for (12) and (13), respectively, and t is the time. Integrating (15), denoting the initial ion fraction of CH_3SiH^+ as X_{44}°, and substituting into (14) yields

$$\frac{dX_{30}}{dt} + k_{13}[M]X_{30} = k_{12}X_{44}^\circ[M]e^{-k_t t[M]} \quad (16)$$

Solution of this equation with the condition that at $t=0$, $X_{30}=X_{30}^\circ$, yields

$$X_{30} = X_{30}^\circ e^{-k_{13}t[M]} - \left(\frac{k_{12}X_{44}^\circ}{k_t - k_{13}}\right)(e^{-k_t t[M]} - e^{-k_{13}t[M]}) \quad (17)$$

Now, at the delay times (or reaction times)[7,8,10,11,13] and ion-source pressures used in this study, the maximum value of the argument of any of the exponentials is ~ 0.3. Hence, with very little error ($\sim 0.04\%$) we may expand the exponentials in (17), and neglect all powers of $(t[M])$ higher than the second. This is easily shown to yield

$$\frac{X_{30}}{X_{30}^\circ} = 1 + t\left(\frac{X_{44}^\circ}{X_{30}^\circ}k_{12} - k_{13}\right)[M] + \frac{t^2}{2}\left[k_{13}^2 - \frac{X_{44}^\circ}{X_{30}^\circ}k_{12}(k_t + k_{13})\right][M]^2 \quad (18)$$

an equation that is a power series in $[M]$ for a constant reaction time t. Such a situation obtains for the data in Figures 1 and 2, since in those experiments a constant delay time (field-free reaction time) of 1.0×10^{-6} sec was used. The derivatives of (18) with respect to $[M]$ are shown in (19) and (20).

$$\frac{d\left(\frac{X_{30}}{X_{30}^\circ}\right)}{d[M]} = t\left(\frac{X_{44}^\circ}{X_{30}^\circ}k_{12} - k_{13}\right) + t^2\left[k_{13}^2 - \frac{X_{44}^\circ}{X_{30}^\circ}k_{12}(k_t + k_{13})\right][M] \quad (19)$$

$$\frac{d^2\frac{X_{30}}{X_{30}^\circ}}{d[M]^2} = t^2\left[k_{13}^2 - \frac{X_{44}^\circ}{X_{30}^\circ}k_{12}(k_t + k_{13})\right] \quad (20)$$

The sign of the second derivative (20) is independent of $[M]$ and since a maximum is observed it must be always negative. This requires

$$\frac{X_{44}^\circ}{X_{30}^\circ}k_{12}(k_t + k_{13}) > k_{13}^2 \quad (21)$$

and, for a maximum, we must have, by setting the first derivative to zero, the result given in (22), namely

$$t[M] = \frac{\left(\frac{X_{44}^\circ}{X_{30}^\circ}\right)k_{12} - k_{13}}{\left(\frac{X_{44}^\circ}{X_{30}^\circ}\right)k_{12}(k_t + k_{13}) - k_{13}^2} \quad (22)$$

Since t and $[M]$ are positive quantities, the inequality (21) requires for the observed maximum the condition expressed by

$$\left(\frac{X_{44}^\circ}{X_{30}^\circ}\right)k_{12} > k_{13} \quad (23)$$

From the nature of the functions comprising numerator and denominator of (22) it is easily shown that if (23) is obeyed, then so is (21). Therefore, a maximum in the plot of the ion fraction of SiH_2^+ *vs.* source pressure is possible if (23) is obeyed. This is a very reasonable condition, since the ratio $X_{44}^\circ/X_{30}^\circ \sim 3$; also since CH_3SiH^+ is the only other observed reactant, the occurrence of reactions such as (12) and (13) is strongly suggested.

In principle, the initial slope and the position of the maximum of the SiH_2^+ curve could be used to calculate k_{12} and k_{13}, since k_t is known from the decay with pressure of the ion fraction of CH_3SiH^+. However, such a treatment leads to computations involving small differences between numbers of poor precision and cannot be considered as giving meaningful results. Thus, although we are confident such reactions are occurring, we are unable to evaluate specific reaction rates of (12) and (13).

B. Effect of Pressure on Secondary Ion Intensities. Numerous products other than $CH_3SiH_2^+$ and SiH_2^+ are observed and appear at m/e values of 58–61, 69–75, and 84–89. Plots of the ion fractions of the most abundant of these products as a function of the ion-source pressure are shown in Figure 3. With the exception of those in the 58–61 range, the m/e value of

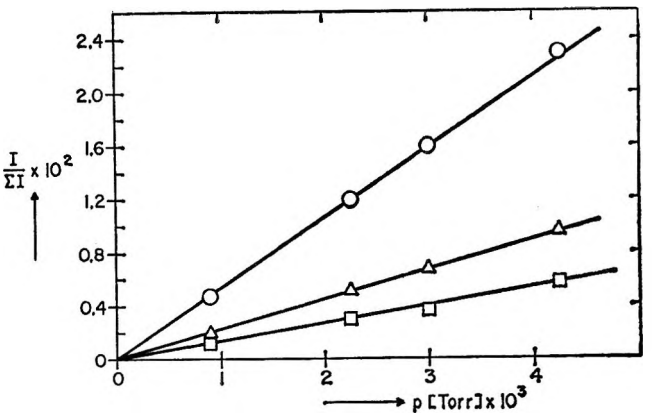

Figure 3. Ion fractions of secondary ions as a function of ion-source pressure at 1.0-μsec delay time: ⊙, m/e 59; △, m/e 72; □, m/e 88.

these product ions is sufficient to identify uniquely its stoichiometric nature, although of course not its structure. For convenience, we assign to the product ions structures based on chemical intuition, on the fact that C–H bonds are generally stronger than SiH bonds,[15–19] and on the assumption that the reaction involving the least atomic rearrangement is the most probable. The assumed product ions are given in Table II, but the arbitrary nature of their implied structure should be borne in mind.

In the case of product ions with m/e values in the 58–61 range, even the stoichiometric nature is ambiguous, although in some cases energetics may be invoked to rule out certain possibilities. The product ion having m/e 58, for example, could be either $(CH_3)_2Si^+$ or $Si_2H_2^+$. If this product arises from CH_3SiH^+, the most favorable reactions, energetically speaking, must be

$$CH_3SiH^+ + CH_3SiH_3 \longrightarrow (CH_3)_2Si^+ + SiH_4 \quad (24a)$$
$$CH_3SiH^+ + CH_3SiH_3 \longrightarrow Si_2H_2^+ + 2CH_4 \quad (24b)$$

So far as is known energetically,[12,23] both are exothermic processes, (24a) by 25 kcal and (24b) by 8 kcal. Reaction 24c, which is 8 kcal exothermic, would also explain the product ion of m/e 58. Although we cannot

$$SiH_2^+ + CH_3SiH_3 \longrightarrow Si_2H_2^+ + CH_4 + H_2 \quad (24c)$$

be sure, we favor (24a) on the basis that it involves the least atomic rearrangement.

In the case of the product with m/e 59, the formation reactions could be either (25a), (25b), or (25c).

$$CH_3SiH^+ + CH_3SiH_3 \longrightarrow (CH_3)_2SiH^+ + SiH_3 \quad (25a)$$
$$CH_3SiH^+ + CH_3SiH_3 \longrightarrow Si_2H_3^+ + CH_4 + CH_3 \quad (25b)$$
$$SiH_2^+ + CH_3SiH_3 \longrightarrow Si_2H_3^+ + CH_3 + H_2 \quad (25c)$$

Table II: Ion–Molecule Reactions and Rate Constants in CH_3SiH_3

Product m/e	Reaction assigned	$k \times 10^{10}$, cm³ molecule⁻¹ sec⁻¹
45	$CH_3SiH^+ + CH_3SiH_3 \longrightarrow CH_3SiH_2^+ + CH_3SiH_2$[a]	6.4 ± 1.3
58	$\longrightarrow (CH_3)_2SiH^+ + SiH_4$	0.44 ± 0.09
59	$\longrightarrow (CH_3)_2SiH^+ + SiH_3$	3.8 ± 0.8
69	$\longrightarrow Si_2CH^+ + CH_4 + 2H_2 + H$	0.19 ± 0.06
70	$\longrightarrow Si_2CH_2^+ + CH_4 + 2H_2$	0.14 ± 0.04
71	$\longrightarrow Si_2CH_3^+ + CH_3 + 2H_2$	0.42 ± 0.13
72	$\longrightarrow CH_3Si_2H^+ + CH_4 + H_2$	1.5 ± 0.3
73	$\longrightarrow CH_3Si_2H_2^+ + H_2 + CH_3$	1.0 ± 0.2
74	$\longrightarrow CH_3Si_2H_3^+ + CH_4$	0.46 ± 0.09
75	$\longrightarrow CH_3Si_2H_4^+ + CH_3$	0.22 ± 0.04
84	$\longrightarrow CH_3Si_2CH^+ + 3H_2$	0.13 ± 0.04
85	$\longrightarrow CH_3Si_2CH_2^+ + 2H_2 + H$	0.25 ± 0.08
86	$\longrightarrow (CH_3)_2Si_2^+ + 2H_2$	0.46 ± 0.09
87	$\longrightarrow (CH_3)_2Si_2H^+ + H_2 + H$	0.36 ± 0.07
88	$\longrightarrow (CH_3)_2Si_2H_2^+ + H_2$	0.92 ± 0.18
89	$\longrightarrow (CH_3)_2Si_2H_3^+ + H$	0.52 ± 0.10
		$\Sigma k_i = 17.2 \pm 1.6$
60	$SiH_2^+ + CH_3SiH_3 \longrightarrow Si_2H_4^+ + CH_4$	0.85 ± 0.25
61	$SiH_2^+ + CH_3SiH_3 \longrightarrow Si_2H_5^+ + CH_3$	0.41 ± 0.12

[a] The rate constant of this reaction has been calculated as if no contribution were made to the formation of $CH_3SiH_2^+$ by reaction of SiH_2^+ with CH_3SiH_3. Such contribution is likely.

Since (25a) is exothermic by 23 kcal and involves much less rearrangement that (25b) or (25c) which, moreover, are endothermic by 7 kcal, we strongly favor (25a) as the process responsible for the formation of m/e 59.

We believe that the product with m/e 60 is $Si_2H_4^+$, because the reaction forming $(CH_3)_2SiH_2^+$ would be ~20 kcal endothermic and therefore very improbable. At the same time, formation of $Si_2H_4^+$ on collisions of CH_3SiH^+ and SiH_2^+ with CH_3SiH_3 could be 16 and 32 kcal exothermic, respectively; we are unable to choose between these alternative routes for formation of $Si_2H_4^+$ (m/e 60).

The product ion at m/e 61 is believed to be $Si_2H_5^+$ since both (26a) and (26b) are exothermic by 10 and 20 kcal, respectively. On the other hand, for the formation of $(CH_3)_2SiH_3^+$ to be energetically feasible it is required that the proton affinity of CH_3SiH_3 be about equal to that of H_2O. This latter possibility is so unlikely as to permit ruling it out. On the basis of the process with the least atomic rearrangement being more probable, we favor (26b) as the source of m/e 61, but we really cannot rule out (26a).

$$CH_3SiH^+ + CH_3SiH_3 \longrightarrow Si_2H_5^+ + C_2H_5 \quad (26a)$$

$$SiH_2^+ + CH_3SiH_3 \longrightarrow Si_2H_5^+ + CH_3 \quad (26b)$$

Some comment about the nature of the possible reactions of SiH_2^+ in this system is warranted. We have examined the product distribution in mixtures of SiD_4 and CH_3SiH_3 and we find that there is no change in distribution (no deuterated products appear) in the 69–75 and 84–89 regions. This means that SiH_2^+ produces on reaction with CH_3SiH_3 only products in the mass region of primary ions and in the m/e 58–61 range. For products in the mass region of primary ions the most likely reactions are those of H^- and H_2^- abstractions from CH_3SiH_3, as shown by (27) and (28). Reaction 27 would only contribute to formation of m/e 45 while (27) would be unobservable, since CH_3SiH^+ is the principal reactant ion in the system. We believe, therefore, that the reactions of SiH_2^+ with CH_3SiH_3 are restricted to (26b), (27), (28), and the reaction shown in Table II that forms $Si_2H_4^+$.

$$SiH_2^+ + CH_3SiH_3 \longrightarrow CH_3SiH_2^+ + SiH_3; \quad \Delta H = -11 \text{ kcal} \quad (27)$$

$$SiH_2^+ + CH_3SiH_3 \longrightarrow CH_3SiH^+ + SiH_4; \quad \Delta H = -11 \text{ kcal} \quad (28)$$

C. Appearance Potentials of Secondary Ions. We have measured the appearance potentials of the product ions having m/e values of 59 and 72. In agreement with our conclusions from the pressure-dependence studies, we find that the appearance potentials of these product ions are, within experimental error, identical with the appearance potentials of CH_3SiH^+ (Table I). We assume the preceding statement applies to all the product ions observed, but we have not made the measurements.

D. Specific Reaction Rates. As described in detail previously,[7,8] the slopes of the straight lines found in plots of ion fraction *vs.* ion-source pressure at constant delay time (reaction time) are proportional to this delay time. If then, such plots as in Figures 1–3 are made for various delay times and the slopes plotted

vs. delay time, a final straight line is obtained whose slope contains the specific reaction rate for ions of thermal kinetic energy (70° in this work). The reactions assigned to the various products, and the reaction rate constants determined, are given in Table II. Comparison of the rate constant for the disappearance of CH_3SiH^+ (1.4×10^{-9} cm^3 molecule^{-1} sec^{-1}) with the sum of the rate constants for product formation *via* CH_3SiH^+ reactions indicates that the reactions of CH_3SiH^+ account for about 80% of the product formation. This mass-balance discrepancy indicates that some other ion is reacting in the system. As discussed already, from our pressure-dependence studies we have concluded that this ion is SiH_2^+, although we are not able to measure all the rate constants of its reactions.

E. Energetics. The mass-spectrometric observation of (11), especially with such a large specific reaction rate, leads immediately to the conclusion that the enthalpy change of this reaction is at most zero. With this conclusion, and the assumption that the reaction is indeed as we have written it, we may easily derive the limit: $D(CH_3SiH_2\text{-}H) \leqslant 94$ kcal/mol, a value consistent with the observed silicon–hydrogen bond dissociation energy in monosilane.[15,27] Combining this with the appearance potential of $CH_3SiH_2^+$ (Table I) we find the limit $I_z(CH_3SiH_2) > 7.7$ eV, a value consistent with reported estimates of the ionization potentials of SiH_3[17] and $(CH_3)_3Si$[19] radicals.

Acknowledgmdnt. This work was supported by the United States Atomic Energy Commission under Contract No. AT(30-1)-3570. We also wish to thank the National Science Foundation for providing funds to assist in the original purchase of the mass spectrometers. This is Atomic Energy Commission Document No. NYO-3570-12.

(27) F. E. Saalfeld and H. J. Svec, *Inorg. Chem.*, 3, 1442 (1964).

Effect of Association with Phenol on Rotation around the (Thio) Carbonyl-to-Nitrogen Bond in an Amide and a Thionamide

by T. H. Siddall, III, E. L. Pye, and W. E. Stewart

E. I. du Pont de Nemours and Company, Savannah River Laboratory, Aiken, South Carolina 29801 *(Received May 19, 1969)*

The effect of added phenol on rotation around the carbonyl-to-nitrogen bond in N-methyl-N-benzyl *o*-chlorobenzamide and in its thio analog in *o*-dichlorobenzene is reported. A model to account for the observed effects is proposed. Quantitative data are reported for the first time for the rate of rotation around the benzene-to-carbonyl bond.

Introduction

The entropy of activation (ΔS^*) is now known to be small, at most a few eu for rotation around the carbonyl-to-nitrogen (amide) bond in amides.[1-6] It now appears certain that there are solvent effects on the rate of rotation around this bond. Chupp and Olin[6] demonstrated that the free energy of activation (ΔF^*) for rotation is about 1 kcal larger in more polar solvents. Earlier work that seemed to demonstrate solvent effects, even on ΔS^* and ΔH^* (the enthalpy of activation), must be viewed with some reserve. There are likely systematic errors in the signal shape analysis used to obtain the rotational rates from proton magnetic resonance (pmr) data.

The small entropy of activation seems to contradict the increased values of ΔF^*. The polar ground state would be more stabilized by greater association with more polar solvents than would the *comparatively* nonpolar transition state for rotation. At the same time, however, the smaller association in the transition state should lead to a significant increase in entropy as compared to the more polar ground state.

The most important purposes of the study were (a)

(1) H. S. Gutowsky, J. Jonas, and T. H. Siddall, III, *J. Amer. Chem. Soc.*, 89, 4300 (1967).

(2) J. A. Weil, A. Blum, A. H. Heiss, and J. K. Kinnard, *J. Chem. Phys.*, 46, 3132 (1967).

(3) A. Mannschreck, A. Mattheus, and G. Rissmann, *J. Mol. Spectrosc.*, 23, 15 (1967).

(4) R. C. Neumann and J. Jonas, *J. Amer. Chem. Soc.*, 90, 1970 (1968).

(5) A. Pines and M. Rabinovitz, *Tetrahedron Lett.*, 3529 (1968).

(6) J. C. Chupp and J. F. Olin, *J. Org. Chem.*, 32, 2297 (1967).

to demonstrate, if possible, the apparent contradiction between small ΔS^* and appreciable solvent effect on ΔF^* and (b) if this contradiction were demonstrated, to provide at least a conceptual basis for resolving this contradiction. This conceptual basis then might lead to still further experimental testing and a detailed kinetic model at a later time.

This paper reports such a study of solvent effects on rotational rates around the amide bond in an amide

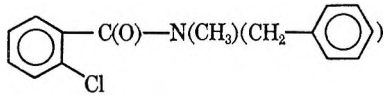

I

and the analogous thionamide

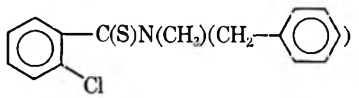

II

These compounds were chosen because of their convenient rotational rates. One pure isomer of each always separates out (in our experience) when these compounds are crystallized. Thus, rotational rates could be measured at low temperature by monitoring the equilibration of the dissolved crystals.

The rotational rates could also be obtained at 100° higher by pmr signal shape analysis. Measurements over such an extended range should yield much more reliable values for ΔS^* than those obtained by either technique alone.[7]

Varying mixtures of phenol and *o*-dichlorobenzene were chosen as the solvent. The *o*-dichlorobenzene has a liquid range (−18 to +179°) that is wide enough for the study, while being a good solvent for the amides and yet being *comparatively* inert at least as compared to phenol or even chloroform. Phenol is known to associate strongly with many amides[8] and should provide strong solvent effects as it is added to the solution. As a demonstration that phenol interacts strongly with the particular amide (I) chosen for this study, the association of phenol with I and II was measured by an infrared technique.

The *ortho* substitution[9-11] of chlorine in these benzamides makes rotation observably slow around the benzene-to-(thio) carbonyl bond also. As an aside to the main investigation, the rotational rates around this bond in I were estimated from pmr signal shape analysis and a lower limit set for this process in II. These are given here as the first report of quantitative measures of this particular rotational process.

Experimental Section

The amides were prepared in a conventional way

$$RC(O)Cl + (R_1)(R_2)NH \xrightarrow[CH_2Cl_2]{Et_3N} RC(O)N(R_1)(R_2) + Et_3N\cdot HCl$$

They were then washed with water and sodium carbonate solution, the solvent evaporated, and the amide crystallized several times. The thionamide was prepared from the amide by adding 100% excess P_2S_5 to the amide and refluxing in xylene for a few minutes and was purified in the same manner as the amides. Both compounds gave correct pmr and ir spectra, free of signals from impurities.

Samples for signal shape analysis were sealed under nitrogen. The *o*-dichlorobenzene and also stock solutions of phenol in *o*-dichlorobenzene were passed through a molecular sieve before use. The phenol concentration in the stock solutions, after sieve treatment, was determined both from ultraviolet absorption and by integrating the OH pmr signal against the signal from cyclohexane that was weighed into samples of the stock solutions. Equilibration of the separated isomer (the more abundant isomer in both cases) was performed as previously described.[7] All nmr measurements were made with a Varian A-60 spectrometer that was equipped with the variable temperature probe. Temperatures were measured by using the methanol and glycol "thermometers" that were supplied with the probe. The response of the thermometers was calibrated against a thermocouple. Pmr spectra for I and II are given in Figure 1.

Signal shape analysis was done only in the central region of intermediate exchange, where the method is least sensitive to error. For studies of rotation around the amide bond, the N-methyl signals were used. These signals are not directly affected by the other rotational process, rotation around the benzene-to-carbonyl bond. The CH_2 signals of the $CH_2C_6H_5$ group were used to follow the rotation around the benzene-to-carbonyl bond. In the limit of slow exchange for this process, the CH_2 signals in both amide isomers ($CH_2C_6H_5$ *cis* to oxygen or sulfur and $CH_2C_6H_5$ *trans*) are AB quartets. These quartets coalesce into singlets in I as the temperature is raised and rapid rotation around this bond causes the protons within the methylene (CH_2) group to become equivalent on the pmr time scale. The coalescence for I is complete at temperatures well below the intermediate exchange region for rotation around the amide bond. The signal shape analysis was done by visually matching experimental with calculated spectra. For the N-methyl signals, Nakagawa's formulation[12] of the

(7) T. H. Siddall, III, and W. E. Stewart, *J. Phys. Chem.*, **73**, 40 (1969).

(8) T. Gramstad and W. J. Fluglevik, *Acta Chem. Scand.*, **16**, 1369 (1962).

(9) G. R. Bedford, D. Greatbanks, and D. B. Rogers, *Chem. Commun.*, 2387 (1966).

(10) T. H. Siddall, III, and R. H. Garner, *Tetrahedron Lett.*, 3513 (1966).

(11) T. H. Siddall, III, and R. H. Garner, *Can. J. Chem.*, **44**, 2837 (1966).

(12) T. Nakagawa, *Bull. Chem. Soc. Jap.*, **39**, 1006 (1966).

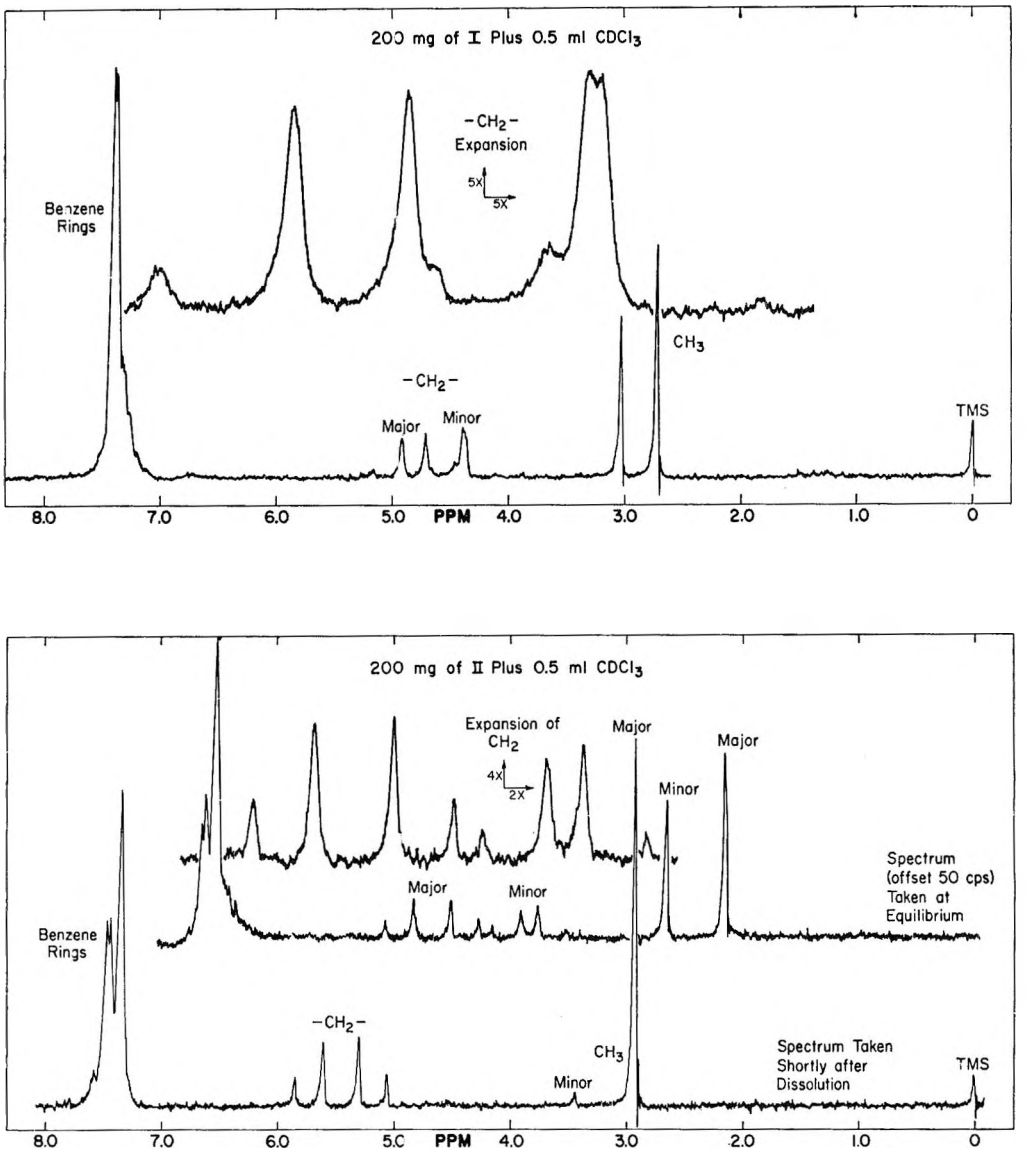

Figure 1. Pmr spectra at −13°.

Gutowsky–Holm equation[13] was used to obtain calculated spectra. The calculated spectra for the AB quartets were obtained according to Heidberg.[14]

The infrared results were all based on the fact that the OH stretching absorption of unassociated (with amide) phenol occurs as a separate, well resolved band[8] and therefore provides a quantitative measure of uncomplexed (free) phenol. The concentrations of free and complexed amide and of complexed phenol could be estimated from solution makeup. The response to phenol concentration was calibrated over the whole temperature range with solutions of phenol in *o*-dichlorobenzene of known composition that contained no amide.

All infrared measurements were made with a Perkin-Elmer 521 spectrometer, equipped with a variable temperature cell.

Results

Results from the pmr measurements are given in Tables I and II and from infrared in Figures 2 and 3. The pmr data were obtained at several time intervals, but on fresh solutions, over a period of months. This happened to have been done as a matter of convenience, but also gives an estimate of the experimental accuracy as opposed to experimental precision. This is a particularly important distinction in signal shape analysis. Both spectrometer performance and also the temperature control in the variable temperature probe tend to be much more reproducible over a single continuous run of experiments than between series of experiments

(13) H. S. Gutowsky and C. H. Holm, *J. Chem. Phys.*, **25**, 1228 (1956).

(14) J. Heidberg, J. A. Weil, G. A. Janusonis, and J. K. Anderson, *ibid.*, **41**, 1033 (1964).

Table I: Kinetic Data

Sample	Composition, mol/l Amide	Phenol	T, °C	ΔF^*, kcal/mol
1	0.64	0	−10	18.5, 18.9
2	0.61	0.61	−13	19.3, 19.7
3	0.62	0.80	−13	19.3, 19.6
4	0.64	0.42	−13	19.0, 19.3
5	0.50	0.80	−2	19.7, 19.9
6	0.62	2.8	13	20.9, 21.1
7	0.60	0	84	18.8, 19.1
			91	18.8, 19.1
8	0.70	0	83	18.3, 18.5
			98	18.2, 18.4
9	0.60	0.44	91	19.1, 19.3
10	0.64	0.42	95	19.0, 19.3
			102	19.0, 19.4
11	0.62	0.47	84	19.6, 19.9
			91	19.6, 19.9
12	0.55	0.80	91	19.4, 19.8
13	0.62	0.80	95	19.3, 19.6
			102	19.3, 19.6
14	0.62	2.8	111	20.5, 20.8
			121	20.6, 20.9
15	0.62	0	97	18.4, 18.7
			106	18.5, 18.8
			111	18.6, 18.9
16	0.62	0.80	97	19.3, 19.6
			106	19.5, 19.8
			111	19.1, 19.4
17	0.62	2.8	97	21.0, 21.3
			106	20.7, 21.0
			111	20.5, 20.8
18	0.64 amide, 0 phenol in $CDCl_3$		−27	19.1, 19.3
	Thionamide	Phenol		
16	0.60	0	49	23.5, 23.7
17	0.60	0.55	50	23.7, 23.9
18	0.60	2.5	53	24.5, 24.7
19	0.60	0	162	23.9, 24.2
			173	23.6, 23.9
20	0.60	0.55	162	24.2, 24.5
			173	24.0, 24.3
21	0.60	2.5	162	25.0, 25.3
			173	24.3, 24.6
22	0.60 amide, 0 phenol in $CDCl_3$		53	23.7, 23.9

performed at widely different times. With temperature control set and flow of nitrogen left alone, ΔF^* measurements reproducible to within 0.2 kcal can be achieved routinely. However, an attempt to return to identical conditions at a later time does not give such good precision.

We achieved a precision of ±0.2 kcal by obtaining signal shapes for each of a series of samples and then repeating measurement on the first of the series immediately. For example, samples 7 and 11 were paired in this way at 84 and 91° and then combined with no. 14 in a series at 111°. Samples 15, 16, and 17 form such a series run at another time. It is for this reason that we can be certain that differences between samples 7, 11, and 14 are real on the one hand and between 15, 16, and 17 on the other, even down to an uncertainty of about 0.2 kcal/mol in ΔF^*. However, sample 8 *vs.* 7 and 9 *vs.* 11 differ by about 0.5 kcal. This comparison, for samples run at different times, is not nearly so "nice" as for samples run in a series. At low temperature, samples 3 and 4 were run the same day with no adjustment of temperature controls between work with the samples. We are inclined to believe, for that reason, that the rotation is really slower in 3 than in 4. However, the observed disparity between samples 3 and 5, very similar solutions, is even greater than between 3 and 4 and yet must not be real. The effect of phenol as measured for sample 6 is so large that it is most certainly real, even though it was run at a different time than the comparison samples.

Although the causes of these errors are not known in detail, it is obvious that the ±2° temperature control claimed for the nmr variable temperature probe must be *the* major source of error (about ±0.2 kcal in ΔF^*) for the equilibration experiments at low temperature. The exact spectrometer performance should be far less critical, subject to normal precautions. Precision in integrating signals is certainly at least as good as 10% with strong signals.

The error at high temperature is more complex. In addition to the temperature error, spectrometer performance and all the assumptions that go into the signal shape analysis must be included. We estimate the error to be ±0.4 kcal based on many signal shape experiments done in this laboratory over an extended period of time. Errors of these magnitudes, at high and low temperatures, combine to give an uncertainty of about 0.5 kcal in ΔH^* and about 5 eu in ΔS^*. These error estimates are based on the simple technique of drawing a scatter of straight lines through the extremes in scatter of data. This should overestimate the error. Alternatively there is a simple way of estimating the error analytically. For example, the difference in ΔF^* at 0 and 100° is

$$|\Delta F^*_{100} - \Delta F^*_0| = |100\Delta S^*|$$

or the error in ΔS^* is

$$100\sigma_{\Delta S^*} = \sqrt{(\sigma_{\Delta F^*,100})^2 + (\sigma_{\Delta F^*,0})^2}$$

$$\sigma_{\Delta S^*} = \frac{1}{100}\sqrt{(400)^2 + (200)^2}$$

$$= \frac{1}{100}\sqrt{20 \times 10^4}$$

$$= \frac{450}{100} = 4.5 \text{ eu}$$

But this simple computation makes no allowance for replication.

Table II: Summary of Kinetic Data for the Amide

Average composition, mol/l		Low temperature (−13°)					High temperature (100°)		
			$\Delta F^* - \Delta F^*_0$, kcal/mol		ΔS^*, eu			$\Delta F^* - \Delta F^*_0$, kcal/mol	
Amide	Phenol	ΔF^*, kcal/mol	Calcd	Obsd	Calcd	Obsd	ΔF^*, kcal/mol	Calcd	Obsd
0.6	0.0	18.5, 18.9	...	...	...	0	18.5, 18.8	...	...
0.6	0.4	19.0, 19.3	1.7	0.5	+9	−3	19.3, 19.6	0.7	0.8
0.6	0.8	19.5, 19.7	1.8	0.9	+9	−1	19.5, 19.9	0.8	1.1
0.6	2.8	20.9, 21.1	2.2	2.4	+12	+3	20.5, 20.8	1.0	2.0

$$\therefore \sigma_{\Delta S^*} < 4.5 \text{ eu or } < \sim 5 \text{ eu}$$

On this basis, our observation that $\Delta S^* \leq 3$ eu (Table II) as compared to a calculated value of about 10 eu is quite significant. The small experimental values for ΔS^* are significantly different from the values predicted from the model in the discussion section. However, a discrimination that requires finer detail than about 5 eu will require improved accuracy, especially in signal shape analysis at high temperature.

The accuracy of the infrared results is not so pertinent to the main purposes of this study. The estimated errors in ΔH are given in Figures 2 and 3. These results do establish beyond any question that I and II are "normal" in their ability to associate with phenol. In fact, their behavior is quite similar to amides of simpler structure.

A Model for the Rotational Process

The effect of added phenol can be used to test a model—one which seems to us to be the most obvious.

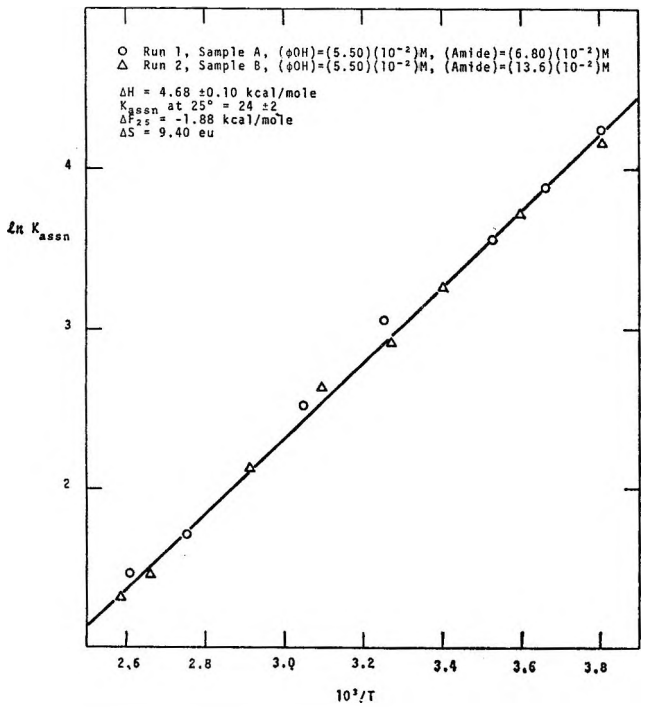

Figure 2. Association constants for N-methyl,N-benzyl-*o*-chlorobenzamide and phenol in *o*-dichlorobenzene.

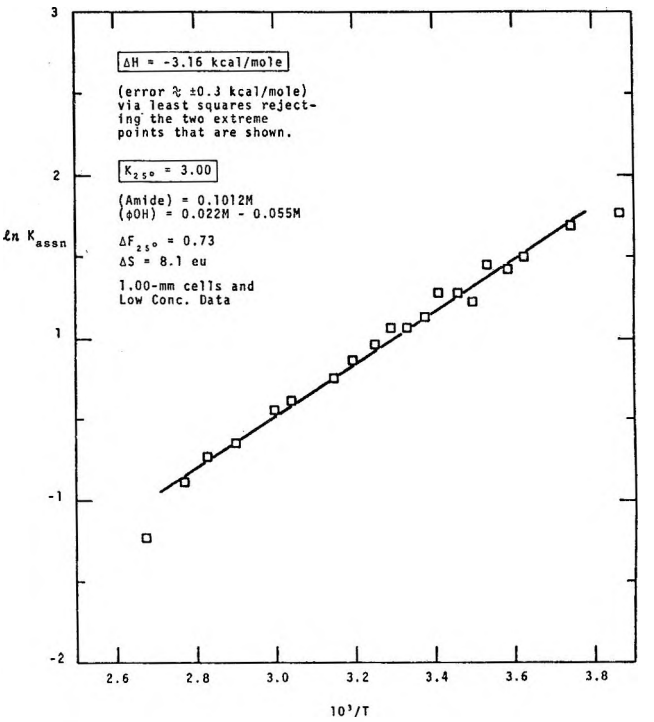

Figure 3. Association constants for N-methyl,N-benzyl-*o*-chlorothiobenzamide and phenol in *o*-dichlorobenzene.

This model assumes (1) that $\Delta S^* = 0$ for *o*-dichlorobenzene solutions with no phenol present and (2) that the association of phenol with the amide transition state is negligible. With phenol present, there are two kinetic routes. The first route (rate constant = k_1) is *via* rotation within free amide molecules. The second route (k_2) is *via* the combination of events—rotation in the associated amide molecule and separation into transition state plus phenol. Then when a = the concentration of unassociated amide, A = the total concentration of amide (subscript zero is for kinetic quantities with no phenol present), and $-\Delta F_a$ = the free energy of association of amide and phenol

$$k_1 = \frac{a}{A} k_0 = \frac{a}{A}\{2.08 \times 10^{10}\, Te^{-\Delta F^*_0/RT}\}$$

$$k_2 = 2.08 \times 10^{10} Te^{-(\Delta F^*_0 + \Delta F_a/RT)}$$

and

$$k \text{ (the observed rate)} = 2.08 \times 10^{10} Te^{-\Delta F^*/RT}$$

but also

$$k = k_1 + k_2$$

therefore

$$e^{-\Delta F^*/RT} = (a/A + e^{-\Delta F_a/RT})(e^{-\Delta F^*_0/RT})$$

In the limit of high phenol concentration as a/A goes to zero, the observed ΔF^* approaches ΔF^*_0 (no phenol) plus ΔF_a (the negative of the free energy of association).

Now at temperatures T_1 and T_2, in this limit

$$\Delta F_1^* - \Delta F_2^* = \Delta F_{a_1} - \Delta F_{a_2}$$

but

$$\Delta F_1^* - \Delta F_2^* = \Delta S^*(T_2 - T_1)$$

or in the limit of high phenol concentration

$$\Delta S^* = \frac{\Delta F_{a_1} - \Delta F_{a_2}}{T_2 - T_1}$$

but

$$\Delta F_{a_1} - \Delta F_{a_2} = (T_1 - T_2)\Delta S_a$$

or

$$\Delta S^* = -\Delta S_a = 9.4 \text{ eu}$$

This analysis assumes that the experimental equilibrium constants for association and derived quantities are applicable at high phenol concentration. This neglect of activity coefficients can affect the analysis. $\Delta S^* = 9.4$ eu must be regarded as a representative value, not as the absolutely correct value.

At lower phenol concentration, $\Delta F^*_0 - \Delta F^*$ must be calculated from the relationship

$$\Delta F^*_0 - \Delta F^* = RT \ln (a/A + e^{-\Delta F_a/RT})$$

Comparison With Experiment

The kinetic data for the amide, I, are summarized in Table II. Data for solutions of near the same composition have been averaged together to give four sets of data. The calculated and observed $\Delta F^* - \Delta F^*_0$ and entropies are listed.

It is immediately obvious that the observations in no way agree with the model. One obvious modification to the model is not adequate. This modification allows the transition state to also be associated with phenol, though to a lesser extent than the ground state. In the transition state, there is certainly less and possibly no contribution of the dipolar resonance form (B) to the molecular description. The transition

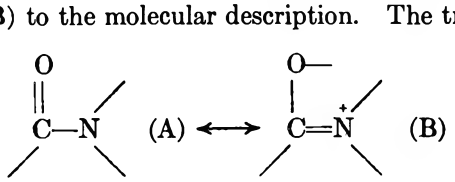

state must be substantially nonplanar as compared to the near planar ground state with a near maximum contribution from B. Even so, the transition state must be at least about as polar as a ketone. Ketones associate with phenol though less so than amides.[15] A polar transition state improves the prospects of a small ΔS^* because phenol is not necessarily released during the rotation. At the same time, a polar transition state, however realistic, decreases the value of $\Delta F^* - \Delta F^*_0$. The fit of model and observed ΔS^* can be improved but only at the expense of the fit of ΔF^*.

Therefore, an expansion of the conceptual basis for the model seems necessary. These solutions must have phenol–amide interactions over larger domains than simple phenol–amide pairs. The phenol must stabilize the ground state more than indicated by measurement of the strength of this pair relationship alone, as is done by the infrared technique. Within this expanded concept, the shell of surrounding molecules is not disturbed during the time of rotation. There is then no reason to expect any large ΔS^*. The transition state is destabilized relative to the ground state by up to about 2 kcal in the presence of phenol. However, the entropy change between the pairs (amide, phenol–amide*, phenol) is small because of the similarity of the states and is nonexistent in the surrounding structure over the rest of the domain.

The small entropy effect on the shell may be due to (a) the shells being nearly the same on an equilibrium basis for the two states or alternatively (b) the relaxation time of this shell being long compared to the time of the rotational event itself. (The time of the rotational event is, of course, many factors of ten shorter than lifetime of the ground state.)

One key requirement to the expanded model can be tested in an obvious fashion. This experimental test requires an amide and a ketone that distribute between two immiscible solvent phases of quite different polarity. If the ketone is assumed to be an adequate stand-in for the transition state, the distribution measurements should predict approximately the increased barrier for rotation in the more polar solvent as compared to the less polar solvent. We are searching for a satisfactory system.

It is interesting to note that $CDCl_3$ increases the barrier (sample 18), though by only about 0.5 kcal. We have observed similar effects for other amides and similar solvent pairs.

The effects of phenol on II are much less marked and close to our experimental error. However, there does seem to be a small effect—an effect consistent with the smaller association with phenol. These smaller effects suggest that thionamides will not be suitable for model testing.

(15) T. Gramstad, *Spectrochim. Acta*, 19, 497 (1963).

Rotation Around the Benzene-to-(Thio) Carbonyl Bond

For rotation around the benzene-to-carbonyl bond in I in $CDCl_3$, $\Delta F^*(20°)$ = 14.5 kcal/mol for the major isomer and 16 kcal/mol for the minor isomer. The shifts induced by benzene added to $CDCl_3$ solutions[16] yield equivocal results as to isomer assignment. *Both* methyl signals are shifted *downfield*. However, we believe the major isomer places the benzyl group *cis* to oxygen. The chemical shift within the AB quartet is larger for the major isomer because the anisotropic carbonyl group is closer. The barrier is slightly larger in the minor isomer for steric reasons. The $C_6H_5CH_2$ group is "larger" than the methyl group and increases the barrier to rotation when it is *cis* to the *o*-chlorobenzene ring.

The barrier to rotation around this bond in II is at least as large as the barrier around the amide bond itself. As coalescence begins for the N-methyl signals, indicating intermediate exchange for rotation around the amide bond, it also begins for the two AB quartets, but not until then. Perhaps both exchange processes broaden the quartets. Rotation may occur around both of these bonds in a synchronous or sequential manner. The fast exchange region (possibly 200° and above) was not accessible in *o*-dichlorobenzene.

The substantial increase ($\geq$8 kcal/mol) for rotation around this bond in II as compared to I must reflect two effects. Sulfur stiffens the amide framework, as is seen from the larger barrier to rotation around the amide bond. This must be an electronic effect. However, the larger sulfur atom must also make a steric contribution to the increase. The benzene ring is out of the amide plane in the ground state. The presence of the larger sulfur atom, approximately in plane, must increase the barrier.

Acknowledgment. The information contained in this article was developed during the course of work under Contract AT(07-2)-1 with the United States Atomic Energy Commission.

(16) J. V. Hatton and R. E. Richards, *Mol. Phys.*, 3, 253 (1960).

The Use of Differential Reaction Kinetics in Determining Rate Constants of Hydroxyl–Isocyanate Reactions

by Friso Willeboordse

Union Carbide Corporation, Chemicals and Plastics, Bound Brook, New Jersey 08805 *(Received August 11, 1969)*

Two differential reaction rate methods, the graphical logarithmic extrapolation method and the differential pseudo-first-order reaction rate approach, have been applied simultaneously in the kinetic analysis of a reacting system of a polyol and phenyl isocyanate under carefully controlled conditions. The combination of the two methods yields basic information on the reactivities of primary and secondary hydroxyl groups in a variety of polyether and polyester polyols. The approach can be applied to other binary systems of active hydrogen-containing compounds, and is particularly useful for the determination of a reaction rate constant not obtainable by other methods. Rate constants of the reactions between phenyl isocyanate and the primary and secondary hydroxyl groups of model compounds are reported. Ethylene glycol shows the highest reactivity with a rate constant of 3.01×10^{-2} l./mol min. Derivatives of ethylene glycol, diethylene glycol, and triethylene glycol have primary hydroxyl group rate constants ranging from 2.21 to 2.78×10^{-2} l./mol min. The secondary hydroxyl group rate constants are of the order of 0.56 to 0.59×10^{-2} l./mol min. The usefulness of the technique of combining the two differential reaction rate methods is illustrated by a kinetic analysis of several compositions of each of three types of polyols where ethylene oxide and ϵ-caprolactone are the polymerizing moieties forming the primary hydroxyl group, and propylene oxide and ϵ-methyl-ϵ-caprolactone the polymerizing moieties forming the secondary hydroxyl group.

Introduction

The knowledge of reaction rates between polyols and isocyanates, and the study of effect of conditions on these rates, has far-reaching implications in urethane technology. Kinetic information on such a reactive system provides us with a tool to increase or decrease the rate of reaction by varying the conditions employed. By judicious selection of these conditions, *e.g.*, type and composition of reactants, type of catalyst present, temperature, solvent polarity, the reaction rate of any particular species in a mixture may be focused upon for accurate study. Conversely, the kinetic data thus generated yield information to the polymer chemist in his goals of product definition, structure analysis, and ultimately product improvement.

This investigation is concerned with the application of two kinetic methods of analysis, and describes a novel approach by combining the two methods to yield kinetic parameters of a particular system which cannot be obtained in other ways. The isocyanate group containing reactant of the system is a singular species whereas the hydroxyl group containing reactant is mostly a binary mixture of alcohols. This binary mixture consists of either a faster and slower reacting alcohol or a multifunctional polymeric alcohol (polyol) containing both primary and secondary hydroxyl groups.

The kinetics of some model reactions between isocyanates and alcohols has been studied extensively, and various reaction mechanisms have been proposed.[1–10] However, comparatively few investigations have yielded data on the rates of isocyanate–polyol reactions,[11–13] and extremely little has been done to determine the *individual* rates of reaction of the different OH species (primary and secondary hydroxyl groups) with an isocyanate[14] with the objective to obtain a fundamental and conceptual picture of the reactivities with a polyester or polyether polyol molecule.

Experimental Section

Materials. The solvents used in the kinetic experiments were invariably checked for reactivity toward phenyl isocyanate in a blank run. Only if they showed

(1) J. W. Baker and J. B. Holdsworth, *J. Chem. Soc.*, 713 (1947); J. W. Baker and J. Gaunt, *ibid.*, 9, 19, 27 (1949).

(2) E. Dyer, H. A. Taylor, S. J. Mason, and J. Sampson, *J. Amer. Chem. Soc*, 71, 4106 (1949).

(3) M. E. Bailey, V. Kirss, and R. G. Spaunburg, *Ind. Eng. Chem.*, 48, 794 (1956).

(4) J. Burkus and C. F. Eckert, *J. Amer. Chem. Soc.*, 80, 5948 (1958).

(5) M. Sato, *ibid.*, 82, 3893 (1960).

(6) W. G. P. Robertson and J. E. Stutchbury, *J. Chem. Soc.*, 4000 (1964); J. N. Greenshields, R. H. Peters, and R. F. T. Stepto, *ibid.*, 5101 (1964).

(7) F. Willeboordse and F E. Critchfield, *Anal. Chem.*, 36, 2270 (1964).

(8) A. Farkas and P. F. Strohm, *Ind. Eng. Chem., Fundam.*, 4, 32 (1965).

(9) D. Benson and N. Fletcher, *Talanta*, 13, 1207 (1966).

(10) S. G. Entelis, O. V. Nesterov, and R. P. Tiger, *J. Cellul. Plastics*, 3, 360 (1967).

(11) K. J. Rauterkus, H. J. Schimmel, and W. Kern, *Makromol. Chem.*, 50, 166 (1961).

(12) H. A. Smith, *J. Appl. Polymer Sci.*, 7, 85 (1963).

(13) H. G. Wissman, L. Rand, and K. C. Frisch, *J. Appl. Polymer Sci.*, 8, 2971 (1964).

(14) F. Willeboordse and R. L. Meeker, *Anal. Chem.*, 38, 854 (1966).

less than 0.4% consumption of the isocyanate in the presence of the catalyst over a period of 2 hr at room temperature were they used for kinetic measurements. The solvents passed this test only after having been purified according to the procedure described below. Toluene (Matheson Coleman and Bell) was redistilled from stannous octoate (catalyst T-9 from M and T Corporation), 100 g per gallon of toluene, and stored in a capped bottle. N,N-Dimethylformamide (Du Pont) was redistilled from Linde Molecular Sieve, Type 5A, under reduced pressure until the water content was less than 0.01% and also stored in a capped bottle. Phenyl isocyanate, reagent grade (Matheson Coleman and Bell), was used fresh. If any crystalline precipitate (dimer and/or trimer) formed, the material was discarded or redistilled under reduced pressure (20 mm) collecting the fraction between 60 and 62°. The alcohols were reagent grade chemicals, and were used without further purification with the exception of the primary and secondary alcohol isomers of the monomethyl ether of dipropylene glycol. From UCAR solvent 2LM, the two isomers were obtained by preparative gas chromatography utilizing a low-temperature (100°) column, 2 m × 1/4 in diameter, of 20% Carbowax 20M on GC-22 Super Support (40/60 mesh). The polyester polyols and polyether polyols were used without further purification after it was ascertained that the water content was less than 0.01%.

The catalyst used in all the kinetic experiments was DABCO, 1,4-diazabicyclo[2.2.2]octane (Houdry Process and Chemical Company), also known as triethylenediamine.

Procedure. The catalyst solution is made by dissolving 4.480 g of DABCO in 200 ml of toluene. The concentration of this solution is 0.200 *M*. The amine content of this solution is checked daily by titrimetric analysis with perchloric acid in glacial acetic acid medium. The catalyst solution can be kept without any detrimental effect for 3–4 days in our experience. The isocyanate reagent solution is prepared by dissolving 10.0 ml (10.95 g) of phenyl isocyanate in 100 ml of toluene. The solution is stable for at least 3 days if stored in the dark, as absorbance measurements will show. The reagent solution is discarded if any crystalline precipitate is formed upon standing. The concentration of this solution is 0.919 *M*.

The procedure is based on following the reaction of the OH group with the NCO group provided by phenyl isocyanate in an anhydrous, binary solvent system consisting of 9:1 (v/v) toluene–DMF, at constant temperature (24.9 ± 0.1°). At regular intervals during the reaction, the isocyanate concentration is determined by measuring the absorbance value of the isocyanate peak in the infrared region. From a predetermined calibration curve, the instantaneous isocyanate concentration can be calculated. Detailed experimental conditions have been described earlier.[14]

Objectives and Evaluation of Test Data

The starting point of this investigation was based on two observations. (a) Rauterkus and coworkers[11] found the reaction rate of the hydroxyl group in poly(oxyethylene) glycols, $HO-(CH_2-CH_2-O)_n-H$, with phenyl isocyanate in dioxane to be independent of the chain length of the oligomer. (b). It was observed in our laboratories[14] that the rate of reaction of the secondary hydroxyl with either acetic anhydride or phenyl isocyanate proved to be a constant for a group of seven widely differing polyether polyols with a molecular weight of about 2000 to about 5000. Table I shows the results obtained for the extrapolated values of the reaction rate constants for the secondary hydroxyl groups in these polyether polyols. Since the use of triethylenediamine as catalyst yields by far the greatest precision in extrapolated k values for polyether polyols, all further kinetic measurements were realized with this catalyst.

The catalyzed urethane reaction shows second-order kinetics in the DMF–toluene binary solvent system.[7] However, the magnitude of the specific rate constants depends generally on the concentration of the reactants[1] as well as specifically on the molar ratio (alcohol)/(catalyst) in this solvent system.[7] In spite of this variability, it has become customary in the literature to report rate data in terms of the "apparent second-order constant." By use of the graphical extrapolation method[15] (GEM) of analyzing second-order reactions, the rate constants of the alcohols and glycols for a catalyst–alcohol ratio was maintained invariably at 1:10, both in the GEM approach as well as in the approach of the method of Roberts and Regan[14,16,17] (MRR). The MRR approach is a pseudo-first-order approximation of an irreversible second-order reaction for simultaneous reactions of two compounds A and B of a binary mixture with a common reagent R. The concentration of R is very much smaller than those of A and B but is to be detected with high sensitivity since the change in concentration of R is followed with time.[14] The MRR approach yields the following expression[14,17]

$$\frac{[A]_0}{[A]_0 + [B]_0} = \frac{\ln\{[R]_t/[R]_0\}}{(k_B - k_A)\{[A]_0 + [B]_0\}t} + \frac{k_B}{k_B - k_A} \quad (1)$$

where k_A and k_B ($k_B > k_A$) are the second-order rate constants of A and B reacting with R; $[A]_0$, $[B]_0$, and

(15) S. Siggia and J. G. Hanna, *Anal. Chem.*, 33, 896 (1961).

(16) J. D. Roberts and C. Regan, *ibid.*, 24, 360 (1952).

(17) H. B. Mark, Jr., and G. A. Rechnitz, "Kinetics in Analytical Chemistry," Interscience Publishers, New York, N. Y., 1968, pp 119–130.

Table I: Rate Constants for Secondary Hydroxyl Group Reactions, $k \times 10^2$, l. mol^{-1} min^{-1}

Alcohol	Av mol wt of polyol	PhNCO reagent, 25° catalyzed[f] by— Stannous octoate	Dibutyltin dilaurate	DABCO
2-Propanol		5.07	2.33	0.918
2-Butanol		5.64	2.45	0.870
NIAX polyol PPG-2025[a]	2010	6.41	2.35	0.528
NIAX polyol LG-56[a]	2890	6.60	2.28	0.529
Voranol CP 3000[b]	2940	6.76		0.521
Actol 31-56[c]	3040	6.43		0.534
Poly-G 4031 PG[d]	3820	6.27		0.539
NIAX polyol LC-45[a]	3950	6.85	2.33	0.537
Pluracol TPE 4542[e]	4700	6.37		0.530
Polyether polyols, average value and standard deviation	2000 to 5000	6.53 ± 0.22	2.59 ± 0.29	0.531 ± 0.007

[a] Union Carbide Corp. [b] Dow Chemical Co. [c] Allied Chemical Co. [d] Olin Mathieson Chemical Corp. [e] Wyandotte Chemicals Corp. [f] Catalyst concentration is 1/200th of alcohol concentration.

$[R]_0$ are the initial concentrations of the two components and the reagent, respectively. $[R]_t$ is the concentration of the reagent at time t.

Equation 1 stipulates that a plot of $1/\{[A_0 + [B_0\}t$ *vs.* $[A]_0/\{[A]_0 + [B]_0\}$, the mole fraction of A, at a given fraction of reagent reacted, $[R]_t/[R]_0$, gives a straight line which can serve as a calibration curve for the determination of the composition of binary systems. Ordinarily, when one deals with binary mixtures of pure compounds, these compositions could be compounded and analyzed. The data points are then plotted in the manner described above to obtain the calibration line. However, when binary mixtures cannot be compounded, the MRR approach cannot be used as is the case with polymeric materials with unknown quantities of primary and secondary hydroxyl groups. Under those circumstances, we have to utilize the data points obtained by the GEM approach. For polymeric hydroxyl compounds, this consists of plotting the logarithm (second-order kinetics) of the total hydroxyl concentration (sum of the primary and secondary OH's) as a function of time.[15] The plot yields a straight line *after* the faster (primary OH) reacting component has completely reacted. The extrapolated intercept at time $t = 0$ equals log $[A]_0$, the initial concentration of the slower reacting component. The value of $[B]_0$ may then be obtained by subtracting $[A]_0$ from the total initial concentration of the hydroxyl groups.

The rate constants for the primary hydroxyl group in the polyether or polyester polyol as well as for the secondary hydroxyl group in the same molecule are obtained by combining the two differential reaction rate methods: the results of the GEM procedure are plotted as abscissa whereas the MRR data are plotted as the ordinate for any particular polymeric compound consisting of two different hydroxyl species. Since the *ratio* of the k values of primary OH reactivity to secondary OH reactivity is about 4 to 5 in polyether and polyester polyols, no limitations for the applicability of both methods appear to exist.[18]

Results

A number of ethylene glycol based model compounds were treated with phenyl isocyanate in the same solvent system. The rate constants for these reactions are reported in Table II. It appears that the diols are more reactive than the monofunctional ethylene glycols. Ethylene glycol exhibits a higher rate constant than the other poly(oxyethylene) glycols of the same oligomer series. However, the rate constants of the other members of the series are not significantly different. The second series in Table II, the ethylene glycol monoalkyl ethers, shows uniform rate constants for the first two members, but the butyl group and more dramatically the hexyl group appear to lower the rates. The same trend is observed with the oligomer series of diethylene glycol monoalkyl ethers and the triethylene glycol monoalkyl ethers. The only deviation appears to be that the rate constant of the diethylene glycol monobutyl ether is hardly any different from either the monomethyl ether or the monoethyl ether. This infers that the bulkiness of the end group has a lesser influence in lowering the rate constant for a longer oxyethylene chain.

A comparison of the rate constants in Table III of primary and secondary hydroxyl groups in selected model glycol compounds showed the reactivity of the primary hydroxyl group to be vastly different from that of the secondary hydroxyl group in its reaction with phenyl isocyanate, and to be practically unaffected by the presence of a β-methyl group. The similarity in rate constants for the primary hydroxyl groups in

(18) R. A. Greinke and H. B. Mark, Jr., *Anal. Chem.*, **39**, 1577 (1967).

Table II: Rate Constants for the Reaction of the Primary Hydroxyl Group with Phenyl Isocyanate at 25°

Alcohol		$k \times 10^2$, l. mol^{-1} min^{-1}
$HOCH_2CH_2OH$	Ethylene glycol	3.01
$HO(CH_2CH_2O)_2H$	Diethylene glycol	2.76
$HO(CH_2CH_2O)_3H$	Triethylene glycol	2.65
$HO(CH_2CH_2O)_4H$	Tetraethylene glycol	2.68
$HOCH_2CH_2OCH_3$	Ethylene glycol monomethyl ether	2.70
$HOCH_2CH_2OC_2H_5$	Ethylene glycol monoethyl ether	2.78
$HOCH_2CH_2OC_4H_9$	Ethylene glycol monobutyl ether	2.53
$HOCH_2CH_2OC_6H_{13}$	Ethylene glycol monohexyl ether	2.21
$HO(CH_2CH_2O)_2CH_3$	Diethylene glycol monomethyl ether	2.57
$HO(CH_2CH_2O)_2C_2H_5$	Diethylene glycol monoethyl ether	2.61
$HO(CH_2CH_2O)_2C_4H_9$	Diethylene glycol monobutyl ether	2.52
$HO(CH_2CH_2O)_3CH_3$	Triethylene glycol monomethyl ether	2.50
$HO(CH_2CH_2O)_3C_2H_5$	Triethylene glycol monoethyl ether	2.54

Table III: Rate Constants for the Reaction of Primary and Secondary Hydroxyl Groups with Phenyl Isocyanate at 25°

Alcohol		$k \times 10^2$, l. mol^{-1} min^{-1}
$HOCH_2CH_2OCH_3$	2-Methoxyethanol	2.70
$HOCH_2CH(CH_3)OCH_3$	2-Methoxypropanol	2.56
$HOCH(CH_3)CH_2OCH_3$	Methoxy-2-propanol	0.58
$HOCH_2CH_2OCH_2CH_2OH$	Diethylene glycol	2.76
$HOCH(CH_3)CH_2OCH_2CH(CH_3)OH$	Dipropylene glycol	0.59
$HOCH_2CH(CH_3)OCH_2CH(CH_3)OCH_3$	Primary {dipropylene glycol	2.44
$HOCH(CH_3)CH_2OCH_2CH(CH_3)OCH_3$	Secondary {monomethyl ether	0.56

ethoxylated or propoxylated glycols, and likewise for the secondary hydroxyl groups, opened the opportunity to compare the two kinetic analysis approaches in the general case of polyols which invariably contain both primary and secondary hydroxyl groups. The principle of combining the results of the two differential reaction rate techniques is illustrated in Figure 1. Three sets of data are included in the diagram: (1) polyols obtained by copolymerization of ethylene oxide and propylene oxide resulting in $-OCH_2CH_2OH$ and $-OCH_2CH(CH_3)OH$ groups, respectively, (2) polyols obtained by copolymerization of ϵ-caprolactone and propylene oxide resulting in $-OCO(CH_2)_4CH_2OH$ and $-OCH_2CH(CH_3)OH$ groups, respectively, and (3) polyols obtained by copolymerization of ϵ-caprolactone and ϵ-methyl-ϵ-caprolactone resulting in $-OCO(CH_2)_4CH_2OH$ and $-OCO(CH_2)_4CH(CH_3)OH$ groups, respectively.

Polyol groups 1 and 2 contain the same secondary hydroxyl configuration whereas groups 2 and 3 contain the same primary hydroxyl configuration. The data points obtained for the three types of polyols suggest three corresponding straight lines drawn through the respective points. Lines 1 and 2 coincide on the $100/t_e$ axis for zero per cent primary hydroxyl content indicating that the secondary hydroxyl group configuration has the same, extrapolated rate value on the $100/t_e$ axis for both types of polyols. Line 3 is drawn through the three data points and a fourth point obtained by extrapolation (drawing line 2) on the $100/t_e$ axis for 100% primary hydroxyl content. The fourth point is in actuality obtained by regression analysis. To effect the statistical analysis, an equation of the form

$$Y = F_0 + F_1P_1 + F_2P_2 \qquad (2)$$

is tested where Y is the $100/t_e$ value. P_1 and P_2 are the primary hydroxyl contents (determined by GEM) for lines 1 and 2, respectively, F_1 and F_2 the corresponding slopes for these lines, and F_0 the intercept with the $100/t_e$ axis.

Figure 1 shows optimum differentiation for the rate values of primary and secondary hydroxyl groups in glycerine-started ethylene oxide–propylene oxide copolymers (line 1) and glycerine-started ϵ-caprolactone–propylene oxide copolymers (line 2). Catalyzed by 0.100 M DABCO solution eq 2 yielded by multiple regression analysis

$$Y = 5.943115 + 0.662927P_1 + 0.522106P_2 \qquad (3)$$

for the combination of lines 1 and 2 ($P_2 = 0$ for line 1, $P_1 = 0$ for line 2). The intersection of line 2 with the 100% primary hydroxyl content (58.15368 in this case) is then used to determine the slope and intercept at 0% primary hydroxyl content of line 3 by regression analysis. The data for a glycerine-started ϵ-caprolac-

Table IV: Extrapolated Values for the Rate Constants of Primary and Secondary Hydroxyl Groups in Polyether and Polyester Polyols[a]

Starter material	Polymerizing moiety forming — Primary hydroxyl group	Polymerizing moiety forming — Secondary hydroxyl group	$k \times 10^2$, l. mol^{-1} min^{-1} — Primary hydroxyl group	$k \times 10^2$, l. mol^{-1} min^{-1} — Secondary hydroxyl group
Propylene glycol	Ethylene oxide	Propylene oxide	2.46	0.531
Glycerine	Ethylene oxide	Propylene oxide	2.46	0.531
Diethylenetriamine	...	Propylene oxide	...	0.588
Sorbitol	...	Propylene oxide	...	0.517
Sucrose	Ethylene oxide	Propylene oxide	2.2	0.50
Dipropylene glycol	ϵ-Caprolactone	Propylene oxide	1.9	0.53
Glycerine	ϵ-Caprolactone	Propylene oxide	2.0	0.53
Glycerine	ϵ-Caprolactone	ϵ-Methyl-ϵ-caprolactone	2.0	0.32

[a] Reagent, phenyl isocyanate; catalyst, 0.200 *M* DABCO.

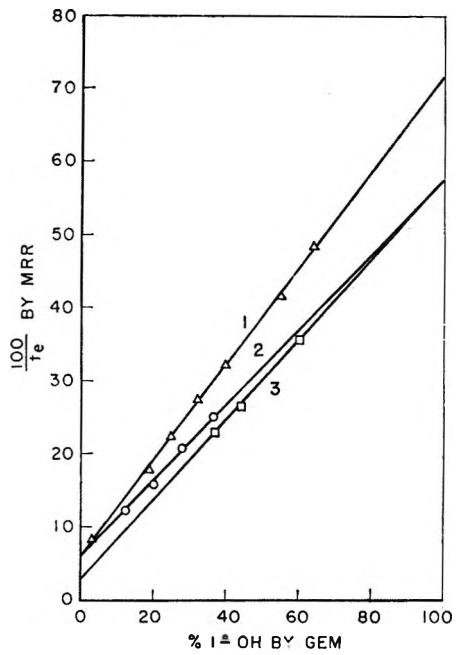

Figure 1. Extrapolated curves for the interrelation of the method of Roberts and Regan (MRR) and the graphical extrapolation method (GEM): △, primary hydroxyl $-OCH_2CH_2OH$, secondary hydroxyl $-OCH_2CH(CH_3)OH$; ○, primary hydroxyl $-OCO(CH_2)_4CH_2OH$, secondary hydroxyl $-OCH_2CH(CH_3)OH$; □, primary hydroxyl $-OCO(CH_2)_4CH_2OH$, secondary hydroxyl $—OCO(CH_2)_4CH(CH_3)OH$.

tone–ϵ-methyl-ϵ-caprolactone polyester polyol thus yielded

$$Y = 2.137 + 0.56017P_3 \quad (4)$$

Discussion

The extrapolation procedure provides us with a useful tool, namely the determination of the rate constant of a functional group, *i.e.*, hydroxyl group, in a particular structural configuration which cannot be obtained in any other way. It is either impossible or in most cases impractical to produce a polyol with only one type of hydroxyl group configuration. The second objective of the principle of combining the MRR and GEM procedures is to determine with greater precision second-order rate constants, amply illustrated by Figure 1. Only three data points are known for line 3. Far greater precision is obtained by establishing a fourth point, the intersection of line 2 (and line 3) with the $100/t_e$ ordinate at 100% primary hydroxyl content. The feasibility of acquiring such an extra datum point is dependent on the precision, *i.e.*, number of data points, with which the curves 1 and 2 are obtained.

The knowledge of the values of the rate constants of the various primary and secondary hydroxyl groups gives us an insight into the comparative reactivities of these polyol end groups; it also provides us with basic data from which we can calculate the overall reactivity of a polyol with the isocyanate group by combination of the respective rate contributions of the primary and secondary hydroxyl groups. The reaction rate constants of the primary and secondary hydroxyl groups in a selected number of commercially available polyols are summarized in Table IV. The rate constants were all obtained by extrapolation. The degree of precision with which the rate values for the first four types of polyols are obtained is far greater than those for the four types in the second group of polyols: a greater number of different compositions are available for each of the first four types of polyols.

The mixed oxide polymer products of propylene glycol and of glycerine show identical rate constants, which implies that the reactivity of the hydroxyl groups is not hampered by a steric hindrance factor and that it is immaterial which one of the two glycols is chosen as starter material. The reactivity of the secondary hydroxyl group in diethylenetriamine-based polyols is significantly enhanced, most probably due to the synergistic catalyst action of the inner amine groups with the catalytic species used in the reaction, DABCO. A decrease in the secondary hydroxyl group rate constant is observed for the sorbitol and sucrose type polyether polyols. The higher functionality of the starter product demands a lesser number of polymerizing moieties in each branch of the molecule, and hence a closer prox-

imity of the terminal hydroxyl groups. Steric hindrance could thus very well be the only factor affecting the hydroxyl group's rate constant. Table IV also shows that the rate constants of the primary hydroxyl groups in polyether polyols are invariably higher than those in polyester polyols. It appears likewise that the reactivities of the secondary hydroxyl groups in polyether polyols are significantly higher than the methyl caprolactone induced ones in a polyester polyol.

Acknowledgment. The author is indebted to L. J. Priestley, Jr., for the preparation of sufficient amounts of pure glycols by preparative gas chromatography and to E. T. Bishop, who helped much in the experimental work.

Ionic Polymerization under an Electric Field. XIII. Living Anionic Polymerization of Styrene in the Binary Mixtures of Benzene and Dimethoxyethane by the Three-State Mechanism

by Norio Ise, Hideo Hirohara, Tetsuo Makino, Katsuhiko Takaya, and Masatoshi Nakayama

Department of Polymer Chemistry, Kyoto University, Kyoto, Japan *(Received February 19, 1969)*

The living anionic polymerization of styrene was studied in the binary mixtures of benzene and dimethoxyethane (DME) at 25° in the presence and absence of an electric field. Under the present experimental conditions, the field influence on the apparent propagation constant (k_p) was negligible, in contrast with benzene–tetrahydrofuran cases previously studied. At a DME content of 50%, the following linear relation held, $k_p = k_p' + k_p''K^{1/2}/[\text{L.E.}]^{1/2}$, where k_p' and k_p'' are the ion pair and free ion rate constants, respectively, K is the dissociation constant of the ion pairs, and [L.E.] the concentration of the living ends. At DME contents below 40%, however, the above equation was no longer valid, and k_p increased with increasing [L.E.]. This concentration dependence was satisfactorily accounted for by the formation of triple ions $\sim\!S^-$, Li^+, $S^-\!\sim$, where $\sim\!S^-$ denotes the carbanion at the end of a polystyrene chain. From the conductance data, the dissociation constants of the ion pairs and the triple ions were estimated. In the DME content range between 50 and 40%, the propagation rate constant of the triple ions (k_p''') was about $10^5\ M^{-1}\ \text{sec}^{-1}$, whereas k_p'' was approximately $3 \times 10^4\ M^{-1}\ \text{sec}^{-1}$. The values of k_p' were 78, 46, and 32 $M^{-1}\ \text{sec}^{-1}$ at DME contents of 50, 45, and 40%, respectively. Reasons for large rate constants of the triple ions were discussed. The desolvation of the growing chain ends was suggested to be an important factor in determining the field-accelerating effects.

In this laboratory, the influence of an electric field on various types of polymerization has been studied.[1,2] Experimental work on cationic systems showed that the field in most cases increased the rate of polymerization, but the interpretation was not clear because of the complicated nature of this type of polymerization. Recently much simplified systems were chosen, namely living anionic polymerizations of styrene,[3] in which the field influence on the propagation step can directly be observed. The results showed that the apparent propagation rate constant of the anionic polymerization of polystyryllithium in the binary mixtures of benzene and tetrahydrofuran (THF) increased in the presence of an electric field when the dielectric constant was high. To be strict, the field did not affect the ion pair rate constant k_p', but it increased the $k_p''K^{1/2}$ term where k_p'' is the free ion rate constant and K the dissociation constant of the ion pair. This observation was in qualitative agreement with our previous interpretation that the field influence on ionic polymerization in general is due to the field-facilitated dissociation[4] of the ion pairs at the growing chain ends. However, the agreement of the observed field effect with the calculated value by Onsager's theory[5] was so poor that we were led to the conclusion that desolvation by the field of

(1) I. Sakurada, Y. Tanaka, and N. Ise, *J. Polymer Sci., A-1*, **6**, 1463 (1968). For earlier references, see this article.

(2) I. Sakurada, N. Ise, Y. Hayashi, and M. Nakao, *Macromolecules*, **1**, 265 (1968).

(3) N. Ise, H. Hirohara, T. Makino, and I. Sakurada, *J. Phys. Chem.*, **72**, 4543 (1968).

(4) (a) M. Wien, *Ann. Physik.*, **83**, 327, 795 (1927); (b) M. Wien, *Physik. Z.*, **28**, 751, 834 (1927).

(5) L. Onsager, *J. Chem. Phys.*, **2**, 599 (1934).

solvent molecules weakly bound to the free carbanion causes the k_p'' value to increase with field. As the rate constant of "naked" free ions we obtained $\simeq 10^5\ M^{-1}\ \text{sec}^{-1}$.

This conclusion is, however, questionable on the basis of the following reasons. First, the Onsager theory is derived for the metallic sphere model for ions, and would not hold for randomly coiled and partially free-draining living polymers. Second the nature and strength of solvation forces, especially between the carbanion and THF, are not clear. Therefore, there is no positive proof that the electric field applied in our experiments would be strong enough to cause the desolvation. Thus, it was thought interesting to carry out the experiment using a solvent which is believed to solvate the carbanion more strongly than THF.[6,7] In this paper, dimethoxyethane (DME) is chosen as a component of the binary solvent containing benzene. It has been reported that, in living anionic polymerization of styrene, the fraction of solvent-separated ion pairs is higher in DME than in THF, and DME can solvate the carbanion.[8]

Experimental Section

Commercial DME was dried over sodium, refluxed over CaH_2 for a week or so, and distilled under nitrogen atmosphere onto a Na–K alloy. Using a high vacuum line, the DME was dried under violent stirring at room temperature, cooled down to the Dry Ice–methanol temperature, and deaerated in the liquid state. Several cycles of drying and deaeration were repeated until the DME showed a stable dark blue color of a charge transfer complex with the Na–K alloy. Then the DME was vacuum distilled onto a Na mirror, deaerated again after confirming the brightness, and distilled into ampoules with break-seals, and the ampoules were sealed off from the vacuum line. If the unadequately purified DME was used, the living ends were rapidly killed and no reproducible results were obtained. Thus, special attention was paid to the purification.

The methods of purification of styrene and benzene have been already described.[3] *n*-Butyllithium was prepared by the method earlier described.[3] Polystyryllithium of a degree of polymerization of 15 was prepared and used as the seed of the polymerization reaction as before.[3] Polystyryllithium was allowed to contact with DME just before the polymerization experiments. The rate of polymerization and the concentration of the living ends were determined spectrophotometrically as in the previous paper.[3]

The procedure and apparatus employed in the kinetic study have been described already.[3] The electric conductivity was calculated from the intensity of the applied field and the current strength. The dielectric constant and viscosity of the solvent mixtures were determined in the same way as described earlier.[3]

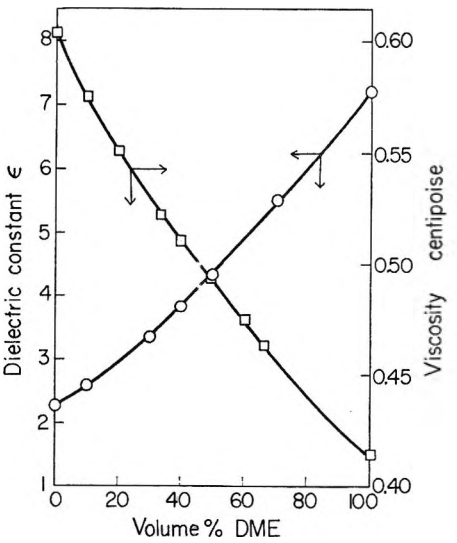

Figure 1. Dielectric constant ○ and viscosity □ of dimethoxyethane–benzene mixture at 25°.

Results and Discussion

Field Effect. Figure 1 shows the dielectric constant and viscosity of the benzene–dimethoxyethane mixtures. The viscosity value of DME is lower by about 10% than that reported earlier[9] whereas the density and dielectric constant are in excellent agreement with the literature values.[9]

According to the two-state polymerization mechanism, the apparent rate constant of propagation k_p can be written as

$$k_p = k_p' + k_p''K^{1/2}/[\text{L.E.}]^{1/2} \qquad (1)$$

where [L.E.] is the concentration of the active chain end.[8,10,11] Equation 1 shows that k_p increases with $1/[\text{L.E.}]^{1/2}$. Our experimental results shown in Figure 2, however, indicate that (1) k_p decreases with $1/[\text{L.E.}]^{1/2}$ for DME contents of 30 and 40%, (2) the k_p–$1/[\text{L.E.}]^{1/2}$ plot has a minimum at 45%, and (3) k_p increases monotonously at 50%. This implies that a reactive species with a large rate constant of propagation participates in the polymerization both in solvents

(6) F. Cafasso and B. R. Sundheim, *J. Chem. Phys.*, **31**, 809 (1959).

(7) T. E. Hogen-Esch and J Smid, *J. Amer. Chem. Soc.*, **88**, 307 (1966).

(8) T. Shimomura, J. Smid, and M. Szwarc, *ibid.*, **89**, 5743 (1967).

(9) C. Carvajal, K. J. Tölle, J. Smid, and M. Szwarc, *ibid.*, **87**, 5548 (1965).

(10) (a) D. N. Bhattacharyya, C. L. Lee, J. Smid, and M. Szwarc, *J. Phys. Chem.*, **69**, 612 (1965); (b) M. Van Beylen, D. N. Bhattacharyya, J. Smid, and M. Szwarc, *ibid.*, **70**, 157 (1966); (c) S. Bywater and D. J. Worsfold, *ibid.*, **70**, 162 (1966); (d) T. Shimomura, K. J. Tölle, J. Smid, and M. Szwarc, *J. Amer. Chem. Soc.*, **89**, 796 (1967).

(11) (a) H. Hostalka, R. V. Figini, and G. V. Schulz, *Makromol. Chem.*, **77**, 240 (1964); (b) H. Hostalka and G. V. Schulz, *Z. Physik. Chem.*, **45**, 286 (1965); (c) W. K. R. Barnikol and G. V. Schulz, *ibid.*, **47**, 89 (1965); (d) L. Böhm, W K. R. Barnikol, and G. V. Schulz, *Makromol. Chem.*, **110**, 222 (1967).

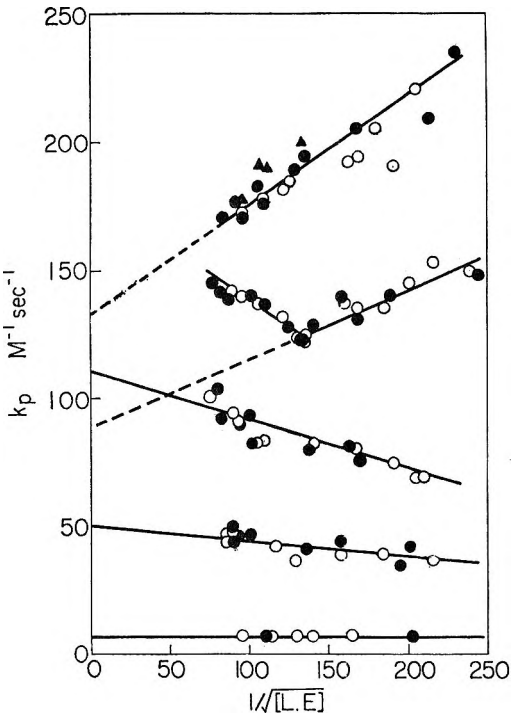

Figure 2. Dependence of the apparent propagation rate constant on the polystyryllithium concentration in, from the top, 50, 45, 40, 30, and 10% dimethoxyethane–benzene mixtures at 25°: ▲, 5 kV/cm; ●, 3 kv/cm; O, 0 kV/cm.

of low dielectric constant and at higher concentrations of the living end. In the light of the present state of the knowledge concerning electrolyte solutions, it is reasonable to conclude that triple ions play an important role as the reactive species,[12] as was earlier discussed by the Syracuse group.

The living end concentration dependence of the apparent propagation constant would be expressed by a curve with a minimum, which was rather fortunately found at a DME content of 45% as shown in Figure 2. If experiments can be carried out at smaller values of $1/[\text{L.E.}]^{1/2}$ for 50% DME, we would observe both a steeper negative slope and a minimum point. Furthermore, experiments at larger values of $1/[\text{L.E.}]^{1/2}$ for 30 and 40% would give positive slopes and minima. In other words, as the DME content increases, the negative slope becomes steeper and the minimum point shifts toward small values of $1/[\text{L.E.}]^{1/2}$.

According to the theory of electrolyte solutions, these changes in the slope and minimum point with composition of the solvent can be accounted for in terms of the triple ion formation, if the triple ions have a larger propagation constant than free ion and ion pairs.

It is to be noted that the field acceleration effect was barely observable for the present systems, in contrast with benzene–tetrahydrofuran systems previously studied. As mentioned above, we were led to the conclusion that the fairly large field acceleration effects observed for the latter systems were due to an increase in k_p'' with field intensity which was believed to be caused by desolvation of solvent molecules weakly bound to free carbanion. This interpretation appears to be strongly supported by the experimental results obtained for benzene–dimethoxyethane systems; DME molecules have higher solvating tendencies than THF molecules not only to cations but also to anions.[8] Therefore the DME molecules cannot be removed from the carbanion by an electric field applied in our experiments.

The finding that the field did not give an acceleration effect for the benzene–dimethoxyethane systems leads us to the following discussion. Intuitively, the solvent-separated ion pair is more dissociable than the contact ion pair. The fraction of the solvent-separated ion pair in DME, however, is larger than that in THF according to the Syracuse group.[7,8] Thus, the finding mentioned above indicates that the field-faciliated dissociation of the solvent-separated ion pair is not the main factor responsible for the field effect.

Triple Ion Formation. In the foregoing section, the k_p increase with increasing concentration of the living ends, which was observed at DME contents below 45% and in ranges of higher concentration, was attributed to the triple ion formation. It is well established that ionic aggregates higher than ion pairs, *i.e.*, triple ions, can be formed in the solvents of low dielectric constants and at higher concentrations of electrolytes.[14]

In this connection, it is useful to examine the electric conductivity data. In Figure 3, the logarithm of the equivalent conductance is plotted against the logarithm of the living end concentration. The conductance was determined conveniently from the intensity of the current passing through the solution in the presence of an electric field of 3 kV/cm. The conductivity should increase by about 4% at 3 kV/cm under the present experimental conditions, according to the Onsager theory. This increase is believed to be within the experimental error, so that no correction was effected. If the polymerizing solutions contain only ion pairs and free ions, the log Λ–log [L.E.] plot should have a slope of -0.5.[15] The slopes shown in Figure 3 are -0.44, -0.42, and -0.39 at DME fractions of 50, 45, and 40%, respectively, being slightly larger than -0.5. From this, it is suggested that the triple ions participate in the polymerization reaction under consideration.

The lowest concentration (C_0), at which the triple ions can exist, can be written as

(12) The triple ions referred to here are of an *inter*molecular type, as will be mentioned below. We should mention that triple ions of an *intra*molecular type were earlier suggested by the Syracuse group.[10a,13]

(13) D. N. Bhattacharyya, J. Smid, and M. Szwarc, *J. Amer. Chem. Soc.*, 86, 5024 (1964).

(14) R. M. Fuoss and C. A. Kraus, *ibid.*, 55, 2387 (1933).

(15) R. M. Fuoss and F. Accascina, "Electrolytic Conductance," 1st ed, Interscience, New York, N. Y., 1959, p 253.

$$C_0 = 3.2 \times 10^{-7}\epsilon^3$$

for 1–1 electrolytes, where ϵ is the dielectric constant of the solvent.[15] The C_0 values at DME fractions of 50, 45, and 40% are 2.6×10^{-5}, 2.2×10^{-5}, and 1.8×10^{-5} M, respectively, being smaller than the concentrations used in the present experiments.

Two types of triple ions can exist, namely (+)(−)(+) and (−)(+)(−). They would differ in stability, because of the asymmetric structures of the cations and anions.[16,17] Since the charge is located at one end of a bulky ion (polystyryl ion), the triple ion (~~S⁻)(+)(S⁻~~) is more stable than (+)(S⁻~~)(+), as was discussed by Fuoss–Kraus[14] and Wooster.[16] Thus we assume the following equilibria

$$\sim\!\sim S^-, Li^+ \overset{K}{\rightleftharpoons} \sim\!\sim S^- + Li^+$$

$$\sim\!\sim S^-, Li^+, S^-\!\sim\!\sim \overset{k}{\rightleftharpoons} \sim\!\sim S^-, Li^+ + S^-\!\sim\!\sim$$

with the dissociation constants K and k. Note that this type of triple ion has two active centers. If the fractions of the free anions and the triple ions are denoted by α and γ, respectively, the mass action equations are

$$K = [\text{L.E.}](\alpha^2 + \alpha\gamma)/(1 - \alpha - 2\gamma)$$

and

$$k = [\text{L.E.}]\alpha[1 - \alpha - 2\gamma)/\gamma$$

The apparent rate constant k_p is

$$k_p = (1 - \alpha - 2\gamma)k_p' + \alpha k_p'' + \gamma k_p'''$$

If we take into consideration $\alpha \ll 1$, and $\gamma \ll 1$

$$k_p = k_p' + \frac{k_p'' K^{1/2}}{\left(1 + \frac{[\text{L.E.}]}{k}\right)^{1/2}}[\text{L.E.}]^{1/2} + \frac{k_p''' K^{1/2}}{\left(1 + \frac{[\text{L.E.}]}{k}\right)^{1/2} k}[\text{L.E.}]^{1/2} \quad (2)$$

This equation is generally valid, and our following discussion is based thereon. As is easily seen, k_p depends on [L.E.] in a complicated manner so that graphical treatments of the kinetic data by means of eq 2 are rather difficult; eq 2 shows that k_p cannot generally be a linear function of, for example, $[\text{L.E.}]^{1/2}$ or of $1/[\text{L.E.}]^{1/2}$. If $[\text{L.E.}]/k$ is negligible, however, eq 2 simplifies to

$$k_p = k_p' + \frac{k_p'' K^{1/2}}{[\text{L.E.}]^{1/2}} + \frac{k_p''' K^{1/2}}{k}[\text{L.E.}]^{1/2} \quad (3)$$

In the solvents of low DME content, where the contribution of the triple ions is so large that free ions can be neglected, the second term on the right-hand side of eq 3 would be dropped. Then, k_p should increase linearly with increasing $[\text{L.E.}]^{1/2}$. In Figure 4, the k_p values are replotted against $[\text{L.E.}]^{1/2}$. A linear relation is seen to hold, though approximately. Evidently, the slight curvature, if it exists, is due to the incorrectness of the simplifying assumption $[\text{L.E.}]/k \approx 0$ and to the unnegligible contribution of free ions. If exact curves could be drawn, we would be able to determine the rate constant values. Unfortunately, the experimental scatter of the data prevents us from following such a method of analysis. Therefore, we *conveniently* adopt a linear approximation, as was shown in Figure 4. Then, the intercept gives k_p' and the slope $k_p''' K^{1/2}/k$. If K and k are known from conductivity data, the approximate values of k_p' and k_p''' can be determined.

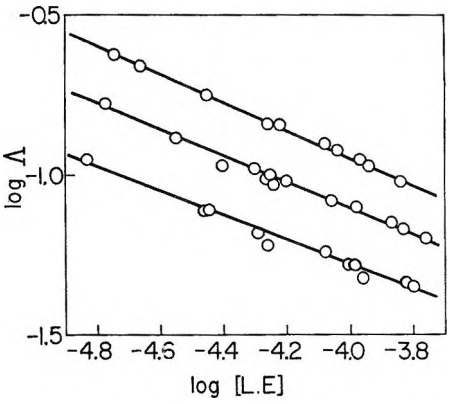

Figure 3. Dependence of the equivalent conductance on the polystyryllithium in, from the top, 50, 45, and 40% dimethoxyethane–benzene mixtures.

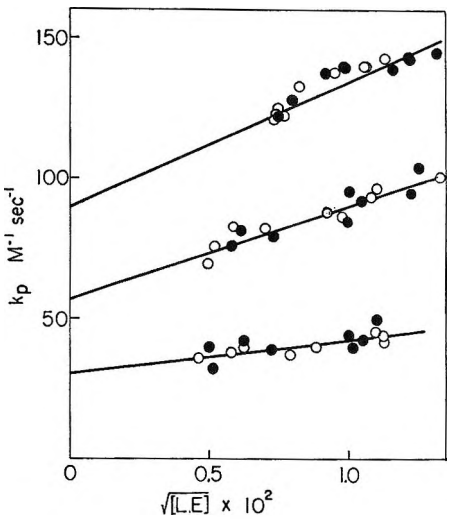

Figure 4. Triple ion formation. Dependence of the apparent rate constant on the polystyryllithium concentration in, from the top, 45, 40, and 30% dimethoxyethane–benzene mixtures at 25°: ●, 3 kV/cm; ○, 0 kV/cm.

It should be mentioned here that an increasing

(16) C. B. Wooster, *J. Amer. Chem. Soc.*, 59, 377 (1937); *ibid.*, 60, 1609 (1938).

(17) M. Dole, *Trans. Electrochem. Soc.*, 77, 385 (1940).

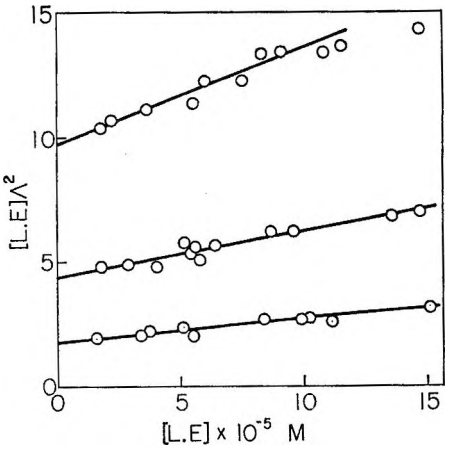

Figure 5. Conductivity data showing triple ion formation in, from the top, 50, 45, and 40% dimethoxyethane–benzene mixtures at 25°.

tendency of k_p with $1/[\text{L.E.}]^{1/2}$ (Figure 2) might not be approximated by a straight line. This is due to the incorrectness of the assumption $[\text{L.E.}]/k \approx 0$ and to the unnegligible contribution of triple ions.

When the triple ions are formed, the equivalent conductance can be written as

$$\Lambda\left(1 + \frac{[\text{L.E.}]}{k}\right)^{1/2} = (\Lambda_0 K^{1/2})/[\text{L.E.}]^{1/2} + (\Lambda_0 K^{1/2}/k)[\text{L.E.}]^{1/2}$$

In solvents of low dielectric constants and at low concentrations, the conductance equation becomes[16]

$$[\text{L.E.}]\Lambda^2 = \Lambda_0^2 K + (2\Lambda_0\lambda_0 - \Lambda_0^2)(K/k)[\text{L.E.}] \quad (4)$$

where Λ_0 is the sum of the limiting conductances of Li^+ ion $[\Lambda_0^+(Li^+)]$ and $\sim\!\!\sim S^-$ ion $[\Lambda_0^-(\sim\!\!\sim S^-)]$ and λ_0 the sum of $\Lambda_0^+(Li^+)$ and the limiting conductance of the triple ion $[\lambda_0^-(\sim\!\!\sim S^-, Li^+, S^-\!\!\sim)]$. According to eq 4, a plot of the $[\text{L.E.}]\Lambda^2$ is linear in [L.E.]. Our results are shown in Figure 5. The intercept and slope give k and K values, if Λ_0 and λ_0 are known.

In order to evaluate Λ_0, we used the Walden rule. According to Nicholls, *et al.*,[18] $\Lambda_0^+(Na^+) = \Lambda_0^+(Li^+)$ in THF. The Walden product $\Lambda_0\eta$ for polystyryl-sodium in THF at 25° was 0.294.[10d] If one assumes $\Lambda_0^+(Na^+) = \Lambda_0^+(Li^+)$ in DME, $\Lambda_0^+(Li^+) = \Lambda_0^+(Na^+) = 55.7$ according to Carvajal, *et al.*[9] If one further assumes that $\Lambda_0^-(\sim\!\!\sim S^-) = 15.0$, we obtain 0.293 as the Walden product at 25° for DME, which is in excellent agreement with that obtained for THF. Thus Λ_0 was calculated using the Walden product thus obtained, and shown in Table I.

λ_0 and Λ_0 are mainly determined by a factor, namely $\Lambda_0^+(Li^+)$. Therefore, it is not erroneous to assume $\lambda_0 = \Lambda_0$.

Thus we have the K and k values which are listed in Table I.

Table I: Dissociation and Reactivity of Lithium Salt of Living Polystyrene in Benzene–Dimethoxyethane Mixtures at 25°

DME, %	ϵ	Λ_0, cm² ohm⁻¹ equiv⁻¹	$K \times 10^{10}$, M	$k \times 10^4$, M	$k_p'' \times 10^{-4}$, M^{-1} sec⁻¹	$k_p''' \times 10^{-4}$ M^{-1} sec⁻¹
40.0	3.81	57.7	0.51	1.88	...	8.5[a]
					2.7[b]	11[b]
45.0	4.08	58.4	1.29	2.30	2.4[a]	9.0[a]
					3.0[b]	12[b]
50.0	4.33	59.5	2.77	2.75	2.4[a]	...
					3.3[b]	12[b]

[a] Observed (first approximation). [b] Corrected.

By combining the K and k values with the slopes of plots shown in Figures 2 and 4, k_p'' and K_p''' can be obtained. The rate constant values thus derived may not be true because a simplified equation such as eq 3 was used and the contributions of the triple ions and of the free ions were neglected for k_p'' and k_p''', respectively. It is highly plausible, however, that the free ions contribute to the polymerization, though to a small extent, under the present experimental conditions under which the polymerization proceeds substantially through the triple ions. Thus, it was necessary to take into account the triple ions and the free ions in the k_p'' and k_p''' determinations, respectively. In practice, expansion of eq 2 in series of $[\text{L.E.}]/k$ (which is much smaller than unity under the present conditions) approximately gives

$$k_p = k_p' + \frac{K^{1/2}}{[\text{L.E.}]^{1/2}} k_p'' + \frac{K^{1/2}}{k}\left(k_p''' - \frac{1}{2}k_p''\right)[\text{L.E.}]^{1/2}$$

into which the first approximation of k_p''' obtained from Figure 4 was substituted. Then $[k_p - K^{1/2}/k \cdot (k_p''' - {}^1/_2 k_p'')[\text{L.E.}]^{1/2}]$ was plotted against $1/[\text{L.E.}]^{1/2}$ in order to obtain a second approximation for k_p''. (In this plot, ${}^1/_2 k_p''$ was calculated by using the first approximation for k_p''. This was not a source of serious error.) Using this newly obtained k_p'' value, $[k_p - K^{1/2} k_p''/[\text{L.E.}]^{1/2}]$ was plotted against $[\text{L.E.}]^{1/2}$ to determine a second approximation for k_p'''. This k_p''' value was recycled to obtain a third approximation for k_p'', which was further used for higher approximations. This cycle was broken when k_p'' and k_p''' converged to the respective constant values and furthermore when k_p' obtained in the k_p'' determination agreed with that derived in the k_p''' determination. The final results are given in Table I. We note that the k_p''' is about four times larger than the k_p''.

The larger rate constant of triple ions invites some comments. According to the classical "sphere in continuum" model, the dissociation constant K can be written as[15]

(18) D. Nicholls, C. Sutphen, and M. Szwarc, *J. Phys. Chem.*, 72, 1021 (1968).

$$K^{-1} = 4\pi Na^3e^b/3000$$

with

$$b = e^2/a\epsilon kT$$

where N is the Avogadro number, and a the center-to-center distance. A thermodynamic derivation based on Born's cycle shows that $K^{-1} \propto e^b$.[19] A similar treatment for triple ions leads to the equation of the form $k^{-1} \propto e^{b/2}$. A plot of log K or log k against $1/\epsilon$ should give a straight line. Our experimental data show that this is the case, as is seen from Figure 6. From the slope, we obtain 10.5 Å as the center-to-center distance for ion pair formation. Though this value appears to be too large, we should note that the experimental data reported for benzene–tetrahydrofuran by Bywater[10c] give also $a \simeq 10$ Å in solvents of low dielectric constants. As the distance parameter for triple ion formation, we obtain $a = 21$ Å. This value is also larger than that derived from the ion pair dissociation, namely 10.5 Å × 1.5 = 15.8 Å.

It is important to discuss why the triple ions are formed in the binary mixtures of benzene and DME. The explanation that the formation of the triple ions is due to coulomb forces alone seems to be inaccurate, since the triple ions were not found in the benzene–tetrahydrofuran mixtures having dielectric constants as low as the benzene–dimethoxyethane mixtures. Thus, it is suggested that DME molecules may play an important role. As was mentioned above, DME molecules have a higher solvating ability than THF molecules not only to cations but also to anions. Two DME molecules coordinate to a cation as a result of the interactions with the negative cavity,[6] and an anion is coordinated to the positive site of the outside of the cavity. Thus a solvent-separated ion pair will be formed. Then the vacant positive site will now be occupied by another anion. Thus, solvent-separated triple ions are formed in our experimental conditions. The large value of the distance parameter, 21 Å, may reflect this situation. On the other hand, THF molecules are unable to solvate simultaneously both cations and anions. Therefore, triple ions cannot be formed in the benzene–tetrahydrofuran mixtures.

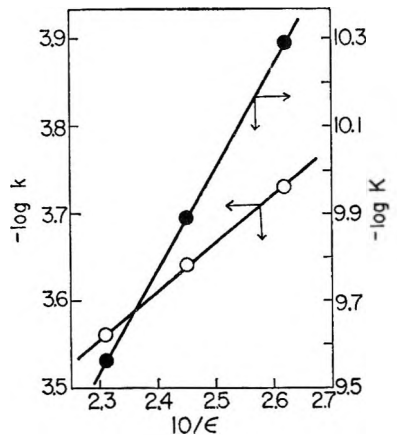

Figure 6. Dependence of the triple ion and ion pair dissociation constants on dielectric constant at 25°: ○, triple ion constant; ●, ion-pair constant.

It would be reasonable that the spreading of the center-to-center distance of the triple ion results in a large rate constant of propagation. As was seen above, k_p''' is about four times larger than k_p''. The conclusion, $k_p''' > 2k_p''$, follows from the first differential derivative of k_p (eq 2) when k_p has a minimum value as is seen in Figure 2. If $k_p''' < 2k_p''$, on the other hand, a minimum value of k_p does not exist, and the slope of the k_p–$[\text{L.E.}]^{1/2}$ plot becomes smaller than can be expected from the two-state polymerization mechanism, as was found by Szwarc, *et al.*[10a,13] They found that two-ended polystyrylcesiums, $Cs^+, S^-\sim\sim S^-, Cs^+$, formed intramolecular triple ions in THF, and reported a value of about 2000 M^{-1} sec^{-1} as k_p''', in contrast with $k_p'' \approx 65{,}000$ M^{-1} sec^{-1}, and $k_p' = 22$ M^{-1} sec^{-1}. These intramolecular triple ions were about 100 times more reactive than the ion pairs. The Syracuse group believe that these triple ions and ion pairs are of a contact type. Therefore, it would be reasonable to suppose that the solvent-separated triple ions found in our system are also much more reactive than solvent-separated ion pairs. The latter have a propagation constant only one-third lower than that of free ions.[8] The distance parameter (21 Å) of the solvent-separated triple ions in our systems was larger than that of the solvent-separated ion pairs, because of the electrostatic repulsive forces between two negative charges of the triple ion. Hence, the rate constant of the triple ions is much larger than that of the ion pairs. On the other hand, the free ions are bounded more firmly by DME than by THF so that their rate constant in the former solvent is smaller than in the latter. The binding of DME in the triple ions is expected to be weaker because of the repulsive forces between negative charges than that in the case of free ions. As a consequence, k_p''' is larger than k_p'', as was observed.

We recall here that the k_p''' value for polystyrylcesium was found to be much smaller than the k_p'' by the Syracuse group,[10a,13] in contrast with our finding for the lithium salt. It would be useful to remember that the cesium salts give the triple ions of a contact type having a low reactivity whereas the lithium salts produce highly reactive solvent-separated triple ions. We believe the discrepancy between the two groups is essentially not due to the difference in the form of the triple ions (intra- or intermolecular), but due to the difference in the solvation state of the gegenions. It is interesting that k_p''' appears

(19) J. T. Denison and J. R. Ramsey, *J. Amer. Chem. Soc.*, 77, 2615 (1955).

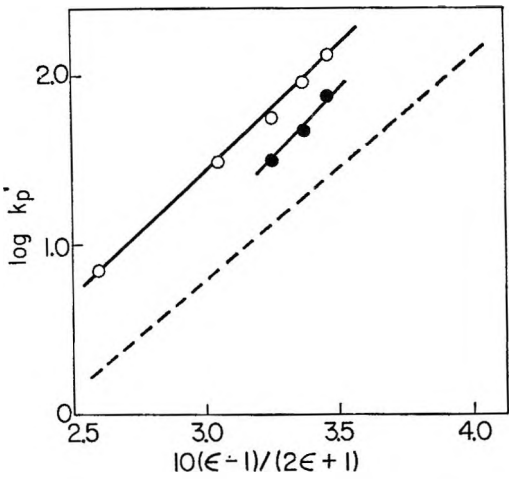

Figure 7. Dependence of the ion-pair rate constant on dielectric constant at 25°: ○, dimethoxyethane–benzene (obsd), – – –, tetrahydrofuran–benzene; ●, dimethoxyethane–benzene (corrected).

to be very strongly influenced by the gegenions, in contrast with k_p'' cases. Further systematic study is in progress in this laboratory.

We should not overlook the fact that one triple ion has two active centers. From the observed value of k_p''' ($11 \sim 12 \times 10^4\ M^{-1}\ \text{sec}^{-1}$), we have $5.5 \sim 6 \times 10^4\ M^{-1}\ \text{sec}^{-1}$ for each active center. It is interesting that this value is close to the k_p'' value ($6.5 \times 10^4\ M^{-1}\ \text{sec}^{-1}$) found in THF by Szwarc, *et al.*[10a]

Ion Pair Rate Constant. The ion pair rate constant k_p' was not affected by the electric field, as was previously the case for benzene–tetrahydrofuran systems.[3] The k_p' values obtained from the intercept of Figure 2 or 4 were 135, 90, 57, 30, and 7.0 $M^{-1}\ \text{sec}^{-1}$ for DME fractions of 50, 45, 40, 30, and 10%, respectively. The k_p' value should be corrected by the same manner as for k_p'' and k_p'''. The final values of k_p' were 78, 46, and 32 $M^{-1}\ \text{sec}^{-1}$, for DME fractions of 50, 45, and 40% respectively.

Following Laidler and Eyring's theory on rate of reaction between dipolar molecules,[20] the ion pair rate constant k_p' is plotted against the dielectric constant in Figure 7. At a given dielectric constant, DME gives larger k_p' than THF. This implies that the fraction of solvent-separated ion pair in DME is larger than in THF.

It would be useful to sum up the present investigation as follows. In contrast with the tetrahydrofuran–benzene cases, the electric field did not increase the overall propagation rate constant (k_p) in the dimethoxyethane–benzene systems. We recall here that the field acceleration observed for the tetrahydrofuran–benzene cases was tentatively ascribed to desolvation of THF molecules bound to the free-ion type living end caused by the electric field. Since DME molecules have a stronger solvating power than THF, the observed fact, that no field acceleration was noticed in the DME containing systems, is quite understandable. Under some conditions in the present system, the k_p–$1/[\text{L.E.}]^{1/2}$ plot showed a feature quite different from that found for tetrahydrofuran–benzene systems. In other words, k_p increased with increasing [L.E.]. Thus, it was deduced that the two-state mechanism accepted in some living anionic systems is not generally valid. The conductivity data showed that the log Λ–log [L.E.] plots gave slopes larger than -0.5, indicating a contribution of triple ions in the propagation process in addition to free ions and ion pairs. In the light of the relatively strong solvating power of DME toward anions as well as cations resulting from the cavity structure of this molecule,[6] we suggested that the triple ion was of a solvent-separated type. This was supported by the large charge-to-charge distance of the triple ion calculated from the conductivity data (and hence the dissociation constant). By taking into consideration the simultaneous contribution of free ions, ion pairs, and triple ions, an equation (eq 2) was derived for k_p. When the triple ion contribution was substantial, this equation was reduced to a relation, which was linear with respect to $[\text{L.E.}]^{1/2}$. The experimental data were found to satisfy this relation, though approximately. From this plot and the conductivity data, the triple-ion rate constants were $\sim 10^5\ M^{-1}\ \text{sec}^{-1}$. This value is larger than the free-ion rate constant ($\sim 3 \times 10^4\ M^{-1}\ \text{sec}^{-1}$), so that it accounts for the above-mentioned deviation from the relationship usually observed between k_p and $1/[\text{L.E.}]^{1/2}$. In short, the interesting features found in the present systems can ultimately be attributed to the molecular geometry of DME, which results in the specific solvating power and simultaneously the triple ion formation in media of low dielectric constants.

Acknowledgments. Our sincere thanks are due to Professor Ichiro Sakurada for his reading of the manuscript.

(20) K. J. Laidler and H. Eyring, *Ann. N. Y. Acad. Sci.*, 39, 303 (1940).

Addition of Oxygen Atoms to Olefins at Low Temperature.

IV. Rearrangements

by Ralph Klein and Milton D. Scheer

National Bureau of Standards, Washington, D. C. 20234 *(Received July 28, 1969)*

Rearrangements in the $O^3(P)$ atom addition to internal, straight-chain olefins involve, as one of the processes, internal rotations resulting in configurational changes. Symmetrical *cis*-olefins at 90°K were found to show greater stereospecificity in the oxygen atom addition reaction as the chain length was increased. Rearrangements involving migration of alkyl groups and localization of oxygen on one of the carbon atoms of the olefinic pair occur in a concerted manner. This was shown from the reactions of 3-ethyl-2-methyl-2-pentene and two of its isomers. Clearly independent rates cannot be associated with migrating alkyl groups, and additional factors, other than electron density, determine the position of addition of the oxygen atom.

Introduction

Reactions below about 150°K in the oxygen atom–olefin system occur without the formation of fragmentation products. A very decided advantage to studies in this temperature region is that the distinction between concurrent reaction paths characterized by small energy differences is emphasized. An example is provided in the comparison of the reactions of *cis*- and *trans*-2-butenes with $O(^3P)$ at 90°K. *cis*-2-Butene gives approximately equal quantities of *cis*- and *trans*-2,3-epoxybutane. Of the epoxybutanes produced from *trans*-2-butene, 90% are *trans*.[1,2] It is well established that oxygen atom addition to olefins gives carbonyls as well as epoxides.[1,3] Carbonyl compounds can arise only by rearrangements in which either a hydrogen atom or an alkyl group is shifted from its original position on one of the olefinic carbon atoms. Both rearrangement processes, namely, the change of configuration in the epoxides from that of the parent olefin and the migration of a hydrogen atom or an alkyl group, are amenable to observation by previously developed, low-temperature methods. Several olefins were selected for study of the O atom addition to illuminate the nature of these rearrangements.

Straight-Chain, Internal Olefins

The addition of $O(^3P)$ to straight-chain, internal olefins is interesting because of *cis–trans* isomerism in the olefin and in the resulting epoxide compounds. A consideration of the O atom addition to *cis*- and *trans*-2-butene in the temperature region 77 to 113°K led to the formulation of a new transition intermediate.[2] In this intermediate, the oxygen atom is represented as bound in a loose, three-membered ring with, and in the plane of, the olefinic structure of the reactant. An interaction between the oxygen atom and the adjacent hydrogen atoms bonded to the olefinic carbon atoms is also postulated. The necessity for the assumption of this interaction arises from the observation that, for both *cis*- and *trans*-2-butene, the ratio of *cis*-2,3-epoxybutane to isobutyraldehyde, as well as that of *trans*-2,3-epoxybutane to 2-butanone, remains constant. The relationship holds over a wide temperature range (77–300°K), despite large differences in the ratios of *trans*- to *cis*-2,3-epoxybutane produced from *cis*- compared to *trans*-2-butene (1.25–8.3). Observations on 2-butenes have been extended to several more straight-chain, internal olefins in the low-temperature region. The results are given in Table I. Comparison of the *trans*-epoxide to ketone ratios from the *cis*- *vs.* the *trans*-olefin with increasing size of the olefin indicates that these ratios diverge. However, the larger olefins show greater stereospecificity in their reactions. Thus, *cis*-3-hexene gives about 2.5 times as much *cis*-3,4-epoxyhexane as the *trans*-epoxide. Even a relatively small quantity of 3-hexanone from the *cis* intermediate could easily account for the difference in the *trans*-epoxide/ketone ratio between the reactions of *cis*- and *trans*-3-hexene. It is noted that the recently proposed "epoxide-like" transition complex implies that, although only one form of the complex is possible from the *trans*-, two forms are possible from the *cis*-olefin

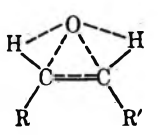

a

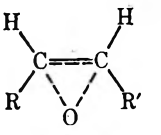

b

Of these, form b could readily lead to the ketone, because of easy migration of H, but form a would

(1) A. N. Hughes, M. D. Scheer, and R. Klein, *J. Phys. Chem.*, **70**, 798 (1966).

(2) M. D. Scheer and R. Klein, *ibid.*, **73**, 597 (1969).

(3) R. J. Cvetanović, *Advan. Photochem.*, **1**, 115 (1963).

Table I: Fractional Product Yields for the O(^{3}P) Addition to Internal, Straight-Chain Olefins at 90°K[a]

Products	2-Butene		2-Pentene		3-Hexene		4-Octene	
	cis	*trans*	*cis*	*trans*	*cis*	*trans*	*cis*	*trans*
trans-Epoxide	0.30	0.50	0.26	0.59	0.17	0.65	0.09	0.68
cis-Epoxide	0.24	0.06	0.34	0.04	0.42	0.02	0.82[c]	0.03[c]
Aldehyde	0.21	0.06	0.20	0.04	0.28	0.03		
Ketone	0.25	0.38	0.20[b]	0.33[b]	0.13	0.30	0.09	0.29
trans-Epoxide/ketone	1.2	1.3	1.3	1.8	1.3	2.2	1.0	2.3
cis-Epoxide/aldehyde	1.1	1.0	1.7	1.0	1.5	0.7		
cis-Epoxide/*trans*-epoxide	0.8	0.12	1.3	0.07	2.5	0.03		
Total epoxide/total carbonyl	1.2	1.3	1.5	1.7	1.4	2.0		

[a] The olefins were diluted 10:1 in propane prior to condensation on a 100-cm^2 Pyrex surface. [b] Sum of 2-pentanone and 3-pentanone, not separated on the glpc. [c] Sum of 2-propylpentanal and *cis*-4,5-epoxyoctane, not separated on the glpc.

be expected to preponderate from the energetic viewpoint.

An indication of the importance of these forms, within the framework of the transition states specified and the assumption that form a gives only the aldehyde in its rearrangement to the carbonyl end product, whereas form b gives mostly ketones, is obtained from the data of Table I. The *trans*-olefin compounds, as may be noted, produce epoxides that contain 90–97% of the *trans* form. If the same ratio of *cis*-epoxide to aldehyde obtained from the *cis*-3-hexene is maintained in the *trans*-3-hexene products, the residual aldehyde presumed to arise from the *trans* intermediate may be calculated. Accordingly a ratio of 50:1 for the *trans*-epoxide/aldehyde compounds derived from the *trans* complex is obtained. Clearly, aldehyde formation from the *trans* intermediate is negligible. All of the straight-chain olefins of Table I conform to this generalization. The *trans*-epoxide/ketone ratio obtained from the *cis*- as compared to the *trans*-olefin shows the largest difference with 4-octene. The correct value, 2.3, is obtained from *trans*-4-octene, because a contribution from the *cis* complex possible is virtually absent. This factor was used to calculate the ketone residual from the *cis* complex, starting with the *cis*-4-octene. Although the *cis*-epoxide and aldehyde were not separated, the ratio of the two may be assumed to be the same as the corresponding one from *cis*-3-hexene. The aldehyde/ketone ratio resulting from the *cis*-4-octene–oxygen complex is calculated to be about 7. It may be concluded that of the two forms of the transition complex derived from the *cis*-olefin, form a is the principal one and b is unimportant.

Two generalizations are apparent from Table I. The first is that retention of configuration of products becomes more pronounced with increasing chain length of the olefin. The second is that reaction of oxygen atoms in the low-temperature region tends to be more stereospecific with *trans*- than with *cis*-olefins. A stereotransformation of the transition intermediate requires a rotation of 180°, about the modified olefinic bond, of one of the carbon atoms of the double bond with its attached groups. Obviously, this process occurs with the *cis*-olefins. The extent to which stereotransformation will occur depends on the rates of ring closure and the rates of rearrangements leading to final products, compared to the rate of the *cis*–*trans* interchange in the complex. It seems reasonable to postulate that the rate of ring closure is independent of the size of the olefin. The ratio of total epoxide to total carbonyl products shows little change with size, and, hence, the rate of rearrangement to carbonyls is also size independent. The frequency of rotation of the portion of the complex

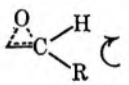

is then directly proportional to the extent of stereotransformation observed in the products. A measure of these transformations is the ratio of *cis*- to *trans*-epoxide, tabulated in Table I. In a rotationally unhindered system, the frequency is inversely related to the moment of inertia of the rotating group. Qualitatively, it would be expected that because of the higher moment of inertia associated with the larger olefin, the stereospecificity should increase with size; this is indeed the case. It is interesting that *cis*-2-pentene shows more stereospecificity than *cis*-2-butene. Despite the fact that both compounds have a methyl group adjacent to the olefinic site, a larger rotational barrier is inferred to be associated with the 2-pentene. A quantitative consideration of the relationship of size and stereo effects would require that potential barriers for rotation be taken into account also, but the qualitative conclusions remain unaffected.

Group Migrations

Carbonyl compounds constitute a sizable fraction of the products of the oxygen atom addition to olefins in the low-temperature region and, as has been noted, an intramolecular group migration is required for carbonyl formation. The principal carbonyl product in the *trans*-2-butene reaction at 90°K is 2-butanone.

The formation of this ketone requires the migration of H. Compared to migration of the methyl group, that of H is highly favored. *cis*-2-Butene is not useful for the comparison, as both of the hydrogen atoms attached to the olefinic carbon pair are suppressed through interaction with oxygen in the complex. The relative quantities of 2-butanone to isobutyraldehyde, after correction of the latter for the contribution from the *cis* complex, is taken as a measure of the ratio of migration of the hydrogen atom to migration of the methyl group. At 90°K, it is about 30. Similar considerations for *trans*-3-hexene lead to a value of about 20 for the ratio of migration of hydrogen with respect to the ethyl group. If rates of migration are independent quantities, to be associated with the specific groups, the rate of migration of ethyl should be the same as, or slightly higher than, that of the methyl group. These ratios are imprecise, because of the small quantities of the aldehyde produced in each case. A direct comparison between methyl and ethyl migrations is desirable if their relative rates are to be established; this can be done through the use of 3,4-dimethyl-3-hexene (DMH). The $O(^3P)$ reaction gives, in addition to 3,4-epoxy-3,4-dimethylhexane, two ketones, namely, 4,4-dimethyl-3-hexanone and 3-ethyl-3-methyl-2-pentanone, depending on whether the methyl or ethyl group migrates. The reaction gives no other products.

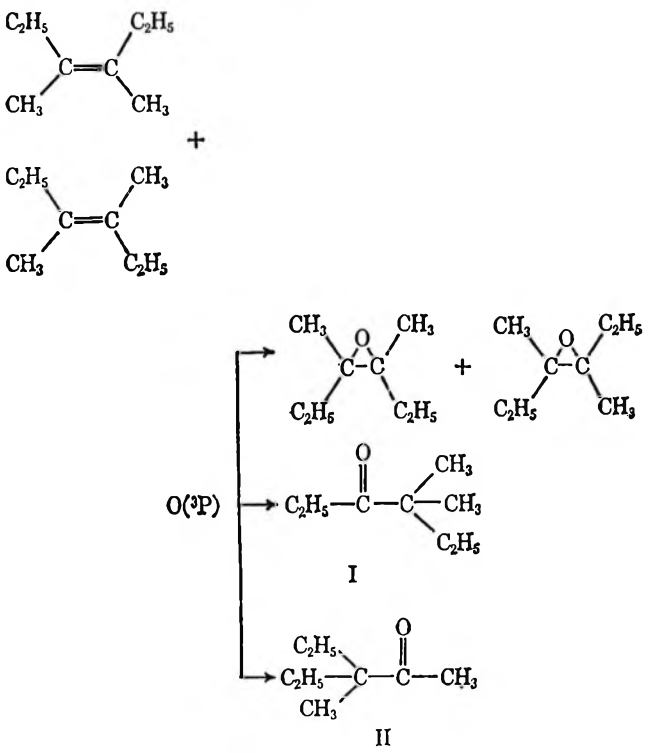

Both *cis*- and *trans*-3,4-dimethyl-3-hexene were used. The two ketone products, 4,4-dimethyl-3-hexanone and 3-ethyl-3-methyl-2-pentanone, will be referred to as I and II. The use of 3-ethyl-2-methyl-2-pentene (MEP) furnishes further data for assessing the validity of the concept of relative rates of migration of groups in establishing the product ratios.

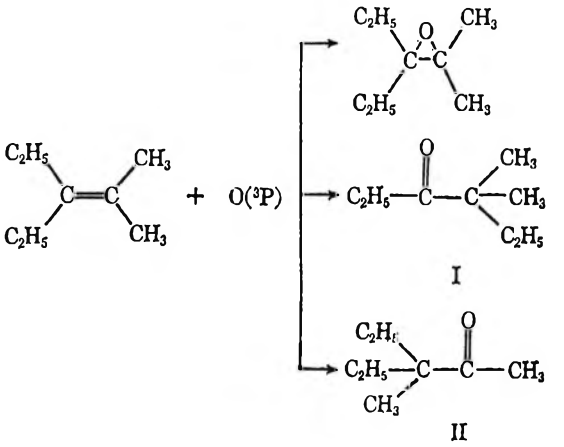

The same two ketones are produced from MEP as from *cis*- and *trans*-DMH. The important difference is that, whereas I results from the reactions of DMH with a rearrangement wherein a methyl group migrates, it is the migration of the ethyl group that gives I from MEP. Ketone II results from ethyl migration starting withD MH, or methyl migration starting with MEP. Therefore, if independent rates of migration are to be associated with these alkyl groups, the ketone ratio (I/II) produced from *cis*- or *trans*-DMH should be equal to (II/I) formed from MEP. It is emphasized that this follows if the presumed migration rates determine the position at which the O becomes localized. On the other hand, strong forces favoring addition to one of the olefinic carbons could control the alkyl group migrations.

Reactions were effected at 90°K in the apparatus routinely used for this purpose.[1] The olefins were diluted 10 to 1 with propane. The exposure time to oxygen atoms was 5 min, and about 1% of the olefin was reacted. The products were determined, after warmup, on a column (0.25 in. × 12 ft glpc) of Carbowax-6000, at 135° and a helium flow of 100 cc/min. The *cis* and *trans* isomers of 3,4-epoxy-3,4-dimethylhexane were not separable. Ketones I and II were easily separable. Retention times were determined with authentic samples of the two ketones. For all three olefins, only three glpc peaks were obtained for the products. These corresponded to the epoxides and the ketones I and II. Ratios of yield of product from the oxygen atom addition are given in Table II.

The notable feature of these results is that, of the two ketones, I and II, I is the major product; (I/II) = 2.5:1. Furthermore, this ratio is virtually independent of the starting olefin. Thus, the concept of independent rates of migration of groups in the rearrangement occurring in the O atom addition to olefins *must be abandoned.* The other alternative would require that the directive effect of the alkyl groups in MEP is such that the O adds to the carbon with the two

ethyl groups 2.5 times more rapidly than to the carbon with the two methyl groups. It would appear that, insofar as the ratio of ketones is concerned, it is their relative stabilities that control the rearrangement processes. Transformation to final products is a migration of an alkyl group concerted with the localization of the oxygen atom on one of the carbon atoms. Localization of the oxygen atom in the transition complex *preceding* alkyl group rearrangement is not in accord with the experimental results. If, in fact, localization did occur, the migration would be determined, in part (completely, if, as in MEP, the groups bonded to each of the olefinic carbon atoms occurred in pairs), by the directive factors, such as electron densities that are postulated as controlling the site of addition. It has been previously stated that oxygen atoms add mainly to the less-substituted carbon atom and that a methyl group confers "less substitution" than an ethyl group.[4] The directive influence of ethyl *vs.* methyl has been noted[5] for hydrogen atom addition to 2-pentene. At 90°K, the ratio of addition to C-2 is 1.6 times that to C-3. For MEP, addition of the O atom to that carbon atom of the double bond to which the two methyl groups are attached would be expected to be favored. Ketone II would, perforce, be formed in greater amounts than I; the data show unequivocally that this is incorrect.

Table II: Product Yield Ratios for the O(^{3}P) Addition to Some Isomeric Octenes at 90°K

Reactant	Product ratios: Ketone ratio (I/II)	Product ratios: Epoxides/ketones
cis-DMH	2.5	1.9
trans-DMH	2.7	1.1
MEP	2.6	2.4

The concerted rearrangement, in which oxygen localization and group migration occur, requires both electronic and spatial reorganization. The addition of ground-state, triplet oxygen to singlet-state olefin to give singlet-state products requires a relaxation process, as represented by a crossing of states on a potential surface. The recently introduced representation of the initial transition intermediate as a loose epoxide structure seems especially appropriate. Migration of groups probably involves a transient bridging of the double bond carbon pair. The path by which the intermediate relaxes to final products could even involve steric effects. The formation of the grouping

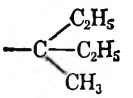

in II is sterically less favorable than

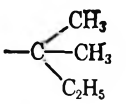

in I, and it may be speculated that the preponderance of I over II in the reactions of the *cis*- and *trans*-DMH and MEP can be ascribed to such steric effects.

Table II shows an interesting variation among the three olefins as regards the epoxide/ketone ratio. The interpretation of these results, and, particularly, why MEP exhibits such a high epoxide/ketone ratio, is not yet at hand.

(4) R. J. Cvetanović, *Can. J. Chem.*, 36, 623 (1958).

(5) R. D. Kelley, R. Klein, and M. D. Scheer, *J. Phys. Chem.*, 69, 905 (1965).

A Concentration-Jump Relaxation Method Study on the Kinetics of the Dimerization of the Tetrasodium Salt of Aqueous Cobalt(II)-4,4′,4″,4‴-Tetrasulfophthalocyanine

by Z. A. Schelly, R. D. Farina, and E. M. Eyring

Department of Chemistry, University of Utah, Salt Lake City, Utah 84112 *(Received August 1, 1969)*

The monomer–dimer equilibrium $2M \underset{{}_0k_{-1}}{\overset{{}_0k_1}{\rightleftharpoons}} D$ of the tetrasodium salt of Co(II)–4,4′,4″,4‴-tetrasulfophthalocyanine (Co(II)–TSPC) has been investigated by equilibrium spectrophotometric measurements and by the stopped-flow relaxation method at 58° in aqueous solution. The ratio of the ionic strength independent forward and reverse rate constants which are ${}_0k_1 = 5.36 \pm 0.15 \times 10^2\ M^{-1}\ \text{sec}^{-1}$ and ${}_0k_{-1} = 2.8 \pm 0.10 \times 10^{-3}\ \text{sec}^{-1}$, respectively, is in good agreement with the spectrophotometrically determined thermodynamic equilibrium constant $K = 2.05 \pm 0.05 \times 10^5\ M^{-1}$. The effect of ionic strength on the equilibrium and kinetics is discussed.

Introduction

Macrocyclic systems with four pyrrole rings have attracted the interest of many investigators due to their biological and industrial importance. A number of water-soluble metal complexes of tetrasulfonated phthalocyanines (see Figure 1) were chosen as models for a spectrophotometric study on this class of compounds by Bernauer and Fallab.[1] The dimerization of sulfonated metal phthalocyanines, like many other charged dye molecules, has been described in the literature.[2] However, very little has been done on the kinetics of the dimerization.[3] The present work describes a kinetic study of the monomer–dimer equilibrium of aqueous Co(II)–TSPC solutions using the concentration-jump relaxation technique.[4]

Experimental Section

All of the chemicals were reagent or analytical grade except the monosodium salt of 4-sulfophthalic acid obtained from Aldrich Chemical Co. which was used without further purification.

The tetrasodium salt of Co(II)-4,4′,4″,4‴-tetrasulfophthalocyanine dihydrate ($C_{32}H_{12}N_8O_{12}S_4Na_2Co \cdot 2H_2O$) was synthesized according to Weber and Busch.[5] The result of the elemental analysis on the compound is in agreement with the calculated theoretical values. *Anal.* Calcd: C, 37.82; H, 1.59; N, 11.03; S, 12.62; Co, 5.80. Found: C, 37.50; H, 1.82; N, 10.73; S, 12.47; Co, 5.80.

The optical measurements were obtained on a Cary 14 recording spectrophotometer. The relaxation experiments were carried out on a Durrum-Gibson stopped flow and a Joule-heating single beam type temperature-jump apparatus.[6] All stopped-flow experiments were performed at 58° where appreciable amounts of monomer and dimer are both present.

Results and Discussion

Equilibrium Experiments. The absorption spectra of Co(II)–TSPC aqueous solutions are shown in Figure 2. In the concentration range of 10^{-7} to $10^{-5}\ M$ the absorption curves form an isosbestic point at λ 639 nm, which we attribute to a monomer–dimer equilibrium. The possibility of further association was excluded in this concentration range.[1] The dimerization constant K of Co(II)–TSPC at 58° has been reported in the literature[1] without any reference to the ionic strength which changes appreciably in the concentration range used, if no salts are added. Their method of determination[1] suggests the equilibrium constant is a concentration quotient $Q = C_D/C_M^2$, where $C_D \equiv$ concentration of dimer and $C_M \equiv$ concentration of monomer. If this is so, then the equilibrium constant reported is valid only at a certain concentration and ionic strength.

One way to obtain the thermodynamic equilibrium constant is to determine the monomer concentration C_M at several different total concentrations C_T of the dye

(1) K. Bernauer and S. Fallab, *Helv. Chim. Acta*, **44**, 1287 (1961).

(2) S. E. Sheppard and A. L. Geddes, *J. Amer. Chem. Soc.*, **66**, 1995 (1944); H. Kobayashi, Y. Torrii, and N. Fukuda, *J. Chem. Soc. Jap.*, **81**, 694 (1960).

(3) R. D. Farina and J. H. Swinehart studied the dimerization of V(IV)–TSPC; to be published.

(4) J. H. Swinehart and G. W. Castellan, *Inorg. Chem.*, **3**, 278 (1964).

(5) J. H. Weber and D. H. Busch, *ibid.*, **4**, 469 (1965).

(6) G. G. Hammes and J. I. Steinfeld, *J. Amer. Chem. Soc.*, **84**, 4639 (1962).

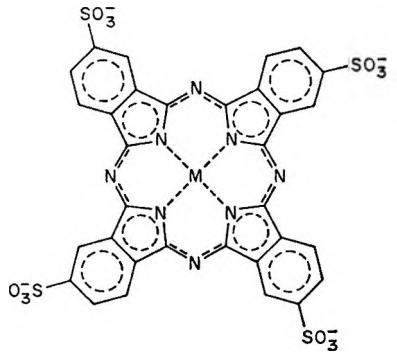

Figure 1. Formula of metal(II)-4,4',4'',4'''-tetrasulfophthalocyanine ion.

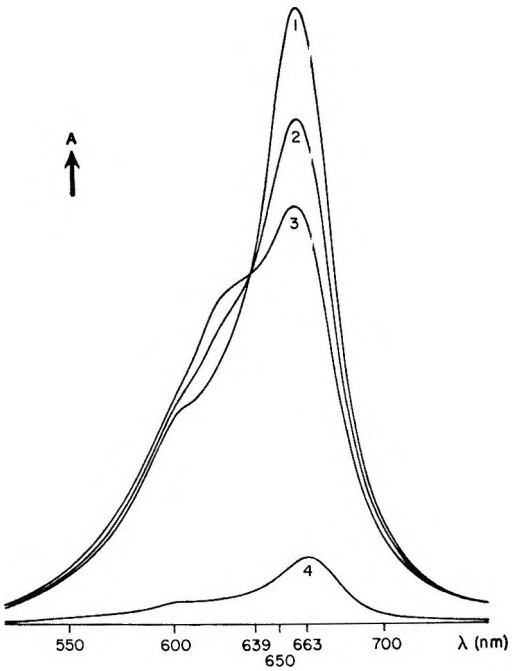

Figure 2. Visible absorption spectra of Co(II)-TSPC at 58°: curve 1 is for a 10^{-6} M concentration in a 10-cm optical path length cell; curve 2 is 10^{-6} M in a 1-cm cell; curve 3 is 5 × 10^{-5} M in a 0.2-cm cell; curve 4 is a 10^{-7} M solution in a 10-cm cell at 81°.

at 58°. This allows the calculation of the quotient Q to be made for different C_T values. Extrapolation of Q to infinite dilution yields $K = 2.05 \pm 0.05 \times 10^{-5}$ M^{-1} (see Figure 3), since

$$\lim_{C_T \to 0} \frac{f_D}{f_M^2} = 1, \text{ hence } \lim_{C_T \to 0} Q = K = \frac{C_D}{C_M^2} \frac{f_D}{f_M^2}$$

where f_D and f_M represent the activity coefficients of the dimer and monomer, respectively. We unsuccessfully attempted to calculate the activity coefficients using the Debye–Hückel limiting law and Davies' equation.[7] The values obtained for f_D/f_M^2 were not in agreement with the experimentally determined ratios K/Q indicating that either the equations are not applicable for so highly charged ions and/or

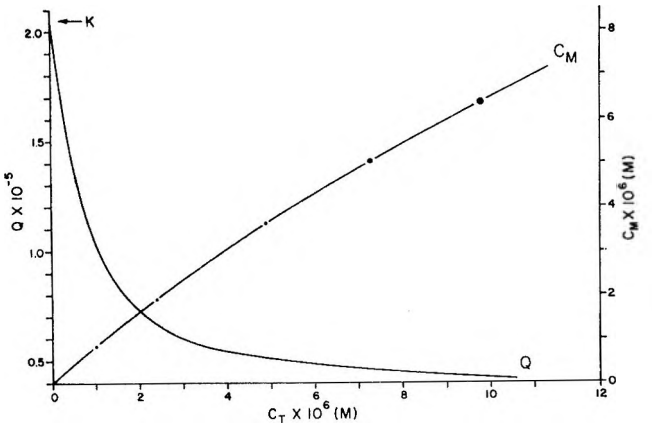

Figure 3. Equilibrium concentration of monomer, C_M (determined), and concentration quotient, Q (calcd), plotted *vs.* total dye concentration, C_T, at 58°.

the charges are different from what we assumed, namely −4 and −8 for monomer and dimer, respectively.

Determination of the Monomer Concentration C_M. Since the absorption bands of the dimer and monomer are strongly overlapping there is no wavelength λ where the molar decadic absorptivity of the monomer ϵ_M and/or dimer ϵ_D can be accurately obtained. We calculated ϵ_M at different λ's by shifting the equilibrium $2M \rightleftharpoons D$ completely in favor of the monomer. This was accomplished by raising the temperature of a highly dilute (10^{-7} M) solution until no increase in absorbance at the monomer absorption maximum λ_{max} was observed. This occurred at about 81°, and the absorbance was measured with a 10-cm cell. The calculated value of ϵ_M at λ_{max} 663 nm is 1.03 ± 0.01 × 10^5 M^{-1} cm^{-1}.

The temperature dependence of ϵ is described implicitly by the function $\epsilon(t)$ = constant × $(n^2 + 2)^2/n$, where n is the refractive index of the solvent.[8] Calculations showed that over the temperature range of 58 to 81° ϵ changes only within the experimental error. Thus $\epsilon_M(81°)$ was used in the spectral determinations at 58°.

The shape of the pure monomer band is defined by the ratio ${}_{max}\epsilon_M/{}_{\lambda_i}\epsilon_M$, where ${}_{max}\epsilon_M$ and ${}_{\lambda_i}\epsilon_M$ are the molar decadic absorptivities at λ_{max} and λ_i, respectively. Assuming that the dimer band is symmetrical about its maximum, one can successively reduce the composite band and approximate to its additive components until there is no overlapping at the desired analytical wavelength.[9]

We could find no way to shift the equilibrium completely in favor of the dimer to obtain the pure dimer

(7) C. W. Davies, "Ion Association," Butterworths, Washington, D. C., 1962, p 41.

(8) G. Kortüm, "Kolorimetrie, Photometrie und Spektrometrie," Springer-Verlag, Berlin, 1962, p 23.

(9) In a very similar way as described by W. West and S. Pears, *J. Phys. Chem.*, **69**, 1894 (1965).

band. But, since $C_T = C_M + 2C_D$, one clearly needs no independent determination of C_D. Absorption spectra and temperature-jump relaxation spectra have indicated that at higher concentrations ($C_T > 5 \times 10^{-5}$ M) and ionic strength ($10^{-2} < I < 10^{-1}$ M) new equilibria are established. This may be due to formation of species with a degree of polymerization greater than two.

Kinetics. Because at high concentration and/or ionic strength further polymerization occurs, we had to restrict our kinetic experiments to low concentrations ($C_T < 10^{-5}$ M) and low ionic strength ($I < 10^{-4}$ M). We perturbed the equilibrium $2M \rightleftharpoons D$ of solutions at 58° by sudden dilutions using the stopped-flow apparatus.[4] The change of the monomer concentration was followed photometrically at λ_{max} 663 nm. No effort was made to maintain a constant ionic strength because of the uncertainty in the charges of the reacting ions. The change in concentration during the reactions was small enough (less than 4%) so that the rate equations could be linearized.

In this system different charged species are present in equilibrium namely $2M^z \underset{{}_0k_{-1}}{\overset{{}_0k_1}{\rightleftharpoons}} D^{2z}$, where $z = -4$ at vanishing concentration. Consequently, shifting the equilibrium changes the ionic strength and activity coefficients f_i during the course of the reaction.[10] If the ionic strength were constant, the reciprocal relaxation time τ^{-1} at any ionic strength can be expressed by

$$\tau^{-1} = {}_0k_{-1}\frac{f_D}{f^{\pm}} + 4{}_0k_1\frac{f_M^2}{f^{\pm}}{}_\infty C_M \qquad (1)$$

where ${}_\infty C_M$ symbolizes C_M at time $t = \infty$, and $f^{\pm}$ is the activity coefficient of the activated complex. The charge of the activated complex is the sum of the charges of the reacting ions which, in our case, is $2z$. Assuming the ionic radii of the activated complex and that of the product (dimer) are very similar, $f_D/f^{\pm}$ becomes unity and eq 1 simplifies to

$$\tau^{-1} = {}_0k_{-1} + 4{}_0k_1\frac{f_M^2}{f^{\pm}}{}_\infty C_M \qquad (2)$$

However, as pointed out earlier, the activity coefficients are changing during the course of the reaction as a function of the instantaneous concentration of the reactants. In this case the relaxation expression 1 modifies to

$$\tau^{-1} = {}_0k_{-1}\beta\left(1 + \frac{\mathrm{d}\ln\beta}{\mathrm{d}\ln C_D}\right) + 2{}_0k_1\left(2 + \frac{\mathrm{d}\ln\alpha}{\mathrm{d}\ln C_M}\right)C_M \qquad (3)$$

where $\alpha \equiv f_M^2/f^{\pm}$ and $\beta \equiv f_D/f^{\pm}$. Applying the previous simplification $\beta \simeq 1$ eq 3 reduces to

$$\tau^{-1} = {}_0k_{-1} + 2{}_0k_1\left(2 + \frac{\mathrm{d}\ln\alpha}{\mathrm{d}\ln C_M}\right)C_M \qquad (4)$$

All activity coefficients converge to unity as one approaches infinite dilution. Consequently, each of eq 1 through 4 yield the same limits

$$\lim_{C\to 0}\frac{\mathrm{d}(\tau^{-1})}{\mathrm{d}C_M} = 4{}_0k_1 \text{ and } \lim_{C_T\to 0}\tau^{-1} = {}_0k_{-1}$$

Hence, the intercept of the τ^{-1} *vs.* C_M plot yields ${}_0k_-$ and the slope of the curve at the intercept is equal to $4{}_0k_1$. Equation 4 provides instantaneous τ^{-1} values as a function of C_M. Thus, in a series of experiments, one has to plot initial (${}_0\tau^{-1}$), final (${}_\infty\tau^{-1}$), or some intermediate (${}_i\tau^{-1}$) reciprocal τ values corresponding to a definite extent of the reaction *vs.* the corresponding C_M.

As was mentioned earlier, the calculation of the activity coefficients was not possible using the Debye–Hückel limiting law or Davies' equation. However, at any equilibrium concentration $Q/K = f_M^2/f_D = \alpha/\beta$. Since $\beta \simeq 1$, Q/K yields $f_M^2/f^{\pm}$ which can be used in eq 2. Similarly, slopes of the curve ln (Q/K) *vs.* ln ${}_\infty C_M$ provide the required values of d ln α/d ln ${}_\infty C_M$ to be substituted into eq 4. Hence a theoretical curve τ^{-1} *vs.* ${}_\infty C_M$ can be calculated using ${}_0k_{-1}$ and ${}_0k_1$ obtained experimentally.

In our experiments single relaxation times were observed resulting in linear plots of log Δ(light intensity) *vs.* time. This indicates that the perturbations were so small that the change of the ionic strength during the reaction did not affect the relaxation times within the experimental error. Therefore, eq 2 was used to calculate the theoretical curve. Figure 4 shows the plot of the experimental and calculated results. The intercept of the experimental curve yields ${}_0k_{-1} = 2.8 \pm 0.10 \times 10^{-3}$ sec^{-1} and from the limiting slope one obtains ${}_0k_1 = 5.36 \pm 0.15 \times 10^{-2}$ M^{-1} sec^{-1}. A

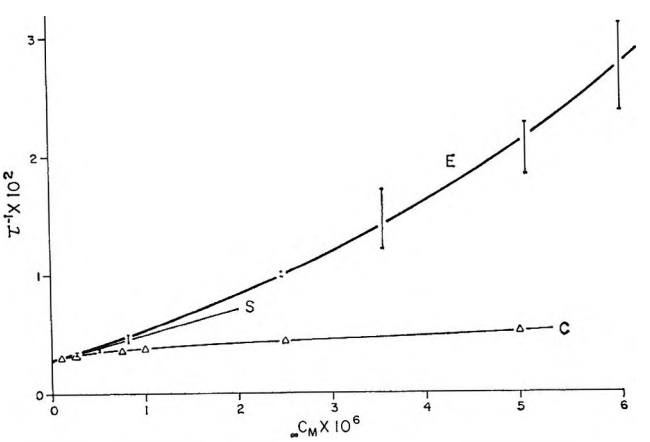

Figure 4. Reciprocal relaxation time, τ^{-1} (E, experimental; C, calculated) *vs.* ${}_\infty C_M$. Line S is the limiting tangent of curve E.

(10) The effect of changing ionic strength on the form of the relaxation equation has been discussed in general by M. Eigen and L. DeMaeyer in A. Weissberger's "Technique of Organic Chemistry," Vol. VIII, part II, Interscience Publishers, New York, N. Y., 1963, p. 904.

ratio ${}_0k_1/{}_0k_{-1}$ of $1.92 \pm 0.12 \times 10^5\ M^{-1}$ is the kinetically determined equilibrium constant. This is in good agreement with the equilibrium constant obtained by the optical method ($K = 2.05 \pm 0.05 \times 10^5\ M^{-1}$). The ratio ${}_0k_1/{}_0k_{-1}$ is presented as the mean of the extreme values of the quotients. Uncertainties associated with numerical values are given as average deviations from the mean, not standard deviations.

At monomer concentrations greater than $5 \times 10^{-7}\ M$ the experimental curve deviates appreciably from the calculated one. This deviation is qualitatively plausible, because the extent of ion-pair formation between Na^+ and the highly charged metal complex ions increases with increasing total concentration. Therefore, the ionic strength independent rate constants ${}_0k_1$ and ${}_0k_{-1}$ are changing as a function of the charges z of the reacting species.

Assume the nonelectrostatic interaction between reactants is substantially independent of their charges, and that the change in the dielectric constant D of the solution is negligible for small changes of the ionic charges at high dilution. Under these conditions one can obtain

$$\mathrm{d} \ln {}_0k_{\pm 1} = -\frac{2ze_0^2N}{DRTr^{\ddagger}}\,\mathrm{d}z \qquad (5)$$

using Scatchard's work[11] as a basis for the derivation. In addition to the familiar symbols N, e_0, R, and T in eq 5, $r^{\ddagger}$ is the radius of the activated complex. It is considered constant for small changes of the charges. In our case z is negative and $\mathrm{d}z$ is positive in eq 5. Therefore, both ${}_0k_1$ and ${}_0k_{-1}$ have to increase with increasing total concentration. Consequently, the rate constants determined experimentally and used in the calculations of the theoretical r's represent the smallest possible values. These rate constants are valid only at infinite dilution where the complex ions have their highest possible charges. This qualitatively explains why the calculated reciprocal relaxation times are lower than the experimental values.

Acknowledgment. This work has been sponsored by AFOSR(SRC)-OAR, USAF, Grant No. 69-1717.

(11) G. Scatchard, *Chem. Rev.*, **10**, 229 (1932); *cf.* A. A. Frost and R. G. Pearson, "Kinetics and Mechanism," 2nd ed, John Wiley & Sons, Inc., New York, N. Y., 1965, p 145.

Angular Dependence of Long-Range Proton Hyperfine Coupling Constants in Aliphatic Radicals

by Michael Barfield

Department of Chemistry, University of Arizona, Tucson, Arizona 85721 *(Received July 24, 1969)*

A theoretical study of the angular dependence of the γ- and δ-proton hyperfine coupling constants in aliphatic radical fragments is presented. A spin density formalism based on the generalized product approximation with intergroup configuration is developed and specialized to valence-bond wave functions. The calculated results for aliphatic radicals in which the unpaired electron is concentrated on a single carbon atom are indicative of the importance of a variety of spin polarization mechanisms. In contrast to previous calculations both positive and negative signs are obtained for a_γ depending on conformation. Calculated results are compared with the available experimental data, and their significance in terms of mechanisms is discussed.

I. Introduction

The observation of long-range hyperfine coupling constants in aliphatic fragments[1-7] has led to a number of theoretical descriptions which include molecular orbital (MO) treatments[8-11] in which extended Hückel theory[12] has been used to calculate hyperconjugative contributions to the long-range proton hyperfine coupling constants. Theoretical calculations of the importance of the spin polarization mechanism for an aliphatic chain have been based on a Dirac vector model[13] and an MO perturbation formulation[14] with valence-bond (VB) parameters for the configuration interaction.

Since the extended Hückel calculations[8-11] ignored exchange interactions, the calculated long-range coupling constants were invariably positive in sign. In the descriptions which included exchange, the calculated γ-hyperfine coupling constants were found to be negative, but both positive and negative values have been inferred[15,16] from nmr contact shifts. Although the relative importance of spin delocalization *via* electron transfer *vs.* spin exchange has been investigated[17,18] for β protons, similar studies have not been given for the long-range hyperfine coupling constants.

The long-range hyperfine proton coupling constants in aliphatic fragments are highly dependent on conformation[1-7] and a correspondence has been noted[13,19,20] with long-range proton–proton coupling constants in nmr spectroscopy. This paper presents a theoretical VB description of the angular dependence of the γ- and δ-hyperfine coupling constant based on the spin polarization mechanism. The theoretical formulation which is presented here uses the generalized product approximation with intergroup configuration interaction,[21-23] and is closely related to a general theoretical formulation[24] which has been used to calculate[25-27] a variety of long-range H–H coupling constants.

II. Theoretical Formulation

A. Spin Density Matrix in the Generalized Product Approximation with Intergroup Configuration Inter-

(1) R. W. Fessenden and R. H. Schuler, *J. Chem. Phys.*, **39**, 2147 (1963).

(2) G. A. Russell and K. Y. Chang, *J. Amer. Chem. Soc.*, **87**, 4381 (1965).

(3) G. A. Russell, K. Y. Chang, and C. W. Jefford, *ibid.*, **87**, 4383 (1965).

(4) R. O. C. Norman and B. G. Gilbert, *J. Phys. Chem.*, **71**, 14 (1967).

(5) G. A. Russell, G. Holland, K. Y. Chang, and L. M. Zalkov, *Tetrahedron Lett.*, **21**, 1955 (1967).

(6) P. J. Krusic and J. K. Kochi, *J. Amer. Chem. Soc.*, **90**, 7155 (1968).

(7) J. J. Windle, J. A. Kuhnle, and B. H. Beck, *J. Chem. Phys.*, **50**, 2630 (1969).

(8) G. A. Petersson and A. D. McLachlan, *ibid.*, **45**, 628 (1966).

(9) R. S. Drago and H. Peterson, Jr., *J. Amer. Chem. Soc.*, **89**, 3978 (1967).

(10) G. R. Underwood and R. S. Givens, *ibid.*, **90**, 3713 (1968).

(11) R. E. Cramer and R. S. Drago, *ibid.*, **90**, 4790 (1968).

(12) R. Hoffman and W. N. Lipscomb, *J. Chem. Phys.*, **36**, 2179 (1962).

(13) Z. Luz, *ibid.*, **48**, 4186 (1968).

(14) J. P. M. Bailey and R. M. Golding, *Mol. Phys.*, **12**, 49 (1967).

(15) E. de Boer and H. van Willigen, "Progress in Nuclear Magnetic Resonance Spectroscopy," Vol. 2, Pergamon Press, Ltd., Oxford, 1967, p 111.

(16) D. R. Eaton, A. D. Josey, and R. E. Benson, *J. Amer. Chem. Soc.*, **89**, 4040 (1967).

(17) J. P. Colpa and E. de Boer, *Mol. Phys.*, **7**, 333 (1964).

(18) P. Lazdins and M. Karplus, *J. Chem. Phys.*, **44**, 1600 (1966).

(19) D. Kosman and L. M. Stock, *Chem. Commun.*, **10**, 551 (1968); R. Z. Sagdeev, Yu. N. Molin, and E. G. Rozantsev, *Teor. Eksp. Khim.*, **5**, 234 (1969).

(20) M. Barfield and M. Karplus, *J. Amer. Chem. Soc.*, **91**, 1 (1969).

(21) R. McWeeny, *Proc. Roy. Soc.*, **A253**, 242 (1959).

(22) R. McWeeny and Y. Mizuno, *ibid.*, **A259**, 554 (1961).

(23) R. McWeeny and B. T. Sutcliffe, *Mol. Phys.*, **6**, 493 (1963).

(24) M. Barfield, *J. Chem. Phys.*, **49**, 2145 (1968); **51**, 2291 (1969).

(25) M. Barfield and B. Chakrabarti, *J. Amer. Chem. Soc.*, **91**, 4346 (1969).

action. Consider the case of two groups designated A and B with N_A and N_B electrons, respectively. If group A is in a level with multiplicity $2S + 1$, then in the generalized product approximation[21-23] a single configuration wave function of the same multiplicity can be written

$$^{2S+1}\Phi_{Aa_M} = \mathcal{A}[^{2S+1}\phi_{Aa_M}(1,2,\ldots,N_A) \times {}^1\phi_{B0}(N_A + 1,\ldots,N_A + N_B)] \quad (1)$$

where $\mathcal{A}$ is an operator which produces a normalized, antisymmetric wave function, M assumes the $2S + 1$ values, $-S$, $-S + 1$, ..., S, and $^{2S+1}\phi_{Aa_M}$ denotes the Mth component of the ath level in the manifold of group A, which has multiplicity $2S + 1$. In eq 1, $^1\phi_{B0}$ denotes the lowest singlet state wave function for group B.

Nonvanishing spin density will arise within the B group on including configuration interaction (CI) between the groups.[23] Consider those configurations formed by spin coupling of the A group with triplet states of the B group

$$^{2S+1}\Phi(Aa\mathrm{B}b)_M = \begin{pmatrix} S & 1 & S \\ M & 0 & M \end{pmatrix}\Phi(Aa_M\mathrm{B}b_0) + \begin{pmatrix} S & 1 & S \\ M+1 & -1 & M \end{pmatrix}\Phi(Aa_{M+1}\mathrm{B}b_{-1}) + \begin{pmatrix} S & 1 & S \\ M-1 & 1 & M \end{pmatrix}\Phi(Aa_{M-1}\mathrm{B}b_{+1}) \quad (2)$$

where, for example

$$\Phi(Aa_M\mathrm{B}b_0) = \mathcal{A}[^{2S+1}\phi_{Aa_M}{}^3\phi_{Bb_0}] \quad (3)$$

For symmetry in the resulting expressions (the calculations are based on a method developed for triplet states) we also include mixing with those configurations in which the B group has multiplicity $2S + 1$

$$^{2S+1}\Phi_{Bb_M} = [^1\phi_{A0}{}^{2S+1}\phi_{Bb_M}] \quad (4)$$

Restricting the configurational mixing to these three functions gives

$$^{2S+1}\Psi_{Aa_M} = \sum_a c_{a,a}{}^{2S+1}\Phi_{Aa_M} + \sum_b c_{a,b}{}^{2S+1}\Phi_{Bb_M} + \sum_{ab}{}' c_{a,ab}{}^{2S+1}\Phi(Aa\mathrm{B}b)_M \quad (5)$$

where the coefficients are determined by solving a secular determinant or by perturbation methods.[21-23] By means of a density matrix description analogous to that developed by McWeeny and Sutcliffe,[23] it readily follows that the spin-density matrix for the standard state ($M = S$) is given by

$$Q_1(\alpha_S\alpha_S|1;1') = \sum_a c_{a,a}{}^2 Q_1(a_Sa_S|1;1') + \sum_b c_{a,b}{}^2 Q_1(b_{+1}b_{+1}|1,1') + 2^{1/2}\delta_{1,S}\sum_{a,b}{}' c_{a,ab}[c_{a,b}Q_1(0a_0|1;1') - c_{a,a}Q_1(0b_0|1;1')] + [1 - \{S(S+1)\}^{-1}]\sum_{a,b}{}' c_{a,ab}{}^2 Q_1(a_Sa_S|1;1') + [S+1]^{-1}\sum_{a,b} c_{a,ab}{}^2 Q_1(b_{+1}b_{+1}|1,1') \quad (6)$$

where $Q_1(a_Sa_S|1;1')$ is the spin-density matrix for the A group, and $Q_1(0b_0|1;1')$ is the transition spin-density matrix for the B group. The term which multiplies the Kronecker delta, $\delta_{1,S}$, only appears if $S = 1$. In this case the spin-density matrix is

$$Q_1(\alpha_{+1}\alpha_{+1}|1;1') = \sum_a c_{a,a}{}^2 Q_1(a_{+1}a_{+1}|1;1') + \sum_b c_{a,b}{}^2 Q_1(b_{+1}b_{+1}|1;1') + \sqrt{2}\sum_{a,b}{}' c_{a,ab}[c_{a,b}Q_1(0a_0|1;1') - c_{a,a}Q_1(0b_0|1,1')] + \frac{1}{2}\sum_{a,b}{}' c_{a,ab}{}^2[Q_1(a_{+1}a_{+1}|1,1') + Q_1(b_{+1}b_{+1}|1;1')] \quad (7)$$

The expression derived by McWeeny and Sutcliffe[23] conforms to the first term in brackets under the third summation sign in eq 6 and 7. These terms give the most important contributions to the B-group spin densities. If the two groups are only weakly interacting, then contributions from the second and last terms in eq 7 will be negligible.

Most of the matrix element expressions which arise for intergroup CI in eq 5 have been given in a previous paper.[24] In addition to these, it is necessary to evaluate the triplet diagonal matrix elements

$$H'_{AB,AB} = \langle {}^3\Phi(Aa\mathrm{B}b)_{+1}|\mathcal{H}|{}^3\Phi(Aa\mathrm{B}b)_{+1}\rangle \quad (8)$$

These can be obtained most simply by the *equivalent operator technique*[23]

$$H'_{AB,AB} = H^A(a_{+1}a_{+1}) + H^B(b_{+1}b_{+1}) + J^{AB}(a_{+1}a_{+1},b_{+1}b_{+1}) - K_0{}^{AB}(a_{+1}a_{+1},b_{+1}b_{+1}) + K^{AB}(a_{+1}a_{+1},b_{+1}b_{+1}) \quad (9)$$

where $H^A(a_{+1}a_{+1})$ is the energy of the A group alone

$$H^A(a_{+1}a_{+1}) = tr[h(1)\rho_1{}^A(a_{+1}a_{+1}|1;1)] + \frac{1}{2}tr[g(1,2)\rho_2{}^A(a_{+1}a_{+1}|1,2;1,2)] \quad (10)$$

in which $h(1)$ and $g(1,2)$ are the one- and two- electron parts of the Hamiltonian operator, respectively. The integrals in eq 9 can be written in terms of spinless density matrices

$$J^{AB}(a_{+1}a_{+1},b_{+1}b_{+1}) = \int g(1,2)P_1{}^A(a_{+1}a_{+1}|1;1)P_1{}^B(b_{+1}b_{+1}|\ 2;2)d\tau_1d\tau_2 \quad (11)$$

(26) M. Barfield and B. Chakrabarti, *Chem. Rev.*, 69, 757 (1969).
(27) M. Barfield and J. J. Reed, *J. Chem. Phys.*, 51, 3039 (1969).

$$K_0^{AB}(a_{+1}a_{+1},b_{+1}b_{+1}) =$$
$$^1/_2\int g(1,2)P_1^A(a_{+1}a_{+1}|2;1)P_1^B(b_{+1}b_{+1}|1;2)d\tau_1 d\tau_2 \quad (12)$$
$$K^{AB}(a_{+1}a_{+1},b_{+1}b_{+1}) =$$
$$^1/_2\int g(1,2)Q_1^A(a_{+1}a_{+1}|2;1)Q_1^B(b_{+1}b_{+1}|1;2)d\tau_1 d\tau_2 \quad (13)$$

The additional off-diagonal elements which are needed are those of the type

$$H_{A,AB} = \langle {}^3\phi_{Aa_{+1}}|\mathcal{H}|{}^3\Phi_{(AaBb)_{+1}}\rangle \quad (14)$$

From eq 2 these elements can be expanded as

$$H_{A,AB} = 2^{-1/2}\{\langle {}^3\Phi_{Aa_{+1}}|\mathcal{H}|\Phi(Aa_{+1}Bb_0)\rangle - \langle {}^3\Phi_{Aa_{+1}}|\mathcal{H}|\Phi(Aa_0Bb_{+1})\rangle\} \quad (15)$$

The wave functions in eq 15 differ in one or two groups, but only the two electron exchange integrals are nonvanishing in the spin integrations

$$H_{A,AB} = -2^{-1/2}\{K^{AB}(a_{+1}a_{+1},0b_0) - K^{AB}(a_{+1}a_0,0b_{+1})\} \quad (16)$$

where, for example

$$K^{AB}(a_{+1}a_{+1},0b_0) =$$
$$\int g(1,2)\rho_1^A(a_{+1}a_{+1}|2;1)\rho_1^B(0b_0|1;2)dr_1dr_2 \quad (17)$$

The transition densities are related to the transition spin densities by[22]

$$\rho_1(0b_{+1}|1;1') = -2^{-1/2}Q_1^B(0b_0|1;1')\beta(1)\alpha^*(1') \quad (18)$$
$$\rho_1(0b_0|1;1') =$$
$$2^{-1}Q_1^B(0b_0|1;1')\{\alpha(1)\alpha^*(1') - \beta(1)\beta^*(1')\} \quad (19)$$
$$\rho_1(a_{+1}a_{+1}|1;1') =$$
$$2^{-1}Q_1^A(a_{+1}a_{+1}|1;1')\{\alpha(1)\alpha^*(1') - \beta(1)\beta^*(1')\} \quad (20)$$
$$\rho_1(a_{+1}a_0|1;1') = 2^{-1/2}Q_1^A(a_{+1}a_{+1}|1;1')\alpha(1)\beta^*(1') \quad (21)$$

On substituting eq 18–21 into the expressions for the exchange integrals and performing the spin integrations, the off-diagonal elements are simply given by

$$H_{A,AB} = 2^{1/2}K^{AB}(a_{+1}a_{+1},0b_0) \quad (22)$$

where

$$K^{AB}(a_{+1}a_{+1},0b_0) =$$
$$\frac{1}{2}\int g(1,2)Q_1^A(a_{+1}a_{+1}|2;1)Q_1^B(0b_0|1,2)d\tau_1 d\tau_2 \quad (23)$$

B. Valence-Bond Wave Functions. To calculate spin densities in radicals with a single unpaired electron we make use of the fact that the use of VB wave functions with configuration interaction between the groups approximates the usual VB bond diagram methods.[24] In addition, if the exchange integral between a terminal electron pair in the perfect-pairing structure is set equal to zero, one of the spins is uncoupled from the system. The remaining fragment is a doublet-state radical.

Triplet VB wave functions are written as a linear combination of nonionic, canonical structures

$${}^3\phi_{Aa_M} = \sum_l c_{a_M,l}{}^3\psi_l \quad (24)$$

An explicit expression for the VB spin density matrix is[24,28]

$$Q_1(a_{+1}a_{+1}|1;1') = \sum_{jl} c_{a_0,j}c_{a_0,l}(1/2)^{n-i_{jl}}\sum_r r(1)r^*(1')g_{jl}{}^r \quad (25)$$

where r denotes an atomic orbital in A, and in the superposition diagrams of the triplet canonical structures i_{jl} is the number of islands and $g_{jl}{}^r = 1$ if both broken bonds are in the same island and r is connected to a broken bond by an even number of bonds. If both broken bonds are in the same island and r differs from the nearest atom which is connected to a broken bond by an odd number of bonds, then $g_{jl}{}^r = -1$. In all other cases $g_{jl}{}^r = 0$. The VB transition density matrix was given previously by

$$Q_1(0a_0|1;1) = \sum_{jl} c_{aj}c_{a_0,l}(1/2)^{n-i_{jl}}\sum_r r(1)r^*(1')f_{jl}{}^r \quad (26)$$

where the notation conforms to that in eq 25, but in the superposition diagrams of singlet and triplet canonical structures $f_{jl}{}^r = -1$ if atomic orbital r is part of an island which contains a broken bond and is in the even subset. The factor $f_{jl}{}^r = -1$ if r is part of an island which contains a broken bond but is in the odd subset. In all other cases this factor is zero. More general expressions for the various density matrices are also available.[29-31]

The various types of intergroup exchange integrals are obtained from eq 25 and 26

$$K^{AB}(0a_0,0b_0) = \frac{1}{2}\sum_{jklm} c_{aj}c_{aok}c_{bl}c_{bom}(1/2)^{n-i_{jk}-i_{lm}} \times \sum_{r,s} f_{jk}{}^r f_{lm}{}^s K(r,s) \quad (27)$$

$$K^{AB}(a_{+1}a_{+1},b_{+1}b_{+1}) = \frac{1}{2}\sum_{jklm} c_{aoj}c_{aok}c_{bol}c_{bom}(1/2)^{n-i_{jk}-i_{lm}} \times \sum_{r,s} g_{jk}{}^r g_{lm}{}^s K(r,s) \quad (28)$$

$$K^{AB}(a_{+1}a_{+1},0b_0) = \frac{1}{2}\sum_{jklm} c_{aoj}c_{aok}c_{bl}c_{bom}(1/2)^{n-i_{jk}-i_{lm}} \times \sum_{r,s} g_{jk}{}^r f_{lm}{}^s K(r,s) \quad (29)$$

where

$$K(r,s) = \int r(1)s(2)\,\mathcal{H}\,r(2)s(1)d\tau_1 d\tau_2 \quad (30)$$

A computer program was written in FORTRAN IV to calculate spin densities by the methods described

(28) M. Barfield, *J. Chem. Phys.*, 47, 3831 (1967).
(29) I. L. Cooper and R. McWeeny, *ibid.*, 45, 226 (1966).
(30) B. T. Sutcliffe, *ibid.*, 45, 235 (1966).
(31) F. A. Matsen and A. A. Cantu, *J. Phys. Chem.*, 72, 21 (1968).

here. Proton hyperfine coupling constants, a_H, were obtained from the expression[32]

$$a_H = 506.8\, Q_1(\alpha_{1/2}\alpha_{1/2}|1_H;1_H)\ \text{G} \qquad (31)$$

Exchange integrals for the aliphatic radical fragment depicted in Figure 1 are entered in Table I. These include the σ–π and σ-exchange integrals of McLachlan,[33] Karplus[34] and Karplus and Fraenkel.[35] As the exchange integral parameters for the geminal interaction parameters are not known accurately, the values adopted here are those which are consistent[26] with the signs and magnitudes of proton–proton coupling over four bonds in propanic fragments.[36]

Table I: Molecular and Atomic Exchange Integrals $K(r,s)$ for Orbitals r and s in the Aliphatic Radical Fragment Depicted in Figure 1

$K(p,\sigma_\alpha)$ =	1.26[a] eV
$K(p,\sigma_\beta)$ =	0.932[a]
$K(p,\sigma_{\beta'})$ =	$-0.827\cos^2\phi$[b]
$K(p,c_\beta)$ =	$-0.827\cos^2(\phi - 120°)$[b]
$K(p,c_{\beta'})$ =	$-0.827\cos^2(\phi + 120°)$[b]
$K(\sigma_\alpha,\sigma_\beta) = K(\sigma_{\beta'},\sigma_{\gamma'})$ =	
$K(c_\beta,h_\beta) = K(c_\gamma,h_\gamma)$ =	−3.80[c]
$K(h_\beta,h_{\beta'})$ =	−1.00[c]
$K(c_\beta,c_{\beta'})$ =	1.01[c]
$K(h_\beta,c_{\beta'}) = K(h_\beta,\sigma_\beta) = K(h_\gamma,\sigma_{\gamma'})$ =	0.14[d]
$K(h_\beta,\sigma_\alpha) = K(h_\beta,\sigma_{\gamma'}) = K(h_{\ },\sigma_{\beta'})$ =	−1.00[d]
$K(\sigma_\beta,c_\gamma)$ =	$-0.287\cos^2\theta + 0.016\cos\theta + 0.015$[e]
$K(c_\beta,c_\gamma)$ =	$-0.287\cos^2(\theta + 120°) + 0.016\cos(\theta + 120°) + 0.015$[e]
$K(c_{\beta'},c_\gamma)$ =	$-0.287\cos^2(\theta - 120°) + 0.016\cos(\theta - 120°) + 0.015$[e]

[a] Reference 35. [b] Reference 33. [c] M. Karplus and D. H. Anderson, *J. Chem. Phys.*, **30**, 6 (1959). [d] Parameters which were used to calculate[4] $J_{HH'}$ in propanic fragments, ref 26. [e] Reference 34.

III. Results and Discussion

A. γ-Proton Hyperfine Coupling. Calculations of the γ-hyperfine coupling constants were based on the eleven orbital fragment depicted in Figure 1. Calculations were performed at 30° intervals of the dihedral angle, ϕ, for $\theta = 60°$ and 180°. The angle ϕ is measured clockwise from the C_3–C_2–C_1 plane and the axis of the unpaired 2p electron as depicted schematically in Figure 2a. The angle θ is measured clockwise between the planes formed by H_γ–C_3–C_2 and C_3–C_2–C_1 as shown in Figure 2b.

Calculated values for a_γ are plotted in Figure 3 as a function of ϕ for $\theta = 60°$ and 180°. A significant feature of these calculations is the appearance of γ-hyperfine coupling constants of either sign depending on the conformation. From studies of nmr contact shifts[15,16] both positive and negative values of a_γ have been inferred, but previous calculations based on the hyperconjugative mechanism with MO wave functions[8–11] gave only positive values while those based on the spin polarization mechanism[13,14] gave only negative values.

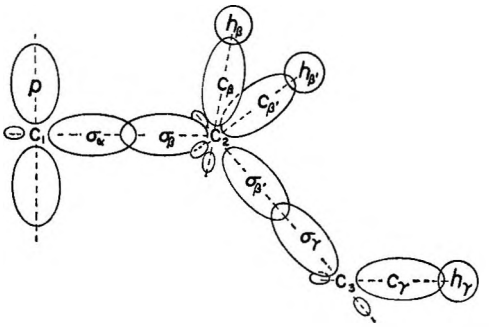

Figure 1. Labeling of orbitals for the propyl radical fragment.

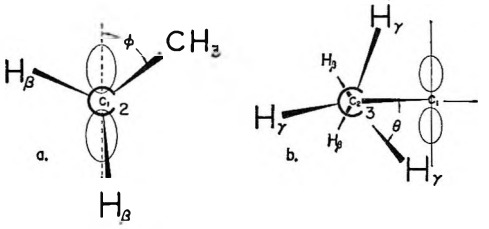

Figure 2. Specification of the dihedral angles θ and ϕ for the propyl radical. (a) Where carbon C_2 eclipses carbon C_1, the dihedral angle ϕ is measured from the axis of the 2p orbital and the C_1–C_2–C_3 plane. (b) Where carbon C_3 eclipses carbon C_2, the dihedral angle θ is measured clockwise from C_3–C_2–C_1 plane to the H_γ–C_3–C_2 plane.

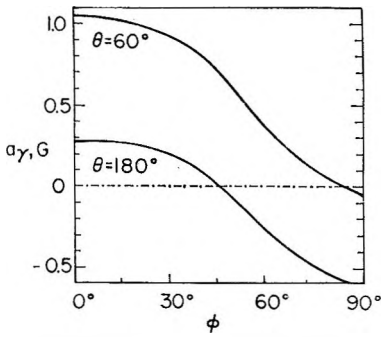

Figure 3. A plot of calculated γ-proton hyperfine coupling constants, a_γ, *vs.* ϕ for $\theta = 60$ and 180°.

A good fit to the calculated values is given by the polynomial

$$a_\gamma = 1.65\cos^2\phi - 0.84\cos^4\phi + 2.62K(\theta) - 0.68\cos^2\phi[K(\theta + 120°) + K(\theta - 120°)] + 0.15[\cos^2(\phi + 120°)K(\theta + 120°) + \cos^2(\phi - 120°)K(\theta - 120°)] + 0.17 \qquad (32)$$

(32) A. Carrington and A. D. McLachlan, "Introduction to Magnetic Resonance," Harper and Row, New York, N. Y., 1967, p 81.
(33) A. D. McLachlan, *Mol. Phys.*, **1**, 233 (1958).
(34) M. Karplus, *J. Chem. Phys.*, **30**, 11 (1959); **33**, 316 (1960).
(35) M. Karplus and G. K. Fraenkel, *ibid.*, **35**, 1312 (1961).
(36) M. Barfield, *ibid.*, **41**, 3825 (1964).

where

$$K(\theta) = -0.287 \cos^2\theta + 0.016 \cos\theta + 0.015$$

Equation 32 is indicative of the various mechanisms leading to the coupling. The first and third terms give contributions of opposite signs and arise from the second-order terms along the paths

$$\{h_\gamma - c_\gamma\} \ldots \{\sigma_\gamma - \sigma_\beta'\} \ldots \{p\}$$
$$\{h_\gamma - c_\gamma\} \ldots \{\sigma_\beta - \sigma_\alpha\} \ldots \{p\}$$

respectively. The fifth term includes contributions from the paths

$$\{h_\gamma - c_\gamma\} \ldots \{c_\beta - h_\beta\} \ldots \{p\}$$
$$\{h_\gamma - c_\gamma\} \ldots \{c_\beta' - h_\beta'\} \ldots \{p\}$$

The second, fourth, and last terms in eq 32 presumably arise from a number of third-order mechanisms which include the paths

$$\{h_\gamma - c_\gamma\} \ldots \{c_\beta - h_\beta\} \ldots \{\sigma_\beta - \sigma_\alpha\} \ldots \{p\}$$
$$\{h_\gamma - c_\gamma\} \ldots \{c_\beta' - h_\beta'\} \ldots \{\sigma_\beta - \sigma_\alpha\} \ldots \{p\}$$
$$\{h_\gamma - c_\gamma\} \ldots \{\sigma_\gamma - \sigma_\beta'\} \ldots \{\sigma_\beta - \sigma_\alpha\} \ldots \{p\}$$

In Table II, calculated values of a_γ are compared with experimental values. Since the conformations of the radicals are not known, it is necessary to make some assumptions. From the temperature dependence of the β-hyperfine coupling constants for the propyl radical, an anisotropic averaging over the rotation about the bonds between the C_1 and C_2 carbon atoms has been suggested.[37] However, the change in a_β over the temperature range of 120° was only about 10%, which is undoubtedly less than the error in the present calculations. As a consequence, the simplest procedure is to assume free rotation about the C_1–C_2 bond. With

Table II: Comparison of Calculated and Experimental Values of a_γ for Aliphatic Radicals

Radical	ϕ	θ	a_γ, calcd, G	a_γ, exptl, G
$CH_3\dot{C}H_2CH_2$	...[a]	...[b]	0.42	(+) 0.38[c,d]
	...[a]	60°	0.65	(+) 0.69[c,d]
	...[a]	180°	−0.04	≤0.15[c]
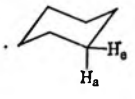	50°	...[e]	0.24	≤0.15[c]
	50°	60°	0.54	±0.65[f]
	50°	180°	−0.05	≤0.05[f]

[a] Free rotation about β carbon is assumed. [b] Calculated value is based on either a threefold barrier or free rotation. [c] Reference 1. [d] Signs sssumed positive from nmr contact shift measurements, ref 15 and 16. [e] Equilibration between two chair conformations assumed. [f] Reference 7.

this assumption, eq 32 can be written

$$a_\gamma(\theta) = 0.69 + 2.62\,K(\theta) + 0.26[K(\theta + 120°) + K(\theta - 120°)] \quad (33)$$

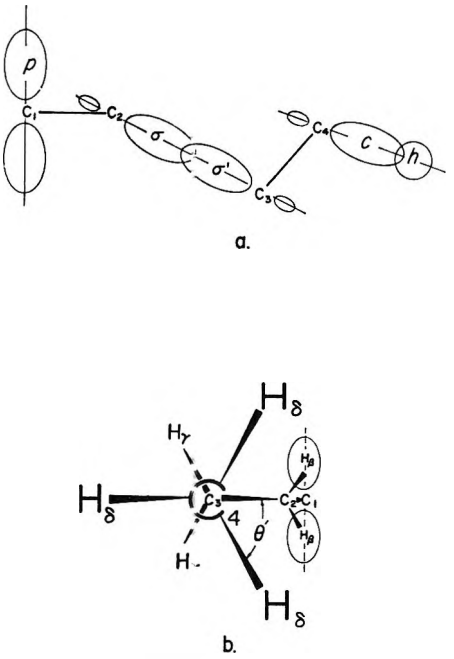

Figure 4. (a) Labeling of orbitals for a fragment of the butyl radical. (b) The dihedral angle θ' is measured clockwise from the C_2–C_3–C_4 plane to the H_δ–C_4–C_3 plane.

Calculated values for $\theta = 60°$ and 180° are 0.65 and −0.04 G, respectively. These values are consistent with the low-temperature esr spectrum[1] of the propyl radical which exhibits γ-hyperfine coupling of 0.69 G to two equivalent protons. Splitting from the third proton was not resolved and was presumed to be less than 0.15 G.[1]

At higher temperature, the esr spectrum exhibits coupling to three equivalent protons. The γ-hyperfine coupling could be calculated either by assuming free rotation or by assuming that most of the coupling arises from conformations which are staggered with respect to the β-methylene carbon

$$\langle a_\gamma \rangle = 3^{-1}\{2a_\gamma(60°) + a_\gamma(180°)\} \quad (34)$$

Both methods give the result, 0.42 G, which is in good agreement with the values observed[1,6] in a number of aliphatic hydrocarbon radicals. Furthermore, on the basis of nmr contact shift measurements[15,16] the signs are expected to be positive

Of particular interest are hyperfine couplings in the cases in which the conformations of the radical are fixed. Significant γ-hyperfine coupling constants have been observed in strained bicyclic molecules,[2-5] but it would not be reasonable to compare these with the calculated values, as the exchange integral parameters in Table I are based on the unstrained hydrocarbons. In the esr spectrum of the cyclohexyl radical no splitting from the γ protons was observed.[1] Assuming equilibrium between two chair conformations[38] and a "nom-

(37) R. W. Fessenden, *J. Chim. Phys.*, **61**, 1570 (1964).
(38) S. Ogawa and R. W. Fessenden, *J. Chem. Phys.*, **41**, 994 (1964).

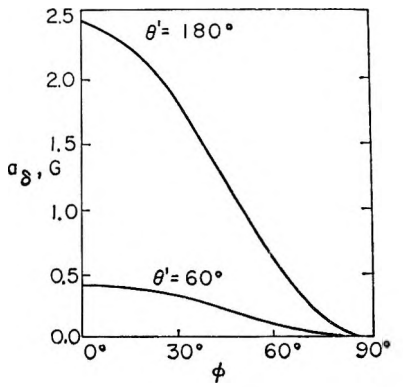

Figure 5. A plot of the calculated δ-proton hyperfine coupling constants, a_δ, *vs.* ϕ for $\theta' = 60$ and 180°.

inal" value of 50° for ϕ gives $a_\gamma = 0.24$ G which is close to the limit of resolution. It is important to note that recent studies[7] of substituted piperidine iminoxyls indicate a single chair conformation and measurable γ-hyperfine coupling to only two axial protons. The calculated results for any reasonable value of ϕ are consistent with this observation.

Hyperfine coupling to γ protons has also been observed in alkylphenoxy radicals[39,40] and alkylxanthyl radicals.[41] The calculated results which are reported here are not easily comparable with these data because of the possibility of long-range contributions associated with appreciable spin density on other carbons of the extended π-electron systems.

B. δ-Proton Hyperfine Coupling. Calculations of the δ-hyperfine coupling constant were based on the simple five-orbital fragment depicted in Figure 4a. Calculations were performed for 30° intervals of the dihedral angle ϕ, and $\theta' = 60°$ and 180°. The dihedral angle ϕ has the same interpretation as before, but θ' is the dihedral angle measured between the H_δ–C_4–C_3 plane and the C_4–C_3–C_2 plane as depicted in Figure 4b.

Calculated values of a_δ which are plotted in Figure 5 are completely consistent with the simple expression

$$a_\delta = -8.42K(\theta') \cos^2 \phi \text{ G} \quad (35)$$

where

$$K(\theta') = -0.287 \cos^2 \theta' + 0.016 \cos \theta' + 0.015$$

Assuming free rotation about the β-carbon methylene this becomes

$$a_\delta = -4.21K(\theta') \quad (36)$$

which gives a_δ (60°) = 0.21 G, and a_δ (180°) = 1.22 G. The average for free rotation or a hindered threefold barrier is 0.54 G. Presumably this is an overestimate since coupling to δ protons in aliphatic hydrocarbon radicals is not normally observed.

For the case of the cyclohexyl radical equilibration between the two chair conformations with $\phi = 50°$ gives $a_\delta = 0.67$ G, which is in good agreement with the observation[1,38] of coupling of magnitude 0.71 G to two equivalent δ protons in this radical. Calculated values to axial and equatorial protons are 0.17 and 1.00 G, respectively. Furthermore, these results are consistent with the experimental observation of coupling to a single δ proton in the chair form of the piperidine-1-oxyl radical.[7]

Acknowledgments. Appreciation is expressed to Professor G. Vincow for a helpful discussion, to the National Science Foundation for partial support of this work, and to the University of Arizona Computer Center for providing computer facilities.

(39) R. W. Kreilick, *J. Amer. Chem. Soc.*, 90, 5991 (1968).
(40) F. Yamauchi and R. W. Kreilick, *ibid.*, 91, 3249 (1969)
(41) M. D. Sevilla and G. Vincow, *J. Phys. Chem.*, 72, 3647 (1968).

The Relative Stabilities of Perchlorate, Perbromate, and Periodate Ions

by Margaret M. Cox and John W. Moore

Contribution No. 1761 from the Department of Chemistry, Indiana University, Bloomington, Indiana 47401
(Received August 14, 1969)

Several explanations of the instability of perbromate salts and perbromic acid have been examined using Hartree–Fock–Slater atomic wave functions and self-consistent charge and configuration (extended Hückel) MO calculations. It is concluded that perbromates should be similar to perchlorates and periodates in stability. The molecular orbital treatment, although highly approximate, corresponds well with observed properties of BrO_4^- and in the case of ClO_4^- is in agreement with previous calculations.

The synthesis of perbromates and the mass spectrum of perbromic acid[1] indicate that these compounds are not extremely unstable, despite many unsuccessful attempts to prepare them.[2] Prior to the reports by Appleman and Studier we had begun a study of a number of "explanations" of the absence of perbromates. The results are reported here.

There have been at least four different rationalizations of the difficulty of preparation of perbromates. Hugus[3] suggested that the normal trend would be a decrease in stability in the order $ClO_4^- > BrO_4^- > IO_4^-$, but that periodate was unusually stable because f orbitals were available for bonding. The f orbitals should be contracted by increasing charge on iodine and would therefore stabilize higher oxidation states. Nyholm showed[4] that s → p promotion energies for arsenic are larger than those for phosphorus or antimony. He argued that the general instability of the highest oxidation states of representative elements in the fourth period is due to this effect. Because of the difficulty of unpairing the s electrons, sp^3 hybridized bromine should be less stable than sp^3 chlorine or iodine. Urch[5] argued that the promotion energy problem could be overcome provided that strong π bonds were formed using vacant d orbitals on the central atom. Using hydrogenic functions for the bromine d orbitals, Urch showed that a radial node might occur in the bonding region, making d_π–p_π overlap very small. Ferreira[6a] found that d_π–p_π overlap between Kr and O was not noticably smaller than between Ar and O, which would appear to invalidate Urch's argument. In order to explain the absence of perbromate Ferreira used Pitzer's inner shell repulsions[6b] and suggested that the electronegativities of I and O differ enough so that coulombic attractions overcome the electron repulsions in IO_4^-.

It appeared to us that the difference in stabilities of ClO_4^-, BrO_4^-, and IO_4^- should be a result of differences in atomic properties of the halogens. Atomic energy levels and radial behavior of atomic wave functions constitute the basis of all of the arguments listed above. Since numerical Hartree–Fock–Slater atomic wave functions[7] can be obtained for most atoms and ions without excessive computation, we decided to examine explanations of the nonexistence of perbromate in terms of the results obtained from the Herman–Skillman Hartree–Fock–Slater formalism.

Atomic Wave Functions and Orbital Energies

Numerical radial wave functions were obtained using the Fortran program of Herman and Skillman[7] modified for use on the Control Data 3400-3600 System of the Indiana University Research Computing Center. Radial functions were calculated for mono- and dipositive ions as well as for neutral halogen atoms, and were approximated by a sum of Slater-type orbitals using a least-squares procedure.[8] Oxygen 2s and 2p functions were obtained from the paper by Clementi,[9] and halogen–oxygen overlaps were evaluated in the usual way.[8] Bond lengths were obtained from Wells[10] for Cl–O and I–O. A Br–O length of 1.62 Å was obtained by interpolation, using the relative lengths of ClO_3^-, BrO_3^-, and IO_3^- as a guide. Table I gives positions of radial

(1) E. H. Appelman, *J. Amer. Chem. Soc.*, **90**, 1900 (1968); M. H. Studier, *ibid.*, **90**, 1901 (1968).

(2) See, for example, W. F. DeCoursey, "Preparation of Perbromates," Doctoral Dissertation, State College of Iowa, Cedar Falls, Iowa, 1953; G. M. Bancroft and H. D. Gesser, *J. Inorg. Nucl. Chem.*, **27**, 1545 (1965).

(3) Z Z. Hugus, Jr., *J. Amer. Chem. Soc.*, **74**, 1076 (1952).

(4) R. S. Nyholm, *Proc. Chem. Soc.*, **273** (1961).

(5) D. S. Urch, *J. Inorg. Nucl. Chem.*, **25**, 771 (1963).

(6) (a) R. Ferreira, *An. Acad. Bresileira de Ciencias*, **38**, 407 (1966); (b) K. S. Pitzer, *J. Amer. Chem. Soc.*, **70**, 2140 (1948).

(7) F. Herman and S. Skillman, "Atomic Structure Calculations," Prentice-Hall, Inc., Englewood Cliffs, N. J., 1963.

(8) H. Johansen, "Algol Programs for Molecular Calculations," H. C. Ørsted Institute, University of Copenhagen, Denmark, 1965.

(9) E. Clementi, C. C. J. Roothaan, and M. Yoshimine, *Phys. Rev.*, **127**, 1618 (1962).

(10) A. F. Wells, "Structural Inorganic Chemistry," 3rd ed, Oxford University Press, London, 1962, p 334.

Table I: Atomic Wave Functions and Overlap Integrals

Function	Distance to outermost radial node, Å	Bond length, Å	Magnitude of Overlap O2sσ	O2pσ	O2pπ
Cl 4s	0.944	1.43	0.182	0.076	...
Cl^+ 4s	0.842	1.43	0.254	0.059	...
Cl 3d	...	1.43	0.284	0.048	0.260
Cl^+ 3d	...	1.43	0.408	0.051	0.354
Br 5s	1.06	1.62[a]	0.178	0.062	...
Br^+ 5s	1.11	1.62[a]	0.242	0.044	...
Br 4d	0.40	1.62[a]	0.262	0.058	0.218
Br^+ 4d	0.39	1.62[a]	0.432	0.051	0.341
I 6s	1.22	1.79	0.146	0.069	...
I^+ 6s	1.18	1.79	0.203	0.061	...
I 5d	0.59	1.79	0.322	0.033	0.244
I^+ 5d	0.59	1.79	0.429	0.064	0.313
I 4f	...	1.79	0.046	0.021	0.048
I^+ 4f	...	1.79	0.267	0.037	0.264
I 5d ($4f^1$)	0.59	1.79	0.433	0.067	0.315
I^+ 5d ($4f^1$)	0.58	1.79	0.430	0.077	0.313

[a] Obtained by interpolation (see text).

nodes and magnitudes of overlap integrals for neutral and monopositive halogen functions.

Using orbital energies derived from the HFS treatment it is possible to estimate s → p, s → d, and s → f promotion energies. This has been done for neutral halogens and monopositive ions. The results appear in Table II. Higher charges were not considered because it is unlikely that the charge on the central halogen in XO_4^- will exceed unity (*vide infra*). Although not all of the required terms in the atomic spectra[11] have been observed, it is possible to estimate empirical promotion energies by extrapolation along isoelectronic series. The empirical values are about 15% below the HFS results in all cases where comparisons have been made, but the trends in HFS values follow the trends in empirical promotion energies.

Extended Hückel Calculations

In order to translate the atomic properties of the halogens into more readily understandable chemical terms we have carried out self-consistent charge and configuration calculations as described by Ballhausen and Gray.[12] The corrections to group overlap formulas noted by Bishop[13] were applied. Calculations were performed initially using basis functions for the neutral halogens. Since charges on all of the halogens were between +0.6 and +0.9 the final results were obtained by interpolation of overlaps between those obtained for univalent and zerovalent halogen functions. The final calculation, therefore, is a function of VSIE's and overlaps which are appropriate to the charges and configurations of the atoms involved. Pertinent results are shown in Table III.

Discussion

From the data reported in Table I, it is clear that radial nodes in the bromine 4d and iodine 5d functions do not have an adverse effect on d_π–p_π overlap relative to the nodeless chlorine 3d. While d_π–p_π overlap for neutral bromine is smaller than for chlorine or iodine, this may be due partly to inaccuracy in fitting a sum of Slater functions to the numerical HFS results. The situation is reversed for Cl^+, Br^+ and, I^+ where d_π–p_π overlap decreases in the order $Cl^+ > Br^+ > I^+$. Since the results of extended Hückel calculations often underestimate the positive charge on the central atom,[14] overlaps for the unipositive halogens should be more appropriate than for the neutral atoms. Urch's suggestion that poor d_π–p_π overlap makes perbromate unstable is incorrect.

Several interesting facts about the behavior of atomic wave functions are implicit in the results in Table I. First of all, an increase in nuclear charge can cause a drastic contraction of diffuse atomic orbitals. The most striking case is shown in Figure 1 where f orbitals for I^0 and I^+ are compared. This contraction causes an increase of about a factor of ten in overlap of the 4f orbital with oxygen functions at an appropriate distance. A second very interesting result is that if f orbitals are occupied they tend to make the d functions much more suitable for bonding. Because the f electron has a high probability of being far from the nucleus it tends to contract the d function beneath it as shown in Figure 2. Together with the rather high energy of the f orbital this effect guarantees that d orbital bonding will be more important than f orbital bonding in periodate. Although Hugus' suggestion that utilization of f orbitals should stabilize higher valence states for iodine was based correctly on the fact that these orbitals are greatly contracted by increasing charge, our results indicate that f orbitals will not be nearly as efficacious as d orbitals in stabilizing IO_4^-.

The HFS results in Table II indicate that s → p promotion energies for Br^0 and Br^+ are 4% larger than for Cl^0 and Cl^+ and 15% larger than for I^0 and I^+. This places the bromine s → p promotion energy 10% above the value to be expected on the basis of a linear periodic trend. Based on the empirical promotion energies the difference is only about 5%. In the case of s → d promotion energies the bromine value is only 7% above a linear interpolation. These figures can be compared with promotion energies for Se (s → p 12%, s → d 9% high) and As (s → p 13%, s → d 10% high). Difficulty of s → p and s → d promotion relative to other members

(11) C. E. Moore, "Atomic Energy Levels," National Bureau of Standards Circular 467, U. S. Government Printing Office, Washington, D. C., 1955.

(12) C. J. Ballhausen and H. B. Gray, "Molecular Orbital Theory," Benjamin, New York, N. Y., 1964.

(13) D. M. Bishop, *Theoret. Chim. Acta*, **8**, 285 (1967).

(14) R. F. Fenske, *Inorg. Chem.*, **4**, 33 (1965).

Table II: Promotion Energies

Type of promotion		Energy, 10^3 cm^{-1} Cl^0	Cl$^+$	Br^0	Br$^+$	I^0	I$^+$
$ns \longrightarrow np$	HFS[a]	101	105	106	110	91	95
	Empirical[b]	85	93	87	95	79	78
$ns \longrightarrow nd$	HFS[a]	233	249	229	250	193	210
$ns \longrightarrow (n-1)f$	HFS[a]	...	...	...	...	229	257

[a] Obtained from Herman–Skillman program (ref 7). [b] Obtained from atomic spectra (ref 11, see text).

Table III: Self-Consistent Charge and Configuration Calculations for XO_4^-

X	Charge	Electron populations, Atomic ns	np	nd	(n − 1)f	(n + 1)s	Overlap σ	π	Orbital energies, 10^3 cm^{-1} Δ^a	$\Sigma\epsilon_i$
Cl	0.64	1.42	3.56	1.38	...	...	0.65	0.43	73.6	−5315
Br	0.72	1.54	3.53	1.22	...	...	0.53	0.41	73.3	−5295
I	0.81	1.48	3.37	1.34	...	...	0.53	0.43	80.1	−5218
I[b]	0.83	1.46	3.37	1.39	−0.05	...	0.47	0.44	68.1	−5237
Cl[c]	0.57	1.41	3.62	1.14	...	0.26	0.68	0.37	77.1	−5346
Br[c]	0.65	1.52	3.62	1.01	...	0.19	0.57	0.37	67.9	−5355
I[c]	0.75	1.46	3.41	1.22	...	0.15	0.54	0.42	65.4	−5226

[a] Energy of lowest fully allowed electronic transition ($^1T_2(t_1^5t_2^1) \longleftarrow {}^1A_1(t_1^6)$). [b] Including 4f orbitals. [c] Including (n + 1)s orbital.

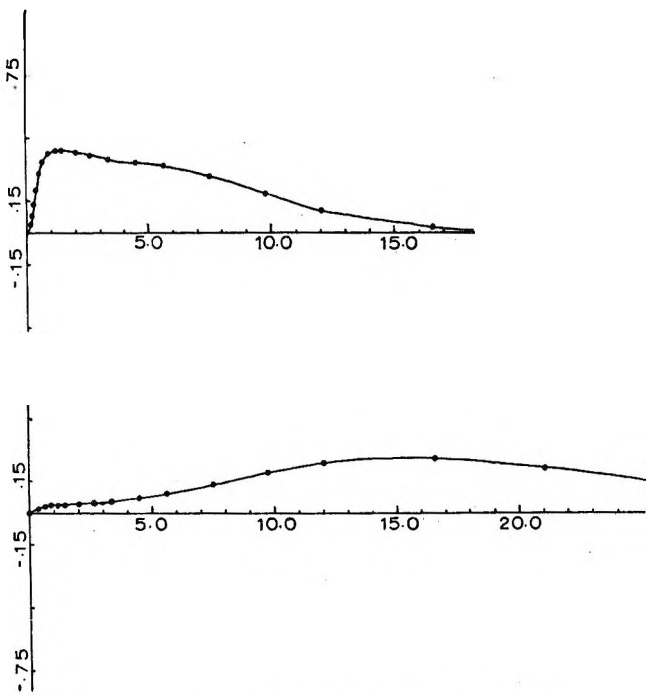

Figure 1. Plots of amplitude of radial wave function *vs.* distance from nucleus (Å) for I^+ [Kr]$4d^{10}4f^15s^25p^3$ (upper) and I^0 [Kr]$4d^{10}4f^15s^25p^4$ (lower). Italicized orbital is plotted.

of a periodic group decreases in the order As > Se > Br. Since selenates and arsenates have been well characterized for some time, it would appear that these relatively small differences are not sufficient to preclude formation of a stable tetrahedral ion.

An estimation of the contribution of inner shell repulsions[6b] to the instability of the perhalate ions can be made. One would expect inner shell repulsions to increase as the radius of the inner shell increases. The distance from the nucleus to the outermost radial maximum of the highest energy closed shell orbitals of each halogen is given in Table IV. If anything, the bromine

Table IV

Atom	Distance to outermost radial maximum, Å (n − 1)s	(n − 1)p	(n − 1)d
Cl (n = 3)	0.19	0.16	...
Br (n = 4)	0.26	0.25	0.22
I (n = 5)	0.37	0.38	0.41

radii are smaller than would be expected on the basis of a linear interpolation between Cl and I. Unusually large inner shell repulsions do not appear to be a viable explanation for the difficulty of preparation of perbromates.

An estimation of the stabilization of XO_4^- anions by partial ionic character in the bonds can be made by calculating coulombic attractions and repulsions assuming point charges in a tetrahedral array with the X–O distances in Table I. The stabilizations are 27.0×10^3 cm^{-1}, 32.2×10^3 cm^{-1}, and 39.9×10^3 cm^{-1}, respectively, for ClO_4^-, BrO_4^-, and IO_4^-, using charges generated by the extended Hückel calculation including (n + 1)s orbitals. Using the radii in Table IV as a

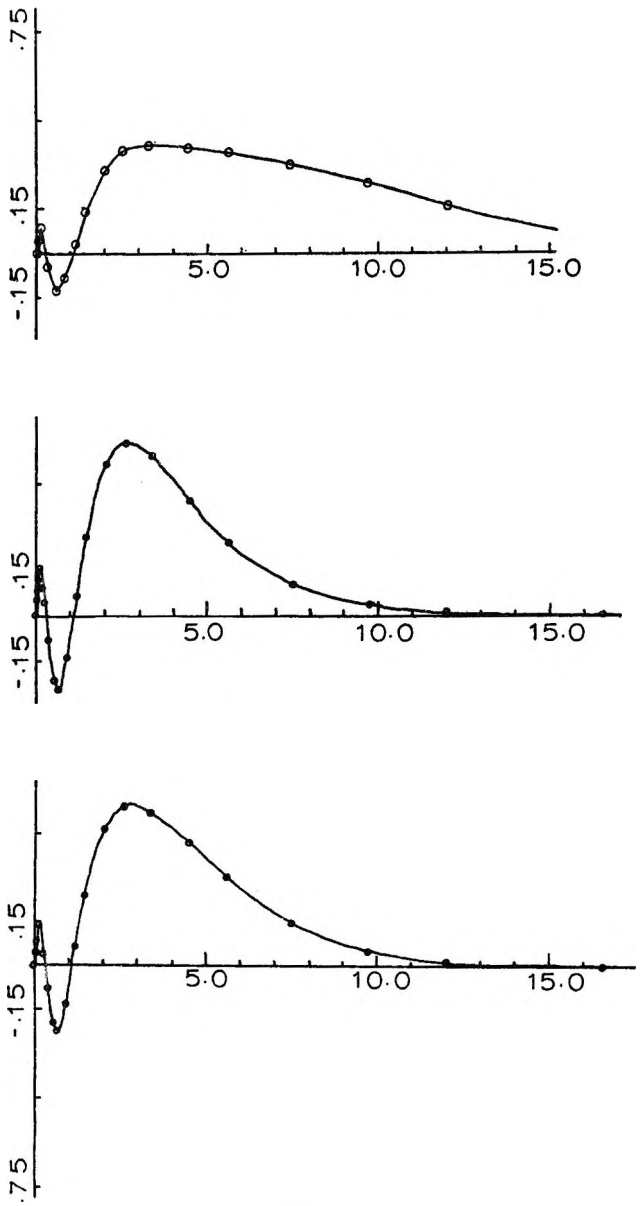

Figure 2. Plots of amplitude of radial wave functions *vs.* distance from nucleus (Å) for $I^0[Kr]4d^{10}5s^25p^4\mathit{5d}^1$ (upper), $I^0[Kr]4d^{10}4f^15s^25p^3\mathit{5d}^1$ (middle), and I^+ $[Kr]4d^{10}5s^25p^3\mathit{5d}^1$ (lower). Italicized orbital is plotted.

guide, inner shell repulsions should be in the ratio 1:1.4:1.9, which is of the same order as the ratio (1:1.2:1.5) of ionic stabilizations for ClO_4^-, BrO_4^-, and IO_4^-, respectively. From these ratios it would appear that BrO_4^- is neither stabilized nor destabilized by the combination of effects.

Using the results of the extended Hückel calculations, a number of predictions can be made regarding the properties of the perhalates. Further discussion is based on the calculations involving $(n + 1)$s orbitals. From Table III it can be seen that the energies of the first fully allowed transitions ($^1T_2(t_1^5t_2^1) \leftarrow {}^1A_1(t_1^6)$ in all cases) decrease in the order $\Delta_{Cl} > \Delta_{Br} > \Delta_I$. This is in accord with the ultraviolet spectra of the ions. Perchlorate does not absorb significantly below 56,000 cm^{-1}, perbromate has a peak at 53,200 cm^{-1},[15] and periodate has a maximum absorbance at 45,000 cm^{-1}. The observed trend is reflected by the Δ values, although they are somewhat too large because of overestimation[14] of off-diagonal matrix elements involving the low-lying s orbitals on halogen and oxygen by the geometric mean approximation. If these functions are removed from the basis set, the lowest virtual orbitals of t_2 and a_1 symmetry become much more stable. The effect on the a_1 level is so large that it drops below the highest filled level, producing a paramagnetic ground state. Obviously the *ns* orbitals on halogens and oxygen must be included in the basis set, but their effect is probably not as great as our results indicate.

An estimate of the Br–O stretching frequency can be made by assuming a linear relation between force constant and bond order and using the equation derived by Gillespie and Robinson.[16] Since total overlap populations should be proportional to bond orders,[17] extrapolation on a plot of force constant *vs.* total overlap population for ClO_4^- and IO_4^- was used to obtain a force constant of 5.40×10^5 dyn cm^{-1} for the Br–O stretch.[18] This corresponds to a weighted average frequency of 829 cm^{-1} for the symmetric and antisymmetric stretching vibrations, which can be compared with the weighted average of 862 cm^{-1} for the observed ν_1 and ν_3.[15] These Br–O frequencies give a force constant of 5.83×10^5 dyn cm^{-1}, nearly the same as the I–O force constant of 5.87×10^5 dyn cm^{-1}, but much smaller than the Cl–O value of 7.45×10^5 dyn cm^{-1}. Despite the absence of any major discontinuity in the atomic properties of Cl, Br, and I, our calculation predicts a slightly weaker Br–O bond than is actually observed.

The smaller overlap population and force constant calculated for BrO_4^- suggest that the bond distance might be slightly larger than the average of Cl–O and I–O. Calculation of overlap integrals as a function of X–O distance indicates that Br–O overlaps are less dependent on this parameter than Cl–O or I–O. Should the experimental bond distance prove to be slightly different from 1.62 Å our results would probably not be grossly different.

The results reported here may be compared with previous work in the case of perchlorate. Wagner[19] has treated a series of chlorine oxyanions using a molecular orbital method. By using a somewhat arbitrary choice of the off-diagonal matrix element for d_π–p_π bonding he obtained a final charge of 0.44 on chlorine and a π-bond

(15) E. H. Appelman, *Inorg. Chem.*, **8**, 223 (1969).

(16) R. J. Gillespie and E. A. Robinson, *Can. J. Chem.*, **41**, 2074 (1963).

(17) R. S. Mulliken, *J. Chem. Phys.*, **23**, 1833 (1955).

(18) K. Nakamoto, "Infrared Spectra of Inorganic and Coordination Compounds," John Wiley and Sons, Inc., New York, N. Y., 1963, pp 103–110.

(19) E. L. Wagner, *J. Chem. Phys.*, **37**, 751 (1962).

order of 0.21. Our results indicate that this choice of β_{d-p} may be somewhat high. Manne[20] has applied an approximate LCAO–MO–SCF calculational scheme to sulfur and chlorine oxyanions, but d orbitals on the central atoms were not included. This results in a considerably higher residual charge on chlorine ($\sim+2.1$) than we obtain. However, it is interesting to note that if the population analysis in our calculation were confined to 3s and 3p orbitals, the charge on chlorine would be +2.02 (not including $(n + 1)$s) or +2.03 (including $(n + 1)$s). Thus the difference is accounted for almost exactly by the amount of charge transferred from the oxygens to chlorine orbitals not included in Manne's calculation. The same ordering of the one-electron levels (except for the additional virtual orbitals produced by expansion of the basis set) is obtained from both calculations.

We do not claim to know the extent of d-orbital participation in bonding in the perhalates. There are two indications that we may have overestimated d-orbital bonding. First, as Fenske[14] has pointed out, the geometric mean approximation for off-diagonal matrix elements is poor when large diagonal terms are involved. Second, we have underestimated the force constant for bromine–oxygen stretching. Since all overlaps except those involving d orbitals are in the order Cl:Br:I for both zero- and univalent ions, the discrepancy may be due to an overemphasis on d-orbital bonding. Nevertheless, the rapid increase in d_π–p_π overlap with increasing charge on the halogen indicates that some charge neutralization *via* π bonding should occur before the charge reaches +2. The answer probably lies between our results and Manne's. A more rigorous calculational scheme involving atomic basis functions appropriate to the atoms in the molecule or ion will be necessary in order to decide this issue.

We have been unable to find any reasonable explanation for the difficulty of preparation of perbromates nor have we been able to confirm previous suggestions.[3-6] While our results indicate that perbromate may be slightly less stable than periodate or perchlorate, the differences are small. We suggest that unfavorable reaction rates, rather than the intrinsic instability of perbromate, may account for the facts. Heating of bromates has probably not worked because the perbromate formed decomposes rapidly at high temperatures, and oxidation of bromine by perchlorate or periodate is an unlikely method because both of the latter are slightly more stable than perbromate. Our conclusions are supported by the successful isolation of perbromate at a low temperature and the apparent stability of perbromic acid in the mass spectrometer,[1] and we are in agreement with those reached by Appelman.[15]

Acknowledgment. We wish to thank Mr. John Kindsvater for his interest in this problem and several helpful discussions. Formulas for f orbital overlap integrals were derived by Mr. Douglas Shepard. The help of Mr. Charles Flowers of the Indiana University Research Computing Center in modifying the Herman–Skillman program is gratefully acknowledged. This work was supported in part by a Frederick Gardner Cottrell grant-in-aid from the Research Corporation.

(20) R. Manne, *J. Chem. Phys.*, **46**, 4645 (1967).

Surface and Interfacial Tensions of Polymer Melts. II.

Poly(methyl methacrylate), Poly(*n*-butyl methacrylate), and Polystyrene

by Souheng Wu

Fabrics & Finishes Department, Experimental Station, E. I. du Pont de Nemours & Company, Wilmington, Delaware 19898 *(Received June 23, 1969)*

The surface tensions of poly(methyl methacrylate), poly(*n*-butyl methacrylate), and polystyrene, and the interfacial tensions of poly(methyl methacrylate)–polyethylene, poly(*n*-butyl methacrylate)–polyethylene, polystyrene–polyethylene, poly(methyl methacrylate)–polystyrene, poly(*n*-butyl methacrylate)–poly(vinyl acetate), and poly(methyl methacrylate)–poly(*n*-butyl methacrylate) systems have been measured by the pendant drop method in the temperature range of 100 to 180°. The parachor equation is found to be applicable to poly(methyl methacrylate) and polystyrene, but not applicable to poly(*n*-butyl methacrylate). The equations of Fowkes and of Good and Girifalco are approximately applicable to polymer systems. However, the simplified forms of these equations are not applicable. The interfacial tensions between polymers are found to be quite high, arising mainly from the effects of the "mismatching" of the nature of the molecular forces and the chain stiffness of the polymer molecules. These two effects are included in the interaction parameter of Good and Girifalco, $\Phi = (1 - 2\delta)[(f_1^d f_2^d)^{1/2} + (f_1^p f_2^p)^{1/2}]$, where δ is the fractional increment of the interfacial distance over the arithmetic mean of the intermolecular distances of the two phases, f_i^d is the fraction of the dispersion-force component of the surface tension of phase i, and f_i^p is that of the polar-force component of phase i. The interfacial region between polymers is relatively discrete. The high interfacial tensions between polymers greatly influence various surface quantities such as contact angle, spreading coefficient, and work of adhesion. The temperature coefficient of the contact angle may be either positive or negative depending on the difference in the surface entropies of the two phases. The polymer having a lower surface tension does not necessarily spread (exhibiting zero contact angle) on the polymer having a higher surface tension. The work of adhesion between polymers can be smaller than the work of cohesion of either phase. The data provide an opportunity to examine polymer adhesion in the light of the interfacial properties of polymer systems.

I. Introduction

Knowledge of interfacial tension can provide information on the intermolecular forces and the interfacial structure between two phases. Although surface tensions of several molten polymers[1-9] have been measured recently, the interfacial tensions between polymers have been virtually unknown. In a previous paper,[1] we reported the first interfacial tension measurements made on polymer systems, *i.e.*, polyethylene, polyisobutylene, and poly(vinyl acetate). The results enabled us to calculate various surface quantities such as spreading coefficient, contact angle, and work of adhesion, and gave information on the interphase attractive forces and the interfacial structure between polymers.

In this paper we report the measurements made on six additional polymer systems, *i.e.*, poly(methyl methacrylate)–polyethylene, poly(methyl methacrylate)–poly(*n*-butyl methacrylate), poly(methyl methacrylate)–polystyrene, poly(*n*-butyl methacrylate)–poly(vinyl acetate), poly(*n*-butyl methacrylate)–polyethylene, and polystyrene–polyethylene. Some of these six systems exhibit zero contact angle in contrast to the large contact angles exhibited by the systems reported in the previous paper.[1] The interfacial tensions between two polymers are found to be quite high due to the "mismatching" of the nature of the intermolecular forces and the conformational restriction of the polymer molecules. These effects are discussed in terms of a modified form of the equations of Fowkes[10] and of Good and Girifalco.[11,12]

II. Experimental Section

A. Pendant Drop Apparatus. The pendant drop method was adopted for the measurements. The method permits attainment of equilibrium of the viscous melts within a reasonable length of time of about 20–40 min. The attainment of equilibrium was tested by checking the constancy of the shape correction

(1) (a) S. Wu, presented at the 43rd National Colloid Symposium Case-Western Reserve University, June 1969; (b) *J. Colloid Interfac. Sci.*, **31**, 153 (1969).

(2) R. J. Roe, *J. Phys. Chem.*, **72**, 2013 (1968).

(3) H. Edwards, *J. Appl. Polym. Sci.*, **12**, 2213 (1968).

(4) R. H. Dettre and R. E. Johnson, Jr., *J. Colloid Interfac. Sci.*, **21**, 367 (1966).

(5) (a) H. Schonhorn, F. W. Ryan, and L. H. Sharpe, *J. Polym. Sci.*, **4**, 538 (1966); (b) *ibid.*, *A*, **3**, 569 (1965); *Polym. Lett.*, **3**, 235 (1965).

(6) T. Sakai, *Polymer*, **6**, 659 (1965).

(7) F. J. Hybart and T. R. White, *J. Appl. Polym. Sci.*, **3**, 118 (1960).

(8) N. Ogata, *Bull. Chem. Soc. Jap.*, **33**, 212 (1960).

(9) H. Tarkow, *J. Polym. Sci.*, **28**, 35 (1958).

(10) F. M. Fowkes in "Chemistry and Physics of Interfaces," American Chemical Society, Washington, D. C., 1965, pp 1–12.

(11) L. A. Girifalco and R. J. Good, *J. Phys. Chem.*, **61**, 904 (1957).

(12) R. J. Good in "Treatise on Adhesion and Adhesives," Vol. I, R. L. Patrick, Ed., Marcel Dekker, New York, N. Y. 1967, pp 9–68.

factor.[1,13] The pendent drop was protected from oxidation in an atmosphere of high purity argon. The details of the construction of the apparatus and the experimental procedure have been discussed previously.[1]

B. Mercury Dilatometer. The densities of the molten polymers were determined by a conventional dilatometric method similar to those of Bekkedahl[14] and Marker, *et al.*[15] The sample size used was about 5 g and a true-bore capillary of 2.000-mm diameter was used. The reproducibility of the results was within 0.5%.

C. Materials. 1. Poly(methyl methacrylate). Because of the very high viscosity of poly(methyl methacrylate), it was necessary to use a low molecular weight polymer. The polymer used was prepared by polymerizing the monomer in toluene with azobisisobutyronitrile as the initiator and had a viscosity-average molecular weight of 3000.

2. Poly(n-butyl methacrylate). The polymer used was prepared by polymerizing the monomer in toluene with azobisisobutyronitrile as the initiator, and had a viscosity-average molecular weight of 37,000.

3. Polystyrene. The polymer used was obtained from Borden Chemical Company and had a viscosity-average molecular weight of 44,000.

4. Poly(vinyl acetate). The polymer used was Union Carbide Vinylite AYAC poly(vinyl acetate) having a weight-average molecular weight of 11,000, or AYAA poly(vinyl acetate), having a weight-average molecular weight of 45,000. All the above polymer samples were purified by twice precipitating into a large quantity of nonsolvent (*n*-hexane or methanol) from toluene solutions. The resulting precipitates were vacuum dried at 80° to remove all the volatile liquids.

5. Polyethylene. The polymer used was Du Pont Alathon 7050 linear polyethylene having a melt index of about 20, 0.2 methyl group per 100 carbon atoms, and a weight-average molecular weight of 67,000. The sample was purified by extraction with cyclohexane in a Soxhlet extractor. The low molecular weight fraction removed by the extraction amounted to about 0.16% of the sample.

III. Results

A. Densities of Molten Polymers. Calculation of the surface and the interfacial tensions from the pendant drop measurements requires density data. The densities of the polymer samples used were determined by the mercury dilatometer.

For poly(methyl methacrylate), the values obtained were $v = 0.8148 + 4.62 \times 10^{-4}t$, 120–180°, where v is the specific volume in cc/g, and t is the temperature in °C. For poly(*n*-butyl methacrylate) $v = 0.9497 + 6.10 \times 10^{-4}(t - 25)$, 100–180°; for polystyrene, $v = 0.9802 + 5.43 \times 10^{-4}(t - 100)$, 100–200°. The data for polystyrene agree well with those of Hellwege, *et al.*[16] For poly(vinyl acetate), the values obtained were $v = 0.8230 + 6.44 \times 10^{-4}t$, 100–180°, for polyethylene $v = 1.152 + 8.80 \times 10^{-4}t$, 140–180°. The data for polyethylene agree well with those of Richardson, *et al.*[17]

B. Surface and Interfacial Tensions. The surface and the interfacial tension values, γ, were calculated by the equation[18]

$$\gamma = g\Delta\rho(d_e)^2/H \qquad (1)$$

where g is the gravitational acceleration, $\Delta\rho$ is the density difference between the liquid of the drop and the surrounding medium, d_e is the equatorial diameter of the drop, and $1/H$ is a correction factor determined by the shape of the drop. In this work, the attainment of equilibrium was tested by checking the constancy of $1/H$ values as determined by a series of shape parameters S_n defined by $S_n = d_n/d_e$ ($n = 8, 9, 10, 11, 12$) where d_n is the diameter of the drop measured at a distance equal to $d_e(n/10)$ up from the bottom of the drop. $1/H$ values as a function of S_n have been tabulated.[13] Variations of $1/H$ values within ±0.5% were taken as the criterion for the attainment of equilibrium which usually takes 20–40 min depending on the viscosity of the system. Examples have been given previously.[1] The systems were all incompatible and sharp phase boundaries were observed. All the surface and the interfacial tension measurements were duplicated or triplicated. Reproducibility was within 0.5 dyn/cm. The effect of the possible degradation of the polymers was probably negligible, since the surface and the interfacial tension values remained constant over an extended period of time after the attainment of equilibrium.

The results are plotted in Figures 1 and 2. For the surface tension values γ in dyn/cm, as a function of temperature in °C, we have poly(methyl methacrylate), $\gamma = 41.1 - 0.076(t - 20)$; poly(*n*-butyl methacrylate); $\gamma = 31.2 - 0.059(t - 20)$; polystyrene; $\gamma = 40.7 - 0.072(t - 20)$.

For the interfacial tension values γ in dyn/cm as a function of temperature in °C, we have: poly(methyl methacrylate)–polyethylene; $\gamma = 11.9 - 0.018(t - 20)$; poly(*n*-butyl methacrylate)–polyethylene; $\gamma = 7.1 - 0.015(t - 20)$; polystyrene–polyethylene; $\gamma = 8.3 - 0.020(t - 20)$; poly(methyl methacrylate)–polystyrene; $\gamma = 3.2 - 0.013(t - 20)$; poly(*n*-butyl methacrylate)–poly(vinyl acetate); $\gamma = 4.2 - 0.010 \cdot (t - 20)$; and poly(methyl methacrylate)–poly(*n*-butyl methacrylate); $\gamma = 3.4 - 0.012(t - 20)$.

(13) R. J. Roe, V. L. Bacchetta, and P. M. G. Wong, *J. Phys. Chem.*, 71, 4190 (1967).

(14) N. Bekkedahl, *J. Res. Nat. Bur. Stand.*, 42, 145 (1949).

(15) L. Marker, R. Early, and S. L. Aggarwal, *J. Polym. Sci.*, 38, 369 (1959).

(16) K. H. Hellwege, W. Knappe, and P. Lehmann, *Kolloid-Z. Z. Polym.*, 183, 110 (1962).

(17) M. J. Richardson, P. J. Flory, and J. B. Jackson, *Polymer*, 4, 221 (1963).

(18) A. W. Adamson, "Physical Chemistry of Surfaces," 2nd ed, Interscience, Publishers Inc., New York, N. Y., 1967, pp 30–37.

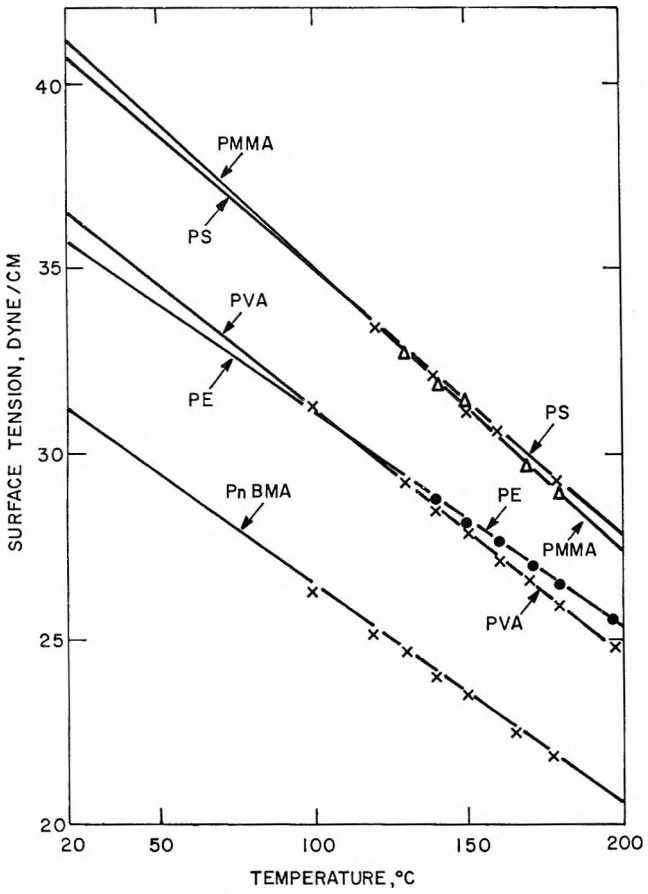

Figure 1. Surface tensions of some polymer melts. PMMA; poly(methyl methacrylate); PS, polystyrene; PnBMA, poly(*n*-butyl methacrylate); PE, polyethylene; PVA, poly(vinyl acetate). The data for PE and PVA are from ref 1.

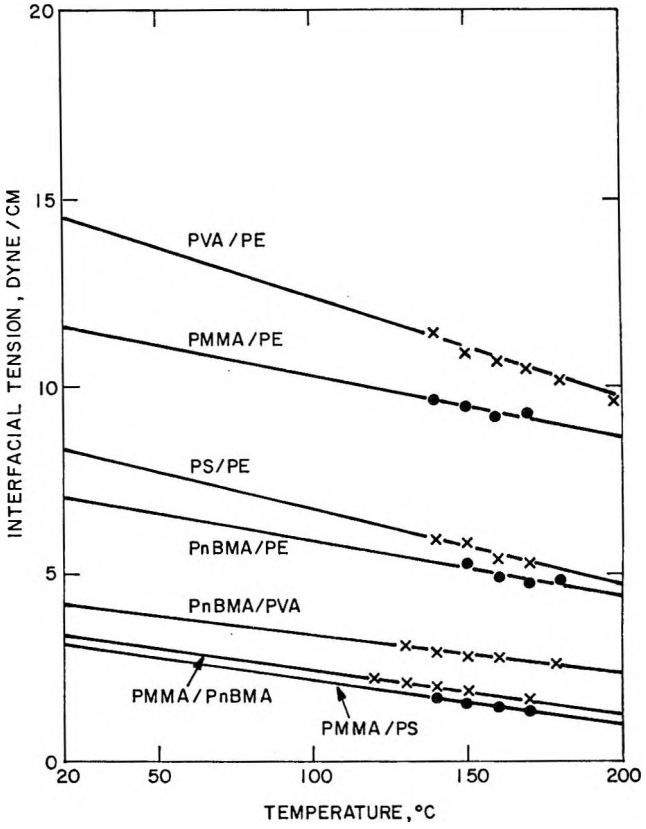

Figure 2. Interfacial tensions between some polymer melts. PMMA, poly(methyl methacrylate); PS, polystyrene; PnBMA, poly(*n*-butyl methacrylate); PE, polyetheylene; PVA, poly(vinyl acetate). The data for PVA–PE are from ref 1.

IV. Discussion

A. Surface Tensions. The experimental and the parachor-calculated values of the surface tension, the temperature coefficients, and the critical surface tensions are tabulated in Table I. The temperature coefficients are very small, *i.e.*, in the vicinity of −0.06, indicating a small entropic contribution to the surface tension. The atomic parachor values used are those recommended by Quayle,[19] *i.e.*, 40.0 for CH_2, 9.0 for C, 15.5 for H, 54.8 for O_2 in esters, 17.7 for double bond, −3.7 per chain branching, and 0.8 for six-membered ring closure. Good agreement between the experimental and the parachor-calculated values is obtained for poly(methyl methacrylate) and polystyrene. But considerable departure is found for poly(*n*-butyl methacrylate). It is interesting to see that for poly(methyl methacrylate) and poly(*n*-butyl methacrylate) the critical surface tensions[20] agree well with the experimental surface tensions. But a large difference is found for polystyrene. However, Fowkes' value[10] of the dispersion-force contribution to the surface tension for polystyrene agrees fairly well with the experimental surface tension value.

B. Interfacial Tensions. The interfacial tension values and some derived quantities for the systems poly(methyl methacrylate)–polyethylene, poly(*n*-butyl methacrylate)–polyethylene, polystyrene–polyethylene, poly(methyl methacrylate)–polystyrene, poly(*n*-butyl methacrylate–poly(vinyl acetate), and poly(methyl methacrylate)–poly(*n*-butyl methacrylate) are tabulated in Tables II–VII.

It can be seen that the interfacial tensions between polymers are quite high and are never negligible. For instance, the interfacial tension amounts to 9.7 dyn/cm at 140° for the poly(methyl methacrylate)–polyethylene system. The high interfacial tension will impart a great influence on various surface quantities such as contact angle, spreading coefficient, and work of adhesion, as will be discussed later.

Fowkes[10] proposed that the interfacial tension γ_{12} can be expressed in terms of the surface tensions of the two individual phases γ_1 and γ_2

$$\gamma_{12} = \gamma_1 + \gamma_2 - 2(\gamma_1^d\gamma_2^d)^{1/2} - I_p \qquad (2)$$

(19) O. R. Quayle, *Chem. Rev.*, 53, 439 (1953).

(20) W. A. Zisman in "Contact Angle, Wettability and Adhesion," Advances in Chemistry Series, No. 43, American Chemical Society, Washington, D. C., 1964, pp 1–51.

Table I: Surface Tension Values and Some Derived Quantities

Polymer	Surface tension, dyn/cm 20°	140°	180°	Temperature coefficient $-d\gamma/dt$, dyn/cm-deg	Surface tension values calcd from parachor,[a] dyn/cm 20°	140°	180°	Critical surface tension, dyn/cm
Poly(methyl methacrylate)	41.1	32.0	28.9	0.076	41.1	32.0	28.9	39–40[b]
Poly(*n*-butyl methacrylate)	31.2	24.1	21.7	0.059	38.1	28.6	26.0	32[c]
Polystyrene	40.7	32.1	29.2	0.072	37.5	30.9	28.5	33,[b] 44[d]
Polyethylene[e]	35.7	28.8	26.5	0.057	35.3	25.0	22.4	31,[b] 35[d]
Poly(vinyl acetate)[e]	36.5	28.6	25.9	0.066	38.8	27.7	24.8	36[c]

[a] The parachor values recommended by O. R. Quayle, *Chem. Rev.*, **53**, 439 (1953) are used. [b] Reference 20. [c] S. Wu, *J. Phys. Chem.*, **72**, 3332 (1968). [d] Values obtained by Fowkes-type plot of contact angle data.[10] [e] Reference 1.

Table II: Interfacial Tension Values and Some Derived Quantities for Poly(methyl methacrylate)–Polyethylene System

T, °C	Interfacial tension, dyn/cm γ_{12}	γ_{12}^d	$(\gamma_{12}^d - \gamma_{12})$	Contact angle, deg $\theta_{PMMA-PE}$	$\theta_{PE-PMMA}$	Φ	Spreading coefficient, erg/cm² $S_{PMMA-PE}$	$S_{PE-PMMA}$	Work of adhesion, erg/cm², W_a	$Q = \frac{\text{work of Adhesion}}{\text{work of cohesion}}$ $W_a/W_{c(PMMA)}$	$W_a/W_{c(PE)}$
20	11.9	~0	−11.9	55	35.5	0.845	−17.3	−6.5	64.9	0.79	0.91
140	9.7	~0	−9.7	53	39	0.841	−12.9	−6.5	51.1	0.80	0.89
180	9.0	~0	−9.0	53	40	0.838	−11.4	−6.6	46.4	0.80	0.88

Table III: Interfacial Tension Values and Some Derived Quantities for Poly(*n*-butyl methacrylate)–Polyethylene System

T, °C	Interfacial tension, dyn/cm γ_{12}	γ_{12}^d	$(\gamma_{12}^d - \gamma_{12})$	Contact angle, deg $\theta_{PnBMA-PE}$	$\theta_{PE-PnBMA}$	Φ	Spreading coefficient, erg/cm² $S_{PnBMA-PE}$	$S_{PE-PnBMA}$	Work of adhesion, erg/cm², W_a	$Q = \frac{\text{work of adhesion}}{\text{work of cohesion}}$ $W_a/W_{c(PnBMA)}$	$W_a/W_{c(PE)}$
20	7.1	~0.1	−7.0	22	46	0.896	−2.6	−11.6	59.8	0.96	0.84
140	5.3	~0.1	−5.2	14	49	0.903	−0.6	−10.0	47.6	0.99	0.83
180	4.7	~0.2	−4.5	~0	49	0.906	0.1	−9.5	43.5	1.00	0.82

Table IV: Interfacial Tension Values and Some Derived Quantities for Polystyrene–Polyethylene System

T, °C	Interfacial tension, dyn/cm γ_{12}	γ_{12}^d	$(\gamma_{12}^d - \gamma_{12})$	Contact angle, deg θ_{PS-PE}	θ_{PE-PS}	Φ	Spreading coefficient, erg/cm² S_{PS-PE}	S_{PE-PS}	Work of adhesion, erg/cm², W_a	$Q = \frac{\text{work of adhesion}}{\text{work of cohesion}}$ $W_a/W_{c(PS)}$	$W_a/W_{c(PE)}$
20	8.3	~0	−8.3	47	24	0.893	−13.3	−3.3	68.1	0.84	0.96
140	5.9	~0	−5.9	45	24	0.905	−9.2	−2.6	55.0	0.86	0.96
180	5.1	~0	−5.1	43	24	0.907	−7.8	−2.4	50.6	0.87	0.96

Table V: Interfacial Tension Values and Some Derived Quantities for Poly(methyl methacrylate)–Polystyrene System

T, °C	Interfacial tension, dyn/cm γ_{13}	γ_{12}^d	$(\gamma_{13}^d - \gamma_{13})$	Contact angle, deg $\theta_{PMMA-PS}$	$\theta_{PS-PMMA}$	Φ	Spreading coefficient, erg/cm² $S_{PMMA-PS}$	$S_{PS-PMMA}$	Work of adhesion, erg/cm², W_a	$Q = \frac{\text{work of adhesion}}{\text{work of cohesion}}$ $W_a/W_{c(PMMA)}$	$W_a/W_{c(PS)}$
20	3.2	~0	−3.2	21	24	0.962	−3.6	−2.8	78.6	0.96	0.97
140	1.7	~0	−1.7	18	19	0.974	−1.8	−1.6	62.4	0.97	0.97
180	1.2	~0	−1.2	17	19	0.976	−1.5	−0.9	56.9	0.98	0.97

where the superscript d means the dispersion force component and I_p is the polar force contribution.

If we assume that eq 2 is applicable to polymer systems, then the dispersion force component for poly(methyl methacrylate), poly(*n*-butyl methacrylate), and polystyrene can be calculated using the interfacial tension data of the first three systems. Since polyethylene may be regarded as completely nonpolar,

Table VI: Interfacial Tension Values and Some Derived Quantities for Poly(*n*-butyl methacrylate)–Poly(vinyl acetate) System

	Interfacial tension, dyn/cm			Contact angle, deg			Spreading coefficient, erg/cm²		Work of adhesion,	$Q = \frac{\text{work of adhesion}}{\text{work of cohesion}}$	
T, °C	γ_{12}	γ_{12}^d	$(\gamma_{12}^d - \gamma_{12})$	$\theta_{PnBMA-PVA}$	$\theta_{PVA-PnBMA}$	Φ	$S_{PnBMA-PVA}$	$S_{PVA-PnBMA}$	erg/cm², W_a	$W_a/W_{c(PnBMA)}$	$W_a/W_{c(PVA)}$
20	4.2	0.3	−3.9	0	42	0.941	1.1	−9.5	63.5	1.02	0.87
140	2.9	0.2	−2.7	0	42	0.950	1.6	−7.4	49.8	1.03	0.87
180	2.5	0.1	−2.4	0	42	0.950	1.7	−6.7	45.1	1.04	0.87

Table VII: Interfacial Tension Values and Some Derived Quantities for Poly(methyl methacrylate)–Poly(*n*-butyl methacrylate) Systems

	Interfacial tension, dyn/cm			Contact angle, deg			Spreading coefficient, erg/cm²		Work of adhesion,	$Q = \frac{\text{work of adhesion}}{\text{work of cohesion}}$	
T, °C	γ_{12}	γ_{12}^d	$(\gamma_{12}^d - \gamma_{12})$	$\theta_{PMMA-PnBMA}$	$\theta_{PnBMA-PMMA}$	Φ	$S_{PMMA-PnBMA}$	$S_{PnBMA-PMMA}$	erg/cm², W_a	$W_a/W_{c(PMMA}$,	$W_a/W_{c(PnBMA)}$
20	3.4	0.5	−3.4	48	0	0.960	−13.3	6.5	68.9	0.84	1.10
140	1.9	0.5	−1.4	46	0	0.975	−9.8	6.0	54.2	0.85	1.12
180	1.4	0.5	−0.9	45	0	0.982	−8.6	5.8	49.2	0.85	1.13

Table VIII: γ^d Values for Some Polymers as Calculated from the Surface and the Interfacial Tension Data Using Equation 2

T, °C	γ^d, dyn/cm	γ^d/γ
Poly(methyl methacrylate), from poly(methyl methacrylate)–polyethylene data		
20	29.5	0.72
140	22.6	0.71
180	20.3	0.70
Poly(*n*-butyl methacrylate), from poly(*n*-butyl methacrylate)–polyethylene data		
20	25.0	0.80
140	19.7	0.82
180	17.8	0.82
Polystyrene, from polystyrene–polyethylene data		
20	32.5	0.80
140	26.2	0.82
180	24.2	0.83
Poly(vinyl acetate), from poly(vinyl acetate)–polyethylene data (ref 1)		
20	23.2	0.64
140	18.5	0.64
180	16.8	0.64

the term I_p in eq 2 vanishes. The values of the dispersion force component γ^d thus calculated for the three polymers and poly(vinyl acetate) are tabulated in Table VIII. Poly(methyl methacrylate) thus contains about a 20% polar contribution. Poly(vinyl acetate) contains about a 35% polar contribution according to a similar calculation made before.[1] Furthermore, the calculation shows that polystyrene contains about a 20% polar contribution in contrast to the common belief that polystyrene should be quite nonpolar. The γ^d values for the polymers thus calculated and listed in Table VIII are considerably smaller than the values obtained by the "Fowkes-type" plot[10] using the contact angle data of ordinary liquids on the polymers.

If we use the γ^d values for the four polymers as found above and apply eq 2 letting $I_p = 2(\gamma_1^p\gamma_2^p)^{1/2}$ where γ^p is the polar force contribution assumed to be $\gamma^p = \gamma - \gamma^d$, then the interfacial tension values for the last three systems can be calculated. The results are tabulated in Table IX. The agreement between the calculated and the experimental values is fairly good. However, the calculated values are consistently smaller than the experimental values, probably resulting from the effect of the conformational restriction of the polymer molecules on the interfacial contact, as will be discussed later. It should be noted that when the Fowkes' γ^d values (obtained from the contact angle data of ordinary liquids) are used in eq 2 to calculate the interfacial tensions between polymers, large discrepancies between the calculated and the experimental values are found.

Table IX: Interfacial Tension Values Calculated by Equation 2, Letting $I_p = 2(\gamma_1^p\gamma_2^p)^{1/2}$

T, °C	Interfacial tension, dyn/cm Calcd	Exptl
Poly(methyl methylacrylate)–polystyrene system[a]		
20	0.5	(3.2)[b]
140	0.5	1.7
180	0.6	1.2
Poly(*n*-butyl methacrylate)–poly(vinyl acetate) system[a]		
20	1.3	(4.2)[b]
140	1.2	2.9
180	1.1	2.5
Poly(methyl methacrylate)–poly(*n*-butyl methacrylate) system[a]		
20	1.0	(3.4)[b]
140	1.0	1.9
180	0.9	1.4

[a] All γ^d values are from Table VIII. [b] Extrapolated values.

C. An Implication on the Interfacial Structure between Polymers. The simplified equation such as by letting $\gamma^d = \gamma$ in eq 2, *i.e.*

$$\gamma_{12} = \gamma_1 + \gamma_2 - 2(\gamma_1\gamma_2)^{1/2} \quad (3)$$

cannot be used for the present polymer systems. The interfacial tension values calculated by eq 3, which we denote as γ^d_{12}, are always negligibly small as compared with the experimental γ_{12} values, as shown in Tables II–VII. This indicates that the interfacial tension between two polymer phases arises mainly from the effects of the "mismatching" of the nature of the intermolecular forces and the polymer molecular conformational restriction on the interfacial contact. These two effects can be included in the equation of Good and Girifalco[11,12]

$$\gamma_{12} = \gamma_1 + \gamma_2 - 2\phi_A\phi_V(\gamma_1\gamma_2)^{1/2} \quad (4)$$

where the parameters ϕ_A and ϕ_V are determined by the "matching" or "mismatching" of the nature of the intermolecular forces and by the intermolecular distances, respectively. If we assume that both the dispersion force and the polar forces obey Berthelot's geometric mean rule, then the parameter ϕ_A is given by

$$\phi_A = (f_1^d f_2^d)^{1/2} + (f_1^p f_2^p)^{1/2} \quad (5)$$

where f^d is the fraction of the dispersion force component of the surface force (*i.e.*, $= \gamma^d/\gamma$) and f^p is the fraction of the polar force component of the surface force (*i.e.*, $= \gamma^p/\gamma$). Equation 5 indicates that ϕ_A will be approximately equal to unity when the intermolecular forces in the two phases are "matched," *i.e.*, $f^d_1 \cong f^d_2$ and $f^p_1 \cong f^p_2$, and will be less than unity when the intermolecular forces are "unmatched." Thus, the interfacial tension will be higher when the nature of the intermolecular forces in the two phases are "unmatched."

On the other hand, the parameter ϕ_V is given by[12]

$$\phi_V = (z_{11}z_{22})/(z_{12})^2 \quad (6)$$

where z's are the intermolecular distances. If we let $z_{12} = (1/2)(z_{11} + z_{22})(1 + \delta)$, where δ is the fractional increase of the intermolecular distance between the phases 1 and 2 over that of the arithmetic mean value, then it can be shown that for small δ values, we have

$$\phi_V = 1 - 2\delta \quad (7)$$

Equation 7 indicates that the fractional increase or decrease of the interfacial intermolecular distance directly determines the value of ϕ_V. When the interfacial intermolecular distance is greater than the arithmetic mean value (*i.e.*, $\delta > 0$ and the interface is discrete), the interfacial tension will be higher. When the interfacial intermolecular distance is smaller than the arithmetic mean value (*i.e.*, $\delta < 0$ and the interface is diffuse), the interfacial tension will be lower.

By using the experimental interfacial tension data in eq 4–7, the δ values are estimated to be in the vicinity of 0.02–0.05, suggesting that the interfacial region between polymers is discrete. On the other hand, similar calculations made on the organic liquid–water systems give δ values in the vicinity of -0.02 to -0.05, suggesting that the interfacial region between ordinary liquids is diffuse.

D. Some Derived Quantities and Adhesion. Successful formulation of adhesion theory requires knowledge of the interfacial structure of polymer systems. Our data here provide an opportunity to calculate various quantities of importance to adhesion (contact angle, spreading coefficient, and work of adhesion), and examine polymer adhesion in the light of these interfacial properties.

The contact angle θ_{12} of polymer 1 on polymer 2 can be calculated by

$$\cos\theta_{12} = 2\Phi(\gamma_2/\gamma_1)^{1/2} - 1 \quad (8)$$

where we have assumed no deformation of the substrate phase and Φ is the interaction parameter defined by

$$\Phi = \frac{\gamma_1 + \gamma_2 - \gamma_{12}}{2(\gamma_1\gamma_2)^{1/2}} \quad (9)$$

It can be seen in Tables II–VII that only poly(*n*-butyl methacrylate) exhibits zero contact angle on poly(vinyl acetate) and on poly(methyl methacrylate), but the contact angles in the reverse situations, *i.e.*, poly(vinyl acetate) on poly(*n*-butyl methacrylate) and poly(methyl methacrylate) on poly(*n*-butyl methacrylate), are quite high. It is also noted that the contact angles of one polymer on another are, in most cases, quite insensitive to temperature variation except for the contact angles of poly(*n*-butyl methacrylate) on polyethylene and those of poly(methyl methacrylate) on polystyrene. However, we note that the contact angles of polyethylene on poly(*n*-butyl methacrylate) and those of polystyrene on poly(methyl methacrylate) are quite insensitive to temperature variation. Of special interest is that the contact angle of poly(*n*-butyl methacrylate) on polyethylene is about 14° at a temperature of 140°, but decreases to 0° at about 180°. The insensitivity of the contact angle of one polymer on another has been noted in our previous paper.[1] For ordinary organic liquids on polymer surfaces, negligible effect of temperature on the contact angle has been reported before.[21,22] However, a significant dependence of the contact angle on temperature has also been found for ordinary organic liquids.[23,24] It is interesting to point out that the contact angle may either decrease

(21) R. E. Johnson, Jr., and R. H. Dettre, *J. Colloid Interfac. Sci.*, **20**, 173 (1965).

(22) (a) H. Schonhorn, *J. Phys. Chem.*, **70**, 4086 (1966); (b) *Nature*, **210**, 896 (1966); (c) *J. Adhesion*, **1**, 38 (1969).

(23) C. L. Sutula, R. Hautala, R. W. Dalla Betta, and L. A. Michell, Abstracts, 153rd National Meeting of the American Chemical Society, Miami, Florida, April 1967.

(24) J. B. Jones and A. W. Adamson, *J. Phys. Chem.*, **72**, 646 (1968).

or increase with increasing temperature. For instance, the contact angle of poly(methyl methacrylate) on polyethylene decreases, but the contact angle of polyethylene on poly(methyl methacrylate) increases with increasing temperature.

The effect of temperature on contact angle can be expressed by the following equation which is obtained by differentiating eq 8 with respect to temperature

$$\frac{\mathrm{d}\cos\theta_{12}}{\mathrm{d}T} = \Phi(1/\gamma_1\gamma_2)^{1/2}[a_1(\gamma_2/\gamma_1) - a_2] \qquad (10a)$$

where

$$a_1 = -\left(\frac{\mathrm{d}\gamma_1}{\mathrm{d}T}\right) \text{ and } a_2 = -\left(\frac{\mathrm{d}\gamma_2}{\mathrm{d}T}\right) \qquad (10b)$$

and we have let

$$\frac{\mathrm{d}\Phi}{\mathrm{d}T} \cong 0 \qquad (10c)$$

Equation 10c is justified experimentally as shown in Tables II–VII and in a previous paper.[1] Since the temperature coefficients of the surface tensions, a_1, a_2, are usually very small, the quantity $[a_1(\gamma_2/\gamma_1) - a_2]$ is therefore usually small (~0.01 dyn/cm or less). This is why the temperature coefficient of the contact angle is usually quite small. However, since the cosine function has a steeper slope near $\theta = 0$, the temperature coefficient for systems having small contact angles tends to be greater as in the case of the contact angle of poly(*n*-butyl methacrylate) on polyethylene shown in Table III. Equation 10a also indicates that the temperature coefficient of the contact angle can be either negative or positive, depending on the sign of the quantity $[a_1 \cdot (\gamma_2/\gamma_1) - a_2]$. This explains why the contact angle of poly(methyl methacrylate) on polyethylene decreases with increasing temperature, but the contact angle of polyethylene on poly(methyl methacrylate) increases with increasing temperature as can be seen in Table II.

The spreading coefficient of polymer 1 on polymer 2 is given by[25]

$$S_{1/2} = \gamma_2 - \gamma_1 - \gamma_{12} \qquad (11)$$

It is interesting to see that poly(*n*-butyl methacrylate) spreads on poly(vinyl acetate), but not *vice versa;* poly(*n*-butyl methacrylate) spreads on poly(methyl methacrylate), but not *vice versa*. No spreading occurs for any of the other systems except for poly(*n*-butyl methacrylate) which spreads on polyethylene at 180°. It is noted that the interfacial tensions between polymers are by no means negligible. Therefore, the polymer having a lower surface tension does not necessarily spread on the polymer having a higher surface tension. For instance, the interfacial tension between poly(methyl methacrylate) and polyethylene amounts to 9.7 dyn/cm at 140°. This high interfacial tension results in the mutual nonspreading of the system. Whether spreading will occur in a system is primarily determined by the magnitude of the interfacial tension which is in turn determined by the "matching" or "mismatching" of the polarity of the two phases and the packing density at the interface. Thus, we may say qualitatively that spreading is favored by matching the polarity and molecular geometry of the two phases.

The work of adhesion W_a and the ratio of the work of adhesion to the work of cohesion W_c as defined below are tabulated in Tables II–VII

$$W_{a12} = \gamma_1 + \gamma_2 - \gamma_{12} \qquad (12)$$

$$W_{c1} = 2\gamma_1 \qquad (13)$$

and

$$Q_{12/1} = \frac{W_{a12}}{W_{c1}} = \Phi\left(\frac{\gamma_2}{\gamma_1}\right)^{1/2} \qquad (14)$$

It can be seen that in many cases both $Q_{12/1}$ and $Q_{12/2}$ are smaller than unity, indicating that the work of adhesion can be smaller than the work of cohesion of either phase in polymer systems.

The theoretical adhesive strength can be given in terms of the work of adhesion by[12,26]

$$\sigma_{a12} = 1.03W_{a12}/z_{12} \qquad (15a)$$

$$= 2.06\Phi(\gamma_1\gamma_2)^{1/2}/z_{12} \qquad (15b)$$

where σ_{a12} is the theoretical adhesive strength and z_{12} is the equilibrium separation of the two phases. On the other hand, the theoretical cohesive strength of phase 1 is given by [12,26]

$$\sigma_{c1} = 1.03W_{c1}/z_{11} \qquad (16a)$$

$$= 2.06\gamma_1/z_{11} \qquad (16b)$$

where σ_{c1} is the theoretical cohesive strength of phase 1 and z_{11} is the equilibrium separation of two neighboring interacting sites.

The values of the work of adhesion for the present systems are in the range of 40–80 ergs/cm^2 between 20 and 180°. If we assume that $z_{12} = 5$ Å, then the theoretical adhesive strength is found to be 12,000–24,000 psi according to eq 15.

(25) W. D. Harkins, "Physical Chemistry of Surface Films," Reinhold Publishing Corp., New York, N. Y., 1952.

(26) J. L. Gardon in "Treatise on Adhesion and Adhesives," Vol. I, R. L. Patrick, Ed., Marcel Dekker, New York, N. Y., 1967, pp 269–324.

Electron Acceptor–Electron Donor Interactions. XV. Examination of Some Weak Charge-Transfer Interactions and the Phenomenon of Thermochromism in these Systems[1,2]

by P. R. Hammond and L. A. Burkardt

Chemistry Division, Code 6056, Michelson Laboratories, Naval Weapons Center, China Lake, California 93555
(Received May 12, 1969)

Electron acceptor and electron donor mixtures that display extremely weak or just contact interaction in a number of solvents are examined. Such acceptors—tetranitromethane, trinitromesitylene—and such donors—tetrakis(dimethylamino)ethylene, tetramethyl-2-tetrazene, triphenylamine, and the sterically hindered alkylbenzenes—are selected mainly on the basis that bulky substituents on π donors and π acceptors markedly reduce their complexing ability. Solution equilibria, temperature effects, phase diagrams, and X-ray diffraction patterns are studied. Colors of many of the liquid two-component acceptor–donor mixtures vanish in the frozen solid. The mixtures exhibit simple eutectic phase diagrams and the thermochromic effect is interpreted as a randomized structure in the liquid permitting intermolecular contacts or very weak association, whereas the solid is a two-phase aggregate of isolated acceptor and donor crystals. On the whole, phase separation and thermochromism occur for systems exhibiting a minimal interaction in solution, whereas chemically related species showing even weak association produce complexes. Exceptions are emphasized, in particular the retention of color in frozen glasses. Contrary to widespread belief, tetranitromethane interacts only weakly with aromatic hydrocarbons; it does not form isolable complexes.

Interpretation of measurements on weakly interacting donor–acceptor systems is limited when the magnitude of the property ascribed to complex formation becomes comparable to the deviations from ideality for the components. For example, although an exothermic heat of mixing is quite good evidence for complexing, a positive excess enthalpy can be ambiguous, merely showing that the escaping tendency for a regular solution pair is sufficient to overcome any possible mutual attraction. Criteria for the existence of new species depend on accurate assessments of the "physical" and "chemical" contributions to the property measured. A method capable of giving a certain answer to the question "Do the materials A and D form an adduct?" is a precise solid/liquid two component phase diagram, where for example a simple eutectic demonstrates the absence of complexing. A limitation here though is that information pertaining to the solid is not necessarily appropriate to the very different and more idealized environments of solution or gas phase. Even for a system that shows no "chemical" contribution according to a number of measurements, a definite statement of truly contact interaction in most cases will be very difficult. Rather, the less precise expression will apply "If there are residual attractive forces, they are very weak."

We seek to show that such weakly interacting systems are common. Previous reports on extremely weak associations that show new bands, attributed solely to the joint interaction of the components, include the halogens[3] and tetranitromethane[4] with aliphatic hydrocarbons, oxygen systems,[5] and possibly amines[6] and aromatic hydrocarbons[7] with the perhalomethanes. Thus, the appearance of absorptions, even though no

(1) For a preliminary account see P. R. Hammond and L. A. Burkardt, *Chem. Commun.*, 986 (1968).

(2) As we shall be examining a number of weakly interacting species, the original title "Studies on Complexes" for the series is inappropriate. In this and the following articles we employ the term "charge-transfer (electron-transfer) interaction" for referring to systems that exhibit intermolecular charge-transfer spectra, whether or not there is bonding between the partners, and, when there is bonding, whether or not charge-transfer forces (*i.e.*, resonance forces of the type $D,A \leftrightarrow D^+ - A^-$) contribute to it. In this respect they are particular examples of "donor–acceptor" interactions (R. S. Mulliken and W. B. Person, *Ann. Rev. Phys. Chem.*, 13, 107 (1962); "Molecular Complexes," John Wiley and Sons, Inc., New York, N. Y., 1969).

Also we employ ionization potential and electron affinity as the criteria of electron-donor and electron-acceptor strength, respectively. This corresponds, in some instances (ref 9c, pp 137–140), with conventional criteria of Lewis acidity and Lewis basicity that relate to the strength of association in adducts. In terms of complex formation, however, the compounds of this article must be disqualified, for they show little evidence of intermolecular bonding in the solid and liquid phases. For example, tetranitromethane and tetrakis(dimethylamino)ethylene must be regarded as very weak acid and base species, respectively, even though they readily demonstrate charge-transfer spectra and are reactive chemically and electrochemically, particularly in regard to oxidation or reduction. Such examples, perhaps exceptions among organic materials, are common among the inorganic. Many of the highest valency halides, oxyhalides, and oxides of the elements (for the most part reactive materials—*e.g.*, the metal hexafluorides, osmium tetroxide) must be described as very weak acceptors with respect to their interactions with aromatic hydrocarbons and fluorocarbons (P. R. Hammond and R. R. Lake, *Chem. Commun.*, 987 (1968)). Although numerous molecular ionization potentials are available, electron affinity values are not, and conclusions with regard to electron-acceptor strength must be based on properties generally agreed to represent them, such as the position of intermolecular charge-transfer spectra and reversible one-electron reduction potentials.

(3) D. F. Evans, *J. Chem. Phys.*, 23, 1424, 1426 (1955).

appreciable concentration of complex is present, is not new to the study of molecular interactions and has been ascribed to transitions occurring when donor and acceptor molecules are merely near to or in contact with each other.[3,8]

Although the phase diagram approach is a familiar one, we emphasize here a property for systems that produce eutectics, yet show transitions in the visible—namely, the colors of the pure liquid samples vanish on freezing. This very simple phenomenon, we think, is significant with regard to its value as an experimental probe of new systems, and in terms of the insight it gives of the physical processes. It has not received the emphasis it deserves, however. It is not found in the elementary chapters (or elsewhere) of the textbooks on molecular complexes,[9] although some comments of Pfeiffer[9a] (p 273), attributed to Kreman, are relevant.

The behavior observed for customary acceptor–donor molecular complexes on changing the temperature is, in solution, an increase of absorption intensity at lower temperature, a consequence of the enthalpy of association, and a freezing of a colored melt of the two components, to a solid complex of a similar hue. A note[10] of Wiberg's referred to a disappearance of color in a frozen nitrobenzene–tetrakis(dimethylamino)ethylene system and has been confirmed[11] and extended to other interactions of the base. A white, opaque solid could be obtained when the deep magenta, almost black, mixture of the base with nitrobenzene was immersed in liquid nitrogen. Melting immediately produced the original color and the cycle could be repeated many times. Moreover, all equilibria in *n*-hexane were characterized by close to zero association constants. An early paper by Tinkler[12a] described the disappearance of color when some mixtures of nitro compounds with amines were frozen. In particular the diphenylamine–*p*-chloronitrobenzene system was studied with respect to viscosity, density, and melting point diagrams. In an extensive study of a microscopic fusion method for the analysis of hydrocarbons and other materials, Laskowski[12b] found a number of systems that are colored in the fused mixtures, which he ascribed to molecular compound formation, but gave solids the color of the components, which he ascribed to separate crystallization. For the most part, we agree with these views although the specific problem of association in the liquid is examined more closely.

A number of weakly interacting species are examined; many are shown to exhibit thermochromism and are compared with a few, chemically related known complexing systems. We measure equilibria for a number of solvents, the effect of temperature on solution absorption intensities, phase diagrams, X-ray diffraction patterns, and the effect of freezing the pure mixed materials alone and in glass media. Selection of pairs is made on the basis of (a) literature, small solution *K* values for tetranitromethane[13] (I) and trinitromesitylene[14] (II) systems; (b) a reported eutectic for tetranitromethane–benzene;[15] or (c) simply on the basis that bulky substituents on π donors and π acceptors markedly reduce their complexing ability, while not

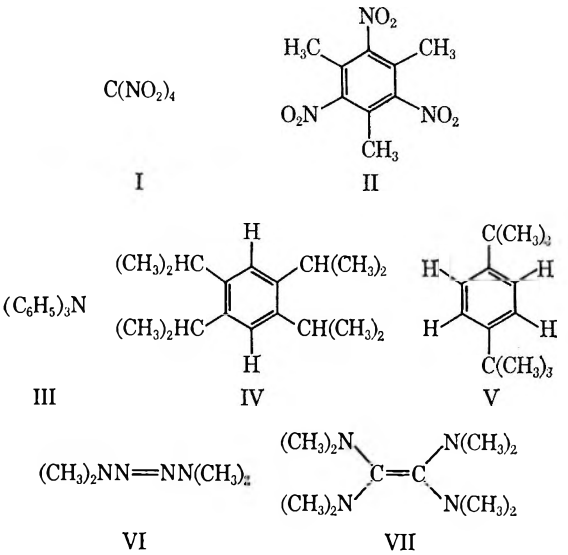

I II III IV V VI VII

(4) G. Kortum, *Z. Phys. Chem.*, (Leipzig), **B43**, 271 (1939); D. F. Evans, *J. Chem. Soc.*, 4229 (1957).

(5) A. U. Munck and J. F. Scott, *Nature*, **177**, 587 (1956); H. Tsubomura and R. S. Mulliken, *J. Amer. Chem. Soc.*, **82**, 5966 (1960).

(6) D. P. Stevenson and G. M. Coppinger, *ibid.*, **84**, 149 (1962).

(7) F. Dorr and G. Buttgereit, *Ber. Bunsenges. Phys. Chem.*, **67**, 867 (1963).

(8) (a) R. S. Mulliken, *Rec. Trav. Chim. Pays-Bas*, **75**, 845 (1956); (b) L. E. Orgel and R. S. Mulliken, *J. Amer. Chem. Soc.*, **79**, 4839 (1957).

(9) (a) P. Pfeiffer, "Organische Molekülverbindungen," 2nd ed, Verlag von Ferdinand Enke, Stuttgart, 1927; (b) G. Briegleb, "Zwischenmolekulare Kräfte und Molekülstruktur," Verlag von Ferdinand Enke, Stuttgart, 1937, reproduced by Edwards Brothers, Inc., Ann Arbor, Mich., 1944; (c) G. Briegleb, "Elektronen-Donator-Acceptor-Komplexe," Springer-Verlag, Berlin 1961; (d) L. J. Andrews and R. M. Keefer, "Molecular Complexes in Organic Chemistry," Holden-Day Inc., San Francisco, Calif., 1964; (e) J. Rose, "Molecular Complexes," Pergamon Press, London, 1967.

(10) N. Wiberg and J. Buchler, *Chem. Ber.*, **97**, 618 (1964).

(11) (a) P. R. Hammond and R. H. Knipe, U. S. Naval Ordnance Test Station, China Lake, Calif., NOTS TP 4123, July 1966. (b) In a recent paper (M. Hor i,K. Kimura, and H. Tsubomura, *Spectrochim. Acta*, **24A**, 1397, (1968)) it was reported there were no spectral changes for solutions of tetrakis(dimethylamino)ethylene (TMAE) with acceptors such as nitrobenzene. New absorptions ascribed to intermolecular charge-transfer transitions have been clearly demonstrated however (P. R. Hammond and R. H. Knipe, *J. Amer. Chem. Soc.*, **89**, 6063 (1967) and in ref 10 and 11a above). The reactive nature of TMAE requires that measurements with it be made with extreme carefulness; nevertheless, the color changes with the nitrobenzenes are difficult to miss. Their conclusions as to the structure of this interesting molecule, its excited states, and its ions are in close agreement with ours.

(12) (a) C. K. Tinkler, *J. Chem. Soc.*, 2171 (1913); (b) D. E. Laskowski and W. C. McCrone, *Anal. Chem.*, **26**, 1497 (1954); D. E. Laskowski, *ibid.*, **32**, 1171 (1960); U. S. Patent 2,809,116 (1957); *Cancer Res.*, **27**, 903 (1967).

(13) It is noteworthy that tetranitromethane interacts only weakly with aromatic hydrocarbon donors, as discussed in the Appendix.

(14) B. Dale, R. Foster, and D. Ll. Hammick, *J. Chem. Soc.*, 3986 (1954).

(15) T. Urbanski, M. Piskorz, W. Cetner, and M. Maciejewski, *Bull. Acad. Pol. Sci., Ser. Sci. Chim.*, **10**, 263 (1962).

necessarily changing the position of the transition a great deal. An acceptor found to show thermochromic effects with one donor responds similarly toward a range of donors. We have chosen systems containing compounds I–VII. Colored mixtures containing 1,1,3,3-tetramethyl-2-thiourea (*e.g.*, with trinitrobenzene), 1,3,5-tri-*t*-butylbenzene (*e.g.*, with tetracyanoethylene), and hexanitrodiphenyl (*e.g.*, with anthracene and pyrene) similarly give colorless solids but are not examined closely here.

Experimental Section

Most materials were commercial samples, further purified. They had analytical data in accord with literature values.

Matheson Coleman and Bell Spectroquality Reagent *n*-hexane and dichloromethane were left overnight in contact with freshly dried Molecular Sieve 4A, and were decanted, distilled, and stored prior to use in polythene sealed screw-capped bottles. Eastman Spectroquality Reagent cyclohexane was used without further purification.

Solution temperature studies were performed with the aid of a thermally insulated jacket containing the cuvette, into which could be poured a liquid of suitable boiling point around the sample. The windows were prevented from frosting by isolating the cell within the jacket and the whole was fitted within the sample compartment of a Cary 14 spectrometer. Temperatures of 35, 30, 0, and −30° were attained by using warm water, ice, and Freon 12. Equilibrium measurements were conducted on the less precise Perkin-Elmer 202 spectrometer at room temperature 27 ± 1°.

Equilibrium measurements were conducted according to a dilution equation, described previously,[16] and the points were weighted according to an assumption of a constant variance in absorbances. The first, highest density measurement was repeated at the end of the run and in some cases at later intervals to check the stability of the spectra. For the experimental conditions used, tetranitromethane runs with anthracene and pyrene had, thus, to be rejected, whereas similar runs with hexamethylbenzene and naphthalene were insufficiently stable for a prolonged solution temperature study. Preliminary examinations on the choice of solvents showed that the spectra of diphenylamine in carbon tetrachloride and particularly in chloroform were not sufficiently stable for the experiment, and colored solutions slowly developed.

For melting point diagrams, time–temperature warming curves rather than cooling curves were used, to avoid extrapolation across a supercooled region. Mixtures of 250–300 mg were melted in platinum crucibles in an all-steel container and preliminary cooling curves were recorded by thermocouples on a chart recorder. Heating was controlled by the temperature of the sample so that the environment was always at a predetermined, slightly higher temperature. A more detailed description of the apparatus will be given elsewhere.

X-Ray powder patterns were determined on a North American Philips Debye–Scherrer powder camera.

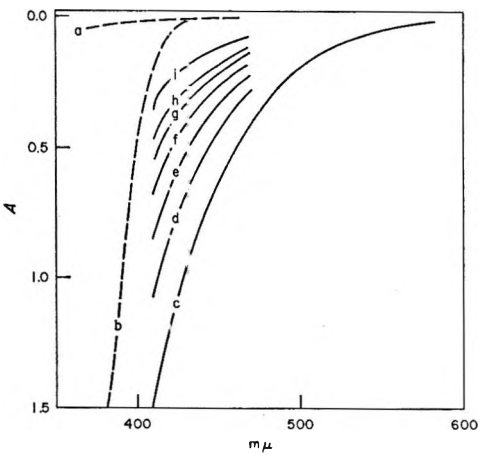

Figure 1. Spectra of the diphenylamine–*p*-chloronitrobenzene system in cyclohexane. Absorptions of 1.0-cm cells of a, 0.40 *M* diphenylamine; b, 0.04 *M* *p*-chloronitrobenzene; c, combined concentrations a plus b; and d–i, solution c at dilutions[17] 1.2, 1.4, 1.6, 1.8, 2.0, and 2.5.

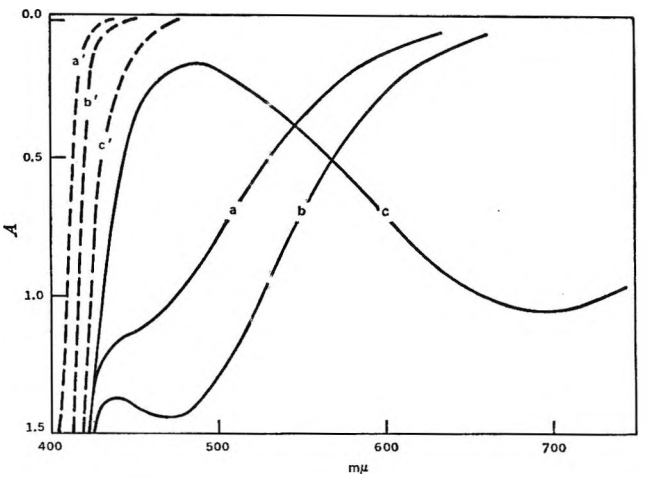

Figure 2. Spectra of triphenylamine–acceptor systems in dichloromethane. Absorptions of 1.0-cm cells of a, 0.13 *M* triphenylamine with 0.13 *M* *p*-dinitrobenzene; b, 0.023 *M* triphenylamine with 0.40 *M* trinitrobenzene; c, 0.417 *M* triphenylamine with 0.017 *M* *p*-chloranil; a, 0.13 *M* *p*-dinitrobenzene; b′, 0.40 *M* trinitrobenzene; and c′, 0.017 *M* *p*-chloranil.

Results

Spectral Studies. The diphenylamine–*p*-chloronitrobenzene interaction produced the spectra of Figure 1 and showed very weak associations in both dichloromethane and cyclohexane.[17] Other systems produced the spectra of Figures 2 and 3, or have been described

(16) P. R. Hammond, *J. Phys. Chem.*, **72**, 2272 (1968).

(17) The term "dilution" we employ here has the specific and self-explanatory meaning "the ratio of the volume of a diluted solution to its original volume"—see ref 16.

Table I: Equilibria, Positions of Absorption, and Color Changes of Some Acceptor–Donor Systems

Donor	Acceptor	Solvent	K, l. mol^{-1}	σ	Position of absorption measurement, mμ	Solution or melt color	Color of solid	Ref
Diphenylamine	*p*-Chloronitrobenzene	Cyclohexane	0.32	0.08	420	Orange	White	*a*
Diphenylamine	*p*-Chloronitrobenzene	Dichloromethane	0.15	0.05	430	Orange	White	*a*
Triphenylamine	*p*-Dinitrobenzene	Dichloromethane	0.20	0.03	450	Red	White	*a*
Triphenylamine	1,3,5-Trinitrobenzene	Dichloromethane	0.21	0.04	468 (max)	Red	Very pale pink	*a*
Triphenylamine	*p*-Chloranil	Dichloromethane	0.16	0.03	696 (max)	Blue-green	Pale cream	*a*
Tetramethyl-2-tetrazene	*p*-Dinitrobenzene	Dichloromethane	0.10	0.03	450,460,470	Orange	White	*b*
Tetrakis(dimethylamino)-ethylene	*p*-Nitroanisole	*n*-Hexane	−0.07	0.04	474 (max)	Red	White	*c*
Tetrakis(dimethylamino)-ethylene	Nitrobenzene	*n*-Hexane	0.01	0.02	493 (max)	Magenta	White	*c*
Tetrakis(dimethylamino)-ethylene	*p*-Chloronitrobenzene	*n*-Hexane	0.08	0.04	533 (max)	Violet	White	*c*
Tetrakis(dimethylamino)-ethylene	Acridine	*n*-Hexane	−0.02	0.04	462 (max)	Red	White	*c*
Tetrakis(dimethylamino)-ethylene	Hexafluorobenzene	Cyclohexane	−0.07	0.05	490	Orange-red	Very pale cream	*d*
Tetrakis(dimethylamino)-ethylene	Hexachlorobenzene	Cyclohexane	0.01	0.04	450	Red	White	*d*
Tetramethyl-2-thiourea	1,3,5-Trinitrobenzene	...	...	...	...	Orange	Very pale cream	*a*
p-Di-*t*-butylbenzene	Tetracyanoethylene	Dichloromethane	0.06	0.03	419 (max)	Orange-red	White	*a*
Tri-*t*-butylbenzene	Tetracyanoethylene	Dichloromethane	...	...	427 (max)	Orange-red	White	*a*
Tetraisopropylbenzene	Tetracyanoethylene	Dichloromethane	−0.21	0.09	496 (max)	Violet	White	*a*
Hexamethylbenzene	Tetranitromethane	Dichloromethane	0.12	0.04	430	Orange-red	White	*a*
Naphthalene	Tetranitromethane	Dichloromethane	0.13	0.06	450	Yellow-orange	White	*a*
Naphthalene	Tetranitromethane	Cyclohexane	−0.07	0.05	460,470,480	Yellow-orange	White	*b*
N,N-Dimethylaniline	Trinitromesitylene	Dichloromethane	0.14	0.04	430	Yellow-orange	White	*a*
Anthracene	Trinitromesitylene	Dichloromethane	...	...	430	Yellow	White	*a*
N,N-Dimethylaniline	1,3,5-Trinitrobenzene	Dichloromethane	0.75	0.08	481 (max)	Red	Magenta	*a*
Anthracene	1,3,5-Trinitrobenzene	Dichloromethane	2.61	0.12	450	Orange-red	Orange	*a*
Durene	Tetracyanoethylene	Dichloromethane	3.31	0.15	480 (max)	Magenta	Magenta	*a*

[a] This work. [b] Ref 16. [c] Ref 11. [d] Ref 18.

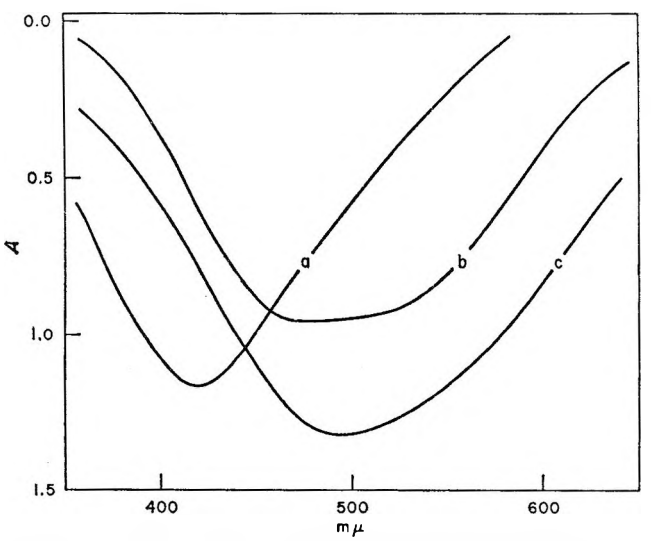

Figure 3. Spectra of tetracyanoethylene–hydrocarbon systems in dichloromethane. Absorptions of 1.0 cm cells of a, 0.02 *M* tetracyanoethylene with 1.00 *M* *p*-di-*t*-butylbenzene; b, 0.0027 *M* tetracyanoethylene with 0.054 *M* durene; and c, 0.025 *M* tetracyanoethylene with 1.00 *M* 2,3,5,6-tetra-*i*-propylbenzene.

previously.[11,16,18] All colors were produced immediately on mixing and were stable over the period of measurement. The absorbances decreased much more rapidly on dilution than would be expected if Beer's law were to apply. Thus, all colors are ascribed to charge-transfer transitions between the acceptor and donor components. Estimates of association constants, determined from weighted least-squares regression calculations, are displayed in Table I, together with standard errors, σ, which are typically ± 0.05 l. mol^{-1}. Molar absorptivities are quite unreliable from a two-parameter equilibrium equation when the interactions are weak, and are found here as large positive and negative values. Independent measurements of ϵ are required for such conditions.

Colors of the melts and of the solids are also set out in Table I. In all cases the changes were distinct, sufficiently so to make the subjective examination reliable. Thus the change from a deep violet liquid of tetracyanoethylene–tetraisopropylbenzene to a clean, white, crystalline solid could not have been mistaken. Moreover, microscope slides of the diphenylamine–*p*-chloronitrobenzene, trinitromesitylene–anthracene, triphenylamine–*p*-dinitrobenzene, and tetracyano-

(18) P. R. Hammond, *J. Chem. Soc., A*, 145 (1968).

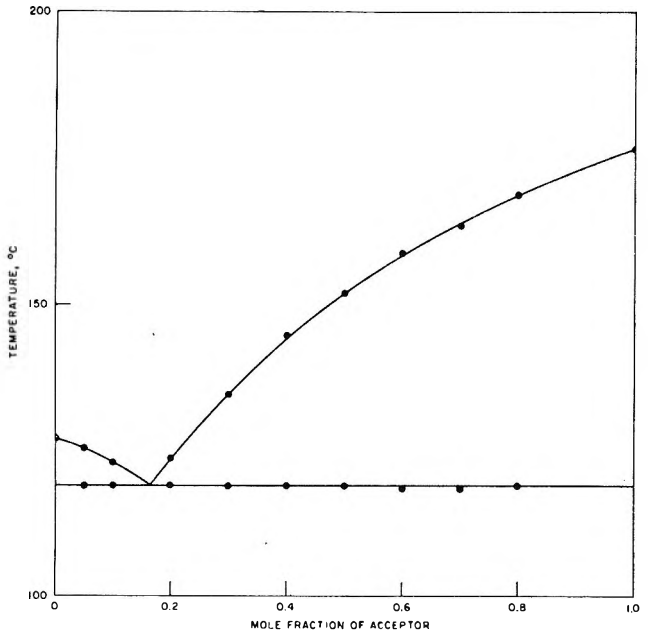

Figure 4. Melting point diagram for the triphenylamine–*p*-dinitrobenzene system.

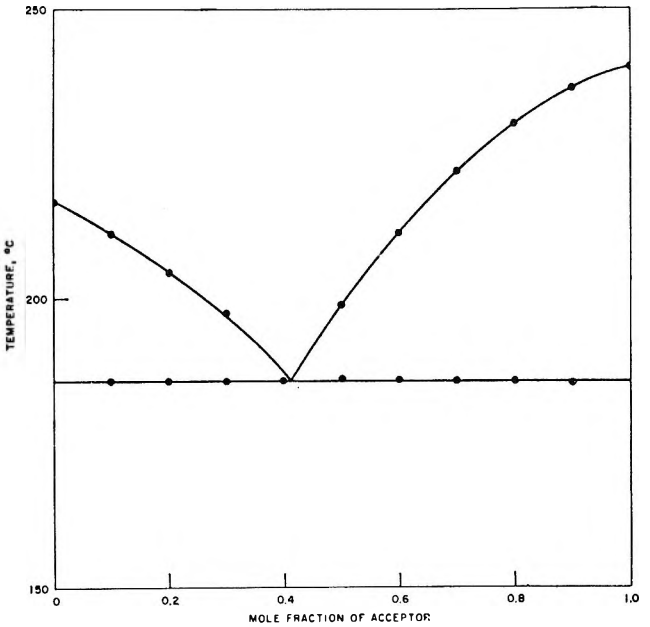

Figure 5. Melting point diagram for the anthracene–trinitromesitylene system.

ethylene–tetra-isopropylbenzene systems, although colored in the hot liquid state, were colorless by both transmitted and reflected light. The tetracyanoethylene–durene and trinitrobenzene–anthracene mixtures were magenta and orange under these conditions. Separate donor or acceptor crystals in the mixtures were not seen on microscope slides. The colors of the solids were the colors of the original components, although a very faint pink could be obtained on rapid freezing of the deep red trinitrobenzene–triphenylamine

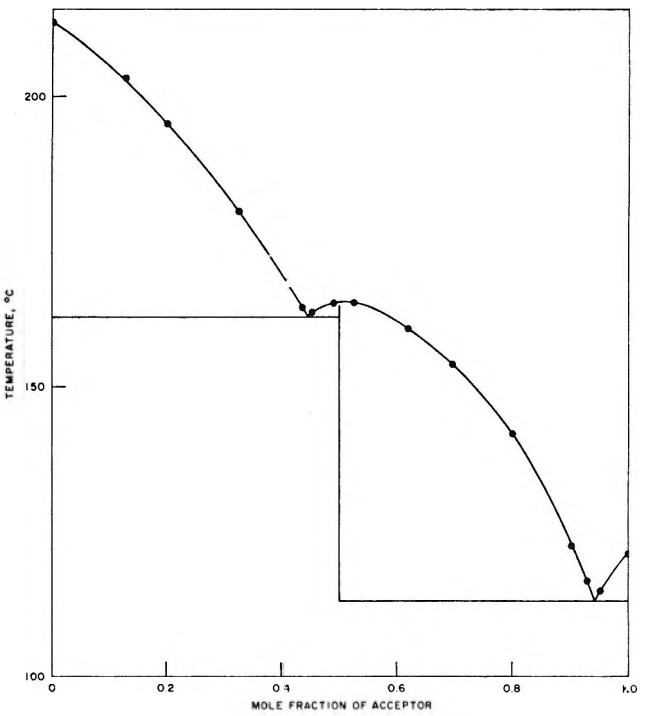

Figure 6. Melting point diagram for the anthracene–1,3,5-trinitrobenzene system.

liquid. Moreover, all changes occurred during the solidification. Results for systems known to form stable complexes are also shown in Table I.

Melting Point Diagrams, X-Ray Diffraction Studies, and Behavior in Glasses. The triphenylamine–*p*-dinitrobenzene and the anthracene–trinitromesitylene systems produced the eutectics of Figures 4 and 5. In most cases the liquidus and solidus curves were clearly defined, although for runs just on the acceptor side of the triphenylamine–*p*-dinitrobenzene eutectic, where very little of the dinitrobenzene was coming into the liquid phase, they were difficult to determine. In contrast, the trinitrobenzene–anthracene phase diagram taken in part from the data of Kreman and Muller[19] is shown in Figure 6.

X-Ray diffraction diagrams of the solidified mixtures diphenylamine–*p*-chloronitrobenzene, triphenylamine–*p*-dinitrobenzene, anthracene–trinitromesitylene, and 1,2,4,5 - tetra - iso - propylbenzene–tetracyanoethylene showed patterns that were superpositions of the components. On the other hand the anthracene–trinitrobenzene and durene–tetracyanoethylene showed changed patterns.

The color loss that occurred in the crystalline systems above was in marked contrast to the behavior in high-viscosity media. Clear glasses, of about the same hue and intensity as the solutions from which they were formed, were made by liquid nitrogen freezing of tetranitromethane–hexamethylbenzene in methylcyclohexane, tetrakis(dimethylamino)ethylene–nitrobenzene

(19) R. Kreman and R. Muller, *Monatsh. Chem.*, **42**, 181 (1921).

Table II: Temperature Effect on the Absorption of Some Donor–Acceptor Systems in Solution[a]

System	Stability	Temp, °C 1	2	3	Absorption type	Lower temperature absorption changes	Lower temperature intensity changes	$-\Delta H$, kcal mol^{-1}
Naphthalene–tetranitromethane	Slow change	30	0	−30	Edge of absorption band	Unstable, only small change with temp		...
Triphenylamine–1,3,5-trinitrobenzene	Small change, may be corrected	30	0	−30	Max., close to acceptor absorption	Max. shift, 465 to 475 mμ	Increase 28%	0.28
Tetraisopropylbenzene–tetracyanoethylene	Stable	35	15	0	Max., broad	No change	Increase 31%	0.95
Durene–tetracyanoethylene	Stable	30	0	−30	Max., broad	No change	Off-chart, 30–0° increase 126%	5.42
p-Di-*t*-butylbenzene–tetracyanoethylene	Stable	35	15	0	Max., sharp	No change	Increase 15%	0.30
Tri-*t*-butylbenzene–tetracyanoethylene	Stable	35	15	0	Max.	Max. shift, 439 to 427 mμ	Increase 3%	...
Tetrakis(dimethylamino)-ethylene–nitrobenzene	Stable	30	0	−30	Max., close to donor absorption	Max. shift, 490 to 500 mμ	Increase 28%	0.28
Tetrakis(dimethylamino)-ethylene–*p*-chloronitrobenzene	Stable	30	0	−30	Max., close to donor absorption	Max. shift, 521 to 536 mμ	Increase 25%	0.23
Tetrakis(dimethylamino)-ethylene–acridine	Stable	30	0	−30	Max., close to donor absorption	From shoulder 460 to max. 465 mμ	Increase 23%	0.18

[a] Allsystems were in dichloromethane with the exception of those containing tetrakis(dimethylamino)ethylene which were in *n*-hexane.

in ether–isopentane (1:1), *p*-di-*t*-butylbenzene–tetracyanoethylene in ether–isopentane, and tetramethyl-2-tetrazene–nitrobenzene in the butane diols. Rapid freezing of the orange nitrobenzene–tetramethyl-2-tetrazene in 2-butanol, a system which changed from a glassy to a crystalline state prior to melting, gave first an orange glass, became white and opaque on warming, and then changed to an orange liquid.

Effect of Temperature on Solution Spectra. Systems that appeared sufficiently stable for a prolonged temperature examination and which did not precipitate at the boiling point of Freon 12 were studied, and the results are displayed in Table II. For an example that showed evidence of complexing (tetracyanoethylene–durene), a decrease in temperature caused a marked increase in intensity. This is attributed mainly to a finite enthalpy of interaction. The other systems showed small increases, little more than predicted from contraction of the solvents. Thus a coefficient of thermal expansion of 0.00137 for both dichloromethane and *n*-hexane produces 8 and 10% intensity increases for temperature decreases from 30 and 35°, respectively, to 0°, on the assumption of an absorption decrease according to the inverse square of the dilution. The quoted enthalpy values were corrected for this.

Discussion

Further evidence that the observed spectra are charge-transfer transitions comes from their position. Thus absorptions of tetracyanoethylene with the sterically hindered alkylbenzenes resembled those with the corresponding methyl derivatives. Absorptions for the triphenylamine systems were displaced to lower energies with increasing strength of the acceptor, and appeared in the visible spectrum as would be predicted from the low ionization potential[20] of 6.86 eV. The weaker complexing properties of trinitromesitylene compared with trinitrobenzene are rationalized in terms of weaker acceptor properties for the molecule with respect to a methyl substituent effect and a reduced interaction of the nitro groups with the aromatic nucleus, caused by a twisting of these groups out of the aromatic plane, and possibly a methyl bulk effect that hinders slightly a close plane-to-plane molecular approach. Colors with triphenylamine systems were obtained in other solvents—carbon tetrachloride, chloroform, hexane, and cyclohexane. The green color reported[21] for triphenylamine with trinitrobenzene in chloroform could not be confirmed, but concentrated solutions of the base in Baker and Adamson Reagent grade chloroform became green over 10 min. The reported instability[21] for triphenylamine interactions is relevant here, although a sensitive electron spin resonance technique was required to show reactivity. Our studies showed that if there were chemical impurities, they were not apparent in the dichloromethane spectra over the period of measurement, about 0.5 hr. On the other hand, a small increase in intensity (2%) was observed for the triphenylamine–trinitrobenzene system after 12 hr at room temperature. The triphenylamine–*p*-dinitrobenzene melting point measurements could be repeated several times on one sample without a notice-

(20) F. I. Vilesov and V. M. Zaitsev, *Dokl. Phys. Chem.*, **154**, 117 (1964).

(21) D. N. Stamires and J. Turkevich, *J. Amer. Chem. Soc.*, **85**, 2557 (1963).

able change in properties, and all melts froze to colorless solids. Continuous variation measurements for the tetranitromethane–naphthalene and trinitrobenzene–triphenylamine mixtures imply that the spectra arise from 1:1 interactions and the other systems are probably in this category.

Solution Measurements. With regard to the small K measurements in Table I, and the question whether they show evidence of complexing, the following considerations are pertinent. Spectrophotometric studies of weak equilibria are hampered by a "conspiracy of errors" that serves to obscure the derived K and ϵ values.[22] Even systems exhibiting purely contact interaction may require association constants greater than zero, although small (about 0.2 l. mol^{-1}).[23] For a complex in solution, where competitive solvation of the donor, acceptor, and complex species occurs,[24a] or just for the displacement of solvent molecules from around the acceptor or donor during the formation of a complex,[24b] a customary equilibrium study may underestimate the true thermodynamic association constant, and even negative K values should be possible. The K estimates of Table I are typically in the region 0.1 l. mol^{-1}, and the relative errors in these are quite large. Even for a 100% error though, we may still characterize such an interaction as extremely weak. Larger values occur for the three complexing systems at the bottom of the table (although still small $\Delta F_c^\circ \simeq 0$), and perhaps for the diphenylamine–chloronitrobenzene in cyclohexane. We find no decidedly negative K values (with just the possible exception of the tetraisopropylbenzene–tetracyanoethylene system in dichloromethane), systems displaying weak interaction in one solvent are weak in others, although for solubility reasons the feebly polar dichloromethane was used in many cases. With the exception of the tetracyanoethylene–durene system, the absorptions changed very little for decreasing temperature. Where distortions of band shape occurred, for example in the neighborhood of the tetraaminoethylene absorption edge, the reported measurements in Table II are for a remote part of the charge-transfer band where such distortions are minimal. After correction for solvent expansion, and expressing the changes as enthalpies, very small ΔH values are found, typically in the region of -250 cal mol^{-1}. The tetraisopropylbenzene–tetracyanoethylene and certainly the complexing system durene–tetracyanoethylene are larger than this. The small ΔH may be interpreted as minute enthalpies of association, changes of band shape, or perhaps solvation changes.[25] The tri-*t*-butylbenzene–tetracyanoethylene interaction appears to be an extreme example within the "zero K" systems of this study. High concentrations are necessary to produce measurable absorptions, and, after correction for solvent contraction, this is the only system that shows a positive temperature coefficient, though small. The total oscillator strength increased with increasing temperature. Moreover an identical effect was observed for the solvent *s*-tetrachloroethane, together with a marked shift of the absorption (a change of color from orange to magenta)! This system may warrant further study.

Phase Diagrams. The condition essential for the loss of color is seen to be the separation of acceptor and donor molecules into two phases in the solid, a behavior typical of systems showing simple eutectic diagrams such as Figures 4 and 5. Diffraction patterns are those of the pure materials. The proportion of acceptor and donor molecules in contact, and hence capable of contributing to the absorption intensity, are the relatively few at crystal interfaces. As an example of a system producing a colored solid, anthracene–trinitrobenzene shows evidence of complexing in both solution and solid phases[19] (Figure 6), and its crystals are built of columns of alternating donor and acceptor molecules.[26] For the association of donor and acceptor in the solid, mutual attraction and packing must overcome the tendency of identical molecules to combine in the same crystal lattice. Where solution studies show these attractive forces are weak, freezing with color loss may occur.

Conclusions

Certainly, most of the solution measurements of Tables I and II show extremely weak interactions. Their description as "contact" appears most appropriate, and these are the systems that exhibit phase separation and color loss. It is reemphasized that color appearance in the liquid state does not necessarily indicate chemical binding.[12b] In contrast, chemically related species showing even feeble association produce complexes. However, not all of the systems should be classified as "contact," for example the enthalpy measurement on tetracyanoethylene–tetraisopropylbenzene. A further, noteworthy exception is Laskowski's demonstration[12b] of the lack of solid complexes for benzoquinone with hexamethylbenzene and anthracene, where solution measurements show weak association.[27,28]

(22) P. R. Hammond, *J. Chem. Soc.*, 479 (1964).

(23) (a) J. E. Prue, *ibid.*, 7534 (1965). (b) Steric limitation may also be important. Thus a naphthalene molecule alongside a compact acceptor such as tetranitromethane, where for favorable orientation the plane of the aromatic faces toward the center of the acceptor sphere, somewhat restricts the number of additional contacts simply because of lack of space—it is far removed from a close-packed equal sphere situation for example. For increasing donor concentration, as site saturation occurs for a contact system, the absorbance falls below a linear dependence on the donor, and a small, finite K may be measured.

(24) (a) S. Carter, J. N. Murrell, and E. J. Rosch, *J. Chem. Soc.*, 2048 (1965); (b) R. L. Scott and D. V. Fenby, *Ann. Rev. Phys. Chem.*, 20, 126 (1969).

(25) Another possible contribution to the change of absorption with temperature for a weakly interacting system, namely the free volume or coordination change in the solvent, is discussed in the following article.

(26) D. S. Brown, S. C. Wallwork, and A. Wilson, *Acta Crystallogr.*, 17, 168 (1964).

(27) P. R. Hammond, *J. Chem. Soc.*, 471 (1964).

Important exceptions to the thermochromic behavior occur for systems tending to produce glasses or solid solutions. The persistence of color in a glass is ascribed to the random structure of the medium leaving acceptor and donor molecules in contact, and should be sensitive to factors impeding crystallization, such as the rapidity of freezing or a molecular geometry which does not lend itself to packing easily into a lattice structure. A limited solubility would account for the faint color of the triphenylamine–trinitrobenzene solid.

That the transitions associated with donor–acceptor pairs are truly intermolecular is now beyond dispute. Evidence for this includes the polarization in crystals of molecular complexes,[29] the dependence of the absorption position on the medium for ion–ion, ion–neutral, neutral–neutral systems,[30] the dependence on I_d of the donor and E_a of the acceptor, and the highly ionic character of the excited state for neutral–neutral pairs.[31] The phenomena described here provide further proof. Moreover, they afford a convincing demonstration of the concept of "contact" interaction.

Acknowledgment. We thank Dr. H. F. Cordes for some suggestions and Mr. C. D. Stanifer for assistance.

Appendix. Tetranitromethane–Aromatic Hydrocarbon Interactions

There appears to be no certain evidence, from spectral measurements in the literature, for tetranitromethane–unsaturated hydrocarbon complexes. The more usual counter view, which may have its early origin in the reasoning that such colored systems must be associated, is favored even when the data suggest the contrary. Estimates were made[32] of the relative equilibrium constants for the tetranitromethane–aromatic hydrocarbon interactions on the assumption that extinction coefficients throughout the series were the same, and such relative values were tabulated in a review[33] and numerous texts.[9c,d,34] The conclusions of these studies may be criticized on two counts. The optical density measurements were all performed at 430 mμ and no account was taken of a displacement of absorption for the different donors. Moreover, even if similar positions of absorption had been compared (for example, maxima), the interactions were weak and the transitions were close to the local donor and acceptor transitions, where the effect most likely is to produce large and varying extinction coefficients. Estimates of relative equilibrium constants made as above are, therefore, unreliable although the papers characterize all the tetranitromethane interactions as having very small K values in the region of 0.07 l. mol^{-1}, the value obtained for the mesitylene system. Secondly, such small equilibrium constants, for carbon tetrachloride solutions[35a] as above, for n-heptane solutions[35b] and for the measurements of this article, cannot be considered as evidence for complexing (see ref 22 and 23). The small ΔH estimates in the Hammick papers suggest weak association, although the measurements are on the edges of absorption bands and may be subject to considerable ϵ changes with temperature; moreover solvent expansion is not considered. It appears certain that the nitro groups rather than the saturated carbon atoms receive the electron in the charge-transfer process, and these are able to contact the π system of the donor without hindrance. Thus the attraction is weak even though there should be no restriction to resonance or polarization mechanisms of bonding. Molecular shape (ball–plane) rather than bulk must determine the weakness of the tetranitromethane–aromatic hydrocarbon interactions.

(28) M. Chowdhury, *Trans. Faraday Soc.*, **57**, 1482 (1961).

(29) K. Nakamoto, *J. Amer. Chem. Soc.*, **74**, 1739 (1952); B. G. Anex and L. J. Parkhurst, *ibid.*, **85**, 3301 (1963); R. M. Hochstrasser, S. K. Lower, and C. Reid, *J. Mol. Spectrosc.*, **15**, 257 (1965); H. Kuroda, T. Kunii, S. Hiroma, and H. Akamatu, *ibid.*, **22**, 60 (1967).

(30) S. F. Mason, *Quart. Rev.* (London), **15**, 354 (1961); E. M. Kosower, *J. Amer. Chem. Soc.*, **80**, 3253, 3261, 3267 (1958).

(31) J. Czekalla and K. O. Meyer, *Z. Phys. Chem.* (Frankfurt am Main), **27**, 185 (1961).

(32) D. Ll. Hammick and R. P. Young, *J. Chem. Soc.*, 1463 (1938); D. Ll. Hammick and R. B. M. Yule, *ibid.*, 1539 (1940).

(33) L. J. Andrews, *Chem. Rev.*, **54**, 713 (1954).

(34) C. N. R. Rao in "The Chemistry of the Nitro and Nitroso Groups," Part I, S. Patai, Ed., Interscience Publishers, New York, N. Y., 1969, p 119.

(35) (a) R. W. Maatman and M. T. Rogers, *Am. Chem. Soc., Div. Petroleum Chem., General Papers*, **33**, 5 (1955); (b) V. A. Gorodyskii and V. V. Perekalin, *Dokl. Phys. Chem.*, **173**, 179 (1967).

Electron Acceptor–Electron Donor Interactions. XVI. Charge-Transfer Spectra for Solutions of Tungsten and Molybdenum Hexafluorides and Iodine Heptafluoride in *n*-Hexane and Cyclohexane. Donor Properties of the Aliphatic Hydrocarbons[1,2]

by P. R. Hammond

Chemistry Division, Code 6056, Michelson Laboratories, Naval Weapons Center, China Lake, California 93555
(Received May 12, 1969)

In an earlier article, demonstration of intermolecular charge-transfer spectra with reactive, high electron affinity compounds had to be conducted with perfluoro- rather than perhydroaromatics.[3] Cyclohexane and *n*-hexane whose ionization potentials are close to that of hexafluorobenzene also show such spectra, even though the electron of the transition must come from a σ rather than a π orbital; for example, solutions of molybdenum hexafluoride in *n*-hexane and cyclohexane are yellow and orange, respectively. Iodine heptafluoride systems are unstable, although the transient yellow of solutions in hexane or cyclohexane may be compared with orange solutions in the perfluorobenzenes. Even carbon tetrachloride and perfluoromethylcyclohexane solutions differ, with the cut-off for the former occurring at lower energies, and this is attributed to a CCl_4 donor–WF_6 or MoF_6 acceptor transition. Equilibrium and enthalpy measurements indicate that if there are attractive forces for these systems in excess of normal dispersion forces they are very weak.

Materials of exceptional reactivity, for example very strongly protonating media, are able to overcome the familiar inertness of the aliphatic hydrocarbons. For such conditions chemical exchange is pronounced to the extent that rejection of the name "paraffin" has been proposed.[4] A well recognized, frequently vigorous reaction of the hydrocarbons is their activity toward powerful oxidizing systems, for example the halogen fluorides. Here we report that such molecules on contact can exhibit intermolecular charge-transfer transitions, where the hydrocarbon functions as an electron donor.

A recent examination[3] found that many of the highest valency halides, oxyhalides, and oxides of the elements exhibit intermolecular transitions with aromatic hydrocarbons and fluorocarbons. The lowest energy of appearance of the bands, and by implication[5] the highest molecular electron affinity species of the compounds chosen for study, were for tungsten and molybdenum hexafluorides, iodine heptafluoride, and iodine oxide pentafluoride. For these, demonstration of charge-transfer spectra had to be conducted with the aromatic perfluorocarbons in most cases, rather than with the more reactive perhydro derivatives. Figure 1 shows spectra used in the dilution studies of the yellow and orange solutions of tungsten and molybdenum hexafluorides with hexafluorobenzene. Iodine heptafluoride and iodine oxide pentafluoride similarly produce colored solutions with the perfluoromethylbenzenes, orange and yellow, respectively, with hexafluorobenzene, although the systems are chemically less stable.

The energy $h\nu_{CT}$ of the maximum of a charge-transfer transition has been related[5] to the donor ionization potential I_d and the acceptor electron affinity E_a by the proposed relation

$$h\nu_{CT} = I_d - E_a - G_1 - G_0 + X_1 - X_0 \qquad (1)$$

G_1 and G_0 are the interaction energies between donor and acceptor in the dative state and in the ground state, and $X_1 - X_0$ is the resonance energy of interaction between the two states. For consideration of a series of related compounds, eq 1 has been simplified to

$$h\nu_{CT} = I_d - E_a + \text{constant} \qquad (2)$$

Even for materials of quite different electronic structures, however, eq 2 appears to be a useful qualitative guide. For example, the ionization potentials of hexafluorobenzene[6] (9.97–9.88 eV), cyclohexane[7] (9.88

(1) Presented at the 157th National Meeting of the American Chemical Society, Inorganic Division, Minneapolis, Minn., April 1969.

(2) This article is also considered as Part VI of a series "Studies on High Electron Affinity Molecules." Earlier papers in this series are (a) *J. Chem. Soc.*, 3113 (1963); (b) *Science*, **142**, 502 (1963), (c) *Nature*, **206**, 891 (1965), (d) *J. Chem. Soc.*, A145 (1968), (e) *Tetrahedron*, **25**, 2549 (1969).

(3) P. R. Hammond and R. R. Lake, *Chem. Commun.*, 987 (1968).

(4) G. A. Olah and R. H. Schlosberg, *J. Amer. Chem. Soc.*, **90**, 2726 (1968).

(5) R. S. Mulliken and W. B. Person, *Ann. Rev. Phys. Chem.*, **13**, 107 (1962).

(6) R. Bralsford, P. V. Harris, and W. C. Price, *Proc. Roy. Soc.*, **258A**, 459 (1960); I. D. Clark and D. C. Frost, *J. Amer. Chem. Soc.*, **89**, 244 (1967).

(7) K. Watanabe, T. Nakayama, and J. Mottl, *J. Quant. Spectrosc. Radiat. Transfer*, **2**, 369 (1962).

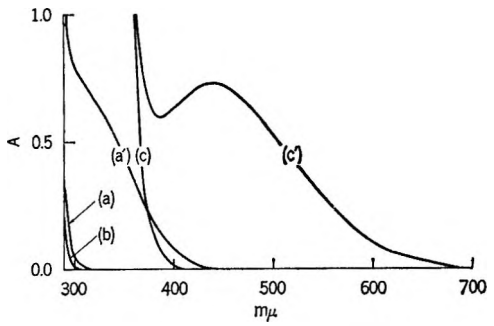

Figure 1. Spectra of hexafluorobenzene–WF_6 or –MoF_6 systems in carbon tetrachloride. Absorptions of 2.0-cm cells. a, WF_6, 0.125 *M*; a', WF_6 0.125 *M* plus hexafluorobenzene 0.125 *M*; b, hexafluorobenzene, 0.125 *M*; c, MoF_6 0.02 *M*; and c', MoF_6 0.02 *M*, hexafluorobenzene, 0.50 *M*.

eV), and *n*-hexane (10.18 eV) are close although the first is probably[6,8] a π-electron ionization whereas the electron can come only from the σ framework for the others. New absorptions appear in the hydrocarbon solutions of the above acceptors at positions comparable to those with hexafluorobenzene.

Studies of tungsten hexafluoride interactions in cyclohexane solvent showed an absorption cut-off for all systems, apart from the π-donor–acceptor charge-transfer transition, which was not present in carbon tetrachloride. Indeed, concentrated solutions of the hexafluoride show an immediate, stable, very pale yellow color, even though the two liquids are colorless. Similarly, the solvents *n*-hexane and cyclohexane give immediate yellow colors with iodine heptafluoride, and yellow and orange solutions respectively with molybdenum hexafluoride, in the latter cases fairly stable.

Earlier, related studies showed that the acceptors iodine,[9,10] bromine,[11] oxygen,[12] and tetranitromethane[10] gave stable absorptions in aliphatic hydrocarbons and cyclohexane, altered slightly from their spectra in the gas phase or solution in the solvents perfluoroheptane or chloroform. Solvent shifts of the acceptor absorptions were ruled out on the basis of the small concentrations required to produce changes, and because of similarity of the gas and solution spectra despite differences in media refractive indices. The absorptions were ascribed to charge-transfer transitions and in most cases close-to-zero equilibrium constants or contact interactions were found. The perfluoride acceptors of this study are more transparent in the visible and ultraviolet regions and show much more dramatic effects.

Properties of a donor–acceptor combination that are responsible for the appearance of a charge-transfer transition also appear to be responsible, in a general sense, for its chemical reactivity.[13] As part of our continuing interest in this area, the hydrocarbon interactions are characterized with respect to stability, stoichiometry, equilibria, and temperature effects in the solvents carbon tetrachloride and perfluoromethylcyclohexane.

Experimental Section

Carbon tetrachloride, *n*-hexane, and cyclohexane were Matheson Coleman, and Bell Spectroquality grade. The carbon tetrachloride was left overnight with freshly dried Molecular Sieve 4A, decanted, fractionally distilled, and stored over the sieve, from which any fine powder had been carefully removed. Dry nitrogen was bubbled rapidly for several minutes through smaller samples for use in the drybox, where they were similarly stored over the granular sieve. Hexane and cyclohexane (100 ml) were hydrogenated overnight at 60 psi in the presence of 1 g of platinum oxide. Such excessive purification was later shown to be unwarranted, however. The samples were degassed and stored as for the carbon tetrachloride. Gas chromatography of the hexane and cyclohexane at 50° over a Silicone SE 52 column indicated impurities were less than 2×10^{-3} *M*. Onset of absorption for 1-cm lengths compared with an air reference in the Cary 14 spectrophotometer occurred at 240 and 230 mμ for cyclohexane and hexane, respectively.

A perfluoromethylcyclohexane sample as obtained directly from the Pierce Chemical Company showed no hydrogen content in a proton magnetic resonance spectrum compared with tetramethylsilane internal standard down to 1%, and showed no absorption for a 1-cm sample compared with a nitrogen gas reference up to 190 mμ; also solutions containing antimony pentafluoride did not darken—a behavior contrasting with most perfluoroalkane sources. Chromatography at 60° over fluorosilicone oil or over a charcoal column of steadily increasing temperature showed a more volatile impurity at about 0.3%. The solvent was degassed, stored over the sieve in the drybox, and used without further purification. The fluorides were readily soluble, and concentrations beyond 0.2 *M* were readily attainable for the hydrocarbons and carbon tetrachloride under the temperature conditions of the experiment. Enthalpy studies required density determinations of this solvent, and the hydrometer measurements show a linear variation over the temperature range, where the densities were 1.739, 1.788, 1.827, 1.858, and 1.908 at 44.9, 27.5, 11.6, 0.0, and −19.5°, respectively.

Tungsten hexafluoride (high purity) and iodine heptafluoride, both from Alfa Inorganics, Inc., and

(8) M. J. S. Dewar and J. Kelemen, *Tetrahedron Lett.*, 2341, 3888 (1967).

(9) S. H. Hastings, J. L. Franklin, J. C. Schiller, and F. A. Matsen, *J. Amer. Chem. Soc.*, 75, 2900 (1953); D. F. Evans, *J. Chem. Phys.*, 23, 1424 (1955); L. M. Julien and W. B. Person, *J. Phys. Chem.*, 72, 3059 (1968); S. N. Bhat, K. R. Bhaskar, and C. N. R. Rao, *Proc. Indian Acad. Sci.*, 66A, 97 (1967).

(10) D. F. Evans, *J. Chem. Soc.*, 4229 (1957).

(11) D. F. Evans, *J. Chem. Phys.*, 23, 1426 (1955).

(12) D. F. Evans, *J. Chem. Soc.*, 345 (1953); A. U. Munck and J. F. Scott, *Nature*, 177, 587 (1956).

(13) R. S. Mulliken, *J. Phys. Chem.*, 56, 801 (1952).

molybdenum hexafluoride, sold as 99% purity from Research Inorganic Chemical Corporation, were used directly. A sample of iodine oxide pentafluoride, free from the heptafluoride, was made available by the courtesy of Dr. D. Pilipovich of Rocketdyne, Canoga Park, Calif. Tungsten and molybdenum hexafluorides were handled in both carbon tetrachloride and perfluoromethylcyclohexane solutions, whereas the iodine fluorides were handled only in the latter. Tungsten hexafluoride in the fluorocarbon solvent was stable indefinitely in borosilicate flasks, stored and manipulated in the drybox. Such molybdenum hexafluoride solutions could be handled over a 2–3 day period; longer than this, a blue precipitate slowly developed on the walls of the flask. The hexafluorides in carbon tetrachloride were less stable, the tungsten starting to darken slightly over a week, whereas the molybdenum began to develop a blue precipitate within a day. For spectral measurements, all solutions were freshly prepared, and certainly showed no absorption changes over the period of study. The iodine fluorides could be handled as colorless solutions in perfluoromethylcyclohexane using borosilicate or silica apparatus in the drybox. For example, tests of these by the addition of perfluorobenzenes produced transiently colored liquids up to several hours. On the other hand, turbidity developed quite rapidly (over 10–15 min) and etching of the glass was apparent. Etching of the silica cuvettes was found for the iodine fluorides, to only a minor extent for molybdenum hexafluoride, and not at all for tungsten hexafluoride. An etched cell appeared to be more sensitive to further corrosion than a fresh one, and for quantitative study only the latter were used. In one example where the silica parts of a cuvette were sealed by a lower-melting borosilicate glass, iodine heptafluoride solutions preferentially attacked and disrupted the borosilicate. An improvement in technique would have been the addition of traces of sodium fluoride to the molybdenum and iodine fluoride solutions. All experiments with the iodine fluorides and the initial tests of the metal hexafluorides in hydrocarbons were conducted behind safety screens, although no violent reactions were found.

Solutions were prepared in an all borosilicate glass apparatus containing Teflon stopcocks and connector seals. A known volume of the solvent was added in the drybox; the fluoride cylinder was connected by means of Teflon tubing that had been thoroughly flushed with dry nitrogen, and the exit was capped with a drying tube. Vapor from the cylinder (which was gently warmed in the case of molybdenum hexafluoride) was collected in the chilled solvent and the concentration was estimated by gain in weight. Solutions, typically 0.1 M, were then handled by conventional pipet techniques. The drybox was constructed of Plexiglass and had neoprene gloves. Dry nitrogen, introduced *via* a long tube of Molecular Sieve 4A pellets, was circulated over trays of concentrated sulfuric acid, sodium hydroxide, and Drierite pellets. During the brief periods when solutions were open to the atmosphere of the box, any traces of escaping fluoride vapor were absorbed by the hydroxide. The hexafluorides were very soluble in the solvents chosen and their volatility was insufficient to cause detectable variations in the low concentrations suitable for measurement. Linear plots could be obtained in the dilution experiments, and maxima clearly indicating 1:1 interactions were found in continuous variation studies. For temperature measurements, the cuvette (capacity ~18 ml) was filled to within 2 ml and was firmly stoppered, so keeping to a minimum the quantity of tungsten hexafluoride escaping from solution into the empty space. Nevertheless, some exchange of vapor must occur for the temperature range employed, 40 to −30°, hence the extremely small enthalpy reported is likely to be an overestimate.

For equilibria and continuous variation studies a dilution cell[14] was used. With these techniques, very few solutions had turbidities in clear regions of the spectra as great as 0.01 absorbance unit, and any over 0.02 were rejected. A careful check (and correction if necessary) for turbidity was made for each measurement within a dilution run; moreover the A^4 weighting of points employed was aimed to minimize the effect of such an error.

Results

The absorption spectra, taken for 1.00, 0.10, and 0.01 cm path length cells, of tungsten and molybdenum hexafluoride solutions in (a) perfluoromethylcyclohexane, (b) carbon tetrachloride, (c) *n*-hexane, and (d) cyclohexane are shown in Figures 2 and 3 (corrected for solvent absorption where necessary). All, where sufficiently stable for examination, obeyed Beer's law. Tungsten hexafluoride spectra were unaltered the following day. Molybdenum hexafluoride spectra in the perfluorocarbon and carbon tetrachloride solvents were stable, although both of the hydrocarbon systems, particularly the cyclohexane, showed changes within 0.5 hr, and increases of the base line were attributed to turbidity. Significant in both of these figures is the displacement of the absorption edge in the order cyclohexane > *n*-hexane > carbon tetrachloride > perfluoromethylcyclohexane, the probable order of increasing ionization potential. Even for the 11.47-eV carbon tetrachloride species, marked shifts from the fluorocarbon are seen. Gas phase absorptions[15] for the hexafluorides are close to and cross curve a in each case, although they rise more steeply.

Figure 4 shows plots according to the method of continuous variations for the tungsten hexafluoride–

(14) P. R. Hammond, *J. Phys. Chem.*, **72**, 2272 (1968).

(15) K. N. Tanner and A. B F. Duncan, *J. Amer. Chem. Soc.*, **73**, 1164 (1951).

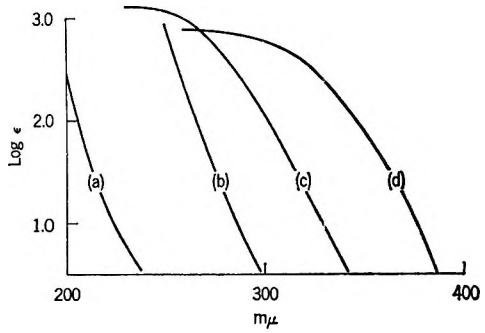

Figure 2. Molar absorptivities of tungsten hexafluoride solutions: a, perfluoromethylcyclohexane, 0.021 *M*; b, carbon tetrachloride, 0.020 *M*; c, *n*-hexane, 0.038 *M*; and d, cyclohexane, 0.069 *M*.

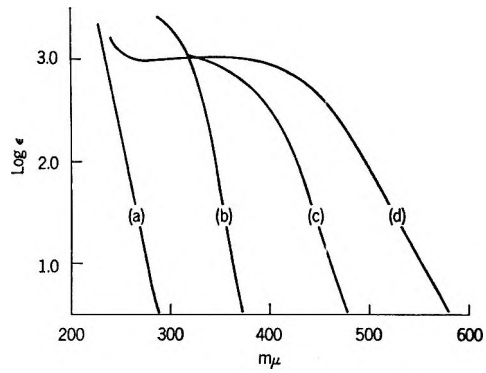

Figure 3. Molar absorptivities of molybdenum hexafluoride solutions: a, perfluoromethylcyclohexane, 0.064 *M*; b, carbon tetrachloride, 0.062 *M*; c, *n*-hexane, 0.139 *M*; and d, cyclohexane, 0.086 *M*.

n-hexane or -cyclohexane systems in perfluoromethylcyclohexane or carbon tetrachloride, and the molybdenum hexafluoride–*n*-hexane system in the fluorocarbon. Thus the species producing the absorptions (assumed monomeric), and by implication the remaining interactions of this article, are of 1:1 character. Representative spectra of tungsten hexafluoride combinations suitable for dilution studies are shown in Figure 5, in particular the cyclohexane system producing a clear absorption shoulder (curve d) was selected for further examination with respect to the effect of temperature. The shoulder was not seen when carbon tetrachloride was used as a solvent. For these concentrations the spectrum resulting from the carbon tetrachloride interaction in C_7F_{13} was readily distinguishable for molybdenum hexafluoride (Figure 6), but was displaced very little from the intrinsic chloride absorption for tungsten hexafluoride. The least stable chemically of the systems measured was MoF_6–*n*-hexane in C_7F_{17} where a 1% decrease in absorbance at 300 mμ over 1 hr and no change in base line were observed.

All absorbances decreased fairly closely by the inverse square of dilution and Table I lists the results of equilibria studies according to

$$\frac{1}{nA} = \frac{n}{K\epsilon' ad} + \frac{1}{\epsilon' a} + \frac{1}{\epsilon' d}$$

where n is the dilution of the solution (the ratio of the volume of a diluted solution to its original volume), A is the absorbancy (here measured for 2-cm cells), ϵ' and K are the molar absorptivity at the wavelength of measurement and association constant, respectively, and a and d are the acceptor and donor concentrations originally put into solution (n and $1/n$ A are the independent and dependent variables). K and ϵ' values were estimated by a weighted least-squares procedure based on the assumption that the variance in the absorbance was independent of magnitude. The weights of the points were thus in the ratio A^4. The table includes the number of points per run for each K and ϵ' pair evaluated and the weighted standard deviation of the ordinate residuals.

The clear absorption shoulder for the tungsten hexafluoride–cyclohexane system in perfluoromethylcyclohexane (curve d of Figure 5) permitted examination of both the distortion of band shape and overall gain in intensity for decreasing temperature. A change from

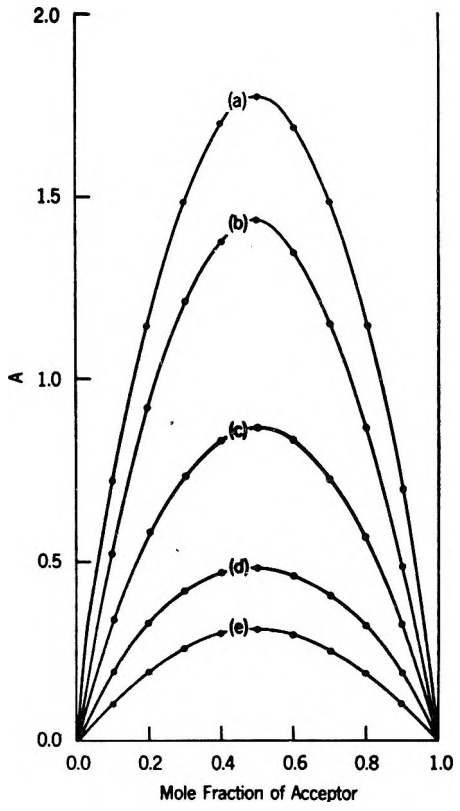

Figure 4. Continuous variation plots, 2.0-cm cells, for tungsten hexafluoride solutions a, b, c, and d, A + D = 0.2 *M*, with a, cyclohexane in perfluoromethylcyclohexane at 250 mμ; b, *n*-hexane in perfluoromethylcyclohexane at 260 mμ; c, cyclohexane in carbon tetrachloride at 300 mμ; d, *n*-hexane in carbon tetrachloride at 300 mμ; and e, molybdenum hexafluoride with *n*-hexane in perfluoromethylcyclohexane, A + D = 0.1 *M*, at 350 mμ.

Table I: Dilution Plots and Equilibria for Some Tungsten and Molybdenum Hexafluoride Systems at 26°

Donor	Acceptor	Solvent	mμ	a	d	Points per run	10^3SD	K, l. mol^{-1}	ϵ'
n-Hexane	WF_6	C_7F_{13}	250	0.10	0.10	8	3	0.57	174
n-Hexane	WF_6	C_7F_{13}	260	0.10	0.10	8	4	0.67	120
n-Hexane	WF_6	C_7F_{13}	270	0.10	0.10	8	8	0.58	100
Cyclohexane	WF_6	C_7F_{13}	250	0.10	0.10	8	1	0.32	282
Cyclohexane	WF_6	C_7F_{13}	260	0.10	0.10	8	3	0.37	230
Cyclohexane	WF_6	C_7F_{13}	270	0.10	0.10	8	1	0.31	234
Cyclohexane	WF_6	C_7F_{13}	280	0.10	0.10	8	2	0.36	178
Carbon tetrachloride	WF_6	C_7F_{13}	250	0.10	0.10	4	28	0.16	298
Carbon tetrachloride	WF_6	C_7F_{13}	255	0.10	0.10	4	31	0.20	218
n-Hexane	WF_6	CCl_4	300	0.10	0.10	4	10	0.19	250
n-Hexane	WF_6	CCl_4	310	0.10	0.10	4	42	0.16	190
Cyclohexane	WF_6	CCl_4	300	0.10	0.10	6	5	0.47	118
Cyclohexane	WF_6	CCl_4	310	0.10	0.10	6	11	0.41	102
Cyclohexane	WF_6	CCl_4	320	0.10	0.10	6	5	0.36	84
n-Hexane	MoF_6	C_7F_{13}	320	0.05	0.10	8	9	0.58	194
n-Hexane	MoF_6	C_7F_{13}	330	0.05	0.10	8	9	0.54	186
n-Hexane	MoF_6	C_7F_{13}	340	0.05	0.10	8	13	0.50	176
Carbon tetrachloride	MoF_6	C_7F_{13}	300	0.05	0.10	6	3	0.22	348
Carbon tetrachloride	MoF_6	C_7F_{13}	310	0.05	0.10	6	16	0.21	302

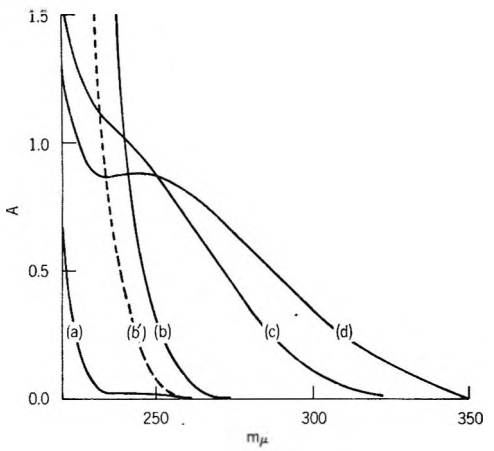

Figure 5. Representative spectra in the dilution study of tungsten hexafluoride systems in perfluoromethylcyclohexane, all species concentrations 0.071 *M*: a, WF_6; b, WF_6 plus CCl_4; b′, CCl_4; c, WF_6 plus *n*-hexane; and d, WF_6 plus cyclohexane.

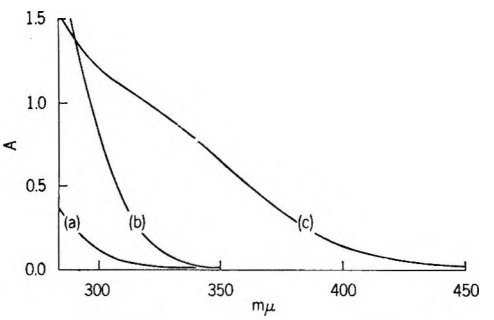

Figure 6. Representative spectra in the dilution study of molybdenum hexafluoride systems in perfluoromethylcyclohexane: a, MoF_6, 0.05 *M*; b, MoF_6 0.05 *M* plus CCl_4 0.10 *M*; and c, MoF_6 0.05 *M* plus *n*-hexane 0.10 *M*.

44° (warm water) to −30° (Freon 12) produced an essentially uniform, reversible increase of absorption of 40% and no distortion. From the contraction of the solvent alone, however, for this temperature range an increase of 24% is expected based on an inverse square of dilution absorbancy relation. An estimate of ΔH from standard formulas[2d] was made by reducing all absorbances and concentrations to lower temperatures and by employing the 250-mμ ϵ' value for this system of Table I. The figure obtained, −252 cal/mol^{-1}, was little affected by changes in ϵ', for example a doubling of ϵ' produced only a 4% decrease in magnitude of ΔH.

Iodine heptafluoride bubbled into *n*-hexane or cyclohexane at room temperature immediately produced bright yellow solutions. The colors faded within 10 sec for cyclohexane and 30 sec for hexane, became cloudy, effervesced slightly, and within minutes produced iodine (at least as a minor product), as seen by the color and by its disappearance on shaking with aqueous sodium thiosulfate. The yellow colors were more stable at lower temperatures; for example, the hexane system persisted for 10 min at −30°. Iodine oxide pentafluoride produced no color change with cyclohexane. Instead the solution became cloudy, effervesced slightly, and within 10 min produced an iodine color. The material exhibits an electron-transfer spectrum in hexafluorobenzene, which for concentrated solutions appears yellow. The behavior in this case resembles tungsten hexafluoride. The absence of color with cyclohexane is not unexpected although transitions in the ultraviolet should be apparent. Because of the instability, difficulty of handling, and a limited supply of the fluoride, further studies were not made.

The effect of freezing molybdenum hexafluoride in *n*-hexane and cyclohexane, and iodine heptafluoride in

hexane, was considerable, but never complete, color-loss. Freon 12, where feasible, or liquid nitrogen was the coolant. Each system was tested a number of times with respect to freezing rates, degrees of immersion, agitation, and duplication of results. Of two possible explanations for the color retention, namely molecular compound formation of the acceptors with the hydrocarbons or partial-glass formation, the second is preferred. Rapid freezing of the MoF_6–hexane system, for example, produced a clear, colored glassy solid.

In accordance with the reported marked difference in solubility parameters between the perfluoromethylcyclohexane and other systems,[16] the activity coefficients for dilute solutions, defined according to deviations from Raoult's law, should be high. The dilution technique showed closely linear, small K plots in all cases, however, in accordance with little change in the activity coefficient product over the concentration range.

Discussion

New, in most cases stable, absorptions, not present in either component separately, appear immediately after the solutions are prepared. On dilution they do not obey Beer's law; indeed many decrease closely by the inverse square of dilution. The changes are striking, often resulting in colored mixtures, and are produced by quite low concentrations, too low to commend solvent shift of the component absorptions as an explanation. The displacements in cyclohexane, *n*-hexane, carbon tetrachloride, and perfluoromethylcyclohexane are in the probable order of increasing ionization potentials and are not related to changing molecular polarizability for example. The small perturbation for the CCl_4 spectrum in perfluoroalkane caused by WF_6 (Figure 5b) is markedly enhanced in the presence of MoF_6—a stronger acceptor (Figure 6b). On the other hand, intensity borrowing effects, in this case from the strong, neighboring CCl_4 absorption, should be much more important than for the hydrocarbon interactions. The absorptions are therefore ascribed to intermolecular charge-transfer transitions with the fluorides acting as acceptors. For a particular hydrocarbon donor the order of appearance of the transitions parallels the order of appearance with perfluoroaromatic donors, implying, according to eq 2, a sequence of molecular electron affinities iodine heptafluoride $\sim$ molybdenum hexafluoride > tungsten hexafluoride.

It is of interest to consider whether the measurements of this article provide evidence of acceptor–donor association in excess of that corresponding to random collisions. Anticipating the following discussion it is proposed that no definite statement can be made concerning solely contact interaction or of attractive forces in the ground state in excess of normal dispersion forces. Rather, the results suggest that attraction, if there is any, is certainly very weak. Measurements having lowest standard deviations from linear plots, namely the tungsten hexafluoride–cyclohexane interaction in perfluoromethylcyclohexane, show in Table I small K values, typically 0.3 l. mol^{-1}, and some scatter of ϵ' for the different wavelengths of measurement. Recalculation of these taking into account the quite accurate, relative ϵ' values available from the spectra, *e.g.*, Figures 5 and 6, afford consistent K measurements within each run. Nevertheless, scatter of points causes a minor effect on the gradient of the plot[17] (and hence $K\epsilon'$) but a major effect on a small intercept, and the magnitude of K and ϵ' could be in error. Criticisms that such small K values may not represent complexing are as follows. For weak associations a "conspiracy" of experimental errors obscures the derived K and ϵ' values, so that little reliance can be placed upon them.[18] Even for a system where there is no net attraction, a small experimental K should be expected.[19] For the cyclohexane–WF_6 in C_7F_{13} interaction the association constant is just a little larger than such a probable critical value ($\sim$0.2 l. mol^{-1}). Measurements having slightly higher standard deviations (WF_6 with hexane in C_7F_{13}, WF_6 with cyclohexane in CCl_4, and MoF_6 with hexane in C_7F_{13}) exhibit a slight falling away of points from the line of eq 3 at higher dilutions. This implies too high absorbancy values which could result from turbidity, although such a possible source of error was treated at least in the clear region of the spectrum; moreover, the weighting of points was chosen to minimize its effect. The deviation produces a larger intercept, hence, a larger K, and indeed these association constants are more than for the WF_6–cyclohexane in C_7F_{13} interaction. The absorptions of WF_6 and MoF_6 in the hydrocarbon and carbon tetrachloride solvents, Figures 2 and 3, afford additional estimates of the extinction coefficients, and require ϵ' values of the table to be upgraded and hence K values to be downgraded. For the association constants discussed above and for the other less reliable measurements, there is no certain evidence that complexing occurs in solution. Also a change from the perfluoroalkane to carbon tetrachloride as a solvent, where charge-transfer spectra with the hexafluorides have been demonstrated, makes little difference in the interactions toward hexane and cyclohexane.

There is also the question whether a finite enthalpy is to be expected for a noncomplexing D, A, S system. Extending Prue's argument[19a] of representing the statistics of the medium by a free volume (V_f) model, V_f decreases with decreasing temperature,[20] and the distance r_s each molecule is constrained to move without encountering a neighbor becomes smaller. The small

(16) R. L. Scott, *J. Phys. Chem.*, **62**, 136 (1958).

(17) W. B. Person, *J. Amer. Chem. Soc.*, **87**, 167 (1965).

(18) P. R. Hammond, *J. Chem. Soc.*, 479 (1964).

(19) (a) J. E. Prue, *ibid.*, 7534 (1965); (b) preceding article.

(20) J. F. Kincaid, H. Eyring, and A. E. Stearn, *Chem. Rev.*, **28**, 301 (1941).

finite K value of a contact system is dependent on Δr (the leeway permitted in the distance separating centers of A and D for which a transition is permissible—this is temperature independent) and although sensibly independent of temperature for a gas phase study, should be responsive to the ratio of Δr to r_s in a liquid. For decreasing temperature, the proportion of molecular pairs disposed to undergo transition increases, the intensity increases, and assuming a constant ϵ, a finite $-\Delta H$ is expected. The solvent expansion correction described earlier accounts merely for the over-all volume change and disregards any possible additional molecular separation effect. For a uniform potential within the liquid cell, the ratio $\Delta r/r_s$, which from the above reasoning is proportional to the concentration of pairs counted as associated, increases as much as 20% for a decrease in temperature similar to that employed here.[20] An alternative approach is to consider the change of coordination for a molecule in a liquid.[21] If this decreases with increasing temperature, the effective number of contacts contributing to the absorption intensity decreases and hence a finite enthalpy is adduced. Steps in the reasoning may be disputable; nevertheless, small enthalpies are expected and the experimental 250 cal/mol^{-1} value indicates that if there is complexing it is very weak. The freezing experiments were also inconclusive, probably as a result of glass formation, as stated earlier.

Molar absorptivities ϵ' are also sensitive to experimental inaccuracies for small K values,[18] and measurements independent of the equilibrium equation are preferable. Figures 2 and 3, from which lowest estimates of ϵ' may be made, indicate values typically of the order 10^3 and oscillator strengths (from frequency–ϵ curve areas) approximately in the region $2\text{–}5 \times 10^{-2}$. It is conceivable that smaller mixing with upper states of the donor or acceptor occurs than for the corresponding systems involving iodine.

Because of chemical reaction, evidence that the yellow colors of solutions of iodine heptafluoride in *n*-hexane and cyclohexane are of intermolecular charge-transfer character is less definite. There seems to be little doubt, however, in terms of the immediate appearances of the colors; the orange charge-transfer absorptions produced with hexafluorobenzene, octafluorotoluene, and perfluoro-*p*-xylene, donors of comparable ionization potential; and, indeed, the similarity of its behavior to molybdenum hexafluoride, which is concluded to be an acceptor of comparable electron affinity.

The interesting question of classification of donor and acceptor types will be examined more closely in later articles. The present experiments provide further evidence of sacrificial σ-donor properties for the aliphatic hydrocarbons. In terms of Mulliken's classification,[22] it seems likely that carbon tetrachloride functions as an increvalent n-type donor, whereas iodine heptafluoride may perhaps be described as a sacrificial acceptor (possibly σ). The present study has been restricted to the highest oxidation state (tetra- and higher coordinate) halides, oxyhalides, and oxides of the elements[3] and has avoided materials of such exceptional reactivity that they would be incompatible with perfluoroaromatic donors. In particular, the bulk of the second and third series transition metal hexafluorides, such as platinum hexafluoride, have not been examined. These are certainly high electron affinity molecules,[23] probably higher than most of the acceptors studied here. It is likely that some of them, for example rhenium hexafluoride, would show similar charge-transfer spectra with aliphatic hydrocarbons and aromatic perfluorocarbons.

Acknowledgment. The author thanks Dick Knipe for many healthy arguments.

(21) J. D. Bernal, *Trans. Faraday Soc.*, **33**, 27 (1937); J. D. Bernal and S. V. King, *Discussions Faraday Soc.*, **43**, 60 (1967).

(22) R. S. Mulliken, *J. Chim. Phys.*, **61**, 20 (1964).

(23) N. Bartlett, *Angew. Chem. Intern. Ed. Engl.*, **7**, 433 (1968).

Acid–Base Catalysis of Dielectric Relaxation of Zwitterions

by Gerhard Schwarz[1]

Max Planck-Institut für physikalische Chemie, Göttingen, Germany *(Received May 26, 1969)*

It is shown that for dipoles of zwitterions preferential orientation due to an applied electric field may be established by two different mechanisms. One refers to the well known effect of rotational diffusion; the other is based on chemical reactions, namely fast protonation and deprotonation processes with an appropriate proton donor–acceptor system. These reactions result in the disappearance of some unfavorably oriented zwitterions and the production of an equal number of more favorably oriented ones. The phenomenon can be interpreted as general acid–base catalysis of dipolar orientation. Accordingly, it should be reflected by corresponding dielectric relaxation properties of the zwitterions. This is favored by slow rotational diffusion (as, for instance, displayed by macromolecular zwitterions, *e.g.*, proteins) and fast chemical relaxation (due to high concentration of the catalyst). Since the zwitterions themselves can accept (or donate) protons, autocatalysis is possible. This is confirmed by some preliminary experimental data. The general theory can easily be extended to such reactions which do not involve zwitterion formation, but some other change of molecular dipole moments.

Introduction

In certain circumstances, orientation of permanent dipoles in an electric field may proceed by means of chemical reaction processes. This implies a chemical mechanism of dielectric relaxation which can be expected to occur in the case of reaction systems resulting in changes of the overall electric dipole moment, provided that the rate of chemical relaxation is sufficiently high compared with that of rotational diffusion.[2] Thus, fast macromolecular reaction processes offer the most favorable conditions to demonstrate the phenomenon. As a matter of fact, first experimental evidence for an effect of this kind was obtained in a pertinent investigation dealing with the conformational change of a polymer molecule.[3]

In this article it will be shown that analogous chemical mechanisms may essentially contribute to dielectric relaxation of a frequently encountered class of molecular dipoles, namely zwitterions (*e.g.*, such formed by amino acids, proteins, etc.). The underlying reactions are proton exchange processes with an appropriate acceptor–donor system. Since the concentration of the latter is not altered, the effect simply represents a case of general acid–base catalysis of dipolar orientation.

The Chemical Rate Processes

Let us consider a molecule with an acidic and a basic group. It may be denoted HZ (where H represents the acidic hydrogen atom). The two protolytic dissociation constants are assumed to have such values that, depending on the pH of the solution, essentially only the following states occur

$$HZH^+ \quad (1)$$

$$^-ZH^+ \quad (2)$$

$$^-Z \quad (3)$$

(*i.e.*, low pH favors state 1, medium pH state 2, high pH state 3). This is frequently encountered in practical cases. At some lower intermediate pH ($\approx pK_1$, *cf.* eq 4b) the zwitterion state 2 primarily behaves as a proton acceptor according to

$$H^+ + {}^-ZH^+ \rightleftharpoons HZH^+ \quad (4a)$$

with

$$K_1 = \frac{\bar{c}_1}{\bar{c}_H \bar{c}_2} \quad (\log K_1 = pK_1) \quad (4b)$$

(the bar indicates equilibrium values of the concentrations of the states 1, 2, and the hydrogen ion, respectively). At a higher intermediate pH ($\approx pK_2$, *cf.* eq 5b) on the other hand, there is mainly deprotonation of the zwitterion described by

$$H^+ + {}^-Z \rightleftharpoons {}^-ZH^+ \quad (5a)$$

where

$$K_2 = \frac{\bar{c}_2}{\bar{c}_H \bar{c}_3} \quad (\log K_2 = pK_2) \quad (5b)$$

Owing to our fundamental assumption we have

$$K_2 \gg K_1 \quad (6)$$

Let us assume that some additional acid–base system

$$H^+ + A^- \rightleftharpoons HA \quad (7a)$$

(involving no zwitterions) is present, which has the equilibrium constant

$$K_A = \frac{\bar{c}_{HA}}{\bar{c}_H \bar{c}_A} \quad (\log K_A = pK_A) \quad (7b)$$

Direct proton transfer between the two systems must be

(1) Physikalisch-Chemisches Institut der Universität Basel, Switzerland.

(2) G. Schwarz, *J. Phys. Chem.*, **71**, 4021 (1967).

(3) G. Schwarz and J. Seelig, *Biopolymers*, **6**, 1263 (1968).

taken into account. In the low pH region this refers primarily to

$$HZH^+ + A^- \underset{k_{21}}{\overset{k_{12}}{\rightleftharpoons}} {}^-ZH^+ + HA \qquad (8a)$$

As is easily seen

$$K_{12} = \frac{k_{12}}{k_{21}} = \frac{K_A}{K_1} \qquad (8b)$$

Hence appreciable concentrations of the reaction partners on both sides of (8a) can only be expected for

$$pK_A \approx pK_1 \ (\approx pH) \qquad (9)$$

(example: HZ = amino acid; HA = carboxylic acid, *e.g.*, acetic acid; pH ≈4.) The analogous process at higher pH is

$${}^-Z + HA \underset{k_{23}}{\overset{k_{32}}{\rightleftharpoons}} {}^-ZH^+ + A^- \qquad (10a)$$

where

$$K_{32} = \frac{k_{32}}{k_{23}} = \frac{K_2}{K_A} \qquad (10b)$$

Both processes, (8a) and (10a), obviously result in the formation or annihilation, respectively, of a zwitterion and its inherent electric dipole moment. Accordingly, application of an electric field must lead to a shift of chemical equilibrium, depending on the angle θ between the directions of the zwitterion dipole $\vec{\mu}_z$ and the field E. For $\theta < 90°$ an increase of the number of zwitterions is favored, while, on the other hand, for $\theta > 90°$ the equilibrium will be shifted toward a decrease of such states. Consequently, the system tends to develop preferential orientation of dipoles parallel to the electric field. Proton transfer of the kind in question has generally proved to be practically diffusion controlled so that the reaction rates can be extremely high.[4] Therefore the implied chemical mechanism of dielectric polarization may be faster than the conventional one based on rotational diffusion. Apparently it then represents a case of acid–base catalysis of dielectric relaxation which should be reflected by the frequency dependence of the dielectric properties. Under these circumstances, pertinent measurements can, in principle, be utilized to determine kinetic data of the underlying chemical rate processes. The general theoretical basis of the phenomenon as well as some fundamental examples have been treated in detail elsewhere.[2] Accordingly, we may now restrict ourselves to particularities of the special problem.

The Relaxation Problem

We direct our attention to process 8a and assume that the molecular states (1) and (2) have the permanent dipole moments μ_1 and μ_2, both of them pointing in the same direction. The latter is to be introduced as a fixed molecular axis which is not affected by the reaction. Consequently, the dipole moment due to zwitterion formation

$$\mu_z = \mu_2 - \mu_1 \qquad (11)$$

also points in this direction (for the sake of simplicity, any components of permanent dipoles perpendicular to it are neglected for the time being, but will be taken into account later on). Permanent dipoles of HA and A^- are assumed to be negligible.

The concentration of the two kinds of dipoles within the solid angle $d\Omega = 2\pi \sin\theta d\theta$ may be expressed as $dc_i = \gamma_i d\Omega$ ($i = 1, 2$). The distribution functions γ_i are subject to the equations of continuity

$$\frac{\partial \gamma_i}{\partial t} = (-1)^i v_{12} + D_r \nabla^2 \gamma_i - (\mathrm{div}\, j_E)_i \qquad (12)$$

($i = 1, 2$). These take into account the chemical rate term

$$-\left(\frac{\partial \gamma_1}{\partial t}\right)_{chem} = \left(\frac{\partial \gamma_2}{\partial t}\right)_{chem} = v_{12} =$$

$$k_{12} c_A \gamma_1 - k_{21} c_{HA} \gamma_2 \qquad (13)$$

the contribution of rotational diffusion

$$D_r \nabla^2 \gamma_i = \frac{D_r}{\sin\theta} \frac{\partial}{\partial \theta} \left\{ \sin\theta \frac{\partial \gamma_i}{\partial \theta} \right\} \qquad (14)$$

(assuming that the rotational diffusion D_r is the same for both states), and the net influx due to the torque exerted by the applied field

$$-(\mathrm{div}\, j_E)_i = \frac{\mu_i E_{or}}{kT} D_r \frac{1}{\sin\theta} \frac{\partial}{\partial \theta} \{ \gamma_i \sin^2\theta \} \qquad (15)$$

(E_{or} = density of the directing field responsible for the orientation of the permanent dipoles.)

The solution of (12) can be obtained by a procedure strictly analogous to that discussed recently (*cf.* section III of ref 2). The electric field densities are usually so small that

$$u_i E_{or} \ll kT \qquad (16)$$

Hence only slight deviations from random distribution of dipole axes will occur, while the over-all concentrations remain constant. We set

$$\gamma_i = \gamma_i^\circ + u_i(t) \cos\theta \qquad (17a)$$

where

$$|u_i(t)| \ll \gamma_i^\circ = c_i/4\pi \qquad (17b)$$

(γ_i° corresponds to statistical orientation at $E = 0$). Under these circumstances we find

$$v_{12} = (k_{12} c_A u_1 - k_{21} c_{HA} u_2) \cos\theta + k_{21} c_A \gamma_1^\circ \delta K \qquad (18)$$

with δK representing the small deviation of

(4) M. Eigen, *Ang. Chem. Int. Ed.*, **3**, 1 (1964); *Discussions Faraday* **39**, 7 (1965).

$$K = \frac{k_{12}}{k_{21}} = \frac{\bar{c}_{HA}\bar{\gamma}_2}{\bar{c}_A\bar{\gamma}_1} \tag{19}$$

at given θ and E from its value at $E = 0$. Based on general thermodynamic theory[2] we have

$$\delta K/K = \frac{\partial \ln K}{\partial E_{or}} E_{or} = \frac{\mu_z E_{or}}{kT} \cos\theta \tag{20}$$

Inserting this in (18), it finally follows that

$$v_{12} = \{k_{12}c_A(u_1 - \bar{u}_1) - k_{21}c_{HA}(u_2 - \bar{u}_2)\} \cos\theta \tag{21}$$

The quantities

$$\bar{u}_i = \frac{\mu_i E_{or}}{kT} \gamma_i^\circ \quad (i = 1,2) \tag{22}$$

apparently represent the instantaneous equilibrium values of the u_i (as determined by the instantaneous values of the applied field). By application of (14) and (15) to (17a) we obtain

$$D_r\nabla^2\gamma_i - (\operatorname{div} j_E)_i = -2D_r(u_i - \bar{u}_i)\cos\theta \tag{23}$$

With (21) and (23), eq 12 lead to linear differential equations for the $u_i(t)$, namely

$$\dot{u}_1 = -(k_{12}c_A + 2D_r)(u_1 - \bar{u}_1) + k_{21}c_{HA}(u_2 - \bar{u}_2) \tag{24a}$$

$$\dot{u}_2 = k_{12}c_A(u_1 - \bar{u}_1) - (k_{21}c_{HA} + 2D_r)(u_2 - \bar{u}_2) \tag{24b}$$

The negative eigenvalues of this system yield the two reciprocal relaxation times

$$\frac{1}{\tau_1} = \frac{1}{\tau_r}; \quad \frac{1}{\tau_2} = \frac{1}{\tau_{ch}} + \frac{1}{\tau_r} \tag{25a, b}$$

(note that always $\tau_2 < \tau_r$) where $1/\tau_r = 2D_r$, *i.e.*, the reciprocal relaxation of the rotational mechanism of orientation, while

$$\frac{1}{\tau_{ch}} = k_{12}c_A + k_{21}c_{HA} = k_{12}c_A^0 \frac{1 + y_1}{1 + y_A} \tag{26}$$

($c_A^0 = c_A + c_{HA}$ = weighing-in concentration of the catalyst; $y_1 = K_1c_H = \bar{c}_1/\bar{c}_2$; $y_A = K_Ac_H = \bar{c}_{HA}/\bar{c}_A$) refers to the chemical relaxation process.

In the case of a periodical electric field with the angular frequency ω we may use the complex notation and put $\dot{u} = i\omega u$ (this $i = \sqrt{-1}$ is not to be confused with the running index used before). Then it follows from (24) that

$$u_1 = \frac{1}{1 + y_1}\left\{\frac{y_1(\bar{u}_1 + \bar{u}_2)}{1 + i\omega\tau_r} + \frac{\bar{u}_1 - y_1\bar{u}_2}{1 + i\omega\tau_2}\right\} \tag{27a}$$

$$u_2 = \frac{1}{1 + y_1}\left\{\frac{\bar{u}_1 + \bar{u}_2}{1 + i\omega\tau_r} + \frac{y_1\bar{u}_2 - \bar{u}_1}{1 + i\omega\tau_2}\right\} \tag{27b}$$

Dielectric Dispersion

After inserting the expressions 27 in (17a), we may calculate the complex dielectric increment due to dipole orientation, $\Delta\epsilon^*$, by utilizing the relation for the corresponding average dipole moment per unit volume which reads

$$\epsilon_0 \Delta\epsilon^* E = g_\alpha N_A \int_0^\pi (\mu_1\gamma_1 + \mu_2\gamma_2)\cos\theta \cdot 2\pi \sin\theta d\theta \tag{28}$$

(ϵ_0 = absolute dielectric constant of vacuum, g_α = factor taking into account the effect of the reaction fields of the dipoles on the induced polarization of the molecule; N_A = Avogadro's number). The result can be written

$$\Delta\epsilon^* = \frac{\Delta\epsilon_r^0}{1 + i\omega\tau_r} + \frac{\Delta\epsilon_2^0}{1 + i\omega\tau_2} \tag{29}$$

where

$$\Delta\epsilon_r^0 = g\frac{N_Ac_0}{3\epsilon_0 kT}\mu_r^2 \tag{30a}$$

($g = g_\alpha$ times the factor E_{or}/E, the latter being the ratio of the directing and the applied field density; $\bar{c}_0 = \bar{c}_1 + \bar{c}_2$ = weighing-in concentration of HZ) with

$$\mu_r = x_1\mu_1 + x_2\mu_2 = \tilde{\mu}_1 + \tilde{\mu}_2 \tag{30b}$$

(x_i = mole fraction of state i; $\tilde{\mu}_i = x_i\mu_i$), while

$$\Delta\epsilon_2^0 = g\frac{N_Ac_0}{3\epsilon_0 kT} x_1x_2\mu_z^2 \tag{31}$$

(note that $x_2 = 1 - x_1$.)

So far we did not take into account components of the permanent dipole moments perpendicular to the direction of the zwitterion dipole. In order to abolish this rather restrictive condition we take advantage of a result obtained by Perrin.[5] It says that in the case of an ellipsoidal molecule, dielectric relaxation can simply be represented as a superposition of the effects contributed by the three principal axes. Thus, we may approximate our molecule by an ellipsoid and compose $\Delta\epsilon^*$ accordingly. We then have a different rotational relaxation time for each axis.

If the lengths of the principal axes are not extremely different, we could nevertheless use a common rotational relaxation time τ_r. Under these circumstances the general expression for $\Delta\epsilon^*$ turns out to be formally identical with the above relations (29, 30a, and 31) provided μ_r and μ_z are defined so that they comply with the fact that the dipole moments of the molecular states 1 and 2 do not necessarily point in the same direction. Actually we have to employ the vector versions of (11) and (30b)

$$\vec{\mu}_z = \vec{\mu}_2 - \vec{\mu}_1; \quad \vec{\mu}_r = \vec{\tilde{\mu}}_1 + \vec{\tilde{\mu}}_2 \tag{32a, b}$$

resulting in

(5) F. Perrin, *J. Phys. Radium*, **7**, 497 (1934).

$$\mu_s^2 = \mu_1^2 - 2\mu_1\mu_2 \cos\psi + \mu_2^2 \quad (33a)$$

$$\mu_r^2 = \tilde{\mu}_1^2 + 2\tilde{\mu}_1\tilde{\mu}_2 \cos\psi + \tilde{\mu}_2^2 \quad (33b)$$

(ψ = angle between $\vec{\mu}_1$ and $\vec{\mu}_2$.) Thus, we may finally write

$$\Delta\epsilon^* = \left\{\frac{\beta_r}{1 + i\omega\tau_r} + \frac{\beta_2}{1 + i\omega\tau_2}\right\}\Delta\epsilon^0 \quad (34a)$$

where

$$\Delta\epsilon^0 = \Delta\epsilon_r^0 + \Delta\epsilon_2^0 = g\frac{N_A c_0}{3\epsilon_0 kT}\{x_1\mu_1^2 + x_2\mu_2^2\} \quad (34b)$$

and

$$\beta_r = \beta_1 = \frac{\mu_r^2}{x_1\mu_1^2 + x_2\mu_2^2}; \quad \beta_2 = \frac{x_1x_2\mu_z^2}{x_1\mu_1^2 + x_2\mu_2^2} = 1 - \beta_1 \quad (34c, d)$$

It is quite clear that an analogous effect as discussed so far with respect to process 8a must also occur due to process 10a (at higher pH). For its quantitative description the above results can be used after changing the original subscripts according to $1 \rightarrow 2$, $2 \rightarrow 3$ (in other words, state 2 takes the place of state 1, while state 3 takes that of state 2).

Experimental Aspects

As can be easily realized from relations 34, the amplitude of the chemically induced dielectric increment, *i.e.*, $\Delta\epsilon_2^0 = \beta_2\Delta\epsilon^0$, should display a maximum for $x_1 = x_2 = 0.5$ which is the case at pH = pK_1 (or at pH = pK_2, analogously). The range around this point would be most favorable for pertinent experimental investigation, provided, however, that τ_2 is sufficiently smaller than τ_r to permit a discrimination between the two dielectric relaxation mechanisms. The latter requires fairly fast chemical relaxation with $\tau_{ch} \lesssim \tau_r$, as can be gathered from (25b).

A discussion of (26) clarifies how τ_{ch} may be minimized. One obvious way, of course, consists in increasing c_A^0 as much as possible. In addition, we could attempt to achieve a maximum value of the factor $k_{12}/(1 + y_A)$ by an appropriate choice of catalyst. From the general kinetic treatment of proton transfer processes given by Eigen,[4] we conclude that k_{12} approaches its diffusion-controlled upper bound if $K_A > K_1$. However, K_A must not become too large since this would so increase y_A that the factor under consideration would be reduced. Favorable values of y_A are found for $K_A < K_1$, but in this case k_{21} will be close to its upper bound so that k_{12} would finally be lowered too much (*cf.* eq 8b). Accordingly, the best choice of HA requires p$K_A \approx$ pK_1, which is equivalent to $k_{12} \approx k_{21}$. These rate constants may exceed 10^9 M^{-1} sec^{-1}, at least in those frequent cases which involve a favorable hydrogen bond structure of the reaction complex. Thus a 1 M solution of the HA–A$^-$ system might well yield a τ_{ch} in the order of magnitude of 10^{-10} sec. This is smaller by orders of magnitude than the τ_r of macromolecular zwitterions (*e.g.*, proteins). Under these circumstances a distinct separation of the two relaxation ranges should be encountered.

For small zwitterions, rotational diffusion is also very fast ($\tau_r \approx 10^{-10}$ sec). In such cases one can hardly expect clearly separated rotational and chemical relaxation ranges. However, a potential $\tau_{ch} \approx \tau_r$ would be reflected by a broadening of the relaxation curves (in comparison with pure rotational relaxation). Instead of a direct and independent experimental determination of τ_r and τ_2 we may then evaluate the mean (reciprocal) relaxation time τ^* (*cf.* the general discussion given elsewhere)[6] according to

$$\lim_{\omega\to\infty}\frac{\omega\Delta\epsilon''}{\Delta\epsilon^0} = \frac{1}{\tau^*} = \frac{\beta_r}{\tau_r} + \frac{\beta_2}{\tau_2} \quad (35a)$$

($\Delta\epsilon''$ = increment of the dielectric loss.) Because of (25b) and (26) we find that

$$\frac{1}{\tau^*} = \frac{1}{\tau_r} + k_{12}\frac{c_A^0}{1 + y_A}\frac{x_1\mu_z^2}{x_1\mu_1^2 + x_2\mu_2^2} \quad (35b)$$

Thus $1/\tau^*$ should be a linear function of c_A^0. Taking advantage also of the pH dependencies of $\Delta\epsilon^0$ (*cf.* eq 34b) and τ^*, a quantitative analysis of pertinent experimental data yields, in principle, the dipole moments μ_1, μ_2, and μ_z as well as the kinetic parameters τ_r and k_{12}.

Let us now stress potential autocatalysis of dipolar orientation due to direct proton transfer between states 1 and 2. Clearly, the reactions

$$HZH^+(\theta) + {}^-ZH^+(\theta') \underset{k_{21}}{\overset{k_{12}}{\rightleftharpoons}} {}^-ZH^+(\theta) + HZH^+(\theta') \quad (36)$$

($k_{12} = k_{21}$ at $E = 0$!) lead to exchange of the zwitterion dipole between the angles θ and θ'' without any material alteration of the reaction system. The chemical rate term for (36) becomes

$$v_{12}' = k_{12}\gamma_1(\vartheta)\gamma_2(\theta') - k_{21}\gamma_1(\theta')\gamma_2(\theta) \quad (37a)$$

The molar change of the dipole moment parallel to the field is $N_A\mu_z(\cos\theta - \cos\theta')$. Employing analogous procedures as before, we find that at small field densities

$$v_{12} = \int_0^\pi v_{12}'\cdot 2\pi \sin\theta' d\theta' \quad (37b)$$

is identical with the expression derived in (21). Accordingly, the above results also apply here. One has only to substitute HZH^+ for HA. In this case the condition of favorable pK is, of course, automatically satisfied ($K_A = K_1$). Furthermore, (26) becomes

(6) G. Schwarz, *Rev. Mod. Phys.*, **40**, 206 (1968).

$$\frac{1}{\tau_{ch}} = k_{12}c_z^0 \qquad (38)$$

($c_z^0 = \bar{c}_1 + \bar{c}_2$ = weighing-in concentration of HZ). This indicates that the autocatalytic effect will be significant only for zwitterion systems of sufficiently high concentration (where $\tau_{ch} \lesssim \tau_r$).

Preliminary experimental evidence of the latter phenomenon was obtained with 1 M aqueous solutions of ϵ-amino caproic acid (measured value of $pK_1 \approx 4.0$).[7] For neutral pH (implying $x_2 = 1$) dielectric relaxation in the GHz range can be described by a superposition of two Debye processes. One of them (around 15 GHz) is interpreted as the effect of water dipoles, while the other process must be attributed to rotational relaxation of the zwitterions. Its reciprocal relaxation time is $1/\tau_r = 2\pi \times 0.7$ GHz. At pH 4.14 ($x_2 \approx 0.6$) a distinct broadening of this part of the relaxation curve is observed, resulting in $1/\tau^* = 2\pi \times 0.9$ GHz. Assuming $\mu_1 \approx 0$, application of (35b) then yields $k_{12} \approx 3 \times 10^9\ M^{-1}\ \text{sec}^{-1}$ which is in excellent agreement with analogous data known from other sources.[4] Moreover, the ratio of the measured $\Delta\epsilon^0$ is found to be 0.67, while about 0.6 is predicted by eq 34b.

Generalization of the Effect and the Theory

Finally, it should be emphasized that the dielectric mechanism pointed out above is by no means restricted to zwitterion systems. The general theory can apparently be applied to any reaction process of the type

$$A_1 + B_1 \underset{k_{21}}{\overset{k_{12}}{\rightleftharpoons}} A_2 + B_2 \qquad (39)$$

where A_1 and A_2 have different dipole moments while B_1 and B_2 have none (or, at least, display no dielectric relaxation interfering with that of A_1 and A_2). Zwitterion formation merely represents a frequently encountered special case of (39) which is most interesting because of the potential dramatic change of the dipole moment.

Acknowledgment. The author is greatly indebted to Dr. R. Pottel and Mr. D. Adolph of the University of Göttingen for informing him of their unpublished experimental data.

(7) R. Pottel and D. Adolph (3. Physikalisches Institut, University of Göttingen) to be published.

Volume–Temperature Relationships of Hydrophobic and Hydrophilic Nonelectrolytes in Water

by J. L. Neal and D. A. I. Goring

Physical Chemistry Section, Pulp and Paper Research Institute of Canada, and Department of Chemistry, McGill University, Montreal, Quebec, Canada *(Received April 17, 1969)*

The change in apparent specific volume, ϕ_2, with temperature, T, was measured dilatometrically for 15 nonelectrolytes in water between −4 and 60°. Hydrophobic compounds generally had lower values of the derivative, $d\phi_2/dT$, than hydrophilic compounds. The derivative increased with increasing concentration dependence of apparent specific volume and was proportional to the enthalpy of solution in water. An explanation is offered based on the concept that hydrophobic compounds promote structure in water while hydrophilic compounds tend to reduce structure. It is proposed that $d\phi_2/dT$ is a useful measure of the effect of a nonelectrolyte on the structure of water.

Introduction

A number of the exceptional properties of pure water can be accounted for in terms of a "mixture" hypothesis. Water is assumed to consist of a structured, low-density form and an unstructured, high-density form. Unusual changes with temperature are said to result from a displacement of the equilibrium.

$$H_2O_{structured} \rightleftharpoons H_2O_{unstructured} \qquad (1)$$

Abnormalities in the properties of aqueous solutions are also attributed to changes in the water structure caused by the added components. Solutes which displace the equilibrium in eq 1 in favor of structure are referred to as structure promoters. Structure breakers have the opposite effect.

In aqueous solution, the temperature dependence of apparent specific volume, $d\phi_2/dT$, of carbohydrates is much greater than the bulk thermal expansion, dv_2/dT. On the basis of this behavior, carbohydrates have been classified as structure breakers[1] because the thermal expansion of the unstructured species in water is higher than that of the structured form. The ability of glucose to destructure water was attributed to its abundance of hydrophilic, hydroxyl groups. On the other hand, higher alcohols have been classified as structure formers because of their negative entropies and enthalpies of mixing with water,[2] their enhancement of the solubility of noble gases in water,[3] and other properties.[4] The structure-promoting tendency of these compounds is attributed to their hydrophobic, alkyl group. Some sparse published data[5,6] indicate that in contrast to the behavior of carbohydrates dv_2/dT is greater than $d\phi_2/dT$ for the aliphatic alcohols in aqueous solution.

From the above it seemed likely that the derivative of the apparent specific volume with respect to temperature would be a useful and sensitive measure of the effect of a particular substance on the structure of water. Also, measurement of $d\phi_2/dT$ is versatile since it can be applied to soluble or insoluble, solid or liquid, and hydrophobic or hydrophilic substances. Since there is no firmly established direct measure of structural interaction by which to test the general validity of $d\phi_2/dT$ as a structural parameter, an indirect approach was taken. The $d\phi_2/dT$ values of a diverse series of compounds were determined and compared with other properties which might be considered indicative of structural interaction. These properties included the concentration dependence of ϕ_2 and the change in solubility with temperature.

The relative scarcity of published thermal expansion data stems in part from the high labor content of conventional measurements. Therefore an automatic dilatometer was developed[7] and used to record changes in volume at tightly spaced temperature intervals.

Experimental Section

Materials. The limiting factor in determining apparent specific volumes of solutes of 1% concentration is not the effect of minor impurities. Consequently, the solutes, which were reagent grade except for tetrahydropyran, THP (bp 86.5–88.5), and hexamethylene tetramine, HMT (N.F.), were used without further purification. The conductivity of the distilled water was 2×10^{-6} ohm^{-1} cm^{-1}.

Dilatometry. The change of solution density with temperature was measured between −4 and 60° with capillary dilatometers. Measurements were possible at temperatures as low as −6° without freezing. Readings were usually taken at temperature intervals of 2°. Details of dilatometry and calculations are given elsewhere.[7]

The results of the dilatometer measurements were expressed as volumes relative to a solution volume at a given temperature. The specific volume of the solution was determined by independent measurement or from literature data at this given temperature, and the relative volumes at other temperatures converted to specific volumes.

The apparent specific volume, ϕ_2, of the solute was derived from

$$v_{12} = w_1 v_1 + w_2 \phi_2 \qquad (2)$$

in which v_1 and v_{12} are the specific volumes of water and the solution and w_1 and w_2 the weight fractions of water and the solute. It is interesting to note that eq 2 is not restricted to solutions. It can be applied with equal validity to colloidal suspensions, water-swollen gels, or even bulk solids under water (*e.g.*, Archimedes) provided the nonaqueous component is totally immersed. In two-phase systems, w_2 and ϕ_2 are, respectively, the weight fraction and apparent specific volume of the nonaqueous component and v_{12} becomes the total volume divided by the total weight of the mixture.

Trial runs with sucrose solutions established that the reproducibility in the present investigation was about 0.8×10^{-5} g ml^{-1} in density. For a 1% solution this corresponds to a precision of ±0.001 ml g^{-1} in ϕ_2. Precise measurement of the density of water has been reported by Kell.[8] His error was about 10^{-6} g ml^{-1}. Since the measurements reported in this paper are less exact, an estimate of our error can be made by comparing our results for pure water with those of Kell. Over the temperature range of interest, the root-mean square difference between Kell's data and ours for pure water was 5×10^{-6} ml g^{-1} in v_1, 1.2×10^{-6} ml g^{-1} deg^{-1} in dv_1/dT, and 1.1×10^{-7} ml g^{-1} deg^{-2} in d^2v_1/dT^2. Most of the measurements reported are based on solutions having $w_2 = 0.01$, for which the corresponding errors are 10^{-3} ml g^{-1} in ϕ_2, 10^{-4} ml g^{-1} deg^{-1} in $d\phi_2/dT$, and 10^{-5} ml g^{-1} deg^{-2} in $d^2\phi_2/dT^2$. The errors in ϕ_2 and its derivatives are proportionately less in more concentrated solutions.

In sucrose solutions ϕ_2 is not especially sensitive to changes in concentration. At 5% concentration of sucrose in water, ϕ_2 is 0.617 ml g^{-1} and at 1% it

(1) M. V. Ramiah and D. A. I. Goring, *J. Polym., Sci., Part C*, 11, 27 (1965).
(2) F. Franks and D. J. G. Ives, *Quart. Rev.* (London), 20, 1 (1966).
(3) A. Ben-Naim, *J. Phys. Chem.*, 71, 4002 (1967), and earlier papers.
(4) G. Nemethy and H. A. Scheraga, *J. Chem. Phys.*, 36, 3382 (1962).
(5) D. M. Alexander, *J. Chem. Eng. Data*, 4, 252 (1959).
(6) M. E. Friedman and H. A. Scheraga, *J. Phys. Chem.*, 69, 3795 (1965).
(7) J. L. Neal, Thesis, McGill University, 1969.
(8) G. S. Kell, *J. Chem. Eng. Data*, 12, 66 (1967).

Table I: Temperature Coefficients of Polynomials of Apparent Specific Volumes of Various Solutes in Water
[ϕ_2 (or v_2) = $A_0 + A_1T \times 10^3 + A_2T^2 \times 10^{-4} + A_3T^3 + 10^{-7} \pm$ Std Dev]

Solute	Concentration (wt. fraction)	A_0 (ml gm^{-1})	A_1 (ml $gm^{-1}°C^{-1}$)	A_2 (ml $gm^{-1}°C^{-2}$)	A_3 (ml $gm^{-1}°C^{-3}$)	S.D. x 10^3 (ml gm^{-1})	Data reference	Calibration reference
t-Butanol	0.0104	1.180	-0.365	0.159	-0.384	0.5	This work	11
"	0.0182	1.175	-0.272	0.153	-0.353	0.5	" "	11
"	0.0472	1.162	0.095	0.110	0.0	0.4	" "	11
"	0.1028	1.130	0.784	0.106	-0.662	2.	" "	11
"	1.0	1.236	1.656	0.0277	0.0	0.7	12	-
I-Butanol	0.01	1.1576	0.2516	0.06915	0.0	0.8	This work	13
"	0.0203	1.1500	0.3763	0.08222	0.0	0.5	" "	13
"	1.0	1.2137	1.051	0.00581	0.0058	-	12	-
Chloroform	0.0065	0.5980	0.3076	0.0	0.0	0.4	This work	14
"	1.0	0.6552	0.7860	0.0142	0.0	0.5	12	-
Neopentanol	0.01127	1.114	0.3495	0.1438	-0.423	0.7	This work	15
Cyclohexanol	0.01022	1.0170	0.4440	0.0089	0.0	0.6	This work	This work
"	1.0	1.0440	0.4115	0.0629	0.0	-	12	-
HMT*	0.01115	0.7741	0.7693	-0.0967	0.931	0.8	This work	16
"	0.02618	0.7728	0.8622	-0.0912	0.764	0.5	" "	16
"	1.0	0.747	0.0	0.0	0.0	-	16	-
Sucrose	0.0101	0.6027	0.8583	-0.1667	1.8	0.5	This work	9
"	1.0	0.6580	0.00916	-0.0315	-0.098	0.3	17	-
Glucose	0.00831	0.6037	0.9403	-0.1086	-0.7335	0.6	This work	18
"	0.021	0.6039	0.9796	-0.1191	0.8068	0.5	" "	18
"	1.0	0.6553	0.00914	0.0384]	-0.1638	0.5	19	
THF**	0.0109	1.0395	0.9057	-0.0382	0.776	0.6	This work	This work
"	1.0	1.0923	1.382	0.0	0.0	0.2	" "	20
t-Butylamine	0.0112	1.2023	0.8315	0.0724	-0.89	1.0	This work	This work
THP***	0.02	1.0291	0.9136	0.0	0.0	0.5	This work	21
"	1.0	1.109	1.294	0.0	0.0	0.2	" "	21
Glycerol	0.00994	0.7469	1.116	-0.2603	4.5	0.1	This work	22
"	0.0105	0.7463	1.056	-0.15	0.98	0.7	" "	22
"	0.01438	0.7468	0.9626	-0.0957	0.0	0.2	" "	22
"	0.01965	0.7484	0.845	-0.0428	0.0	0.2	" "	22
"	0.0466	0.7486	0.968	-0.0757	0.0	0.1	" "	22
"	0.1	0.7540	0.760	-0.0532	0.21	1.2	22	22
"	1.0	0.7859	0.3434	0.0072	0.0	0.2	22	22
i-Inositol	0.0106	0.6390	1.3061	-0.1137	0.0	0.1	This work	This work
Urea	0.0106	0.6992	1.8064	-0.1198	0.0	1.0	This work	23
"	1.0	0.7495	0.116	0.0	0.0	-	23	23
Formamide	0.01175	0.8096	2.5704	-0.3349	2.6	0.9	This work	24
"	0.0223	0.8118	2.479	-.3512	3.18	1.	" "	24
"	1.0	0.86907	0.6639	0.0	0.0	0.1	12	12

* Hexamethylene Tetramine
** Tetrahydrofuran
*** Tetrahydropyran

0.616 ml g^{-1}.[9] However, in the case of *t*-butyl alcohol,[10] ϕ_2 changes sharply with concentration and estimates of intrinsic properties were possible only by extrapolation to zero concentration for measurements on dilute solutions.

Results

The results of the dilatometry measurements were reduced to the corresponding apparent specific volumes and expressed as polynominal functions of temperature, T. The coefficients of the polynomials of the

Table II: Regression Coefficients of Apparent Specific Volume on Temperature and Concentration
($\phi_2 = A_0 + A_1T + A_2w_2 + A_3T^2 + A_4w_2^2 + A_5w_2T + A_6T^3$

Sample	A_0, ml g^{-1}	$A_1 \times 10^3$, ml g^{-1} deg^{-1}	$A_2 \times 10^3$, ml g^{-1}	$A_3 \times 10^4$, ml g^{-1} deg^{-2}	$A_4 \times 10^4$, ml g^{-1}	$A_5 \times 10^5$, ml g^{-1} deg^{-1}	$A_6 \times 10^7$, ml g^{-1} deg^{-3}	Std dev ml g^{-1}
Sucrose	0.5984	1.263	0.2736	−0.2917	0.0	0.0	2.8	0.0017
Glycerol	0.7464	0.9678	0.6079	−0.0783	0.0	−0.862	0.4	0.0022
HMT	0.7736	0.8465	−0.1428	−0.1162	0.0	0.0	1.2	0.0011
t-Butyl alcohol	1.1850	−0.3571	−5.773	0.1495	0.6293	8.531	−0.05	0.0014

Table III: Comparison of Apparent Specific Volume at 4° with Other Properties of 15 Solutes

Solute	Concentration, wt fraction	ϕ_2, ml g^{-1}[a]	$d\phi_2/dT \times 10^3$, ml g^{-1} deg^{-1}[a]	$d^2\phi_2/dT^2 \times 10^4$, ml g^{-1} deg^{-2}[a]	$dv_2/dT - d\Phi/dT \times 10^3$, ml g^{-1} deg^{-1}[a]	$d\phi_2/dw_2 \times 10^2$, ml g^{-1}	$-\frac{d \ln s}{d(1/T)}$, deg	Ref	Solute no.
t-Butyl alcohol	0.0	1.179	−0.240	0.31	1.92	−0.595	(−1900)	25	1
1-Butanol	0.0	1.159	0.307	0.14	0.75	−0.637	−1098	26	2
Chloroform	0.0065	0.599	0.308	0.00	0.50	...	−1483	14	3
Neopentanol	0.01	1.116	0.463	0.28	...	...	−1193	15	4
Cyclohexanol	0.01	1.019	0.489	0.18	0.27	...	−1163	26	5
HMT	0.0	0.777	0.696	−0.17	−0.696	−0.070	− 55	27	6
Sucrose	0.0	0.606	0.734	−0.29	−0.70	−0.027	177	14	7
Glucose	0.0	0.607	0.857	−0.20	−0.82	−0.051	1582	14	8
THF	0.01	1.043	0.878	−0.06	0.50	...	...	...	9
t-Butylamine	0.011	1.206	0.885	0.12	...	...	...	...	10
THP	0.02	1.033	0.914	0.00	0.38	...	−1700	23	11
Glycerol	0.0	0.750	0.941	−0.09	−0.592	0.030	(− 550)	28	12
i-Inositol	0.0106	0.644	1.215	−0.23	...	...	...	...	13
Urea	0.01	0.706	1.711	−0.24	−0.74	0.119[30]	(30)[b]	28	14
Formamide	0.0	0.819	2.315	−0.61	−1.651	0.171	(180)	29	15

[a] At 4°; [b] $\Delta H_{\text{dissolution}} - \Delta H_{\text{fusion}}$.

solutes considered are listed in Table I. Individual values of ϕ_2 at specific temperatures are given elsewhere.[7] Since the deviations of the fits of the polynomials are comparable to the errors expected in the determination, the polynomials can be accepted as valid to about ±0.002 ml g^{-1} in apparent specific volume for the 1% solutions and somewhat better for more concentrated solutions. Terms of higher order than cubic were not justified and in some cases even lower orders sufficed.

Also included in Table I are coefficients for the pure materials based in most cases on data compiled from the literature. References 11–24 are given in Table I to the sources of both the thermal expansion data and the calibration points for specific volume.

The data for solutes which were measured at more than one concentration are amenable to a regression analysis on concentration and temperature. The coefficients of the resultant equations are listed in Table II. In the cases of sucrose and hexamethylene tetramine (HMT) it was possible to include data from other sources and thereby extend the range of validity of the equation.

Values of ϕ_2, $d\phi_2/dT$, $d^2\phi_2/dT^2$, and $(dv_2/dT - d\phi_2/dT)$ as well as other properties of each of the solutes

(9) F. Schneider, D. Schliephake, and A. Klimmer, *Zucker*, **16**, 7 (1963).

(10) K. Nakanishi, *Bull. Chem. Soc. Jap.*, **33**, 793 (1960).

(11) K. Nakanishi, N. Kato, and M. Maruyama, *J. Phys. Chem.*, **71**, 814 (1967).

(12) J. Timmermans, "Physico-Chemical Constants of Pure Organic Compounds," Elsevier Publishing Co., Amsterdam, 1965.

(13) W. H. Pasfield, *J. Phys. Chem.*, **69**, 2406 (1965).

(14) H. Stephen and T. Stephen, "Solubilities of Inorganic and Organic Compounds," The Macmillan Co., New York, N. Y., 1963.

(15) P. M. Ginnings, *J. Amer. Chem. Soc.*, **59**, 1112 (1937).

(16) V. Crescenzi, F. Quadrifoglio, and V. Vitagliano, *J. Phys. Chem.*, **71**, 2313 (1967).

(17) F. Schwers, *J. Chem. Soc.*, **99**, 1478 (1911).

(18) D. Schliephake, *Die Stärke*, **17**, 44 (1965).

(19) G. S. Parks, *J. Phys. Chem.*, **32**, 1366 (1928).

(20) H. Bohme and W. Schurhoff, *Ber.*, **84**, 41 (1951).

(21) G. M. Bennet, and W. J. Philip, *J. Chem. Soc.*, 1939 (1928).

(22) C. S. Miner and N. N. Dalton, Ed., "Glycerol," American Chemical Society Monograph No. 117, Reinhold Publishing Corp., New York, N. Y., 1953.

(23) F. T. Gucker, F. W. Gage, and C. E. Moser, *J. Amer. Chem. Soc.*, **60**, 2582 (1938).

(24) J. G. Albright and L. S. Gosting, *J. Phys. Chem.*, **64**, 1537 (1960).

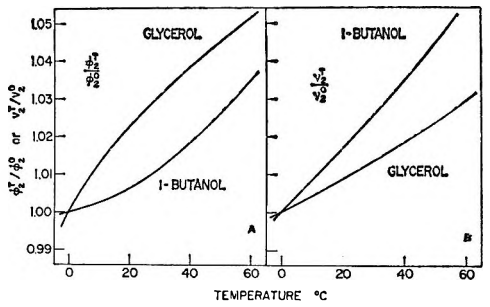

Figure 1. A. The apparent specific volume relative to the apparent specific volume at 0° in water *vs.* temperature for 1-butanol and for glycerol. B. The specific volume relative to the specific volume at 0° *vs.* temperature for 1-butanol and glycerol for comparison with corresponding aqueous solution property shown in A.

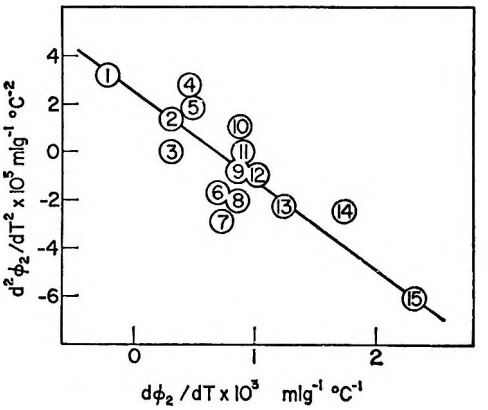

Figure 2. The curvature in apparent specific volume in water, $d^2\phi_2/dT^2$, *vs* the slope $d\phi_2/dT$. The numbers identify the solutes in Table III.

studied are listed in Table III.[25-30] The volume–temperature properties were derived from the polynomials in Table I at 4°. The choice of 4° as standard temperature of comparison has been discussed earlier,[31] but comparisons at any low (0–15°) temperature yield substantially the same result. Where extrapolation was possible the values were calculated for zero concentration. The result at a single low (usually 1%) concentration was used when the data were insufficient to warrant extrapolation.

Column 7 contains $d\phi_2/dw_2$, the change in ϕ_2 with concentration. The difference in sensitivity of ϕ_2 to concentration mentioned earlier is apparent. In column 8 the change in solubility with temperature, $(d \ln s)/(d(1/T))$, is given and column 9 shows the literature reference to it. In the case of liquids which are miscible with water, column 8 is a published value of a calorimetrically determined partial molar heat of mixing divided by R, $\Delta H_m/R$. These values are in parentheses. The final column in Table III gives a code number useful in identifying points in subsequent graphs.

Discussion

The behavior of 1-butanol is typical of solutes such as neopentanol and cyclohexanol which contain major hydrophobic moieties. The apparent specific volume in water, ϕ_2, is less than the bulk specific volume. The slope, $d\phi_2/dT$, is less than the corresponding thermal expansion of the pure compound, dv_2/dT, and the curvature, $d^2\phi_2/dT^2$ is positive. The behavior of glycerol is typical of compounds containing polar groups such as formamide, urea, inositol, glucose, and sucrose. These compounds also show a net loss of volume when dissolved in water but, in contrast to the hydrophobic compounds, $d\phi_2/dT$ is greater than dv_2/dT and $d^2\phi_2/dT^2$ is negative. The difference in volume–temperature behavior of the two classes of compounds is illustrated in Figure 1 in which ϕ_2^T/ϕ_2^0 or v_2^T/v_2^0, the values of apparent specific volume and specific volume relative to their values at 0°, are plotted against temperature for 1-butanol and glycerol.

The trends in volume shown in Table III and Figure 1 are entirely compatible with the concept of dissolved substances altering the structure of water. Molecules which are rich in hydroxyl groups or polar molecules disrupt the structure of water adjacent to them.[1] The change in volume with temperature of this water is high.[4] The net effect on the mixture is that $d\phi_2/dT$ appears to be abnormally high when compared with dv_2/dT.

In contrast, hydrophobic molecules become surrounded with a layer of increased structure, the thermal expansion of which is low, like that of ice.[4] The net effect is that these structure promoters appear to have abnormally low $d\phi_2/dT$. Thus the temperature coefficient of apparent specific volume appears to be a useful and sensitive measure of the structural interaction of a solute with water.[32]

Figure 2 illustrates the correlation between the slopes $d\phi_2/dT$, and curvatures, $d^2\phi_2/dT^2$, and suggests that the curvature is positive for structure promoters and

(25) J. Kenttamaa, E. Tommila, and M. Martti, *Ann. Acad. Scient. Fennicea, A*, **93**, 1 (1959).

(26) A. E. Hill and W. M. Malisoff, *J. Amer. Chem. Soc.*, **48**, 918 (1926).

(27) J. F. Walker, "Formaldehyde," Reinhold Publishing Corp., New York, N. Y., 1953.

(28) J. Perreu, *Compt. Rend.*, 210, 293 (1940).

(29) I am indebted to Dr. D. Patterson and Dr. J. Kow of the Chemistry Department, McGill University, for this measurement.

(30) R. H. Stokes, *Aust. J. Chem.*, 20, 2087 (1967).

(31) J. L. Neal and D. A. I. Goring, *J. Polym. Sci., Part C*, **28**, 103 (1969).

(32) In a previous treatment[1,7] of carbohydrate molecules as structure breakers it was assumed that $d\phi_2/dT$ contains a component representing the thermal expansion of the pure material. This component was allowed for simply by substracting dv_2/dT from $d\phi_2/dT$. It might be expected that the difference $(d\phi_2/dT - dv_2/dT)$ would in fact be a more meaningful structural parameter than $d\phi_2/dT$ alone. However, it was found for the liquid samples examined in the present work that $d\phi_2/dT$ and $(d\phi_2/dT - dv_2/dT)$ are themselves so highly correlated (coefficient = 0.98) that no particular advantage can be claimed for the use of the difference instead of the single derivative.

negative for structure breakers. These trends would be expected if the extent of the structurally perturbed layer of water molecules decreased with increase in temperature. Such a decrease for hydrophobic structure promoters has been predicted quantitatively by Némethy and Scheraga.[33] Ramiah and Goring[1] have also found a decrease at higher temperatures in the extent of the perturbed layer for carbohydrates as have Ihnat, Szabo, and Goring.[34] Significantly in Figure 1 $d(\phi_2^T/\phi_2^0)/dT$ for 1-butanol and glycerol become equal at ~60°.

The data presented in Figure 3 show that a quantitative relationship exists between $d\phi_2/dT$ and $d\phi_2/dw_2$, and that $d\phi_2/dw_2$ is positive for structure breakers and negative for structure promoters. This latter trend furnishes graphic support to the view expressed by Buijs and Choppin,[35,36] who stated that "structure forming solutes affect water structure in a way formally equivalent to a decrease in temperature." The apparent specific volume usually decreases with a decrease in temperature and thus, addition, of increasing quantities of a structure promotor to water, being equivalent to a lowering of the temperature, produces a reduction in ϕ_2 ($d\phi_2/dw_2$ negative). This concept can be extended in the light of Figure 3 to include the equivalence of structure disrupting solutes to a temperature increase. Successive additions of a structure breaker will correspond to an increase in the temperature of the solution and thus to an increase in ϕ_2 ($d\phi_2/dw_2$ positive). It must be emphasized that the foregoing observations are purely descriptive and are not meant as a substitute for a quantitative treatment based on solute–solute interactions and their effect on water structure.

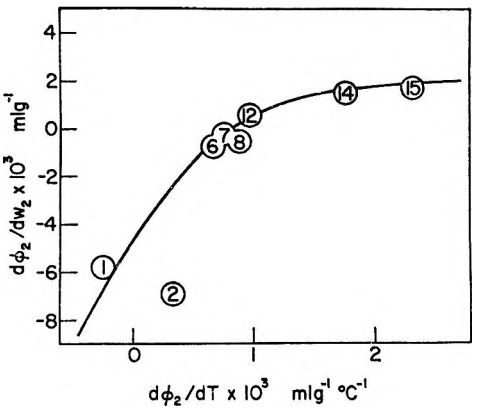

Figure 3. The change in apparent specific volume with concentration, $d\phi_2/dw_2$ *vs.* the change in apparent specific volume with temperature, $d\phi_2/dT$ for a number of solutes.

The correlation of d ln s/d(1/T) with $d\phi_2/dT$ in Figure 4 can be interpreted thermodynamically. The temperature coefficient of solubility is related to the partial molar heat of mixing of the solute, $\overline{\Delta H}_M$.[7,37] Values of $\overline{\Delta H}_M$ calculated from the change in solubility with temperature are negative for the hydrophobic solutes. The structuring of water corresponds to the formation of ice and thus it is not surprising that

$$\frac{d \ln s}{d(1/T)} = -\frac{\overline{\Delta H}_M}{R} \quad (3)$$

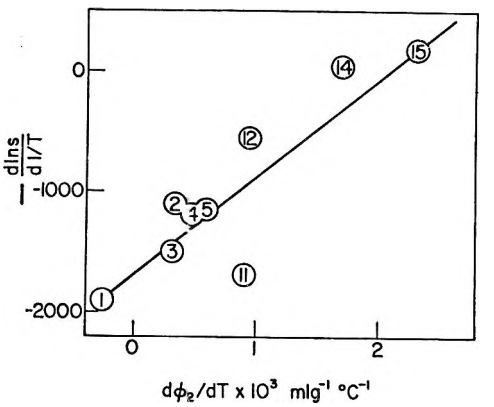

Figure 4. The temperature dependence of solubility, d ln s/d(1/T) *vs.* the change in apparent specific volume with temperature, $d\phi_2/dT$, for a number of solutes.

solution of a hydrophobic structure promoter is exothermic. If structure promoters act in a way equivalent to freezing water then structure breakers should act in a way equivalent to melting ice and would be expected to show positive values of $\overline{\Delta H}_M$[38] and correspondingly negative values of d ln s/d(1/T). Thus either d ln s/d(1/T) or $\overline{\Delta H}_M$ can be regarded as a measure of the nature and extent of structural interactions and the good correlation of Figure 4 supports the validity of $d\phi_2/dT$ as a quantitative indication of structural changes produced by an aqueous solute.[39,40]

(33) G. Némethy and H. A. Scheraga, *J. Chem. Phys.*, **36**, 3415 (1962).

(34) M. Ihnat, A. Szabo, and D. A. I. Goring, *J. Chem. Soc.*, 1500 (1968).

(35) K. Buijs and G. R. Choppin, *J. Chem. Phys.*, **39**, 2035 (1963).

(36) G. Barone, V. Crescenzi, and V. Vitagliano, *J. Phys. Chem.*, **72**, 2588 (1968).

(37) J. H. Hildebrand, and R. L. Scott, "The Solubility of Nonelectrolytes," 3rd ed, Reinhold Publishing Corp., New York, N. Y., 1950, p 134

(38) H. S. Frank and F. Franks, *J. Chem. Phys.*, **48**, 4746 (1968).

(39) It is interesting to note that cyclohexanol and neopentanol lie on the line even though they are solids and might be expected to be displaced by d ln s/d(1/T) by an amount equivalent to their heats of fusion. For these solutes the "solubility" represents the equilibrium composition of the liquid aqueous phase in contact with an organic liquid phase.[15,26] Thus no change of state accompanies dissolution in the solution from which d ln s/d(1/T) is calculated. If $\overline{\Delta H}_M$ for the other solids in Table III could be resolved into fusion and dissolution components, $\Delta H_{dissolution}$ should reflect the enthalpy of changes in water structure caused by the addition of the solute and, therefore, be in accord with the trend shown in Figure 4. When ΔH_{fusion}[40] is subtracted from the $\Delta H_{dissolution}$ of urea, the result lies close to the line drawn in Figure 4. The points for HMT, sucrose, and glucose are not included in Figure 4 since $\overline{\Delta H}_M$ for these solids includes unknown and (probably) large heats of fusion.

(40) F. W. Miller and H. R. Dittmar, *J. Amer. Chem. Soc.*, **56**, 848 (1934).

In the foregoing interpretation, it is assumed that heat effects due to interaction of water with the solute are small compared with the enthalpy changes produced by perturbation of the water structure near the surface of the solute molecule. In the absence of specific interactions, mixing with water would be expected to be athermal for hydrophilic compounds and endothermal for hydrophobic compounds. Specific interactions with hydrophilic compounds would be expected to produce heat. The opposite trend illustrated in Figure 4 indicates that the contributions to the enthalpy arise predominantly from structural changes in the water.

It is interesting to note that the temperature of maximum density, TMD, of a solution is related to $d\phi_2/dT$ since from eq 2

$$dv_{12}/dT = w_1\, dv_1/dT + w_2\, d\phi_2/dT \qquad (4)$$

At TMD

$$dv_{12}/dT = 0$$

and

$$d\phi_2/dT = -\frac{w_1}{w_2}\, dv_1/dT \qquad (5)$$

It is therefore not surprising that some workers[41-43] have related TMD with structural effects. However, TMD changes sharply with concentration and $d\phi_2/dT$ is a more direct measure of the effect of the solute on the structure of water.

At this stage it should be noted that there is no significant correlation between $d\phi_2/dT$ and ϕ_2 or $\phi_2 - v_2$. Almost without exception ϕ_2 was smaller than v_2 for both hydrophobic and hydrophilic substances. This is expected for the latter since hydrophilic solutes are structure breakers and the water destructured becomes more compact, leading to a decrease in the apparent specific volume. However, a contraction is also observed for structure promoters in spite of the fact that such solutes increase the proportion of the high volume component.[44]

The hydrophobic contraction has been accounted for by some authors[6] as a result of the space conserving mechanism of filling empty clathrate cages. Friedman and Scheraga[6] have pointed out that complete caging is not necessary to account for the contraction. It can also arise from partial caging because of the ability of the solute to occupy volume otherwise unoccupied by water molecules. The negative value of $d\phi_2/dT$ for *t*-butyl alcohol may arise from an exceptionally strong structuring tendency of this molecule at low temperatures. Here the high-volume structured layer may be several water molecules thick near 0°. When the temperature is increased, rapid destructuring (melting) of the icelike layer may produce a decrease in ϕ_2 similar to the decrease in volume of pure water in this temperature range.

Concluding Remarks

The change in apparent specific volume with temperature, $d\phi_2/dT$, of a substance in water is an index of its structural interaction with water. This is the main conclusion of the present work. Moreover, measurements of $d\phi_2/dT$ are applicable to a wide variety of nonelectrolytes—solid and liquid, hydrophobic and hydrophilic, large and small molecules, and even dispersed insoluble[1,31] substances.

A simple extension of the hydrophobic, structure promotion hypothesis[4] to hydrophilic substances accounts for the relationship between structuring tendency and $d\phi_2/dT$. Good correlations were found between $d\phi_2/dT$ and the curvature $d^2\phi_2/dT^2$, the concentration dependence of ϕ_2, and the temperature coefficient of solubility. Each of these relationships could be explained in terms of the structural hypothesis.

Although hydrophobic and hydrophilic compounds generally were opposite in their behavior, the change was continuous from one extreme to the other. This continuity supports the view that the ranking of a particular molecule as a structure promoter or a structure breaker will depend on the net result of contributions from both the hydrophobic and hydrophilic parts of the molecule.

(41) G. Wada and S. Umeda, *Bull. Chem. Soc. Jap.*, **35**, 647, 1797 (1962).

(42) F. Franks and B. Watson, *J. Chem. Soc.*, 329 (1967).

(43) D. A. Armitage, M. J. Blandamer, K. W. Morcom, and N. C. Treloar, *Nature*, **219**, 718 (1968).

(44) A. Holzer and M. F. Emerson, *J. Phys. Chem.*, **73**, 27 (1969).

NOTES

Secondary Valence Force Catalysis. X. Fluorine-19 Chemical Shifts as a Probe for Localization of Organic Substrates in Micellar Systems[1]

by Paul A. Arrington, A. Clouse, David Doddrell, R. B. Dunlap, and E. H. Cordes[2]

Department of Chemistry, Indiana University, Bloomington, Indiana 47401 *(Received June 9, 1969)*

A series of investigations from this laboratory has established that the acid-catalyzed hydrolysis of ortho esters and acetals is subject to catalysis by anionic surfactants.[3] While several features of these reaction systems have been elucidated,[3] the principal habitat of these substrates within the micellar phase remains conjectural (arguments suggesting that the reaction site is very likely the micellar surface and not the micellar interior do not, of course, settle this question[3d]). The utility of nuclear magnetic resonance as a tool for the study of micelle formation and structure[4] suggests that it might serve as a probe for the localization of ortho esters and acetals within aqueous solutions of micellated anionic surfactants. Data reported herein bear out the accuracy of this supposition.

Experimental Section

Materials. Organic solvents employed in these experiments were obtained commercially, were either of reagent or spectral grade, and were generally employed without further purification. Water was glass distilled using a Corning Model Ag-1a still. Fluorinated substrates including fluorobenzene, *p*-fluorobenzaldehyde, *p*-fluoroacetophenone, and *p*-fluoroanisole were obtained commerically and were reagent grade. Methyl ortho-*p*-fluorobenzoate was kindly supplied by Professor R. W. Taft. *p*-Fluorobenzaldehyde diethyl acetal was prepared according to the method of Fife and Jao.[5] Proton and fluorine nmr spectra failed to reveal any impurities in the fluorinated substrates. Sodium dodecyl sulfate was obtained from Distillation Products Industries and dodecyldimethyl ammonia propane sulfonate was a generous gift from the Miami Valley laboratories of Procter and Gamble, Inc. Dodecyltrimethyl ammonium bromide was prepared in this laboratory by Mr. L. R. Romsted according to the method of Scott and Tartar.[6]

Nmr Measurements. Unless otherwise noted, all measurements were made at approximately 27° in solutions containing approximately 0.01 *M* substrates. Solutions of methyl ortho-*p*-fluorobenzoate and *p*-fluorobenzaldehyde diethyl acetal in organic solvents were approximately 0.1 *M*. Shielding parameters reported are relative to fluorobenzene in the same environment and were calculated as described by Taft, *et al.*[7]

^{19}F chemical shifts were recorded at 56.4 MHz relative to external trifluoroacetic acid with a Varian DA 60 nmr spectrometer equipped with a Varian V4350A internal lock system. A Hewlett-Packard 200AB audio generator was used as the external lock frequency. Due to the low concentration of some samples, and hence the large number of sweeps to be made, an external sweep audio was used to replace that normally taken from the recorder. The external audio was generated from the C-1024 ramp using a Hewlett-Packard 5100B frequency synthesizer to convert the dc voltage sweep ramp to a 2600 to 2500 Hz ±1 Hz sweep range, that is a 100-Hz sweep width. All chemical shifts are from the most intense peak of the multiplets obtained in all cases. The resolving power of this system may be appreciated from inspection of Figure 1 in which a ^{19}F nmr spectrum of a dilute solution of methyl ortho-*p*-fluorobenzoate in aqueous methanol following 1347 sweeps is shown. Chemical shifts have not been corrected for bulk diamagnetic susceptibility effects, which are expected to be very small.

(1) Supported by Grant AM-08232 from the National Institutes of Health and Grant GB 8162 from the National Science Foundation.

(2) Career Development Awardee of the National Institutes of Health (Grant K3 GM 10-248-03). Fellow of the Alfred P. Sloan Research Foundation.

(3) (a) J. G. Fullington and E. H. Cordes, *Proc. Chem. Soc.*, 224 (1964); (b) M. T. A. Behme, J. G. Fullington, R. Noel, and E. H. Cordes, *J. Amer. Chem. Soc.*, 87, 266 (1965); (c) L. R. Romsted, R. B. Dunlap, and E. H. Cordes, *J. Phys. Chem.*, 71, 4681 (1967); (d) R. B. Dunlap and E. H. Cordes, *J. Amer. Chem. Soc.*, 90, 4395 (1968); (e) R. B. Dunlap and E. H. Cordes, *J. Phys. Chem.*, 73, 361 (1969); (f) R. B. Dunlap, G. A. Ghanim, and E. H. Cordes, *ibid.*, 73, 1898 (1969).

(4) (a) R. Haque, *J. Phys. Chem.*, 72, 3056 (1968); (b) J. C. Eriksson, A. Johansson, and L. O. Andersson, *Acta. Chem. Scand.*, 20, 2301 (1966), and references therein; (c) B. R. Donaldson and J. C. P. Schwarz, *J. Chem. Soc.* (Phys. Org. Sect.), 395 (1968); (d) N. Muller and R. H. Birkhahn, *J. Phys. Chem.*, 71, 957 (1967); N. Muller and B. H. Birkhahn, *ibid.*, 72, 583 (1968).

(5) T. H. Fife and L. K. Jao, *J. Org. Chem.*, 30, 1492 (1965).

(6) A. B. Scott and H. V. Tartar, *J. Amer. Chem. Soc.*, 65, 692 (1943).

(7) R. W. Taft, F. Prosser, L. Goodman, and G. T. Davis, *J. Chem. Phys.*, 38, 380 (1963).

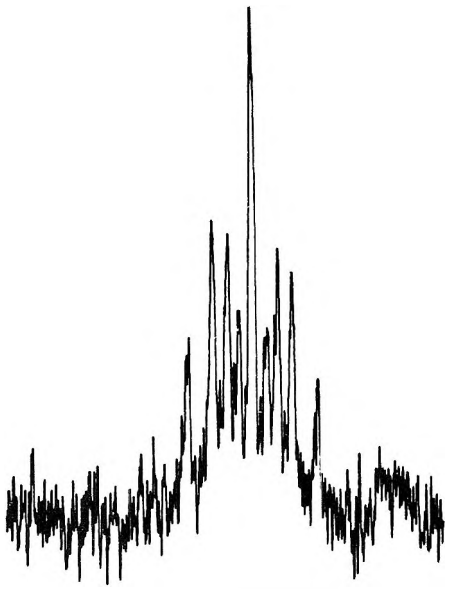

Figure 1. ^{19}F nmr spectrum of a dilute solution of methyl-*p*-orthofluorobenzoate in 15% methanol:85% water solution recorded following 1347 sweeps.

Results and Discussion

In Table I, ^{19}F chemical shifts for methyl ortho-*p*-fluorobenzoate and *p*-fluorobenzaldehyde diethyl acetal in a variety of organic solvents, water–methanol mixtures, and aqueous solutions of sodium dodecyl sulfate are collected. Both kinetic studies and molecular sieve chromatography have revealed that, at the concentrations of surfactant employed, these substrates are incorporated substantially completely into the micellar phase.[3b,d,f] In all cases involving partially aqueous media, the pH was maintained sufficiently high to prevent appreciable hydrolysis of either substrate during the time period necessary to make the experimental measurements.

While these data alone are inadequate to establish those factors most important in determining variability of chemical shift from solvent to solvent, they are consistent with an important contribution from hydrogen bond formation between protic solvent molecules and the ortho ester or acetal functions as one such factor. Note that most considerations suggest that the micellar surface has properties not unlike those of aqueous solution;[8] this would suggest that the substrates are localized at the micellar surface, not the micellar interior. Hydrogen bond formation between substrate and solvent can account for the nature of the shifts observed since such bonding will tend to deplete the aromatic system of electrons and, hence, reduce the screening at the fluorine nucleus. For atoms of the second row, including fluorine, the paramagnetic screening tensor is dominant and, to a first approximation, most other contributions to the chemical shift, such as anisotropy or electric field effects, can be neglected.[9]

Table I: ^{19}F Chemical Shifts for Methyl Ortho-*p*-fluorobenzoate and *p*-Fluorobenzaldehyde Diethyl Acetal for Several Solvent Systems

Solvent	Chemical Shifts, ppm[a]	
	Methyl ortho-*p*-fluorobenzoate	*p*-Fluorobenzaldehyde diethyl acetal
Hexane	36.42 (25)	37.55 (31)
Decane	37.67	...
Benzene	35.74 (25)	36.68
Pyridine	35.92	36.97
Triethylamine	36.06 (25)	37.34
n-Butylamine	36.49	37.64
N-Methylacetamide	36.22	37.45
2,4-Dimethylphenol	33.95 (26)	35.32
o-*t*-Butylphenol	34.04 (25)	34.68 (25)
Methanol	36.58	38.33
80% Aq. methanol[b]	36.19 (39)	38.12 (25)
60% Aq. methanol[b]	35.74 (40)	37.48 (25)
53% Aq. methanol[b]	35.64 (100)	...
47% Aq. methanol[b]	35.53 (100)	...
40% Aq. methanol[b]	...	36.72 (100)
30% Aq. methanol[b]	35.74 (768)	36.38 (435)
15% Aq. methanol[b]	35.23 (1347)	...
Dimethylformamide	...	37.82 (16)
Dimethyl sulfoxide	...	36.13
Acetone	...	38.44
0.1 *M* SDS[b,c]	33.88 (150)	35.82 (87)
0.1 *M* SDS, 0.01 *M* substrate	34.02 (110)	35.43 (1125)
0.075 *M* SDS, 0.0075 *M* substrate	34.10 (223)	35.57 (2106)
0.05 *M* SDS, 0.005 *M* substrate	34.02 (200)	...
0.10 *M* SDS, 0.005 *M* substrate	33.87 (301)	...

[a] All chemical shifts are upfield with respect to an external standard of neat trifluoroacetic acid. Number of sweeps of each spectrum is given in parentheses following chemical shift for those cases in which more than one sweep was employed. See the text for details of the measurement process. [b] Measured in the presence of 0.042 *M* sodium carbonate buffer. [c] SDS is sodium dodecyl sulfate. Measured in the presence of saturating concentrations of the substrates.

However, effects of solvent dielectric constant can be important.[9b]

In order to probe these points more thoroughly, we have extended measurements of chemical shifts to fluorobenzene and *para*-substituted fluorobenzenes containing weakly basic oxygen atoms capable of hydrogen bond formation with appropriate solvents, specifically *p*-fluorobenzaldehyde, *p*-fluoroacetophenone, and *p*-fluoroanisole. By focusing attention on shielding parameters with respect to fluorobenzene rather than on the chemical shifts themselves, Taft and his associates have demonstrated that specific interactions between solvent and substituent, including polar interactions, proton transfer equilibria, Lewis acid–base equilibria, and hydrogen bond formation, may be

(8) For a summary, see P. Mukerjee, *Advan. Colloid Interface Sci.*, **1**, 241 (1967).

(9) (a) M. Karplus and T. P. Das, *J. Chem. Phys.*, **34**, 1683 (1961). (b) J. W. Emsley and L. Phillips, *Mol. Phys.*, **11**, 437 (1966).

Table II: ^{19}F Chemical Shifts and Shielding Parameters for a Series of *para*-substituted Fluorobenzenes in a Variety of Organic Solvents and Aqueous Surfactant Solutions. Values Are Expressed in ppm Upfield from the External Lock Signal of Trifluoroacetic Acid[a]

Solvent	H	O ‖ CH	O ‖ CCH$_3$	OCH$_3$	C(OCH$_3$)$_3$	CH(OC$_2$H$_5$)$_2$
n-Hexane	35.05	26.35	28.72	46.67		
		8.70	6.33	−11.62	−1.37	−2.50
n-Octane	34.72	25.66	28.10	46.29		
		8.06	6.62	−11.57	...	...
Carbon tetrachloride	33.63	24.15	27.07	45.00		
		9.48 (9.40)	6.56 (6.60)	−11.37 (−11.50)	...	...
Benzene	34.88	25.62	28.37	46.36		
		9.26	6.51 (6.50)	−11.48 (−11.45)	−0.86	−1.8
Methanol	36.97	26.65	29.13	48.37		
		c	7.86 (7.65)	−11.40 (−11.45)	+0.40	−1.35
75% Aq. methanol	36.54	25.67	28.40	47.94		
		10.87 (10.50)	8.14 (8.50)	−11.40 (−11.20)	+0.35	−1.58
2,4-Dimethylphenol[b]	35.21	22.87	25.53	45.12		
		12.34	9.68	−9.81	+1.26	−0.10
Sodium dodecyl sulfate	35.23	23.35	26.85	47.34		
		11.88	8.38	−12.11	+1.19	−0.19
Dodecyltrimethylammonium bromide	34.47	23.71	26.45	45.51		
		10.76	8.02	−11.04	...	...
Dodecyldimethylammonia-propane sulfonate	34.33	23.79	26.54	45.41		
		10.54	7.79	−11.08	...	...

[a] All spectra were taken on solutions containing 0.01 *M* solute. Surfactants were present at a concentration of 0.2 *M* in the appropriate solutions. Shielding parameters are given directly below the chemical shift values. [b] Diluted 1:1 with carbon tetrachloride. [c] A rapid reaction took place.

identified.[10] Our choice of substrates and solvents attempts to focus attention specifically on the last of these effects since ability to form hydrogen bonds ought to clearly distinguish the micellar surface from the micellar interior.[9]

In Table II, ^{19}F chemical shifts and shielding parameters for the compounds of interest in various organic solvents and in aqueous solutions of an anionic, cationic, and zwitterionic surfactant are collected. Both the effect of electron-donating power of the substituent and the effect of solvent on the chemical shifts are consistent with previous findings.[10] Several of the values in Table II have previously been measured under similar conditions by Taft, *et al.*;[10c] satisfactory agreement between the two sets of values is generally found.

The data in Table II bear out the expectation that formation of hydrogen bonds between protic solvents and *para* substituents will cause the shielding parameters to become more positive. With *p*-fluoroacetophenone, for example, the shielding parameters in hexane, octane, carbon tetrachloride, and benzene vary within the limits 6.35 to 6.51. In methanol, in contrast, the value is 7.83, in 75% aqueous methanol, 8.16, and in 2,4-dimethylphenol, the strongest hydrogen bonding agent in this series, 9.68. Related results are obtained with the other substrates with the single exception of *p*-fluoroanisole, previously recognized as rather insensitive to solvent effects.[10c] Hydrogen bond formation, of course, may not account for the total effects observed.

The shielding parameters collected in Table II for the micellar solutions clearly bear out the conclusion that *para*-substituted fluorobenzenes occupy a site in the micellar phase in which hydrogen bond formation with the solvent can occur We can be certain that the fluorobenzenes are incorporated into the micellar phases both by analogy with the behavior of the ortho ester and acetal and from the observation that the surfactants solubilize these compounds. These observations are fully consistent with the proton nmr studies of Eriksson and Gillberg who concluded that molecules such as benzene and nitrobenzene are solubilized at the surface of cationic micelles while less polar materials such as cumene and cyclohexane are incorporated into the micellar interior.[11]

Finally, the shielding parameters of Table II suggest that the environment of organic substrates associated with micellar surfaces does depend on the nature of the micelle-forming surfactant. One might tentatively

(10) (a) D. Gurka, R. W. Taft, L. Joris, and P. von R. Schleyer, *J. Amer. Chem. Soc.*, 89, 5957 (1967), and references therein; (b) R. W. Taft, E. Price, I. R. Fox, I. C. Lewis, K. K. Andersen, and G. T. Davis, *ibid.*, 85, 3146 (1963); (c) R. W. Taft, E. Price, I. R. Fox, I. C. Lewis, K. K. Andersen and G. T. Davis, *ibid.*, 85, 709 (1963).

(11) J. C. Eriksson and G. Gillberg, *Acta Chem. Scand.*, 20, 2016 (1966).

conclude that the substrates are in a better hydrogen bonding environment on the surface of the anionic and cationic micelles than on the surface of the zwitterionic micelle. These data do suggest that a more extended investigation into the properties of the micellar surface employing fluorine magnetic resonance may yield information important for the interpretation of kinetic data for reactions occurring in micellar systems.

On the Interaction of Solute Molecules with Porous Networks

by A. G. Ogston

Department of Physical Biochemistry, John Curtin School of Medical Research, Australian National University, Canberra, A.C.T. Australia *(Received June 30, 1969)*

Giddings, Kucera, Russell and Myers[1] have given an elegant and penetrating account, on the basis of statistical mechanics, of "exclusion" interactions between rigid molecules and inert porous networks. Because the network is considered as *random* (whatever forms of surface compose it), their treatment does not appear to demand that it need also be *rigid*, since variation of the distribution of its elements with time would not affect the time-average of interactions of molecules with it. The treatment is not, therefore, so asymmetrical with regard to the distinction between "network" and "molecules" as might appear at first sight.

In such a context as gel chromatography, there is of course a very practical distinction between solute and gel. Nevertheless, the findings of Edmond, Farquhar, Dunstone and Ogston[2] and of Ogston and Silpananta[3] show that real cross-linked gels (specifically Sephadex) have thermodynamic properties, both in themselves and in their interactions with solute molecules, very similar to those of equivalent *solutions* of uncross-linked molecules. This opens the possibility of treating gel–solute interactions by the same (symmetrical) approach as is used for solute–solute interactions and, consequently, of comparing results obtained on both types of system by experimental methods appropriate to each.

A basis for this treatment is provided by Flory's[4] "dilute solution" theory; by this, the molecular covolume of a pair of molecules, whose interaction is purely entropic, can be identified with their *molar* second virial coefficient (interaction between like molecules) or the corresponding *molar* interaction coefficient (interaction between unlike molecules).[5] The chemical potentials of solutes vary with exponentials of the products of these coefficients and the relevant concentration.[5]

Molar covolumes are easily evaluated in simple cases.

(1). Sphere–Sphere. (The molecules have radii r_1 and r_2). The molar covolume is

$$U_{1,2} = \frac{4\pi}{3}(r_1 + r_2)^3 N \qquad (1)$$

(2) Sphere–Rod. (The sphere has radius r_1; the rod has cylindrical half-length l_2, cylindrical radius r_2, and hemispherical ends of radius r_2). The covolume is most simply obtained from the volume that the center of a sphere cannot enter, *i.e.*

$$U_{1,2} = \left\{2\pi(r_1 + r_2)^2 l_2 + \frac{4\pi}{3}(r_1 + r_2)^3\right\} N \qquad (2)$$

However, the same result can be arrived at (i) by considering the probability of placement of a sphere of radius $(r_1 + r_2)$ in a random arrangement of thin rods of length $2l_2$;[6] (ii) with rather greater difficulty, by considering the average limitation of the rotation of a rod whose center lies between $(r_1 + r_2)$ and $(r_1 + r_2 + l_2)$ from the center of a sphere; or (iii) by considering the rod to be generated by movement of a sphere of radius r_2 through distance $2l_2$ in a random distribution of spheres of radius r_1. (It can be shown that the probability of "collision" in this case, for unit swept volume, is the same as for the infinitesimal radial expansion of a sphere of radius r_2, so that the argument of ref 6 can be applied). The last method is of special interest because it shows that the movement of the sphere need not be rectilinear; therefore, the "rod" need not be straight or stiff, provided that multiple exclusion of a sphere by parts of the same rod does not occur.

(3) Rod–Rod. (Each rod is as in *2*, with radii r_1, r_2 and cylindrical half-lengths l_1, l_2). Route 2 (ii) could no doubt be followed in this case also, though with greater difficulty still, but it is easily solved by route (iii). One rod is considered to be generated by movement through distance $2l_1$ of a sphere of radius $(r_1 + r_2)$ in a random suspension of thin rods of length $2l_2$. Application of the argument of ref 6 then leads directly to

$$U_{1,2} = \left\{2\pi(r_1 + r_2)l_1 l_2 + 2\pi(r_1 + r_2)^2(l_1 + l_2) + \frac{4\pi}{3}(r_1 + r_2)^3\right\} N \qquad (3)$$

Equation 3 is (like expression 1) symmetrical, as it should be. Putting $l_1 = 0$ reduces eq 3 to eq 2, and putting l_2 also $= 0$, reduces eq 2 to eq 1. Putting $r_1 =$

(1) J. C. Giddings, E. Kucera, C. P. Russell, and M. N. Myers, *J. Phys. Chem.*, **72**, 4397 (1968).

(2) E. Edmond, S. Farquhar, J. R. Dunstone, and A. G. Ogston, *Biochem. J.*, **108**, 755 (1968).

(3) A. G. Ogston and P. Silpananta, *ibid.*, in press.

(4) P. J. Flory, "Principles of Polymer Chemistry," Cornell University Press, Ithaca, N. Y., 1953.

(5) E. Edmond and A. G. Ogston, *Biochem. J.*, **109**, 569 (1968).

(6) A. G. Ogston, *Trans. Faraday Soc.*, **54**, 1754 (1958).

r_2 and $l_1 = l_2$ gives the covolumes for self-interaction of spheres or rods. These expressions should also hold good for systems in which rods are cross-linked to form a gel, provided that the randomness of their distribution is unaffected and that the cross links themselves do not contribute significantly to the exclusion.

A fascinating consequence of these expressions is that they show that any system of two solutes which interact only entropically will satisfy the conditions for "incompatible" phase separation provided only that the molecules are of different size. This condition is[5]

$$\mu_{11}\,\mu_{22} - \mu^2_{12} < 0$$

With spheres, for example, this condition is satisfied by the algebraically necessary condition

$$(2r_1)^3(2r_2)^3 - (r_1 + r_2)^6 < 0$$

which depends only on the ratio r_1/r_2, not on their absolute magnitude. Similar relationships can be shown to hold for the sphere–rod and rod–rod cases. Ogston and Silpananta[3] have shown that incompatible phase separation occurs in a Sephadex–polyethylene glycol system under conditions similar to those under which it occurs in a dextran–polyethylene glycol system.

An Electron Spin Resonance Study of Acetate Dianion and Acetamide Anion[1]

by Michael D. Sevilla

Atomics International Division of North American Rockwell Corporation, Canoga Park, California 91304
(Received June 30, 1969)

Reactions of the electron with amino acids and dipeptides are under investigation in this laboratory through use of electron spin resonance (esr) spectroscopy.[2] To elucidate the structure of the anion radicals formed it was desirable to investigate model compounds for these systems. Acetate ion and acetamide were chosen because the acetate dianion should have a π-electronic structure similar to anions of amino acids[3] and the acetamide anion should closely approximate the electronic structure of an anion of the peptide bond. These species were prepared through electron attachment in an alkaline glass. They are found to exhibit interesting properties owing to restricted rotation of their methyl groups which are described in this note.

Experimental Section

The experimental procedure was essentially that of Ayscough, Collins, and Dainton[4] as modified by Holroyd and Glass.[5] In this method a deoxygenated 8 N NaOD (92% D_2O) solution containing 5 mM $K_4Fe(CN)_6$ and 1–10 mM solute is cooled to 77°K. The glass formed is photolyzed with 2537-Å uv light at 77°K for approximately 1 min. The photolysis produces a dark blue color due to the electron. At this point, an esr spectrum is taken of the sample to ensure that photolysis of the organic solute is minimal. The sample is then photobleached at 77°K with light from an infrared lamp for approximately 4 min. The electrons become mobile, attach to the solute, and the esr spectrum of the anion can be then observed.

A Varian V4510 esr spectrometer equipped with a dual cavity and Fieldial magnetic field regulator was employed in this work. Measurements of hyperfine splittings and g values were made *vs.* potassium peroxylamine disulfonate (A_N = 13.0 G and g = 2.0056).

Results

Photolysis of the deuterated alkaline glass containing sodium acetate (10 mM) produces mainly the electron. Photobleaching results in a radical whose esr spectrum shows a large doublet splitting (*ca.* 27 G) (Figure 1a). A small amount of methyl radical is formed in the

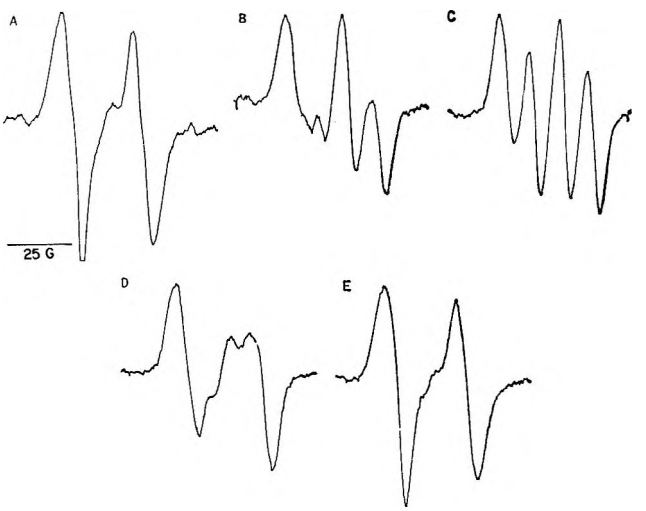

Figure 1. First derivative esr spectra of the acetate dianion in a deuterated alkaline glass at various temperatures: A, spectrum taken immediately after photobleaching, T = 85°K. (The very weak outer lines are due to the methyl radical); B, spectrum after warming to 150°K; C, spectrum at 180°K; D, spectrum after cooling to 150°K; E, spectrum at 85°K. After first warming to 180°K repeated cycling results in reproducible spectra.

(1) This work was supported by the Division of Biology and Medicine of the U. S. Atomic Energy Commission.

(2) M. D. Sevilla, Abstracts, The 158th National Meeting of the American Chemical Society, New York, N. Y., 1969.

(3) (a) J. W. Sinclair and M. W. Hanna, *J. Phys. Chem.*, **71**, 84 (1967); (b) P. B. Ayscough and A. K. Roy, *Trans. Faraday Soc.*, **64**, 582 (1968).

(4) P. B. Ayscough, R. G. Collins, and F. S. Dainton, *Nature*, **205**, 965 (1965).

(5) R. A. Holroyd and J. W. Glass, *Int. J. Radiat. Biol.*, **14**, 445 (1968).

photolysis.[6] Photobleaching results in no increase in the methyl radical concentration; thus, this species is not produced by a reaction of the electron. Upon warming the sample, the doublet spectrum changes gradually (Figure 1b) until at 180°K it appears as a quartet whose lines have approximately the same intensity (Figure 1c).[7] Cooling the sample after initially warming to 180°K does not reproduce the line intensities in the intermediate temperature region (Figure 1d); however, at 85°K a doublet splitting, 26.5 G, similar to that initially formed is found (Figure 1e). After this first annealing of the sample repeated cycling of the temperature between 85 and 180°K results in reproducible spectra at each temperature identical with those found in Figures 1c, d, and e. Increasing the temperature to 190°K results in a loss of the esr signal.

The results for acetamide are shown in Figure 2. The results are similar to those found for "annealed" samples of sodium acetate. Photolysis again produces electrons and only a small amount of methyl radical. Photobleaching at 77°K results in a radical whose esr spectrum at 85°K consists of a large 30.8-G doublet splitting. Warming the sample to 180°K produces a 13.5-G quartet in the intensity ratio 1:3:3:1. At intermediate temperatures (85°K $< T <$ 180°K) a gradual change from doublet to quartet is observed (Figures 2b, c) which is reversible. Again at temperatures near 190°K, the esr signal is lost.

At 180°K the g values of acetate dianion and acetamide anion are 2.0032 ± 0.0003 and 2.0030 ± 0.0003, respectively.

Preparation of samples of acetate and acetamide in alkaline H_2O solutions results in spectra with larger line widths. At lower temperatures both species show resolved doublets with splittings similar to those found in D_2O solutions. At 180°K the spectrum of acetamide anion appears as a singlet, $\Delta H_{m.s.} \simeq 35$ G, while that of acetate dianion is only partially resolved.

Discussion

The results show that reaction with the electron at 77°K produces the acetate dianion and acetamide anion. Further, the doublet spectra at 85°K show that the methyl groups of these anions are not free to rotate rapidly at this temperature and can be considered locked in a spatial configuration corresponding to a potential minimum so as to produce one large splitting. The spectra at 180°K indicate that the methyl groups are rotating more rapidly. The results are complicated by the change in line intensities noted in the spectra of acetate dianion before and after annealing. This is considered to be due to either a relaxation of the acetate molecular framework to a more stable configuration accompanied by an adjustment in the electronic wave function[8] or a change in the nature of the alkaline glass immediately about the dianion to accommodate the extra negative charge. The fact that this effect was not found for acetamide anion argues against the latter. Further discussion of the results found for the acetate dianion after annealing and acetamide anion is given below.

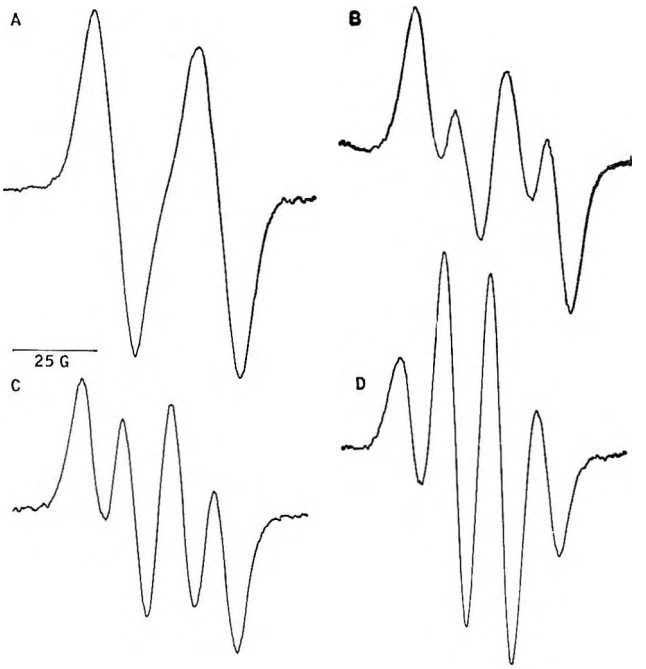

Figure 2. First derivative esr spectra of the acetamide anion in a deuterated alkaline glass at various temperatures: A, 85°K (the weak methyl radical signal has been removed by warming); B, 133°K; C, 146°K; D, 180°K.

The orientation of the methyl group protons in the locked configuration found at 85°K can be determined by recourse to relation (1) which describes the β-proton splitting, A_β^H, as a function of angle[9]

$$A_\beta^H(\theta) = B_0\rho^\pi + B_2\rho^\pi\cos^2\theta \qquad (1)$$

where B_0 and B_2 are empirical constants with $B_2 \gg B_0$, ρ^π is the spin density in the p_z orbital of the π-carbon atom, and θ represents the dihedral angle between the z axis of the p_z orbital and the alkyl C–H bond axis. The doublet spectrum observed would result only if the three methyl protons were at angles near 0, 120, and 240°. This would produce a large splitting for the proton at $\theta = 0°$ and two small (apparently unresolved) splittings for the protons at $\theta = 120$ and 240°.

As the temperature is increased above 85°K, the

(6) Since a small amount of dianion was also produced in this step the formation of methyl radicals could be due to uv photolysis of $CH_3CO_2^{2-}$.

(7) The signal due to the methyl radical is lost as the sample is warmed. Experiments in which a high concentration of methyl radicals was produced by photolysis of the dianion yielded an esr spectrum of the $\cdot CH_2CO_2^-$ radical upon warming to 180°K. This species proved to be more stable than the dianion and could be observed free from the dianion.

(8) A similar phenomenon found in irradiated crystalline alanine (ref 3a) also has been explained in terms of a change in hybridization.

(9) See M. D. Sevilla and G. Vincow, *J. Phys. Chem.*, **72**, 3647 (1968), and references therein.

methyl group undergoes increasingly rapid reorientation between potential minima until in the case of acetamide anion at 180°K, "free" rotation occurs (rapid reorientation in comparison to the hyperfine splitting in cycles per second). In the case of acetate dianion, the methyl group does not rapidly reorient even at 180°K. Consequently, observed line intensities for acetate at 180°K are similar to those for acetamide anion at 146°K. By comparison to the acetamide anion spectral behavior, the splitting for a freely rotating methyl in the acetate dianion is estimated to be 11.8 G.[10]

The lack of resolution of the two protons at 120 and 240° in the low-temperature spectrum of both anions can be understood by first solving for values of $B_0\rho^\pi$ and $B_2\rho^\pi$ using eq 1 and the experimental splittings for the "locked" and "freely" rotating cases. The assumption is made that there is no significant temperature dependence in $B_0\rho^\pi$ and $B_2\rho^\pi$. It is found that $B_0\rho^\pi \cong -3.2$ and $B_2\rho^\pi \cong 29.4$ for acetate dianion, and $B_0\rho^\pi \cong -3.8$ and $B_2\rho^\pi \cong 34.6$ for the acetamide anion. The calculated splittings of the protons at 120 and 240° in the low-temperature case are then +3.9 G (acetate) and +4.8 G (acetamide), values which are well within the observed line width of 10 and 13 G, respectively.

Since theoretical spin densities are essential to the computation of theoretical values of the methyl proton splittings for comparison to experiment, McLachlan SCF–MO calculations were performed for the acetate and acetamide radical ions (Table I).[11] The effect of the methyl group is simulated by the use of typical hyperconjugation parameters and a small inductive effect. The results of this calculation are given in Table I. The coulomb (h) and resonance (k) parameters employed are: $k_{\dot{C}-O} = (k_{C-O} + k_{C=O})/2 = 1.2$, $k_{C=O} = 1.6$, $h_O = 1.5$, $k_N = 0.8$, and $h_N = 1.5$.[12] Moderate changes in these parameters are not found to affect the spin density distribution significantly. For example, a value of $h_O = 2.5$ instead of 1.5 raised ρ_3^π by only 0.09 for acetate dianion. Two methods are available to obtain theoretical methyl splittings for comparison with experiment. First the spin density on the carboxyl carbon, ρ_3^π can be used to estimate the methyl group hyperfine splittings for free rotation assuming a relation of the form $A_{CH_3}^H = Q_{CH_3}\rho_3^\pi$ where $Q_{CH_3} \cong 20$ G.[13] Second, the methyl proton hyperfine splitting can also be calculated from the spin density in the pseudo-π orbital composed of a linear combination of methyl hydrogen 1s orbitals, by use of the relation $A_{CH_3}^H = 217\rho_H^\pi$.[14] For acetate dianion it is found that $A_{CH_3}^H = 13.9$ and 14 G for the first and second calculation, respectively. The results for acetamide anion are slightly lower, 13.7 and 13.8 G. The two types of calculations are in excellent agreement with one another and in reasonable agreement with experiment. Thus the calculated and "experimental" spin density distributions should also be in reasonable agreement.

Table I: McLachlan Spin Density Calculations[a]

Position	Acetate dianion	Acetamide anion
	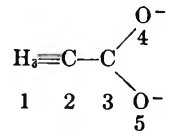	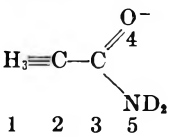
1	0.0646	0.0636
2	−0.032	−0.033
3	0.693	0.685
4	0.137	0.228
5	0.137	0.057

[a] Hyperconjugation parameters used were: $h_1 = 0.5$, $h_2 = -0.10$, $h_3 = -0.10$, $k_{12} = 2.5$, $k_{23} = 0.9$.

The spectra of acetamide anion show no resolution of nitrogen hyperfine splittings whether isotropic or anisotropic. This is explained by the spin density calculations which predict only a small spin density and consequently a small splitting for nitrogen. The deuteriums bonded to nitrogen of course should give rise to negligible hyperfine splittings.

The results found in this work show that anions can be made of small molecules quite easily. Further, they show that by a suitable choice of the molecular species and use of a deuterated alkaline glass, esr spectra can be obtained which are well resolved and easily interpretable.

Radicals structurally related to acetate dianion have been reported as products of the radiolysis of acetic acid[15] and a number of other carboxyl-containing compounds.[16] A protonated acetate dianion was reported in the radiolysis study of acetic acid at 77°K. The results found for this species are in good agreement with those found here but suggest a moderate effect of the protonation (and dimerization) on the methyl proton hyperfine splitting. The acetate dianion has also been reported as a product of the radiolysis of sodium acetate;[17] however, the species observed has been shown to

(10) The spectra in the intermediate temperature range between the locked and freely rotating cases can be understood in terms of the effect of hindered rotation on line widths and splittings of methyl groups. See J. H. Freed, *J. Chem. Phys.*, **43**, 1710 (1965), and references therein for quantum mechanical and classical treatments of this phenomenon.

(11) A. D. McLachlan, *Mol. Phys.*, **3**, 233 (1960).

(12) (a) A. Streitwieser, "Molecular Orbital Theory for Organic Chemists," John Wiley & Sons, Inc., New York, N. Y., 1962, p 135. (b) G. Vincow in "Radical Cations," E. T. Kaiser and L. Kevan, Ed., Interscience, New York, N. Y., 1968, p 175.

(13) Reference 12b, p 165.

(14) (a) D. Lazdins and M. Karplus, *J. Chem. Phys.*, **44**, 1600 (1966); (b) D. H. Levy, *Mol. Phys.*, **10**, 233 (1966).

(15) I. Miyagawa and W. Gordy, *J. Amer. Chem. Soc.*, **83**, 1036 (1961).

(16) J. Sinclair and M. W. Hanna, *J. Chem. Phys.*, **50**, 2125 (1969), and references therein.

(17) D. G. Cadena, V. Mendez, and J. R. Rowlands, *Mol. Phys.*, **13**, 157 (1967).

be the methyl radical through ^{13}C substitution studies.[18,19] Up to the present time neither the acetate dianion nor the acetamide anion have been shown to be products of the radiolysis of sodium acetate and acetamide. Since these anions would be expected to be products of radiolysis, the results reported here should aid in their future identification.

(18) M. T. Rogers and L. D. Kispert, *J. Chem. Phys.*, 46, 221 (1967).

(19) M. T. Rogers and L. D. Kispert in "Radiation Chemistry," Advances in Chemistry Series, No. 82, American Chemical Society, Washington, D. C., 1968, p 327.

Ultrasonic Attenuation in Aqueous Triethylamine

by Robert Scott Brundage and Kenneth Kustin

Department of Chemistry, Brandeis University, Waltham, Massachusetts 02154 *(Received July 7, 1969)*

We wish to report on a new design for a small acoustic attenuator using the pulse technique and the determination of the rate constants for the reaction

$$(C_2H_5)_3N \cdot H_2O \underset{k_{-b}\ (M^{-1}\ sec^{-1})}{\overset{k_b\ (sec^{-1})}{\rightleftharpoons}} (C_2H_5)_3NH^+ + OH^- \quad (1)$$

by this method.

Apparatus

The application of ultrasonic attenuation to chemical systems for the purpose of measuring rate constants has been described, from theoretical and practical viewpoints, by Eigen and De Maeyer.[1] Of the various methods that have been, or may be, used in this technique, the pulse method was chosen because it appears to work best throughout a greater frequency range than any other ultrasonic method.[2] Essentially, the method works as follows (Figure 1). A power pulser forms the main signal which is sent into the transmitting side of the cell (T). There, it is partially absorbed by the liquid sample and then reemitted from the receiver side (R), as an attenuated pulse. This signal can be observed directly on a suitable oscilloscope (7–60 MHz). This type of broad amplification detection becomes severely limited with increasing frequency.[2] Therefore, the higher frequency signals are sent into a tuned heterodyne amplifier–rectifier and then detected. A signal generator then feeds a comparison signal of identical frequency and similar shape to the amplifier after a distinctly well-separated time interval. The variable attenuator controlling the size of this comparison signal yields measurements independent of amplifier nonlinearities.[3]

The most serious losses of signal occur within the sample cell. Of utmost concern is that the sound

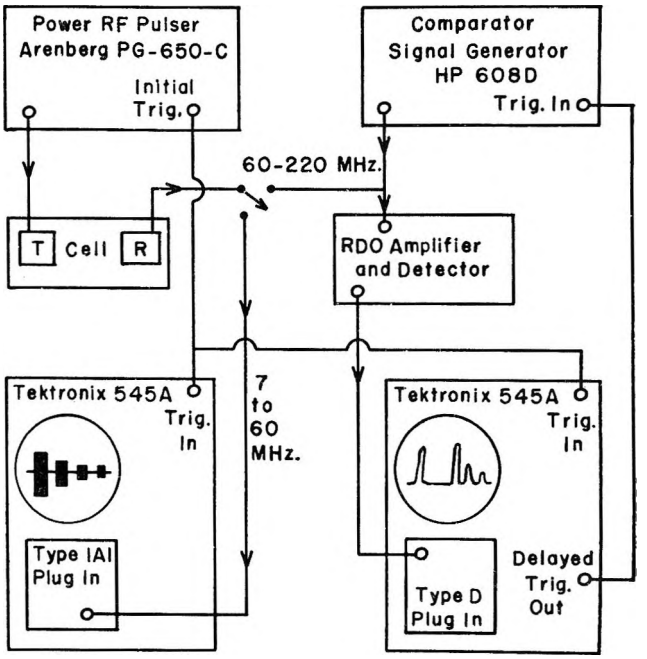

Figure 1. Electronic components for pulse technique.

wave plane must intersect the receiving crystal within an error of parallelism between transmitting and receiving crystals equivalent to one-third of a wavelength. The necessary alignment is usually obtained by adjusting a set of screws referenced to a fixed plane.[4–6] A simpler alternative arrangement is an optical bench, with free, separately housed transducers (Figure 2). An earlier arrangement using free housings did not employ an optical bench with that arrangement's inherent advantages in achieving parallelism.[7]

Accuracy can be readily calculated once the tolerances of the machining are determined. The over-all parallelism of the milling of the trough sides, the turning of the cylinders, and the boring of the quartz window hole could be done to nearly a mil over several inches at the Brandeis University machine shop. To ensure mutual parallelism of 10^{-4} radian between the transmitter and receiver transducers, 2.5-in. housings were chosen. This machining error leaves a play of another 3×10^{-4} radian or 1 min for the perpendicularity of the quartz windows which are commercially available within this degree of accuracy from the Dell Optical Co.

(1) M. Eigen and L. De Maeyer in "Technique of Organic Chemistry," Vol. VIII, part II, 2nd ed, A. Weissberger, Ed., Interscience, New York, N. Y., 1963, p 895 (see pp 952 and 1005).

(2) F. Eggers and K. Kustin in "Fast Reactions," K. Kustin, Ed., Academic Press, New York, N. Y., 1969.

(3) For more details, see R. S. Brundage, Ph.D. Thesis, Brandeis University, 1969.

(4) R. N. Barfield and W. G. Schneider, *J. Chem. Phys.*, 31, 488 (1959).

(5) S. S. Yun, R. T. Beyer, and M. W. Dill, *ibid.*, 36, 2737 (1962).

(6) J. H. Andreae, R. Bass, E. L. Heasell, and J. Lamb, *Acustica*, 8, 131 (1958).

(7) J. R. Pellam and J. K. Galt, *J. Chem. Phys.*, 14, 608 (1946).

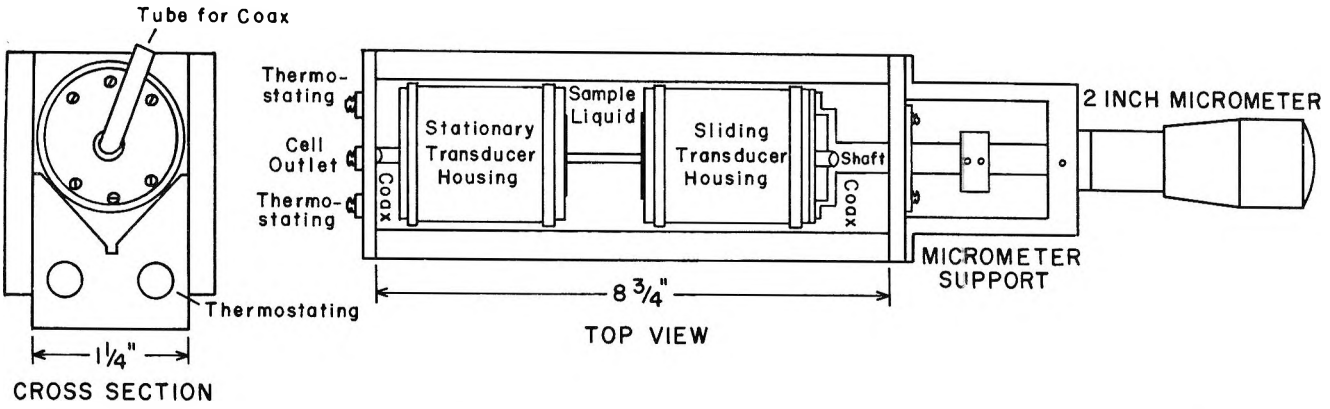

Figure 2. Diagram of ultrasonic absorption cell. The 1.25-in. stainless steel stock for the "V-block" bed must be carefully annealed to prevent warping. The "V" is milled in one operation, using the face and side of a large tool. The 2.5-in. long cylindrical housings, also annealed, were each bored and faced in the same chucking to ensure parallelism.

One cylinder was constructed with freedom to rotate to cancel equivalent nonparallelism between the two window pieces. Consequently, the over-all accuracy approaches the best attained in an ultrasonic absorption cell.[8]

An additional advantage of this design is its relatively small sample size, requiring about 100 ml of liquid. This volume can be reduced by a third or more with suitable fillers at each end. It is also relatively easy to change transducer crystals since they are automatically aligned against the inside window faces.

The simplest system to use for calibration purposes is pure water, for which there are no chemical relaxation processes in the frequency range covered by this apparatus. In this case the quotient α/f^2, where α is the acoustic attenuation coefficient (nepers per centimeter) and f is frequency (Hertz), should be equal to a constant, as shown by the data in Table I.

Table I: Ultrasonic Absorption Readings of Water at 25°

f, MHz	$\alpha/f^2 \times 10^{17}$, nepers sec²/cm	f, MHz	$\alpha/f^2 \times 10^{17}$, nepers sec²/cm
18.7	22.7	115.3	21.0
30.7	21.9	127.3	21.3
42.9	22.2	140.5	21.6
55.2	22.5	151.5	22.1
66.9	21.4	163.7	21.0
78.9	21.6	176.0	20.9
91.2	21.2	220	21.1
103.2	22.1	Av	21.6 ± 2.3%

Further comparison of the water data with known values indicates wavelength and frequency accuracies of 1%. A trial system of aqueous ammonia was chosen as a further calibration of the apparatus. Curves of

$$(\alpha\lambda)_{chem} = (\alpha\lambda)_{solution} - (\alpha\lambda)_{water} = \text{constant} \times \omega\tau/(1 + \omega^2\tau^2) \quad (2)$$

($\alpha\lambda$ is the attenuation coefficient per wavelength λ, $\omega = 2\pi f$ (radians per second), and τ is the relaxation time (second)) expected for a single relaxation process, were obtained, yielding positions and sizes of relaxation peaks, as well as an $\alpha\lambda$ accuracy, which agrees well with the measurements by Tamm, *et al.*[9] In addition to a measurement of relaxation maxima, from which the pertinent rate constants may be found, the $\alpha\lambda$ values also yield the standard volume change, $\Delta V°$, for the reaction.[10] This value, although less accurately determined by ultrasonic measurements in the case of ammonia than are the kinetic data, is also in reasonable agreement with ref 10.

Kinetics of the Aqueous Triethylamine Dissociation Equilibrium

The kinetics of OH^- binding to triethylammonium ion Et_3NH^+ is of interest because the attack is hindered by steric compression in comparison to ammonium ion. Nuclear magnetic resonance techniques were recently used in *acidic* solutions of triethylammonium ion to determine rates of proton exchange, from which the rate constants of eq 1 could be calculated.[11] The relaxation spectra of the attenuation of ultrasound in *basic* solutions provide a direct measure of the rate constants for the hydroxide reaction.

The experimental procedure for determining τ was to distil a stock sample of Et_3N and prepare an aqueous solution. A Corning Model 12 pH meter was used to determine the pH, which was measured before and after the acoustic experiment, and proved to be relatively constant during this time. The $(\alpha\lambda)_{chem}$ plots, according to eq 2, shown in Figure 3 yield the relaxation times.

Analysis of eq 1 without activity coefficients did not

(8) J. L. Hunter and H. D. Dardy, *J. Acoust. Soc. Amer.*, 36, 1914 (1964).

(9) K. Tamm, G. Kurtze, and R. Kaiser, *Acustica*, 4, 380 (1954).

(10) M. Eigen, *Z. Phys. Chem.* (Frankfurt am Main), 1, 176 (1954).

(11) E. K. Ralph, III, and E. Grunwald, *J. Amer. Chem. Soc.*, 89, 2963 (1967).

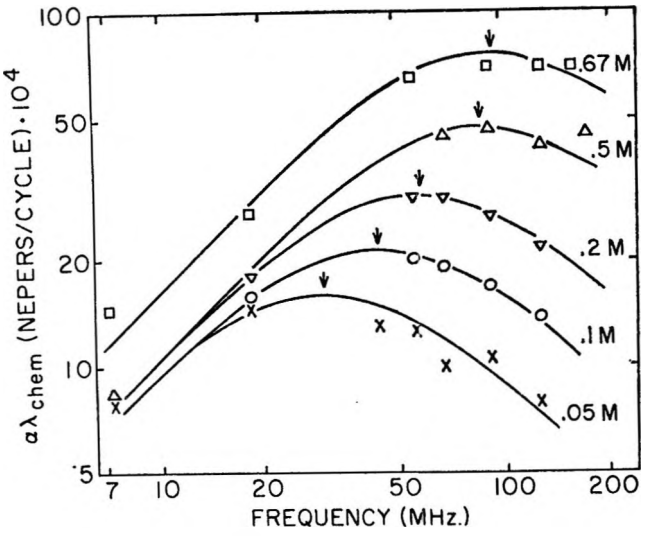

Figure 3. Ultrasonic absorption in aqueous triethylamine at 25°: ×, 0.05 *M*, 34 MHz, 1505 m/sec; ○, 0.1 *M*, 46 MHz, 1510 m/sec; ▽, 0.2 *M*, 60 MHz, 1520 m/sec; △, 0.5 *M*, 85 MHz, 1545 m/sec; □, 0.67 *M*, 93 MHz, 1565 m/sec.

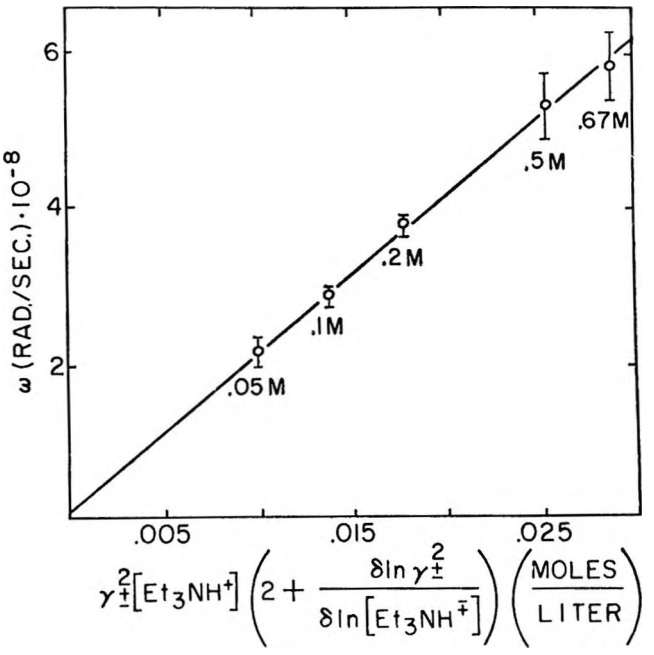

Figure 4. Concentration dependence of acoustic absorption maxima according to eq 3. The slope of this line is $k_{-b}°$ and the intercept is $k_b°$.

lead to self-consistent rate constants for all the data points nor was the quotient of the forward and reverse rate constants in agreement with the independently determined dissociation constant.[11] The ionic strength of these solutions shows a strong variation, going from essentially zero to about 0.025 *M*. The activity coefficients for the species in these solutions are known from potentiometric data.[11] The result, using the standard treatment for obtaining relaxation times, is[12]

$$1/\tau = k_{-b}°\gamma_{\pm}^2[Et_3NH^+]\left(2 + \frac{\partial \ln \gamma_{\pm}^2}{\partial \ln [Et_3NH^+]}\right) + k_b° \quad (3)$$

where $k_b°$ and $k_{-b}°$ are the rate constants at zero ionic strength, $\gamma_{\pm}$ is the mean activity coefficient, and the other symbols have their usual meaning. Figure 4 is a plot of the experimental values for eq 3. The straight line is based on a standard least-squares analysis of these values. The slope of this line is $k_{-b}°$ and the intercept is $k_b°$. The results at 25° are

$$k_{-b}° = (2.03 \pm 0.08) \times 10^{10}\ \text{sec}^{-1}\ M^{-1}$$

$$k_b° = (8 \pm 6) \times 10^6\ \text{sec}^{-1}$$

so that

$$K_B° = k_b°/k_{-b}° = (4 \pm 3) \times 10^{-4}\ M$$

These results corroborate the nmr and differential potentiometric values. Also, $\Delta V°$ was calculated to be -20 ± 2 cm³/mol.

Pure triethylamine has been studied by ultrasound to observe structural transitions, first at atmospheric pressure[13] and then to 3000 atm, yielding less than 5% variation of the 90-MHz relaxation peak.[14] Highly concentrated solutions of the triethylamine have been further investigated by McKellar and Andreae in an attempt to determine the mechanism of an absorption of similar magnitude.[15,16] The present study in dilute aqueous medium explained the presence of a single relaxation peak by relating it to reaction 1.

The rate constants of protolytic reactions have been reviewed by Eigen, *et al.*[17] Although the combination of hydroxide ion with a protonated amine base is generally diffusion controlled, interesting variations occur with differently substituted amine bases. In particular, a monotonic decrease in k_{-b} would be anticipated for the series NH_4^+ to $(CH_3)_3NH^+$. However, the formation of H bonds, which would effectively increase the minimum encounter distance, compensates to some extent for the loss of binding sites. Steric hindrance, which retards the rate of proton transfer,[11] is more pronounced for triethylamine than for trimethylamine. Nevertheless, the k_{-b} rate constants are $3.4 \times 10^{10}\ M^{-1}\ \text{sec}^{-1}$ (20°) for NH_4^+,[8] and $2.1 \times 10^{10}\ M^{-1}\ \text{sec}^{-1}$ (20°) for $(CH_3)_3NH^+$.[17] At 25° these rate constants would be slightly larger, indicating only a small additional retarding effect on the rate of hydroxide ion recombination by increasing the size of the aliphatic substituted group.

(12) J. Stuehr and E. Yeager in "Physical Acoustics," Vol. 2A, W. P. Mason, Ed., Academic Press, New York, N. Y., 1965, p 387.

(13) E. L. Heasell and J. Lamb, *Proc. Roy. Soc.*, A237, 233(1956).

(14) T. A. Litovitz and E. H. Carnevale, *J. Acoust. Soc. Amer.*, 30, 134, 610 (1958).

(15) J. F. McKellar and J. H. Andreae, *Nature*, 195, 778 (1962).

(16) D. Sette, *Nuovo Cimento, Ser. 10*, 1, 800 (1955).

(17) M. Eigen, W. Kruse, G. Maass, and L. De Maeyer, *Progr. Reaction Kinetics*, 2, 287 (1964); (see Table 2, p 308).

Acknowledgment. We gratefully acknowledge partial support from Public Health Service Research Grant GM-08893-07 from the National Institute of General Medical Sciences, Public Health Service.

Retention of Configuration during Recoil Tritium Reactions at Asymmetric Carbon Positions in 2,3-Dichlorobutane[1]

by Yi-Noo Tang, C. T. Ting, and F. S. Rowland

Department of Chemistry, University of California, Irvine, California 92664 *(Received July 15, 1969)*

One of the most important, and common, reactions of energetic tritium atoms from nuclear recoil is the substitution for hydrogen in a C–H bond, as in eq 1.[2-5] Earlier experiments have demonstrated that this substitution at an asymmetric carbon atom is accompanied by retention of optical configuration in both the crystalline and gaseous phases.[6-9] However, the experimental procedures have generally involved (a) numerous chemical reactions and separations and (b) sufficiently high specific radioactivity to permit measurement following all of these steps, together with the heavy radiation damage that accompanies such high specific activity. Consequently, measurements have been performed on very few systems, and confirmatory experiments with other systems are thus desirable.

$$T^* + RH \longrightarrow RT + H \qquad (1)$$

The most significant of the previous experiments have involved the reactions of recoil tritium atoms with an optically active molecule, addition of both *d*- and *l*-carriers, optical resolution of the *dl* mixture, and degradation of each to determine the intramolecular distribution of tritium activity.[6-9] Target molecules containing two or more asymmetric carbon atoms substitute the much simpler chemistry involved in the separation of diastereomers for the resolution of optical isomers. Since the *meso* and *dl* forms of 2,3-dichlorobutane (DCB) can be readily separated and analyzed by radio gas chromatography,[10] the experiments can be carried out with lower radiation damage (and specific activity) in the sample. We have carried out a series of experiments in all three phases designed to measure the retention–inversion characteristics of the recoil tritium substitution reaction with these molecules. The experiments have not involved actual determination of the intramolecular location of the tritium in 2,3-DCB.

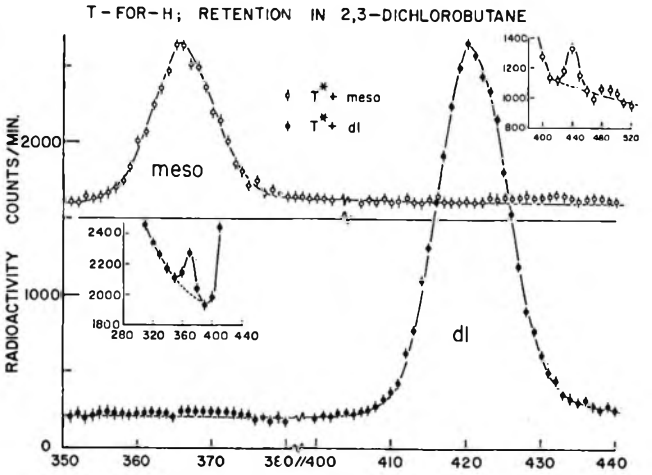

Figure 1. Radio gas chromatograms of tritiated 2,3-dichlorobutane-*t* molecules from reactions of recoil tritium with 2,3-dichlorobutane in 1,3-butadiene plus O_2-scavenged gas phase experiments. Upper diagram (displaced upward by 1500 cpm); T* + *meso*-DCB; Lower diagram, T* + *dl*-DCB; insets, same chromatograms with counts summed over 10-min intervals.

Experimental Section

The *dl* and *meso* forms of 2,3-DCB were prepared by low-temperature stereospecific addition of Cl_2 to *trans*- and *cis*-2-butene, respectively, and were then purified further by preparative glpc. The measured macroscopic *meso* content of *dl* samples, *after* irradiation, was approximately 0.5% for condensed phase samples, and less than 0.1% for gas samples. Neutron irradiations were performed on liquid phase samples of DCB in capillaries containing LiF powder and on gaseous samples with ^3He as the tritium source.[2-5] Enough argon was added to the gas-phase samples to minimize losses of activity by recoil into the walls.

The irradiated samples were analyzed in the usual manner by radio gas chromatography, without any special difficulties.[11] The *meso*- and *dl*-2,3-DCB peaks separate very satisfactorily on a 35-ft tritolyl phosphate column, as shown in Figure 1.

(1) This research was supported by A. E. C. Contracts No. AT-(11-1)-407 and AT-(11-1)-34, Agreement No. 126.

(2) R. Wolfgang, *Progr. Reaction Kinetics*, **3**, 97 (1965).

(3) R. Wolfgang, *Ann. Rev. Phys. Chem.*, **16**, 15 (1965).

(4) F. Schmidt-Bleek and F. S. Rowland, *Angew. Chem., Int. Ed.*, **3**, 769 (1964).

(5) "Chemical Effects of Nuclear Transformations," Vol. 1 and 2, International Atomic Energy Agency, Vienna, 1965.

(6) F. S. Rowland, C. N. Turton, and R. Wolfgang, *J. Amer. Chem. Soc.*, **78**, 2354 (1956).

(7) H. Keller and F. S. Rowland, *J. Phys. Chem.*, **62**, 1373 (1958).

(8) J. G. Kay, R. P. Malsan, and F. S. Rowland, *J. Amer. Chem. Soc.*, **81**, 5050 (1959).

(9) M. Henchman and R. Wolfgang, *ibid.*, **83**, 2991 (1961).

(10) C. M. Wai and F. S. Rowland, *J. Phys. Chem.*, **71**, 2752 (1967).

(11) J. K. Lee, E. K. C. Lee, B. Musgrave, Y.-N. Tang, J. W. Root, and F. S. Rowland, *Anal. Chem.*, **34**, 741 (1962).

Results

Under all conditions of irradiation as summarized in Table I, the radioactivity of the tritiated parent molecule was at least 20 times larger than that of the isomer corresponding to inversion at one carbon atom. In each experiment, however, a measurable yield of the tritiated "inversion" compound was obtained. These small yields show up more clearly when the observed counts are accumulated into 10-min interval plots than in the 1-min plots used for the parent molecules. Many other labeled compounds are also observed, usually not in positions which interfere with the determination of the *dl*- and *meso*-DCB activities. An extra, unidentified radioactivity peak was found between the *meso* and *dl* peaks in some O_2-scavenged samples; this peak was completely suppressed by the inclusion of 1,3-butadiene as an additional scavenger. In the absence of information about I_2–DCB solid solubilities, the intracrystal scavenging situation is unknown for the solid samples. Small correction factors, proportional to the relative masses, have been applied to the *meso* data for the macroscopic mass conversion of *dl* to *meso* during liquid phase irradiations.

Table I

(A) Ratio of *meso*- and *dl*-2,3-Dichlorobutane-*t* from Recoil Tritium Reactions with 2,3-Dichlorobutanes

Phase	Sample composition, cm Hg *dl*-DCB	Scavenger	Ar	^{3}He	Relative yield of *meso*-DCB-*t* (*dl*-DCB-*t* = 100)
Gas	1.4	O_2(1.8)	13.2	1.6	1.4 ± 0.4
Gas	1.4	O_2(3.7)	11.3	1.6	~2
Gas	1.5	O_2(4.4)	57.9	3.4	1.2 ± 0.4
Gas	1.5	O_2(8.0)	55.4	7.2	1.3 ± 0.4
Liquid		None	...	LiF	3.2 ± 0.8
Liquid		I_2	...	LiF	2.3 ± 0.6
Solid		I_2	...	LiF	4.5 ± 1.0

(B) Butadiene/O_2 Scavenger

Phase	DCB	Scavengers	^{3}He	Relative Yields *dl*-DCB-*t*	*meso*-DCB-*t*
Gas	*dl*(1.4)	O_2(4.0) 1,3-Bu(2.6) O_2(3.6)	1.9	100	1.2 ± 0.3
Gas	*meso*(1.4)	1,3-Bu(3.1)	2.0	4.6 ± 0.5	100

Configurations Following T-for-H Substitution at an Asymmetric sp³ Carbon Atom. The data of Table I confirm completely the general conclusion from the previous experiments—substitution of T-for-H occurs very preferentially with retention of configuration at the asymmetric sp³ carbon atom. Inversion of configuration during substitution would require appreciable motion by the other substituent atoms and groups, and has been postulated to be highly disfavored because insufficient time is available during the substitution process for completion of the requisite atomic motions.[2-5] Retention of configuration, on the other hand, need not involve extensive adjustment of position by the other substituents and could readily occur on a time scale of $\sim 10^{-14}$ sec. The present experiments are completely consistent with this hypothesis;[2-5] in this, as in the earlier experiments, all of the other substituents are at least as heavy as a methyl group and the question of retention *vs.* inversion with light substituents (*i.e.*, H or D atoms) has not been studied.

Formation of the "Opposite" Isomer in Gas Phase. All of the experiments demonstrate the presence of the "opposite" radioactive isomer in small yield. Precise determination of the per cent retention/inversion at the asymmetric carbon atom would require a determination of the intramolecular distribution of tritium between the CH_3– and –CHCl– positions of each product molecule. Comparisons with other inter- and intramolecular competitions suggests that the *per-bond* substitution of T-for-H will be quite similar for both bond types (perhaps from 70 to 100% as much –CTCl– as CH_2T–, compared per bond),[12,13] and thus that 18–25% of the tritium activity of the parent stereoisomer is actually in the asymmetric C–H position. Even if *all* of the tritium activity of the *meso* isomer from the reaction of T* with *dl*-DCB is in the asymmetric position, the gas-phase preference for retention of configuration is $\geq 93\%$ with this parent molecule. The corresponding lower limit for the *meso* isomer is approximately $\geq 80\%$.

The presence of the labeled opposite isomer is clearly demonstrated by the data of Figure 1 and Table I, keeping open the question of the possible existence of some *bona fide* hot substitution-with-inversion reactions. However, similar gas-phase experiments involving the stereochemistry of the substitution of ^{38}Cl or ^{39}Cl for Cl in 2,3-DCB have shown[10] (a) low, but detectable, yields of the opposite isomer (opposite/parent ~0.02) in butadiene–O_2-scavenged systems and (b) substantial yields of the opposite isomer (ratios from 0.50–1.0) unless butadiene is present. Since the gas-phase yield of the opposite isomer in the tritium experiments is very small (absolute yield ~0.1%), and some small uncertainties exist concerning the detailed scavenging mechanisms under (a) and (b), we do not consider that the small peaks observed in these experiments are positive proof of the presence of a substitution-with-inversion mechanism. The desirability, and great difficulty, of intramolecular determination of the tritium location in the opposite isomer makes further experiments with the 2,3-DCB molecules less advantageous than experiments with similar *dl*, *meso*

(12) T. Smail and F. S. Rowland, *J. Phys. Chem.*, **72**, 1845 (1968).

(13) J. W. Root and F. S. Rowland, *J. Amer. Chem. Soc.*, **84**, 3027 (1962).

pairs containing hydrogen *only* in the asymmetric positions, *e.g.*, CHFClCHFCl.

Inversion Products in Condensed Phases. The yields of *meso*-2,3-DCB-*t* from the reactions of T* with the *dl* parent are definitely higher in the condensed phases than in the gas phase, even though still small. The most probable explanation for these increased yields is that some *dl*-2,3-DCB-*t* molecules, initially formed by T-for-H substitution, are sufficiently excited to decompose by C–Cl bond rupture. The residual C_4H_7TCl radical can then undergo either (a) immediate recombination with the Cl atom, retaining the original stereochemistry; or (b) racemization to a mixture of radicals of both "*dl*" and "*meso*" form, and then recombination with the Cl atom, providing additional yields of both labeled isomeric forms. These recombination processes can be facilitated in the condensed phase by the surrounding solvent or crystal cage, capable of retaining atom and radical in close proximity to one another.

Studies of ^{38}Cl reactions with 2,3-DCB in the condensed phases show large yields of both labeled isomers, in both liquid and solid. The presence of *both* labeled forms in nonequilibrium amounts in the ^{38}Cl experiments has been attributed in close competition between the time scales for racemization of newly-formed $CH_3CHClCHCH_3$ radicals and combination of these radicals with others in the cage. With ^{38}Cl in the liquid phase at room temperature, about 30% of the reformed molecules have the "opposite" configuration from that of the parent.[14] Such cage recombinations, however, play only a small percentage role in the tritium experiments. Assuming similar competitive rates for racemization and recombination, the contribution of cage reactions to the total parent yield is no more than 8% in recoil tritium reactions with 2,3-dichlorobutane.

An alternate hypothesis seems much less likely, but cannot be eliminated by present data. If a substitution-with-inversion mechanism is postulated to *require* the simultaneous deposition of very large amounts of excitation energy,[15] the fraction of such molecules surviving in the gas phase could be substantially smaller than for labeled molecules formed by substitution-with-retention, in agreement with the observations of Table I. Such a postulate is not wildly unreasonable when inversion would be accompanied by motion of CH_3, Cl, and $CHClCH_3$ groups. In any event, the total yield corresponding to stabilized "inversion" product, as measured in condensed phases, is very much smaller than that of the "retention"product, and the heavily predominant mechanism of T-for-H substitution must still be identified as the retention mode.

(14) F. S. Rowland, C. M. Wai, C. T. Ting, and G. Miller, "Chemical Effects on Nuclear Transformations," Vol. I, IAEA, Vienna, 1965, p 333.

(15) See E. K. C. Lee and F. S. Rowland, *J. Amer. Chem. Soc.*, **85**, 897 (1963).

A Multilayer Isotherm with Sensible Spreading Pressure Limits

by C. M. Greenlief and G. D. Halsey

Department of Chemistry, University of Washington, Seattle, Washington 98105 (*Received July 28, 1969*)

Isotherm equations that cover the entire range of adsorption have exhibited one of two types of thermodynamic difficulties: either the lack of a Henry's law region at low coverage, or in the case of the BET equation a spreading pressure that approaches infinity as the pressure tends toward the saturation vapor pressure, P_0.[1]

One of us has proposed an equation that has the virtue of having the correct limiting behavior at both low and high coverage.[2] It is the purpose of this note to explore this equation further.

The isotherm is a linear combination of a virial expansion at low coverage and a term at high coverage due to the decay of surface energy with the third power of the distance. Specifically

$$P = bn \exp[(c/b)n] + P_0 \exp[-a(v/v_m)^{-3}] \quad (1)$$

where c is negative and a and b are positive. n is the amount of gas adsorbed, v is the volume of gas adsorbed, and v_m is the volume of a monolayer of gas; a is a measure of the adsorption potential.

For low coverages, eq 1 becomes

$$P = bn + cn^2 + \ldots \quad (2)$$

These constants can be expressed in terms of gas–solid virial coefficients,[3] ($b = KT/B_{AS}$ and $c = kTC_{AAS}/B^3_{AS}$). The expansion is valid only if c is negative, but this is to be expected in the temperature range below the critical temperature of the adsorbate, in the region where a multilayer isotherm becomes appropriate.[4]

At high coverages eq 1 approaches the limit

$$\ln (P/P_0) = -a/\theta^3 \quad (3)$$

where $\theta = v/v_m$, the surface coverage in monolayers.

Typical isotherms of eq 1 are shown in Figure 1. The isotherm as proposed has no empirical parameters, and its only arbitrary feature is the choice of a simple exponential blending function.

In Figure 2, experimental data of Prenzlow and Halsey[5] for the adsorption of argon on one layer of xenon preadsorbed on graphitized carbon black are fitted to eq 1. The constants have been adjusted to the

(1) H. M. Cassel, *J. Phys. Chem.*, **48**, 195 (1944).

(2) G. D. Halsey, "The Solid–Gas Interface," E. A. Flood, Ed., Marcel Dekker, New York, N. Y., 1967.

(3) W. A. Steele, *Advan. Colloid Interfac. Sci.*, **1**, 3 (1967).

(4) G. D. Halsey, *J. Chem. Phys.*, **36**, 1688 (1962).

(5) C. F. Prenzlow and G. D. Halsey, *J. Phys. Chem.*, **61**, 1158 (1957).

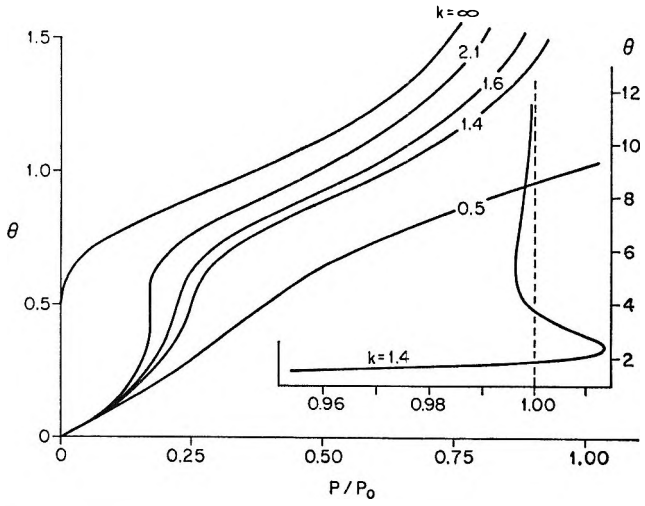

Figure 1. Adsorption isotherms for the equation $P/P_0 = \theta e^{-k\theta} + e^{-1/\theta^2}$.

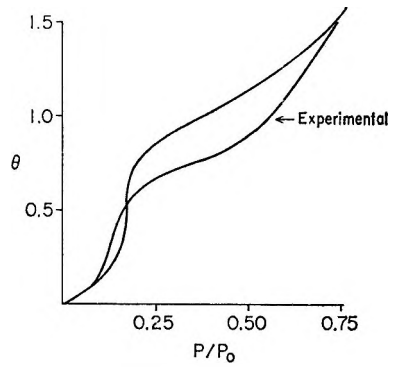

Figure 2. Adsorption isotherms of argon on xenon and eq 1 in the form $P/P_0 = (1.0)\,\theta e^{-2.15\,\theta} + e^{-1.35/\theta^2}$.

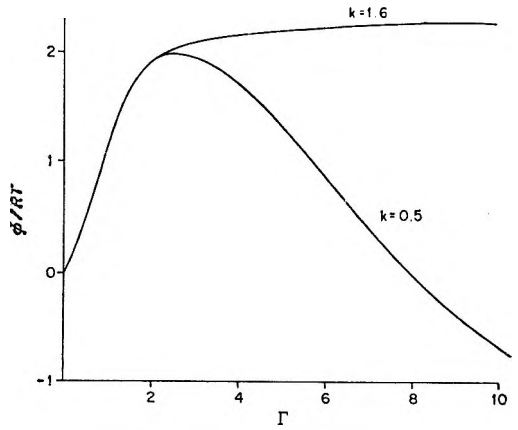

Figure 3. Spreading pressure curves based on the isotherm $P/P_0 = \theta e^{-k\theta} + e^{-1/\theta^2}$.

initial slope and ultimate cube-law regions. The agreement in the intermediate region is reasonable.

It is clear from the shape of the examples of the isotherm that unstable regions are a possibility. Aside from the obvious two-dimensional phase change in the $k = 2.1$, 1.4 isotherms in Figure 1, another type of behavior is encountered in the $k = 0.5$ isotherm of this figure. Because of the nature of this loop, it is not possible to find two phases of equal spreading pressure. Indeed, a calculation of spreading pressure, shown in Figure 3, indicates that the spreading pressure, although it follows the ideal gas law at low coverages, may ultimately pass through zero and become negative. The thick film cannot be in equilibrium with the thin film; this situation corresponds to a liquid not wetting a surface. At saturation the surface would be covered with a rarified film, given by the lowest intersection of the isotherm with the saturation line.

We are indebted to Dr. J. P. Hobson, who sent us a preprint that contains an isotherm of xenon on silver quite similar to the upper part of the $k = 1.4$ isotherm in Figure 1. However, there is a strongly held first layer and a resultant knee in the isotherm that our equation in its simple form cannot fit.

Radiation-Induced Chain Decomposition of Hexachloroethane in Cyclohexane Solutions. Reactions of the Pentachloroethyl Radical

by A. Horowitz and L. A. Rajbenbach

Soreq Nuclear Research Centre, Yavne, Israel
(Received March 3, 1969)

Investigation of the kinetics of chlorine atom elimination from chloro-substituted alkyl radicals

$$C_nH_{2n+1-m}Cl_m \rightleftharpoons C_nH_{2n+1-m}Cl_{m-1} + Cl \quad (1)$$

has been so far limited to several studies in the gas phase.[1-6] Such reactions can appropriately be studied in the gas phase since they require relatively high temperatures, mainly because the activation energy of the forward step of reaction 1 is quite high[2,3] (~20 kcal mol^{-1}) while that of the reverse step is negligible.[5]

The purpose of this study was to investigate the kinetics of the chlorine elimination reaction from

(1) (a) P. B. Ayscough, A. J. Cocker, and F. S. Dainton, *Trans. Faraday Soc.*, **58**, 1128 (1962); (b) P. B. Ayscough, A. J. Cocker, F. S. Dainton, and S. Hirst, *ibid.*, **58**, 295 (1962); (c) *ibid.*, **58**, 318 (1962); (d) F. S. Dainton, D. A. Lomax, and M. Weston, *ibid.*, **58**, 308 (1962).

(2) (a) S. Dusoleil, P. Goldfinger, A. M. Van der Auwera, G. Martens, and D. Van der Auwera, *ibid.*, **57**, 2917 (1961); (b) P. Goldfinger, G. Huybrechts, and G. Martens, *ibid.*, **57**, 2200 (1961); (c) P. Goldfinger and G. Martens, *ibid.*, **57**, 2210 (1961).

(3) G. Huybrechts, L. Meyers, and G. Verbeke, *ibid.*, **58**, 1128 (1962).

(4) J. H. Knox and J. Riddick, *ibid.*, **62**, 1190 (1966).

(5) P. B. Ayscough, F. S. Dainton, and B. E. Fleischfreser, *ibid.*, **62**, 1838 (1966).

(6) C. Cillien, P. Goldfinger, G. Huybrechts, and G. Martens, *ibid.*, **63**, 1631 (1967).

Table I: The Radiolytic Yields of the Main Products of the Radiolysis of C_2Cl_6 Solutions in Cyclohexane[a]

$[C_2Cl_6]$, mM	Temp, °C	$G(C_2Cl_4)$	G(HCl)	$G(C_2Cl_5H)$	G(c-$C_6H_{11}Cl$)	$G(-C_2Cl_6)$[b]	$\frac{G(C_2Cl_4)}{G(C_2Cl_5H)}$	$\frac{G(C_2Cl_4)+G(C_2Cl_5H)}{G$(c-$C_6H_{11}Cl$)}
100	24	102	100	180	255	...	0.57	1.10
25	50	342	368	206	546	...	1.66	1.00
50	50	416	461	240	644	...	1.74	1.02
75	50	550	578	323	795	...	1.70	1.10
100	50	587	632	352	844	...	1.67	1.12
100	75	1600	1510	490	1990	1900	3.24	1.02
25	100	1200	1270	192	1450	1495	6.25	0.96
50	100	2375	2470	366	2575	2700	6.50	1.06
75	100	3400	3410	510	3580	3850	6.65	1.09
100	100	4100	4050	595	4480	4050	6.90	1.04

[a] Total dose: 3.3×10^{18}, 1.6×10^{18}, 6.6×10^{17}, and 2.2×10^{17} eV ml^{-1} for experiments at 24, 50, 75, and 100°, respectively. [b] Average of four determinations.

pentachloroethyl radicals (reaction 1) in the liquid phase. Chlorine atoms react readily with alkanes and therefore the use of alkane solvent would prevent the back reaction and thus destroy the equilibrium. Such conditions would favor the study of the above elimination reaction in the liquid phase.

The reaction between alkyl radicals and hexachloroethane was found[7] to lead to the formation of pentachloroethyl radicals. The irradiation of dilute solutions of hexachloroethane in cyclohexane would thus seem to offer a convenient way to generate pentachloroethyl radicals through the interaction of radiolytically generated cyclohexyl radicals with the solute.

Experimental Section

Materials. Hexachloroethane (Fluka technical grade) was purified by sublimation. The purified material was more than 99.9% pure as determined by analytical gas chromatography and did not contain free chlorine.

Phillips Research grade cyclohexane, stated purity 99.99%, was used as received after it was found that treatment with sulfuric acid[8] did not affect, within experimental error (±5%), the yield of products.

Procedure. Sample preparation and irradiation techniques were identical with those described by us previously.[8,9] The irradiations were carried out at a dose rate of 2.1×10^{17} eV ml^{-1} min^{-1}. The compounds C_2Cl_6, C_2Cl_5H, C_2Cl_4, and c-$C_6H_{11}Cl$ were determined gas chromatographically, using a 12-ft column of 20% silicon oil DC-200 on Diatoport S, 60–80 mesh. They were identified by comparison of retention times with those of corresponding pure samples on both the silicon and on a 12-ft, 20% Ucon column.

To determine the yield of hydrogen chloride, the irradiated samples were kept at liquid air temperature and opened under a layer of water. The aqueous layer was separated, and its HCl content was determined coulometrically using the Aminco-Cotlove chloride titrator.

Results and Discussion

The main radiolytic products at 24, 50, 75, and 100° were found to be pentachloroethane, chlorocyclohexane, tetrachloroethylene, and HCl. The yields of these products are given in Table I. They are expressed in terms of G values and refer to the total number of molecules formed or disappearing per 100 eV of energy deposited into the solution.

Mechanism of Product Formation

The radiolysis of alkanes results in the formation of alkyl radicals *via* carbon–carbon and carbon–hydrogen bond fission. In the case of pure cyclohexane, the C–C bond breakage is relatively small, and the radiolysis of cyclohexane results primarily in the formation of cyclohexyl radicals and hydrogen atoms. Subsequently, the reaction between the hydrogen atoms and the solvent leads to the formation of hydrogen molecules and cyclohexyl radicals. Therefore, per one hydrogen molecule formed through this mechanism, two cyclohexyl radicals are formed. The radiolytic generation of cyclohexyl radicals can thus be represented by

$$2c\text{-}C_6H_{12} \rightsquigarrow 2c\text{-}C_6H_{11} + H_2 \qquad (2)$$

It is possible in the radiolysis of dilute solutions of C_2Cl_6 in cyclohexane that a part of the energy initially deposited in the solvent may be transferred to the solute, leading to its enhanced decomposition. Such energy transfer processes would not be expected to decrease the over-all rate of formation of radicals. The high yields of C_2Cl_5H, C_2Cl_4, HCl, and especially of c-$C_6H_{11}Cl$ (the G value of the latter product approaching 4500 at 100° at 0.1 M solute concentration,

(7) J. P. West and L. Schmerling, *J. Amer. Chem. Soc.*, 72, 3525 (1950).

(8) L. A. Rajbenbach and U. Kaldor, *J. Chem. Phys.*, 47, 242 (1967).

(9) A. Horowitz and L. A. Rajbenbach, *J. Amer. Chem. Soc.*, 91, 4626 (1969).

as compared with approximately 5 for cyclohexyl radicals in the radiolysis of cyclohexane) indicate that all these products are formed by a long chain reaction mechanism. The free-radical nature of the chain mechanism is further supported by the finding that in the radiolysis at 100° of 0.025 M solutions of hexachloroethane in cyclohexane the addition of cyclohexene (0.1 M) depressed the yield of all major products by approximately 90%. The length of the chain and the fact that the radicals involved in the chain mechanism are the same as those that are expected to be formed mainly as result of the radiolytic decomposition of C_2Cl_6 show that no significant error is introduced when reaction 2 is considered as the initiation step of the chain sequence. The fact that within experimental error, the following equalities are observed

$$G(c\text{-}C_6H_{11}Cl) = G(C_2Cl_5H) + G(C_2Cl_4) \quad (I)$$

$$G(-C_2Cl_6) = G(c\text{-}C_6H_{11}Cl) \quad (II)$$

suggests the following propagation steps of the chain reaction

$$c\text{-}C_6H_{11} + C_2Cl_6 \longrightarrow c\text{-}C_6H_{11}Cl + C_2Cl_5 \quad (3)$$

$$C_2Cl_5 + c\text{-}C_6H_{12} \longrightarrow C_2Cl_5H + c\text{-}C_6H_{11} \quad (4)$$

$$C_2Cl_5 \longrightarrow C_2Cl_4 + Cl \quad (5)$$

$$Cl + c\text{-}C_6H_{12} \longrightarrow HCl + c\text{-}C_6H_{11} \quad (6)$$

The chain termination can be expected to result from radical–radical interactions.

It should be noted that according to our reaction scheme the only reaction in which chlorine atoms participate is the abstraction of hydrogen from the solvent (reaction 6). This assumption seems to be justified in view of the very high values of k_6 and the large excess of cyclohexane over the reaction products and intermediates which could react with the chlorine atom.

As far as the cyclohexyl radical is concerned we have not considered the possibility of its addition to tetrachloroethylene. We have recently reported[9] that the addition of alkyl radical to C_2Cl_4 proceeds quite readily and leads to the formation of alkyltrichloroethylene, RC_2Cl_3. Cyclohexyltrichloroethylene, however, was not found among the products in the present system, its absence indicating that under the experimental conditions the addition of cyclohexyl radical to tetrachloroethylene can be discounted. Similarly, one would not expect the addition of the bulky C_2Cl_5 radicals to tetrachloroethylene. The fact that within experimental error $G(HCl) \approx G(C_2Cl_4)$ is consistent with the assumption that C_2Cl_4 is not removed from the system by secondary reactions.

The steady-state treatment of reactions 2–6 leads to the following expressions.

$$G(C_2Cl_5H) = \frac{1}{1 + k_5/k_4[c\text{-}C_6H_{12}]} G(c\text{-}C_6H_{11}Cl) \quad (III)$$

$$G(C_2Cl_4) = \frac{1}{k_4[c\text{-}C_6H_{12}]/k_5 + 1} G(c\text{-}C_6H_{11}Cl) \quad (IV)$$

Thus the yields of C_2Cl_5H and C_2Cl_4 should be proportional to the c-$C_6H_{11}Cl$ yield. The fact that expressions III and IV are obeyed (see Figure 1) lends further support to the chain mechanism proposed.

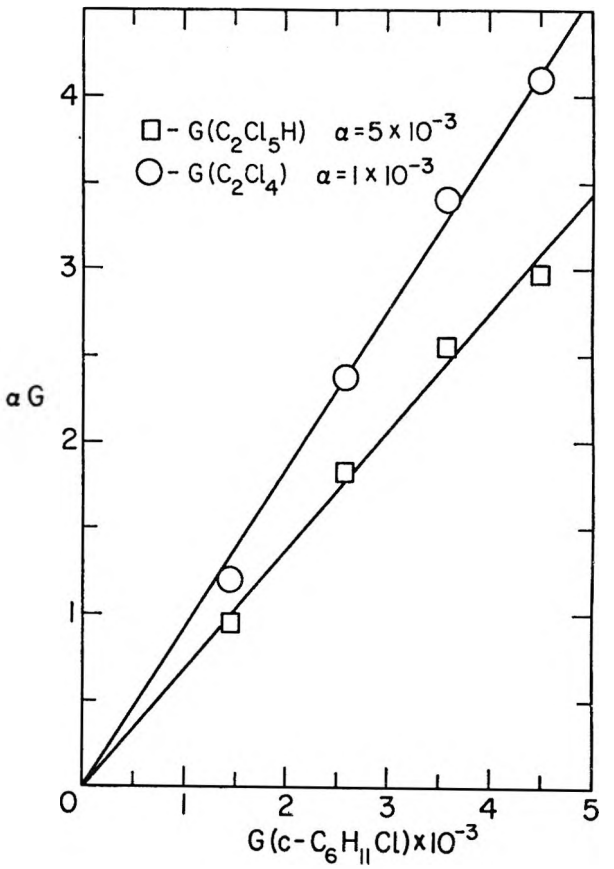

Figure 1. The yields of pentachloroethane and tetrachloroethylene at 100° as a function of the yield of chlorocyclohexane, expressions III and IV.

Determination of the Relative Arrhenius Parameters of Reactions 4 and 5 and the Estimation of E_5

Combining eq III and IV with the Arrhenius formulation for k_5 and k_4, we obtain

$$\log \frac{G(C_2Cl_4)}{G(C_2Cl_5H)} = \log A_5/A_4 - \frac{E_5 - E_4}{RT} \log e - \log [c\text{-}C_6H_{12}] \quad (V)$$

From the plot of $\log [G(C_2Cl_4)/G(C_2Cl_5H)]$ as a function of $1/T$ (see Figure 2) we obtain $A_5/A_4 = 10^{5.9 \pm 0.2} M$ and $E_5 - E_4 = 7.0 \pm 0.2$ kcal mol^{-1}.

The activation energy of the monomolecular elimination of chlorine atom from the pentachloroethyl radical has been determined in the gas phase[2] and

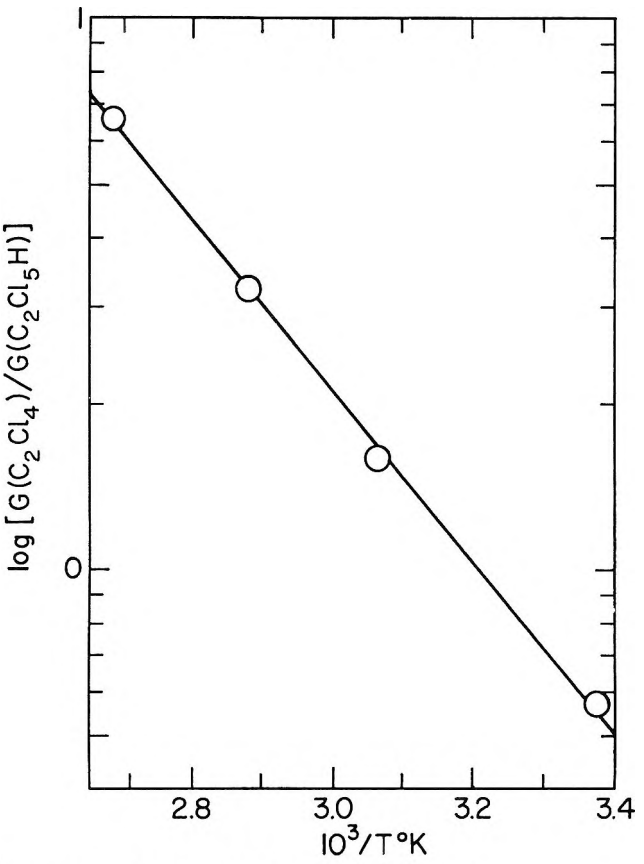

Figure 2. Arrhenius plot for k_5/k_4, expression V.

was found to be 16.8 kcal mol^{-1}. It would therefore be interesting to compare our results with those obtained in the previous study.

The determination of E_5 requires knowledge of the Arrhenius parameters for the abstraction of the hydrogen atom from cyclohexane by the C_2Cl_5 radical. Unfortunately, these parameters are not known. However, the Arrhenius parameters of the analogous reaction of the CCl_3 radical, which may be expected to be fairly close to that of the C_2Cl_5 radical, have been reported. Henglein, *et al.*,[10] arrived at the Arrhenius parameters of the reaction of CCl_3 radicals with cyclohexane by studying the temperature dependence of the chlorocyclohexane yield obtained by a chain mechanism in the radiolysis of CCl_4 solution in cyclohexane. The chain propagation reactions in the c-C_6H_{12}–CCl_4 system were

$$CCl_3 + c\text{-}C_6H_{12} \longrightarrow CCl_3H + c\text{-}C_6H_{11} \quad (7)$$

$$c\text{-}C_6H_{11} + CCl_4 \longrightarrow c\text{-}C_6H_{11}Cl + CCl_3 \quad (8)$$

Assuming the activation energy of reaction 8 to be negligible, the over-all activation energy of 9.6 kcal mol^{-1} for the formation of c-$C_6H_{11}Cl$ was assigned to reaction 7. Using this value of E_7 as equal to E_4, we get 16.9 kcal mol^{-1} for E_5, in close agreement with the results in the gas phase.

(10) A. Henglein, E. Heckel, Y. Ojima, and G. Meisner, *Ber. Bunsenges. Phys. Chem.*, **67**, 988 (1963).

The Wavelength Dependence of the Primary Processes in the Photolysis of Sulfur Dioxide

by T. Navaneeth Rao and Jack G. Calvert

Chemistry Department, The Ohio State University, Columbus, Ohio 43210 *(Received July 22, 1969)*

Recent studies of the photolysis of sulfur dioxide within the first allowed absorption band are in accord with the following reaction mechanism.[1-3]

$$SO_2 + h\nu \longrightarrow {}^1SO_2 \quad (I)$$

$${}^1SO_2 + SO_2 \longrightarrow (2SO_2) \longrightarrow (\text{ground-state } SO_2) \quad (1)$$

$$\longrightarrow {}^3SO_2 + SO_2 \quad (2)$$

$${}^1SO_2 \longrightarrow SO_2 + h\nu_f \quad (3)$$

$$\longrightarrow SO_2 \quad (4)$$

$$\longrightarrow {}^3SO_2 \quad (5)$$

$${}^3SO_2 \longrightarrow SO_2 + h\nu_p \quad (6)$$

$$\longrightarrow SO_2 \quad (7)$$

$${}^3SO_2 + SO_2 \longrightarrow (2SO_2) \longrightarrow (\text{probably } SO_3 + SO) \quad (8)$$

The $^1SO_2$ and $^3SO_2$ represent the first excited singlet (presumably $^1B_1$) and triplet ($^3B_1$) states, respectively, of sulfur dioxide. Very recent work from this laboratory suggests that the dominant ultimate product of reaction 1 is ground-state sulfur dioxide molecules, while that of reaction 8 is SO_3 and SO.[4]

Although there is agreement on the major features of the mechanism, there remains considerable uncertainty as to the importance of reactions 4 and 5 relative to reaction 3. Rao, Collier, and Calvert concluded that the rate of singlet removal by internal conversion and intersystem crossing, (4) and (5), outweighed that by radiative decay, reaction 3.[3a] On the other hand, Mettee concluded that reaction 3 was the only fate of $^1SO_2$ at low pressures of sulfur dioxide.[1a] Strickler and Howell presented no evidence on this matter, but for theoretical reasons they accepted the dominance of (3) in their discussions.[2]

It is very important that further evidence bearing on this feature of the mechanism be obtained, since the significant contribution of first-order, nonradiative decay processes to the deactivation paths in a molecule as simple as sulfur dioxide is unexpected in terms of present

(1) (a) H. D. Mettee, *J. Chem. Phys.*, **49**, 1784 (1968); (b) H. D. Mettee, *J. Phys. Chem.*, **73**, 1071 (1969).

(2) S. J. Strickler and D. B. Howell, *J. Chem. Phys.*, **49**, 1947 (1968).

(3) (a) T. N. Rao, S. S. Collier, and J. G. Calvert, *J. Amer. Chem. Soc.*, **91**, 1609 (1969); (b) T. N. Rao, S. S. Collier, and J. G. Calvert, *ibid.*, **91**, 1616 (1969).

(4) S. Okuda, T. N. Rao, D. H. Slater, and J. G. Calvert, *J. Phys. Chem.*, **73**, 4412 (1969).

theory. In this work we present such evidence based on the measurement of the fluorescence quantum yields of sulfur dioxide at wavelengths 2650, 2750, 2963, and 3020 Å. The methods employed were similar to those described in detail previously in our study of sulfur dioxide photochemistry at 2875 A.[3a]

Many features of the data are in good agreement with the results of the previous workers. Thus the ratios of the quantum yield of phosphorescence to that of fluorescence at each wavelength estimated in this work check well with those reported by Mettee. See the data of Table I. Also the wavelength dependence of the

Table I: Ratio of Phosphorescence to Fluorescence Quantum Yields (ϕ_p/ϕ_f) in Sulfur Dioxide Photolysis at Several Wavelengths for $[SO_2] \geq 10^{-5}$ M

Wavelength, Å	ϕ_p/ϕ_f This work	ϕ_p/ϕ_f Mettee[a]
2650	0.08 ± 0.02	0.08
2750	0.09 ± 0.02	0.10
2850	...	0.14
2875	0.14 ± 0.02[b]	...
2963	0.26 ± 0.02	0.26
3020	0.35 ± 0.05	0.39

[a] Average data for $p_{SO_2} \geq 200$ μ as read from Figure 4 of Mettee.[1a] [b] Data of Rao, Collier, and Calvert.[3a]

ϕ_f values at a given concentration of sulfur dioxide shows the same trends as those reported by Mettee and Strickler and Howell. See Table II. For a given pressure of

Table II: Quantum Yields of Fluorescence from Pure SO_2 Vapor Excited at Several Wavelengths and 25°

$[SO_2]$, $M \times 10^5$	Quantum yield of fluorescence, $\phi_f \times 10^3$ 2650 Å	2750 Å	2963 Å	3020 Å
0.285	53	38	18	14
0.39	39	30	14	11.7
0.62	26	20	8.8	9.0
0.84	19	16	6.8	5.8
1.72	9.5	7.0	3.4	3.3
3.44	5.5	...	...	...
5.16	3.5	2.7	...	1.23
6.90	2.7	2.1	1.03	...
8.62	...	1.6	0.82	0.76
10.40	1.8	...	...	0.57

sulfur dioxide, fluorescence is less efficient at the longer wavelengths.

The slopes of the Stern–Volmer plots of the fluorescence data, shown in Figure 1, provide new estimates of the rate constant ratios, $(k_1 + k_2)/k_3$, as a function of wavelength. These data are summarized in Table III

Table III: Comparison of Ratios of Rate Constants Involving Excited Singlet SO_2 Quenching Reactions at Several Wavelengths and 25°[a]

Wavelength, Å	$(k_1 + k_2)/k_3$, l./mol × 10^5 This work	$(k_1 + k_2)/k_3$, l./mol × 10^5 Mettee[b]	$(k_1 + k_2)/(k_3 + k_4 + k_5)$,[c] l./mol × 10^5
2650	5.3 ± 0.1	1.9 ± 0.4	...
2750	7.0 ± 0.2	3.4 ± 0.3	...
2850–2894	6.6 ± 0.3[d]	5.6 ± 0.6	2.7 ± 0.5
2963–2967	13.8 ± 0.4	10.2 ± 1.0	3.4 ± 0.8
3020–3021	15.9 ± 0.9	10.7 ± 0.8	3.9 ± 1.2
3130–3132	...	20.1 ± 0.7	7.2 ± 2.0

[a] The error limits shown are the 95% confidence limits; those quoted for the data of Strickler and Howell were derived for the data of their Figure 4 by the authors. All data points were used in deriving the estimates for this work. [b] Reference 1a. [c] Reference 2. [d] Reference 3a.

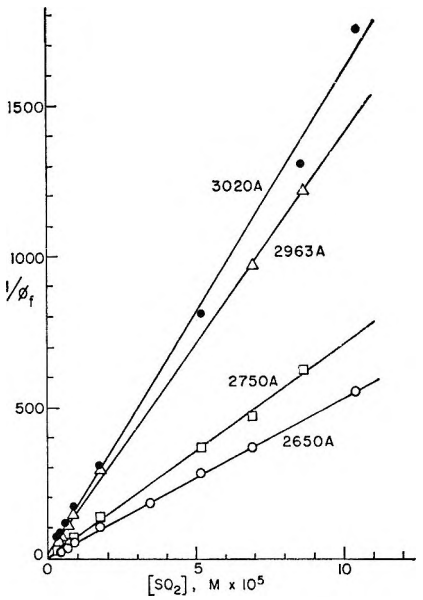

Figure 1. Stern–Volmer plot of the quantum yields of fluorescence for SO_2 excited at several wavelengths and at 25°. Open circles, 2650 Å; squares, 2750 Å; triangles, 2963 Å; closed circles, 3020 Å; the lines drawn through the data are the least-squares fits using all of the points; the slopes of these lines were used to derive the estimates of $(k_1 + k_2)/k_3$ given in Table IV.

where they are compared with previous estimates of this ratio by Mettee[1a] and the related ratio $(k_1 + k_2)/(k_3 + k_4 + k_5)$, determined by Strickler and Howell.[2] The agreement of our data and those of Mettee at the 2850–2875, 2963, and 3020-Å regions is reasonably good, but at 2650 and 2750 Å the agreement is only within a factor of about 2. Obviously there are some undetermined errors other than random errors which contribute to one or both of these sets of estimates.

The previous conclusion of Rao, Collier, and Calvert[3a] that the limiting quantum yield of fluorescence is much less than unity at $[SO_2] = 0$, is supported by these new findings. Table IV summarizes these data. ϕ_f

Table IV: Comparison of Data for Limiting Quantum Yields of Fluorescence of SO_2, $[SO_2] = 0$, at Several Wavelengths and 25°.

Wavelength, Å	Quantum yield of fluorescence at $[SO_2] = 0$[a] This work	Mettee[b]	Estimated from $^1SO_2$ quenching rate data[c]
2650	0.55 ± 0.43	1.4 ± 0.6	
2750	0.13 ± 0.05	1.2 ± 0.4	
2850–2894	0.14 ± 0.06[d]	1.0 ± 0.6	0.44 ± 0.11
2960–2967	0.15 ± 0.14	0.86 ± 0.45	0.28 ± 0.09
3020–3021	0.061 ± 0.12	0.97 ± 0.43	0.29 ± 0.11
3130–3132	...	0.67 ± 0.72	0.36 ± 0.40

[a] Error limits shown are the 95% confidence limits. Only the low concentration data ($[SO_2] \leq 0.84 \times 10^{-5} M$) were used in this case since these give the most accurate intercept determination. [b] Reference 1a. [c] Estimated in this work from the ratio at each wavelength of the Strickler and Howell data[2] for $(k_1 + k_2)/(k_3 + k_4 + k_5)$ to the average of the rate constant estimates of $(k_1 + k_2)/k_3$ for that wavelength range from this work and that of Mettee.[1a] The error limits shown in this case are estimated by the authors from the original Strickler and Howell data, those reported by Mettee, and those found in this work. [d] Reference 3a.

at $[SO_2] = 0$, as derived from the intercept of the Stern–Volmer plots, is well below unity at all the wavelengths employed. The comparable data of Mettee suggest $\phi_f \cong 1$ within the error limits at each wavelength.

A further check on the two divergent results is possible from a combination of the $^1SO_2$-quenching rate data of Strickler and Howell[2] and those of Mettee and our present work. The slope of the Strickler and Howell plot of the function $(I^\infty_f/I_f) - 1$ *vs.* $1/p_{SO_2}$ gives directly $(k_3 + k_4 + k_5)/(k_1 + k_3)$. An average of the rate constant estimates of Mettee and our data can provide a best estimate of $(k_1 + k_2)/k_3$ for several wavelength regions common to all the studies. The reciprocal of the product of these two functions gives an independent estimate of ϕ_f at $[SO_2] = 0$ ($\phi_f = k_3/(k_3 + k_4 + k_5)$ for these conditions). The estimates derived in this fashion are shown in the last column of Table IV. In each case the data suggest an efficiency of process 3 which is well below unity. However, this check is of questionable validity. Mettee has compared his work directly with that of Strickler and Howell by plotting his raw fluorescence data in the Strickler and Howell form.[1a] The original data, the actual plots, and the values of $(k_1 + k_2)/(k_3 + k_4 + k_5)$ are not shown, but Mettee indicates that the rate constant ratios are from two to three times those obtained by Strickler and Howell. Since Mettee's estimates of $(k_1 + k_2)/k_3$ are also in general two to three times the value of $(k_1 + k_2)/(k_3 + k_4 + k_5)$ from Strickler and Howell, Mettee's data seem consistent within themselves and reflect a value of ϕ_f at $[SO_2] = 0$ near unity and $k_4 + k_5 \ll k_3$. Mettee suggests that the difference between his own work and that of Strickler and Howell may result from systematic errors in pressure measurements.

We have been unable to rationalize the large difference between our and Mettee's intercepts of the Stern–Volmer plots. In our opinion the low values for ϕ_f at $[SO_2] = 0$ obtained in our work are not caused by some artifact of the instrument or the methods employed by us, since the results of analogous experiments with biacetyl are entirely consistent with those of previous workers.

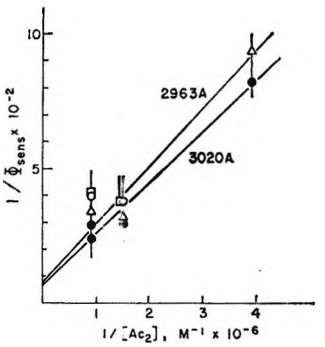

Figure 2. Plot of the reciprocal of the quantum yield of the $^3SO_2$-sensitized phosphorescence from biacetyl *vs.* the reciprocal of the $[Ac_2]$. Open circles, 2650-Å excitation; squares, 2750 Å; triangles, 2963 Å; closed circles, 3020 Å.

In any case the present findings require that one accept with reservation the conclusion of Mettee of a perfect efficiency of fluorescence of SO_2 at zero pressure. The present data continue to support the contention made by Rao, Collier, and Calvert previously[3a] that internal energy dissipation in sulfur dioxide can compete favorably with fluorescence emission even in the limit of zero pressure. Our previous work at 2875 Å suggested that the rate of internal conversion far outweighed that for intersystem crossing $k_4 > k_3 > k_5$. Our present results can be explained at least qualitatively by assuming that the extent of coupling which occurs between the vibronic levels of the $^1SO_2$ and the ground-state molecule is sufficiently great to override the intrinsic low density of states in the molecule. The abnormally long lifetime[5] of $^1SO_2$ has been rationalized in these terms.[2,6,7]

(5) K. F. Greenough and A. B. F. Duncan, *J. Amer. Chem. Soc.*, **83**, 555 (1961).
(6) A. E. Douglas, *J. Chem. Phys.*, **45**, 1007 (1966).
(7) D. P. Chock, J. Jortner, and S. A. Rice, *ibid.*, **49**, 610 (1968).

Two additional features of this work are worthy of note. In the process of establishing the needed wavelength dependence of the fluorescence intensity envelope at the wavelengths of excitation employed in this work, we carried out experiments with added biacetyl. The quantum yields of the SO_2-sensitized phosphorescence in biacetyl (ϕ_{sens}) were calculated from these runs as reported in Table V. Biacetyl at low concentrations

Table V: Quantum Yields of SO_2-Sensitized Biacetyl Phosphorescence (ϕ_{sens}) in the Photolysis of SO_2 in SO_2–Biacetyl Mixtures at Several Wavelengths and 25°; $[SO_2] = 8.62 \times 10^{-5}\ M$

Exciting wavelength, Å	$[Ac_2]$, $M \times 10^5$	$\phi_{sens} \times 10^3$
2650	0.0665	2.6
2650	0.111	2.5
2750	0.0665	2.6
2750	0.111	2.4
2963	0.0259	1.06
2963	0.0665	3.1
2963	0.111	2.9
3020	0.0259	1.2
3020	0.0665	3.5
3020	0.111	3.5
3020	0.111	4.2

quenches the triplet sulfur dioxide molecule efficiently without serious depletion of the singlet molecule concentration. Presumably reactions 9, 10, and 11 describe the additional events which occur on addition of small quantities of biacetyl to sulfur dioxide

$$^3SO_2 + Ac_2 \longrightarrow SO_2 + {}^3Ac_2 \quad (9)$$

$$^3Ac_2 \longrightarrow Ac_2 + h\nu'_p \quad (10)$$

$$\longrightarrow Ac_2 \quad (11)$$

According to the proposed mechanism, the intercept of the $1/\phi_{sens}$ *vs.* $1/[Ac_2]$ plot should give $(k_{10} + k_{11})(k_1 + k_2)/k_{10}k_2$.[3a] At the two wavelengths where an intercept determination can be made realistically, the data give ~78 for 2963 Å and ~66 for 3020 Å. Taking $k_{10}/(k_{10} + k_{11}) = 0.15$[8] we estimate that $k_2/(k_1 + k_2) \cong 0.09$ at 2963 Å and ~0.10 at 3020 Å. These estimates are very similar to the previous estimate for this rate constant ratio (0.08) made in experiments at 2875 Å.[3a] One may conclude tentatively that there is no dramatic wavelength dependence to the fraction of $^1SO_2$ which form triplets on undergoing a quenching collision with sulfur dioxide.

It is interesting to speculate as to the origin of the variation of the ϕ_p/ϕ_f ratio at high $[SO_2]$ with wavelength. See Table I. In theory $\phi_p/\phi_f = k_6k_2/k_3k_8$ for these conditions. All the previous studies[1-3] suggest that the triplet emission occurs from a vibronically relaxed $^3SO_2$ species for all energies (within the first allowed band) of $^1SO_2$ excitation employed. Hence, it seems unlikely that either k_6 or k_8 varies significantly with wavelength used in the sulfur dioxide photolysis. Also the present work shows that the $k_2/(k_1 + k_2)$ ratio is rather insensitive to wavelength change; unless $k_1 + k_2$ varies proportional to k_2 as the exciting wavelength is changed, then k_2 is approximately independent of the exciting wavelength. Thus it seems reasonable to suspect that the variation of k_3 is the major cause of the ϕ_p/ϕ_f ratio change with wavelength. This is in agreement with the conclusions of Mettee[1a] and Strickler and Howell.[2] Such a view is also in accord with the qualitative experimental observations of Douglas that the lifetime of the $^1SO_2$ state decreases with decrease in wavelength, and the theoretical expectations of Dexter and Fowler[9] and Strickler and Howell.[2] If the observed changes are due to k_3 alone, then k_3 increases by a factor of about 4.4 in magnitude over the range 3020 to 2650 Å. The present data for the ratio of $k_3/(k_3 + k_4 + k_5)$ are not sufficiently accurate to test this hypothesis well, but the trend of values for our data shown in Table IV is consistent with it.

Experimental Section

The experimental methods of fluorescence and phosphorescence measurement were essentially the same as those described in detail previously.[3a] All measurements were made on the Turner Model 210 absolute spectrophosphorimeter. One minor modification of the basic equipment was made. The quartz cell used in the previous study was replaced with a special Supracil cell (1 × 1 × 4 cm) which gave less scatter and fluorescence background.

Light absorption by sulfur dioxide at each of the wavelength regions followed the Beer–Lambert law well. The apparent extinction coefficient, as determined on the Turner Model 210 using the same excitation band width as that employed in the fluorescence work, are as follows: 2650 Å, 86.5; 2750 Å, 154; 2963 Å, 180; and 3020 Å, 120 l./mol-cm.

In the integration of the emission envelope we used the following wavelength limits: excitation at 2650 Å, 3000–5100 Å; excitation at 2750 Å, 3100–5200 Å; excitation at 2963 Å, 3250–5200 Å; and excitation at 3020 Å, 3300–5200 Å. The measured area represented the following fractions of the total areas of the emission envelope ($1/a$ as defined previously[3a]): 2650 Å, 0.877; 2750 Å, 0.856; 2963 Å, 0.784; and 3920 Å, 0.844. Calculations of both the fluorescence and phosphorescence

(8) (a) G. M. Almy and P. R. Gillette, *J. Chem. Phys.*, 11, 188 (1943); (b) S. S. Collier, D. H. Slater, and J. G. Calvert, *J. Photochem. Photobiol.*, 7, 737 (1968).

(9) D. L. Dexter and W. B. Fowler, *J. Chem. Phys.*, 47, 1379 (1967).

yields were carried out using the method detailed previously.[3a]

Acknowledgment. The authors acknowledge gratefully the support of this work through a research grant from the National Air Pollution Control Administration, U. S. Department of Health, Education, and Welfare, Public Health Service, Arlington, Va. We wish to thank Drs. George Jackson and David Slater for help in the treatment of data.

COMMUNICATIONS TO THE EDITOR

Entropies of Sodium and Hydroxide Ions and the Thermodynamics of Ionization of Water

Sir: There is significant disagreement between the reported values for the heat of ionization of water obtained from two different methods of determination. The equilibrium constant for the self-ionization of water (reaction 1) has been determined over a wide temperature range from an extensive series of measurements.[1]

$$H_2O(l) = H^+(aq) + OH^-(aq) \qquad (1)$$

By use of the van't Hoff equation, a value of $\Delta H_1° = 13.52$ kcal/mol is obtained from the temperature dependence of the equilibrium constant. Directly measured values for the heat of this same reaction at 25°, obtained from the calorimetric results of many investigators,[2] lead to a value of $\Delta H_1° = 13.34$ kcal/mol. This discrepancy is more than five times the "quoted" uncertainties in the values of $\Delta H_1°$.

For comparison with later calculations, the values of $\Delta H_1°$ are now combined witht he value of $\Delta G_1° = 19.093$ kcal/mol, obtained from the equilibrium constant for the self-ionization of water at 25°,[1] to give $\Delta S_1°$. Further combination of these values with the entropy of $H_2O(l)$[3,4] results in values for the partial molal entropy, $\bar{S}_2°$ of the $OH^-(aq)$ ion of -1.97 gibbs/mol from the temperature dependence of the equilibrium constant for reaction 1 and $\bar{S}_2° = -2.57$ gibbs/mol from the calorimetrically determined $\Delta H_1°$. In view of the care taken in the work that led to both of the above values, an independent path that leads to the value of $\bar{S}_2°$ of $OH^-(aq)$ would prove useful in resolving the small but important discrepancy in the thermodynamics of ionization of water.

Such a path is available from data recently reported in the literature. To ensure that no data are used in this calculation of $\bar{S}_2°$ of $OH^-(aq)$ which depend on measured values of $\Delta H_1°$, a calculation is first presented that leads to the $\bar{S}_2°$ of $Na^+(aq)$. For the reaction

$$NaCl(c) = Na^+(aq) + Cl^-(aq) \qquad (2)$$

the standard free energy change is calculated from the equation

$$\Delta G° = -RT \ln \gamma_\pm^2 s^2 \qquad (3)$$

where $\gamma_\pm$, the mean activity coefficient of NaCl in the saturated solution, is obtained from Robinson and Stokes' tabulation[5] and s, the molal solubility of NaCl(c), is taken from Seidell.[6] This leads to $\Delta G_2° = -2.160$ kcal/mol. The standard heat of solution of NaCl(c) is 0.928 kcal/mol.[7] Combining these two values leads to $\Delta S_2° = 10.36$ gibbs/mol. The entropy of $Cl^-(aq)$ is taken from a third-law analysis of the Ag/AgCl potential by Ahluwalia and Cobble[8] to be 13.51 gibbs/mol. This value is dependent only on $\bar{S}_2°$ defined as 0 for $H^+(aq)$ and third-law entropies for pure compounds. A value of $S° = 17.33$ gibbs/mol for NaCl(c) was obtained from low-temperature heat capacity measurements.[9] These are then combined with

(1) Data reviewed in H. S. Harned and B. B. Owen, "The Physical Chemistry of Electrolytic Solutions," 3rd ed, Reinhold Publishing Corp., New York, N. Y., 1958.

(2) Data reviewed in J. W. Larson and L. G. Hepler, "Solute–Solvent Interactions," C. D. Ritchie and J. F. Coetzee, Ed., Marcel Dekker, Inc., New York, N. Y., 1969.

(3) D. D. Wagman, W. H. Evans, V. B. Parker, I. Halow, S. M. Bailey, and R. H. Schumm, National Bureau of Standards Technical Note 270-3, U. S. Government Printing Office, Washington, D. C., 1968.

(4) The value of the entropy of $H_2O(l)$ is derived from the spectroscopic value for the entropy of $H_2O(g)$ and is completely independent of the thermodynamics of reaction 1. Private communication with V. B. Parker.

(5) R. A. Robinson and R. H. Stokes, "Electrolyte Solutions," 2nd ed, Revised, Butterworth and Co., Ltd., London, 1961.

(6) A. Seidell, "Solubilities of Inorganic and Metal Organic Compounds," 3rd ed, D. Van Nostrand Co., Inc., New York, N. Y., 1940.

(7) V. B. Parker, "Thermal Properties of Aqueous Uni-univalent Electrolytes," NSRDS-NBS2, U. S. Government Printing Office, Washington, D. C., 1965.

(8) J. C. Ahluwalia and J. W. Cobble, *J. Amer. Chem. Soc.*, **86**, 5381 (1964).

(9) K. K. Kelly and E. G. King, U. S. Bureau of Mines Bulletin 592, U. S. Government Printing Office, Washington, D. C., 1961.

$\Delta S_2°$ to give $\bar{S}_2° = 14.18$ gibbs/mol for $Na^+(aq)$. This value is in good agreement with the value reported in reference 3, a value which might have involved the entropy of $OH^-(aq)$.

Because the monohydrate of sodium hydroxide is the hydrate in equilibrium with the saturated solution at 25°, for reaction 4

$$NaOH \cdot H_2O(c) = Na^+(aq) + OH^-(aq) + H_2O(liq) \quad (4)$$

$\Delta G_4°$ may be calculated from the equation

$$\Delta G° = -RT \ln \gamma_\pm^2 s^2 a_w \quad (5)$$

where s is the molal solubility of $NaOH \cdot H_2O(s)$ in water at 25°, $\gamma_\pm$ is the mean activity coefficient of NaOH in the saturated solution, and a_w is the activity of H_2O in the saturated solution. Substituting the value of the solubility reported by Siemens and Giauque[10] and the values of a_w and $\gamma_\pm$ from Stokes[11] leads to $\Delta G_4° = -6.342$ kcal/mole. The standard heat of solution of $NaOH \cdot H_2O(s)$ is reported as $\Delta H_4° = -5.118$ kcal/mol.[7,12] These values may then be combined to give $\Delta S_4° = 4.41$ gibbs/mol. This value is then further combined with the entropy of $Na^+(aq)$, calculated above, the entropy of $H_2O(l)$,[3] and the entropy of $NaOH \cdot H_2O(c)$[12] to give $\bar{S}_2° = -2.70$ gibbs/mol for the $OH^-(aq)$ ion.

The value of $\bar{S}_2°$ of $OH^-(aq)$ obtained by this calculation is in good agreement with the calorimetrically measured heat of ionization of water but not with the value obtained from the temperature dependence of the equilibrium constant. The apparently erroneous value of $\Delta H_1°$ obtained from the temperature dependence of this equilibrium data is indicative of the severe strain placed on even good data by differentiation. A small systematic error that resulted in the value of $\Delta G_1°$ determined at 50° being 0.05% too low and the value of 0° being 0.05% too high would lead to a value of $\Delta H_1°$ that was 1% too high. Such an error would, of course, be difficult to detect and, therefore, to eliminate.

Acknowledgment. The author wishes to thank Professor L. Hepler for discussions and useful suggestions on the subject of this paper and the Benedum Foundation for financial support.

(10) P. R. Siemens and W. F. Giauque, *J. Phys. Chem.*, **73**, 149 (1969).

(11) R. H. Stokes, *J. Amer. Chem. Soc.*, **67**, 1689 (1945).

(12) L. E. Murch and W. F. Giauque, *J. Phys. Chem.*, **66**, 2052 (1962).

DEPARTMENT OF CHEMISTRY
MARSHALL UNIVERSITY
HUNTINGTON, WEST VIRGINIA 25701

JOHN W. LARSON

RECEIVED OCTOBER 29, 1969